ISSN 0021-9673

VOL. 599 NOS. 1 + 2 MAY 22, 1992

COMPLETE IN ONE ISSUE

11th Int. Symp. on HPLC of proteins, peptides and polynucleotides Washington, DC, October 20–23, 1991

JOURNAL OF CHROMATOGRAPHY

INCLUDING ELECTROPHORESIS AND OTHER SEPARATION METHODS

SYMPOSIUM VOLUMES

ELSEVIER

JOURNAL OF CHROMATOGRAPHY

INCLUDING ELECTROPHORESIS AND OTHER SEPARATION METHODS

Scope. The *Journal of Chromatography* publishes papers on all aspects of chromatography, electrophoresis and related methods. Contributions consist mainly of research papers dealing with chromatographic theory, instrumental development and their applications. The section *Biomedical Applications*, which is under separate editorship, deals with the following aspects: developments in and applications of chromatographic and electrophoretic techniques related to clinical diagnosis or alterations during medical treatment; screening and profiling of body fluids or tissues with special reference to metabolic disorders; results from basic medical research with direct consequences in clinical practice; drug level monitoring and pharmacokinetic studies; clinical toxicology; analytical studies in occupational medicine.

Submission of Papers. Manuscripts (in English; *four* copies are required) should be submitted to: Editorial Office of *Journal of Chromatography*, P.O. Box 681, 1000 AR Amsterdam, Netherlands, Telefax (+31-20) 5862 304, or to: The Editor of *Journal of Chromatography, Biomedical Applications*, P.O. Box 681, 1000 AR Amsterdam, Netherlands. Review articles are invited or proposed by letter to the Editors. An outline of the proposed review should first be forwarded to the Editors for preliminary discussion prior to preparation. Submission of an article is understood to imply that the article is original and unpublished and is not being considered for publication elsewhere. For copyright regulations, see below.

Publication. The *Journal of Chromatography* (incl. *Biomedical Applications*) has 39 volumes in 1992. The subscription prices for 1992 are:

J. Chromatogr. (incl. *Cum. Indexes, Vols. 551–600*) + *Biomed. Appl.* (Vols. 573–611):
Dfl. 7722.00 plus Dfl. 1209.00 (p.p.h.) (total *ca.* US$ 4880.25)

J. Chromatogr. (incl. *Cum. Indexes, Vols. 551–600*) only (Vols. 585–611):
Dfl. 6210.00 plus Dfl. 837.00 (p.p.h.) (total *ca.* US$ 3850.75)

Biomed. Appl. only (Vols. 573–584):
Dfl. 2760.00 plus Dfl. 372.00 (p.p.h.) (total *ca.* US$ 1711.50).

Subscription Orders. The Dutch guilder price is definitive. The US$ price is subject to exchange-rate fluctuations and is given as a guide. Subscriptions are accepted on a prepaid basis only, unless different terms have been previously agreed upon. Subscriptions orders can be entered only by calender year (Jan.–Dec.) and should be sent to Elsevier Science Publishers, Journal Department, P.O. Box 211, 1000 AE Amsterdam, Netherlands, Tel. (+31-20) 5803 642, Telefax (+31-20) 5803 598, or to your usual subscription agent. Postage and handling charges include surface delivery except to the following countries where air delivery via SAL (Surface Air Lift) mail is ensured: Argentina, Australia, Brazil, Canada, China, Hong Kong, India, Israel, Japan*, Malaysia, Mexico, New Zealand, Pakistan, Singapore, South Africa, South Korea, Taiwan, Thailand, USA. *For Japan air delivery (SAL) requires 25% additional charge of the normal postage and handling charge. For all other countries airmail rates are available upon request. Claims for missing issues must be made within three months of our publication (mailing) date, otherwise such claims cannot be honoured free of charge. Back volumes of the *Journal of Chromatography* (Vols. 1–572) are available at Dfl. 217.00 (plus postage). Customers in the USA and Canada wishing information on this and other Elsevier journals, please contact Journal Information Center, Elsevier Science Publishing Co. Inc., 655 Avenue of the Americas, New York, NY 10010, USA, Tel. (+1-212) 633 3750, Telefax (+1-212) 633 3990.

Abstracts/Contents Lists published in Analytical Abstracts, Biochemical Abstracts, Biological Abstracts, Chemical Abstracts, Chemical Titles, Chromatography Abstracts, Clinical Chemistry Lookout, Current Contents/Life Sciences, Current Contents/Physical, Chemical & Earth Sciences, Deep-Sea Research/Part B: Oceanographic Literature Review, Excerpta Medica, Index Medicus, Mass Spectrometry Bulletin, PASCAL-CNRS, Pharmaceutical Abstracts, Referativnyi Zhurnal, Research Alert, Science Citation Index and Trends in Biotechnology.

See inside back cover for Publication Schedule, Information for Authors and information on Advertisements.

0021-9673/92/$05.00

This issue is printed on acid-free paper

Printed in the Netherlands

For Contents, see p. VII.

FOR ADVERTISING INFORMATION PLEASE CONTACT OUR ADVERTISING REPRESENTATIVES

USA/CANADA

Weston Media Associates

Mr. Daniel S. Lipner
P.O. Box 1110, GREENS FARMS, CT 06436-1110
Tel: (203) 261-2500, Fax: (203) 261-0101

GREAT BRITAIN

T.G. Scott & Son Ltd.

Tim Blake
Portland House, 21 Narborough Road
COSBY, Leicestershire LE9 5TA
Tel: (0533) 753-333, Fax: (0533) 750-522

Mr. M. White or Mrs. A. Curtis
30-32 Southampton Street, LONDON WC2E 7HR
Tel: (071) 240 2032, Fax: (071) 379 7155,
Telex: 299181 adsale/g

JAPAN

ESP - Tokyo Branch

Mr. S. Onoda
20-12 Yushima, 3 chome, Bunkyo-Ku
TOKYO 113
Tel: (03) 3836 0810, Fax: (03) 3839-4344
Telex: 02657617

REST OF WORLD

ELSEVIER SCIENCE PUBLISHERS

Ms. W. van Cattenburch
P.O. Box 211, 1000 AE AMSTERDAM,
The Netherlands
Tel: (20) 515.3220/21/22, Telex: 16479 els vi nl
Fax: (20) 683.3041

Wilson and Wilson's Comprehensive Analytical Chemistry Volume XXVIII

Analysis of Substances in the Gaseous Phase

by **E. Smolková-Keulemansová** *and* **L. Feltl**, *Charles University, Department of Analytical Chemistry, Prague, Czechoslovakia*
Series Editor **G. Svehla**, *Department of Chemistry, University College, Cork, Ireland*

Nowadays, there are increasing demands for the control and specification of all aspects of industrial manufacturing. There is also a growing need to understand various biological processes and conditions for agricultural production, and concern for protection of the environment and human health. These factors have made it imperative to develop adequate methods for the analysis of gaseous substances or substances that can be converted to the gaseous state. It is not only necessary to apply known and developed methods correctly, but novel analytical procedures must also be found. Instrumentation should be improved and the applications of these methods will have to be extended.

The present volume provides a comprehensive description of the state-of-the-art and of future possibilities in the analysis of gaseous substances. In the individual chapters the following themes have been discussed: the theoretical basis for the methods, a description of the instrumentation and the steps necessary in actual analyses and an outline of the principal areas in which each method can be employed. Both classical methods that are still useful for the solution of analytical problems using simple instrumentation, and the newest methods in the field are described. Special attention is paid to modern electrochemical and spectroscopic methods, and to methods based on a number of physical principles. Gas chromatography is discussed in the greatest detail because of its specially important position in modern analytical chemistry.

The book should be well received by the analytical public and should be extremely useful to students and workers in scientific research laboratories and in fields dealing with environmental protection.

1991 xiv + 480 pages
Price: US $ 205.00 / Dfl. 400.00
Subscription price:
US $ 184.50 / Dfl. 360.00
ISBN 0-444-89122-6

Elsevier Science Publishers
P.O. Box 211, 1000 AE Amsterdam, The Netherlands
P.O. Box 882, Madison Square Station, New York, NY 10159, USA

JOURNAL OF CHROMATOGRAPHY

VOL. 599 (1992)

JOURNAL of CHROMATOGRAPHY

INCLUDING ELECTROPHORESIS AND OTHER SEPARATION METHODS

SYMPOSIUM VOLUMES

ELSEVIER
AMSTERDAM — LONDON — NEW YORK — TOKYO

J. Chromatogr., Vol. 599 (1992)

Washington, DC, The Patent Office in 1884

0021-9673/92/$05.00

Printed in the Netherlands

SYMPOSIUM VOLUME

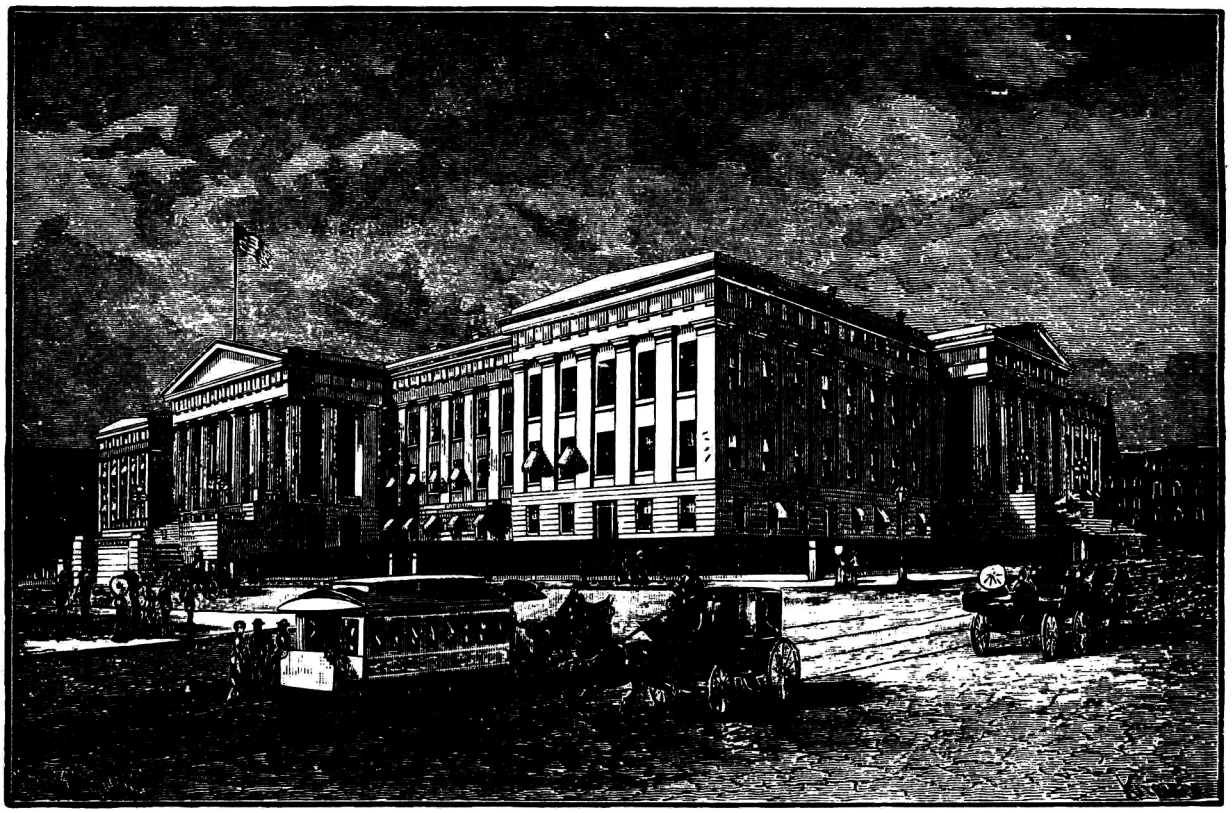

11TH INTERNATIONAL SYMPOSIUM ON HIGH-PERFORMANCE LIQUID CHROMATOGRAPHY OF PROTEINS, PEPTIDES AND POLYNUCLEOTIDES

Washington, DC (USA), October 20–23, 1991

Guest Editors

FRED E. REGNIER
(West Lafayette, IN, USA)

JOSEPH J. DeSTEFANO
(West Chester, PA, USA)

MILTON T. W. HEARN
(Melbourne, Australia)

JAN-CHRISTER JANSON
(Uppsala, Sweden)

B. R. ÖSTERLUND
(Uppsala, Sweden)

KLAUS K. UNGER
(Mainz, Germany)

CONTENTS

11TH INTERNATIONAL SYMPOSIUM ON HIGH-PERFORMANCE LIQUID CHROMATOGRAPHY OF PROTEINS, PEPTIDES AND POLYNUCLEOTIDES, WASHINGTON, DC, OCTOBER 20–23, 1991

In articles with more than one author, the name of the author to whom correspondence should be addressed is indicated in the article heading by a 6-pointed asterisk (*).

Journal of Chromatography, 599 (1992) 1
Elsevier Science Publishers B.V., Amsterdam

CHROMSYMP. 2560

Foreword

The *Eleventh International Symposium on High-Performance Liquid Chromatography of Proteins, Peptides and Polynucleotides* was held at the Sheraton Washington Hotel in Washington, DC, USA, from October 20th to 23rd, 1991. Washington showed its absolute best side with beautiful fall weather, friendly atmosphere and superb hospitality. The approximately 300 participants were able to enjoy a very successful meeting, with 32 lectures and 100 posters in 8 different sessions. High-performance liquid chromatography (HPLC) of macromolecules continues to be an interesting and ever-developing area of research. The structure of packing materials and the dynamic processes occurring between macromolecules and particulate surfaces still attract much interest. The integration of HPLC with other techniques is another area of interest. Most notably among the techniques used are mass spectrometry for increasing the sensitivity of detection and chemometric methods for designing experiments and evaluating chromatographic results.

The participants were also able to enjoy a good social programme, from a welcome reception, through a reception and buffet at the historic Union Station, to a farewell dinner at the Sheraton Washington Hotel.

The intensive three-day programme provided a stimulating forum for the exchange of new research findings, ideas and concepts in many areas of the life sciences, where HPLC continues to play an important role. I would like to thank all those who contributed to the meeting and shared their research results, thoughts and knowledge in both presentations and discussions. I would also like to thank the members of the Scientific Committee (M. T. W. Hearn, K. K. Unger, F. E. Regnier, J. J. DeStefano and J.-C. Janson) for their tireless efforts in composing a scientific programme of high quality. Thanks are also due to Dr. Erich Heftmann, Editor of the *Journal of Chromatography* Symposium Volumes, for his editing of this proceedings volume. The generous support of Pharmacia LKB Biotechnology, Tosoh Co. and Bio-Rad Laboratories in sponsoring the social programme is much appreciated. Finally, I want to thank Ms. Janet Cunningham of Barr Enterprises for her assistance in the organization of the meeting.

Uppsala (Sweden) Bengt R. Österlund

Journal of Chromatography, 599 (1992) 3–11
Elsevier Science Publishers B.V., Amsterdam

CHROMSYMP. 2518

Measurement of amino acid compositions of glycoprotein systems by gas-phase hydrolysis and reversed-phase high-performance liquid chromatography

Deborah E. H. Palladino*, Robin M. House and Kenneth A. Cohen

Boehringer Ingelheim Pharmaceuticals, Inc., 900 Ridgebury Road, P.O. Box 368, Ridgefield, CT 06877-0368 (USA)

ABSTRACT

Interest in glycoproteins and their compositions has increased in recent years. Work described in this report illustrates the use of an amino acid analysis protocol involving gas-phase hydrolysis and reversed-phase high-performance liquid chromatography of glycoprotein systems at microgram levels. In other amino acid analysis protocols the problem of losses of amino acids of glycoproteins has been documented. These losses were due to various reactions, referred to as browning or Maillard reactions, which yielded a residue from which amino acids were not recoverable.

In our work, three glycoprotein systems are examined: ovalbumin, sICAM-1, and bovine serum albumin —which is naturally unglycosylated, but is spiked with about 30% saccharides. In all three cases, the compositional agreement between the molar ratio of amino acids determined empirically and that predicted is greater than 90%. Thus it is shown that the adverse effects of Maillard-type reactions are avoided, and the presence of carbohydrates causes negligible interferences with amino acid analysis performed under the conditions described herein.

INTRODUCTION

Amino acid analysis is an extremely valuable technique for characterization and quantitation of polypeptides [1–5]. The technique consists of three basic steps frequently performed in the following order: hydrolysis of peptide bonds to liberate amino acids, derivatization of the liberated amino acids, and separation of the derivatized amino acids. The three steps are carried out with numerous chemistries including hydrolysis by hydrochloric acid or methanesulfonic acid in the gas or liquid phase; derivatization by ninhydrin, *o*-phthalaldehyde, phenylisothiocyanate, dabsyl chloride or fluorenylmethyl chloroformate; and separation by reversed-phase or ion-exchange high-performance liquid chromatography (HPLC).

Pioneered and developed within the last decade, one of the most widely used protocols of amino acid analysis begins with hydrolysis by hydrochloric acid in the gas phase, followed by derivatization by phenylisothiocyanate and then separation by reversed-phase HPLC [3,5–13]. This particular protocol is applicable to the analysis of many classes of polypeptides especially at microgram levels. However, application to the class of glycoproteins remains largely uninvestigated.

Amino acid analysis of glycoproteins demands special consideration. The potential for losses of amino acids due to browning reactions that occur during liquid-phase hydrolysis of milligrams of glycoproteins is extensively documented [1,2,14]. Briefly, browning reactions, which are also referred to as Maillard reactions, lead to brown residue called humin or melanoidins. The humin is composed of products of reactions between amino acids and saccharides, their derivatives (*e.g.*, sialic acid), or their acid-catalyzed degradation intermediates. The exact composition and molecular structure of humin remain unknown. Nonetheless it is clear that

0021-9673/92/$05.00

amino acids as well as saccharides from which humin is derived are virtually irrecoverable for most purposes, including amino acid analysis.

A complicated scheme of reactions, some in series, others in parallel, yields humin [1,2,14]. Both aldoses and ketoses can react with the amine moiety of amino acids or peptides. The nature of the reactions and products depends on moisture, temperature, and pH. For instance at a temperature greater than 100°C and pH less than 1, which occur during hydrolysis with 6 *M* hydrochloric acid, saturated and unsaturated dicarbonyl compounds as well as α-, β-unsaturated carbonyl compounds can form from the constituent saccharides of the glycoproteins and react with amino acids. At a higher pH, such as pH greater than 4, which occurs during the removal of the hydrochloric acid used for hydrolysis, intact reducing sugars or their degradation products can react with amino acids. In either acidic condition, humin can be produced, rendering amino acids (and saccharides, for that matter) essentially irretrievable for consequent analysis.

In view of the potentially adverse browning reactions, the research reported herein addresses the integrity of amino acid analysis that incorporates hydrolysis of glycoprotein by hydrochloric acid in the gas phase, derivatization by phenylisothiocyanate, and separation by reversed-phase HPLC. Three glycoprotein systems at the microgram level are examined. Two are naturally glycosylated proteins, ovalbumin and sICAM-1 (soluble intercellular adhesion molecule 1), the latter being a potent and specific *in vitro* inhibitor of rhinovirus infection [15–17]. The third glycoprotein system is naturally unglycosylated bovine serum albumin which is spiked with saccharides roughly simulating the carbohydrate content of sICAM-1. Compositional agreement, a mathematical parameter that quantifies the correspondence of the amino acid molar ratio determined empirically to that predicted, is used to demonstrate that the presence of saccharides causes negligible interference with the accuracy of amino acid analysis performed under the conditions described.

EXPERIMENTAL

Apparatus

Hydrolysis of proteins and derivatization of amino acids were performed using the Waters Picotag workstation module (Waters/Millipore, Milford, MA, USA). The liquid chromatographic system consisted of a Waters 680 automated gradient controller module, Waters 590 pump, Waters 510 pump, Waters WISP automatic sampling device, Dupont Instruments column compartment (DuPont, Wilmington, DE, USA) and a Kratos spectroflow 757 UV–VIS absorbance detector (Kratos, Ramsey, NJ, USA). Chromatographic data were analyzed by a Hewlett-Packard HP 1000-A600 processor laboratory automation system (Hewlett-Packard, Palo Alto, CA, USA) with HP 3357 software and by a Vectra personal computer (Hewlett-Packard) with custom-designed software for the measurement of amino acids. A Waters Picotag column, C_{18}, 15 × 0.39 cm, was used for HPLC. Pyrex 9820 (50 × 6 mm) culture tubes were from Corning (Corning Glass, Corning, NY, USA) and reaction vials from Waters.

Chromatographic solvents

Picotag eluent A and Picotag eluent B [13] were used for mobile phase solvents. Picotag diluent was used for solubilizing derivatized amino acid samples prior to HPLC injection.

Amino acid analysis solvents

Phenol was ACS-reagent grade (Aldrich, Milwaukee, WI, USA). Water was HPLC grade (Milli Q and Milli-RO, Millipore, Milford, MA, USA). Triethylamine, hydrochloric acid (6 *M*, constant boiling) and phenylisothiocynate were all purchased from Pierce (Rockford, IL, USA). Methanol was HPLC grade high purity (Burdick & Jackson, Musk egon, MI, USA). Ethanol was Absolute-200 proof (AAPer Alcohol & Chemical Co., Shelbyville, KY, USA).

Proteins, saccharides and amino acids

Amino acid standard H was purchased from Pierce. D(+)-Galactosamine (cell culture reagent grade), D(+)-mannose, and N-acetyl-D-glucosamine were all purchased from Sigma (St. Louis, MO, USA). Albumin from bovine serum, and ovalbumin from chicken egg-grade V, were both purchased from Sigma. sICAM-1 was produced recombinantly in Chinese hamster ovary cells and was purified by tangential flow ultrafiltration and

affinity liquid chromatography [18]. All glycoprotein systems were dissolved in Dulbecco's phosphate-buffered saline.

Hydrolysis and derivatization

Hydrolysis and derivatization were performed largely according to Waters Picotag methodology [7,13]. Samples were pipetted into 50 × 6 mm tubes previously pyrolyzed at 500°C for 16 h in a muffle furnace. After the addition of sample, the tubes were placed in a reaction vial and the samples were dried. A 200-μl volume of 6 *M* HCl containing 1% (v/v) liquefied phenol was added to the bottom of the reaction vial. The vial was purged with nitrogen, sealed, and placed in the oven compartment of the workstation for hydrolysis, which was carried out for 0.5 to 2.0 h at 150°C. One reaction vial was used per each duration of hydrolysis. After the appropriate time of hydrolysis, the reaction vial was removed and the tubes were taken out and transferred to a clean reaction vial. The hydrolyzed samples were dried, neutralized by delivering to each tube 20 μl of a solution of methanol–water–triethylamine (2:2:1), and vortexed. The neutralized samples were dried, derivatized by adding to each tube 10 μl of a solution of methanol–water–triethylamine–phenylisothiocyanate (7:1:1:1), and vortexed. The samples were allowed to stand for 20 min at room temperature. The derivatized samples were dried, and unless otherwise noted, each was reconstituted with 200 μl of Picotag diluent and 4 μl were injected onto the HPLC column.

Chromatography

Reversed-phase HPLC of the derivatized amino acids was performed using a Waters Picotag column and Picotag eluents A and B. Gradients were taken from ref. 13. Absorbance was at 254 nm and 0.05 a.u.f.s. Injection volume was 4 μl. The amino acids were identified by retention times and quantified by areas, as compared to those of standards. Customized software, prepared by the Analytical Sciences and Management Information Systems Departments of Boehringer Ingelheim Pharmaceuticals, was used for these identifications and quantifications. In addition, the software calculated an experimental molar ratio of amino acids. This calculation was relative to the predicted or known number of moles of a selected amino acid present in one mole of test polypeptide.

Data collected from the detector was transferred to an analog-to-digital (A/D) converter (118652A, Hewlett-Packard), then to the 1000-A600 processor, and finally to a Vax computer (Digital Equipment Corporation, Maynard, MA, USA) over a LAN ethernet. The customized software ran off of the Vectra personal computer and was written in Turbo Pascal (Borland International, Scotts Valley, CA, USA). The Vectra computer was connected to the VAX computer also over a LAN ethernet and used the VAX computer as a virtual disc drive.

Calculations

Compositional agreement (*CA*), a mathematical parameter defined as follows, was calculated to quantify an overall accuracy of each amino acid analysis.

$$CA = 100\% \times [N_p - (\sum|n_e - n_p|)]/N_p$$

where: N_p = the predicted (known) total number of moles of all amino acids in one mole of polypeptide; n_e = the empirically determined number of moles of a specific amino acid in one mole of polypeptide; n_p = the predicted (known) number of moles of a specific amino acid in one mole of polypeptide.

Compositional agreement as given above is apparently equivalent to per cent correct composition [19] and inversely related to per cent error [5,12] reported previously. These indexes all serve with comparable utility the same substantive purpose of providing a simple and quantitative parameter to assess an overall accuracy of an amino acid analysis.

Semantically, however, we prefer the nomenclature compositional agreement, because it has greater general applicability. Both per cent correct composition and per cent error are nomenclature that imply that the true amino acid content of a sample is definitively known. Frequently there are samples (*e.g.*, synthetic peptides, recombinant fusion proteins) for which the amino acid content is intended but not definitively known. Even for samples of pure standards of polypeptides, it could be argued that the true content of amino acids is not definitely known because of the ubiquitous nature and often unknown magnitude of background amino acid contaminants [5,10,12,13,19]. Thus because it implies less presupposition about the true content of amino acids in a sample, the term compositional agreement is used throughout this report.

RESULTS AND DISCUSSION

Bovine serum albumin as a control

Bovine serum albumin was selected as a control because of its lack of glycosylation. Hence the possibility of interference of carbohydrates with amino acid analysis was precluded. Over the course of several weeks amino acid analyses were performed on a total of 14 samples of bovine serum albumin. Highly reproducible chromatograms similar to that presented in Fig. 1A were obtained.

Measurements of amino acid compositions were also reproducible and generally within 15% agreed with predicted compositions, as illustrated by a typical example given in Table I. Such agreement, representative of the other 13 analyses, was reasonable for a single analysis and was consistent with results reported earlier for commercially available unglycosylated proteins of high purity [5,12,19,20]. For each of the 14 analyses of bovine serum albumin, compositional agreement was also calculated. Values ranged from 88 to 95% and averaged 91%, which again was comparable to results reported previously [5,12,19,20]. Thus, values of approximately 90% for compositional agreement typified amino acid analyses for which there was no possibility of problems attributable to the presence of saccharides.

Glycoprotein systems

The three glycoprotein systems that were analyzed and compared to the control were chicken egg ovalbumin, sICAM-1 and bovine serum albumin to which saccharides were spiked. As ovalbumin and sICAM-1 were naturally glycosylated, no saccharides were added. Ovalbumin was composed of approximately 4% (w/w) saccharides [21,22], while sICAM-1 was composed of approximately 30% saccharides [15]. sICAM-1 was produced recombinantly in Chinese hamster ovary cells, which secreted the sICAM-1 in a soluble form [18]. This form simulated the five extracellular domains of ICAM-1, a naturally occurring, membrane-bound glycoprotein which was identified as a human cellular receptor for the subgroup of rhinoviruses known as major groups [16]. sICAM-1 was found to be a potent and specific *in vitro* inhibitor of rhinovirus infection [16].

The glycoprotein system containing bovine serum albumin included 30% (w/w) saccharides to simulate roughly the carbohydrate content of sICAM-1 [15,17,23]. Mannose, N-acetylglucosamine and galactosamine, in equal amounts (*i.e.*, 10% each) were the added saccharides, because they were common to various types of O-linked and N-linked oligosaccharides [24], and the sequence of amino acids of sICAM-1 exhibited eight potential sites (Asn-X-Ser or-Thr) of N-linked glycosylation [15].

A total of five samples of ovalbumin in three amounts (50, 100 and 185 μg) were hydrolyzed and analyzed (Fig. 1B) for amino acid composition. Compositional agreement ranged from 87 to 89% and averaged 88% (Table II). Also at three levels (35, 70 and 125 μg), a total of eight samples of bovine serum albumin spiked with saccharides were hydrolyzed and analyzed (Fig. 1C, Table II). Compositional agreement ranged from 88 to 95% and averaged 92%. Hydrolysis and analysis of sICAM-1 at 42 μg and 184 μg gave an average compositional agreement of 92% (Fig. 1D, Table II). For each of the three glycoprotein systems and for each of the seven levels spanning 35–185 μg, compositional agreement was equivalent to that obtained with the control of bovine serum albumin that was not spiked with saccharides (*cf.* above and Table I). Therefore the potentially adverse effects of browning reactions were negligible.

Variation of hydrolysis time

The study of the effects of browning reactions on amino acid analysis of sICAM-1 was extended to encompass various durations of hydrolysis, which have been recommended [1,2,19,25,26] in order to assess as accurately as possible amino acid composition. Rates and extents of hydrolytic cleavage of peptide bonds have depended on the specific amino acids participating in the bonds [1,2,25,26]. Also, the stabilities of amino acids liberated from peptide bonds have depended on the specific amino acid. Thus for sICAM-1 hydrolysis durations of 0.5, 0.75, 1.0, 1.5 and 2.0 h were employed, with recoveries given in Table III for each amino acid.

As expected, levels of Tyr, Ser and Thr (Table III) decreased 15–40% with increased time of hydrolysis, ostensibly because of a greater susceptibility of these three amino acids to progressive hydrolytic destruction [1,2,25,26]. Levels of Glx and Asx decreased 30–50% as well with increased duration of

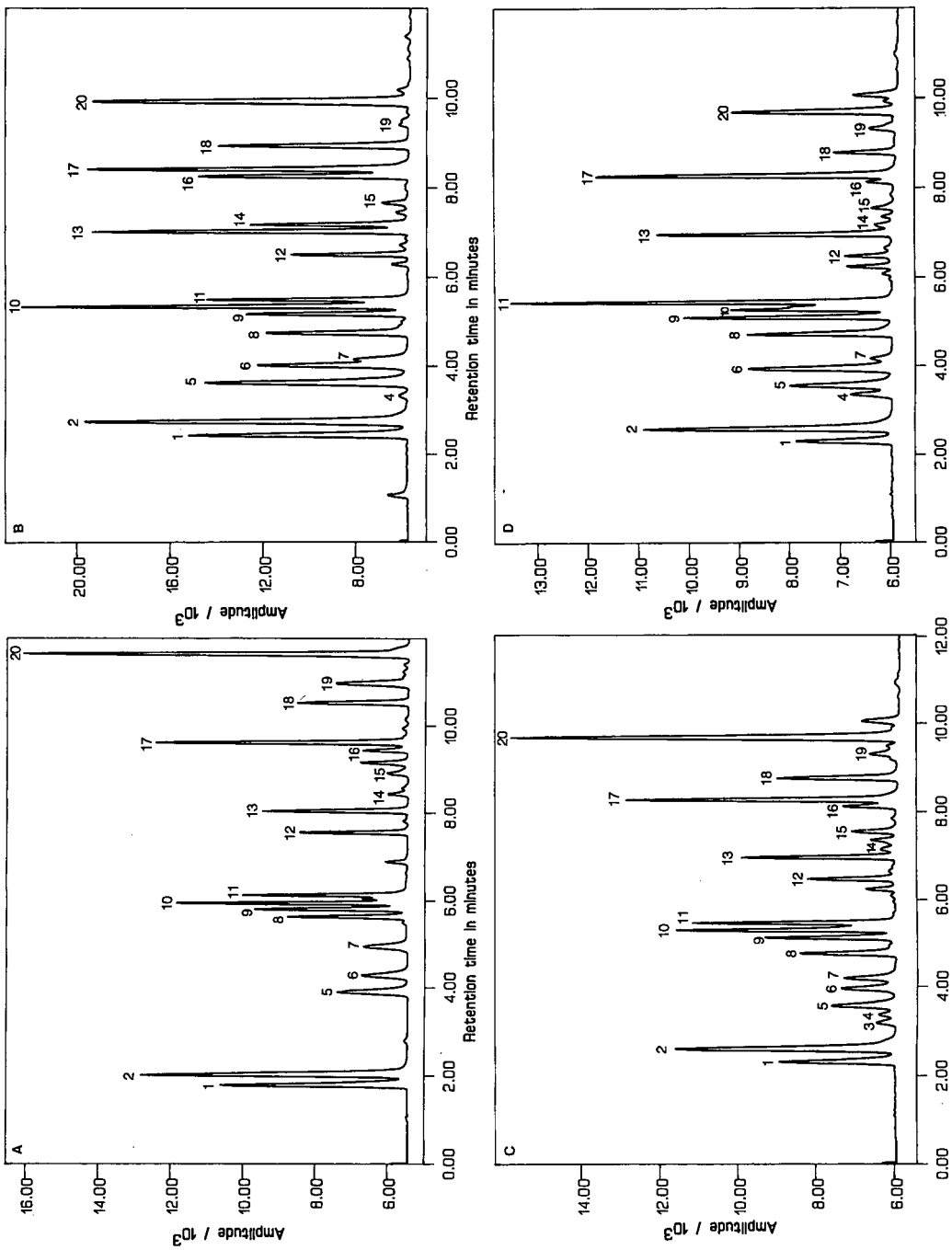

Fig. 1. Typical amino acid analysis chromatograms of (A) bovine serum albumin, (B) ovalbumin, (C) bovine serum albumin, spiked with saccharides, and (D) sICAM-1. All were hydrolyzed for 1 h at 150°C. A was generated using conventional Picotag methodology which includes a column oven temperature of 38°C [13]. B, C and D were generated using the gradient, the addition of extra triethylamine to eluent A, and the column oven temperature (42°C) recommended in advanced Picotag methodology for amino sugars [13]. Peaks: 1 = aspartic acid (Asp); 2 = glutamic acid (Glu); 3 = galactosamine (GalN); 4 = glucosamine (GlcN); 5 = serine (Ser); 6 = glycine (Gly); 7 = histidine (His); 8 = arginine (Arg); 9 = threonine (Thr); 10 = alanine (Ala); 11 = proline (Pro); 12 = tyrosine (Tyr); 13 = valine (Val); 14 = methionine (Met); 15 = cysteine (Cys); 16 = isoleucine (Ile); 17 = leucine (Leu); 18 = phenylalanine (Phe); 19 = impurity; 20 = lysine (Lys).

TABLE I

TYPICAL AMINO ACID ANALYSIS OF BOVINE SERUM ALBUMIN (WITHOUT SACCHARIDES)

Amino acid[a]	Measured (pmol)[b]	n_e[c]	n_p	$\lvert n_e - n_p \rvert$
Asx	924	59	48	11
Glx	1280	81	75	6
Ser	404	26	28	2
Gly	271	17	15	2
His	267	17	17	0
Arg	372	24	23	1
Thr	487	31	34	3
Ala	722	46	46	0
Pro	484	31	28	3
Tyr	314	20	19	1
Val	484	31	36	5
Met	71	5	4	1
Cys	—[d]	—[d]	35[e]	—[d]
Ile	182	12	14	2
Leu	912	58	61	3
Phe	409	26	26	0
Lys	966	62	59	3
Trp	—[d]	—[d]	2[e]	—[d]
Total $CA = 92\%$	—	—	$N_p = 533$	$\sum \lvert n_e - n_p \rvert = 43$

[a] Definitions of abbreviations are given in the key in the legend of Fig. 1. In addition Asx is the sum of asparagine and aspartic acid, and Glx is the sum of glutamine and glutamic acid.

[b] 10 μg of bovine serum albumin in 10 μl of water were hydrolyzed at 150°C for 1 h, derivatized, reconstituted in 100 μl, and 10 μl were injected.

[c] Calculated relative to the predicted number of residues of phenylalanine (26).

[d] Not determined.

[e] Disregarded in the calculation of N_p and compositional agreement.

hydrolysis, possibly because of longer exposure to metal ions [8,19,20,27]. Indeed in our experiments no precautions (*e.g.*, addition of EDTA) were taken to offset losses of Asp and Glu due to interactions with ionic calcium, magnesium, sodium, and potassium, which were present in the sample matrix after sICAM-1 was purified prior to amino acid analysis [18,23].

Interestingly levels of Leu, Ile and Val also decreased 30–40% with increased duration of hydrolysis (Table III). This was surprising. The hydrophobic side chains of Leu, Ile and Val were reported to shield proximal peptide bonds from hydrolytic attack by hydronium ions [2]. Longer times of hydrolysis were therefore suggested [1,2,25,26] in order to achieve greater cleavage of peptide bonds relatively resistant to hydrolysis and, consequently, to liberate more completely Leu, Ile, Val and adjacent amino acids sharing these bonds. Thus, that recoveries of Leu, Ile and Val of sICAM-1 decreased with increased hydrolysis time was not anticopated. It was possible that Leu, Ile and Val preferentially reacted with saccharides in a time-dependent fashion and that longer hydrolysis times resulted in greater losses. However inspection of the sequences of amino acids in the vicinities of the eight potential glycosylation sites of sICAM-1 revealed no particular preponderance of Leu, Ile or Val [15].

From the data presented in Table III, an optimized determination of amino acid composition of sICAM-1 was made. A molar ratio of amino acids was calculated by taking for each amino acid the largest amount measured as a function of hydrolysis time. This approach exploited the highest recovery achieved for every residue [2]. The molar ratio of amino acids determined empirically in sICAM-1 (Table IV) closely approximated that predicted. For 13 of 16 amino acids the agreement between experimental and predicted was within 15%. Indeed compositional agreement was 92%. Thus the potentially adverse effects of browning reactions were not evident.

From the data presented in Table III, compositional agreements were calculated for each of the individual durations of hydrolysis. For the longer hydrolyses (*e.g.*, 1.5 and 2.0 h), the compositional agreements were poor, *i.e.*, less thn 80%, evidently due to losses of Tyr, Ser, Thr, Glx, Asx, Leu, Ile and Val, as mentioned above. However, the compositional agreements achieved for the shorter hydrolysis times were greater than 90%, which was equivalent to that obtained in the optimized determination of molar ratio depicted in Table IV. Thus an accuracy of measurement as good as that obtained in the extensive hydrolysis study was attainable with single short hydrolyses, although this was not predictable, making it prudent to conduct the hydrolysis time study [25,26].

The study of the effects of browning reactions on amino acid analysis was extended further to include various durations of hydrolysis of bovine serum albumin spiked with saccharides. Trends similar to those illustrated in Table III were obtained for

TABLE II

COMPOSITIONAL AGREEMENT OF GLYCOPROTEIN SYSTEMS

	Spiked (μg)			Saccharide content (%)	Compositional agreement[a]
	Mannose	N-Acetylglucosamine	Galactosamine		
Ovalbumin (185 μg)[b]	0	0	0	4	87, 87 ($n=2$)
Ovalbumin (101 μg)	0	0	0	4	89 ($n=1$)
Ovalbumin (50 μg)	0	0	0	4	88, 89 ($n=2$)
Bovine serum albumin (125 μg)	20	20	20	32	93, 91, 91 ($n=3$)
Bovine serum albumin (70 μg)	10	10	10	30	95, 95 ($n=2$)
Bovine serum albumin (35 μg)	5	5	5	30	88, 89, 92 ($n=3$)
sICAM (184 μg)	0	0	0	*ca.* 30	93 ($n=1$)
sICAM (42 μg)	0	0	0	*ca.* 30	91, 91 ($n=2$)

[a] Cysteine and tryptophan were disregarded.
[b] Amount hydrolyzed at 150°C for 1 h and derivatized.

TABLE III

AMINO ACID ANALYSIS OF sICAM-1 BY VARIOUS TIMES OF HYDROLYSIS

Amino acid[b]	Measured (pmol)[a]				
	Hydrolysis time (h)				
	0.5	0.75	1.0	1.5	2.0
Asx	440	385	252	266	218
Glx	727	700	610	548	483
Ser	370	337	296	282	251
Gly	403	381	356	339	335
His	61	60	55	57	49
Arg	302	302	295	292	270
Thr	406	428	392	403	368
Ala	335	333	354	346	335
Pro	505	504	527	531	521
Tyr	98	87	79	89	58
Val	494	464	394	374	334
Met	46[c]	46	43	45	41
Ile	59	59	48	51	47
Leu	608	593	500	478	429
Phe	128	120	108	114	104
Lys	220	203	185	188	162

[a] Given values are averages of duplicate amino acid analyses, results of which differed for each entry no more than 10%. For each analysis 33 μg of sICAM-1 in 10 μl of phosphate buffered saline were hydrolyzed at 150°C and derivatized.
[b] Definitions of abbreviations are given in the footnotes of Table I and in the key in the legend of Fig. 1.
[c] Single determination rather than an average.

nearly all amino acids, particularly Tyr, Ser, Thr, Asx, Glx, and even Leu, Ile and Val (data not shown). A molar ratio of amino acids was calculated by taking for each amino acid the maximum amount determined as a function of hydrolysis time. The molar ratio determined empirically was in good agreement with that predicted (Table IV), as the compositional agreement was 90%, and for 12 of 16 amino acids experimental values were within 15% of predicted values.

All of the studies described above served to demonstrate that no significantly deleterious effects of browning reactions on overall amino acid analysis of glycoprotein systems as performed were encountered. Possibly insufficient carbohydrate reactant was present, although both sICAM-1 and bovine serum albumin spiked with saccharides contained substantial fractions (30%) of carbohydrate. Alternatively hydrolysis in the gas phase instead of the liquid phase may have effectively immobilized the potential reactants (*i.e.*, amino acids and saccharides and their derivatives) to the wall of the hydrolysis tube such that it became impossible for them to diffuse. Therefore, they could not contact one another to react.

This hypothesis was consistent with several earlier reports. For instance in order to minimize the loss of amino acids during liquid-phase hydrolysis of amino acid analysis, a dilute solution of glycoprotein was

TABLE IV

OPTIMIZED DETERMINATION OF MOLAR RATIOS OF AMINO ACIDS

Amino acid[a]	sICAM-1		Bovine serum albumin spiked with saccharides	
	Experimental[b]	Predicted	Experimental[b]	Predicted
Asx	35.4	34	43.9	48
Glx	57.8	61	68.6	75
Ser	29.4	30	25.1	28
Gly	31.8	30	16.8	15
His	4.8	5	16.0	17
Arg	24.1	26	22.5	23
Thr	32.7	43	28.0	34
Ala	26.5	25	45.9	46
Pro	40.6	40	38.5	28
Tyr	7.7	8	15.8	19
Val	36.9	43	31.0	36
Met	3.7	2	4.4	4
Cys	—[c]	14[d]	—[c]	35[d]
Ile	4.7	7	10.9	14
Leu	48.2	53	54.8	61
Phe	10.0	10	26.0	26
Lys	17.3	17	56.6	59
Trp	—[c]	5[d]	—[c]	2[d]

[a] Definitions of abbreviations are given in the footnotes of Table I and in the key in the legend of Fig. 1.
[b] Calculated relative to the predicted number of residues of phenylalanine.
[c] Not determined.
[d] Disregarded in the calculation of N_p and compositional agreement.

recommended [2]. Presumably, a low concentration of glycoprotein makes it less likely that potential reactants, such as amino acids and saccharides or their derivatives, will collide in solution; without collision, there can be no reaction [2].

More recent reports also implicated the importance of concentration and collision [28,29]. In both of these papers excellent compositional agreements were obtained for glycoproteins, even though the amino acid analysis employed liquid-phase hydrolysis. Precolumn derivatization and reversed-phase HPLC were used. Indeed in one of the reports, phenylisothiocyanate was the derivatizing agent [28]. In the other paper, the derivatizing agent was 4-dimethylaminoazobenzene-4′-sulfonyl chloride [29]. Significantly, common to both papers was the microgram levels of glycoprotein hydrolyzed. Moreover, in the latter paper [29], recoveries of amino acids were decreased only when concentration of glucose was increased ten-fold. These findings induce intriquing questions pertaining to mechanisms of browning reactions, which further work should help to elucidate.

CONCLUSIONS

Amino acid analysis that employs the widely used protocol of hydrolysis by hydrochloric acid in the gas phase, followed by derivatization with phenylisothiocyanate and then separation by reversed-phase HPLC, is applied successfully to glycoprotein systems at the microgram level. Three glycoprotein systems are examined: ovalbumin which is comprised naturally of about 4% carbohydrate, sICAM-1 which is comprised naturally of about 30% carbohydrate, and bovine serum albumin which is naturally unglycosylated but is spiked with about 30% saccharides to simulate roughly the carbohydrate content of sICAM-1. In all three cases the compositional agreement between the molar ratio of amino acids determined empirically and that predicted is typically greater than 90%. Such excellent compositional agreement is comparable to that obtained in the amino acid analysis of proteins lacking carbohydrate. Thus it is concluded that, in amino acid analysis as performed, the adverse effects

of Maillard-type reactions are avoided and the presence of carbohydrates causes no serious problems with the determinations of molar ratios of amino acids in glycoprotein systems.

ACKNOWLEDGEMENTS

The authors gratefully acknowledge K. Maruk, R. Shansky and K. Lubbe for supplying the sICAM-1 and for instructive discussions, S. Marlin for instructive discussions, H. Butler and K. Esche for development of customized software, M. Folderauer and M. Heinicke for preparation of the manuscript, S. Persichilli for preparation of figures, and F. Hatch and F. Hess for support of the work.

REFERENCES

1 S. Hunt, in G. C. Barret (Editor), *Chemistry and Biochemistry of the Amino Acids*, Chapman & Hall, New York, 1985, p. 376.
2 J. E. Eastoe, in A. Gottschalk (Editor), *Glycoproteins, Their Composition, Structure, and Function*, Part A, Elsevier, Amsterdam, New York, 1972, p. 158.
3 S. A. Cohen and D. J. Strydom, *Anal. Biochem.*, 174 (1988) 1.
4 G. Ogden and P. Foldi, *LC·GC*, 5 (1987) 28.
5 J. W. Crabb, L. Ericsson, D. Atherton, A. J. Smith and R. Kutny, in J. J. Villafanca (Editor), *Current Research in Protein Chemistry: Techniques, Structure and Function*, Academic Press, New York, 1990, Ch. 5, p. 49.
6 R. L. Heinrikson and S. C. Meredith, *Anal. Biochem.*, 136 (1984) 65.
7 B. A. Bidlingmeyer, T. L. Tarvin and S. A. Cohen, *J. Chromatogr.*, 336 (1984) 93.
8 R. Mora, K. D. Berndt, H. Tsai and S. C. Meredith, *Anal. Biochem.*, 172 (1988) 368.
9 N. M. Meltzer, G. I. Tous, S. Gruber and S. Stein, *Anal. Biochem.*, 160 (1987) 356.
10 K. L. Stone and K. R. Williams, *J. Chromatogr.*, 359 (1986) 203.
11 R. F. Ebert, *Anal. Biochem.*, 154 (1986) 431.
12 K. A. West and J. W. Crabb, in J. J. Villafanca (Editor), *Current Research in Protein Chemistry: Techniques, Structure and Function*, Academic Press, New York, 1990, Ch. 4, p. 37.
13 S. A. Cohen, M. Meys and T. L. Tarvin, *The Picotag® Method: A Manual of Advanced Techniques for Amino Acid Analysis*, Millipore Corporation, Medford, MA, 4/89 WM 02, Rev. 1., 1989, p. 1.
14 A. Gottschalk, in A. Gottschalk (Editor), *Glycoproteins, Their Composition, Structure, and Function*, Part A, Elsevier, Amsterdam, New York, 1972, p. 141.
15 D. E. Staunton, S. D. Marlin, C. Stratowa, M. L. Dustin and T. A. Springer, *Cell*, 52 (1988) 925.
16 S. D. Marlin, D. E. Staunton, T. A. Springer, C. Stratowa, W. Sommergruber and V. J. Merluzzi, *Nature (London)*, 344 (1990) 70.
17 M. L. Dustin, R. Rothlein, A. K. Bhan, C. A. Dinarello and T. A. Springer, *J. Immunol.*, 137 (1986) 245.
18 K. A. Maruk, K. Lubbe, J. Hopkins, K. Cohen, S. D. Marlin and R. E. Shansky, in preparation.
19 D. Atherton, in T. E. Hugli (Editor), *Techniques in Protein Chemistry*, Academic Press, San Diego, CA, 1989, p. 273.
20 D. R. Dupont, P. S. Keim, A. H. Chui, R. Bello, M. Bozzini and K. J. Wilson, in T. E. Hugli (Editor), *Techniques in Protein Chemistry*, Academic Press, San Diego, CA, 1989, p. 284.
21 *Biochemicals Organic Compounds for Research and Diagnostic Reagents*, Sigma, St. Louis, MO, 1991, p. 71.
22 L. W. Cunningham, R. W. Clouse and J. D. Ford, *Biochim. Biophys. Acta*, 78 (1963) 379.
23 R. E. Shansky and K. A. Maruk, *J. Liq. Chromatogr.*, in press.
24 J. C. Paulson, *Trends Biochem. Sci.*, 14 (1989) 272.
25 C. W. Gehrke, L. L. Wall, Sr., J. S. Absheer, F. E. Kaiser and R. W. Zumwalt, *J. Assoc. Off. Anal. Chem.*, 68 (1985) 811.
26 G. S. Sittampalam, R. M. Ellis, D. J. Miner, E. C. Richard and D. K. Clodfelter, *J. Assoc. Off. Anal. Chem.*, 71 (1988) 833.
27 K. A. West and J. W. Crabb, in T. Hugli (Editor), *Techniques in Protein Chemistry*, Academic Press, San Diego, CA, 1989, p. 295.
28 R. Gupta and N. Jentoft, *J. Chromatogr.*, 474 (1989) 411.
29 K. Muramoto and H. Kamiya, *Anal. Biochem.*, 189 (1990) 223.

Journal of Chromatography, 599 (1992) 13–20
Elsevier Science Publishers B.V., Amsterdam

CHROMSYMP. 2524

Selective high-performance liquid chromatographic purification of bispecific monoclonal antibodies

Laura Tarditi, Maria Camagna, Anna Parisi and Cristina Vassarotto

Biochemical Oncology Laboratories, SORIN Biomedica, 13040 Saluggia (VC) (Italy)

Lucia B. DeMonte

Department of Genetics, Biology and Medical Chemistry, University of Turin, Turin (Italy)

Michelle Letarte

Hospital for Sick Children, Toronto (Canada)

Fabio Malavasi

Department of Genetics, Biology and Medical Chemistry, University of Turin, Turin and Centre for Immunogenetics and Histocompatibility, CNR, Turin (Italy)

Massimo Mariani*

Biochemical Oncology Laboratories, R & D Diagnostic Laboratories, SORIN Biomedica, 13040 Saluggia (VC) (Italy)

ABSTRACT

The recent development of improved production techniques for bispecific monoclonal antibodies (biMAbs) has significantly increased interest in specific purification procedures. In this investigation, a general high-performance liquid chromatographic (HPLC) purification method is proposed that allows highly purified biMAbs to be obtained from mouse ascites fluid containing a mixture of different antibodies, *i.e.*, parental MAbs, active biMAb and a mixture of randomly assembled heavy and light chains. Proteins from ascites fluid were precipitated with ammonium sulphate and applied to a high-performance protein A column to separate the total immunoglobulin fraction. BiMAbs were isolated from other immunoglobulins by two subsequent passages through a high-performance hydroxyapatite (HPHT) column. This purification protocol combines specificity of protein A for immunoglobulin G (IgG) and high selectivity of hydroxyapatite for different IgG idiotypes. All purification steps were performed rapidly and reliably by HPLC. This method was applied to the purification of six different biMAbs with consistently high yields, purity and homogeneity. This general purification method may prove extremely valuable when highly pure preparation of biMAbs is required, as for *in vivo* use.

INTRODUCTION

Bispecific murine monoclonal antobodies (biMAbs) have been developed in the last decade [1] and have found widespread use only recently, mainly in the study of cell–cell interactions and in lymphocyte retargeting. In the former instance, biMAbs can simultaneously recognize molecules expressed on tumour cells and on cytotoxic effector cells. Other models include biMAbs as targeting agents for toxins, drugs or radiopharmaceuticals. BiMAbs are becoming a widely used tool in applied cell biology, in functional studies and in diagnostic and therapeutic applications.

0021-9673/92/$05.00

BiMabs have been obtained both by immunoglobulin G (IgG) heterocross-linking [2] and by the production of hybrid hybridomas [1,3]. The latter method can be achieved either by fusing a hybridoma with splenocytes of mice immunized with the selected antigen or by direct fusion of two hybridomas [4]. Both methods involve cumbersome procedures and show low efficiency. As an alternative, a high-efficiency biological protocol for producing hybrid hybridomas has been devised recently [5]. This approach includes conventional somatic fusion between two hybridoma cell lines, previously made resistant to different metabolic drugs by means of retrovirus-derived shuttle vectors carrying the relevant resistance genes. The resulting hybrid hybridomas secrete a mixture of antibodies, including biMabs, parental MAbs and several inactive or partially active (monospecific) antibodies due to randomly assembled heavy and light parental chains.

Therefore, the critical problem in the production of biMAbs by hybrid hybridomas is purification of active biMAb from other contaminant immunoglobulins. Purification protocols have so far exploited the difference in the isoelectric points of individual immunoglobulins in ion-exchange chromatography [4]. An alternative method is the use of anti-idiotype MAbs to parental MAbs in double affinity chromatography [6]. Neither of the above-mentioned techniques has found general application. In several instances, monoclonal IgGs show differences in isoelectric points that are not sufficient to allow their separation by ion-exchange chromatography. Detailed studies using different stationary phases and elution gradients are essential. Affinity chromatography with anti-idiotype MAbs requires the availability of anti-idiotype reagents to all parental MAbs. Moreover, Regulatory Authorities suggest avoiding affinity chromatography as the last purification step owing to possible leakage of ligands from the columns when the product is intended for *in vivo* use [7,8].

The scope of this work was the definition of the parameters of a purification protocol able to yield large amounts of pure biMAbs to be used as *in vitro* reagents and *in vivo* immunopharmaceuticals. Experience indicated a three-step high-performance liquid chromatographic (HPLC) purification method using a combination of well defined antibody purification procedures: protein A [9–11] and hydroxyapatite [12–14] chromatography. As described previously [15], such a combination resulted in a generally applicable method for MAb purification. This protocol includes (i) protein A affinity chromatography to isolate the total IgG fraction, (ii) a first passage through hydroxyapatite to fractionate different MAb idiotypes and to evidence the biMAb peak and (iii) a second hydroxyapatite chromatography to remove inactive contaminants completely from biMAb preparations.

The selected method has been succesfully tested in the purification of six different biMAbs. The results indicate that the requirements of general application, high yields and product purity have been fully met.

EXPERIMENTAL

Monoclonal antibodies

A set of hybridomas of known specificity were used to obtain hybrid hybridomas. These included F023C5 (anti-CEA IgG_1) [16], Ep2 (anti-HMW-MAA IgG_{2a}) [17], 44C10 (anti-CALLA IgG_{2b}) [18], CBT3 (anti-CD3 IgG_{2a}) [19], AB8.28 (anti-FcR-like molecule IgG_{2a}) [19], CBT11 (anti-CD2 IgG_1) [20], A10 (anti-CD38 IgG_{2a}) [21] and 1LF5 [anti-diethylenetriaminepentaacetic acid (DTPA) metal chelating agent IgG_1] [22].

Generation of hybrid hybridomas

Resistance to geneticin (G418) or methotrexate (MTX) was conferred on hybridoma cells by means of retroviral shuttle vectors carrying the relevant resistance genes. Details were given by DeMonte *et al.* [5]. Hybridomas were infected by co-cultivation with irradiated psi-2 packaging cell lines, previously transfected with the appropriate vectors. The psi-2 packaging cell line, carrying the pMV7 vector [23] or the pSDHT vector [24], was used to confer either G418 or MTX resistance on the parental hybridomas, respectively. PEG-mediated somatic cell fusion and hybrid hybridoma selection were performed according to the literature [5].

The biMAbs produced included AB8.28 × Ep2 [5], CBT3 × Ep2 [5], A10 × Ep2 [25], CBT3 × CBT11 [20], CBT3 × 44C10 [20] and F023C5 × 1LF5 [26]. Massive production of biMAb was obtained by growing the hybrid hybridomas *in vivo* as tumour ascites in pristane-primed BALB/c mice.

Purification of biMAbs

Purification was performed by HPLC with a MAPS 800 system (Bio-RAD Labs., Richmond, CA, USA), equipped with UV–visible and conductivity detectors. The same instrument, equipped with analytical and preparative injection loops, can be used both for analytical and process-scale purification.

Ascites fluid was pretreated with 1 m*M* $CaCl_2$ (final concentration) (2 h at 18–25°C and 16–22 h at 2–8°C) to allow conversion of fibrinogen present in the sample to fibrin. After removing the fibrin clot, ascites specimens were centrifuged at 10 000 *g* and then heat-inactivated at 56°C for 40 min. The samples were further clarified by ultracentrifugation at 100 000 *g* for 60 min at 2–8°C and then precipitated by adding an equal volume of saturated ammonium sulphate solution at pH 6.5.

Pellet was collected after centrifugation (10 000 *g*, 25 min at 2–8°C) and subsequently dissolved in water and dialysed *versus* protein A binding buffer, namely 1.5 *M* glycine–3.0 *M* NaCl (pH 9.0). Dialysed solution was applied to a 100 × 25 mm I.D. Affi-Prep protein A column (Bio-Rad Labs.) at a flow-rate of 5 ml/min. The total IgG fraction was eluted with 0.1 *M* citrate buffer (pH 3.0) and immediately neutralized with 1 *M* Tris (pH 8.5).

After dialysis against 10 m*M* sodium phosphate buffer (pH 6.8), a trace amount of IgG was loaded on to a 100 × 7.8 mm I.D. hydroxyapatite (HPHT) column (Bio-Rad Labs.) to select the appropriate fractionation gradient for each biMAb. Purification was performed at a flow-rate of 0.4 ml/min using 10 m*M* phosphate buffer (pH 6.8) as buffer A and 350 m*M* phosphate buffer (pH 6.8) as buffer B.

After appropriate gradient selection, hydroxyapatite purification of biMAbs was linearly scaled-up and performed on a 50 × 25 mm I.D. HPHT preparative column (Bio-Rad Labs.) at a flow-rate of 4 ml/min. Identification of peaks containing biMAbs was achieved by analysis of eluted peak fractions according to biMAb specificity, *i.e.*, on antigen-coated plates by indirect radioimmunoassay or on effector and target cells by indirect immunofluorescence assay. The fractions corresponding to active biMAbs were dialysed *versus* 10 m*M* phosphate buffer (pH 6.8) and re-chromatographed through a hydroxyapatite column under the same conditions to separate biMAbs further from residual contaminant immunoglobulins. The fractions corresponding to pure biMAbs were finally dialysed *versus* 0.1 *M* phosphate-buffered saline (pH 7.4), sterile filtered and stored deep-frozen.

Sodium dodecyl sulphate–polyacrylamide gel electrophoresis (SDS-PAGE) and isoelectric focusing

Purified bispecific and parental MAbs were analysed by 12.5% SDS-PAGE under reducing conditions (2% dimercaptoethanol) according to Laemmli [27]. Isoelectric focusing was performed with a PhastSystem using PhastGel IEF 3–9 (Pharmacia LKB, Uppsala, Sweden).

IgG determination

Immunoglobulin contents of the ascites fluid was evaluated by means of an in-house enzyme-linked immunosorbent assay (ELISA) method employing affinity-purified rabbit IgG to mouse IgG insolubilized on wells or conjugated to horseradish peroxidase [15]. Calibration graphs were obtained with an irrelevant affinity-purified MAb, class-matched with the antibody under analysis. With biMAbs derived from parental immunoglobulins of different isotypes, the graphs were derived from samples containing 50% mixtures of class-matched irrelevant antibodies.

Purified bispecific and parental MAbs concentrations were evaluated by measuring the UV absorbance at 280 nm using $E^{1\%}_{1cm} = 14.0$ [11].

RESULTS AND DISCUSSION

Pretreatment of ascites before chromatography appears to be a critical step in the whole purification process. Indeed, fibrin removal by $CaCl_2$, lipid and mineral oil (pristane) removal by ultracentrifugation and partial protein purification by ammonium sulphate precipitation proved to be of high relevance in preserving the column lifetime.

In order to evaluate purification yields, immunoglobulin contents of ascites fluids were checked by ELISA. Mean values of the estimated total IgG are reported in Table I. Ammonium sulphate precipitation and protein A purification make it possible to obtain the whole IgG fraction from ascites, with yields ranging from 65 to 75% (see Table III).

HPHT chromatography separates IgGs according to their net charge; this feature confers on hy-

TABLE I

IMMUNOGLOBULIN CONCENTRATIONS IN HYBRID HYBRIDOMA ASCITES FLUID

Immunoglobulin concentrations were evaluated by an ELISA method after ascites fluid ultracentrifugation.

biMAb	Ascites fluid IgG content (mg/ml)
AB8.28 × Ep2	9.2
CBT3 × CBT11	4.3
CBT3 × Ep2	7.5
F023C5 × 1LF5	11.4
A10 × Ep2	3.5
CBT3 × 44C10	2.7

droxyapatite its unique selectivity for IgG idiotypes [13–15]. As the active biMAb secreted by one hybrid hybridoma is formed of two IgG moieties, each corresponding to half of the parental IgG, this combination will have a total net charge intermediate between those of the parental MAbs. Therefore, the biMAb will be eluted from the HPHT column with an ionic strength intermediate between those of the parental MAbs. Thus, a consistent gap between the retention times of parental MAbs becomes a condition that cannot be overlooked in order to obtain a satisfactory separation of biMAbs. The choice of appropriate linear gradients for each biMAb appears to be critical to obtain a significant difference in HPHT retention times of parental MAbs and consequently to achieve pure preparations of biMAbs.

Gradients were selected after evaluating the retention times of parental MAbs on a 100 × 7.8 mm I.D. HPHT column (10–20 mg loading capability). The general gradient range was 0–80% buffer B. The next step was a linear scale-up of selected gradients to a 50 × 25 mm I.D. HPHT preparative column (about 500 mg loading capability) using a ten times faster flow-rate and a twice as long gradient, as reported in Table II.

TABLE II

SELECTED GRADIENT FOR biMAb PURIFICATION ON A 50 × 25 mm I.D. HYDROXYAPATITE COLUMN

BiMAbs were purified through a 50 × 25 mm I.D. Preparative HPHT column at a flow-rate of 4 ml/min. Buffer A, 10 m*M* phosphate (pH 6.8); buffer B, 350 m*M* phosphate (pH 6.8).

biMAb	Phosphate linear gradient		
	Initial B (%)	Final B (%)	Time (min)
CBT3 × CBT11	10	70	110
CBT3 × 44C10	10	70	110
CBT3 × Ep2	20	80	110
A10 × Ep2	20	40	120
AB8.28 × Ep2	15	50	120
F023C5 × 1LF5	0	50	100

The HPHT chromatographic elution profile of protein A-purified immunoglobulin is shown in Fig. 1 for each biMAb. The peak fractions corresponding to active biMAb were identified by appropriate double antigen specificity tests and by isoelectrofocusing. SDS-PAGE under reducing conditions was used to discriminate parental MAbs from bispecific IgGs when the two parental MAbs had differently migrating (fast and slow) light chains, as shown in Fig. 2 for MAbs AB8.28 and Ep2, and previously reported by other workers [13,14].

SDS-PAGE individually performed on peak fractions eluted from HPHT (Fig. 1A) showed that peaks 1 and 5 correspond to parental IgGs, each representing a differently migrating light chain. Peaks 2, 3 and 4 correspond to differently assembled parental heavy and light chains. Peak 3, which displayed light chain with a similar, if not identical, segregation, is the active bispecific fraction (activity data are reported elsewhere [5]).

Total IgG of the CBT3 × CBT11 hybrid hybridoma was also separated into five peaks by HPHT purification (Fig. 1B), two corresponding to parental MAbs (peaks 1 and 5), two to inactive products (peaks 2 and 4) and one to the active biMAb (peak 3). Under the conditions set up for this protocol, the other biMAbs studied were resolved into three main peaks by HPHT chromatography (Fig. 1C, D and E). CBT3 × 44C10 displayed a peculiar behaviour (Fig. 1F), which will be discussed later.

Middle peaks constantly included the active bispecific fraction. Parental Mabs were eluted in the first and third peaks (Fig. 1C, D and E). With A10 × Ep2 (Fig. 1E), the first peak was quantitatively lower than the others. The unbalanced proportion among the peaks probably reflects a different ex-

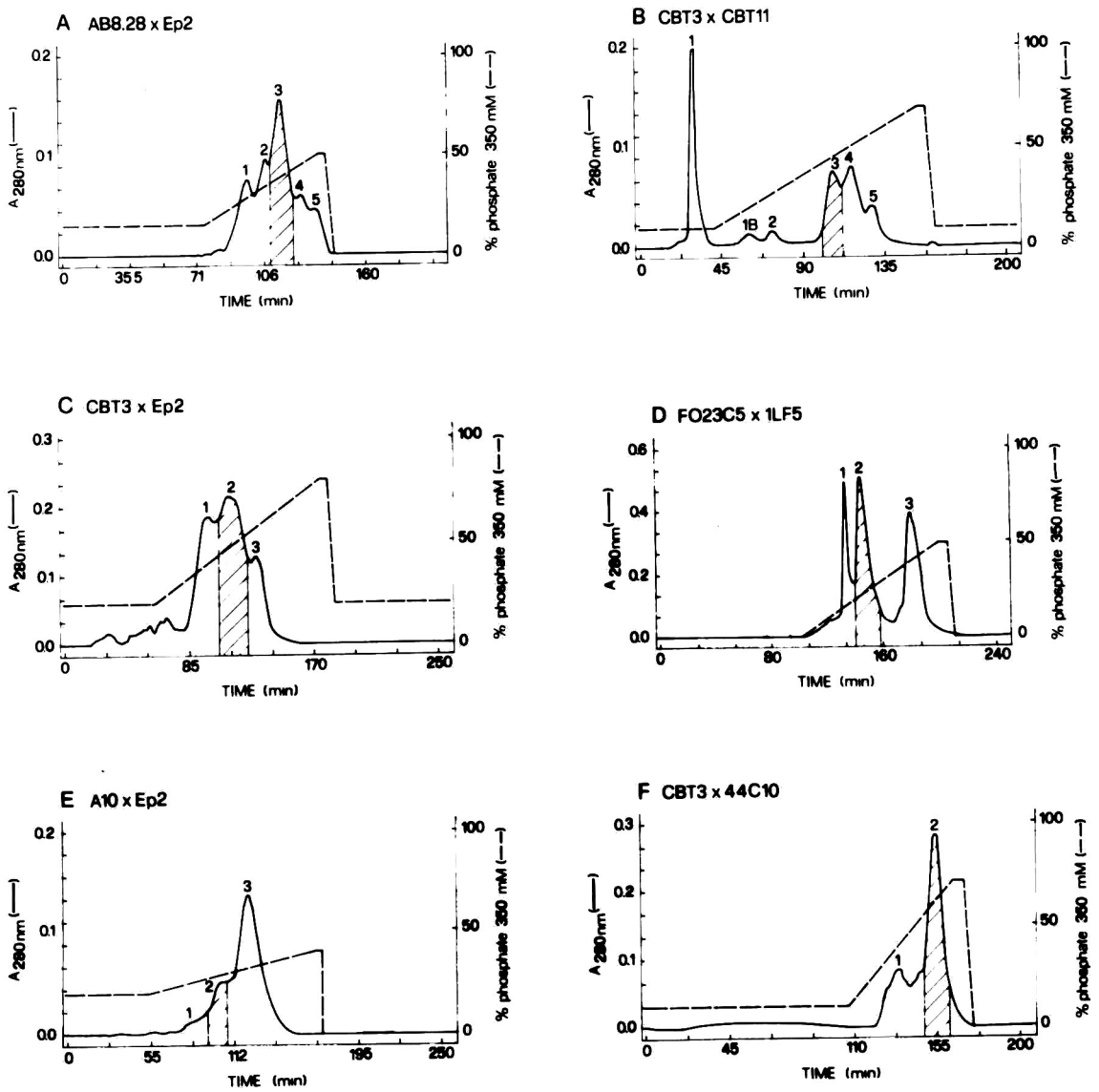

Fig. 1. Elution profiles of hydroxyapatite HPLC of immunoglobulins secreted by hybrid hybridomas. Purification was performed on a 50 × 25 mm I.D. HPHT column at a flow-rate of 4 ml/min. Buffer A, 10 m*M* phosphate (pH 6.8); buffer B, 350 m*M* phosphate (pH 6.8). Hatching indicates the peaks containing the active biMAb fractions. (A) AB8.28 × Ep2: 110-min linear gradient from 15 to 50% B. Peak 3 contains the biMAb; peaks 1 and 5 contain parental MAbs, AB8.28 and Ep2, respectively; peaks 2 and 4 contain inactive rearrangements of parental heavy and light chains. (B) CBT3 × CBT11: 110-min linear gradient from 10 to 70% B. Peak 3 contains the biMAb; peaks 1 and 5 contain parental MAbs, CBT11 and CBT3, respectively; peaks 2 and 4 contain inactive rearrangements of heavy and light parental chains. (C) CBT3 × Ep2: 110-min linear gradient from 20 to 80% B. The middle peak (hatched) contains the biMAb and peaks 1 and 3 correspond to parental MAbs Ep2 and CBT3, respectively. (D) F023C5 × 1LF5: 110-min linear gradient from 0 to 50% B. The middle peak (hatched) contains the biMAb and peaks 1 and 3 correspond to parental MAbs F023C5 and 1LF5, respectively. (E) A10 × Ep2. 120-min linear gradient from 20 to 40% B. The middle peak (hatched) contains the biMAb and peaks 1 and 3 correspond to parental MAbs A10 and Ep2, respectively. (F) CBT3 × 44C10: 110-min linear gradient from 10 to 70% B. Peak 2 corresponds to the active biMAb and peak 1 contains the parental MAb CBT3. The lack of resolution between the parental MAb 44C10 and the peak containing the biMAb is probably due to a characteristic of 44C10 hybridoma to secrete small amounts of IgG; a similar behaviour appeared on the A10 × Ep2 trace (E).

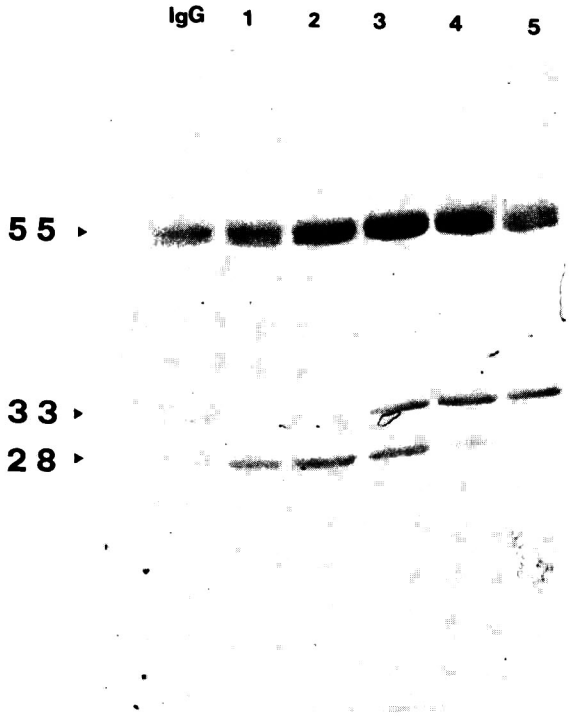

Fig. 2. SDS-PAGE under reducing conditions of the peak fractions derived from AB8.28 × Ep2 fractionation. Lanes 1–5 show the migration patterns of distinct peak fractions obtained by HPHT purification. Parental MAbs AB8.28 (1) and Ep2 (5) show differently migrating light chains. The marked lane shows IgG obtained by protein A affinity chromatography. Numbers on the left are molecular masses × 10^{-3}.

pression of heavy and light chains in the hybrid hybridomas. This evidence was further strengthened by the results of the HPHT purification of CBT3 × 44C10 (Fig. 1F), where only two detectable peaks were obtained. The first corresponds to the parental CBT3 MAb and the second contains the biMAb. A possible explanation of this observation may be the low IgG production of one parental hybridoma. Both A10 and 44C10 were found to be low IgG producers: selection of a high producer sub-clone of the anti-CD38 A10 hybridoma is in progress, in order to evaluate the influence of quantitative levels of immunoglobulin secretion by parental hybridomas in the generation of biMAbs and other molecular hybrid molecules.

IEF analysis of the peaks eluted after the first HPHT run showed low but significant peak-to-peak contamination. This prompted us to include a second application of peak fractions containing biMAbs on to a HPHT column in order to free biMAb preparations from any residual contamination. An example of chromatograms showing the second HPHT runs of peak fractions containing CBT3 × Ep2 and F023C5 × 1LF5 is given in Fig. 3. The retention time of the eluted peak is identical with the same parameter as recorded in the first HPHT run (*i.e.*, 105.3 ± 1.2 min for CBT3 × EP2 and 143.7 ± 0.8 min for F023C5 × 1LF5).

The final step was purity evaluation of biMAb preparations obtained following this protocol. The samples were submitted to SDS-PAGE and IEF, and the gels further tested by densitometric scanning.

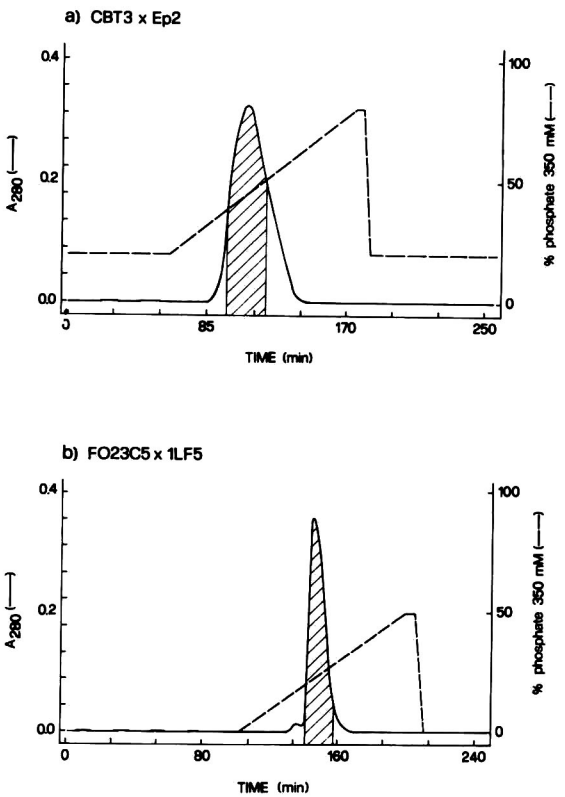

Fig. 3. HPHT second-run chromatographic profile of biMAb-containing fractions. BiMAbs obtained by first-run hydroxyapatite chromatography were re-loaded on a high-performance hydroxyapatite column (50 × 25 mm I.D.) at a flow-rate of 4 ml/min and eluted using the same phosphate gradients selected for the first run. (a) CBT3 × Ep2: 110-min linear gradient from 20 to 80% B. (b) F023C5 × 1LF5: 110-min linear gradient from 0 to 50% B.

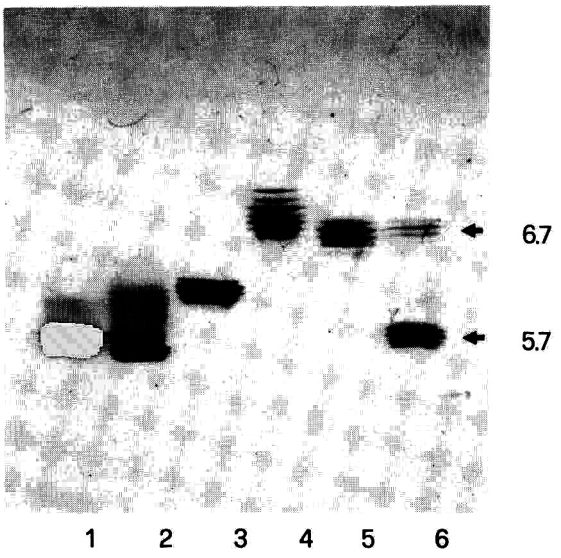

Fig. 4. Isoelectrofocusing of peak fractions collected after HPHT purification of F023C5 × 1LF5 biMAb. Lanes 1 and 5 show the IEF patterns of parental F023C5 and 1LF5 MAbs, respectively. Lane 6 contains an artificial mixture of the same parental MAbs. Lane 2 and lane 4 display an IEF pattern identical with that attributed to the parental MAbs with minimal contamination. The biMAb obtained after two HPHT purification runs (lane 3) is clearly distinguishable from the MAb mixture. It is also free from any apparent contaminating parental IgG. Numbers on the right are molecular masses × 10^{-3}.

Fig. 4 reports the results of the IEF analysis of the peak fractions obtained after purification of F023C5 × 1LF5 biMAb. Peak 1 (lane 2) corresponds to the parental F023C5 MAb and, peak 3 (lane 4) is identical with the parental 1LF5 MAb. Peak 2, confirmedly containing the bispecific MAb (see above), displays bands the p*I* range of which is intermediate between those of the two parental MAbs (lane 3). The IEF pattern of purified biMAbs was unique and markedly different from that of the simple mixture of parental MAbs (lane 6).

A low peak-to-peak contamination was apparent in peak fractions 1 and 3: the highest degree of purification was achieved by the biMAb peak fraction after the second HPHT run (98.7% as highlighted by gel densitometric scanning). At the end of the purification procedure presented here, the purity obtained for each biMAb was >98%. This was achieved by submitting samples to repeated passages through chromatographic columns. However, high purity demands lower yields; in this instance, the yield of the process from ascites to pure biMAb was in the acceptable range 10–35% (Table III).

CONCLUSIONS

This paper has reported the experience acquired so far in the investigation of methods and conditions to be applied in the purification of murine biMAb.The proposed protocol is the result of comparative tests: here, only the final conditions are reported, which allow discrimination between biMAbs and contaminanting ascites IgG. In fact, parental MAb trace contamination may hamper biMAb functional acitivity or mislead its effects in *in vitro* and *in vivo* applications.

TABLE III

biMAb PURIFICATION YIELDS

biMAb	Protein A: total IgG yield[a] (%)	HPHT I			HPHT II: biMAb yield[a] (%)
		total IgG yield[a] (%)	biMAb yield[a] (%)	biMAb/IgG ratio[b] (%)	
AB8.28 × Ep2	61.0	45.7	20.9	45.7	17.7
CBT3 × CBT11	70.0	39.4	13.4	34.0	12.2
CBT3 × Ep2	74.0	59.0	34.0	57.6	25.5
F023C5 × 1LF5	56.1	40.4	16.7	41.3	14.3
A10 × Ep2	69.5	45.7	13.0	28.4	12.1
CBT3 × 44C10	69.4	44.4	33.0	74.3	31.3

[a] Total process yield determined as recovered IgG at the end of each chromatographic step with respect to initial total IgG contents in ascites fluid. Values include centrifugations, precipitation, dialysis and filtrations of processed samples.
[b] Determined as the ratio of mg of purified biMAb recovered to mg of total IgG recovered.

This work focused on an already validated method of IgG isolation [15], which combines IgG specificity of protein A and the peculiar ability of hydroxyapatite to discriminate IgG idiotypes. This two-step chromatographic purification method was also previously shown not to affect IgG-binding capability [15], and it has been successfully submitted to validation for endotoxin, murine DNA and virus removal [28]. In particular, hydroxyapatite was found to remove different viral agents with high efficiency, as suggested by FDA and EEC guidelines [29–31].

All purification steps were performed rapidly and reliably by HPLC. This purification procedure was selected to provide pure reagents meeting the requirements to become immunopharmaceuticals, to be used either *in vitro* or, mainly, *in vivo* for localization and/or the destruction of tumour cells.

ACKNOWLEDGEMENTS

This study was partly supported by a grant from the National Research Programme "Technologies in Oncology" given to SORIN Biomedica by the Italian Ministry of University and Technological Research, and was also supported by grants from AIRC (Associazione Italiana Ricerca Cancro), AIDS Projests (Istituto Superiore Sanità, Rome, 1991) and Target Project "Biotecnologie e Biostrumentazione" (CNR, Rome, 1991). Lucia B. DeMonte is a postdoctoral fellow at Turin University.

REFERENCES

1 C. Milstein and A. C. Cuello, *Nature (London)*, 305 (1983) 537.
2 D. M. Segal and J. R. Wunderlich, *Cancer Invest.*, 6 (1988) 83.
3 U. D. Staerz and M. J. Bevan, *Proc. Natl. Acad. Sci. U.S.A.*, 83 (1986) 1453.
4 M. R. Suresh, A. C. Cuello and C. Milstein, *Methods Enzymol.*, 121 (1986) 210.
5 L. B. DeMonte, P. Nistico, R. Tecce, P. Dellabona, M. Momo, A. Anichini, M. Mariani, P. G. Natali and F. Malavasi, *Proc. Natl. Acad. Sci. U.S.A.*, 87 (1990) 2941.
6 S. M. Pupa, S. Canevari, E. Colzani, E. M. Damgard, S. Menard, S. Miotti and M. I. Colnaghi, *J. Immunol. Res.*, 3 (1991) 16.
7 *Guidelines for the Preparation and Presentation of Applications for General Marketing of Monoclonal Antibodies Intended for Use in Humans*, Australian Drug Evaluation Committee (Department of Community Services and Health), Canberra, 1987, Appendix C.
8 *Code of Federal Regulations*, Title 21, par. 610, 15b (para), Office of Federal Register, National Archives and Records Service, General Services Administration, U.S. Government Printing Office, Washington, DC, 1981.
9 A. Forsgren and J. Sjoquist, *J. Immunol.*, 97 (1966) 822.
10 G. Kronvall and D. Frommel, *Immunochemistry*, 7 (1979) 124.
11 P. L. Ey, S. J. Prowse and C. R. Jenkin, *Immunochemistry*, 15 (1978) 429.
12 D. R. Nau, *BioChromatography*, 4 (1989) 4.
13 H. Juarez-Salinas, S. C. Engelhorn, W. L. Bighee, M. L. Lowry and L. H. Stanker, *BioTechniques*, 2 (1984) 164.
14 H. Juarez-Salinas, G. S. Ott, J. C. Chen, T. L. Brooks and L. H. Stanker, *Methods Enzymol.*, 121 (1986) 615.
15 M. Mariani, F. Bonelli, L. Tarditi, R. Calogero, M. Camagna, E. Spranzi, E. Seccamani, G. Deleide and G. A. Scassellati, *BioChromatography*, 4 (1989) 149.
16 G. L. Buraggi, L. Callegaro, A. Turrin, L. Gennari, E. Bombardieri, G. Mariani, G. Deleide, M.Dovis, M. Gasparini, R. Doci, E. Regalia, E. Seregni and G. A. Scassellati, *Cancer Detect. Prevent.*, 10 (1987) 335.
17 P. Giacomini, O. Segatto and P. G. Natali, *Int. J. Cancer*, 39 (1987) 729.
18 M. Letarte, S. Vera, R. Tran, J. B. L. Addis, R. J. Onizuka, E. J. Quackenbush, C. V. Jongeneel and R. R. McInness, *J. Exp. Med.*, 168 (1988) 1247.
19 F. Malavasi, C. Tetta, A. Funaro, G. Bellone, E. Ferrero, A. Colli Franzone, P. Dellabona, G. Camussi and F. Caligaris Cappio, *Proc. Natl. Acad. Sci. U.S.A.*, 84 (1986) 2443.
20 L. B. DeMonte, M. Momo, A. Funaro, P. Nistico, A. Anchini, E. Bombardieri, F. Cavallo, E. Seccamani, M. Letarte, M. Mariani, P. G. Natali and F. Malavasi, in J. L. Romet-Lemonne, M. W. Fanger and D. M. Segal (Editors), *Proceedings of the Second International Conference on Bispecific Antibodies and Targeted Cellular Cytotoxicity, Seillac, October 1990,* Foundation Nationale de Transfusion Sanguinel, Les Ulis, 1991, p. 149.
21 A. Funaro, G. C. Spagnoli, C. M. Ausiello, M. Alessio, S. Roggero, D. Delia, M. Zaccolo and F. Malavasi, *J. Immunol.*, 145 (1990) 2390.
22 M. Mariani, A. Bartolazzi, M. Camagna, A. Parisi, L. Tarditi, C. Vassarotto and P. G. Natali, *Hybridoma*, (1992) in press.
23 P. T. Kirschemeir, G. M. Housey, M. D. Johnson, A. S. Perkins and J. B. Weinsteinerkins, *DNA*, 7 (1988) 219.
24 A. D. Miller, M. F. Law and I. M. Verma, *Mol. Cell. Biol.*, 5 (1985) 431.
25 L. B. DeMonte, M. Momo, A. Funaro, P. Nistico, A. Anchini, E. Bombardieri, F. Cavallo, E. Seccamani, L. Tarditi, M. Mariani, P. G. Natali and F. Malavasi, *J. Chemother.*, (1991) 3 suppl., 315.
26 M. Mariani, A. Parisi, L. Tarditi, L. DeMonte, A. Bartolazzi, M. Camagna, C. Vassarotto, C. Bonino, G. Paganelli, P. G. Natali and F. Malavasi, submitted for publication.
27 U. K. Laemmli, *Nature (London)*, 227 (1970) 680.
28 M. Mariani and L. Tarditi, *Bio/Technology*, in press.
29 ECC Regulatory Document, Note for Guidance: Validation of Virus Removal and Inactivation Procedures, *Biologicals*, 19 (1991) 247.
30 *Points to Consider in the Characterization of Cell Lines Used to Produce Biologicals*, Department of Health and Services, Food and Drug Administration, Washington, DC, 1987.
31 Guidelines on the Production and Quality Control of Monoclonal Antibodies of Murine Origin Intended for Use in Man, *Trends Biotechnol.*, 6 (1988) G5.

Journal of Chromatography, 599 (1992) 21–24
Elsevier Science Publishers B.V., Amsterdam

CHROMSYMP. 2531

Chromatographic analysis of low-molecular-mass copper-binding ligands from the crab species *Scylla serrata* and *Portunus pelagicus*

Siau-Gek Ang*

Department of Chemistry, National University of Singapore, 10 Kent Ridge Crescent, Singapore 0511 (Singapore)

Victor Wong Thi Wong

Department of Zoology, National University of Singapore, 10 Kent Ridge Crescent, Singapore 0511 (Singapore)

ABSTRACT

Two copper-binding proteins and a zinc-binding ligand were isolated from the hepatopancreas of the crab *Portunus pelagicus*. The copper-binding proteins behave similarly to those from the crabs *Carcinus maenas* and *Scylla serrata*, and were shown to be metallothioneins. Reversed-phase high-performance liquid chromatographic (HPLC) analysis confirmed the relative purity of both proteins with only cross-contamination between the two different forms of metallothioneins, and offers a good method to separate the two forms of metallothioneins. The vast difference in the retention times (and hence the hydrophobicity) in reversed-phase HPLC indicates that the two proteins could be conformationally very different.

INTRODUCTION

Copper and zinc are essential in trace amounts for all life forms, but are toxic when present at inappropriately high concentrations. Metallothioneins are a group of low-molecular-mass, cysteine-rich metal-binding proteins which are thought to occupy a central position in the metabolism of particular trace metals such as copper, cadmium, zinc and mercury [1]. They were first isolated from mammalian species [2] but have since been found in other organisms.

Metallothioneins have also been found in crab species. Two forms of metallothionein proteins (molecular mass 10 000 and 4100) have been isolated from the hepatopancreas of the shore crab *Carcinus maenas* [3], showing great individual variability between crabs as to their presence and their contents of copper, zinc and cadmium. The complete amino acid sequences of metallothioneins 1 and 2 from the crab *Scylla serrata* have also been reported [4]. Comparison of their primary structures with the known sequences of thioneins from equine kidney [5], human liver [6] and mouse liver [7] reveals a high degree of sequence homology among the six proteins, especially with respect to the conservation of the abundant cysteinyl residues.

Copper is regulated in trace levels in most vertebrates and is associated with very specific enzymes. However, numerous invertebrate species, including crustaceans, rely on haemocyanin, a Cu^{2+}-containing molecule [8]. Thus, in these species, Cu^{2+} is incorporated in metabolic and physiological activities in substantial amounts.

As metallothioneins are induced by and bind copper, they could play a central role in copper metabolism in most organisms. However, metallothioneins may be only part of a complex interplay of different compartments for trace metals, as they are ubiquitious in not being able to discriminate between copper, zinc and cadmium.

0021-9673/92/$05.00

EXPERIMENTAL

In the laboratory, live male crabs obtained from local markets were maintained in separate compartments in plastic tanks in aerated artificial sea water (Marinemix), prepared at a salinity of 33.3% and containing 0.5 μg/l of Cu^{2+}, for 2-week periods. The metal was added to the medium as an aliquot of a stock solution of the analytical-reagent grade salt. After the 2-week exposure period, the crabs were killed by freezing and the hepatopancreas was dissected out from each on partical thawing.

It was necessary to maintain reducing conditions throughout extraction with dithiothreitol (DTT) [4], as metallothionein proteins are very prone to the effects of oxidation during isolation owing to their very high cysteine content. To the dissected tissue was added an approximately equal volume of homogenizing buffer, Tris–HCl (0.01 *M* Tris, 0.01 *M* NaCl, HCl added to adjust the pH to 8.6) with 0.1 m*M* phenylmethanesulphonyl fluoride (PMSF) to prevent protease activity and 1 m*M* DTT to maintain reducing conditions. The mixture was homogenized and then centrifuged at 25 000 *g* for 3 h.

The supernatant was applied to a Sephadex G-50 column and eluted with Tris–HCl buffer (pH 8.6) containing 0.5 m*M* DTT to maintain reducing conditions. Pooled fractions corresponding to peaks I and II were then separately loaded on to an ion-exchange column (DEAE-Sephacel) and eluted with a 0.02 *M* Tris–HCl buffer gradient of increasing ionic strength (conductivity 2–35 mS, 0.01–0.4 *M* NaCl). The Cu^{2+}-containing fractions were then freeze-dried and desalted by passage through a Sephadex G-25 column. Metal analysis by flame and graphite furnace atomic absorption spectrophotometry (AAS) with a Shimadzu AA 670 instrument was performed after each purification step to check for the elution position of the metal-binding ligands.

The desalted fractions were then analysed by high-performance liquid chromatography (HPLC) using a Waters reversed-phase C_{18} (Nova-Pak C_{18}, 4 μm, 100 Å) column (300 × 3.9 mm I.D.) with a binary gradient Shimadzu HPLC LC-6A system. Buffer A was 0.1% trifluoroacetic acid (TFA) in water purified with a Milli-Q system (Millipore) and buffer B was 0.1% TFA in HPLC-grade acetonitrile.

Capacity factors, k', were calculated from the equation $k' = (t_R - t_0)/t_0$, where t_R and t_0 are the elution times of a retained and non-retained sample, respectively.

RESULTS AND DISCUSSION

Edible crabs are heavily consumed in the coastal areas in Asia. They are of special interest as the accumulation of heavy metals within their body tissues as a result of high concentrations of metals in sea water from polluting effluents could result in levels unacceptable for human consumption. There is therefore a need to monitor total levels, and also to study further the mechanisms of metal regulation in these tropical decapods.

Although much work has been done on temperate species of crabs, work on tropical species is conspicuous by its absence. This paper serves to redress this imbalance by identifying and isolating trace-metal-binding, low-molecular-mass ligands in selected tropical species of organisms, with the ultimate aim of understanding the proper role of these ligands in the complex physiology of these organisms. We decided to use a local crab species, *Portunus pelagicus*, owing to their ready availability, the large size of the hepatopancreas, convenience and the fact that these ligands have been shown to occur in crabs. In addition, we also obtained a few *Scylla serrata* crabs for comparison studies.

The *Scylla serrata* species of crabs have been studied previously and the metallothioneins from this species have been characterized and sequenced [4]. The chromatographic behaviour of the material obtained from *Portunus pelagicus* is very similar to that from *Scylla serrata* and *Carcinus maenas* crabs [3].

Fig. 1 shows a typical Sephadex G-50 elution profile (molecular mass linear separation range 30 000–1500) derived from hepatopancreas tissue pooled from male *Portunus pelagicus* crabs, reducing conditions being maintained throughout by the addition of DTT. Peaks I and II correspond to metallothioneins as seen in the *Scylla serrata* and *Carcinus maenas* crabs. Although the two peaks are not completely resolved, there is a definite shoulder indicating the presence of two proteins. Peak III binds to zinc, corresponding to a low-molecular-mass non-proteinaceous zinc-binding ligand that had also been found in the latter two species of crabs [9].

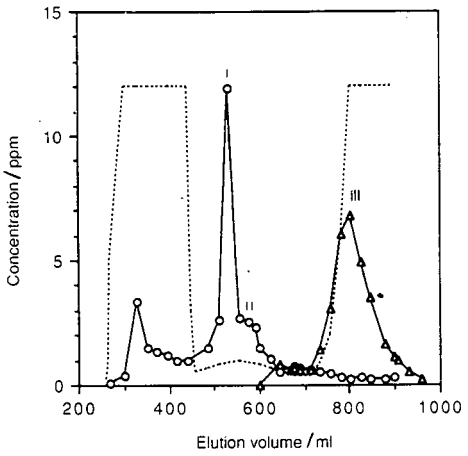

Fig. 1. Sephadex G-50 elution profile of male *Portunus pelagicus* crab hepatopancreas from copper-exposure experiments. The sample was homogenized in Tris–HCl buffer containing 1 m*M* DTT and eluted with Tris–HCl buffer containing 0.5 m*M* DTT. Bed volume, 780 ml; flow-rate, 70 ml/h; detection wavelength, 254 nm. ○ = Copper; △ = zinc. Dashed line, absorbance.

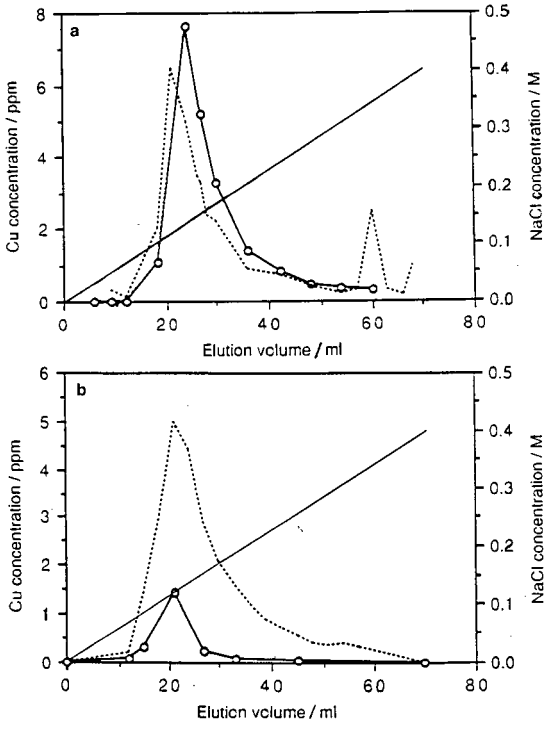

Fig. 2. Elution profile of Sephadex G-50 fractions of (a) peak I and (b) peak II on a DEAE-Sephacel ion-exchange column (12 × 1.2 cm I.D.). Bed volume, 12.5 ml; flow-rate, 18 ml/h; detection wavelength, 254 nm. ○ = Copper. Dashed line, absorbance.

Fig. 2 shows typical ion-exchange chromatograms of material obtained from peaks I and II of the Sephadex G-50 elution and applied separately to a DEAE-Sephacel ion-exchange column (12 × 1.2 cm I.D.). Olafson *et al.* [10] reported two well resolved metal-containing peaks using a 30 × 2.6 cm I.D. Bio-Rad Cellex D DEAE-cellulose column using pooled fractions isolated by gel permeation chromatography. As peaks I and II were not completely resolved peaks on the Sephadex G-50 column, we expected material from peaks I and II to be mixtures of the two metallothioneins. However, we observed that on our DEAE-Sephacel column, the material from both peaks I and II gave single metal-containing peaks on anion exchange. That the two metallothioneins were not resolved at this stage in the purification could be due to the sharp gradient employed on the short ion-exchange column used in the elution of the proteins. Further studies are currently being conducted to examine this more closely. The proteins were desalted with water through a Sephadex G-25 column, with salt detected by conductivity measurements and the metallothionein proteins by AAS.

Analytical reversed-phase HPLC was carried out on purified material (from the *Portunus pelagicus* crabs) from peaks I and II separately to check for homogeneity. For comparison, the material from the *Scylla serrata* crabs was also subjected to the same analysis. Fig. 3a and b show the respective chromatograms for the two species of crabs. The capacity factors (k') of the two proteins from the *Portnunus pelagicus* crabs (2.5 and 8.4) are very similar to those for the proteins isolated from the *Scylla serrata* crabs (2.7 and 8.3), indicating that the two proteins from the hepatopancreas of the *Portunus pelagicus* crabs are therefore metallothionein proteins.

As peaks I and II were not completely resolved on the Sephadex G-50 column, it is not surprising that in both instances the material from the two peaks appeared to contain a mixture of the same two proteins. From the chromatograms, it is obvious that although both peaks consist of mixtures of the two proteins, peak II consists predominantly the protein of $k' = 2.5$. As can be seen from the metal trace using AAS measurement in Fig. 1, peak I is a sharp peak whereas peak II is relatively broad, and it appears that elution of peak II has begun before

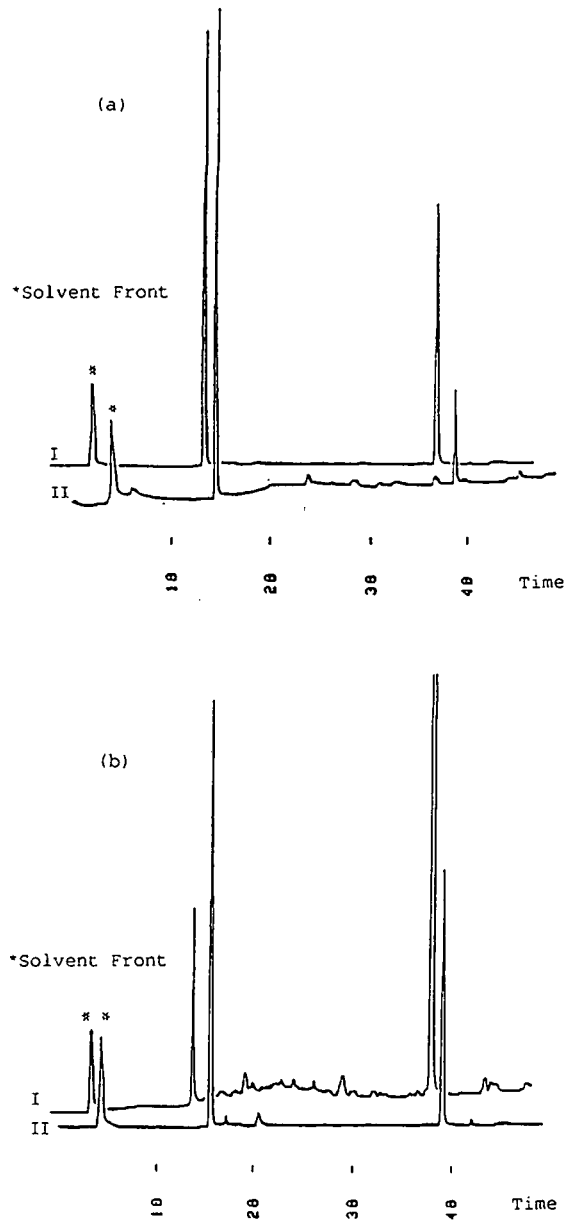

Fig. 3. HPLC analyses of metallothioneins from peaks I and II of (a) *Portunus pelagicus* and (b) *Scylla serrata* on a reversed-phase C_{18} column. Solvents used in elution: (A) 0.1% TFA in Milli-Q-purified water and (B) 0.1% TFA in acetonitrile, with a gradient from 10 to 60% B in 40 min. Flow-rate, 0.5 ml/min; detection wavelength, 254 nm. Time in min.

peak I is completely eluted. Therefore, it is understandable that there is cross-contamination and that peak II is purer than peak I. From this analysis, it is obvious that reversed-phase HPLC would be a good method to isolate pure samples of the two proteins because of the vast difference in the retentions of the two proteins on the reversed-phase C_{18} column used.

In addition to these two metallothionein proteins, hepatopancreas extracts typically contain a zinc-binding complex of low molecular mass, as has also been shown with *Carcinus maenas* [9]. The characterization of this zinc-binding ligand will be presented in a separate paper. We have also observed that the level of induction of the proteins after exposure for 2–5 days to artificial sea water spiked with Cu^{2+} appears to be higher than that for a longer period (14 days). This is based on the results of measurement of metal levels after the first purification step (Sephadex G-50). We are now carrying out time-scale experiments to verify this observation.

ACKNOWLEDGEMENTS

This work was supported by generous grants from the National University of Singapore (RP880603) and the International Atomic Energy Agency (6243/RB).

REFERENCES

1 B. L. Vallee, in J. H. R. Kagi and M. Nordberg (Editors), *Metallothionein*, Birkhauser Verlag, Basel, 1979, pp. 19–40.
2 J. H. R. Kagi, M. Vasak, K. Lerch, D. E. O. Gilg, P. Hunziker, W. R. Bernhard and M. Good, *Environ. Health Perspect.*, 54 (1984) 93.
3 V. W. T. Wong and P. S. Rainbow, *Comp. Biochem. Physiol. A*, 83 (1986) 149.
4 K. Lerch, D. Ammer and R. W. Olafson, *J. Biol. Chem.*, 257 (1982) 2420.
5 Y. Kojima, C. Berger, B. L. Vallee and J. H. R. Kagi, *Proc. Natl. Acad. Sci. U.S.A.*, 73 (1976) 3413.
6 M. M. Kissling and J. H. R. Kagi, *FEBS Lett.*, 82 (1977) 247.
7 I.-Y. Huang, A. Yoshida, H. Tsunoo and H. Nakajima, *J. Biol. Chem.*, 252 (1977) 8217.
8 J.-L. M. Martin, A. van Wormhoudt and H. J. Ceccaldi, *Comp. Biochem. Physiol. A*, 58 (1977) 193.
9 V. W. T. Wong and P. S. Rainbow, *Comp. Biochem. Physiol. C*, 87 (1987) 203.
10 R. W. Olafson, R. G. Sim and K. G. Boto, *Comp. Biochem. Physiol. B*, 62 (1979) 407.

Journal of Chromatography, 599 (1992) 25–33
Elsevier Science Publishers B.V., Amsterdam

CHROMSYMP. 2509

Biosep-SEC-S high-performance size-exclusion chromatographic columns for proteins and peptides

Faizy Ahmed* and Bijan Modrek

Phenomenex, Inc., 2320 West 205th Street, Torrance, CA 90501 (USA)

ABSTRACT

Spherical silica particles (5 μm) of three different pore sizes, 145, 290 and 500 Å (Biosep-SEC-S2000, Biosep-SEC-S3000 and Biosep-SEC-S4000), were bonded with a hydrophilic coating and evaluated for the size-exclusion chromatography of proteins and peptides. The results of experiments with synthetic peptides and lysozyme under different mobile phase conditions indicated very nominal non-specific interaction of proteins with the stationary phases. The recovery of trypsin, protein mass and enzyme activity, determined at mobile phase pH values of 3 and 7, was excellent for all three column types. The new stationary phases showed superior stability towards common protein denaturants and organic modifiers.

INTRODUCTION

Size-exclusion chromatography (SEC) is one of the most widely used techniques for the characterization of proteins and peptides. This versatile procedure is often employed not only for protein purification but also in the determination of their molecular weights [1–3]. Over the past few years, new stationary phases for the SEC of biopolymers have been developed [4–6] and characterized [7]. Silica-based chromatographic supports provide great advantages such as rigidity, well defined pore-size distribution and stability towards a variety of mobile phase solvents. However, depending on the nature of the bonded phase and the presence of unreacted silanols, interaction of proteins or peptides with the stationary phase can occur, resulting in non-ideal size exclusion behavior [8–10]. Such interactions have been shown to be ionic or hydrophobic in nature [4,7,9]. These non-specific interactions can lead to errors in the determination of protein and peptide molecular weights and, in many instances lower recoveries of protein mass and diminished biological activity. We report here the development of a new silica-based support for the SEC of proteins and peptides. The new stationary phases were evaluated using synthetic peptides and natural proteins and were shown to operate essentially with a size-exclusion mechanism.

EXPERIMENTAL

Biosep-SEC-S series columns were prepared by bonding silica of pore sizes 145, 290 and 500 Å with a hydrophilic coating. Synthetic size-exclusion peptide standards were obtained from Synthetic Peptides (Edmonton, Canada). The sequences of five peptides are Ac–(Gly–Leu–Gly–Ala–Lys–Gly–Ala–Gly–Val–Gly)$_n$–amide (Ac = N-acetyl, amide = C-amide), where n = 1–5, giving rise to five peptides consisting of 10–50 residues. The peptides have increasing charge (+1 to +5) and hydrophobicity, with molecular weights of 826, 1595, 2362, 3129 and 3897 dalton, respectively.

All laboratory chemicals used in the preparation of mobile phase buffers were of HPLC grade and purchased from Fisher Scientific (Tustin, CA, USA), except sodium dodecyl sulfate (SDS), which was from Pierce (Rochford, IL, USA). The proteins used were either obtained from Boehringer Mannheim (San Diego, CA, USA) or Sigma (St. Louis, MO, USA). Some of the size-exclusion protein stan-

0021-9673/92/$05.00

dards were also purchased from Bio-Rad Labs (Richmond, CA, USA). Mobile phase buffers were filtered through 0.2-μm Anodisc 47, Anopore membrane disc filters (Phenomenex, Torrance, CA, USA) and degassed by helium sparging before use. Protein standards were prepared in the mobile phase buffer at a concentration of 2 mg/ml and were filtered through 0.2-μm Anotop 10-Plus inorganic membrane syringe filters (Phenomenex) prior to injection.

Chromatographic runs were performed on a Hewlett-Packard 1050 Series pumping system with an HP 1050 multiple wavelength detector. A Phenoflow flow meter (Phenomenex) installed at the outlet of the detector was used to monitor the flow and very stable flow was obtained with this pump.

The partition coefficient, K_D was calculated with the equation $V_e = V_0 + K_D V_i$ [7], where V_e is the elution volume of the analyte, V_0 is the column void volume and V_i is the pore volume of the support. As the total liquid volume, $V_T = V_0 + V_i$, substituting for V_i, then $K_D = (V_e - V_0)/(V_T - V_0)$. The total liquid volume (V_T) of the column was determined by chromatography of ethylene glycol with refractive index detection or dihydroxyacetone with UV detection at 300 nm, using water as mobile phase. The V_T values for the three types of columns (300 × 7.75 mm I.D.) with increasing pore size were calculated to be 11.54, 12.44 and 12.40 ml, respectively. The void volume, V_0, of the column was determined by injecting 10 μl of high-molecular-weight calf thymus DNA (2.5 mg/ml solution from Boehringer Mannheim), with 50 m*M* NaH_2PO_4 buffer (pH 6.8) as mobile phase and UV detection at 260 nm. The V_0 values for the three phases (300 × 7.75 mm I.D. columns) were 5.27, 5.45 and 5.80 ml, respectively.

RESULTS AND DISCUSSION

Recently, synthetic peptides have been introduced to diagnose the surface activities of silica-based chromatographic stationary phases, including reversed-phase, size-exclusion and ion-exchange matrices [11–13]. These peptides provide a very convenient method to test the performance of newly developed chromatographic supports. Two sets of peptide standards, with increasing hydrophobicity and cationic charge, were used to evaluate the behavior of Biosep-SEC-S2000 with a pore size of 145 Å. The sizes of the peptide standards are such that they ideally separate out on this stationary phase. As these peptides have increasing charge and hydrophobicity (see Experimental for the sequence), silica supports containing surface charge due to free silanols or hydrophobic character have been shown to retain the peptides by ionic or hydrophobic binding, resulting in reversal of the order of elution [11]. In extreme cases of such surface activity, the peptides have been shown to elute after the total permeation volume of the column, indicating in such instances that the column is behaving more like a cation exchanger than an SEC support.

Table I shows the effect of mobile phase composition on the retention times of three peptides (+5, +2 and +1) on Biosep-SEC-S2000. Under all the mobile phase conditions used, the peptides showed ideal SEC patterns, eluting in order of increasing molecular weight. The mobile phase composition had virtually no effect on the retention times. If there were unreacted silanols present on this stationary phase, the low ionic strenght of 100 m*M* phosphate buffer at pH 6.8 would have resulted in retention of the peptides due to ionic interactions. This would cause the largest peptide with the highest charge (+5) to elute much later than expected on the basis of size. Increasing the salt concentration in the buffer would suppress ionic interactions with the stationary phase, but could lead to hydrophobic binding and result in a non-ideal elution

TABLE I

EFFECT OF MOBILE PHASE COMPOSITION ON THE ELUTION BEHAVIOR OF SYNTHETIC PEPTIDES

A synthetic peptide mixture containing +5, +2 and +1 peptides was dissolved in water and 10 μl were subjected to SEC on a Biosep-SEC-S2000 column (300 × 7.75 mm I.D.) under the mobile phase conditions described, at a flow-rate of 1 ml/min. UV detection at 210 nm.

Mobile phase	t_R (min)		
	+5 Peptide	+2 Peptide	+1 Peptide
100 m*M* phosphate (pH 6.8)	8.85	9.58	10.04
100 m*M* phosphate (pH 6.8) containing 500 m*M* NaCl	8.91	9.66	10.25
0.1% aqueous TFA	8.87	9.68	10.10

pattern for the peptides. Thus, when the salt concentration in the mobile phase was increased by adding 500 m*M* NaCl to the 100 m*M* NaH_2PO_4 buffer, no effect on the retention time of the peptides was observed, indicating the absence of hydrophobic binding on this stationary phase.

In the separation of peptides, it is convenient to use trifluoroacetic acid (TFA) as an eluent, as it is easily removed by lyophilization. The acidic conditions of the mobile phase also suppress the ionic interaction with the stationary phase, similarly to the effect of increasing the salt content in mobile phase. The synthetic peptide mixture described above was subjected to SEC on the Biosep-SEC-S2000 column in 0.1% TFA. The retention times of the peptides remained unchanged with this mobile phase (Table I) compared with other mobile phases used. Some of the commercial columns require high concentrations of TFA (1%) to suppress completely the ionic activity, and such extreme conditions may have an adverse effect on the column lifetime [11]. The stationary phase described here shows ideal SEC behavior with 0.1% TFA as is normally used for such applications.

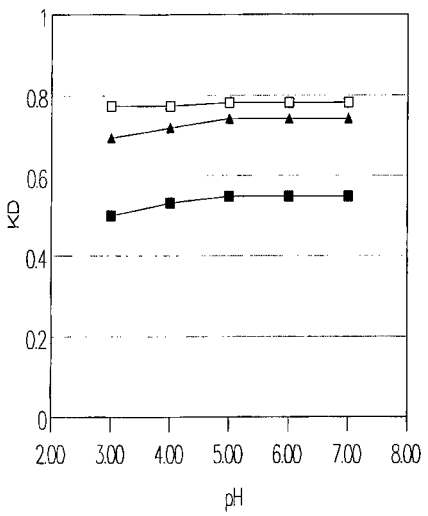

Fig. 1. Effect of mobile phase pH on the K_D of lysozyme. Biosep-SEC-S2000, -S3000 and S4000 columns (300 × 7.75 mm I.D.) were equilibrated with 0.1 *M* NaH_2PO_4 buffer at different pH values between 3 and 7. Lysozyme was dissolved in the same buffer as the mobile phase at 10 mg/ml and 20 μl of the solution were inhected. The flow-rate was 1 ml/min and detection was at 280 nm. Columns: ■ = Biosep-SEC-S2000; ▲ = Biosep-SEC-S3000; □ = Biosep-SEC-S4000.

The synthetic peptides were useful in the evaluation of the surface activity of Biosep-SEC-S2000 (pore size 145 Å) columns. However, because of the larger pore sizes of the supports, the peptide standards would not resolve on the Biosep-SEC-S3000 (pore size 290 Å) and Biosep-SEC-S4000 (pore size 500 Å) columns. Therefore, lysozyme was used as a probe for their evaluation. Biosep-SEC-S2000 was also included, to further confirm the results obtained with synthetic peptides. Lysozyme is a hydrophobic and very basic protein (p*I* = 11.0) and has been recommended as a probe for testing the surface activity of size-exclusion columns [7]. Some SEC supports show drastic changes in retention behavior of lysozyme under mobile phase conditions differing in ionic strength and pH, indicating ionic and hydrophobic interactions with the stationary phase [4,7]. The effect of changing the mobile phase pH on the SEC of lysozyme was tested on Biosep-SEC -S2000, -S3000 and -S4000 columns. The mobile phase pH values were varied between 3 and 7 with an ionic strength of the buffer (0.1 *M*) normally used for size-exclusion chromatography of proteins. Fig. 1 is a plot of mobile phase pH *vs.* K_D of lysozyme on the three types of columns. There was only a nominal increase in K_D of the enzyme with an

TABLE II

RECOVERY OF TRYPSIN FROM BIOSEP-SEC-S COLUMNS

The columns were equilibrated with 0.1 *M* NaH_2PO_4 buffer (pH 3.0 or 7.0). Trypsin was dissolved in NaH_2PO_4 buffer (pH 3.0) at 10 mg/ml. A volume of 20 μl of the solution was injected on to the columns and the peaks were collected. For each pH value, at least five runs were performed. The peaks were assayed for protein concentration and enzyme activity by the UV–VIS method. The enzyme activity was measured using N-benzoyl-L-arginine-*p*-nitroacetanilide as a substrate in Tris–HCl buffer (pH 8.0) containing $CaCl_2$. The hydrolysis was followed by the increase in absorption at 386 nm.

Column	pH	Protein (%)	Specific activity (%)
Biosep-SEC-S2000	3.0	85–100	86–100
	7.0	70–79	95–100
Biosep-SEC-S3000	3.0	98–101	96–100
	7.0	70–78	96–100
Biosep-SEC-S4000	3.0	92–100	95–101
	7.0	69–80	94–100

increase in pH of the mobile phase, suggesting a very low ionic-type interaction with the supports. For some commercial SEC supports, it has been observed that an increase in the ionic strength of the mobile phase above 0.2 *M* leads to binding of lysozyme by hydrophobic interaction [4]. However, when the buffer concentration was increased to 0.2 *M* at pH 7.0, the change in elution time was insignificant with the SEC phases described here (data not shown). These results complement and support earlier experiments with the synthetic peptides, and demonstrate essentially a size-exclusion mechanism operating under the normal mobile phase conditions, with other retention mechanisms having little or no influence.

It is important in any protein chromatographic

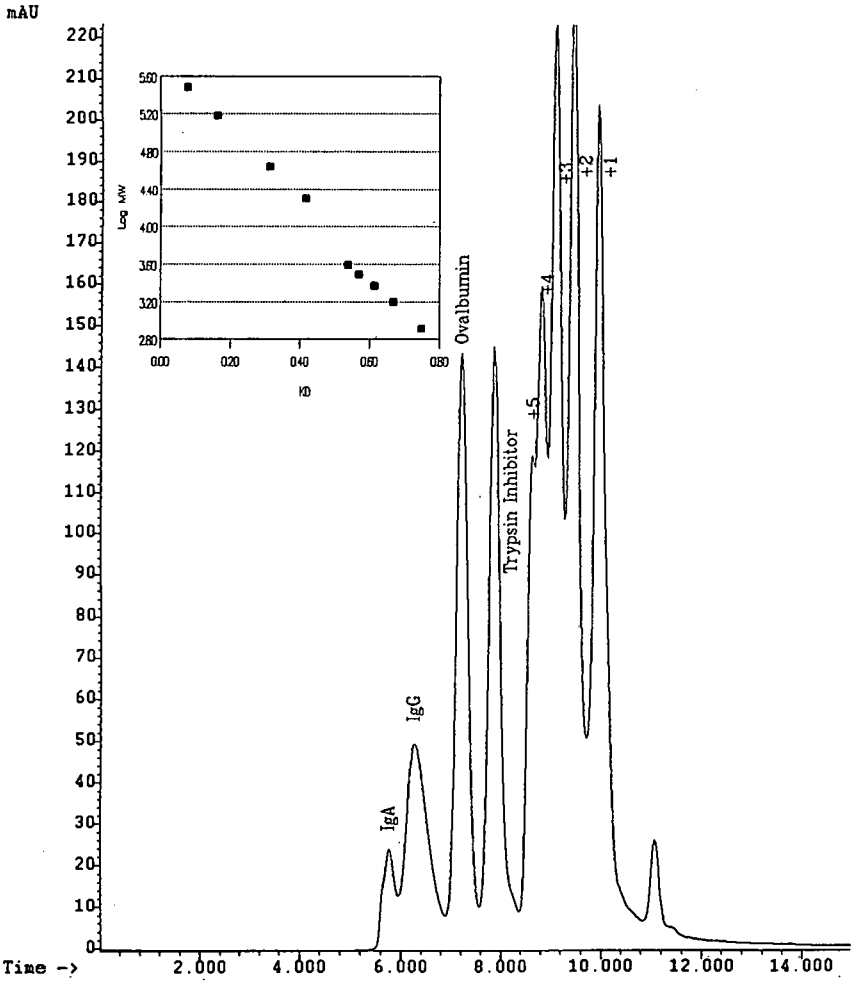

Fig. 2. SEC of proteins and peptides on Biosep-SEC-S2000. A 300 × 7.75 mm I.D. column was equilibrated with 50 m*M* NaH_2PO_4 buffer (pH 6.8) at a flow-rate of 1 ml/min. Protein standard was prepared by dissolving 4 mg each of γ-globulin (a mixture of immunoglobulins IgM, IgA and IgG), ovalbumin and trypsin inhibitor in 1 ml of mobile phase. About 4 μl of this mixture were added to 100 μl of a solution of synthetic peptides. A 10-μl volume of the sample was injected on to the column. The elution of proteins and peptides was followed by UV detection at 215 nm. Peaks identified: IgA (300 000 dalton), IgG (150 000 dalton), ovalbumin (44 000 dalton), trypsin inhibitor (20 100 dalton), peptide +5 (3897 dalton), peptide +4 (3129 dalton), peptide +3 (2362 dalton), peptide +2 (1595 dalton), and peptide +1 (826 dalton). The inset is a plot of log molecular weight (MW) *vs.* K_D for this separation (r^2 = 0.9936). The K_D values were calculated using the equation $K_D = (V_e - V_0)/(V_T - V_0)$, where V_e is the elution volume and V_T and V_0 represent the total liquid volume and void volumes of the column, respectively. Time in min.

procedure to have good recoveries of protein mass from the column. It is equally important to retain the maximum amount of biological activity in the sample following the chromatographic step. In some instances, one may recover all the protein from a column, while losing much of the biological activity because of its interaction with the stationary phase [7]. Trypsin is another basic protein (p*I* 10.5) and is a suitable probe to study such interactions. Therefore, trypsin chromatography on Biosep-SEC-S phases was studied with respect to recovery of protein and enzyme activity, at mobile phase pH values of 3.0 and 7.0. The results are given in Table II. When 200 μg of the enzyme were injected on to the column, the typical recovery of the protein mass ranged from 85–100% at pH 3.0. However, at pH 7.0 the recovery was lower, ranging between 69 and 80% for all the phases. Earlier experiments with synthetic peptides and lysozyme have shown that non-specific interactions are virtually absent in these columns. The loss of trypsin mass may be due to some denaturation or possibly because of autodigestion. The recovery of enzyme activity, however, was excellent at both pH values for all the columns tested and ranged from 85 to 100%.

After ascertaining that there was no apparent surface reactivity of Biosep-SEC-S stationary phases, the separation range of these columns for proteins and peptides under native conditions was determined. First Biosep-SEC-S2000 was evaluated for its resolving capacity. A mixture containing five synthetic peptide standards (charge +1 to +5) and proteins (immunoglobulins, ovalbumin and trypsin inhibitor) was subjected to SEC on this column, equilibrated with 50 m*M* NaH_2PO_4 buffer (pH 6.8). The chromatographic profile is presented in Fig. 2. All the components of the mixture were adequately resolved. The plot of log (molecular weight) *vs.* K_D is given in the inset and shows excellent linearity (r^2 = 0.9936). The separation range for this phase for proteins and peptides can be conveniently set at 1000–300 000 dalton based on these results.

The resolving power of Biosep-SEC-S3000 was tested with a wide range of proteins. The column was equilibrated with 50 m*M* NaH_2PO_4 buffer (pH 6.8) and mixtures containing different proteins were subjected to SEC. For some proteins which co-eluted, such as trypsin inhibitor and carbonic anhydrase, runs were performed to determine and confirm the individual retention times. Fig. 3 is a plot of log (molecular weight) *vs.* K_D for all proteins separated using the Biosep-SEC-S-3000 column and shows linearity with r^2 = 0.977. It is well known that the size of a macromolecule depends not only on its molecular weight but also its conformation [14]. Different shapes, such as solid-sphere, random coil or rod-like structures, with the same molecular weight show different elution behaviors in SEC. Therefore, considering the diversity of the proteins used in this experiment, the correlation coefficient would appear to be acceptable. Thus, when insulin and cyanocobalamin were excluded from the calcu-

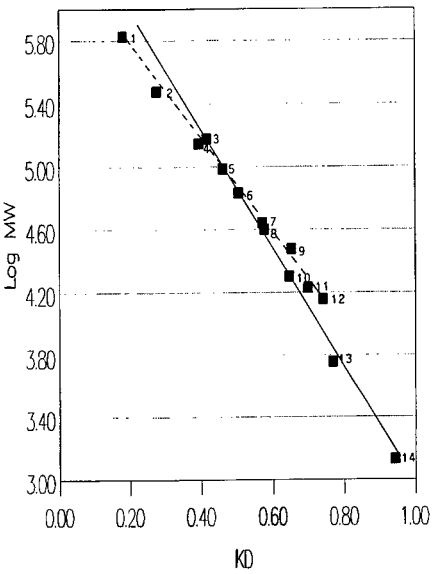

Fig. 3. Cromatography of proteins on Biosep-SEC-S3000. A mixture of different proteins was prepared by dissolving 2 mg each in the mobile phase buffer 50 m*M* NaH_2PO_4 (pH 6.8). A 10-μl volume of the sample was injected into a 300 × 7.75 mm I.D. column which was equilibrated with the buffer at 1 ml/min. UV detection at 280 nm was applied. Three different runs with mixtures of proteins were performed and the log MW *vs.* K_D plotted (solid line, for all proteins, r^2 = 0.977; dashed line, excluding insulin and cyanocobalamin, r^2 = 0.9905). Proteins: 1 = thyroglobulin (670 000 dalton); 2 = IgA (300 000 dalton); 3 = IgG (150 000 dalton); 4 = lactate dehydrogenase (134 000 dalton); 5 = phosphorylase *b* (97 000 dalton); 6 = bovine serum albumin (68 000 dalton); 7 = ovalbumin (44 000 dalton); 8 = horse radish peroxidase (40 000 dalton); 9 = carbonic anhydrase (30 000 dalton); 10 = trypsin inhibitor (20 100 dalton); 11 = myoglobin (17 000 dalton); 12 = lysozyme (14 400 dalton); 13 = insulin (5700 dalton); 14 = cyanocobalamin (1350 dalton).

lations, the correlation coefficient improved to 0.9905 and only carbonic anhydrase seemed to deviate from the best-fit curve in as much as it co-eluted with trypsin inhibitor. Although cyanocobalamin is not a protein and is used as a marker, its elution behavior may not be consistent with proteins or peptides. Insulin, on the other hand, being smaller in size than all the other proteins used in this study, may deviate from the elution pattern of these proteins simply because of differences in the tertiary structure and shape. The deviation of carbonic anhydrase from normal elution is surprising, as it is an acidic protein (pI = 5.3). This may be because of its conformation or its interaction with the stationary phase by a mechanism other than ionic or hydrophobic binding.

When used under denaturing conditions, SEC can be effectively employed for the determination of protein molecular weights. Proteins attain an extended rod-like or random coil structure under de-

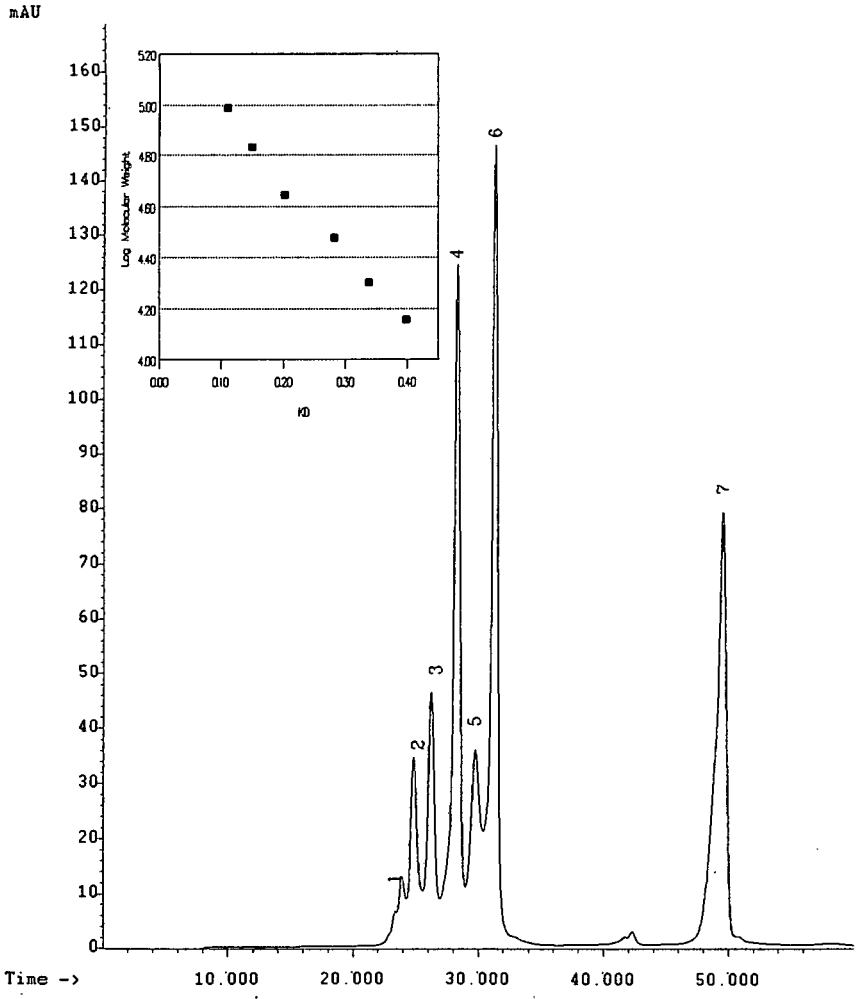

Fig. 4. SEC of proteins on Biosep-SEC-S3000 using 0.5% SDS. Protein mixture was prepared by dissolving 2 mg each of (1) phosphorylase *b* (97 000 dalton), (2) bovine serum albumin (68 000 dalton), (3) ovalbumin (44 000 dalton), (4) carbonic anhydrase (30 000 dalton), (5) trypsin inhibitor (20 100 dalton) and (6) lysozyme (14 400 dalton) in 0.5 ml of 20 mM NaH_2PO_4 buffer (pH 6.5) containing 1% SDS and 1% β-mercaptoethanol. The solution was boiled for 3 min and 20 μl were injected on to the column (600 × 7.75 mm I.D.); equilibrated with 20 mM NaH_2PO_4 buffer (pH 6.5) containing 0.5% SDS at a flow-rate of 1 ml/min. Peak 7 is BME. The inset is a plot of log MW *vs.* K_D with r^2 = 0.9908. Time in min.

naturing conditions, and because of uniformity in the conformation, the determination of molecular weight has been shown to be more accurate [3]. In fact, SEC separations of proteins are often found to be much better under denaturing conditions than when in a native state [15,16]. The Biosep-SEC-S3000 column was evaluated for its ability to separate proteins using 6 *M* guanidine hydrochloride (GnHCl) and SDS, and also for its stability toward these reagents.

The effects of buffer concentration on the retention times of proteins and peptides using SDS in SEC have been described [17]. The mode of separation was shown to be affected by the presence of

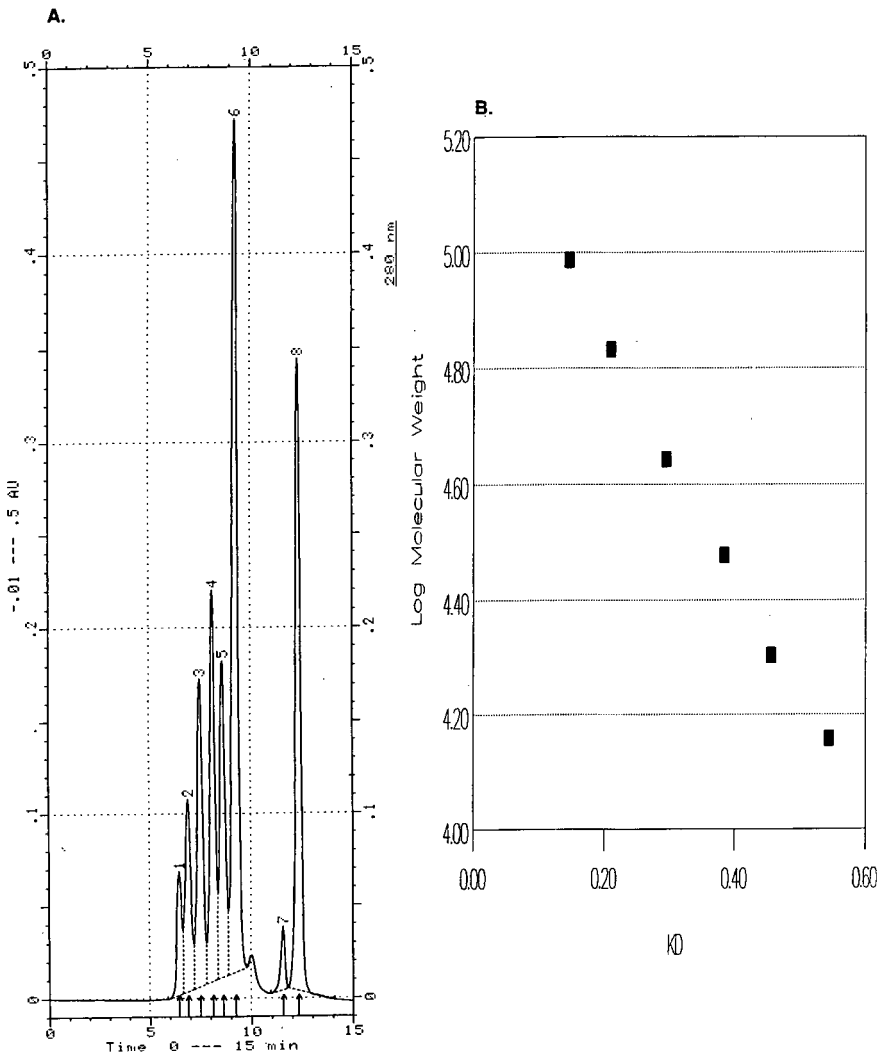

Fig. 5. (A) SEC of proteins on Biosep-SEC-S3000 using 6 *M* guanidine hydrochloride. The same set of proteins as in Fig. 3 was used. The proteins were dissolved in 0.5 ml of 20 m*M* NaH_2PO_4 buffer (pH 6.5) containing 8 *M* guanidine hydrochloride and 1% BME. The solution was boiled for 5 min and 20 μl were injected on to the column, equilibrated with 20 m*M* NaH_2PO_4 buffer (pH 6.5) containing 6 *M* GnHCl at a flow-rate of 1 ml/min. The separation profile was followed by UV detection at 280 nm. Peaks: 1 = phosphorylase *b* (97 000 dalton); 2 = bovine serum albumin (68 000 dalton); 3 = ovalbumin (44 000 dalton); 4 = carbonic anhydrase (30 000 dalton); 5 = trypsin inhibitor (20 100 dalton); 6 = lysozyme (14 400 dalton); 7 = a contaminant; 8 = β-mercaptoethanol. (B) Plot of log MW *vs.* K_D, r^2 = 0.9948.

excess of SDS. The concentration of this denaturant in the mobile phase was ideally kept at its critical micellar concentration, which depended on the buffer concentration. Therefore, the optimum conditions of buffer and SDS for the separation of a mixture of proteins on Biosep-SEC-S3000 was determined. To obtain consistent chromatographic profiles in repeated runs, 20 m*M* NaH_2PO_4 buffer (pH 6.5) containing 0.5% SDS was found to be essential for this support. When a lower concentration of SDS (0.1%) was used, the separation profile varied from run to run. Fig. 4 shows the separation of a mixture of proteins under the optimum, established conditions on a Biosep-SEC-S3000 column. There was a good linear relationship between log (molecular weight) and K_D (r^2 = 0.9908) for this separation, as shown in the inset. The last peak to elute was β-mercaptoethanol (BME) and showed a nearly ideal K_D of 1.09. Proteins are known to have an extended rod-like conformation in SDS, but they become increasingly spherical with decreasing molecular weight. Consequently, the lower limit of the molecular weight of proteins, for the calibration graph using SDS, is about 15 000 dalton [15].

Fig. 5A shows the separation of the same mixture of proteins on a Biosep-SEC-S3000 column using 6 *M* GnHCl in 20 m*M* NaH_2PO_4 buffer (pH 6.5). All proteins were well resolved and a plot of log (molecular weight) *vs.* K_D (Fig. 5B) showed excellent linearity (r^2 = 0.9948). The results conflict with those reported earlier [3], where phosphorylase *b* and serum albumin failed to resolve under similar conditions on a TSK3000SW column. These differences may be related to the pore size of the stationary phases. In this experiment, BME eluted a K_D of 0.98, which is ideal for a small, non-interacting molecule. The two proteins which failed to resolve under native conditions, carbonic anhydrase and trypsin inhibitor (Fig. 3), separated well using 6 *M* GnHCl and 0.5% SDS. These data show the in-

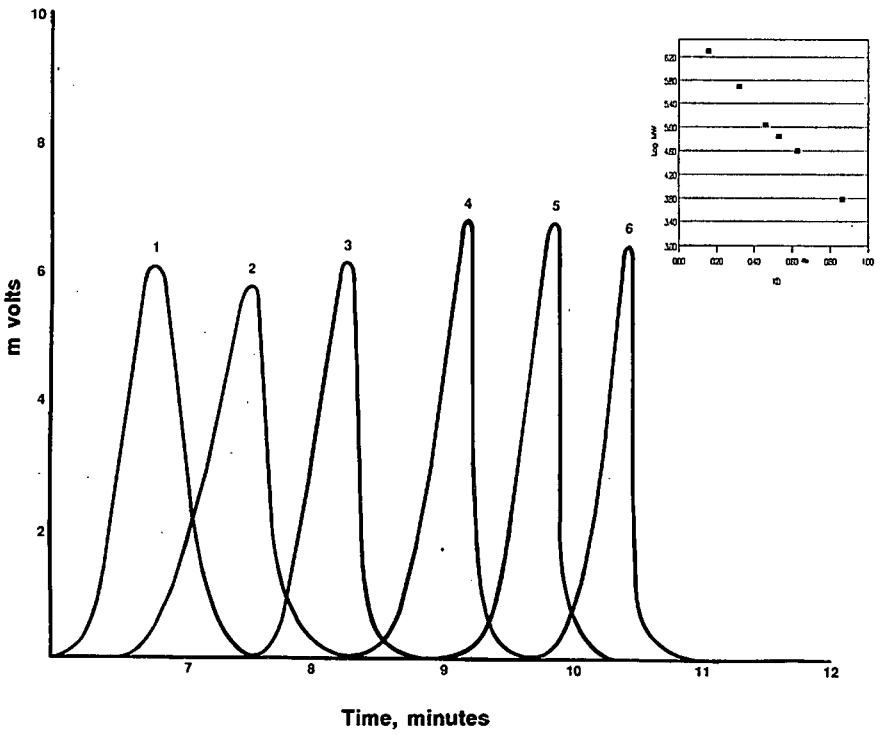

Fig. 6. Separation of dextrans on Biosep-SEC-S4000. Chromatographic runs were performed individually for each dextran. Dextran was dissolved in water at 25 mg/ml and 10 µl were injected on to the column, equilibrated with water at 1 ml/min. Peaks: 1 = blue dextran ($2 \cdot 10^6$ dalton); 2–6 = dextrans of molecular weight 500 000, 110 000, 70 000, 40 000 and 6000 dalton, respectively. The inset is a plot of log MW *vs.* K_D, r^2 = 0.993.

creased resolving power of the stationary phase under denaturing conditions. Following exposure to denaturants, Biosep-SEC-S columns could be easily regenerated by washing them overnight with water at a flow-rate of 0.2 ml/minute. Such regenerated columns could be reused under native conditions for the SEC of proteins without any decrease in resolution.

The resolving power of Biosep-SEC-S4000 with 500 Å pore size was tested with dextrans ranging from 6000 to $2 \cdot 10^6$ dalton. Stationary phases with this pore size are considered to be ideal for the SEC of dextrans [6]. On the other hand, well characterized polymers such as dextrans have been recommended for the calibration of SEC columns [15]. Each dextran sample was run individually on the column after equilibration with water. The separation profile is shown in Fig. 6 and is a composite of individual runs. All the dextrans were resolved with an excellent linear correlation of the log (molecular weight) *vs.* K_D plot ($r^2 = 0.993$). This phase was not able to resolve proteins of molecular weight below 15 000 dalton (data not shown), which permeate into the pores, but is suitable for the separation very high-molecular-weight proteins (15 000–$2 \cdot 10^6$ dalton).

For all the calibration graphs [log (molecular weight) *vs.* K_D plots] obtained here, excellent linearities were observed. It should be pointed out, however, that variation in the properties such as shape and size of macromolecular standards may result in sigmoidal curves for such plots. For a support of given pore size, the plot is suggested to be linear between K_D values of 0.1 and 0.9 [15]. It is therefore important to evaluate critically all the experimental parameters before using such plots for the determination of molecular weights.

CONCLUSIONS

The silica-based supports developed here for the high-performance SEC of proteins and peptides were evaluated for surface activity with synthetic peptides and proteins under different mobile phase conditions. The stationary phases showed excellent SEC properties, such as very low non-specific interaction with proteins and peptides, good resolution and wide molecular weight separation ranges. The supports showed excellent chemical stability toward common buffers and protein denaturants and could be easily regenerated following exposure to these denaturants.

REFERENCES

1 A. J. de Vries, M. Lepage, R. Bean and C. L. Guillemin, *Anal. Chem.*, 38 (1967) 935.
2 K. A. Grauber, J. M. Whittaker and M. Morris, *Anal. Biochem.*, 97 (1979) 176.
3 R. C. Montelaro, M. West and C. Issel, *Anal. Biochem.*, 114 (1981) 398.
4 D. E. Schmidt, R. W. Glese, D. Conron and B. L. Karger, *Anal. Chem.*, 52 (1980) 177.
5 M. Czok and G. Guichon, *J. Chromatogr.*, 506 (1990) 303.
6 H. Engelhardt and D. Mathes, *J. Chromatogr.*, 185 (1979) 305.
7 E. Pfannkoch, K. C. Lu and F. E. Regnier, *J. Chromatogr. Sci.*, 18 (1980) 430.
8 E. Perez-Paya, L. Bruco, C. Abad, V. Soria and A. Campos, *J. Chromatogr.*, 548 (1991) 93.
9 T. E. Eremeva, T. O. Bykova and V. S. Gromov, *J. Chromatogr.*, 522 (1990) 67.
10 T. Mizutani and A. J. Mizutani, *J. Chromatogr.*, 168 (1979) 143.
11 C. T. Mant, J. M. R. Parker and R. S. Hodges, *J. Chromatogr.*, 397 (1987) 99.
12 C. T. Mant and R. S. Hodges, *J. Chromatogr.*, 409 (1987) 155.
13 C. T. Mant and R. S. Hodges, *Chromatographia*, 24 (1987) 805.
14 W. W. Yau, J. J. Kirkland and D. D. Bly, *Modern Size-Exclusion Liquid Chromatography. Practice of Gel Permeation and Gel Filtration Chromatography*, Wiley-Interscience, New York, 1979, p. 43.
15 L. Hagel, in J. C. Janson and L. Ryden (Editors), *Protein Purification, Principles, High Resolution Methods and Applications*, VCH, New York, 1989, pp. 63–106.
16 W. Fish, K. Mann and C. Tanford, *J. Biol. Chem.*, 244 (1969) 4989.
17 T. Takagi, K. Takeda and T. Okuno, *J. Chromatogr.*, 208 (1981) 201.

Journal of Chromatography, 599 (1992) 35–42
Elsevier Science Publishers B.V., Amsterdam

CHROMSYMP. 2517

Separation of synthetic phosphorothioate oligodeoxynucleotides from their oxygenated (phosphodiester) defect species by strong-anion-exchange high-performance liquid chromatography

B. John Bergot*

Therapeutics Group, Applied Biosystems, Inc., Foster City, CA 94404 (USA)

W. Egan ·

Biophysics Laboratory, Center for Biologics Evaluation and Research, Food and Drug Administration, Bethesda, MD 20892 (USA)

ABSTRACT

A method is described which separates synthetic deoxynucleotide phosphorothioates from their oxygenated (phosphodiester, "P=O") defect species by strong-anion-exchange chromatography, using novel "soft-base" anionic eluents. The method enables the qualitative and quantitative assessment of P=O content in phosphorothioate DNA, and represents a rapid and sample-conserving alternative to ^{31}P-NMR.

INTRODUCTION

Synthetic DNA analogues, particularly those which have been modified at the phosphorus internucleotidic linkage, now have become indispensable tools for research in the field of "anti-sense DNA," where blockage of translational gene product (protein) formation can be effected by Watson–Crick binding of a short (15–30 base) strand of DNA to an appropriate complementary sequence within the target mRNA. An analogue showing promise as a potential therapeutic agent is the phosphorothioate [1] congener of DNA, where sulfur replaces the non-bridging oxygen at the pentavalent phosphorus nexus of the polymer (Fig. 1).

The Therapeutics Group at Applied Biosystems has been investigating large-scale synthesis of synthetic DNA, particularly the phosphorothioate analogs. As a potential drug, such material must be rigorously characterized as to its chemical nature, which, in turn, demands stringent analytical criteria for purity (or homogeneity).

High-performance ion-exchange chromatography (IEC) is being increasingly used for relatively rapid qualitative and quantitative profiling of synthetic DNA [2–5]. Agrawal *et al.* [6] have recently reported on a high-performance liquid chromatographic (HPLC) method for characterization of phosphorothioate DNA, though only for octamers. We have extended the use of IEC to the analysis of 20- to 27-mer phosphorothioates, and wish to report a most unusual and unexpected finding. Our synthetic methodology leading to the desired phosphorothioates requires oxidative sulfurization [7,8] at the phosphite linkage during each cycle of synthesis; however, a fractional amount (0.5–1%) of the oxygenated (phosphodiester) species is produced concomitantly. Cumulatively, this imcompleteness of sulfurization leads to the formation of significant populations of oligonucleotide phospho-

0021-9673/92/$05.00

S-d($C_{12}G_5T_{10}$) S-d($A_3C_7G_7T_4$)

1 **2**

S-d($A_1C_8G_2T_9$) S-d($C_{13}G_3T_4$)

3 **4**

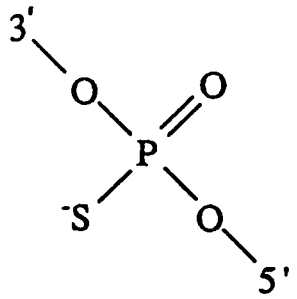

Fig. 1. Empirical formulae for synthetic phosphorothioate DNA used in this study, and detail of phosphorothioate moiety.

rothioates containing phosphoric acid diester ("P=O") linkages. We have developed an ion-exchange method of high-performance chromatographic separation of these various defect species using novel ("soft-base") anionic eluents, and we shall demonstrate the utility of the assay in obtaining accurate profiles of "P=O" contributions to several phosphorothioate synthetic analogues. Relative to ^{31}P-NMR spectroscopy, the conventional method of ascertaining the molecular environment about the phosphate linkage in DNA [9], our IEC method is (a) readily automated, and (b) requires a thousand-fold less sample.

EXPERIMENTAL

Chemicals and reagents

All HPLC buffer salts were reagent grade or better supplied by Aldrich (Milwaukee, WI, USA). Acetonitrile (HPLC grade) was from Burdick and Jackson (Muskegon, MI, USA). All gel electrophoresis reagents came from IBI (New Haven, CT, USA). Stains-all dye was from Eastman Kodak (Rochester, NY, USA).

DNA synthesis and purification

Phosphorothioate DNA was prepared on either an Applied Biosystems Model 380B or 390Z Automated DNA Synthesis instrument using standard protocols [10] as suggested by the manufacturer, except with the substitution of 3H-1,2-benzothiol-3-one 1,1-dioxide [7] (or an equivalent sulfur-donor reagent) for iodine, and reversing the normal oxidation-then-cap sequence within each cycle. The crude DNA is subsequently purified by reversed-phase preparative chromatography as its 5'-O-dimethoxytrityl derivative according to published methods [11]. Following detritylation and sodium chloride–ethanol precipitation, the recovered phosphorothioate DNA is freeze-dried to a powered solid.

NMR

^{31}P-NMR was performed on the following two instruments with their respective operating conditions: (1) JEOL GSX-500; resonance frequency, 202.45 MHz; acquisition time, 0.655 s; pulse delay, 6 s; pulse width, 5 μs (45°) and (2) Varian Unity 3000; resonance frequency, 121.42 MHz; acquisition time, 1.6 s; pulse delay, 0 s; pulse width, 11 μs (90°).

Ion-exchange chromatography

The HPLC instrumentation was as follows: Series 410 BIO LC System, ISS-200 Auto-sampler, Model 1020 Data System (Perkin-Elmer, Norwalk, CT, USA); 759A UV Detector (Applied Biosystems, Foster City, CA, USA). The columns were PL-SAX (Polymer Labs., Church Stretton, UK) strong-anion-exchanger, 10 μm, 100 Å porosity, 15 cm × 7.5 mm I.D., and Nucleogen-DEAE 60-7 (Macherey-Nagel, Düren, Germany), 7 μm, 60 Å porosity, 12.5 cm × 4 mm I.D. Mobile phases: A, 50 m*M* ammonium phosphate pH 8.2–CH_3CN (95:5, v/v); B, 1.5 *M* potassium bromide in 50 m*M* ammonium phosphate pH 6.7–CH_3CN (80:20, v/v); C, CH_3CN; D, 1.0 *M* sodium thiocyanate in 50 m*M* ammonium phosphate pH 8.2. Separation of

the DNA species was achieved by gradient elution, and the various gradient profiles used are summarized in Table I. The UV monitor was set at 260 nm for gradients I and III and 280 nm for gradient II.

Gel electrophoresis

Purified deoxyoligonucleotides (*ca.* 0.05–0.1 optical density units (O.D.)/lane) were analyzed by polyacrylamide gel electrophoresis (PAGE) on 15 × 15 cm gels (20%T, 5%C[a]) using 40 m*M* Tris–borate buffer at pH 8.3. Bands were visualized by staining with Stains-all according to the manufacturer's suggested protocol[b] and quantified by scanning densitometry using a Model 300S Computing Densitometer (Molecular Dynamics, Sunnyvale, CA, USA).

RESULTS AND DISCUSSION

Our orifinal intent was to evaluate various silica- and polymer-based anionic exchange media for their suitability in assessing synthetic phosphorothioate chain-length homogeneity. We assumed only marginal and not unexpected chromatographic differences between the phosphorothioates and their respective phosphodiester congeners; essentially the phosphorothioates as a class are more lipophilic than phosphodiesters [6,12], and somewhat stronger retention of the former was anticipated. However, phosphorothioates **1**–**4** *could not* be eluted from either weak- (WAX) or strong- (SAX) anion-exchange supports using conventional salt gradients, *e.g.* 0–2 *M* sodium chloride, 0–1.5 *M* ammonium sulfate, etc. Neither increasing the mole-fraction of the organic modifier nor varying the type of modifier (acetonitrile, methanol, formamide) had any effect on elution profiles. Conventional denaturants such as 7 *M* urea also were without effect. The corresponding phosphodiester compounds eluted smoothly as expected, however (data not shown).

Changing the eluting anion to either bromide or thiocyanate did in fact promote elution of the phosphorothioates under gradient conditions (Fig. 2). The profiles of compounds **1** and **2** suggested substantial presence of so-called "deletion" or "failure" sequences (a consequence of poor coupling yields and/or incomplete detritylation at the 5′-terminus during each cycle of automated solid-phase synthesis [10]; however, when compound **2** ("high P=O", four components by IEC) was analyzed by PAGE–scanning densitometry, essentially a single band was detected (Fig. 3), inconsistent with a sus-

TABLE I

GRADIENT PROGRAMS USED IN THIS STUDY

Mobile phases are identified in the Experimental section.

Gradient	Time (min)	Flow-rate (ml/min)	Mobile phase (%)			
			A	B	C	D
I	Start	1.5	50	30	20	–
	48	1.5	0	80	20	–
	4	1.5	0	80	20	–
	10	2.0	50	30	20	–
II	Start	1.5	50	–	20	30
	48	1.5	10	–	20	70
	4	1.5	10	–	20	70
	10	2.0	50	–	20	30
III	Start	1.5	80	0	20	–
	70	1.5	0	80	20	–
	10	2.0	80	0	20	–

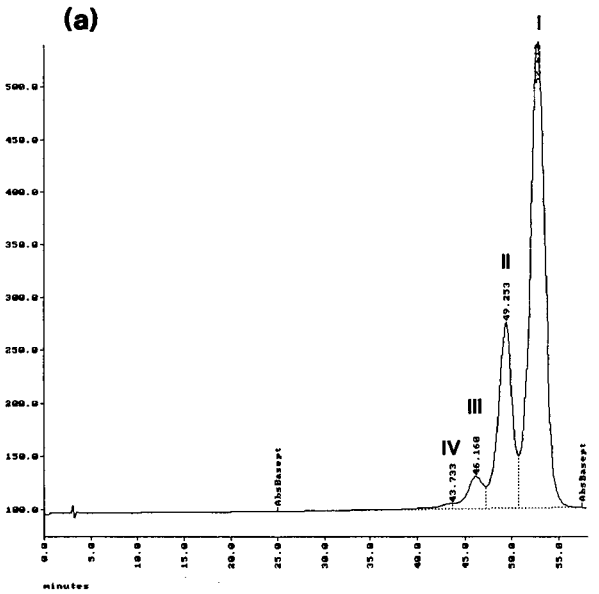

Fig. 2.

(Continued on p. 38)

[a] T = [g acrylamide + g N,N′-methylenebisacrylamide (Bis)]/100 ml solution; C = g Bis/% T.

[b] Kodak Product Publication Number JJ-11.

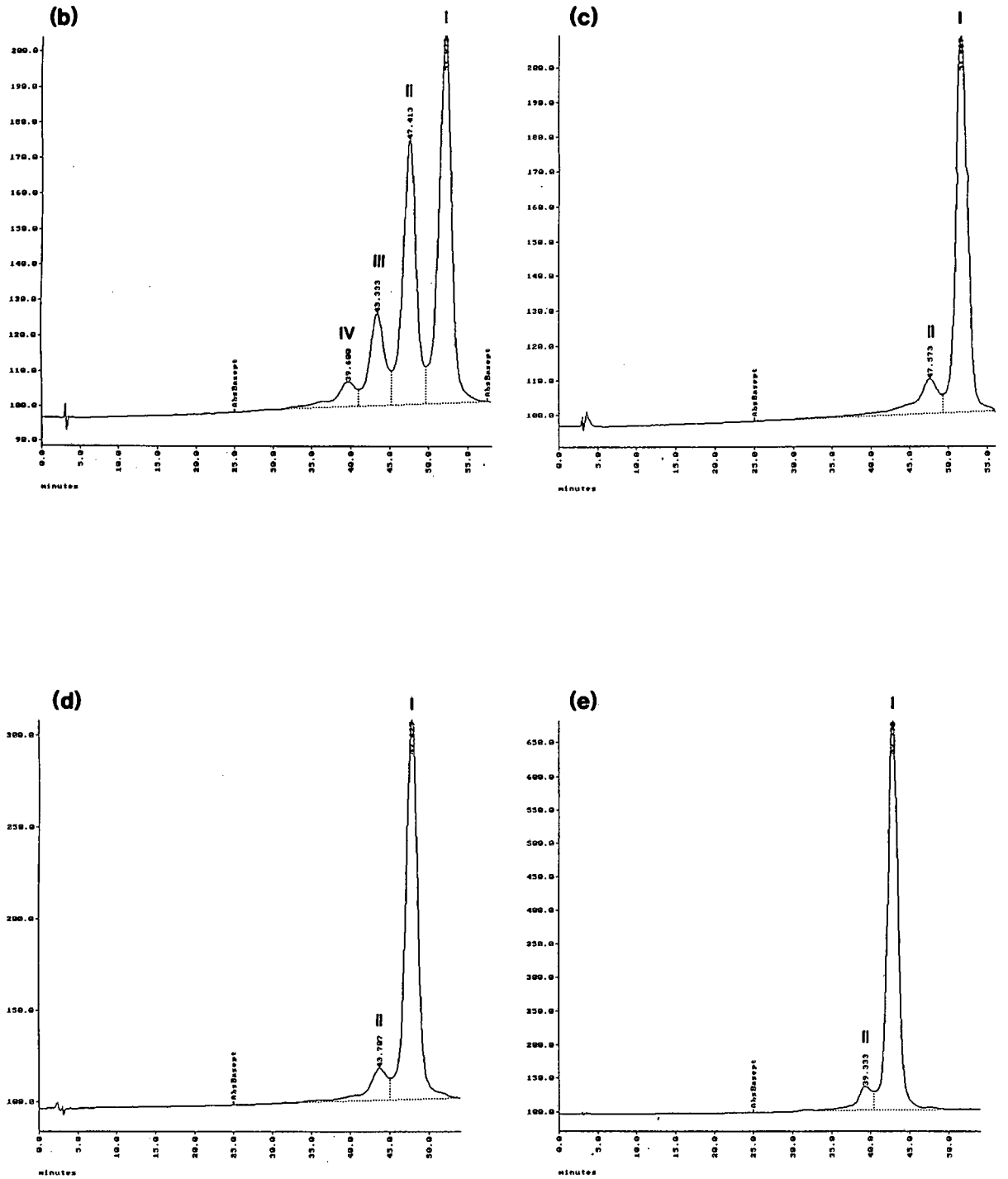

Fig. 2.

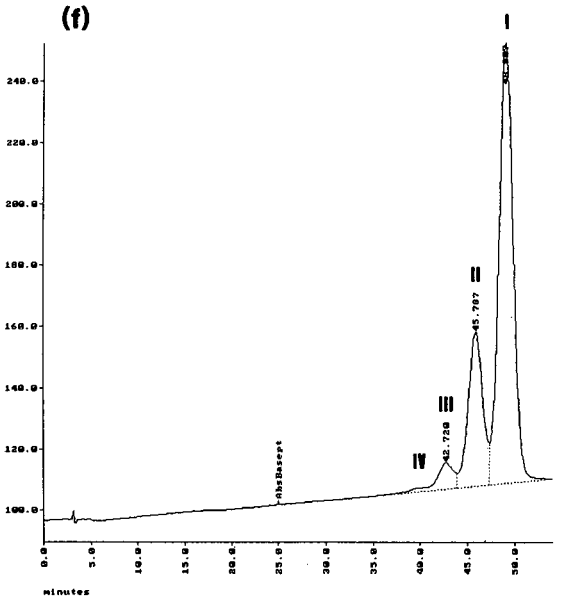

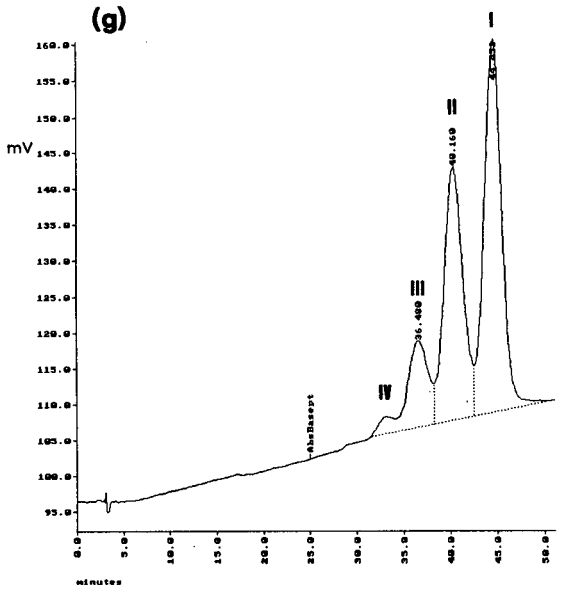

Fig. 2. IEC chromatograms of phosphorothioate DNA: (a) **1**, (b) **2**, "high P=O", (c) **2**, "low P=O," (d) **3**, (e) **4**, conditions per gradient I; (f) **1**, (g) **2**, "high P=O", conditions per gradient III. Roman numerals indicate constitutive peaks of each analogue (see Tables I and II). Column: PL-SAX at 1.5 ml/min flow-rate. Approximately 10–20 μg of DNA was injected on-column per analysis.

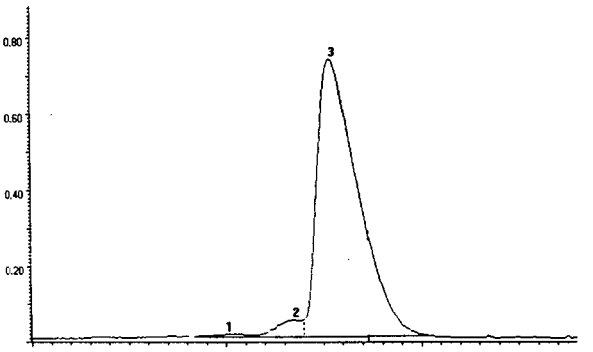

Fig. 3. Computing densitometric scan of compound **2** ("high P=O," see Fig. 2b) following slab-gel electrophoresis and staining. Migration is from right (top) to left (bottom). Band 3 = full-length 21-mer (97%); band 2 = 20-mer ($n-1$) impurity (2.8%); band 1 = 19-mer ($n-2$) impurity (0.2%).

pected high degree of chain-length heterogeneity. IEC was clearly revealing heterogeneity within the molecule, though *not* as a consequence of length variability.

Isolation and ^{31}P-NMR spectroscopy of IEC-resolved components

To examine further the nature of the constitutive elements forming **1** and **2**, approximately 50 mg of each were taken for preparatieve IEC, where 10 mg aliquots were chromatographed on the 15 cm × 7.6 mm I.D. PL-SAX column using Gradient II as described under Experimental. The largest three components (peaks I, II and III) from each compound

TABLE II

DETERMINATION BY ^{31}P-NMR OF % P=O OCCURRING IN CONSTITUTIVE SPECIES OF SELECTED PHOSPHOROTHIOATE DNA ANALOGUES (**1** AND **2**)

Peak	%P=O			
	Found		Theoretical	
	1	**2**	**1**	**2**
I	0.0[a]	0.1[a]	0.0	0.0
II	5.1[a]	3.6[b]	3.8 (1/26)	5.0 (1/20)
III	8.8[a]	7.7[b]	7.7 (2/26)	10.0 (2/20)
IV	N.D.[c]	N.D.	11.5 (3/26)	15.0 (3/20)

[a] 500 MHz, quantified by peak height.
[b] 300 MHz, quantified by resonance integral (area).
[c] N.D. = Not determined.

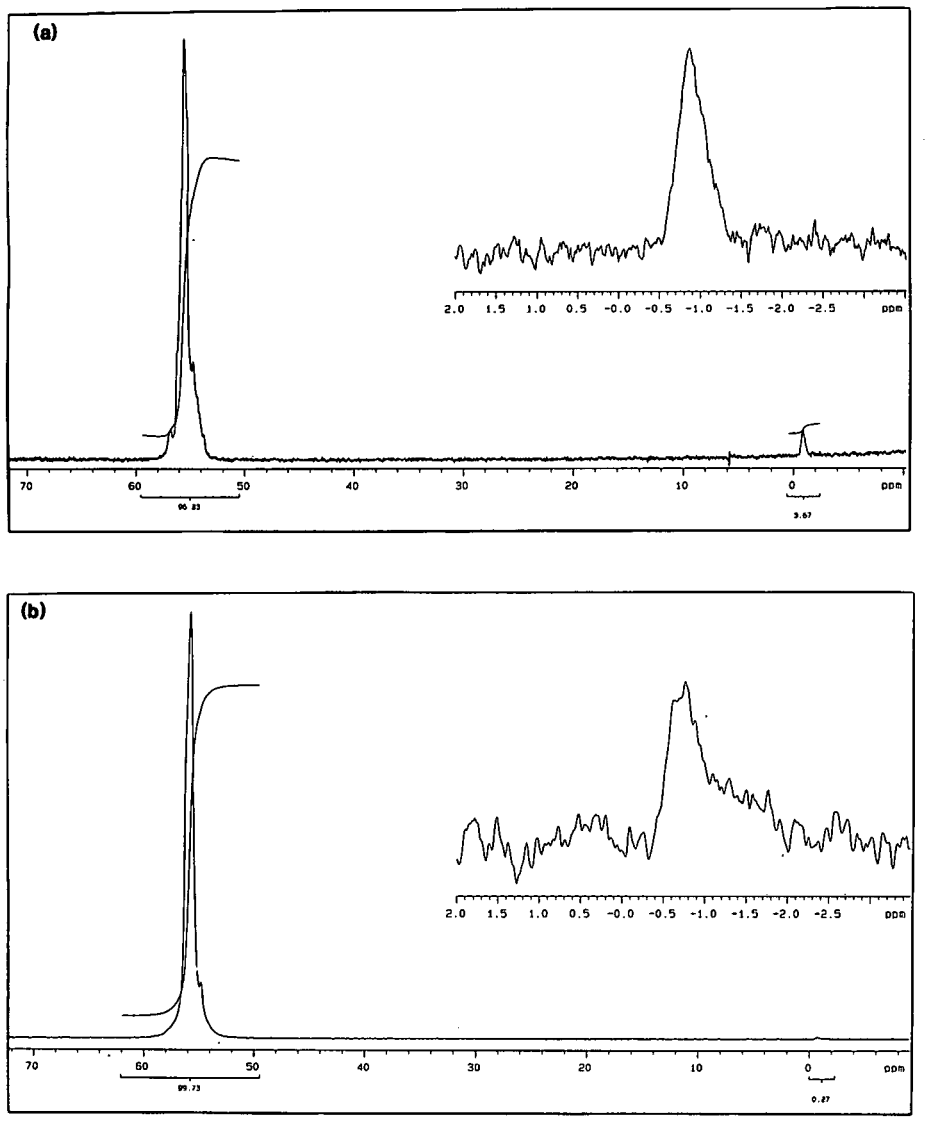

Fig. 4. ^{31}P-NMR spectra of (a) **2**, "high P=O," and (b) **3**. Instrument: Varian Unity 3000, conditions per Experimental. Signal at 54–56 ppm is phosphorothiate P=S, and signal at −1 to −3 ppm is phosphodiester P=O.

were accumulated until 2–12 mg each were recovered. Following desalting and quantification by UV spectrometry the isolated materials (80–95% pure) were lyophilized, then reconstituted in HPLC-grade water or deuterium oxide for ^{31}P-NMR studies. Table II summarizes the results for Peaks I, II and III of **1** and **2**, respectively.

Resonances in the ^{31}P-NMR are well-resolved and conclusive for, (1) $(RO)_2$ P=O(S^-), 50–60 ppm, and (2) $(RO)_2$ P=O(O^-), (−)5–0 ppm [13]. Reference ^{31}P-NMR Spectra for **1** and **2** are shown in Fig. 4. These data clearly show that the IEC profiles are in fact indicating the presence of oxygenated defect species of each parent phosphorothioate, and moreover, the distribution of these defect species can be described mathematically as terms of the binomial expansion series, $(x+y)^n$.

TABLE III

COMPARISONS BETWEEN CALCULATED AND ACTUAL VALUES OF OXYGENATION DISTRIBUTION AT INTERNUCLEOTIDIC PHOSPHATE LINKAGES OF SEVERAL DNA PHOSPHOROTHIOATE ANALOGUES

Calculated values were found by solving the first four terms of the general equation $(x + y)^n$ as developed in the text, where x (P=S) and y (P=O) were obtained from ^{31}P-NMR[a], and actual values were determined by IEC.

Compound	P=S[a]	$(P=S)_n$, Peak I (%)		$(P=S)_{n-1}$, $(P=O)$, Peak II (%)		$(P=S)_{n-2}$, $(P=O)_2$, Peak III (%)		$(P=S)_{n-3}$, $(P=O)_3$, Peak IV (%)	
		Calc.	Found	Calc.	Found	Calc.	Found	Calc.	Found
1	99.3	83.3	83.7	15.3	14.1	1.35	1.9	0.07	0.3
1	98.3	64.03	64.5	28.8	29.0	6.2	5.6	0.9	0.8
1	98.0	59.1	58.1	31.4	29.4	8	9.8	1.3	2.7
2	99.6	92.3	90.0	7.4	7.9	0.3	$\leqslant 2$	$\leqslant 0.1$	<0.5
2	97.3	57.8	52.4	32.1	33.5	8.5	11.3	1.4	2.8
3	99.7	94.4	93.8	5.4	5.9	<0.2	<0.5	<0.1	<0.5
4	99.7	94.4	93.0	5.4	7.0	<0.2	<0.5	<0.1	<0.5

[a] From ^{31}P-NMR, where % P=S = 100 × integral area (P=S)/integral area [(P=S) + (P=O)], and % P=O = 100 × integral area (P=O)/integral area [(P=S) + (P=O)].

Mathematical depiction of peak profiles

Our chemical pathway for phosphorothioate DNA synthesis requires oxidative sulfurization at the tervalent phosphorus (phosphite) intermediate at each cycle of deoxynucleotide monomer addition. Due to adventitious chemical side-reactions, a certain (presumably constant) proportion of phosphite is also converted to the oxo-form [8] per cycle. Letting x and y be the mole-fractions of phosphorothioate and phosphoric acid diester linkages, respectively, then for a 27-mer (26 internucleotidic linkages) $(x+y)^{26} = x^{26} + 26x^{25}y + 325\,x^{24}y^2 + 2600\,x^{23}y^3 + \ldots$ etc. At 98% overall sulfurization ($x = 0.98$) and 2% oxygenation ($y = 0.02$), the numerical values of the first four terms in the binomial expansion are 0.591 + 0.341 + 0.08 + 0.013. The first term represents the relative abundance of the fully thiolated (P(=S) material, the second term represents the relative abundance of the aggregate of all species containing a *single* oxygen, the third term represents all species containing *two* oxygens, the fourth term represents all species containing *three* oxygens, and so forth. Further correlations between ^{31}P-NMR and IEC data are shown in Table III, where very good agreement between expected and actual IEC profiles was obtained. Therefore, by examination of the IEC profile of a synthetic phosphorothioate DNA, one may be able to compute the *net* or *aggregate* P=O contribution to the molecule using the general formula: $\%P=S = (\text{peak height}/100)^{1/n-1} \times 100$, where n = number of deoxynucleotide residues and peak height is that of the last eluted peak in the chromatogram, and $\%P=O = 100 - (\%P=S)$.

General comments

The ability of bromide and thiocyanate to elute smoothly phosphorothioate DNA (16 to 27 bases) from WAX or SAX media, as opposed to the general ineffectiveness of traditional high-salt gradients, may be rationalized by invoking the principle of "hard" *vs.* "soft" bases [14] (or nucleophiles). The sulfur anion is regarded as a "soft" base [15], and, indeed, the net negative charge residing within each phosphorothioate moiety appears to be principally located on sulfur [16]. This suggests that the strong ion-pair formed between the thiolo (−) and quaternary ammonium (+) exchanger can be most efficiently disrupted by a "soft" competitive anionic species, such as thiocyanate or bromide. However, we did note that the latter salts were equally effective (at low molarity) in displacing "natural" phosphodiester congeners of compounds **1–4** (data not shown), implying additional applications for these systems in ion-exchange analysis of synthetic deoxyoligonucleotides.

CONCLUSIONS

We have devised a rapid quantitative and qualitative means for determining the extent of oxygenation (phosphodiester) present in deoxyoligonucleotide phosphorothioate analogues synthesized via contemporary automated solid-phase modalities. The method requires less than 1 O.D. ($< 3\ \mu g$) DNA per analysis, and *ca.* 1 h analysis cycle. ^{31}P-NMR assay, on the other hand, requires typically 20 mg material and a minimum of 2–4 h scanning time for reasonable signal-to-noise peak detection and integration (at the $\leqslant 1\%$ P=O level).

ACKNOWLEDGEMENTS

The authors wish to thank Dr. Steve Menchen, DNA R & D, Applied Biosystems, for his inspired suggestions and helpful discussions, and Ms. Colleen Hansen of the DNA Therapeutics Group for performing the gel electrophoresis analyses.

REFERENCES

1 G. Zon and W. J. Stec, in F. Eckstein (Editor), *Oligonucleotides and Their Analogs: A Practical Approach*, IRL Press, Oxford, 1991, Ch. 4, pp. 87–103.
2 G. Zon and J. A. Thompson, *BioChromatography*, 1 (1986) 22.
3 Y. Kato, T. Kitamura, A. Mitsui, Y. Yamasaki, T. Hashimoto, T. Murotsu, S. Fukushige and K. Matsubara, *J. Chromatogr.*, 447 (1988) 212.
4 H. Sawai, *J. Chromatogr.*, 481 (1989) 201.
5 P. Edwardson, I. Collins, M. Scawen, T. Atkinson, G. Cox, S. Sivakoff and R. Stout, *J. Chromatogr.*, 545 (1991) 79.
6 S. Agrawal, J. Tang and D. Brown, *J. Chromatogr.*, 509 (1990) 396.
7 R. Iyer, L. Phillips, W. Egan, J. Regan and S. Beaucage, *J. Org. Chem.*, 55 (1990) 4693.
8 H. Vu and B. Hirschbein, *Tetrahedron Lett.*, 32 (1991) 3005.
9 F. Eckstein, *Acc. Chem. Res.*, 12 (1979) 204.
10 J. W. Efcavitch, in D. H. Schlesinger (Editor), *Macromolecular Sequencing and Synthesis: Selected Methods and Applications*, Alan R. Liss, New York, 1988, Ch. 17, p. 221.
11 G. Zon, in W. S. Hancock (Editor), *High Performance Liquid Chromatography in Biotechnology*, Wiley, New York, 1990, Ch. 14, pp. 301–397.
12 W. J. Stec and G. Zon, *J. Chromatogr.*, 236 (1988) 263.
13 W. J. Stec, G. Zon, W. Egan and B. Stec, *J. Am. Chem. Soc.*, 106 (1984) 6077.
14 J. March, *Advanced Organic Chemistry*, Wiley-Interscience, New York, 1985, Ch. 8, p. 221
15 R. Pearson, *J. Am. Chem. Soc.*, (1963) 3533.
16 C. Liang and L. Allen, *J. Am. Chem. Soc.*, 109 (1987) 6449.

Journal of Chromatography, 599 (1992) 43–49
Elsevier Science Publishers B.V., Amsterdam

CHROMSYMP. 2538

Influence of different N- and O-linked carbohydrates on the retention times of synthetic peptides in reversed-phase high-performance liquid chromatography

Laszlo Otvos, Jr.*, Laszlo Urge and Jan Thurin

The Wistar Institute of Anatomy and Biology, 3601 Spruce Street, Philadelphia, PA 19104 (USA)

ABSTRACT

Glycopeptides consisting of 6–19 amino acid residues and different mono- and disaccharides attached to single asparagine and serine residues were synthesized on solid-phase and were characterized by reversed-phase high-performance liquid chromatography and circular dichroism. It was shown that the decreased retention times due to glycosylation could be correlated with the increasing length of the sugar moiety. Phosphorylation of the same sequences reduced the retention times 1.6 times more than glycosylation with monosaccharides did. The binding to the column was dependent on the structure of the disaccharide when derivatized and glycosylated asparagine, the building block of N-glycopeptide syntheses was studied. However, this structural dependence of the elution times disappeared in the final glycopeptides. Although both glycosylation and phosphorylation resulted in altered secondary structure of the peptide backbone, it appears that the retention times reflect the increased hydrophilicity more strongly than induced conformational orientation on the surface of the bonded phase.

INTRODUCTION

Recently the chemical synthesis of post-translationally modified peptides has become the center of interest of the biotechnology sector. Although non-modified protein fragments are readily available through procedures of gene technology, the biological function of the proteins can only be fully understood if the characteristic peptide fragments are properly glycosylated and phosphorylated. Most viral proteins are N-glycosylated, for example gp 120 of HIV-1 is extremely heavily glycosylated [1], and the full pathogenic potential of HIV-1 *in vitro* is manifested only if its viral envelope proteins are N-glycosylated [2]. Serine- and threonine-bound carbohydrate systems are found in mucins and in related proteins, and are considered to be tumor-associated antigens [3].

We and others have developed several novel solid-phase synthetic strategies for glycopeptides and phosphopeptides [4–9]. The purification of these post-translationally modified peptides, similarly to the parent, non-modified analogues, is accomplished almost exclusively by reversed-phase high-performance liquid chromatography (RP-HPLC). We regularly use RP-HPLC to quantify the coupling efficiencies, the crucial step for solid-phase glycopeptide synthesis [10]. RP-HPLC separation of glycosylated and non-glycosylated forms of isolated N- and O-glycopeptides has been reported [11–13], and the influence of N-glycosylation on the retention times of peptides has been estimated based on isolated rat neurointermediary lobe peptides [14], but systematic studies on the contribution of different sugars to the RP-HPLC retention times of synthetic peptides have not been reported yet. Furthermore, in this paper we compare the influence of glycosylation and phosphorylation of the same serine residue, and serine-phosphorylation and asparagine-glycosylation of the same peptide backbone to refine the predictive algorithms. The observed differences in retention times are examined in context with the detected conformational changes upon glycosylation to gain insights into a

0021-9673/92/$05.00

possible conformational orientation on the surface of the bonded phase. Finally, we show why caution should be exercised when conclusions from retention time differences, based on RP-HPLC of derivatized sugars [15], are drawn on the contribution of the same sugars when incorporated into final peptides.

EXPERIMENTAL

Peptide synthesis

N^{α}-9-Fluorenylmethoxycarbonyl-asparagine N^{β}-glycosides [Fmoc-Asn(sugar)derivatives] were prepared as described earlier [16]. Asparagine-linked glycopeptides were synthesized on solid phase using a BioSearch SAM2 automated synthesizer. Carbohydrates were incorporated by the building block strategy with different Fmoc-Asn(sugar)-O-pentafluorophenyl derivatives [5]. Unprotected serine residues were introduced for O-glycopeptide synthesis and glycosylated with peracetylated glucose oxazoline after the peptide chain assembly was completed [6]. For phosphopeptide synthesis, the same resin was phosphorylated with dibenzyl phosphochloridate [8]. Peptides were cleaved off the resin with trifluoroacetic acid–anisole/thioanisole (95:5, v/v). The O-glycopeptides were finally deacetylated with 0.1 *M* NaOH. Phosphorylation of VF13 and the varicella peptide (for the sequences see Table II) was made with polyphosphoric acid after the peptides were cleaved from the solid support. Glycopeptides and phosphopeptides were analyzed by fast-atom bombardment mass spectrometry, two-dimensional NMR and phosphate analysis. Amino acid analyses were performed in The Wistar Institute Protein Microchemistry Facility.

Chromatography

Chromatographic system A consisted of two Beckman 110A pumps, regulated by a 421A controller, an Altex Ultrasphere ODS 250 × 10 mm I.D. column, a Beckman 160 fixed-wavelength detector operating at 214 nm, 0.1 a.u.f.s., and a Shimadzu C-R6A integrator. Solvent A was 0.1% aqueous trifluoroacetic acid; solvent B was 0.1% trifluoroacetic acid in acetonitrile. The samples were loaded in 5% solvent B. The flow-rate was 3 ml/min. A linear gradient of 1.33%/min of solvent B was used for screening the N-glycopeptides (gradient a), and 0.67%/min for O-glycopeptide and detailed N-glycopeptide analysis (gradient b). Gradient b with Beckman 114 M pumps was used to analyze the Fmoc-Asn(sugar) derivatives (chromatographic system B). The loads were 10–100 μg.

Circular dichroism (CD)

CD spectra were taken on a Jasco J720 spectrograph. Spectograde trifuoroethanol and water were used as solvents. All measurements were made in 0.02 cm cells. The peptide concentrations were 0.4 mg/ml throughout.

RESULTS

Separation of Fmoc-Asn(sugar)-O-tert.-butyl derivatives

Glycosylated N-fluorenylmethoxycarbonyl-asparagine *tert.*-butyl esters are the starting materials for solid-phase N-glycopeptide synthesis. Since the reaction route to these derivatives proceeds through unpurified intermediate products, their final purification is necessary before cleavage and activation occurs. Although the major factors in binding of these derivatives to RP-HPLC columns are the hydrophobic fluorenylmethyl and *tert.*-butyl groups, structural information of the exposed regions of the sugars can still be obtained through their binding. Table I lists the retention times of a series of Fmoc-Asn(sugar)-O-*tert.*-butyl derivatives. Disaccharide derivatives bind to the column less than monosaccharide derivatives do, as expected. Asparagine with sugars containing 2-acetamido groups bind to the column stronger than sugars without acetamido groups, because of the methyl group. Nevertheless, the acetamido group is still hydrophilic, as the strongly increased retention time of the 2-deoxy de-

[a] Abbreviations for the amino acid residues are: A (Ala) = L-alanine; R (Arg) = L-arginine; N (Asn) = L-asparagine; D (Asp) = L-aspartic acid; C (Cys) = L-cysteine; Q (Gln) = L-glutamine; E (Glu) = L-glutamic acid; G (Gly) = L-glycine; I (Ile) = L-isoleucine; L (Leu) = L-leucine; K (Lys) = L-lysine; M (Met) = L-methionine; F (Phe) = L-phenylalanine; P (Pro) = L-proline; S (Ser) = L-serine; T (Thr) = L-threonine; Y (Tyr) = L-tyrosine; V (Val) = L-valine. Abbreviations for the monosaccharides are: Gal = D-galactopyranose; Glc = D-glucopyranose; GalNAc = 2-acetamido-2-deoxy-D-galactopyranose; GlcNAc = 2-acetamido-2-deoxy-D-glucopyranose; Man = D-mannopyranose.

TABLE I

REVERSED-PHASE SEPARATION OF Fmoc-Asn (SUGAR)-O-*tert.*-BUTYL DERIVATIVES

Carbohydrate	Retention time (min)
Galβ(1→3)GlcNAc	62.59
Glcβ(1→4)Glc (cellobiose)	62.59
Glcα(1→4)Glc (maltose)	62.59
GlcNAcβ(1→4)GlcNAc (chitobiose)	63.14
Glc	65.08
Gal	65.08
GlcNAc	65.72
GalNAc	65.72
Man	65.72
2-Deoxy-Glc	67.83

rivative suggests. While the configuration of the substitutents at C-4 does not affect the observed retention times, the substitutents at C-2 do. The most interesting feature of Table I is the separation of disaccharides conjugated to the asparagine residue. While Galβ(1→3)GlcNAc, Glcβ(1→4)Glc (cellobiose) and Glcβ(1→4)Glc (maltose) derivatives cannot be separated, the GlcNAcα(1→4)GlcNAc (chitobiose) derivative exhibits increased retention time, suggesting that the "outer" sugar plays a role only in binding to the surface of the column. Since monosaccharides still bind, it appears that (regardless of the sterochemistry of the glycosidic bond) the outer sugar prevents contact of the inner sugar with the bonded phase, most probably through folding. The maltose, Galβ(1→3)GlcNAc and chitobiose derivatives were injected together in Fig. 1. Peak a represents the two disaccharide derivatives with Glc or Gal as the outer sugar, peak b represents the disaccharide derivative with GlcNAc as the outer sugar. It should be noted that the Fmoc-Asn(Man) and Fmoc-Asn(Glc) derivatives (differing in the position of the hydroxyl group at C-2) could not be separated once the C-terminal *tert.*-butyl group was removed.

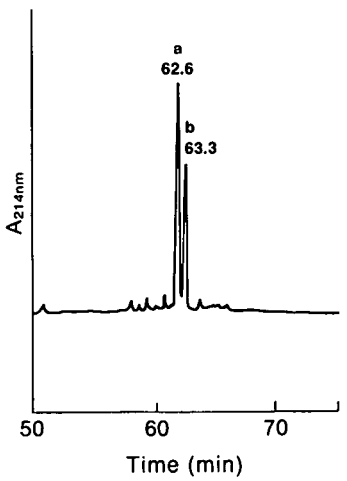

Fig. 1. Co-injection of Fmoc-Asn(maltose)-O-*tert.*-butyl, Fmoc-Asn[Galβ(1→3)GlcNAc]-O-*tert.*-butyl and Fmoc-Asn(chitobiose)-O-*tert.*-butyl. Chromatographic conditions as described under Experimental. Peaks: a = the disaccharide derivatives with glucose or galactose, as the outer sugar moiety; b = the chitobiose derivative with the outer sugar containing 2-acetamido group (GlcNAc). The inner sugar does not seem to play a role in the binding to the column.

The influence of N-glycosylation on the retention times of synthetic peptides

One set of our model peptides is excised from glycoprotein sequences of rabies, heptatis B, and varicella viruses, and contains the natural Asn-Xxx-Ser/Thr consensus glycosylation pattern (Table II). The presence or absence of carbohydrate on the asparagine residues was suggested to be involved in antigenic activity [17,18]. We employed mainly GlcNAc as the sugar moiety, since this carbohydrate is attached to the asparagine in all natural N-glycosylated systems, and the conformational transition due to glycosylation was detected immediately after incorporation of the first moiety [19]. Unnatural glycosylated analogues of the principal neutralizing determinant (PND) of HIV gp 120 were made to break tolerance in the hypervariable region of the V3 loop through slight changes in the conformation caused by the incorporation of the various sugar moieties [20]. As Table II shows, incorporation of monosaccharides reduced the retention times of the parent, non-modified peptides. Phosphorylation of VF13 reduced the retention 1.6 times more than glycosylation with GlcNAc did. The extent of the reduction is heavily sequence dependent and apparently less effective and selective at the termini than in mid-chain positions. As the data of peptides GM12 show, incoporation of disaccharides repeatedly reduced the retention times further than incorporation of monosaccharides did.

TABLE II

THE DECREASE OF THE RETENTION TIME OF SYNTHETIC PEPTIDES ON RP-HPLC DUE TO N-GLYCOSYLATION AND COMPARISON WITH O-PHOSPHORYLATION OF THE SAME SEQUENCES

Conformation of parent and modified peptides as determined by circular dichroism. Chromatographic system A, gradient a was used in all these experiments. Glycosylated asparagine residues are marked with an asterisk; phosphorylated serines are italicized.

Peptide	Sequence	Side-chain modification	Decrease of retention time compared to unmodified analogue (min)	Proposed conformation
GM12[a]N	GKAYTIFN•KTLM	–	–	α-Helical
GM12G		GlcNAc	1.0	Type Iβ-turn
GM12C		Chitobiose	1.4	Stronger type Iβ-turn
GM12B		Cellobiose	1.4	Type I β-turn
VF13[a]N	VVEDEGCTN•L*S*GF	–	–	α-Helical
VF12G		GlcNAc on Asn	0.8	Type I β-turn
VF13P		Phosphate on Ser	1.3	Distorted
Hep71[b]N	TKPSDGN•CTCIPIPS	–	–	Type II β-turn
Hep71G		GlcNAc	0.5	Stronger turn
VgpIV[c]N	VFIGQELPTGTN•Y*S*	–	–	Type II β-turn
VgpIVG		GlcNAc on Asn	0.2	No change
VgpIVP		Phosphate on Ser	0.2	No change
PND[d]N	N•GPGRAFY	–	–	Type II β-turn
PNDGlc		Glc	0.7	Stronger turn
PNDGlcNAc		GlcNAc	0.7	Stronger turn
PNDGal		Gal	0.7	Stronger turn
PNDGalNAc		GalNAc	0.7	Stronger turn
PNDC		Chitobiose	0.8	Stronger turn
PNDB		Cellobiose	0.8	Stronger turn

[a] Corresponding to rabies virus G (glyco-)protein.
[b] Corresponding to hepatitis B virus surface antigen protein.
[c] Excised from varicella virus gp IV (glyco-)protein.
[d] GPGRAFY corresponds to the principal neutralizing determinant of the V3 loop of gp 120 of human immunodeficiency virus (HIV) 1.

In contrast to the glycosylated asparagine residues, however, the selectivity based on the identity of the outer sugar disappeared. Fig. 2 represents a co-injection of equal amounts of GM12C and GM12B where only a single peak could be detected, verifying the identical retention times for these two disaccharide-containing glycopeptides. Co-injection of PND glycopeptides that contained only monosaccharides (GlcNAc and Glc) resulted in a single peak, but co-injection of a PND with both monosaccharide and disaccharide (GlcNAc and chitobiose) resulted in two closely eluting peaks (data not shown).

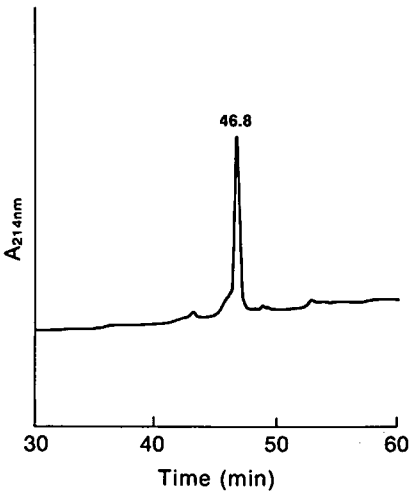

Fig. 2. Co-injection of rabies peptide GM12 glycosylated on its asparagine residue with two disaccharides, chitobiose and cellobiose. Chromatographic system A with gradient b was used. The conditions are found in Experimental. No separation of the two glycopeptides is observed.

Reversed-phase characterization of O-glycopeptide sequences

Abnormal phosphorylation of peptide tau7 (corresponds to amino acid residues 189–207 of human τ protein) may play a role in the deposition process of Alzheimer's disease [21]. To test this possibility

TABLE III

COMPARATIVE CHROMATOGRAPHIC AND CONFORMATIONAL DATA ON O-GLYCOSYLATED AND PHOSPHORYLATED PEPTIDES

Chromatographic system A gradient b was used in all these experiments. Glycosylated and phosphorylated serine residues are marked with an asterisk. Ac = Acetyl.

Peptide	Sequence	Side-chain modification	Decrease of retention time compared to unmodified analogue (min)	Proposed conformation
Tau7[a]	PKSGDRSGYSSPGS*PGTPG	–	–	Type II β-turns
Tau7P		Phosphate	1.44	Mostly random
Actau7	Ac-PKSGDRSGYSSPGS*PGTPG	–	–[b]	
Actau7G		GlcNAc	0.97	Mixture of β-turns
Hexa[c]	Ac-GS*PVEK	–	–	Mostly random
HexaP		Phosphate	4.48	Distorted
HexaG		GlcNAc	2.71	Turn-like

[a] Peptide sequence is excised from human τ protein.
[b] Acetylation was necessary for the successful synthesis of O-glycopeptides but not for phosphopeptides. Phosphorylated and acetylated peptide has not been prepared. In fact, acetylation increased the retention time of the non-acetylated, unmodified peptide by 1.9 min; the retention time of the acetylated and side-chain unmodified peptide served as the starting point for the HPLC study of the glycosylated and acetylated peptide.
[c] Synthetic and chromatographic test sequence.

and to test the specificity of the post-translational modification on antibody recognition, we synthesized tau7, as well as tau7 containing either a phosphate or GlcNAc, on serine 14 (for the sequence see Table III). We also prepared a test hexapeptide which was either O-glycosylated or phosphorylated to further verify the synthetic and chromatographic results [6]. Because of the hydrophilic nature of the peptide sequences, a slower gradient was used in Table III than in the study of N-glycopeptides. Nevertheless, O-glycosylation and N-glycosylation reduced the retention times similarly. It is striking that the ratio of the decrease of the retention times due to phosphorylation compared to glycosylation is consistently 1.6 for both peptide series. Fig. 3 represents a coinjection of the unmodified test hexapeptide and its glycosylated and phosphorylated analogues. All these components are well separated, as expected from the retention time changes determined in Table III.

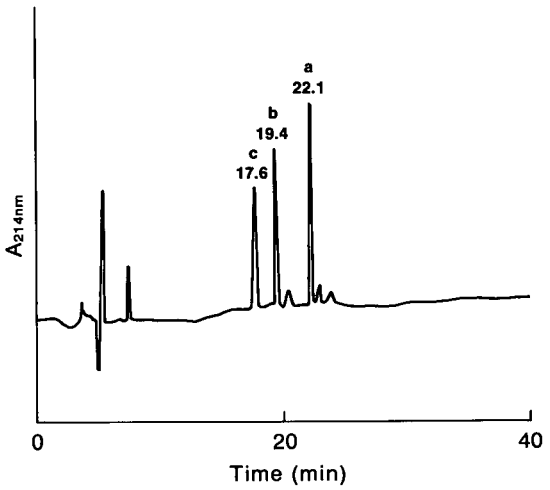

Fig. 3. Co-injection of the unmodified test hexapeptide (peak a), and its glycosylated (GlcNAc, peak b) and phosphorylated (peak c) analogues. Chromatographic conditions as described under Experimental. Phosphorylation reduced the retention time further than glycosylation of the same serine residue did.

DISCUSSION

Prediction of retention times of peptides on RP-HPLC is of great value in the process of isolating and identifying protein fragments [14,22]. Although the use of synthetic peptides offers a much wider database, especially when positional environmental domains alter the retention coefficients [23], the influence of post-translational modifications was

thought to be based on only a few isolated N-glycopeptides and O-phosphopeptides [14]. The quantitative effect of O-glycosylation had not been examined earlier.

In the present study we undertook a detailed analysis of the RP-HPLC retention times of glycopeptides as a function of the identity, number, and location of the sugar moieties. We found that the major determinant in the elution time of N-glycopeptides (corresponding to mainly natural glycosylation sites) on RP-HPLC is the number of sugar moieties incorporated, which is in agreement with earlier reports. Increasing levels of artificial glycosylation of lysine residues reduces the retention times on RP-HPLC and the number of sugars is the main determinant in the elution time [24]. On asparagine, however, the reduction of retention time is not a linear function of the number of carbohydrate moieties. Incorporation of the first sugar reduced the retention time much more than a subsequently added sugar moiety. Glycosylation of the asparagine residue of a pentapeptide IMMNG (our test sequence for studying the coupling efficiency [10]) with a trisaccharide (chitotriose) almost did not decrease the elution time further than glycosylation with a disaccharide (chitobiose) did (data not shown).

Separation of sugars alone on RP-HPLC has been accomplished [25], and the contribution of derivatized carbohydrates on the retention time in RP-HPLC has been estimated [15]. However, as our findings with the separation of sugar-conjugated asparagine derivatives and final glycopeptides suggest, conclusions drawn merely on data concerning the carbohydrate moieties should be handled with caution. Asparagine coupled to disaccharides differing in the outer sugar could be separated, but this difference in the retention times disappeared when the same glycosylated asparagine residues were incorporated into a T cell epitopic peptide of rabies virus. This fact suggests that the general hydrophobicity of unfolded peptides [26] is not the only determining factor of the elution pattern of glycopeptides. Divergencies occurred in the prediction of peptide retention times due to conformation dependent changes in hydrophobic contact area occupancy at the stationary phase surface [27,28]. Peptides with a tendency to assume both β-pleated sheets [29] and α-helices [30] were reported to change their conformation during reversed-phase separation. Later, these conformational change were investigasted by CD studies in polar non-polar solvent systems. In an earlier report, we discussed the possibility that the delay in the elution of a synthetic phosphopeptide isomer was due to a distinctive β-turn formation [31]. A type III β-turn, generally having a class C CD, can be regarded as a single turn of a 3_{10}-helix [32], and a series of these turns can be considered periodic structures. Conformational changes are invaluable tools for RP-HPLC screening of potential T cell epitopes [30]. Our T cell epitopes, GM12 and VF13, exhibit unordered CD spectra in water, but in trifuoroethanol assume typical α-helical structure. Glycosylation results in a two-step conformational change. Incorporation of monosaccharides as a first step breaks the α-helix [19], and the decreased retention times of the glycopeptides is in agreement with this process. The incorporation of the second sugar into GM12 (besides increasing the overall hydrophilicity), however, as a second step stabilizes the newly formed β-turn only slightly [19], and the retention time should increase instead of decreasing further, as has been recorded. Apparently, the increase of the hydrophilicity and the increase of the ordered (turn) structure affect the retention times in opposite directions, and the final result favors the hydrophilicity. This idea is further supported by the data on the hepatitis and PND sequences, where although stronger β-turns were formed after glycosylation, the retention times of the glycopeptides are still decreased.

Glycosylation of serine residues decreases the retention times less than phosphorylation of the same residues does, and this can be explained by both mechanisms. Phosphorylation generally results in a distorted structure [19,33], which can be regarded as a long-range intramolecular turn [33], but not as a periodic structure [19]. On the other hand, the phosphate group is very hydrophilic; it is in anionic form even at pH 2, where the chromatographic runs are made [33]. The definite reduction of retention times due to phosphorylation compared to both types of glycosylation, however, contradicts an earlier algorithm [14] that predicts a much greater effect of glycosylation. Based on our results, it appears that such an algorithm needs major revision or refinement.

ACKNOWLEDGEMENTS

The authors thank Dr. David W. Speicher and Shirley Peterson (editor) for their critical reading of the manuscript. This work was supported by National Institutes of Health grant GM 45011 (to L.O.).

REFERENCES

1 R. A. Gruters, J. J. Neefjes, M. Tersmette, R. E. De Goede, A. Tulp, H. G. Huisman, F. Miedema and H. L. Ploegh, *Nature (London)*, 330 (1987) 74.
2 D. C. Montefiori, W. E. Robinson and W. M. Mitchell, *Proc. Natl. Acad. Sci. U.S.A.*, 85 (1988) 9248.
3 G. F. Springer, P. R. Desai, M. S. Murthy and E. F. Scanlon, *J. Surg. Oncol.*, 11 (1979) 95.
4 V. M.-Y. Lee, B. J. Balin, L. Otvos, Jr. and J. Q. Trojanowski, *Science (Washington, D.C.)*, 251 (1991) 675.
5 L. Otvos, Jr., L. Urge, M. Hollosi, K. Wroblewski, G. Grazyk, G. D. Fasman and J. Thurin, *Tetrahedron Lett.*, 31 (1990) 5889.
6 M. Hollosi, E. Kollat, I. Laczko, K. F. Medzihradszky, J. Thurin and L. Otvos, Jr., *Tetrahedron Lett.*, 32 (1991) 1531.
7 H. Kunz and B. Dombo, *Angew. Chem., Int. Ed. Engl.*, 27 (1988) 711.
8 L. Otvos, Jr., I. Elekes and V. M.-Y. Lee, *Int. J. Pept. Protein Res.*, 34 (1989) 129.
9 H. B. A. DeBont, J. H. VanBoom and R. M. Liskamp, *Tetrahedron Lett.*, 31 (1990) 2497.
10 L. Otvos, Jr., K. Wroblewski, E. Kollat, A. Perczel, M. Hollosi, G. D. Fasman, H. C. J. Ertl and J. Thurin, *Pept. Res.*, 2 (1989) 362.
11 K. H. Strube, F. Lottspeich and R. Geyer, *Eur. J. Biochem.*, 184 (1989) 119.
12 H. Sasaki, N. Ochi, A. Dell and M. Fukuda, *Biochemistry*, 27 (1988) 8618.
13 H. P. J. Bennett, N. G. Seidah, S. Benjannet, S. Solomon and M. Chretien, *Int. J. Pept. Protein Res.*, 27 (1986) 306.
14 C. A. Browne, H. P. J. Bennett and S. Solomon, *Anal. Biochem.*, 124 (1982) 201.
15 Y. C. Lee, B. I. Lee, N. Tomiya and N. Takahashi, *Anal. Biochem.*, 188 (1990) 259.
16 L. Urge, E. Kollat, M. Hollosi, I. Laczko, K. Wroblewski, J. Thurin and L. Otvos, Jr., *Tetrahedron Lett.*, 32 (1991) 3445.
17 R. I. Macfarlan, B. Dietzschold, T. Wiktor, M. Kiel, R. A. Houghten, R. A. Lerner, J. R. Sutcliffe and H. Koprowski, *J. Immunol.*, 133 (1984) 2748.
18 A. Vafai, Z. Wroblewska, R. Mahalingam, G. Cabirac, M. Wellish, M. Cisco and D. Gilden, *J. Virol.*, 62 (1988) 2544.
19 L. Otvos, Jr., J. Thurin, E. Kollat, L. Urge, H. H. Mantsch and M. Hollosi, *Int. J. Pept. Protein Res.*, 38 (1991) 476.
20 I. Laczko, M. Hollosi, L. Urge, K. E. Ugen, D. W. Weiner, H. H. Mantsch, J. Thurin and L. Otvos, Jr., *Biochemistry*, submitted for publication.
21 I. Grundke-Iqbal, Y. C. Tung, M. Quinlan, H. M. Wisniewski and L. I. Binder, *Proc. Natl. Acad. Sci. U.S.A.*, 83 (1986) 4913.
22 J. L. Meek, *Proc. Natl. Acad. Sci. U.S.A.*, 77 (1980) 1632.
23 R. A. Houghten and S. T. DeGraw, *J. Chromatogr.*, 386 (1987) 223.
24 H. Morehead, P. McKay and R. Wetzel, *Anal. Biochem.*, 126 (1982) 29.
25 C. Capon, P. Cache, Y. Leroy, G. Strecker, J. Montreuil and B. Fournet, *J. Chromatogr.*, 425 (1988) 35.
26 C. T. Mant, N. E. Zhou and R. S. Hodges, *J. Chromatogr.*, 476 (1989) 363.
27 M. T. W. Hearn, M. I. Aguilar, C. T. Mant and R. S. Hodges, *J. Chromatogr.*, 438 (1988) 197.
28 G. E. Katzenstein, S. A. Vrona, R. J. Wechsler, B. L. Steadmann, R. V. Lewis and C. R. Middaugh, *Proc. Natl. Acad. Sci. U.S.A.*, 83 (1986) 4268.
29 M. T. W. Hearn and M. I. Aguilar, *J. Chromatogr.*, 392 (1978) 33.
30 K. Buttner, O. Arad, J. Ostresh and R. A. Houghten, in R. Epton (Editor), *Innovation and Perspectives in Solid-Phase Synthesis*, SPCC, Birmingham, 1990, p. 325.
31 L. Otvos, Jr., I. A. Tangoren, K. Wroblewski, M. Hollosi and V. M.-Y. Lee, *J. Chromatogr.*, 512 (1990) 265.
32 F. A. Smith and L. G. Pease, *CRC Crit. Rev. Biochem.*, 8 (1980) 315.
33 L. Otvos, Jr., M. Hollosi, A. Perczel, B. Dietzschold and G. D. Fasman, *J. Protein Chem.*, 7 (1988) 365.

Journal of Chromatography, 599 (1992) 51–63
Elsevier Science Publishers B.V., Amsterdam

CHROMSYMP. 2512

Chromatographic analysis of tropomyosins from rabbit skeletal, chicken gizzard and earthworm muscle

Dan L. Crimmins* and Richard S. Thoma

Howard Hughes Medical Institute, Core Protein/Peptide Facility, Washington University School of Medicine, 660 S. Euclid Ave., Box 8045, St. Louis, MO 63110 (USA)

ABSTRACT

Tropomyosins from rabbit skeletal, chicken gizzard and earthworm muscle all exist as dimeric, *ca.* 100% α-helical coiled-coil species in benign media. Two major tropomyosin isoforms from each muscle source have been identified and can be conveniently designated α (fast) and β (slow) based on electrophoretic mobility under denaturing conditions. The ratio of α to β chains is *ca.* 3–4:1 for rabbit skeletal and *ca.* 1:1 for chicken gizzard and earthworm tropomyosins. Each chain from the former two muscle sources has been sequenced, thus providing a molecular basis for interpreting the *in vivo* population of homo- and hetero-dimers. The characteristics of each purified tropomyosin in weak-anion exchange, strong-cation exchange and reversed-phase high-performance liquid chromatography are described. Binding to and/or elution from the reversed-phase matrix results in dissociation into highly helical monomeric chains. This mode of chromatography separates the α and β chains of earthworm and chicken gizzard tropomyosins, but not those of the rabbit protein. Both anion- and cation-exchange chromatography use mild (benign) elution conditions under which the native, *in vivo* dimer population should be preserved. Only the rabbit protein exhibited peak separation on the anion-exchange resin, with peak assignment corresponding to the known molecular organization of homo- and hetero-dimers. In strong cation-exchange analysis, all three tropomyosins exhibit a chromatographic transition near pH 6.5, possibly the result of histidine(s) titration. Collectively, the chromatographic data confirm the present understanding of the *in vivo* mixture of dimers for tropomyosin from rabbit skeletal and chicken gizzard. It is concluded that native earthworm tropomyosin exists predominantly as an αβ hetero-dimer.

INTRODUCTION

The α-helical coiled-coil motif, once thought to be the sole province of fibrous proteins, has been found in a wide variety of biological systems, *e.g.*, "spike-projections" from bacterial cell walls (streptococcal M) and viral membranes (influenza hemagglutinin), plasma (spectrin and fibrinogen) and cell nuclei (DNA-binding proteins, *e.g.*, "leucine-zippers") [1,2]. Tropomyosin (Tm) is the prototypical protein exhibiting this molecular architecture, consisting of two amphipathic, parallel, in-register and slightly super-twisted chains whose amino acid sequence follows a pseudo-heptad repeat [3–5]. The physical forces responsible for maintaining chain association have been the subject of extensive experimental and theoretical studies and a consensus picture has emerged that invokes hydrophobe–hydrophobe and ionic ("salt-bridge") interactions as the predominant contributors [1,2].

Tm has been isolated and partially characterized from several sources of vertebrate skeletal, cardiac and smooth muscle, and also from a few invertebrate species [6]. The protein from rabbit skeletal muscle [Tm(R)] is the best studied Tm to date. It consists of two distinct protein isoforms differing slightly (39 substitutions/284 total, mostly conservative) in primary structure [7]. These are designated α (fast) and β (slow), respectively, based on electrophoretic mobility on sodium dodecyl sulfate–polyacrylamide gel electrophoresis (SDS-PAGE), and exist in a *ca.* 3–4:1 α:β ratio [4,8,9]. Each chain has a cysteine located at sequence position 190 and the β chain has an additional cysteine at position 36 [7], hence parallel dimer molecules, having adjacent sulfhydryls, can be disulfide cross-linked [3,4,10,11].

0021-9673/92/$05.00

In vitro all three dimeric coiled-coils, $\alpha\alpha$, $\alpha\beta$, and $\beta\beta$, can be produced and these have been studied [10–13] in an effort to explain the observed *in vivo* dimer population of *ca.* 92–96% $\alpha\alpha$ + $\alpha\beta$ and *ca.* 4–8% $\beta\beta$ [14,15].

Tm from chicken gizzard [Tm(C)] has also been sequenced [16,17] and in this instance the two isoforms, designated in this paper as α and β, are present at a *ca.* 1:1 ratio, differ by 72/284 residues, and the α chain has a cysteine at position 36 whereas the β chain has a cysteine at position 190 [16,17]. Hence, only Tm(C) homo-dimers can be disulfide cross-linked. *In vivo,* the $\alpha\beta$ hetero-dimer of Tm(C) is the predominant molecular species [18–24] and this has led to the suggestion that tissue sources containing nearly equal amounts of the two genetic variants will preferentially assemble as $\alpha\beta$ hetero-dimers [25]. In support of this hypothesis are the observations reported for a variety of tissues from fetal and adult rabbit muscle [25] and frog muscle [26].

Earthworm Tm [Tm(W)], on the other hand, has not yet been sequenced and few data on the properties of this invertebrate Tm have appeared [6,27], nor has information appeared regarding the composition of the *in vivo* dimer mixture in terms of the individual, herein designated α and β, chains. Data from a previous study have shown that native Tm (W) cannot be disulfide cross-linked [6].

In this investigation, purified preparations of Tm (R), Tm(C) and Tm(W) were subjected to C_4 reversed-phase (RP) high-performance liquid chromatography (HPLC), weak anion-exchange (WAX) HPLC and strong cation-exchange (SCX) HPLC to compare the chromatographic characteristics of these structurally similar proteins. For all three protein sources, the native, reduced dimer(s) dissociate into individual subunits during binding to and/or elution from the C_4-RP column, as has been previously observed for Tm(R) [14]. Only the cross-linked Tm(R) preparation exhibits a different chromatographic elution profile when compared with its reduced counterpart. WAX-HPLC indicates that only the Tm(R) coiled coils gives a chromatographic separation, with subsequent peak assignment consistent with the known dimer population [14,15]. SCX-HPLC illustrates that all three Tms display a chromatographic transition near pH 6.5, possibly the result of histidine(s) titration. As both ion-exchange systems use non-denaturing elution conditions, the associative dimeric assemblies are expected to be preserved during this mode of chromatography. Therefore, the collective chromatographic data confirm the *in vivo* dimer population for Tm(R) and Tm(C) and suggest that the predominant coiled-coil species for native Tm(W) is the $\alpha\beta$ hetero-dimer.

EXPERIMENTAL

Protein preparation, chemicals and reagents

Tm(R) was purified from rabbit skeletal muscle [28], Tm(W) was purified from earthworm body wall muscle [6] and Tm(C) was purchased from Sigma (St. Louis, MO, USA; T-3026 Lot 66F-9675). Each protein was judged to be satisfactorily pure by SDS-PAGE and UV spectrophotometry, and gave the expected circular dichroism (CD) at low temperature in benign buffer. The lyophilized protein, previously stored desiccated at −20°C, was generally resuspended to a nominal concentration of 3 mg/ml with 1% (v/v) acetic acid (Fisher Scientific, St. Louis, MO, USA) [14]; the resulting solution was then stored at 4°C until use. This low-pH acetic acid reconstitution procedure offers several advantages, including rapid protein solubility, solvent volatility, inhibition of cysteine oxidation and apparent abscence of bacterial growth, but suffers from high UV background absorption. The sources of HPLC solvents, amino acid reagents, water purification and additional materials have been described [29,30].

HPLC instrumentation and chromatography

C_4-RP-HPLC was performed at 37°C on a Vydac 214TP54 C_4 column (25 cm × 0.46 cm I.D.) purchased from the Nest Group (Southborough, MA, USA) with sample elution effected via a linear gradient from 0 to 100% B in 60 min at 1 ml/min, using mobile phases A = 0.1% trifluoroacetic acid and B = 0.095% trifluoroacetic acid in acetonitrile–water (90:10) [14,15].

WAX-HPLC was performed at 28°C on a TSK DEAE-5PW column (7.5 cm × 0.75 cm I.D.) and SCX-HPLC at 28°C on a TSK SP-5PW column (7.5 cm × 0.75 cm I.D.), each purchased from Altex (San Ramon, CA, USA). A linear gradient from 0 to 50% B in 30 min at 1 ml/min was used to elute

samples from the anion-exchange resin and a solvent program from 0 to 100% B in 30 min at 1 ml/min was used to elute samples from the cation-exchange column. For each ion-exchange system, mobile phase A = 10 m*M* sodium phosphate and mobile phase B = 10 m*M* sodium phosphate–1 *M* NaCl, each titrated to the desired pH. Protein samples were either exhaustively dialyzed *vs.* ion-exchange mobile phase A or vacuum-dried (Savant Instruments, Farmingdale, NY, USA) and resuspended in this buffer for preparative chromatography. This was necessary because the larger amounts of acetic acid co-injected in this instance substantially altered the chromatography (*e.g.*, diminished protein binding). All chromatograms from C_4-RP-, WAX- and SCX-HPLC were monitored simultaneously at 214 and 280 nm with fractions collected at 0.25-min intervals (250 μl per fraction) for the preparative runs. The configuration of the chromatographic hardware, temperature control and the data acquisition procedures have been described previously [14,29,30].

SDS-PAGE

Generally, 15 μl of the appropriate ion-exchange fraction was mixed with 15 μl of 2 × loading buffer [180 m*M* sodium phosphate–9 m*M* disodium ethylenediaminetetraacetic acid–3.6% (w/v) SDS–18% (v/v) glycerol–0.036% (w/v) bromophenol blue (pH 7.5)], incubated for 30 min at 45°C and then electrophoresed for 90 min at a constant voltage of 150 V on 4–20% linear acrylamide gradient twelve-well mini-gels (1 mm thick) (Enprotech, Hyde Park, MA, USA) [14,15,31]. This gradient gel system provided better resolution for the two-chain, cross-linked dimers and was employed whenever this type of separation was desired. Otherwise, protein samples were treated as above except that 100 m*M* dithiothreitol was included in the 2 × loading buffer to reduce protein disulfide bonds; the resulting samples were then analyzed on 10–20% gradient mini-gels as this gradient gel system afforded better separations for the various one-chain monomeric species. The sample size was 2–20 μl per well; the gel was stained for 15 min with 0.05% (w/v) Coomassie Brilliant Blue R-250–50% (v/v) methanol–7.5% (v/v) acetic acid, de-stained with 10% (v/v) methanol–7.5% (v/v) acetic acid until the background cleared to an acceptable level and then stored in heat-sealed plastic pouches prior to photography with a Kodak EDP print system (Fisher Scientific). C_4-RP fractions (15 μl) or stock Tm solutions were vacuum-dried, resuspended with 15 μl of water and then mixed with 15 μl of the desired 2 × loading buffer as described above.

Additional analytical techniques

Amino acid compositional analysis of stock Tm solutions and selected C_4-RP fractions was performed by manual precolumn phenylisothiocyanate derivatization of acid hydrolysates as described [29,32]. CD instrumentation, sample measurements (kindly performed by Dr. Marilyn Emerson Holtzer) and subsequent data analysis have been detailed [12,28,33].

RESULTS AND DISCUSSION

C_4-RP-HPLC

The individual purified proteins were subjected to C_4RP-HPLC and fractions collected for further analysis. Previously, it was shown that C_4-RP chromatography of uncross-linked Tm(R) $\alpha\alpha$ dimer resulted in chain dissociation into highly helical monomeric molecules and the individual α and β chains from uncross-linked Tm(R) $\alpha\beta$ dimer were unresolved. In addition, only the disulfide cross-linked forms of the three Tm(R) dimers ($\alpha\alpha$, $\alpha\beta$ and $\beta\beta$) could be separated both from each other and from the uncross-linked monomers [14]. These results and their implications form a basis for interpreting the data presented in this section.

Fig. 1 displays a composite chromatogram for all three of the Tms studied. The retention times for each species of Tm are similar (Fig. 1A–C), and this suggests that either the relevant contact region(s) between protein chain and column support are similar or that the overall hydrophobicity is similar for all six protein chains. Further, it is likely that the individual dissociated chains of Tm(C) and Tm(W) will possess a high degree of helicity as the Tm(R) chain counterparts [14] such that the global chain conformation and accessibility of the hydrophobic residues are expected to be comparable. Clearly, however, other more subtle factors must be present because partial chain separation is observed for Tm (C) (Fig. 1A) and the α and β chains of Tm(W) are almost baseline resolved (Fig. 1B).

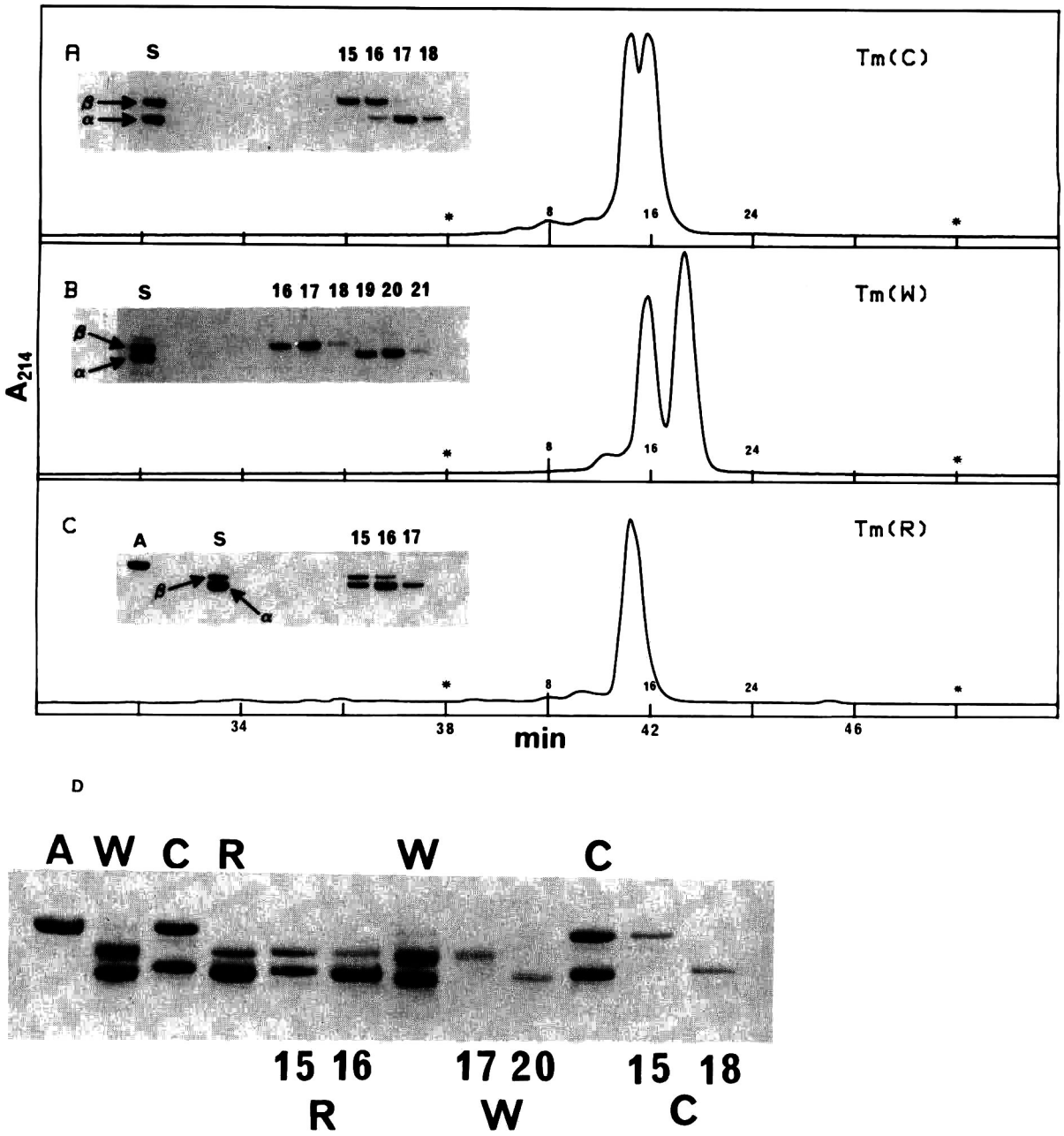

Fig. 1. C_4-RP-HPLC and SDS-PAGE of Tm(C), Tm(W) and Tm(R). All chromatograms were monitored at 214 nm with fractions collected at 0.25-min intervals and asterisks indicate the beginning and end of the collection period. (A) Tm(C), 650 mV full-scale. Inset shows 10–20% SDS-PAGE of indicated fractions and of the unfractionated, stock (S) protein. (B) Tm(W), 850 mV full-scale. Inset shows gel analysis of indicated fractions. (C) Tm(R), 1250 mV full-scale. SDS-PAGE of indicated fractions and an M_r marker protein rabbit actin (A) is shown in the inset. (D) Composite 10–20% SDS-PAGE of selected fractions from the individual C_4-RP-HPLC runs showing the relative electrophoretic mobility of the various Tm molecular species. Left to right: actin, stock Tm(W), stock Tm(C), stock Tm(R), fractions 15 and 16 from Tm(R) chromatogram C, stock Tm(W), fractions 17 and 20 from Tm(W) chromatogram B, stock Tm(C) and fractions 15 and 18 from Tm(C) chromatogram A.

The SDS-PAGE insets from each of these chromatograms indicate that the molecular species designated as the β chain (slower gel component) elutes earlier from the C_4 column than the α chain (faster gel component) for both of these Tms. Attempted disulfide oxidation of Tm(C) and Tm(W) did not result in any retention time changes compared with those shown in Fig. 1. In contrast, Tm(R) did display such a difference, in complete agreement with our earlier results [14] (data not shown). The data for Tm(C) were expected, as the predominant native molecular species is an $\alpha\beta$ hetero-dimer and only homo-dimers can be disulfide cross-linked [16–24]. This information has not been determined for Tm(W), but the above results suggest that, here also, both an $\alpha\beta$ hetero-dimer is the predominant species and cysteines, if present, on the individual chains are not spatially proximal to participate in a disulfide bond (see also below).

A photograph of a 10–20% SDS-PAGE experiment is shown in Fig. 1D for unfractionated stock Tms, selected C_4-RP fractions from the above chromatograms and a relative molecular mass (M_r) 43 000 marker protein, rabbit skeletal actin (A). Note the electrophoretic resolution of the individual α and β chains from a given Tm. The migration order is actin $\approx$ β-Tm(C) < β-Tm(W) $\approx$ β-Tm(R) < α-Tm(C) < α-Tm(W) $\approx$ α-Tm(R). The α and β chains from Tm(R) and Tm(C) are 284 residue, *ca.* M_r 33 000 species and differ in absolute molecular mass by <200 [7,17]. Although the Tm(W) chains have not yet been sequenced, it seems plausible that similar chain characteristics will prevail such that the observed partial resolution of the six Tm chains illustrated in Fig. 1D must reside in a combined subtle effect of the amount of SDS bound to the protein and the overall conformation of this complex. This line of reasoning and cautionary note have been expressed before to rationalize the slight difference in electrophoretic mobility of the Tm(W) and Tm(R) chains when Tm(W) was first isolated [6].

The analytical C_4RP-HPLC profiles for each Tm monitored at both 214 nm and 280 nm are illustrat-

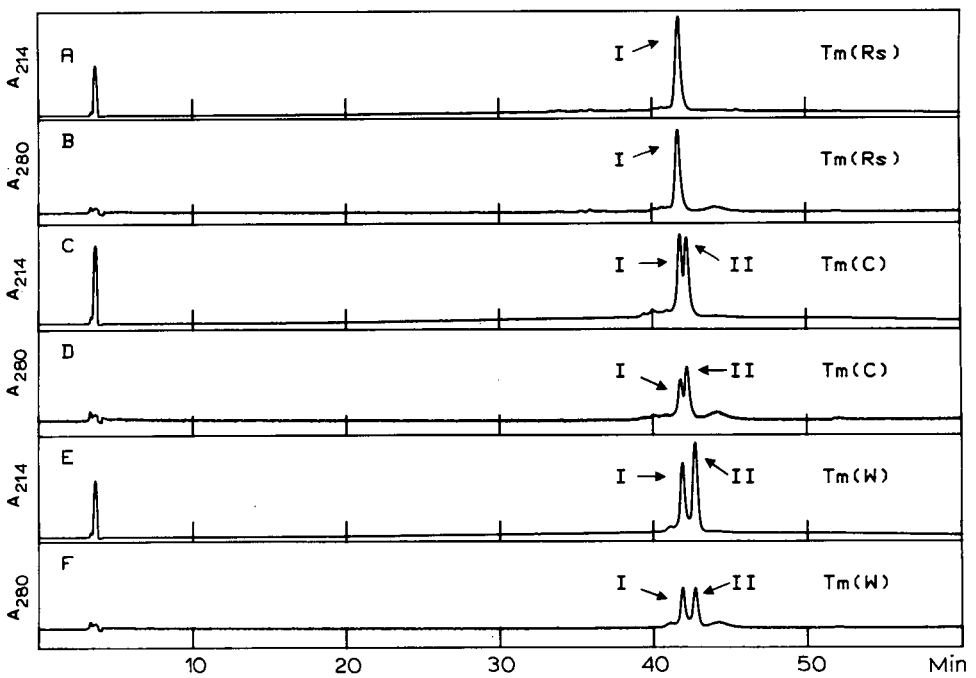

Fig. 2. Analytical C_4-RP-HPLC of Tm(R), Tm(C) and Tm(W). (A) Tm(R_s) = Tm(R) at 214 nm, 800 mV full-scale; (B) Tm(R_s) = Tm(R) at 280 nm, 25 mV full-scale; (C) Tm(C) at 214 nm, 480 mV full-scale; (D) Tm(C) at 280 nm, 15 mV full-scale; (E) Tm(W) at 214 nm, 672 mV full-scale; (F) Tm(W) at 280 nm, 21 mV full-scale. Peaks are labeled for identification purposes. See Table I for amino acid composition of Tm(R) and Tm(W) peaks and Table II for integrated absorbance area ratios of all three Tms.

TABLE I

AMINO ACID COMPOSITION OF Tm(R) AND Tm(W) C_4-RP-HPLC FRACTIONS

Amino acid	Concentration (mol%)						
	Tm(R)			Tm(W)			
	Peak I	Stock	Lit.[a]	Peak I	Peak II	Stock	Lit.[b]
Asx	9.8	10.5	10.3	9.3	11.1	11.6	11.6
Glx	25.3	24.0	25.1	23.7	26.0	25.3	26.4
Ser	4.8	4.8	5.0	5.8	4.6	4.9	5.2
Gly	1.7	2.4	1.2	4.5	3.5	3.4	4.1
His	0.7	0.9	0.6	0.8	0.5	0.6	0.6
Arg	5.3	5.3	4.9	6.0	5.0	5.3	5.0
Thr	2.8	2.7	2.8	6.0	6.8	5.9	6.0
Ala	13.2	12.2	12.5	11.3	9.9	10.8	10.6
Pro	0	0	0	0	0	0	0
Tyr	2.0	2.1	2.1	1.5	1.2	1.3	1.4
Val	3.2	3.6	3.4	3.9	4.5	3.9	4.2
Met	1.9	2.3	2.3	1.9	1.5	1.9	1.4
Ile	3.7	3.6	4.1	2.9	3.3	2.4	3.2
Leu	11.1	11.0	11.2	10.9	10.6	11.0	10.1
Phe	0.4	0.4	0.4	1.3	1.4	1.4	1.5
Lys	14.0	14.3	13.7	10.3	10.1	10.3	8.6
Trp	n.d.[c]	n.d.	0	n.d.	n.d.	n.d.	0
Cys	n.d.	n.d.	0.4	n.d.	n.d.	n.d.	0

[a] Literature values taken from ref. 7.
[b] Literature values taken from ref. 6.
[c] n.d. = Not determined.

ed in Fig. 2. Peaks are labeled I and II for identification purposes and amino acid analysis was performed on Tm(R) peak I (Fig. 2A) and Tm(W) peaks I and II (Fig. 2E). These results are listed in Table I, where it is evident that the compositional analysis of the stock proteins and Tm(R) peak I compares very favorably with literature values and that Tm (W) peak fractions I and II have nearly identical residue numbers. The minor differences observed for these Tm(W) fractions (found in replicate analyses, data not shown) must await sequence analysis of the individual chains for confirmation.

The chromatograms monitored at 280 nm (Fig. 2B, D and F) should only report on the tyrosine content of each chain because no tryptophan residues are found in any of these Tm species [6,7,17] and the phenylalanine contribution at this wavelength is expected to be minimal. Visual inspection of the peptide bond absorption at 214 nm for Tm(C) (Fig. 2C) shows peaks I and II to be virtually identical, in contrast to the apparent tyrosine content (Fig. 2D) as peak II exhibits a greater 280 nm intensity than peak I. The converse of these observations is illustrated for the Tm(W) chromatograms monitored at 214 nm (Fig. 2E) and 280 nm (Fig. 2F). In this instance, the displayed 214-nm profile indicates that peak II has a greater absorbance at 214 nm than peak I, whereas the corresponding 280-nm chromatogram shows essentially identical peak intensities. As discussed below, this implies that the tyrosine content of Tm(C) peak I is less than that of Tm(C) peak II, and for Tm(W) the opposite result holds, *i.e.*, Tm(W) peak I has a greater tyrosine content than Tm(W) peak II.

Table II summarizes the integrated peak areas at 214 and 280 nm as the ratio 214:280 nm for each of the Tms. The number reported for the tyrosine (Tyr) content of the Tm(C) and Tm(W) chains was calculated using the observed 214:280 nm ratio for Tm(R) and a value of six Tyr for both the α and β chains of Tm(R) [7]. It is important to point out that the numbers given in parentheses in Table II were determined with an independent HPLC system. These values are consonant with those obtained with the other HPLC system and so should increase confidence in the validity of this analysis. Peak I (β) from Tm(C) gave a calculated Tyr content of 3.2 compared with the sequence value of 3 (given in brackets) while peak II (α) yielded values of 4.3 and 4 Tyr, respectively [17]. These determina-

TABLE II

ABSORBANCE RATION (214/280 nm) FROM C_4-RP-HPLC AND TYROSINE DETERMINATION FOR Tm(R), Tm(C) AND Tm(W)

Protein	214/280 nm		No. of Tyr	
	Peak I	Peak II	Peak I	Peak II
Tm(R)	36.7/1	–	6	–
	(36.5/1)[a]	–	(6)	–
Tm(C)	67.8/1	50.8/1	3.2[3][b]	4.3[4]
Tm(W)	54.8/1	68.1/1	4.0	3.2
	(52.1/1)	(66.4/1)	(4.2)	(3.3)

[a] Numbers in parentheses were independently determined on a separate HPLC system.
[b] Numbers in brackets are literature values taken form ref. 17.

tions lend further support to the identification and designation of the Tm(C) chains presented above.

A similar set of calculations for the Tm(W) C_4-RP peak fractions gave the opposite analysis for the α (peak II) and β (peak I) species of *ca.* 3 Tyr and *ca.* 4 Tyr, respectively. One can use the averaged numbers for these individual peaks (chains) and the *ca.* 1:1 ratio of chains to calculate a stock protein Tyr value of *ca.* 3.68 for Tm(W). This calculated Tyr content differs by less than 6% from an analysis performed 11 years prior using cruder methodology on unfractionated Tm(W) chains [6]. Additionally, the Tyr mol% for these fractions, 1.5 and 1.2, respectively, and the value of 2.0% measured for the Tm(R) fraction (Table I) can also be used to calculate the Tyr content of Tm(W) α and β chains if one assumes the same degree of polymerization for the Tm(W) and Tm(R) chains, *i.e.*, 284 residues. Performing such an analysis indicates experimentally 5.68 Tyr (compared with the sequence value of 6 [7]) for Tm(R), giving 4.26 Tyr for Tm(W) peak I (β) and 3.41 Tyr for Tm(W) peak II (α). Hence the compositional Tyr analysis (Table I) and the chromatographic peak-area ratio calculations (Table II) provide a consistent set of data for the Tyr content of the α and β chains of Tm(W).

WAX-HPLC

The three purified Tms were subjected to analytical WAX-HPLC over the pH range 8.4–5.0 (Fig. 3). One would then expect as a first approximation that as the pH is lowered from slightly basic (pH 8.4) to mildly acidic (pH 5.0) the retention time of the protein should decrease. This can be rationalized as a concomitant decrease in the net negative charge of the protein (*e.g.*, lysine and histidine protonation). Although net charge is clearly an important factor in determining the extent of protein binding to ion-exchange resins, the three-dimensional protein structure and accessibility of the appropriately signed charged residues to interact with the matrix are equally important [34]. Sample loading and elution for this mode of chromatography are performed under mild solvent conditions such that the protein chains are expected to remain associated as dimers and the native dimer population should be preserved. Interestingly, the Tms appear to be ideal model candidates to test the "contact residue" hypothesis [34], as these molecules exhibit

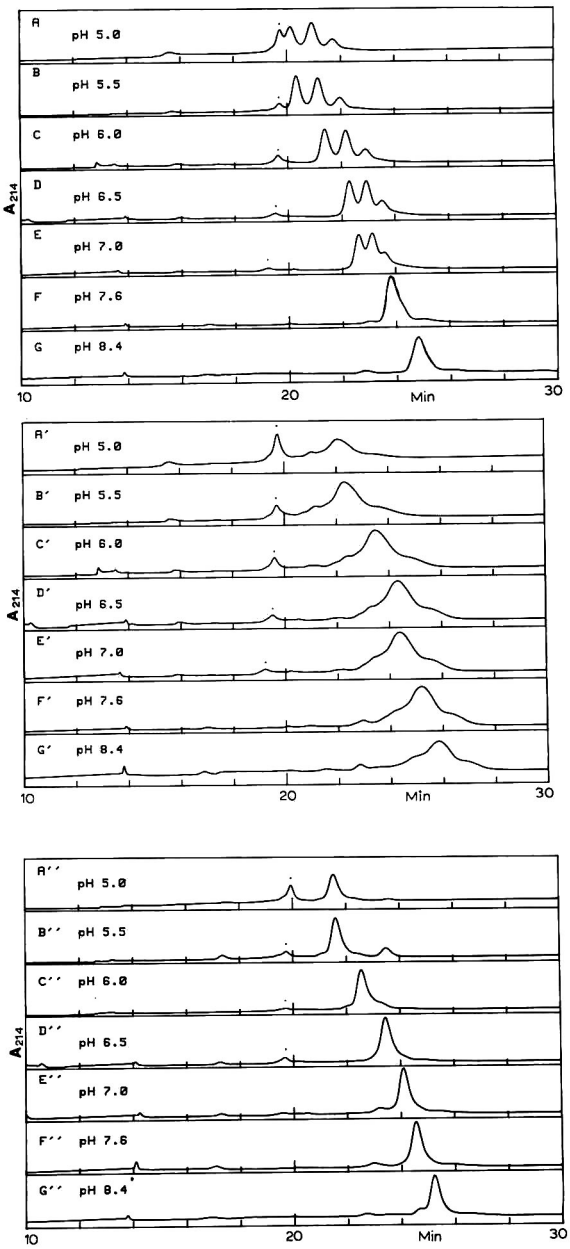

Fig. 3. Analytical WAX-HPLC at different pH values for Tm(R), Tm(W) and Tm(C). Top, unprimed panels: Tm(R_s) = Tm(R) monitored at 214 nm; A–G, 200, 500, 500, 500, 500, 600 and 600 mV full-scale respectively. Dot above peak at *ca.* 19–20 min indicates a gradient-associated UV artifact also observed in "blank" chromatograms. Middle, single-primed panels: Tm(W) monitored at 214 nm; A′–G′, 150, 300, 300, 300, 300, 500 and 300 mV full-scale respectively. Bottom, double-primed panels: Tm(C) monitored at 214 nm; A″–G″, 300, 500, 600, 600, 600, 600 and 600 mV full-scale, respectively.

a particularly simple secondary (α-helix) and quaternary (coiled-coil) structure under the experimental conditions used. Thus, potential complications arising from tertiary structure are absent in this instance such that it may be possible to pinpoint specific regions (sites) of the sequenced Tms in contact with the resin.

The Tm(R) preparation showed a progressive decrease in retention time from WAX-HPLC as the pH was lowered from 8.4 to 5.0 (Fig. 3, top, unprimed panels). Between pH 7.6 (Fig. 3F) and pH 7.0 (Fig. 3E) it is evident that peak resolution for the Tm(R) sample is occurring and that a further decrease in pH improves this resolution. On the other hand, neither Tm(W) (Fig. 3, middle, single-primed panels) nor Tm(C) (Fig. 3, bottom, double-primed panels) displayed such peak separation, although each protein gave the same general trend of decreasing retention time with decreasing pH as Tm (R). Tm(W) chromatographed as a particularly broad peak over this entire pH range (Fig. 3, middle, single-primed panels) whereas Tm(C) eluted (Fig. 3, bottom, double-primed panels) with a peak shape similar to Tm(R) (Fig. 3, top, unprimed panels). The chromatographic profile of Tm(C) at pH 8.4 (Fig. 3G″) appears similar in detail to a previous

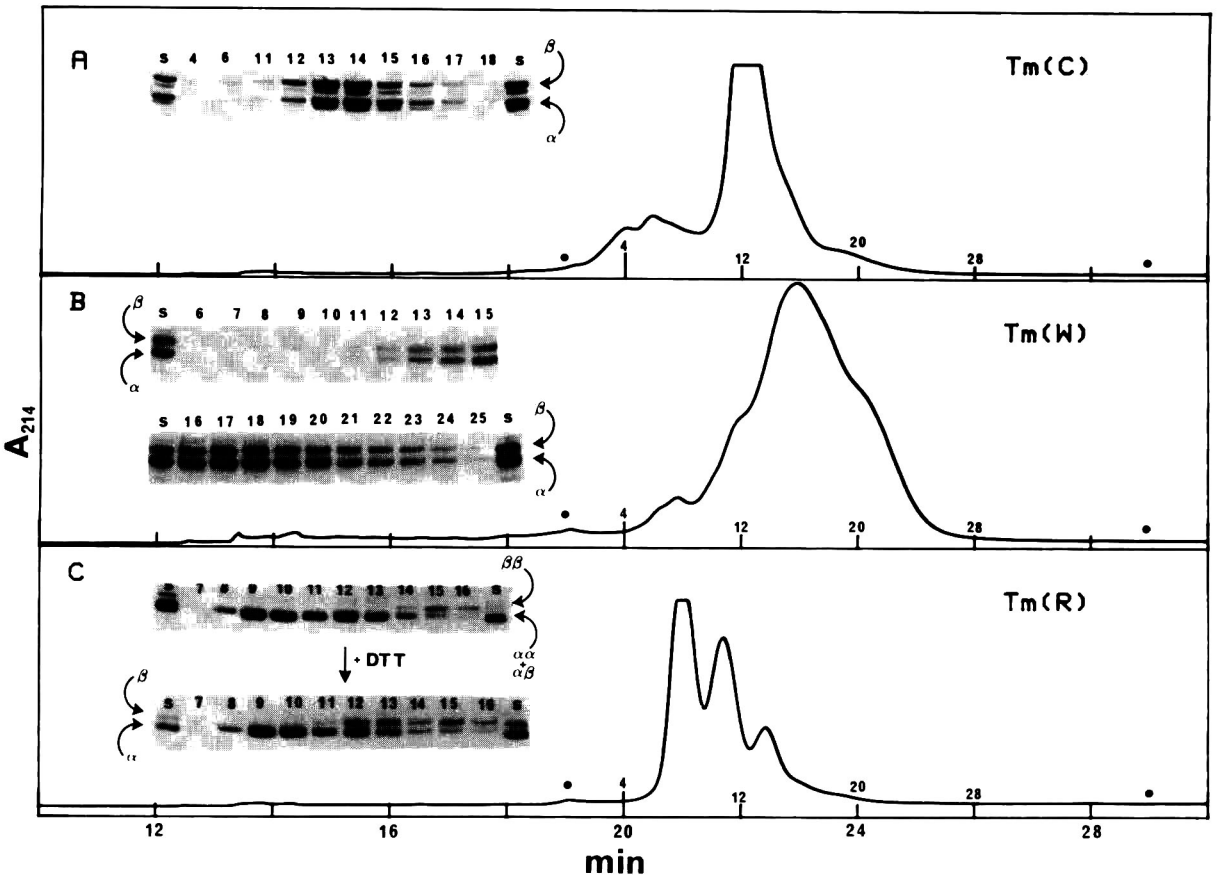

Fig. 4 Preparative WAX-HPLC at pH 6.0 and SDS-PAGE of Tm(C), Tm(W) and Tm(R). All chromatograms were monitored at 214 nm with fractions collected at 0.25-min intervals and dots indicate the beginning and end of the collection period. (A) Tm(C), 2500 mV full-scale. Major peak is off-scale; see Fig. 3C″ for analytical profile. Inset shows 10–20% SDS-PAGE of the indicated fractions and of the unfractionated, stock (S) protein. (B) Tm(W), 2000 mV full-scale. Inset shows gel analysis of indicated fractions. (C) Tm(R), 2500 mV full-scale. Major peak is off-scale; see Fig. 3C for analytical profile. Upper inset shows 4–20% SDS-PAGE of indicated fractions and lower inset shows 10–20% SDS-PAGE of the same samples reduced with dithiothreitol (DTT) prior to electrophoresis.

analysis [21] of the native dimer population of Tm (C), where the main peak was identified as the $\alpha\beta$ hetero-dimer and a small preceding peak was assinged to an $\alpha\alpha$ dimer. Therefore the integrity of the native dimer population in this mode of chromatography is maintained for Tm(C) and Tm(R) (see below).

Prepatative amounts of the three Tms were injected and fractions collected on the WAX resin at pH 6.0 (Fig. 4). The pH was chosen for the preparative runs because the analytical profile for Tm(R) (Fig. 3C) gave acceptable peak resolution without interference from a gradient-associated artifact (dot above peak at *ca.* 19 min) and little change was observed for the other two Tms over the studied pH range. The gel inset for Tm(C) (Fig. 4A) indicates approximately equal intensity and distribution of the α and β chains across the peak fractions, *i.e.*, the majority of the native dimer population of Tm(C) is an $\alpha\beta$ hetero-dimer [18–24]. Some slight chain degradation of the stock sample is more apparent at these higher sample loads, as indicated by minor bands of faster electrophoretic mobility than the major α and β bands.

Tm(W) (Fig. 4B) chromatographed as a broad peak with both leading and trailing shoulders, although the corresponding gel inset showed only the expected two major isoforms of this Tm in roughly equal amounts. The origin of this chromatographic heterogeneity is not readily apparent but may residue in a small population of post-translationally modified chains, *e.g.*, phosphorylated or deamidated, or may represent the partial separation of minor contaminants seen as the slower and faster migrating components relative to the major β and α chains, respectively (see gel inset, Fig. 1B).

The gel analysis of the chromatographic elution profile for Tm(R) (Fig. 4C) showed that the starting sample prepared by dialysis into mobile phase of pH 6.0 was virtually all oxidized, *i.e.*, disulfide cross-linked (upper gel inset, lane S). This was unexpected because sulfhydryl oxidation via molecular oxygen tends to be more efficient at neutral to slightly basic pH. The same UV distribution was observed for an uncross-linked Tm(R) sample (data not shown), suggesting that the oxidation state of the cysteines have no observable effect on WAX-HPLC. Neither Tm(C) nor Tm(W) became disulfide cross-linked after dialysis into pH 6.0 buffer (data not shown). Importantly, the elution order of the three major peaks is $\alpha\alpha$, $\alpha\beta$ and $\beta\beta$, as assessed from the gel analysis. The first-eluting peak contains α chains (+DTT gel inset, lanes 8–10), the next peak contains approximately equal amounts of α and β chains (+DDT gel inset, lanes 12–14), and the third peak is clearly enriched in the β chain component (+DDT gel inset, lanes 15 and 16). Similar conclusions regarding the peak assignments are possible from the upper gel inset for this chromatogram. The elution order at pH 6.0 follows the net negative charge of the Tm(R) dimers: $\alpha\alpha(-50)$, $\alpha\beta(-52)$ and $\beta\beta(-54)$ and is analogous in charge content distribution to the WAX chromatograms for *in vitro* produced homo- and hetero-dimers of Tm(C) [21]. It was not possible to determine the percentage of each dimer species for the Tm(R) preparation owing to insufficient peak resolution, but qualitatively it is obvious that all three Tm(R) dimer species are present in native Tm(R). In addition to the previous C_4-RP-HPLC, SDS-PAGE and capillary electrophoresis data [14,15], the WAX-HPLC data presented here represent the fourth independent analytical technique that unequivocally demonstrates the existence of $\beta\beta$ homo-dimers in native Tm(R).

SCX-HPLC

A set of experiments comparable to those reported above for WAX-HPLC were performed on the three Tms chromatographed on an SCX column. The pH in the instance was varied from 8.0 to 6.0 (Fig. 5). If the "contact residue" hypothesis [34] is correct then, as the pH is lowered from 8.0 to 6.0, the Tm retention time should increase. The composite analytical chromatograms shown in Fig. 5 support this assertion and one possibility is that the protonation of histidine(s) and/or protonation of abnormally high titrating acidic residues may be responsible for these observations. The fact that both Tm(R) (Fig. 5, top, unprimed panels) and Tm(C) (Fig. 5, bottom, double-primed panels) are highly net negatively charged at these pHs (from their known sequence) yet still bind to the cation-exchange column provides further experimental evidence supporting the "contact-residue" hypothesis [34]. All three Tms were tightly bound to the cation-exchange matrix at pH 5.5–4.5 such that no protein eluted using the normal gradient program (data not shown).

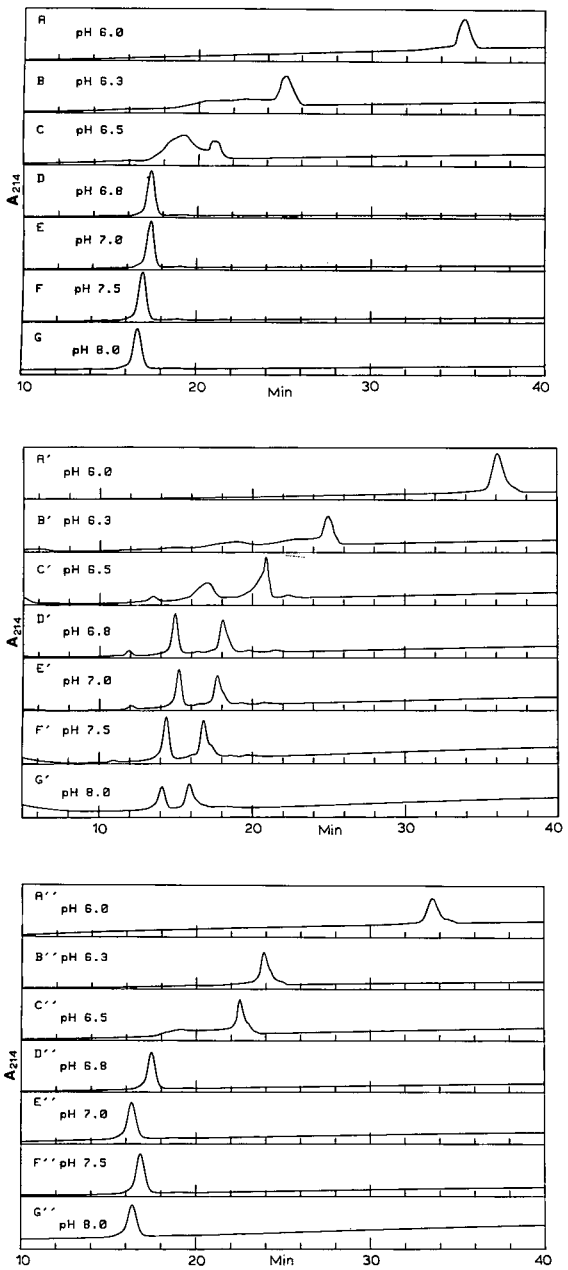

Fig. 5. Analytical SCX-HPLC at different pH values for Tm(R), Tm(W) and Tm(C). Top, unprimed panels: $Tm(R_s)$ = Tm(R) monitored at 214 nm; A–G 350, 300, 300, 900, 800, 600 and 600 mV full-scale, respectively. Middle, single-primed panels: Tm(W) monitored at 214 nm; A′–G′, 600, 300, 300, 300, 300, 200 and 200 mV full-scale, respectively. Bottom, double-primed panels: Tm(C) monitored at 214 nm; A″–G″, 300, 500, 500, 400, 400, 400 and 200 mV full-scale, respectively. Note the broad elution profile near pH 6.5 for all three proteins.

SCX-HPLC of Tm(R) at pH 6.5 resulted in a broad, poorly resolved set of peaks (Fig. 5C). These peaks eventually coalesced into one peak at pH 6.0 (Fig. 5A) whose width, however, was slightly greater than in the chromatograms at pH 6.8–8.0 (Fig. 5, D–G). A set of standard proteins (carbonic anhydrase, ribonuclease A and lysozyme) chromatographed under identical conditions exhibited increased retention times as the pH varied from 8.0 to 6.0 but did not show peak broadening or splitting (data not shown), suggesting that the observed chromatographic transition is Tm specific.

It seems likely that the sites involved in this transition near pH 6.5 (Fig. 5C) are Tm histidine residues, for the following reasons. First, the observed transition occurs in a pH range normally entailing histidine residue titration [35]. Second, extant NMR data on purified $\alpha\alpha$ and $\beta\beta$ Tm(R) indicate that the two α-chain histidines, his-153 and his-276, titrate at different pHs with his-153 exhibiting micro-pK_a states; the β chain has only his-153, which displays a similar titration profile identical with his-153 from the α chain [36] {Tm(R) β chain residue 276 is asparagine [7]}. Further, at pHs outside the transition regon, the NMR resonances could be superimposed [36], an observation compatible with the coalescence of the SCX-HPLC peaks observed at pH 6.0 (Fig. 5A) and pH 8.0 (Fig. 5G). Third, additional NMR experiments have demonstrated that the micro-titration states of his-153 are the result of different conformational states of Tm which have different pK_a values for this histidine residue and are in slow exchange with one another near room temperature [37].

Caution is necessary, however, in merging the NMR and SCX-HPLC results into a unified structural interpretation at these sites on Tm(R) because the experimental parameters prevailing in these distinct analytical techniques are sufficiently different. The obvious differences were in protein concentration, 10–20 mg/ml in NMR *vs.* 0.5–3 mg/ml in SCX-HPLC, and in salt concentration, 1 *M* for NMR where Tm is unaggregated *vs.* 10 m*M* for SCX-HPLC where Tm could be appreciably aggregated. It is also unclear whether both Tm binding to the cation matrix resulting in a high local concentration of protein and Tm elution from the column with high salt would actually bring the two sets of experimental parameters into closer agreement. In any

event, even if the chromatographic transition near pH 6.5 (Fig. 5C) is due to histidine titration, it is far from certain if this derives from micro-pK_a states of his-153 or multiple conformational states, or simply to titration differences between the two histidines of the α chain.

Analytical SCX-HPLC of Tm(C) shows essentially the same chromatographic trend (Fig. 5, A″–G″) as for Tm(R) (Fig. 5, A–G). Specifically, this includes an increased retention time as the pH is decreased from 8.0 to 6.0, a slightly wider peak at pH 6.0 (Fig. 5A″) than pH 8.0 (Fig. 5G″) and a transition region near pH 6.5 (Fig. 5C″). For Tm (C), this chromatographic transition is different in absolute appearance than Tm(R), yet it seems reasonable to expect the two proteins to behave similarly. NMR titration data have not appeared for the histidine residues of Tm(C) and it would be informative to compare the NMR and SCX-HPLC data for both Tm(R) and Tm(C).

The chromatographic profiles displayed for Tm (W) (Fig. 5, middle, single-primed panels) were at first disturbing because of the two distinct peaks observed over the majority of the pH range. There are three possible explanations. First Tm(W), unlike Tm(R) and Tm(C), may be highly susceptible to dissociation into the corresponding α and β chains during binding to and/or elution from the

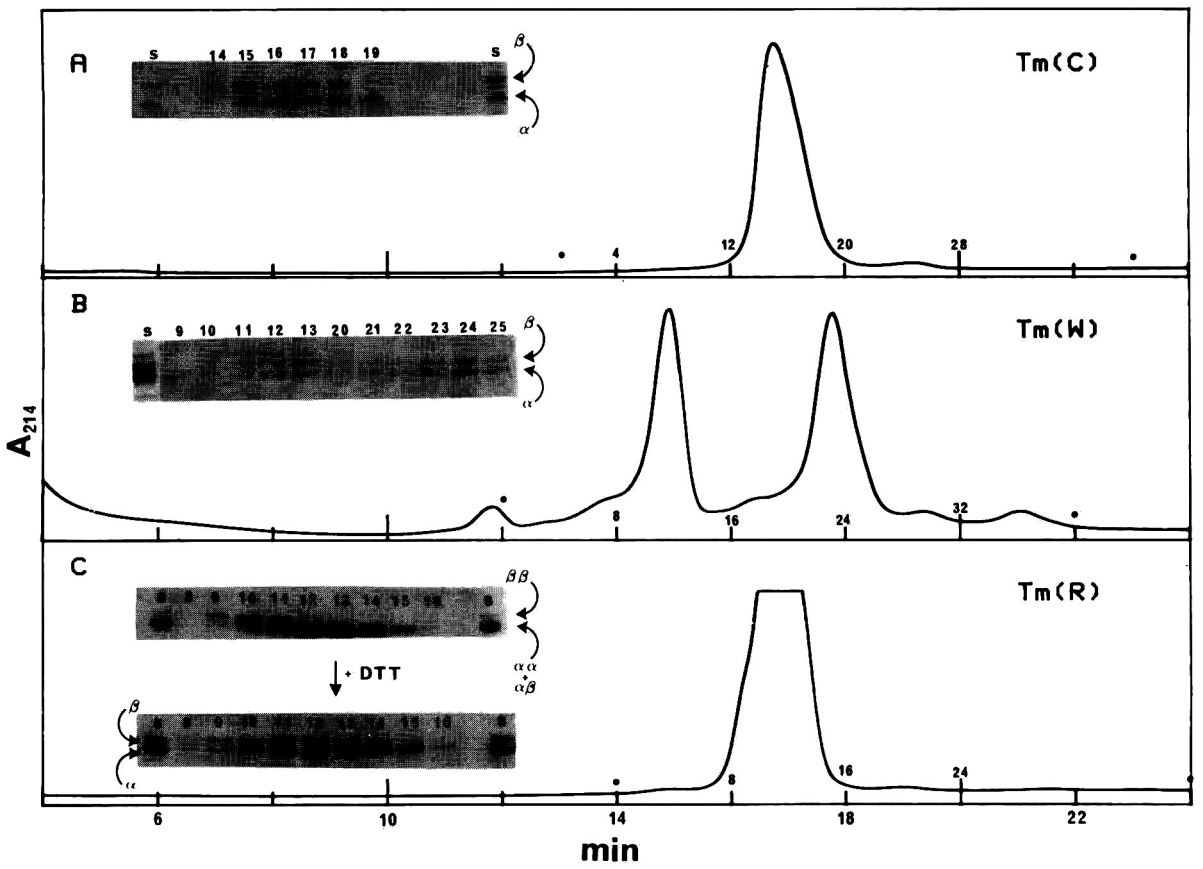

Fig. 6. Preparative SCX-HPLC at pH 7.5 and SDS-PAGE of Tm(C), Tm(W) and Tm(R). All chromatograms were monitored at 214 nm with fractions collected at 0.25-min intervals and dots indicate the beginning and end of the collection period. (A) Tm(C), 1800 mV full-scale. Inset shows 10–20% SDS-PAGE of indicated fractions and of the unfractionated, stock (S) protein. (B) Tm(W), 1200 mV full-scale. Inset shows gel analysis of indicated fractions. (C) Tm(R), 2500 mV full-scale. Major peak is off-scale; see Fig. 5F for analytical profile. Upper inset shows 4–20% SDS-PAGE of the indicated fractions and lower inset shows 10–20% SDS-PAGE of the same samples reduced with DTT prior to electrophoresis.

SCX resin. Second, chain exchange may occur during the chromatographic process. Third, the cation-exchange resin, in contrast to reversed-phase and anion-exchange supports, may actually separate according to subtle differences in the dimer isoforms. It will be seen next that preparative SCX-HPLC of Tm(W) at pH 7.5 points to a variation of the latter possibility as the correct one.

Fig. 6 illustrates preparative SCX-HPLC for all three Tms. The chromatography was performed at pH 7.5 to address the origin of the two peaks observed for Tm(W) in the analytical run (Fig. 5F') and little relevant chromatographic change was evident for Tm(R) and Tm(C) from pH 8.0 to 6.8. No unexpected results occurred for either Tm(C) (Fig. 6A), which gave only the $\alpha\beta$ hetero-dimer band, or Tm(R) (Fig. 6C), where a hint of $\beta\beta$ enrichment as the leading shoulder of the main off-scale peak was observed (upper and lower gel insets, lane 9). The starting Tm(R) sample, again, became almost exclusively oxidized, *i.e.*, disulfide cross-linked, by dialysis into mobile phase A pH 7.5 buffer, but an uncross-linked sample yielded the same UV profile (data not shown) as is shown in Fig. 6C.

Returning to the Tm(W) preparative run (Fig. 6B), we see from the gel inset that the early eluting peak at *ca.* 15 min comprised approximately equal amounts of α and β chains (lanes 10–13) in addition to an upper band of slower electrophoretic mobility originally seen as a minor contaminant in the unfractionated, stock protein (lane S). The second major peak at *ca.* 18 min is exclusively approximately equal amounts of Tm(W) α and β chains (lanes 20–25). Apparently, this minor contaminant becomes highly enriched and is able to interact with Tm(W) α and β chains during SCX chromatography. A similar occurrence has been reported for anion-exchange chromatography of a rabbit actin–Tm(W) complex as binding of actin to Tm(W) dimer resulted in a concomitant decrease in the original Tm(W) peak and the appearance of a new peak representing the actin–Tm(W) complex [27]. If the early-eluting peak in SCX-HPLC really represents a worm actin–Tm(W) complex, then this chromatographic system could provide a general means of assaying such an interaction. Current efforts are focused on identifing this upper band by comparative peptide mapping and immunological studies.

CONCLUSIONS

This study compared the chromatographic characteristics of Tms from two vertebrate [Tm(R) and Tm(C)] and one invertebrate species [Tm(W)]. Three modes of HPLC (C_4RP, WAX and SCX) were used and several conclusions can be drawn from the results. C_4RP-HPLC of all three unoxidized proteins results in chain dissociation into individual α and β subunits. Separation of these isoforms was accomplished for Tm(W) and Tm(C) but not Tm(R). Only Tm(R) could be disulfide cross-linked, and as a consquence gave a distinct C_4RP chromatogram. This confirmed that the predominant native molecular species of Tm(C) is an $\alpha\beta$ hetero-dimer, as each chain has no adjacent cysteine partner to produce as disulfide cross-link. The inability to cross-link Tm(W) suggests that it also exists *in vivo* as the $\alpha\beta$ hetero-dimer and that if cysteines are present here they occur at distinct sequence positions in the α and β chains and are not sufficiently close to form disulfide cross-links. A preliminary denaturation–renaturation experiment [38] on Tm(W) followed by an attempted cross-linking reaction showed identical C_4RP chromatograms for both the native control and experimental test sample. Further, each chain probably contains a single cysteine residue [6]. Hence, under these experimental conditions, the resulting Tm(W) dimer population reached *in vitro* is identical with the native protein, *i.e.*, all $\alpha\beta$.

WAX-HPLC experiments indicate that the retention times for all three Tms progressively decrease as the pH decreases from 8.4 to 5.0. Tm(R) is partially resolved into three peaks corresponding to the known mixture of dimer species found *in vivo*. Gel analysis of the Tm(C) and Tm(W) peaks, on the other hand, indicated that the single Tm(C) peak is exclusively composed of approximately equal amounts of α and β chains, as was the analogous Tm(W) peak which, however, exhibited apparent heterogeneity.

Similar studies using SCX-HPLC showed that all three Tms increased in retention time as the pH was lowered from 8.0 to 6.0, even though at pH 6.0 both Tm(R) and Tm(C) are highly negatively charged. Clearly, these negatively charged molecules are able to bind to a cation-exchange resin supporting the notion that net charge at a given pH is not the sole

determinant in protein–ion-exchange interaction. Near pH 6.5 all three Tms displayed a broad chromatographic transition, possibly as a result of individual histidine residue protonation. Tm(W) produced an anomalous chromatogram with the first-eluting peak containing approximately equal amounts of α and β chains yet highly enriched in a minor contaminant observed in the original protein preparation.

The chromatographic data in their entirety confirm the known *in vivo* dimer population of Tm(R) and Tm(C) and indicate, in addition, that the native *in vivo* dimer population of Tm(W) is an $\alpha\beta$ heterodimer.

ACKNOWLEDGEMENTS

We are indebted to Professor Alfred Holtzer and Dr. Marilyn Emerson Holtzer (Chemistry Department, Washington University, St. Louis, MO, USA) for their generous gift of the Tm(R) and Tm (W) preparations used in this study and for their interest in and critical reading of the manuscript. The excellent manuscript organization of Mrs. Pat Parvin, Ms. Lorraine Whiteley and Mr. James Wrabl (gel photography) is sincerely appreciated.

REFERENCES

1 J. Talbot and R. S. Hodges, *Acc. Chem. Res.*, 15 (1982) 224–230.
2 C. Cohen and D. A. D. Parry, *Proteins*, 7 (1990) 1–15.
3 P. Johnson and L. B. Smillie, *Biochem. Biophys. Res. Commun.*, 64 (1975) 1316–1322.
4 S. S. Lehrer, *Proc. Natl. Acad. Sci. U.S.A.*, 72 (1975) 3377–3381.
5 A. McLachlan and M. Stewart, *J. Mol. Biol.*, 98 (1975) 293–304.
6 D. L. Crimmins, L. L. Isom and A. Holtzer, *Comp. Biochem. Physiol.*, 69B (1981) 35–46, and references cited therein.
7 A. Mak, L. B. Smillie and G. R. Stewart, *J. Biol. Chem.*, 255 (1980) 3647–3655.
6 E. Eisenberg and W. W. Kielley, *J. Biol. Chem.*, 249 (1974) 4742–4748.
9 G. M. Strasburg and M. L. Greaser, *FEBS Lett.*, 72 (1976) 11–14.
10 M. E. Holtzer, T. Breiner and A. Holtzer, *Biopolymers*, 23 (1984) 1811–1833.
11 M. E. Holtzer, K. Askins and A. Holtzer, *Biochemistry*, 25 (1986) 1688–1692.
12 M. E. Holtzer, A. Holtzer and D. L. Crimmins, *Biochem. Biophys. Res. Commun.*, 166 (1990) 1279–1283.
13 M. E. Holtzer, W. C. Bracken and A. Holtzer, *Biopolymers*, 29 (1990) 1045–1056.
14 D. L. Crimmins and M. E. Holtzer, *J. Chromatogr.*, 543 (1991) 327–343.
15 M. E. Holtzer, S. G. Kidd, D. L. Crimmins and A. Holtzer, *Protein Sci.*, (1992) in press.
16 S. Y. M. Lau, C. Sanders and L. B. Smillie, *J. Biol. Chem.*, 260 (1985) 7257–7263.
17 C. Sanders and L. B. Smillie, *J. Biol. Chem.*, 260 (1985) 7264–7275.
18 C. Sanders, L. D. Burtnick and L. B. Smillie, *J. Biol. Chem.*, 261 (1986) 12774–12778.
19 L. D. Burtnick, C. Sanders and L. B. Smillie, *Arch. Biochem. Biphys.*, 266 (1988) 622–627.
20 P. Graceffa, *Biochemistry*, 28 (1989) 1282–1287.
21 A. Jansco and P. Graceffa, *J. Biol. Chem.*, 265 (1990) 5891–5897.
22 S. S. Lehrer and Y. Qian, *J. Biol. Chem.*, 265 (1990) 1134–1138.
23 S. S. Lehrer and W. F. Stafford, III, *Biochemistry*, 30 (1991) 5682–5688.
24 S. Nakamura, T. Sakurai and Y. Nonomura, *J. Biochem.*, 109 (1991) 758–762.
25 D. D. Bronson and F. H. Schachat, *J. Biol. Chem.*, 257 (1982) 3937–3944.
26 S. S. Lehrer, Y. Qian and S. Hvidt, *Science*, 246 (1989) 926–928.
27 A. Ditgens, J. D'Haese, J. V. Small and A. Sobieszek, *J. Muscle Res. Cell Motility*, 3 (1982) 57–74.
28 M. E. Holtzer, A. Holtzer and J. Skolnick, *Macromolecules*, 16 (1983) 173–180.
29 D. L. Crimmins, J. Gorka, R. S. Thoma and B. D. Schwartz, *J. Chromatogr.*, 443 (1988) 63–71.
30 D. L. Crimmins, R. S. Thoma, D. W. McCourt and B. D. Schwartz, *Anal. Biochem.*, 176 (1989) 255–260.
31 D. L. Crimmins, D. W. McCourt, R. S. Thoma, M. G. Scott, K. Macke and B. D. Schwartz, *Anal. Biochem.*, 187 (1990) 27–38.
32 R. S. Thoma and D. L. Crimmins, *J. Chromatogr.*, 537 (1991) 153–165.
33 M. E. Holtzer, S. Kumar, A. Holtzer and D. L. Crimmins, *Biopolymers*, 28 (1989) 1597–1612.
34 W. Kopaciewicz, M. A. Rounds, J. Fausnaugh and F. E. Regnier, *J. Chromatogr.*, 266 (1983) 3–21.
35 J. L. Markley, *Acc. Chem. Res.*, 8 (1975) 70–80.
36 B. F. P. Edwards and B. D. Sykes, *Biochemistry*, 17 (1978) 684–689.
37 B. F. P. Edwards and B. D. Sykes, *Biochemistry*, 19 (1980) 2577–2583.
38 M. E. Holtzer, unpublished results.

Journal of Chromatography, 599 (1992) 65–75
Elsevier Science Publishers B.V., Amsterdam

CHROMSYMP. 2550

Polymer-coated reversed-phase packings with controlled hydrophobic properties

I. Effect on the selectivity of protein separations

Michael Hanson and Klaus K. Unger

Johannes Gutenberg-Universität, Institut für Anorganische und Analytische Chemie, 6500 Mainz (Germany)

Colin T. Mant and Robert S. Hodges*

Department of Biochemistry and the Medical Research Council of Canada Group in Protein Structure and Function, University of Alberta, Edmonton, Alberta T6G 2H7 (Canada)

ABSTRACT

A novel approach to analytical and preparative protein separations by reversed-phase chromatography is described. Porous and non-porous silica supports were coated with polymethacrylate-based polymers or copolymers to produce tailored stationary phases of varying hydrophobicity. Through the application of a model protein mixture of lysozyme, cytochrome *c* and myoglobin, it was demonstrated that selective unfolding of proteins can be achieved by varying the hydrophobicity of the polymer coat permitting manipulation of the chromatographic pattern of analytical protein separations. Thus, proteins may be maintained in their native, folded state or may be partially or completely unfolded, depending on the choice of packing and/or run conditions. In addition, on the non-porous packings, such manipulation of protein elution profiles is achievable at run times of < 5 min. A potential preparative role for the polymer-coated packings was demonstrated through their application to the reversed-phase chromatography of a three-protein complex, rabbit skeletal troponin. Through packing and/or temperature manipulation, it was demonstrated that even such a multi-protein complex, stabilized only by non-covalent interactions, may be maintained during purification by reversed-phase chromatography.

INTRODUCTION

Reversed-phase high-performance liquid chromatography (RP-HPLC) has seen a significant increase in recent years in its application to polypeptides and proteins [1,2]. However, its use in this regard still does not rival the extent of its application to smaller peptide molecules (< 50 residues). Reasons for many researchers' reluctance to utilize RP-HPLC for protein separations have included such concerns as protein denaturation, poor recoveries, broad misshapen peaks, ghosting and loss of activity with biologically active proteins such as enzymes [3].

The most commonly used solvent systems for RP-HPLC of polypeptides involve linear increasing gradients, starting with water and increasing concentrations of organic solvent (usually methanol, acetonitrile or isopropanol) [1,2]. These solvent systems generally employ low concentrations of perfluorinated organic acids [*e.g.*, trifluoroacetic acid (TFA)] at a concentation of 0.05–0.1% (v/v) in both the water and the organic solvent, resulting in a pH of *ca.* 2.0. Although many proteins are susceptible to unfolding in such aqueous organic solutions at acidic pH, particularly during prolonged exposure, Lau *et al.* [4] demonstrated that the primary cause of protein unfolding during RP-HPLC is the hydro-

0021-9673/92/$05.00

phobicity of the stationary phase which disrupts the hydrophobic interactions stabilizing the native conformation.

RP-HPLC separations of polypeptides have generally been carried out on silica-based matrices containing alkyl (*e.g.*, C_3, C_4, C_8, C_{18}) hydrophobic functional ligands. As hydrophobic interactions play a major role in stabilizing the three-dimensional structure of a protein, it is not surprising that the hydrophobicity of such matrices (especially considering the relatively high hydrocarbon loadings typical of such stationary phases) could unfold a protein on binding to the column. As pointed out by Lau *et al.* [4], this may preclude the purification of multi-subunit proteins or of any proteins where a separation in the native conformation is desired.

The development of hydrophobic interaction chromatography (HIC), another separation method base on hydrophobic interactions between the solute and the stationary phase, was spurred by the tendency of proteins to become unfolded during RP-HPLC [5–7]. For HIC, ligands of lower hydrophobicity, lower ligand densities and aqueous solutions (absence of organic modifier) at neutral pH are used, all with the intention of maintaining a protein in its native conformation. In spite of the milder conditions of this technique compared with RP-HPLC, changes in protein tertiary and/or quaternary structure (the stability of which are heavily dependent on hydrophobic interactions), during HIC cannot be ruled out [7]. In addition, the presence of high concentrations of stabilizing salts characteristic of HIC may necessitate a subsequent desalting step prior to further characterization or application.

A major advantage of RP-HPLC, apart from its powerful resolving capability, is the availability of volatile mobile phases, such as the frequently employed aqueous TFA to TFA–acetonitrile gradient elution system. The utility of such a system combined with maintenance of the native state of a protein is clear. In addition, as proteins vary in their degree of stability, packings with various degrees of hydrophobicity would be extremely useful in protein separations by affecting selectivity due to differential induction of conformational change. Indeed, several researchers [7–11] have observed that changes in sorbent hydrophobicity and/or temperature could be used to improve the resolution of proteins with similar retention times through controlled unfolding of proteins in a protein mixture. However, there are practical limits to decreasing the ligand density of silica-based packings containing functional ligands such as alkyl or phenyl moieties [7], since the effectiveness and capacity of the column would decrease simultaneously.

There have been major advances in recent years in the design and development of stationary phases for RP-HPLC, frequently with a focus on novel concepts and improvement of the stationary phase chemistry of RP-HPLC packings [12,13]. One approach has been to immobilize defined polymer layers at the surface of rigid non-porous inorganic or porous inorganic supports in such a way that a solute impermeable layer results [13,14]. The approach described in this paper involved coating porous or non-porous silica supports with polymethacrylate-based polymers or copolymers, such materials lending themselves well for the preparation of stationary phases of controlled hydrophobicity. Employment of monodisperse non-porous silica particles enabled us to take advantage of the rapid analysis times and high recovery of biopolymers typical of such packings, because with such micropellicular sorbents the chromatographic interactions are limited to the outer surface [14–17]. The more commonly employed porous silica support, in addition to its greater sample capacity compared with non-porous silica, also serves as a useful comparison with the micropellicular packings. From the observed RP-HPLC chromatographic profiles of protein mixtures, we have demonstrated the potential value of the novel concept of employing stationary phases with a range of hydrophobicities for both analytical and preparative protein separations.

EXPERIMENTAL

Materials

HPLC-grade water and acetonitrile were obtained from J. T. Baker (Phillipsburg, NJ, USA) and HPLC-grade TFA from Pierce (Rockford, IL, USA). Cyclohexanol, toluene, sodium perchlorate and ammonium sulphate were obtained from Fisher (Fairlawn, NJ, USA). 1,4-Dioxane and sodium chloride were obtained from BDH (Vancouver, BC, Canada). *n*-Pentane was obtained from E. Merck (Darmstadt, Germany), methanol from E. Merck

and J. T. Baker and dicumyl peroxide (DCP) from Aldrich Chemie (Steinheim, Germany). Equine cytochrome *c*, chicken lysozyme and equine myoglobin were obtained from Sigma (St. Louis, MO, USA). Rabbit skeletal whole troponin, troponin C (TnC), troponin I (TnI) and troponin T (TnT) were prepared from tissue extracts in the laboratory of R. S. Hodges.

Apparatus

The HPLC instrument consisted of a Hewlett-Packard (Avondale, PA, USA) HP1090 liquid chromatograph, coupled to an HP1040A detection system, HP9000 Series 300 computer, HP9133 disc drive, HP2225A Thinkjet printer and HP7440A plotter. Columns were packed by means of a Shandon (Sewickley, PA, USA) or a Haskel (Burbank, CA, USA) packing pump.

Supports

Monospher (non-porous silica; 1.7-μm mean particle diameter) and LiChrospher (porous silica; 10 μm; 300-Å pore size) supports were obtained from E. Merck.

Preparation of packings

Preparation of silicas. Pretreatment of the non-porous Monospher support was carried out as described by Hanson *et al.* [13]. The porous LiChrospher support did not require prepreparation.

Preparation of prepolymer of poly(2-hydroxyethyl methacrylate) (P2HEMA). A mixture of 2-hydroxyethyl methacrylate (2-OH-EMA) (20 g) and DCP (0.25 g), the radical starter, was heated under reflux at 100°C for 75 min and cooled, producing oligo-2-OH-EMA, a prepolymer soluble in methanol.

Preparation of precopolymer of ethyl methacrylate–2-hydroxyethyl methacrylate (P2HE-E) copolymer. A mixture of ethyl methacrylate (EMA) (10 g), 2-OH-EMA (10 g) and DCP (0.25 g) was heated under reflux at 100°C for 75 min and cooled, producing oligo-EMA–2-OH-EMA, a precopolymer soluble in methanol.

Preparation of prepolymer of poly(ethyl methacrylate) (PEMA). A mixture of EMA (20 g) and DCP (0.25 g) was heated under reflex at 100°C for 2 h and cooled, producing oligo-EMA, a prepolymer soluble in both diethyl ether and toluene.

Preparation of precopolymer of octadecylmethacrylate–methylmethacrylate copolymer (POMA). Octadecyl methacrylate (OMA) (10 g), a solid at room temperature, was dissolved together with DCP (0.25 g) in methyl methacrylate (MMA) (10 g), heated under reflux for 3 h and cooled. The resulting oligo-OMA–MMA copolymer (25% OMA–75% MMA) was soluble in *n*-pentane.

Coating of silica supports

Monospher. Monospher beads (30 g) were added to a solution of prepolymer (0.3 g) and DCP (15 mg) in 50 ml of the relevant solvent.

LiChrospher. LiChrospher beads (15 g) were added to a solution of prepolymer (1.5 g) and DCP (76 mg) in 50 ml of the relevant solvent.

Following evaporation of the solvent, the coating procedure was carried out as described by Hanson *et al.* [13].

The formulae of the immobilized polymers and copolymers are shown in Fig. 1. Relative hydro-

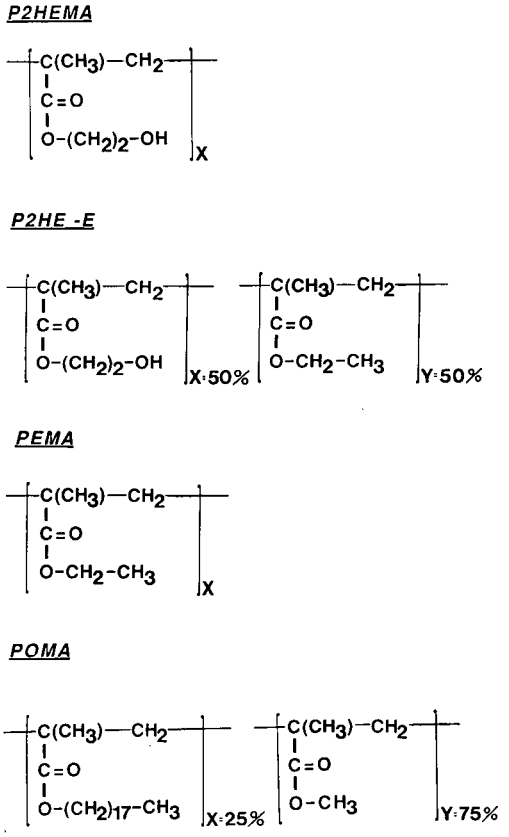

Fig. 1. Structures of methacrylate-based stationary phases synthesized in this study.

phobicities of these packings are P2HEMA < P2HE-E < PEMA < POMA. It should be stressed that these procedures produce stationary phases where the polymers and copolymers are adsorbed on the surface of the supports and are not covalently linked to the silicas in any way.

Clean-up procedure

Monospher. The polymers and copolymer-loaded Monospher supports were cleaned as described by Hanson *et al.* [13].

LiChrospher. The coated LiChrospher supports were subjected to a sedimentation process in toluene–1,4-dioxane, followed by the procedure described by Hanson *et al.* [13] for Monospher packings, except for the elimination of a sonication step.

Column packing

Monospher. Monospher packings were suspended in 1,4-dioxane–toluene–cyclohexanol (1:1:1, v/v/v) and packed by the downward flow method into stainless-steel columns (36 × 4.6 mm I.D.) (Bischoff, Leonberg, Germany) at a packing pressure of 600 bar, using methanol as packing solvent.

LiChrospher. LiChrospher packings were packed identically with the Monospher packings, except that a packing pressure of 350 bar was used.

RESULTS AND DISCUSSION

The reversed-phase packings described above were applied to the separation of two groups of proteins:

(1) Lysozyme, cytochrome *c* and myoglobin: this mixture of monomeric proteins provides a criterion for evaluating the effects of different column packings on changes in protein tertiary structure. These three proteins have frequently been utilized for such purposes [7,10,11]. Myoglobin is particularly useful for demonstrating solvent and/or stationary phase effects on tertiary structure due to the presence of a non-covalently bound haeme group (detectable at 400 nm). In contrast, the haeme of cytochrome *c* is covalently bound to the polypeptide portion of the molecule. Lysozyme is also an ideal protein for these studies as it exists only in two forms (unfolded or native) during chromatography. In addition, they serve to highlight the utility of polymethacrylate-coated silicas for analytical protein separations through selective protein unfolding.

(2) Rabbit skeletal troponin (Tn), consisting of troponin T (TnT), troponin I (TnI) and troponin C (TnC): this thin filament muscle protein, containing three protein subunits, permits the evaluation of the effects of column packings on the chromatographic behaviour of a multi-protein complex stabilized only by non-covalent interactions. In addition, they illustrate potential preparative applications of polymethacrylate-coated silica.

Application of polymethacrylate-coated silicas to analytical protein separations

Fig. 2 shows the changes in the elution profile of the mixture of lysozyme, cytochrome *c* and myoglobin on non-porous (Monospher), polymer-coated packings of varying hydrophobicity (P2HEMA < PEMA < POMA; Fig. 2A, B and C, respectively). The protein mixture was dissolved in water instead of the starting eluent of 0.05% aqueous TFA (pH 2). Although it has been demonstrated that neither lysozyme nor myoglobin is unfolded in 0.1% aqueous TFA [7,11], it was felt that the stability of even these two proteins would be better assured in the absence of acid prior to their injection on the columns.

From Fig. 2, there is a dramatic effect of packing hydrophobicity on the chromatographic profile of the protein mixture, as evidenced by the change in protein elution order as the relative hydrophobicity of the packing is increased. The elution order on the least hydrophobic packing, P2HEMA (Fig. 2A), is native lysozyme (Ln) followed by cytochrome *c* and myoglobin. As the hydrophobicity of the packing is increased to PEMA (Fig. 2B), although the same basic elution order as that observed on P2HEMA is maintained, there is now the appearance of the denatured (unfolded) lysozyme (Ld) peak between cytochrome *c* and myoglobin. As the packing hydrophobicity is increased further to POMA (Fig. 2C), the elution order is now cytochrome *c*, lysozyme (Ld) and myoglobin, with no native lysozyme remaining in the elution profile. On the P2HEMA packing, lysozyme is maintained in its native (folded) state. The surface of a protein is considerably less hydrophobic than its interior, where the majority of hydrophobic residues are located, hence the native lysozyme molecule is eluted prior to the unfolded molecule, where all formerly interior residues are now fully exposed. A similar switch in elu-

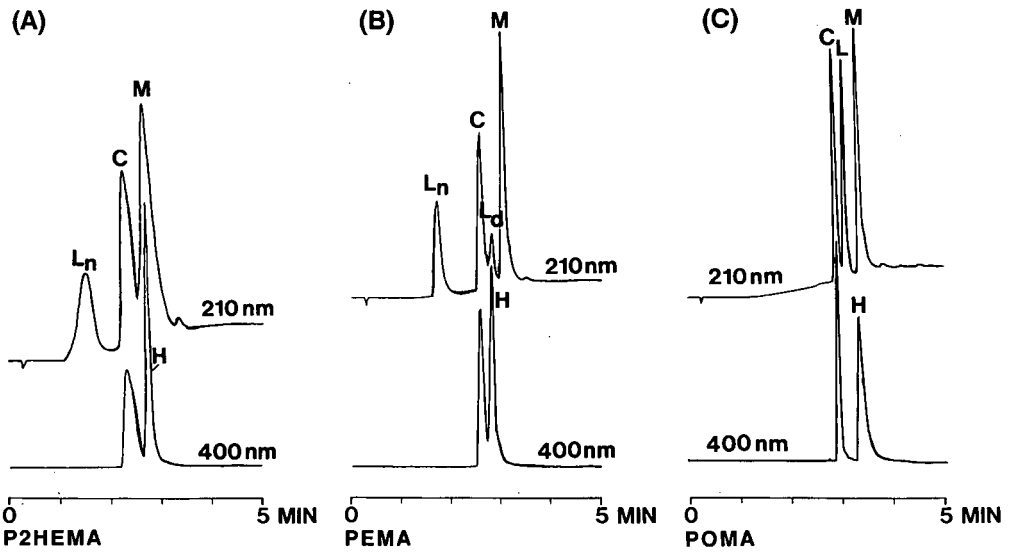

Fig. 2. Effect of hydrophobicity of non-porous Monospher packings on RP-HPLC elution profiles of proteins. (A), (B) and (C) show the elution profiles obtained on the P2HEMA, PEMA and POMA packings, respectively. Mobile phase, linear A–B gradient (20% acetonitrile/min) at a flow-rate of 1 ml/min, where A is 0.05% aqueous TFA and B is 0.05% TFA in acetonitrile; temperature, 25°C. Ln, Ld, C, M and H denote, native lysozyme, denatured lysozyme, cytochrome *c*, myoglobin and haeme, respectively. Sample mixture dissolved in water.

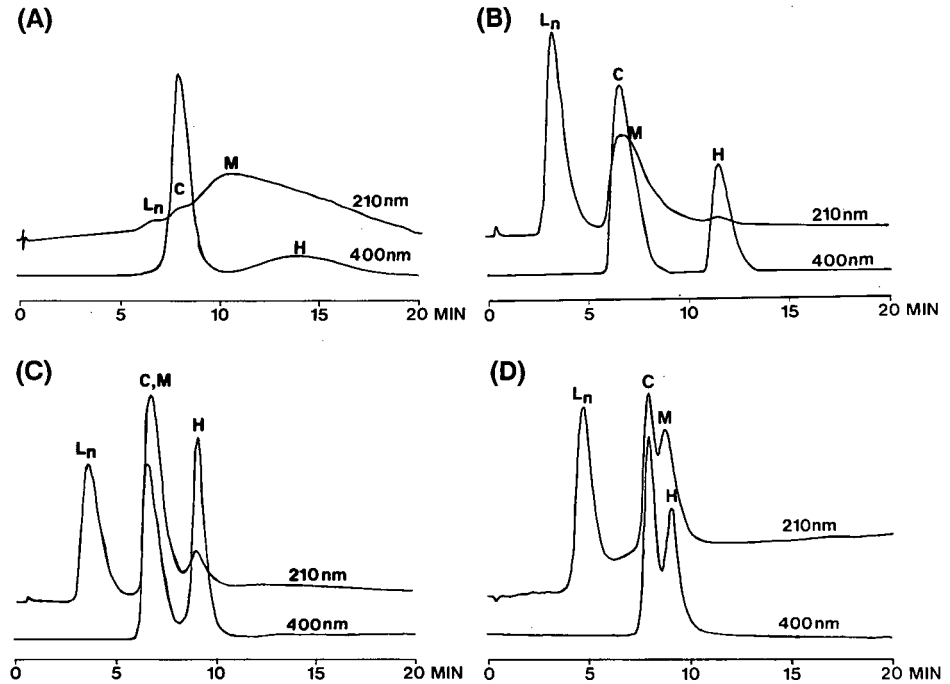

Fig. 3. RPC of proteins on porous LiChrospher P2HEMA packing. Mobile phase: (A) linear A–B gradient (4% acetonitrile/min) at a flow-rate of 1 ml/min, where A is 0.05% aqueous TFA and B is 0.05% TFA in acetonitrile; (B), (C) and (D), linear A–B gradient (4% acetonitrile/min) at a flow-rate of 1 ml/min, where A is 0.05% aqueous TFA and B is 0.05% TFA in 50% aqueous acetonitrile (B), 60% aqueous acetonitrile (C) or 80% aqueous acetonitrile (D), both solvents containing 0.1 *M* $(NH_4)_2SO_4$ (B), 0.1 *M* NaCl (C) or 0.1 *M* $NaClO_4$ (D); temperature, 25°C. The different proportions of acetonitrile to water in solvent B are due to the different solubilities of the various salts. Ln, C, M and H denote lysozyme, cytochrome *c*, myoglobin and haeme, respectively. Sample mixture dissolved in water.

tion order of these three proteins was reported by Mant and Hodges [11] when comparing two silica-based hydrophobic interaction packings differing only in the ligand density of the phenyl functional groups.

The conformational states of cytochrome *c* and myoglobin on the P2HEMA packing cannot be confirmed. The sharpness of the haeme peak of myoglobin compared with the broader myoglobin peak (in contrast to cytochrome *c*, where the protein and haeme peaks are very similar) suggests that this non-covalently bound group may be acting independently from the polypeptide chain, *i.e.*, although the haeme group and the polypeptide portion of myoglobin (apomyoglobin) are co-eluted on the P2HEMA packing under the conditions employed, the myoglobin has probably been either partially or totally unfolded. The different retention times of the haeme group and apomyoglobin on the PEMA and POMA packings indicate unfolding of myoglobin on these more hydrophobic stationary phases.

Fig. 3 illustrates the effect of salt on the chromatographic behaviour of the three proteins on the porous LiChrospher P2HEMA packing. The satisfactory performance of the Monospher P2HEMA packing (Fig. 2A) in separating the three proteins indicated that the responsibility for the poor elution profile shown in Fig. 3A (obtained by a conventional aqueous TFA to TFA–acetonitrile gradient) may lie with the porous LiChrospher support rather than the methacrylate polymer coating. Badly tailing and skewed peaks are frequently the result of non-ideal reversed-phase column behaviour in the form of electrostatic, in addition to hydrophobic, solute–packing interactions. It is well known that underivatized and ionized (negatively charged) silanols on conventional silica-based packings (e.g., alkyl- or phenyl-bonded packings) may cause such non-ideal behaviour [1,2,18]. Even though the low pH (pH 2) of TFA-based mobile phases should ensure protonation of these silanols, this is not always the case [18]. In this study, the silanols on the silica supports were not covalently linked to a functional ligand. Instead, the supports were coated with methacrylate-based polymers. With such packings, it is known that polymer film thickness will affect packing hydrophobicity [13]. The film thicknesses (and carbon coverage/m^2) of the packings prepared in this study were minimized to ensure that the individual stationary phases were not too hydrophobic, as selective protein denaturation was the goal. Owing to the synthesis process, a minimum of *ca.* 1% (w/w) of polymer is required to produce a satisfactory coating on the non-porous Monospher support. As a compromise, for the porous LiChrospher material, 10% (w/w) of polymer was employed during synthesis, with a concomitant loss of some polymer during the synthesis process. This results in a higher relative overall coverage of the Monospher support compared with that of the LiChrospher silica, as the non-porous particles have a much lower interactive surface area compared with the porous silica. Hence it is possible that, whereas the polymer coverage of the Monospher particles was sufficient to prevent potential silanol problems, this was not the case with the porous LiChrospher support.

The addition of almost any salt to the mobile phase will suppress undesired electrostatic solute–packing interactions during RP-HPLC, thereby improving the chromatographic profile [1,2,19]. Fig 3B, C and D show the effects on the protein chromatographic profiles of adding ammonium sulphate, sodium chloride and sodium perchlorate respectively, (all at a 0.1 *M* concentration) to the mobile phase. Although the presence of all three salts produced improved the chromatographic profiles over those obtained in their absence (Fig. 3A), their effectiveness varied considerably. Thus, there was improved peak shape on substituting sodium chloride (Fig. 3C) for ammonium sulphate (Fig. 3B). Whereas lysozyme remains in its native state (Ln), as observed previously on the Monospher P2HEMA packing (Fig. 2A), myoglobin is clearly unfolded, with its haeme group eluted independently of apomyoglobin. Cytochrome *c* and apomyoglobin are co-eluted in the presence of either of these two salts. Not only is there a further improvement in protein peak shape with the addition of sodium perchlorate to the mobile phase (Fig. 3D), but cytochrome *c* and myoglobin are now partly resolved, resulting in the same elution order as that observed on the Monospher P2HEMA packing (Fig. 2A).

Fig. 4 shows the chromatographic profiles of the protein mixture obtained on LiChrospher packings of increasing hydrophobicity (P2HEMA < P2HE-E < PEMA < POMA; Fig. 4A, B, C and D, respectively) in the presence of 0.1 *M* sodium per-

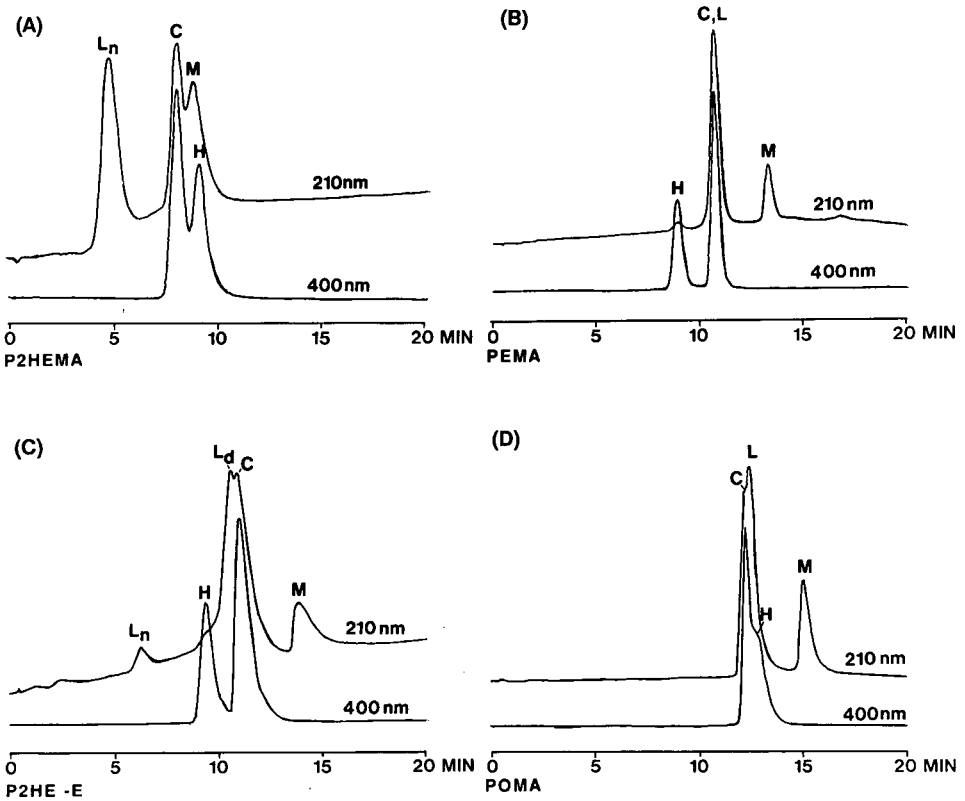

Fig. 4. Effect of hydrophobicity of porous LiChrospher packings Si 300 (10 μm) on RP-HPLC elution profiles of proteins. (A), (B), (C) and (D) show the elution profiles obtained on the P2HEMA, PEMA, P2HE-E and POMA packings, respectively. Mobile phase, linear A–B gradient (4% acetonitrile/min) at a flow-rate of 1 ml/min, where A is 0.05% aqueous TFA and B is 0.05% TFA in 80% aqueous acetonitrile, both A and B containing 0.1 *M* $NaClO_4$; temperature, 25°C. Ln, Ld, C, M and H denote native lysozyme, denatured lysozyme, cytochrome *c*, myoglobin and haeme, respectively. Sample mixture dissolved in water.

chlorate. In a similar manner to that observed for the Monospher packings (Fig. 2), there is a switch in elution order of the three proteins between the P2HEMA packing (Fig. 4A) (native lysozyme, followed by cytochrome *c* and, finally, myoglobin) and the POMA packing (Fig. 4D) (cytochrome *c*, followed by unolded lysozyme and, finally, myoglobin), although, under the run conditions employed, cytochrome *c* and denatured lysozyme are barely separated on the latter column. However, the P2HE-E and PEMA packings exhibit some interesting intermediate profiles. On the P2HE-E column, most of the lysozyme is now eluted in its unfolded form just prior to cytochrome *c*. With the PEMA packing, all of the lysozyme is now in its unfolded form, and is co-eluted entirely with cytochrome *c*. The latter observation is in contrast to the elution behaviour of lysozyme on the Monospher PEMA packing, where the protein is eluted in only a partially unfolded state (Fig. 2B). This apparent greater stability of lysozyme on the Monosper packing compared with the LiChrospher PEMA packing may be due to the inherent properties of the porous packing material (Fig. 4C) compared with the Monospher column (Fig. 2B). Apart from the changes in the chromatographic patterns of the three proteins on the four porous packings, there are also selectivity differences between the non-porous and porous versions of the same polymer coatings even allowing for the different run conditions employed on the porous and non-porous packings. This is especially clear from the elution behaviour of cytochrome *c* and unfolded lysozyme on the LiChrospher PEMA and POMA packings (Fig. 4)

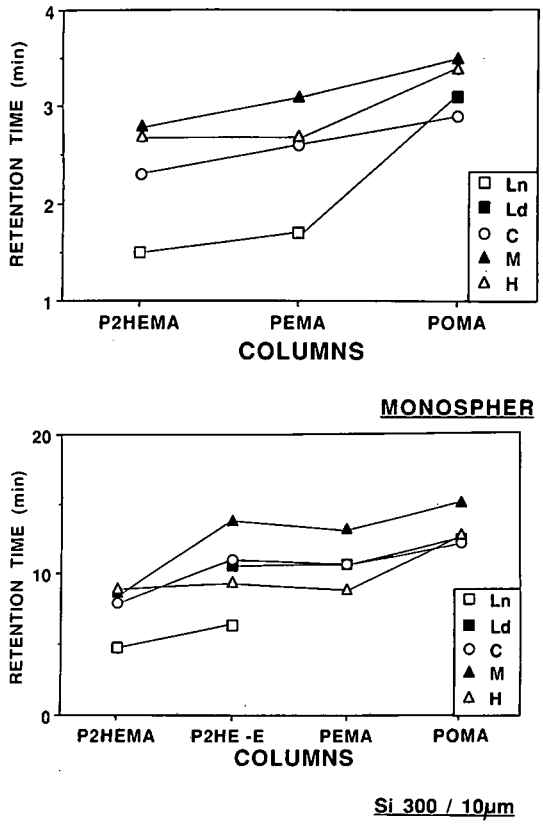

Fig. 5. Summary of stationary phase selectivities for RP-HPLC separation of lysozyme, cytochrome *c* and myoglobin. Mobile phase: Monospher packings, see Fig. 2; LiChrosper packings, see Fig. 4. □ = Ln; ■ = Ld; ○ = C; ▲ = M; and △ = H, denoting, native lysozyme, denatured lysozyme, cytochrome *c*, myoglobin and haeme, respectively.

compared with that observed on their Monospher counterparts (Fig. 2).

Fig. 5 summarizes the retention behaviour of the three proteins on the LiChrospher and Monospher packings. As might be expected, there is a general increase in protein retention times on both series of packings as the hydrophobicity of the polymer coating is increased from P2HEMA to PEMA to POMA. The most dramatic increase occurs with lysozyme as it is converted from its native (□) to its denatured (■) form.

Selective unfolding of proteins by temperature manipulation

Although the primary cause of protein unfolding in standard RPC is the hydrophobicity of a reversed-phase matrix, changes in temperature can also have a dramatic effect on protein stability [2,7,8,10,11]. Proteins are increasingly unfolded as the temperature is raised, the extent of thermally induced unfolding being dependent on the lability of the specific protein involved. Indeed, several researchers have noted that differences on protein lability to temperature changes could be used to improve resolution of proteins with similar retention times [2,7,8,10,11]. Thus, it was felt that temperature manipulation during RP-HPLC of proteins on a specific polymer-coated support, as opposed to their resolution on packings of varying hydrophobicity, may add another dimension to the utility of the stationary phases described in this study.

As an initial test of this approach to RP-HPLC of proteins, lysozyme was subjected to RP-HPLC on the LiChrospher P2HEMA packing at temperatures ranging from 25 to 40°C (Fig. 6A). The P2HEMA stationary phase was chosen as lysozyme had been shown to be in its native state on this packing at room temperature (25°C) (Figs. 3D and 4A). From Fig. 6, a progressive unfolding of lysozyme (native lysozyme, Ln, to unfolded lysozyme, Ld) is observed as the temperature is raised from 25 to 40°C. At 25°C, lysozyme is in a fully native state (Ln), unfolding to a fully unfolded state (Ld) at

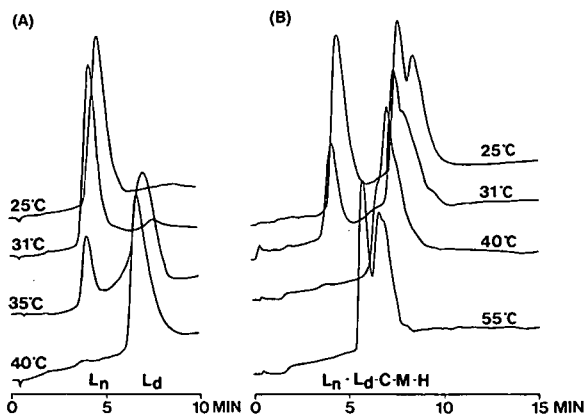

Fig. 6. Effect of temperature on RP-HPLC elution profiles of proteins on porous LiChrospher P2HEMA packing. (A) Lysozyme only; (B) mixture of lysozyme, cytochrome *c* and myoglobin. Mobile phase, linear A–B gradient (4% acetonitrile/min) at a flow-rate of 1 ml/min, where A is 0.05% aqueous TFA and B is 0.05% TFA in 80% aqueous acetonitrile; temperatures as indicated; absorbance at 210 nm. Samples dissolved in water.

40°C, as evidenced by the increase in protein retention time at the higher temperature. Intermediate temperatures of 31°C and, particularly, 35°C, produced chromatographic profiles indicating the presence of both native and unfolded lysozyme.

Fig. 6B shows the effect of increasing temperature on the resolution of the three-protein mixture (lysozyme, cytochrome *c* and myoglobin). Protein retention times in RP-HPLC generally decrease with increasing temperature, owing to increasing solubility of the solute in the mobile phase as the temperature rises [7,10,11,20,21]. In addition sharper protein peaks, often leading to improved resolution due to a more rapid transfer of the solutes between the stationary and mobile phases, generally accompanies a rise in temperature. It is apparent from Fig. 6B that there is indeed an overall sharpening of peptide peaks with an increase in temperature, together with a decrease in retention times of the two proteins (cytochrome *c* and myoglobin) already denatured at room temperature (25°C). However, the resolution of this particular peptide mixture is clearly not improved with increase in temperature, owing to the gradual appearance of unfolded lysozyme in an elution position close to the other two proteins. Wider band widths at room temperature are offset by the excellent separation of lysozyme from the other two proteins owing to the maintenance of its native state. Hence, although temperature manipulation during RP-HPLC of proteins may undoubtedly complement the selective protein unfolding properties of a stationary phase, this approach must be tailored to the specific protein mixture under investigation.

Application of polymethacrylate-coated silicas to preparative purification of proteins in their native conformation

The maintenance of the native protein during the preparative purification of proteins is frequently of concern to researchers, particularly where retention of biological acitivity is desired. The results of this study (Figs. 2–6) (reflecting similar observations of other researchers [7,10,11]) have demonstrated that the native state of proteins may be maintained during RP-HPLC through the employment of a mildly hydrophobic stationary phase and/or low temperatures, suggesting a potential preparative role for such packings. To test this potential further, polymethacrylate-coated silicas were applied to RP-HPLC of a multi-protein complex (stabilized by non-covalent interactions), rabbit skeletal troponin (RsTn), which was felt to be an even greater challenge than isolation of a single monomeric protein in its native conformation.

Isolation of RsTn and its individual protein components (TnT, TnI, TnC) had traditionally been carried out by classical open-column techniques, generally employing combinations of chromatography on ion-exchange resins [22–24]. However, as Cachia *et al.* [25] pointed out, these methods of purification are time consuming and result in the dispersion of the desired product(s) in large volumes of column effluent. The denaturing character of RP-HPLC has so far precluded advantage being taken of the powerful resolving capability of this technique for purifications of this kind.

Fig. 7 shows the elution profile of whole RsTn on Monospher P2HEMA (Fig. 7B), comparing it with the elution profiles of the three individual subunits run separately (Fig. 7A). Although maintenance of the three-protein complex is achieved at 5°C (also the temperature at which the individual subunits were chromatographed), as evidenced by the single peak, gradual dissociation of the subunits was evident as the temperature was raised.

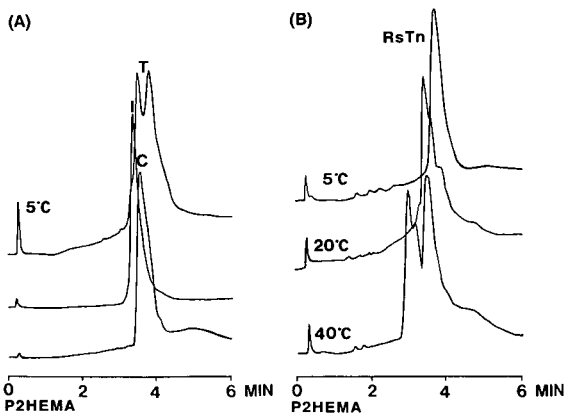

Fig. 7. RP-HPLC of rabbit skeletal whole troponin (RsTn) and individual subunits (TnI, TnT, TnC) on non-porous Monospher packings. (A) Subunits run individually on P2HEMA; (B) whole troponin run on P2HEMA. Mobile phase, linear A–B gradient (16% acetonitrile/min) at a flow-rate of 1 ml/min, where A is 0.05% aqueous TFA and B is 0.05% TFA in 80% aqueous acetonitrile, both A and B containing 0.1 *M* $NaClO_4$; temperatures as indicated; absorbance at 210 nm. Samples dissolved in water.

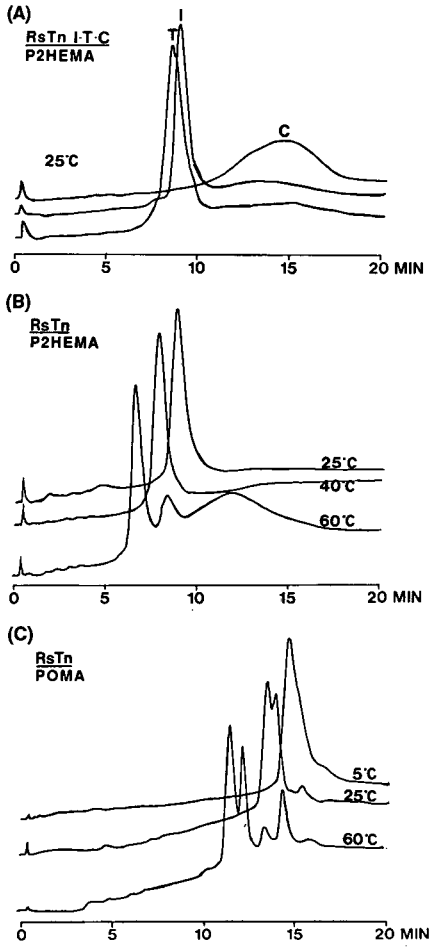

Fig. 8. RP-HPLC of rabbit skeletal whole troponin (RsTn) and individual subunits (TnI, TnT, TnC) on porous LiChrospher Si 300 (10 μm) packings. (A) Subunits run individually on P2HEMA; (B) whole troponin complex run on P2HEMA; (C) whole troponin complex run on POMA. Mobile phase, linear A–B gradient (4% acetonitrile/min) at a flow-rate of 1 ml/min, where A is 0.05% aqueous TFA and B is 0.05% TFA in 80% aqueous acetonitrile, both A and B containing 0.1 *M* $NaClO_4$; temperatures as indicated; absorbance at 210 nm. Samples dissolved in water.

The results in Fig. 8 suggest that the complex is even more stable on the LiChrospher P2HEMA packing, with a single peak being maintained even at 40°C (Fig. 8B). At first glance, this interesting observation is unexpected because, all other things being equal, non-porous materials are usually deemed to be less denaturing than porous materials, owing to an absence of pore effects. However, an explanation may lie with the original preparation of the packings. Thus, a minimum of *ca.* 1% (w/w) of polymer was employed to ensure a complete coating on the non-porous Monospher silica support (see Experimental). On the porous LiChrospher material, 10% (w/w) of polymer was employed (with concomitant loss of material during the prepolymer synthesis process), resulting in a lower value of % carbon/m^2 of support surface area compared with the Monospher material, *i.e.*, it is possible that, in this instance, the porous material is potentially less denaturing than the Monospher packings. The decrease in the retention time of the complex at 40°C compared with 25°C is consistent with previous observations of the effect of temperature on RP-HPLC elution profiles [7,10,11,20,21]. It is interesting that even on the LiChrospher POMA packing (Fig. 8C), containing the most hydrophobic polymer coating synthesized, it appears that the multi-protein complex may be maintained (if only barely, considering the broadness of the peak) at low temperature (5°C).

CONCLUSIONS

We have evaluated the potential of a novel concept for protein separations by reversed-phase chromatography on non-porous and porous polymethacrylate-coated silicas. Selective unfolding of proteins was achieved by varying the hydrophobicity of the polymer coat, permitting manipulation of the chromatographic pattern of analytical protein separations. In addition, it was also demonstrated that maintenance of the native state of a multi-protein complex, stabilized by non-covalent interactions, should be possible during preparative isolation. The results of this preliminary study, together with a companion paper which further characterizes these packings through their employment for separations of model peptides [26], suggests that the potential of these packings for polypeptide separations is very promising.

ACKNOWLEDGEMENTS

This work was supported by the Medical Research Council of Canada Group in Protein Structure and Function and the Deutsche Forschungsgemeinschaft (DFG) and by equipment grants from

the Alberta Heritage Foundation for Medical Research. We acknowledge the International Association for the Exchange of Students for Technical Experience (IAESTE) for enabling M. H. to spend 6 months in the laboratory of R. S. H.

REFERENCES

1 C. T. Mant and R. S. Hodges, in K. M. Gooding and F. E. Regnier (Editors), *High-Performance Liquid Chromatography of Biological Macromolecules: Methods and Applications*, Marcel Dekker, New York, 1990, p. 301.
2 C. T. Mant and R. S. Hodges (Editors), *HPLC of Peptides and Proteins: Separation, Analysis and Conformation*, CRC Press, Boca Raton, FL, 1991.
3 K. D. Nugent, in C. T. Mant and R. S. Hodges (Editors), *High-Performance Liquid Chromatography of Peptides and Proteins: Separation, Analysis and Conformation*, CRC Press, Boca Raton, FL, 1991, p. 279.
4 S. Y. M. Lau, A. K. Taneja and R. S. Hodges, *J. Chromatogr.*, 317 (1984) 129.
5 J. L. Fausnaugh, E. Pfannkoch, S. Gupta and F. E. Regnier, *Anal. Biochem.*, 137 (1984) 464.
6 J. L. Fausnaugh, L. A. Kennedy and F. E. Regnier, *J. Chromatogr.*, 317 (1984) 141.
7 R. H. Ingraham, S. Y. M. Lau, A. K. Taneja and R. S. Hodges, *J. Chromatogr.*, 327 (1985) 77.
8 L. R. Snyder, *J. Chromatogr.*, 179 (1979) 167.
9 R. A. Barford, B. J. Sliwinski, A. C. Breyer and H. L. Rothbart, *J. Chromatogr.*, 235 (1982) 281.
10 C. T. Mant, N. E. Zhou and R. S. Hodges, *J. Chromatogr.*, 476 (1989) 363.
11 C. T. Mant and R. S. Hodges, in C. T. Mant and R. S. Hodges (Editors), *High Performance Liquid Chromatography of Peptides and Proteins: Separation, Analysis and Conformation*, CRC Press, Boca Raton, FL, 1991, p. 437.
12 K. K. Unger (Editor), *Packings and Stationary Phases in Chromatographic Techniques*, Marcel Dekker, New York, 1990.
13 M. Hanson, K. K. Unger and G. Schomburg, *J. Chromatogr.*, 517 (1990) 269.
14 K. K. Unger, in K. K. Unger (Editor), *Packings and Stationary Phases in Chromatographic Techniques*, Marcel Dekker, New York, 1990, p. 331.
15 K. K. Unger, G. Jilge, J. N. Kinkel and M. T. W. Hearn, *J. Chromatogr.*, 359 (1986) 61.
16 K. Kalghatgi and Cs. Horváth, *J. Chromatogr.*, 398 (1987) 335.
17 Y.-F. Maa and Cs. Horváth, *J. Chromatogr.*, 445 (1987) 71.
18 C. T. Mant and R. S. Hodges, *Chromatographia*, 24 (1987) 805.
19 W. S. Hancock and D. R. K. Harding, in W. S. Hancock (Editor), *Handbook of HPLC for the Separation of Amino Acids, Peptides and Proteins*, Vol. 2, CRC Press, Boca Raton, FL, 1984, p. 3.
20 W. C. Mahoney and M. A. Hermodson, *J. Biol. Chem.*, 255 (1980) 11199.
21 K. A. Cohen, K. Schellengerg, K. Benedek, B. L. Karger, B. Grego and M. T. W. Hearn, *Anal. Biochem.*, 140 (1984) 223.
22 M. L. Greaser and J. Gergeley, *J. Biol. Chem.*, 246 (1971) 4226.
23 M. L. Greaser and J. Gergeley, *J. Biol. Chem.*, 248 (1973) 2125.
24 P. C. S. Chong and R. S. Hodges, *J. Biol. Chem.*, 256 (1981) 5064.
25 P. J. Cachia, J. Van Eyk, W. D. McCubbin, C. M. Kay and R. S. Hodges, *J. Chromatogr.*, 343 (1985) 315.
26 M. Hanson, K. K. Unger, C. T. Mant and R. S. Hodges, *J. Chromatogr.*, 599 (1992) 77.

Journal of Chromatography, 599 (1992) 77–85
Elsevier Science Publishers B.V., Amsterdam

CHROMSYMP. 2551

Polymer-coated reversed-phase packings with controlled hydrophobic properties

II. Effect on the selectivity of peptide separations

Michael Hanson and Klaus K. Unger

Institut für Anorganische und Analytische Chemie, Johannes Gutenberg-Universität, 6500 Mainz (Germany)

Colin T. Mant and Robert S. Hodges*

Department of Biochemistry and the Medical Research Council of Canada Group in Protein Structure and Function, University of Alberta, Edmonton, Alberta T6G 2H7 (Canada)

ABSTRACT

We have designed and synthesized novel reversed-phase packings of non-porous and porous polymethacrylate-coated silicas. By varying the hydrophobicity of the polymer coating, selective unfolding of polypeptides may be achieved, thus enabling manipulation of the chromatographic profile. This study characterizes these packings through their employment for separations of model synthetic peptides of defined secondary, tertiary and quaternary structure. Thus, the packings were applied to the reversed-phase separation of α-helical amphipathic and non-amphipathic peptides of the same amino acid composition but different sequences. In addition, selective unfolding of model two-stranded α-helical coiled-coil peptides was achieved with these packings. Through the observation of the chromatographic behaviour of these model peptides on the various polymethacrylate-coated silicas, we were able to confirm the potential of such tailored packings for separations of peptides and proteins.

INTRODUCTION

We have previously evaluated [1] the potential of a novel concept for protein separations by reversed-phase high-performance liquid chromatography (RP-HPLC), where selective unfolding of proteins is achieved by varying the hydrophobicity of the polymer coating on non-porous and porous polymethacrylate-coated silicas. This approach involves manipulation of the chromatographic pattern of a protein mixture containing proteins of different labilities. In addition, maintenance of a multi-protein complex, stabilized by non-covalent interactions, is also possible on such stationary phases.

The present study serves to extend the characterization of these polymer-coated packings through their employment for separations of model synthetic peptides. By observing the chromatographic behaviour of these peptides of defined secondary, tertiary and quaternary structure, we sought to gain further insight into the potential benefits of such packings for polypeptide separations by RP-HPLC.

EXPERIMENTAL

Materials

HPLC-grade water and acetonitrile were obtained from J. T. Baker (Philipsburg, NJ, USA) and HPLC-grade trifluoroacetic acid (TFA) from Pierce (Rockford, IL, USA). Dithiothreitol (DTT) was purchased from Schwarz-Mann Biotech (Cleveland, OH, USA). Potassium chloride and potassium dihydrogenorthophosphate were purchased from BDH (Toronto, Canada).

0021-9673/92/$05.00

Peptides

Peptides were synthesized (structures shown in Table I) on an Applied Biosystems (Foster City, CA, USA) peptide synthesizer, using the general procedure for solid-phase peptide synthesis described by Hodges and co-workers [2,3].

Apparatus

The HPLC instrument consisted of an HP1090 liquid chromatograph (Hewlett-Packard, Avondale, PA, USA) coupled to an HP1040A detection system, HP9000 Series 300 computer, HP9133 disc drive, HP2225A Thinkjet printer and HP7440A plotter.

Reversed-phase packings

Monospher (non-porous silica; 1.7-μm mean particle diamter) and LiChrospher (porous silica; 10 μm; 300-Å pore size) supports from E. Merck (Darmstadt, Germany) were coated with poly-2-hydroxyethylmethacrylate (P2HEMA), polyethylmethacrylate (PEMA) or octadecylmethacrylate–methylmethacrylate copolymer (POMA) as described in ref. 1. The packings were then packed into stainless-steel columns (36 × 4.6 mm I.D.; Bischoff, Leonberg, Germany) as decribed previously [1].

The relative hydrophobicities of these packings are P2HEMA < PEMA < POMA.

RESULTS AND DISCUSSION

Synthetic model peptides

The sequences of two series (G and L series) of synthetic model peptide polymers of 21, 28 and 35 residues employed in this study are shown in Table I. These two series of peptides have the same amino acid composition, but different sequences. Both series of peptides consist of an initial seven-residue sequence containing a cysteine residue [Lys–Cys–Ala–Glu–Gly–Glu–Leu (G series) or Lys–Cys–Ala–Glu–Leu–Glu–Gly (L series)], followed by a repeating seven residue (heptapeptide) repeat: [Lys–Leu–Glu–Ala–Gly–Glu–Leu] for the G series; [Lys–Leu–Glu–Ala–Leu–Glu–Gly] for the L series. All of the synthetic peptides in the present study were acetylated at the N-terminal and amidated at the C-terminal to rule out possible repulsive ionic interactions due to the presence of these end groups. Circular dichroism studies have demonstrated that both sets of peptides have a high potential to form α-helical structure in a non-polar environment, such as the hydrophobic stationary phase of a reversed-phase packing and the organic modifier employed in the mobile phase [4,5]. In Fig. 1, the amino acid sequences of the G and L series peptides are viewed as axial projections of α-helices in an helical wheel. The hydrophobic amino acid residues, *e.g.*, leucine residues, are segregated on one side of the α-helix in L series peptides to form amphipathic helices con-

TABLE I

SYNTHETIC PEPTIDES EMPLOYED IN THIS STUDY

Peptide[a]	Peptide sequence[b]
G21	Ac–Lys–Cys–Ala–Glu–Gly–Glu–Leu–[Lys–Leu–Glu–Ala–Gly–Glu–Leu]$_2$–amide
L21	Ac–Lys–Cys–Ala–Glu–Leu–Glu–Gly–[Lys–Leu–Glu–Ala–Leu–Glu–Gly]$_2$–amide
G28	Ac–Lys–Cys–Ala–Glu–Gly–Glu–Leu–[Lys–Leu–Glu–Ala–Gly–Glu–Leu]$_3$–amide
L28	Ac–Lys–Cys–Ala–Glu–Leu–Glu–Gly–[Lys–Leu–Glu–Ala–Leu–Glu–Gly]$_3$–amide
G35	Ac–Lys–Cys–Ala–Glu–Gly–Glu–Leu–[Lys–Leu–Glu–Ala–Gly–Glu–Leu]$_4$–amide
L35	Ac–Lys–Cys–Ala–Glu–Leu–Glu–Gly–[Lys–Leu–Glu–Ala–Leu–Glu–Gly]$_4$–amide

[a] The "G" and "L" series of peptide polymers represent series of, respectively, non-amphipathic and amphipathic α-helical peptides. For each peptide analogue, the letter represents the series to which it belongs and the number denotes the number of amino acid residues it contains.

[b] Ac = N^{α}-Acetyl; amide = C^{α}-amide. The residues (Gly and Leu) shown between the vertical lines are responsible for the sequence variation of peptides with the same amino acids composition.

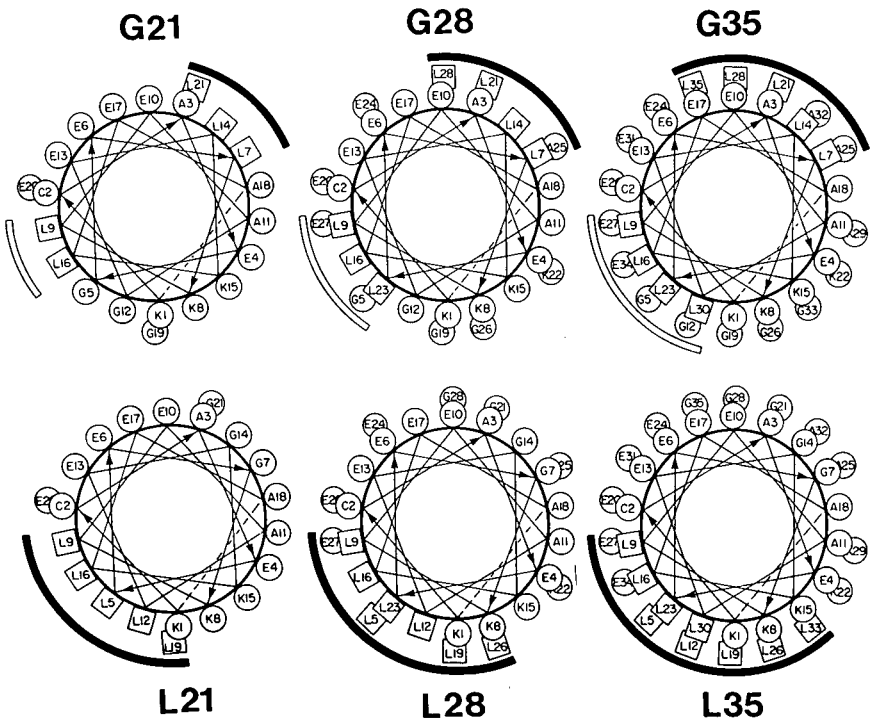

Fig. 1. The amino acid sequence for the G and L series peptides (Table I), represented as helical wheels. The perimeter of a wheel corresponds to the polypeptide backbone and the external circles and squares represent the individual amino acid side chains. The leucine residues are denoted by squares and all other side chains by circles. Since the α-helix has 3.6 residues per turn, adjacent side chains in the sequence are separated by 100° of arc on the wheel. Two hydrophobic surfaces are observed on opposing sides of the helix for the peptides in the G series as indicated by the solid and open bars. The peptides of the L series are amphipathic, containing one dominant hydrophobic surface on one side of the α-helix as indicated by the solid bars. The G and L series peptides are denoted by the letters G and L, respectively, followed by a number which denotes the number of residues in the polypeptide chain.

taining a preferred binding domain [4,5]. In contrast the hydrophobic residues of the G series peptides are more evenly distributed on opposite sides of the α-helix to form non-amphipathic helices.

The sequence about the cysteine residue of the L series peptides (Table I) is identical to that found in tropomyosin (Lys–Cys–Ala–Glu–Leu–Glu), the best understood example of a two-stranded α-helical coiled coil [6–9]. The amino acid sequence of the heptapeptide repeat (Lys–Leu–Glu–Ala–Leu–Glu–Gly) used on the remaining heptads of the L series peptides (Table I) was chosen based on the criteria described by Hodges *et al.* [10]. These criteria were based on the observation that tropomyosin and other two-stranded α-helical coiled-coil proteins were stabilized by hydrophobic residues at positions 2 and 5 of a repeating heptad sequence [(X–N–X–X–N–X–X)$_n$ where N is a non-polar residue]. In the present study, positions 2 and 5 of the repeating heptad of the L series peptides are occupied by Leu residues. Indeed, polymers of a similar heptad sequence, [Lys–Leu–Glu–Ser–Leu–Glu–Ser]$_n$ [10,11] verified the hypothesis of Hodges *et al.* [6] that positions 2 and 5 were responsible for the hydrophobic interactions stabilizing the two-stranded α-helical coiled coils.

The synthetic L-series peptides were deemed to represent an ideal model system for probing the chromatographic properties of the polymer-coated supports described in this study. A straightforward shifting of the residues in the heptad sequences of the amphipathic L series peptides produced the non-amphipathic G series peptides (Table I), enabling a comparison of the ability of the various packing to separate amphipathic and non-amphipathic peptides of the same composition but differ-

ent sequence. The presence of the cysteine residue at position 2 of the first heptad of the L series peptides allows a determination of the effect of varying packing hydrophobicity on the stability of coiled-coil peptides both in the absence and presence of a covalent disulphide bond linking the two polypeptide chains. Finally, the 35-residue L series peptide is small enough for easy synthesis of peptide analogues (and large enough to form a stable three-dimensional structure capable of tolerating sequence changes) [3], allowing an examination of the effect of varying hydrophobicity of the column packing on the stability of peptide analogues, where the one or more leucine residues in the critical 2 and 5 positions of the heptads (Table I) has been substituted with a less hydrophobic residue.

Separation of amphipathic and non-amphipathic peptides of the same amino acid composition but different sequence

Fig. 2 shows the elution profiles of respective pairs of the G and L series peptides on the three chromatographic packings. From a previous study by Hodges and co-workers [4,5], it would be expected that, if the peptides of both series were bound to the reversed-phase packings in their monomeric form, then the amphipathic L series peptides (containing a preferred binding domain) would be eluted later than their respective G series analogues. For the majority of the elution profiles shown in Fig. 2, this is indeed the case, with the POMA packing, particularly, exhibiting good selectivity in separating the monomeric peptide pairs in run times of less than 4 min. However, there is a very interesting selectivity shift for the 35-residue analogues on the P2HEMA packing, the most hydrophilic of the three employed. The elution of peptide L35, which is known to be a coiled-coil dimer in 0.1% aq. TFA [12,13], prior to G35 suggests that the hydrophobic domains of the amphipathic L35 peptide are not being exposed to the P2HEMA packing, *i.e.*, L35 is being maintained as a dimer on this column, even in the absence of a disulphide bond between the L35 monomers. Although Ingraham *et al.* [14] demonstrated that a similar 36-residue peptide was eluted primarily in a dimeric form from an hydrophobic

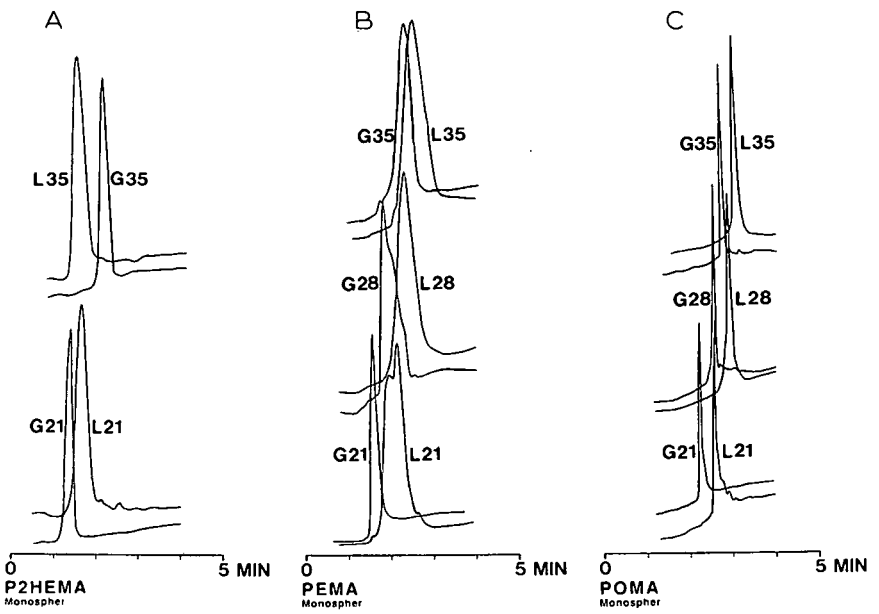

Fig. 2. Reversed-phase chromatography of the G and L series peptides (Table I). Pairs of peptides of the same composition and polypeptide chain length but different sequences were chromatographed on P2HEMA (A), PEMA (B) and POMA (C) packings. Conditions: linear A–B gradient elution (20% acetonitrile/min) at a flow-rate of 1 ml/min, where eluent A is 0.05% aqueous TFA and eluent B is 0.05% TFA in acetonitrile; temperature, 26°C. The peptides were dissolved in 0.05% aq. TFA containing 10 m*M* DTT prior to application to the columns to ensure that the peptides remained in their reduced form.

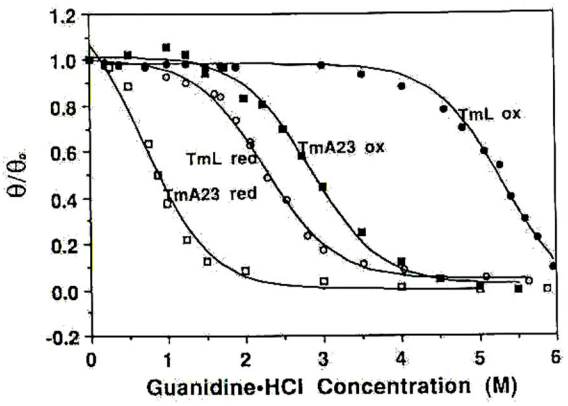

Fig. 3. Guanidine hydrochloride denaturation profiles of synthetic peptide analogues in 0.1 *M* KCl, 0.05 *M* orthophosphate buffer, pH 7. θ/θ_0 represents the ratio of the ellipticity at 220 nm at the indicated molarity of guanidine hydrochloride to the ellipticity without guanidine hydrochloride. TmL Red and TmL Ox refer to the reduced and oxidized forms of peptide L35 (Table I), respectively; TmA23 Red and TmA23 Ox refer to the reduced and oxidized forms of peptide TmA23, respectively, where the leucine at position 23 of TmL has been substituted by alanine.

interaction chromatography column operated in reversed-phase mode, the maintenance of this dimeric state required temperatures as low as 0°C. Even under these conditions, some breakdown of quaternary structure was evident. In contrast, no disruption of the quaternary structure of the 35-residue L series peptide was evident on the P2HEMA packing, even at room temperature. The elution of peptide L21 after its non-amphipathic analogue, G21, could be expected, since the amphipathic L21 is already monomeric in the starting solvent [12,13].

Selective unfolding of model two-stranded α-helical coiled-coil peptides by polymethacrylate-coated packings

The 35-residue L series peptide (now termed TmL) was chosen as the model polypeptide for further characterization of the polymer-coated packings. The effect of the packings on the chromatographic behaviour of the reduced (TmL Red) and oxidized, *i.e.*, disulphide-bridged (TmL Ox) forms of TmL was determined. In addition, an analogue of TmL, denoted TmA23, where the leucine residue at position 23 was substituted by an alanine residue, was also employed. In order to rationalize subsequent peptide chromatographic behaviour, it was necessary to establish, by non-chromatographic means, the relative stabilities of the dimeric forms of the reduced and oxidized forms of the TmL and TmA23 polypeptides.

Stability of coiled-coil dimers of TmL and TmA23. Fig. 3 shows the guanidine hydrochloride denaturation profiles of the oxidized and reduced forms of TmL and TmA23. In non-denaturing (benign) medium, both the reduced and oxidized forms of the two peptides are two-stranded α-helical coiled-coils. However, the effect of increasing concentrations of the denaturating guanidine hydrochloride on the dimers differs dramatically depending upon the stability of the α-helical coiled coils. Clearly, the oxidized, disulphide bridged forms of the TmL and TmA23 are more stable than their respective reduced forms, as evidenced by the higher concentrations of guanidine hydrochloride required to produce the same drop in ellipticity ratio for the oxidized coiled-coils compared to their reduced forms. The marked positive impact of a disulphide bridge to coiled-coil stability has been previously demonstrated by Hodges and co-workers [3,15]. Also clear is the decrease in coiled-coil stability resulting from the leucine to alanine substitution at position 23. Leucine 23 is at one of the key hydrophobic positions which serve to stabilize the coiled-coil structure (Table I), and similar destabilization effects have been reported by Hodges and co-workers [3,15–18], when leucine residues in the hydrophobic positions of the heptad repeats have been replaced by residues with less hydrophobic side-chains.

These results can be better understood by observing the computer-generated three dimensional structures of the coiled-coils (Fig. 4). The left structure of Fig. 4 shows the coiled-coil dimer of TmL. The hydrophobic (leucine) residues of the 3–4 repeat responsible for the formation and stabilization of the two-stranded α-helical coiled-coil are buried between the two polypeptide chains. Oxidation of the cysteine residues at position 2 of each 35-residue chain (TmL Ox), forms a 70-residue disulphide-linked polypeptide and helps to stabilize the coiled-coil structure. In the middle structure of Fig. 4, all side-chains have been removed from the TmL dimer except the leucine side-chains in the 3–4 repeat positions. It can be seen that the leucine side-chains intercalate to form a continuous hydrophobic surface along the inside of the coiled-coil. By compari-

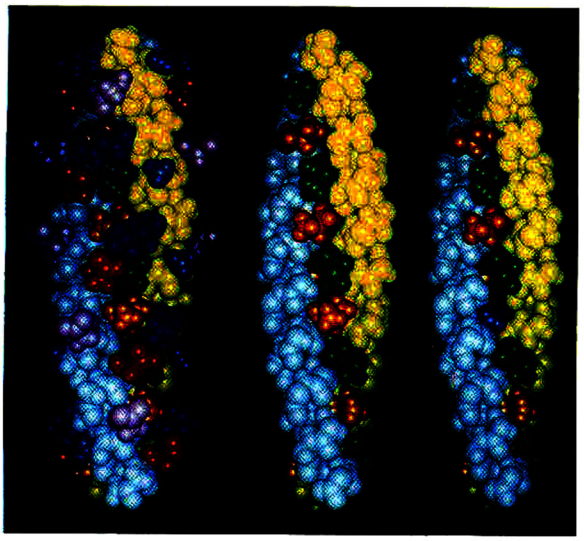

Fig. 4. Space-filling representations of two-stranded α-helical coiled-coils. Left: coiled-coil of TmL. Middle: coiled-coil of TmL with all side-chains removed except the leucine residues in the hydrophobic 3–4 repeat positions of both chains (positions 5, 9, 12, 16, 19, 23, 26, 30 and 33, starting from the top of the polypeptide chains). Right: coiled-coil of TmA23 with all side-chains removed except the leucine residues in the hydrophobic 3–4 repeat positions of both chains (see above); position 23 is now occupied by alanine. The main chain atoms of one α-helix are white and the other yellow. The side-chains are coloured as follows: left and middle coiled-coils of TmL, leucine residues are brown for the white polypeptide chain and green for the yellow chain; alanine residues are purple; glutamic acid residues are red or pink; lysine residues are blue; glycine residues are white; right coiled-coil of TmA23, as for TmL, except that alanine side-chains are now blue. This figure was derived by utilizing molecular dynamics and energy minimization with torsion angles (Φ, ψ) and inter-chain leucine–leucine residue backbone constraints.

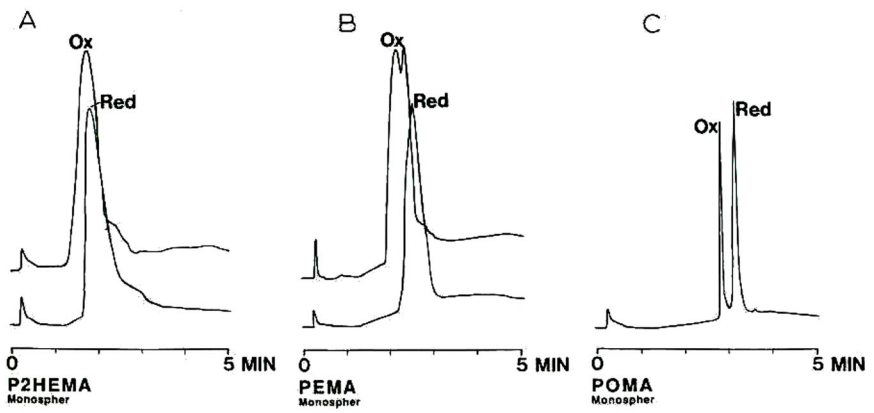

Fig. 5 Reversed-phase chromatography of synthetic model peptide TmL (L35 in Table I). The elution profiles shown are of the oxidized (Ox) and reduced (Red) forms of the peptide on P2HEMA (A), PEMA (B) and POMA (C) packings. Conditions as in Fig. 2. The reduced form of the peptide was obtained by dissolving it in 0.05% aq. TFA containing 10 m*M* DTT prior to application.

sion (Fig. 4, right structure), two leucine residues are replaced by two alanine residues in the centre of the coiled-coil of TmA23. There is now a hole through the centre of the coiled-coil above and below the two interacting alanine residues. Thus, not only are the hydrophobic interactions of lower magnitude in the TmA23 dimer, but water, which is excluded from interaction with hydrogen bonds of the α-helix near the hydrophobic core of TmL, is more accessible to those hydrogen bonds on TmA23. The net result is that both the oxidized and reduced TmA23 coiled-coils are less stable than their TmL counterparts, as has been shown by extensive characterization of the stability of these model peptides, determined by monitoring (by circular dichroism) the ellipticities of the peptides as a function of guanidine hydrochloride concentration [16–18]. Calculated values for the transition midpoint of guanidine hydrochloride concentration (at which the helical content of the peptide has been reduced by 50%) and the free energies of unfolding of the molecules clearly demonstrated the greater stability of the TmL dimer compared to the TmA23 dimer.

RP-HPLC of oxidized and reduced forms of TmL. From Fig. 5, the elution times of the oxidized and reduced forms of TmL are very similar on the least hydrophobic packing, P2HEMA. TmL Red has already been shown to be maintained as a dimer on this packing (Fig. 2, top left elution profile), indicating that both the reduced and oxidized polypeptides maintain their quaternary structure on P2HEMA. On the more hydrophobic PEMA packing, there is evidence that both the oxidized (note the doublet, suggesting conformational changes) and reduced forms of TmL are undergoing at least partial structural change. It would be expected that if the 70-residue disulphide-linked TmL (TmL Ox) was completely unfolded on the surface of the packing, allowing full accessibility of all the side-chains to interact with the stationary phase, then it would be eluted later than the monomers of its reduced form (TmL Red), based upon the increase in hydrophobicity. However, TmL Red is being eluted slightly later than TmL Ox on PEMA, suggesting that at least partial unfolding of the less stable (Fig. 3) TmL Red dimer has been effected. The unfolding of the TmL Red coiled-coil is even more pronounced on the most hydrophobic POMA packing, with baseline resolution of the disulphide-linked TmL and the TmL Red monomers. The observation that TmL Ox is still eluted before the reduced monomers even on the POMA packing is again suggestive of only partial (if any) unfolding on this packing, reflecting similar results by Hodges *et al.* [3] on a traditional C_8 column. This again reflects the stability conferred to the TmL coiled-coil by the presence of a disulphide bond (the guanidine hydrochloride concentration required to denature 50% of the α-helical structure $[G \cdot HCl]_{1/2}$, was 5.3 *M* compared to 2.3 *M* for TmL Red; Fig. 3).

RP-HPLC of reduced and oxidized forms of TmA23. Fig. 6 shows a similar elution pattern of the oxidized and reduced forms of TmA23 on the three

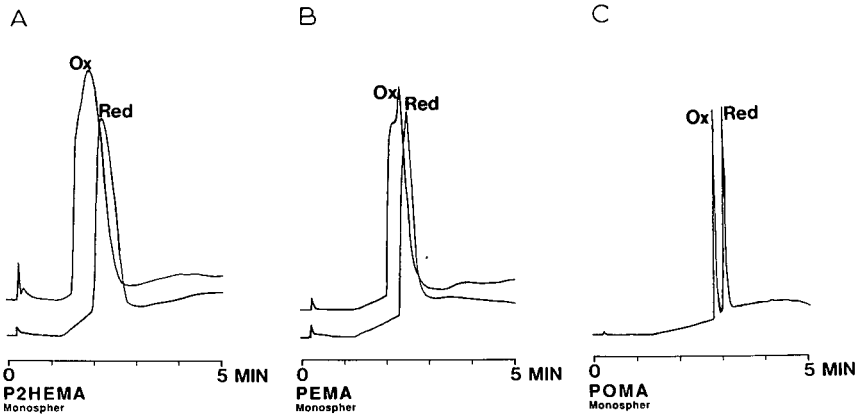

Fig. 6. Reversed-phase chromatography of synthetic model peptide TmA23 in its reduced and oxidized form. This peptide was obtained by substitution of alanine for leucine at position 23 of peptide TmL (L35 in Table I). Conditions as in Fig. 2. Other details as in Fig. 5.

packings as was observed for the respective forms of TmL (Fig. 5). The major difference lies in the distinctly later elution of TmA23 Red than TmA23 Ox on the P2HEMA packing. Thus, the reduced form of the alanine substituted dimer is undergoing at least partial breakdown of quaternary structure even on the least hydrophobic packing, reflecting the destabilizing effect of the leucine to alanine substitution (Figs. 3 and 4). Whether the oxidized TmA23 analogue is maintained as a full coiled-coil on this packing, or whether it undergoes partial unfolding, is difficult to ascertain, although some conformational change is apparent on the more hydrophobic PEMA packing, as was observed for TmL Ox (Fig. 5). The disulphide bridge clearly still confers considerable stability to even the destabilized (compared to TmL) TmA23 analogue, as evidenced by the later elution of the TmA23 Red monomers compared to TmA23 Ox on the most hydrophobic POMA packing.

Comparison of RP-HPLC at TmL and TmA23. Fig. 7 compares the elution behariour of pairs of

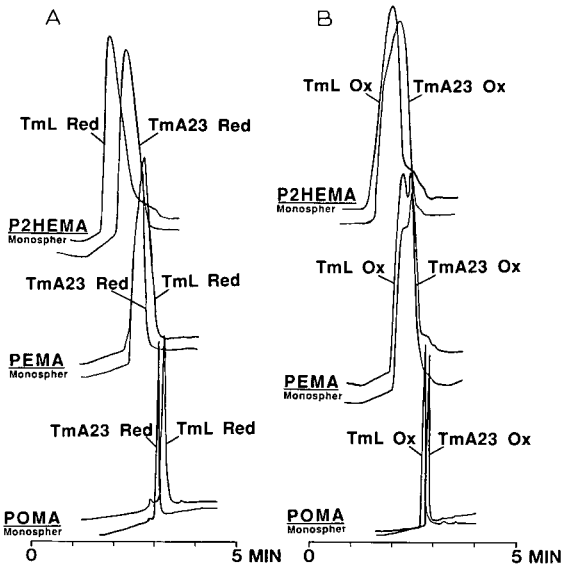

Fig. 7. Reversed-phase chromatography of synthetic model peptides on P2HEMA (top profiles), PEMA (middle profiles) and POMA (bottom profiles) packings. TmL and TmA23 refer, respectively, to peptide L35 (Table I) and peptide L35 containing an alanine substitution (for leucine) at position 23. Ox and Red refer, respectively, to the oxidized (B) and reduced (A) forms of the peptides. The reduced forms of the peptides were obtained by dissolving them in 0.05% aq. TFA containing 10 m*M* DTT prior to application.

reduced (left profiles) and disulphide linked (right profiles) TmL and TmA23 peptides. It would be expected that, because of the greater hydrophobicity of a leucine side-chain compared to that of alanine, that full unfolding of TmL and TmA23 coiled-coils would result in later elution of TmL (oxidized or reduced) compared to the corresponding forms of the alanine substituted analogues. From Figs. 2 and 5, it is known that TmL Red is probably maintained in its native coiled-coil form on the P2HEMA packing; from Fig. 6, at least partial disruption of the coiled-coil of TmA23 Red was apparent. Hence, the later elution of TmA23 Red compared to TmL Red is not surprising, with the hydrophobic core of the former dimer being more fully exposed than that of TmL Red. The elution order is reversed on the most hydrophobic packing (POMA) as would be expected if the more hydrophobic core of TmL, compared to TmA23, was now able to interact more fully with the stationary phase. This result suggests that the reduced coiled-coils are completely unfolded on the POMA column. The co-elution of the peptide analogues on the PEMA packing represents intermediate conformational states of the polypeptides on a packing intermediate in hydrophobicity between P2HEMA and POMA.

The elution profiles of the oxidized analogues (Fig. 7B) serve as another illustration of the stabilizing effect of a disulphide bridge on both the TmL and TmA23 analogues. Considering the stability of the oxidized dimers of TmL (Fig. 5) and TmA23 (Fig. 6) observed previously on P2HEMA, the essential co-elution of TmL Ox and TmA23 Ox is not unexpected. The destabilizing effect of the leucine to alanine substitution is again apparent from the elution profile on the most hydrophobic packing (POMA) where TmA23 Ox is eluted after the more potentially hydrophobic TmL Ox. If disruption of the quaternary structure (if any) of both dimers had occurred to the same extent on POMA, then the more hydrophobic 70-residue TmL polypeptide would have been eluted after the 70-residue alanine-substituted analogue. This result agrees with the $[G \cdot HCl]_{1/2}$ values of 2.9 *M* and 5.3 *M* for TmA23 Ox and TmL Ox, respectively. The elution behaviour of the oxidized analogues on the PEMA packing again suggests intermediate conformational states of the disulphide-linked chains on the PEMA packing.

CONCLUSIONS

In this study, we have extended our original evaluation [1] of the potential of a novel concept for polypeptide separations by examining the effect of polymethacrylate-coated silicas on RP-HPLC of synthetic peptides of defined secondary, tertiary and quaternary structure. By selective unfolding of these model peptides, we have characterized further these packings of varying hydrophobicity, thus confirming the potential of such tailored packings for separation of peptides and proteins.

ACKNOWLEDGEMENTS

This work was supported by the Medical Research Council of Canada Group in Protein Structure and Function, the Deutsche Forschungs-Gemeinschaft (DFG) and by equipment grants from the Alberta Heritage Foundation for Medical Research. We would like to acknowledge the International Association for the Exchange of Students for Technical Experience (IAESTE) for enabling M. H. to spend six months in the laboratory of R.S.H.

REFERENCES

1 M. Hanson, K. K. Unger, C. T. Mant and R. S. Hodges, *J. Chromatogr.*, 599 (1992) 65.
2 J. M R. Parker and R. S. Hodges, *J. Protein Chem.*, 3 (1985) 465.
3 R. S. Hodges, P. D. Semchuk, A. K. Taneja, C. M. Kay, J. M. R. Parker and C. T. Mant, *Pept. Res.*, 1 (1988) 19.
4 N. E. Zhou, C. T. Mant and R. S. Hodges, *Pept. Res.*, 3 (1990) 8.
5 N. E. Zhou, P. D. Semchuk, C. M. Kay and R. S. Hodges, in C. T. Mant and R. S. Hodges (Editors), *High-Performance Liquid Chromatography of Peptides and Proteins: Separation, Analysis and Conformation*, CRC Press, Boca Ration, FL, 1991, p. 643.
6 R. S. Hodges, J. Sodek, L. B. Smillie and L. Jurasek, *Cold Spring Harbor Symp. Quant. Biol.*, 37 (1977) 299.
7 J. Sodek, R. S. Hodges, L. B. Smillie and J. Jurasek, *Proc. Natl. Acad. Sci. USA*, 69 (1972) 3800.
8 J. Sodek, R. S. Hodges and L. B. Smillie, *J. Biol. Chem.*, 253 (1978) 1129.
9 D. Stone and L. B. Smillie, *J. Biol. Chem.*, 253 (1978) 1137.
10 R. S. Hodges, A. K. Saund, P. C. S. Chong, S. A. St.-Pierre and R. E. Reid, *J. Biol. Chem.*, 256 (1981) 1214.
11 S. A. St.-Pierre and R. S. Hodges, *Biochem. Biophys. Res. Commun.*, 72 (1976) 581.
12 S. Y. M. Lau, A. K. Taneja and R. S. Hodges, *J. Chromatogr.*, 317 (1984) 129.
13 C. T. Mant and R. S. Hodges, in C. T. Mant and R. S. Hodges (Editors), *HPLC of Peptides and Proteins: Separation, Analysis and Conformation*, CRC Press, Boca Raton, FL, 1991, p. 437.
14 R. H. Ingraham, S. Y. M. Lau, A. K. Taneja and R. S. Hodges, *J. Chromatogr.*, 327 (1985) 77.
15 R. S. Hodges, N. E. Zhou, C. M. Kay and P. D. Semchuk, *Pept. Res.*, 3 (1990) 123.
16 N. E. Zhou, C. M. Kay and R. S. Hodges, *J. Biol. Chem.*, 267 (1992) 2664.
17 N. E. Zhou, B.-Y. Zhu, C. M. Kay and R. S. Hodges, *Biopolymers*, in press.
18 B.-Y. Zhu, N. E. Zhou, P. E. Semchuk, C. M. Kay and R. S. Hodges, *Int. J. Peptides Protein Res.*, in press.

Journal of Chromatography, 599 (1992) 87–104
Elsevier Science Publishers B.V., Amsterdam

CHROMSYMP. 2545

Theory of perfusion chromatography

A. I. Liapis* and M. A. McCoy

Department of Chemical Engineering and Biochemical Processing Institute, University of Missouri–Rolla, Rolla, MO 65401-0249 (USA)

ABSTRACT

A mathematical model of perfusion chromatography was constructed for column systems. This model could describe the dynamic behavior of single- and multi-component adsorption in columns having perfusive adsorbent particles (the perfusive particles have a non-zero intraparticle fluid velocity). The model expressions for the adsorbent particles include the intraparticle mass transfer mechanisms of convection (intraparticle fluid flow) and diffusion and the mass transfer step involving the interaction between the adsorbate molecules and the active sites on the surface of the porous adsorbent particles. The continuity expression for the fluid flowing stream in the column includes the mechanism of axial dispersion. When the intraparticle fluid velocity is taken to be equal to zero in the model of perfusion chromatography, the resulting expressions could describe single- and multi-component adsorption in columns having purely diffusive particles. The perfusion chromatographic model was solved and used to study the dynamic behavior of column systems for different particle sizes, column lengths, column fluid superficial velocities, intraparticle fluid velocities and different values of the effective pore diffusivity and of the total number of active sites per volume of adsorbent. Columns with perfusive adsorbent particles and columns with purely diffusive adsorbent particles were considered in this work. The dynamics of the interaction mechanisms of the adsorption step of the systems studied in this work are (a) relatively not fast, (b) relatively fast and (c) infinitely fast. The values of certain variables which could be used to evaluate column performance, and also the breakthrough curves obtained from columns having perfusive adsorbent particles, were compared with those obtained from columns involving purely diffusive adsorbent particles. The results from the systems studied in this work suggest that for adsorption systems having relatively fast or infinitely fast interaction kinetics (that is, the dynamics of the interaction step between the adsorbate molecules and the active sites are relatively fast or infinitely fast), the use of perfusive particles could have the potential to provide improved column performance.

INTRODUCTION

The term "perfusion chromatography" was used by Afeyan *et al.* [1] for the technique that involves the flow of liquid through a porous chromatographic particle. Their perfusive particles [1] have a network of large pores (6000–8000 Å) which transect the particles (these pores are called throughpores), and also a network of smaller (500–1500 Å) interconnecting pores between the throughpores. Also, Afeyan *et al.* [1] indicated that scanning electron micrographs show that the pore network is continuous and that no point in the porous matrix is more than 5000–10 000 Å from a throughpore. The experimental data of Afeyan *et al.* [1] suggest that their perfusive particles appear to have a bidisperse [2] porous network. However, Afeyan *et al.* [1] provided no information about the pore-size distribution functions [2,3] of the network of the throughpores and of the network of the smaller interconnecting pores; also, they provided no information about the network pore connectivity [2,3].

Theoretical models have been constructed and used to describe, with reasonable accuracy, the behavior of various single- and multi-component adsorption systems involving purely diffusive porous adsorbent particles [2–16]. The theoretical models have provided significant information about (a) the behavior and the relative importance of the transport mechanisms occurring in the adsorption systems that employ purely diffusive adsorbent particles, (b) the conditions at which percolation

0021-9673/92/$05.00

threshold phenomena may occur in purely diffusive adsorbent particles and (c) the effects that the pore-size distribution, the network pore connectivity and the sizes of the adsorbate molecules and of the active sites on the surface of the adsorbent particles have on the permeability of the adsorbate molecules. Further, the theoretical models have been used to design various small- and large-scale adsorption systems. The intraparticle mass transfer mechanisms that have been considered in the models involving purely diffusive adsorbent particles [2–16] are pore diffusion, surface diffusion and the interaction step(s) between the adsorbate(s) and the active sites on the surface of the adsorbent particles. Different systems involving fast (including infinitely fast) and slow dynamics for the interaction step(s) have been considered [2–16].

In this work, a mathematical model of perfusion chromatography is constructed. The model is then used to study the dynamic behavior of adsorption columns involving perfusive adsorbent particles. It is hoped that the theoretical model of perfusion chromatography, in the first stage of its evolution, will provide useful information about the effects and the relative importance of the different transport mechanisms on the dynamic behavior of adsorption systems employing perfusive adsorbent particles. Further, the models could provide a useful basis for comparing the performance, for a given adsorption system, of perfusive adsorbent particles relative to the performance that could be obtained from purely diffusive porous adsorbent particles.

THEORY

Adsorption is considered to take place from a flowing liquid stream in a fixed bed of perfusive adsorbent particles under isothermal conditions, and the concentration gradients in the radial direction of the bed are considered to be not significant [12,15,17]. The feed solution to the bed is considered to contain n components, and m ($m < n$) solutes may compete for the available active sites for specific adsorption; also, $m + 1 \leqslant i \leqslant l$ ($l < n$) solutes may be non-specifically adsorbed, and $l + 1 \leqslant i \leqslant n$ solutes are simply transported by intraparticle convection and diffusion into the pores of the particles without interacting with the adsorbent [10,12]. A differential mass balance for each component in the flowing fluid stream gives

$$\frac{\partial C_{di}}{\partial t} - D_{Li}\frac{\partial^2 C_{di}}{\partial x^2} + \frac{V_f}{\varepsilon}\cdot\frac{\partial C_{di}}{\partial x} = -\frac{(1-\varepsilon)}{\varepsilon}\cdot\frac{\partial \bar{C}_{psi}}{\partial t}, \qquad i = 1, 2, \ldots, n \tag{1}$$

In eqn. 1, the velocity of the fluid stream, V_f, is taken to be independent of the space variable x, because the liquid solutions encountered in many chromatographic systems are most often very dilute and the main component of the solution is the carrier fluid. For non-dilute solutions a material balance, as shown by Harwell *et al.* [18], would provide the expression for $\partial V_f/\partial x$. The pressure drop through the fixed bed, which is important in the design of an adsorption packed bed (fixed bed) system, can be determined by the methods reported by Geankoplis [19]. The initial and boundary conditions of eqn. 1 are as follows:

$$C_{di} = 0 \text{ at } t = 0,\ 0 \leqslant x \leqslant L, \qquad i = 1, 2, \ldots, n \tag{2}$$

$$\frac{V_f}{\varepsilon}\cdot C_{di} - D_{Li}\cdot\frac{\partial C_{di}}{\partial x} = \frac{V_f}{\varepsilon}\cdot C_{di,in} \text{ at } x = 0,\ t > 0, \qquad i = 1, 2, \ldots, n \tag{3}$$

$$\frac{\partial C_{di}}{\partial x} = 0 \text{ at } x = L,\ t > 0, \qquad i = 1, 2, \ldots, n \tag{4}$$

The value of $C_{di,in}$ may be constant or it may vary with time. An expression for calculating D_{Li} was presented by Arnold *et al.* [20], but in certain systems the axial dispersion is so low that by setting its value equal to zero the error introduced in the prediction of the behavior of an affinity adsorption system is not significant [17,20]. When the axial dispersion coefficient is set equal to zero, eqn. 3 (with $D_{Li} = 0$) becomes

$$C_{di} = C_{di,in} \text{ at } x = 0,\ t > 0, \qquad i = 1, 2, \ldots, n \tag{5}$$

The transport of the species in the perfusive adsorbent particles is considered to involve the following mass transfer mechanisms: (a) intraparticle convection (flow of liquid through the porous perfusive adsorbent particle), (b) diffusion in the pore fluid (pore diffusion), (c) diffusion on the pore surfaces (surface diffusion) and (d) the mass transfer step involving the interaction of the adsorbates with the active sites on the surface of the pores [this step represents the adsorption mechanism; species adsorbed by specific interaction(s), in addition to non-specifically adsorbed components, may be con-

sidered]. The adsorption process is considered to be isothermal as the heats of adsorption apparently do not change the temperature [1,3–10,12,13,15–17,20–23] of the liquid phase even in large-scale systems; this occurs because the total amount of adsorbed material is small and the heat capacity of the liquid phase is high. The differential mass balance for each component i in a perfusive adsorbent particle of slab geometry is given by

$$\varepsilon_p \cdot \frac{\partial C_{pi}}{\partial t} + \varepsilon_p v_p \cdot \frac{\partial C_{pi}}{\partial z} + \frac{\partial C_{si}}{\partial t} = \sum_{j=1}^{n} \frac{\partial}{\partial z}\left(\varepsilon_p D_{pij} \frac{\partial C_{pj}}{\partial z}\right) + \sum_{j=1}^{n} \frac{\partial}{\partial z}\left(D_{sij} \frac{\partial C_{sj}}{\partial z}\right), \qquad i = 1, 2, \ldots, n \tag{6}$$

In eqn. 6, the terms $\partial C_{si}/\partial t$ and $\partial C_{sj}/\partial z$ become equal to zero for species which do not bind by specific or non-specific adsorption. Further, if the particle porosity, ε_p, changes in a significant quantitative way because of the adsorbate(s) loading on the surface of the pores [3], then the first two terms in the left-hand side of eqn. 6 should be replaced by $\partial(\varepsilon_p C_{pi})/\partial t$ and $v_p[\partial(\varepsilon_p C_{pi})/\partial z]$, respectively. Also, if v_p changes in a significant quantitative way, because the adsorbate(s) loading on the surface of the pores may be changing the particle permeability [3], then the term $\varepsilon_p v_p(\partial C_{pi}/\partial z)$ in eqn. 6 should be replaced by $\partial(\varepsilon_p v_p C_{pi})/\partial z$. It is worth mentioning at this point that v_p may also change if the solution is non-dilute and significant amounts of adsorbate(s) are adsorbed within the particle; it is considered that this latter kind of v_p change would not occur often because in most systems the solutions are dilute and the size of the particle is small. It should also be noted that if the loading of the particles changes in a significant way the size of the radii of the pores, and because of that the pore-size distribution and pore connectivity changes, then the values of the diffusion coefficients (like the values of D_{pij}) could be changing with the local loading on the pore surfaces [3], and the phenomenon of percolation threshold [3] could appear to be possible in one or more of the porous networks located between the throughpores of the perfusive particles.

The mixtures of components to be separated by chromatographic systems are usually dilute (this is most often the case for mixtures of biological macromolecules), especially with respect to the component(s) of interest, and therefore it may be possible to set the off-diagonal ($D_{pij}, i \neq j$; $D_{sij}, i \neq j$) elements of the effective pore diffusivity matrix, $\mathbf{D}_p$, and of the surface diffusivity matrix, $\mathbf{D}_s$, equal to zero [13,15,24,25]. In this case, eqn. 6 would take the following form

$$\varepsilon_p \cdot \frac{\partial C_{pi}}{\partial t} + \varepsilon_p v_p \cdot \frac{\partial C_{pi}}{\partial z} + \frac{\partial C_{si}}{\partial t} = \frac{\partial}{\partial z}\left[\varepsilon_p D_{pi} \cdot \frac{\partial C_{pi}}{\partial z} + D_{si} \cdot \frac{\partial C_{si}}{\partial z}\right], \qquad i = 1, 2, \ldots, n \tag{7}$$

In eqn. 7, D_{pi} and D_{si} represent the diagonal terms ($D_{pij}, i = j$; $D_{sij}, i = j$) of the diffusivity matrices $\mathbf{D}_p$ and $\mathbf{D}_s$. If the interaction between the adsorbate(s) and the active sites on the surface of the pores is strong, then the surface diffusion may, in certain systems, be neglected. If the contribution of surface diffusion to mass transfer is insignificant, then eqn. 7 would become

$$\varepsilon_p \cdot \frac{\partial C_{pi}}{\partial t} + \varepsilon_p v_p \cdot \frac{\partial C_{pi}}{\partial z} + \frac{\partial C_{si}}{\partial t} = \frac{\partial}{\partial z}\left(\varepsilon_p D_{pi} \cdot \frac{\partial C_{pi}}{\partial z}\right), \qquad i = 1, 2, \ldots, n \tag{8}$$

It is clear that eqn. 8 cannot be solved if an appropriate expression for the term $\partial C_{si}/\partial t$ is not available. This term represents the accumulation of the adsorbed species i on the internal surface of the perfusive adsorbent particle, and it can be quantified if a thermodynamically consistent mathematical model could be constructed that could describe the mechanism of adsorption for component i. For isothermal adsorption systems, the term $\partial C_{si}/\partial t$ could be of the form

$$\frac{\partial C_{si}}{\partial t} = f_i(\mathbf{C}_p, \mathbf{C}_s, \mathbf{k}), \qquad i = 1, 2, \ldots, m, m+1, \ldots, l \tag{9}$$

where f_i represents the functional form of the dynamic adsorption mechanism for component i; $\mathbf{C}_p$ represents the concentration vector of the adsorbates in the pore fluid, $\mathbf{C}_p = (C_{p1}, C_{p2}, \ldots, C_{pm}, C_{pm+1}, \ldots, C_{pl})$; $\mathbf{C}_s$ denotes the concentration vector of the adsorbates in the adsorbed phase, $\mathbf{C}_s = (C_{s1}, C_{s2}, \ldots, C_{sm}, C_{sm+1}, \ldots, C_{sl})$; and $\mathbf{k}$ represents the

vector of the rate constants that characterize the interaction kinetics between the adsorbates and the active sites. For certain single- and multi-component adsorption systems, dynamic adsorption models of the form given in eqn. 9 have been constructed and presented in the literature [9,10,15,16,21,23,26,27].

In some adsorption systems, the rates of interaction between the adsorbates and the active sites may be much higher than the intraparticle convection and diffusional rates, and in such systems it may be possible to assume that equilibrium exists between the adsorbates in the pore fluid and in the adsorbed phase at each point in the pores. In this case, one would need to have thermodynamically consistent mathematical expressions that could describe the equilibrium adsorption isotherms of the adsorbates. Various mathematical expressions (developed from equilibrium adsorption models) for single- and multi-component equilibrium adsorption isotherms have been presented in the literature [4,6,8–11,14,21,22,26–32]. The term $\partial C_{si}/\partial t$ in eqn. 8, for systems where adsorption equilibrium may be assumed between the adsorbates in the pore fluid and in the adsorbed phase at each point in the pores, is then given by

$$\frac{\partial C_{si}}{\partial t} = \sum_{j=1}^{l}\left(\frac{\partial g_i}{\partial C_{pj}}\right)\left(\frac{\partial C_{pj}}{\partial t}\right), \qquad i = 1,2,\ldots,m, \; m+1,\ldots,l \tag{10}$$

where

$$C_{si} = g_i(\mathbf{C}_p, \mathbf{K}), \qquad i = 1,2,\ldots,m,m+1,\ldots,l \tag{11}$$

The functions g_i represent the equilibrium adsorption isotherms for the adsorbates that may compete for the available (accessible) active sites on the surface of the pores. **K** represents the vector of the equilibrium constants that characterize the equilibrium interactions between the adsorbates and the active sites.

The initial and boundary conditions for eqn. 8 and the initial condition for eqn. 9 are as follows:

at $t = 0$ $C_{pi} = 0$ for $0 \leqslant z \leqslant z_0$, $\quad i = 1,2,\ldots,n$ (12)

at $z = 0$ $C_{pi} = C_{di}$, $t > 0$, $\quad i = 1,2,\ldots,n$ (13)

at $z = z_0$ $C_{pi} = C_{di}$, $t > 0$, $\quad i = 1,2,\ldots,n$ (14)

at $t = 0$ $C_{si} = 0$ for $0 \leqslant z \leqslant z_0$, $\quad i = 1,2,\ldots,m,m+1,\ldots,l$ (15)

Eqns. 13 and 14 were obtained from the assumption that the external mass transfer resistance (the mass transfer resistance in a liquid film that may be located on the external particle surface) is not significant. Detailed calculations [12,16,33,34] for adsorption columns involving purely diffusive particles have shown that the intraparticle mass transfer resistance of a purely diffusive particle is significantly larger than the external mass transfer resistance, for the bulk flow-rates that are usually encountered in adsorption columns, and hence if the external mass transfer resistance is neglected the effect on the breakthrough curve is not significant. Further, in the perfusive particles there is flow in and out of the particles, and hence one may consider that the effect of the external mass transfer resistance will be even less significant than that encountered in purely diffusive particles.

The variable $\bar{C}_{psi}$ in eqn. 1 represents the average concentration of adsorbate in the adsorbent particle and its value is obtained from the equation

$$\bar{C}_{psi} = \frac{1}{V_{pv}}\left[\int_0^{V_{pv}} C_{si}\mathrm{d}V + \int_0^{V_{pv}} \varepsilon_p C_{pi}\mathrm{d}V\right], \quad i = 1,2,\ldots,n \tag{16}$$

where V_{pv} denotes the volume of the adsorbent particle. For particles of slab geometry, eqn. 16 gives

$$\bar{C}_{psi} = \frac{1}{z_0}\left[\int_0^{z_0} C_{si}\mathrm{d}z + \int_0^{z_0} \varepsilon_p C_{pi}\mathrm{d}z\right], \quad i = 1,2,\ldots,n \tag{17}$$

For particles of spherical geometry with radius r_0, eqn. 16 provides the following expression for $\bar{C}_{psi}$ in spherical adsorbent particles:

$$\bar{C}_{psi} = \frac{3}{r_0^3}\left[\int_0^{r_0} r^2 C_{si}\mathrm{d}r + \int_0^{r_0} r^2 \varepsilon_p C_{pi}\mathrm{d}r\right], \quad i = 1,2,\ldots,n \tag{18}$$

In eqn. 18, the variable r represents the radial direction of the coordinate system for the spherical particles. The term $\partial \bar{C}_{psi}/\partial t$ in eqn. 1 is obtained by differentiating the terms of eqn. 16 with respect to time, and this operation gives

$$\frac{\partial \bar{C}_{psi}}{\partial t} = \frac{1}{V_{pv}}\left[\frac{\partial}{\partial t}\left(\int_0^{V_{pv}} C_{si}\mathrm{d}V\right) + \frac{\partial}{\partial t}\left(\int_0^{V_{pv}} \varepsilon_p C_{pi}\mathrm{d}V\right)\right], \quad i = 1, 2, \ldots, n \qquad (19)$$

In order to solve eqn. 8, an expression for the intraparticle velocity v_p is needed. An equation for v_p can be constructed by considering that the driving force for convective flow across a particle is the column pressure gradient, $\Delta P/L$, which imposes a pressure Δp across a particle of length z_0, and thus one could consider that $\Delta P/L = \Delta p/z_0$; however, $\Delta p/z_0 = \mu v_p/K_p$, and $\Delta P/L$ could be obtained from an Ergun-type [35] equation. This approach would give an expression for v_p of the form

$$v_p = K_p(\alpha_1 V_f + \alpha_2 V_f^2) \qquad (20)$$

where K_p is the permeability of the porous adsorbent particle, V_f is the superficial velocity (see eqn. 1) and α_1 and α_2 are constants calculated [34] from the system properties (fluid density, fluid viscosity, bed porosity, particle size).

The dynamic behavior of the column involving perfusive adsorbent particles of slab geometry is obtained by solving simultaneously eqns. 1–4, 8, 9 and 12–15. If the axial dispersion coefficient, D_{Li}, is taken to be zero, then eqn. 5 should be used instead of eqn. 3. Further, if the adsorption step between the adsorbates and the active sites may be considered to occur infinitely fast, then the term $\partial C_{si}/\partial t$ in eqn. 8 should be replaced by the expression in the right-hand side of eqn. 10, and for this case eqns. 9 and 15 are not needed. The solution of the equations of the mathematical model of perfusion chromatography was obtained [34] by employing the numerical method of orthogonal collocation [10,12,16,33,34, 36,37] on the space variables, and the resulting ordinary non-linear differential equations were integrated [34] by using Gear's method [37], which is employed in the LSODES component of the ODEPACK [38] software package.

It should be mentioned that if the intraparticle velocity v_p is set equal to zero in eqn. 8, then the solution of the above-mentioned equations would provide the dynamic behavior of a column having purely diffusive adsorbent particles of slab geometry. If the perfusive adsorbent particles have spherical geometry, then the differential mass balance for each component i in a perfusive adsorbent particle of spherical geometry (a material balance like eqn. 8 but for spherical particles) would be given by

$$\varepsilon_p \cdot \frac{\partial C_{pi}}{\partial t} + \varepsilon_p v_{pr} \cdot \frac{\partial C_{pi}}{\partial r} + \varepsilon_p v_{p\theta} \cdot \frac{1}{r} \cdot \frac{\partial C_{pi}}{\partial \theta} + \frac{\partial C_{si}}{\partial t} = \varepsilon_p D_{pi}\left[\frac{1}{r^2} \cdot \frac{\partial}{\partial r}\left(r^2 \cdot \frac{\partial C_{pi}}{\partial r}\right) + \frac{1}{r^2 \sin\theta} \cdot \frac{\partial}{\partial \theta}\left(\sin\theta \cdot \frac{\partial C_{pi}}{\partial \theta}\right)\right], \quad i = 1, 2, \ldots, n \qquad (21)$$

where v_{pr} and $v_{p\theta}$ represent the intraparticle velocity components in the r and θ directions, respectively. If ε_p and D_{pi} vary with the local loading [3] (the intraparticle velocity may also vary because of the local loading), then the variation of ε_p and D_{pi} has to be considered in eqn. 21. The velocity components v_{pr} and $v_{p\theta}$ could be obtained by solving the continuity and Navier–Stokes equations of the flowing fluid stream in the column together with the continuity and Darcy's equations of the flow in the porous particles. Appropriate initial and boundary conditions for eqn. 21 can be developed; then eqn. 21 could be solved simultaneously with the equations for C_{di} and C_{si} discussed above, in order to predict the dynamic behavior of column systems involving perfusive adsorbent particles of spherical geometry.

RESULTS AND DISCUSSION

In this work, frontal analysis results are presented for systems involving single-component adsorption. The theory of perfusion chromatography that was presented in the previous section could be used, as discussed earlier, to describe the dynamic behavior of multi-component adsorption systems when the values of the parameters in the equations of the multi-component model of perfusion chromatography could be estimated from experimental measurements and/or from appropriate constitutive equations and correlations [2–16,19–23,26–33]. In the work of Afeyan *et al.* [1], experimental data for certain multi-component systems involving perfusive adsorbent particles were presented, but the values of the parameters that characterize the rates of the mass transfer and adsorption mechanisms of those systems have not been measured. Further, the experimental data presented by Afeyan *et al.* [1] are

not sufficient for the appropriate calculation of the values of these parameters through the use of the multi-component mathematical model of perfusion chromatography presented here.

The perfusion chromatographic single-component adsorption systems examined in this work are considered to involve adsorbent particles of slab geometry and the interaction kinetics (adsorption mechanism) between the adsorbate molecules and the active sites are considered to be described by a reversible mechanism of the form

$$A + S \underset{k_2}{\overset{k_1}{\rightleftharpoons}} AS \tag{22}$$

where A represents the adsorbate molecule, S denotes the free active site on the surface, AS represents the adsorbate-active site complex and k_1 and k_2 are the rate constants that characterize the forward and reverse interaction mechanisms, respectively. If the interaction steps in expression 22 are considered to represent elementary interactions, then the dynamic equation for the mechanism in expression 22 is given by [15]

$$\frac{\partial C_s}{\partial t} = k_1 C_p (C_T - C_s) - k_2 C_s \tag{23}$$

The right-hand side of eqn. 23 represents one possible form for the function f_i in eqn. 9 for single-component adsorption; the subscript i is dropped from the equations of the perfusion chromatographic model whenever a single-component adsorption system (as is the case here) is considered. Eqn. 23 has been found to provide, for practical purposes, an adequate expression for the dynamics of the interaction between β-galactosidase and immobilized monoclonal anti-β-galactosidase [10,15, 16], and for the dynamics of the interaction between lysozyme and immobilized monoclonal anti-lysozyme [23]. In the perfusion chromatographic simulation studies in this work we examined the following single-component adsorption systems: (a) β-galactosidase interacting with immobilized monoclonal anti-β-galactosidase and (b) lysozyme interacting with immobilized monoclonal anti-lysozyme.

The monoclonal antibody molecules are considered to be immobilized on the surface of perfusive adsorbent particles of slab geometry and the dynamics of the adsorption step are described by eqn. 23. Two different values for the particle size, z_0, were considered: (i) $z_0 = 8.060 \cdot 10^{-6}$ m and (ii) $z_0 = 16.120 \cdot 10^{-6}$ m.

In Table I, the values of the parameters used in the perfusion model for the simulation of the two different single-component adsorption systems discussed above are presented; in certain simulations, the values of some of the parameters in Table I have been altered, and this is indicated in the appropriate figures by reporting the values of the parameters. Further, the values of other parameters of the perfusion model are reported in the captions of the figures. The values of the parameters in Table I are from adsorption systems reported in the literature [10,12,15,16,23] and, for the purposes of the simulations of this work, are considered to have appropriate magnitudes; it should be mentioned that the value of C_T in Table I represents the largest (maximum) amount of adsorbate that could be adsorbed per unit volume of particle.

In the simulations in this work, the dynamic behavior of the perfusion chromatographic systems was examined for the following intraparticle velocities (for a given superficial velocity, V_f): $v_p = 0$, $v_p = 0.02V_f$, $v_p = 0.03V_f$ and $v_p = 0.05V_f$. The range of the values of V_f examined in this work is similar to the experimental values considered by Afeyan *et al.* [1]. Further, the resulting range of the non-zero values of the intraparticle velocity, v_p, examined in this work is within the range suggested by the data in ref. 1 and by calculations performed

TABLE I

VALUES FOR CERTAIN PARAMETERS OF THE MODEL OF PERFUSION CHROMATOGRAPHY

System[a]	Parameters
A	$C_{d,in} = 0.1$ kg/m^3; $C_T = 2.2$ kg/m^3; $D_L = 0$; $D_p = 6.9 \cdot 10^{-12}$ m^2/s; $k_1 = 2.35 \cdot 10^{-2}$ m^3/kg · s; $k_2 = 5.17 \cdot 10^{-6}$ s^{-1}; $K = k_1/k_2 = 4.545 \cdot 10^3$ m^3/kg; $\varepsilon = 0.35$; $\varepsilon_p = 0.50$; $T = 293$ K
B	$C_{d,in} = 0.1$ kg/m^3; $C_T = 2.2$ kg/m^3; $D_L = 0$; $D_p = 17.885 \cdot 10^{-12}$ m^2/s; $k_1 = 4.108$ m^3/kg · s; $k_2 = 0.2222$ s^{-1}; $K = k_1/k_2 = 18.488$ m^3/kg; $\varepsilon = 0.35$; $\varepsilon_p = 0.50$; $T = 282.5$ K

[a] System A, β-galactosidase and monoclonal anti-β-galactosidase; system B, lysozyme and monoclonal anti-lysozyme.

with eqn. 20. It is worth noting again that the adsorbent particles are considered to be purely diffusive when $v_p = 0$.

If the dynamics of the adsorption step are considered to be infinitely fast, then adsorption equilibrium between the adsorbate in the pore fluid and in the adsorbed phase may be considered at every point in the pores, and hence $\partial C_s/\partial t$ is taken to be zero in eqn. 23. In this case, eqn. 23 would give the following equilibrium ($\partial C_s/\partial t = 0$) adsorption expression:

$$C_s = \frac{C_T K C_p}{1 + K C_p} \tag{24}$$

Eqn. 24 represents the equilibrium Langmuir adsorption expression [4,9,10,15,16,39] and K is the equilibrium adsorption constant ($K = k_1/k_2$). The right-hand side of eqn. 24 represents one possible form for the function g_i in eqn. 11 for single-component adsorption; the subscript i is dropped from the equations of the perfusion chromatographic model whenever a single-component adsorption system (as is the case here) is considered. When eqn. 24 is employed in the right-hand side of eqn. 10, the following expression is obtained for $\partial C_s/\partial t$:

$$\frac{\partial C_s}{\partial t} = \left(\frac{\partial C_s}{\partial C_p}\right)\left(\frac{\partial C_p}{\partial t}\right) = \left[\frac{C_T K}{(1 + K C_p)^2}\right]\left(\frac{\partial C_p}{\partial t}\right) \tag{25}$$

In this work, the dynamic behavior of a perfusion chromatographic system (single-component adsorption system) with infinitely fast dynamics for the adsorption step was also examined (for purposes of comparison with a system having finite dynamics of interaction), and the expression for the term $\partial C_s/\partial t$ in eqn. 8 was represented by eqn. 25. For this adsorption system, the value of C_T was taken to be equal to 2.2 kg/m^3 (this value is the same as that used in the systems in Table I), and the value of the equilibrium adsorption constant K was taken to be equal to the value for the system involving the interaction of lysozyme with immobilized monoclonal anti-lysozyme, and thus $K = k_1/k_2 = 4.108/0.2222 = 18.488$ m^3/kg.

In Figs. 1–10, the breakthrough curves for β-galactosidase and lysozyme are presented for different column lengths, particle sizes, column fluid superficial velocities (V_f) and intraparticle velocities (v_p). The results in Figs. 1 and 2 indicate that there is no significant difference between the breakthrough

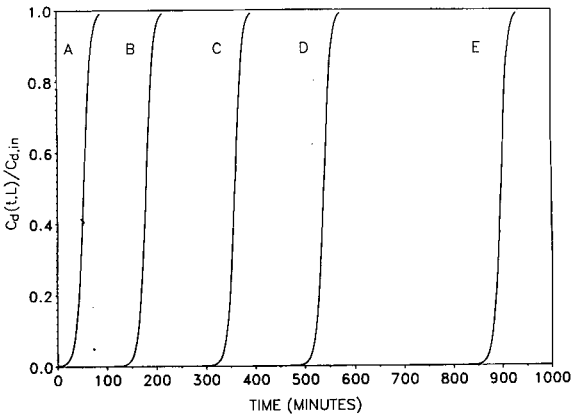

Fig. 1. Breakthrough curve of β-galactosidase: $z_0 = 8.060 \cdot 10^{-6}$ m; $V_f = 0.138 \cdot 10^{-3}$ m/s; $v_p = (0, 0.02, 0.03, 0.05)V_f$. Column lengths: (A) 0.03; (B) 0.1; (C) 0.2; (D) 0.3; (E) 0.5 m.

curves of purely diffusive ($v_p = 0$) and perfusive ($v_p > 0$) particles when $V_f = 0.138 \cdot 10^{-3}$ m/s; it can also be observed that when $z_0 = 16.120 \cdot 10^{-6}$ m, the breakthrough of β-galactosidase begins to occur slightly later for the column systems involving perfusive particles. When the superficial velocity, V_f, in the column is increased to $2.778 \cdot 10^{-3}$ m/s, then the curves in Figs. 3 and 4 clearly show that, for a given column length, the breakthrough of β-galactosidase begins to occur later for the column systems employing perfusive particles. Also, the differences

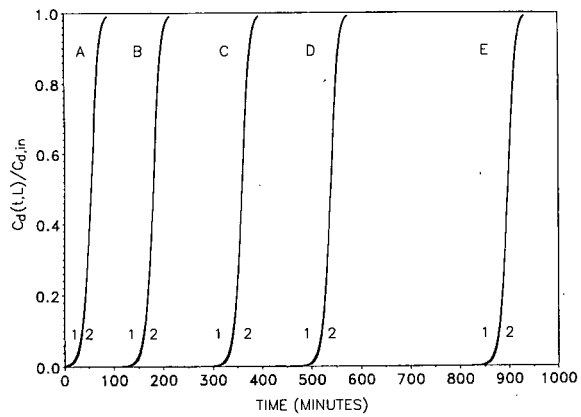

Fig. 2. Breakthrough curve of β-galactosidase: $z_0 = 16.120 \cdot 10^{-6}$ m; $V_f = 0.138 \cdot 10^{-3}$ m/s; (1) $v_p = 0$; (2) $v_p = (0.02, 0.03, 0.05)V_f$. Column lengths, (A) 0.03; (B) 0.1; (C) 0.2; (D) 0.3; (E) 0.5 m.

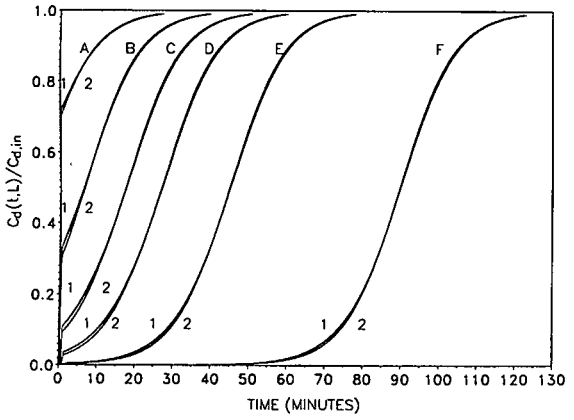

Fig. 3. Breakthrough curve of β-galactosidase: $z_0 = 8.060 \cdot 10^{-6}$ m; $V_f = 2.778 \cdot 10^{-3}$ m/s; (1) $v_p = 0$; (2) $v_p = (0.02, 0.03, 0.05)V_f$. Column lengths: (A) 0.03; (B) 0.1; (C) 0.2; (D) 0.3; (E) 0.5 m; (F) 1.0 m.

between the β-galactosidase breakthrough curves obtained from the columns having perfusive particles and from the columns involving purely diffusive particles increase as the particle size increases. A comparison of the results in Figs. 3 and 4 indicates that, for a given column length, the breakthrough of β-galactosidase starts later when the smaller particle size is used. Further, by comparing the times at which β-galactosidase breakthrough begins (Figs. 3 and 4), it is found that the percentage difference between the initial times (initial time refers to the

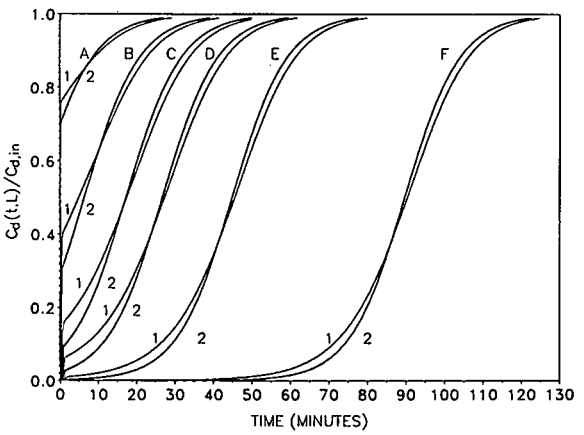

Fig. 4. Breakthrough curve of β-galactosidase: $z_0 = 16.120 \cdot 10^{-6}$ m; $V_f = 2.778 \cdot 10^{-3}$ m/s; (1) $v_p = 0$; (2) $v_p = (0.02, 0.03, 0.05)V_f$. Column lengths: (A) 0.03; (B) 0.1; (C) 0.2; (D) 0.3; (E) 0.5; (F) 1.0 m.

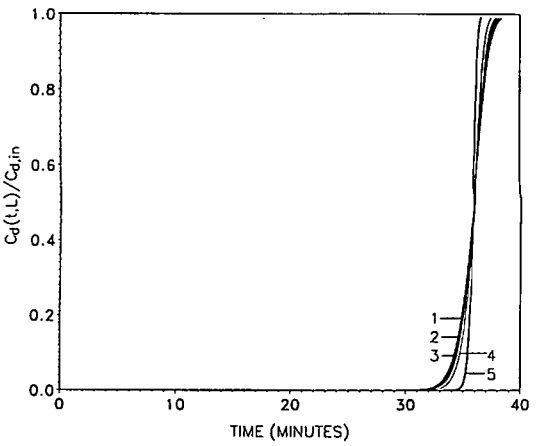

Fig. 5. Breakthrough curve of lysozyme: $V_f = 0.138 \cdot 10^{-3}$ m/s; $L = 0.03$ m; (1) $v_p = 0$, $z_0 = 16.120 \cdot 10^{-6}$ m; (2) $v_p = 0.02V_f$, $z_0 = 16.120 \cdot 10^{-6}$ m; (3) $v_p = 0.03V_f$, $z_0 = 16.120 \cdot 10^{-6}$ m; (4) $v_p = 0.05V_f$, $z_0 = 16.120 \cdot 10^{-6}$ m; (5) $v_p = (0, 0.02, 0.03, 0.05)V_f$, $z_0 = 8.060 \cdot 10^{-6}$ m.

time at which breakthrough begins) obtained from purely diffusive and perfusive particles decreases as the column length increases. In Figs. 2–4, the relative differences in the breakthrough curves obtained from the three different non-zero v_p values are very small and could not be described graphically.

In Fig. 5, the results indicate that the differences in

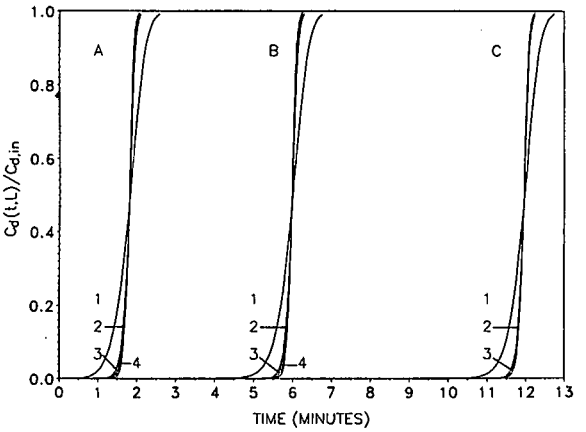

Fig. 6. Breakthrough curve of lysozyme: $V_f = 2.778 \cdot 10^{-3}$ m/s; $z_0 = 8.060 \cdot 10^{-6}$ m. Column lengths and intraparticle fluid velocities: (A) 0.03 m, (1) $v_p = 0$, (2) $v_p = 0.02V_f$, (3) $v_p = 0.03V_f$, (4) $v_p = 0.05V_f$; (B) 0.1 m, (1) $v_p = 0$, (2) $v_p = 0.02V_f$, (3) $v_p = 0.03V_f$, (4) $v_p = 0.05V_f$; (C) 0.2 m, (1) $v_p = 0$, (2) $v_p = 0.02V_f$, (3) $v_p = (0.03, 0.05)V_f$.

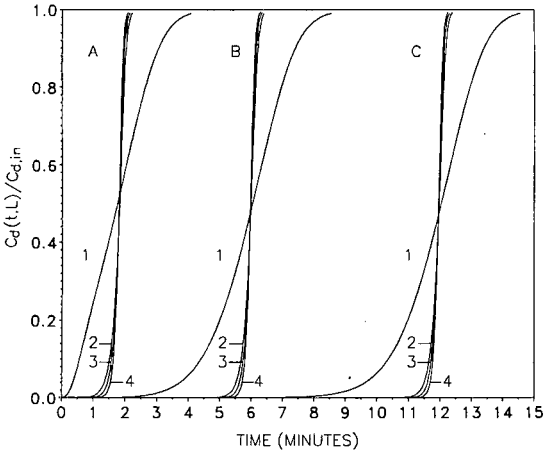

Fig. 7. Breakthrough curve of lysozyme: $V_f = 2.778 \cdot 10^{-3}$ m/s; $z_0 = 16.120 \cdot 10^{-6}$ m. Column lengths: (A) 0.03; (B) 0.1; (C) 0.2 m. For all column lengths: (1) $v_p = 0$; (2) $v_p = 0.02V_f$; (3) $v_p = 0.03V_f$; (4) $v_p = 0.05V_f$.

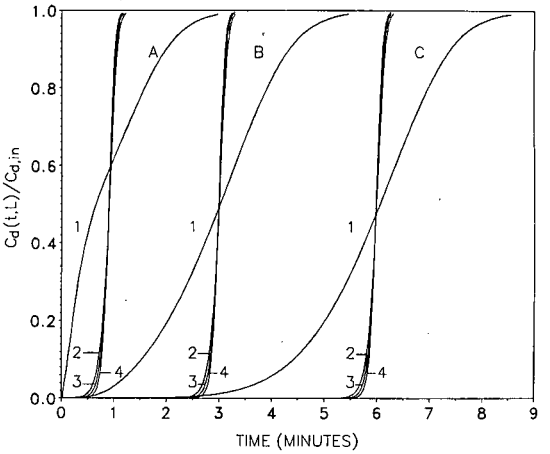

Fig. 9. Breakthrough curve of lysozyme: $V_f = 5.556 \cdot 10^{-3}$ m/s; $z_0 = 16.120 \cdot 10^{-6}$ m. Column lengths: (A) 0.03; (B) 0.1; (C) 0.2 m. For all column lengths: (1) $v_p = 0$; (2) $v_p = 0.02V_f$; (3) $v_p = 0.03V_f$; (4) $v_p = 0.05V_f$.

the lysozyme breakthrough curves obtained from purely diffusive and perfusive particles are insignificant when $z_0 = 8.060 \cdot 10^{-6}$ m and $V_f = 0.138 \cdot 10^{-3}$ m/s. For the larger particles, the data in Fig. 5 imply that the differences in the breakthrough curves are small, and the breakthrough of lysozyme begins at larger times when perfusive particles are used in the column; further, it can be observed that as the intraparticle velocity, v_p, is increased the time at which breakthrough begins is increased. Also, the data in Fig. 5 imply that the utilization of immobilized monoclonal anti-lysozyme (ligand) is higher (higher column performance) when the smaller in size particles are used.

In Figs. 6 and 7, the lysozyme breakthrough curves are shown for different column lengths and particle sizes when $V_f = 2.778 \cdot 10^{-3}$ m/s. It can be observed that the breakthrough curves obtained

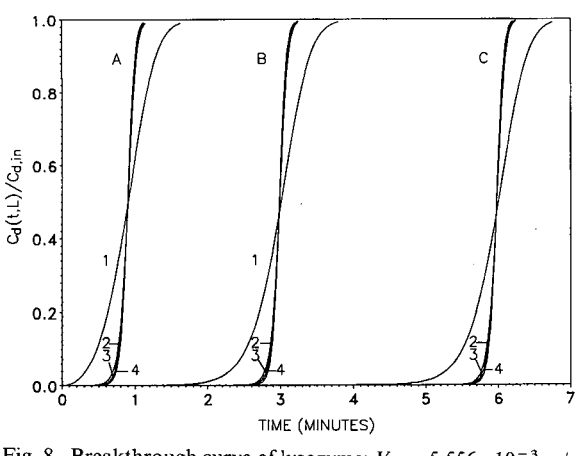

Fig. 8. Breakthrough curve of lysozyme: $V_f = 5.556 \cdot 10^{-3}$ m/s; $z_0 = 8.060 \cdot 10^{-6}$ m. Column lengths: (A) 0.03; (B) 0.1; (C) 0.2 m. For all column lengths: (1) $v_p = 0$; (2) $v_p = 0.02V_f$; (3) $v_p = 0.03V_f$; (4) $v_p = 0.05V_f$.

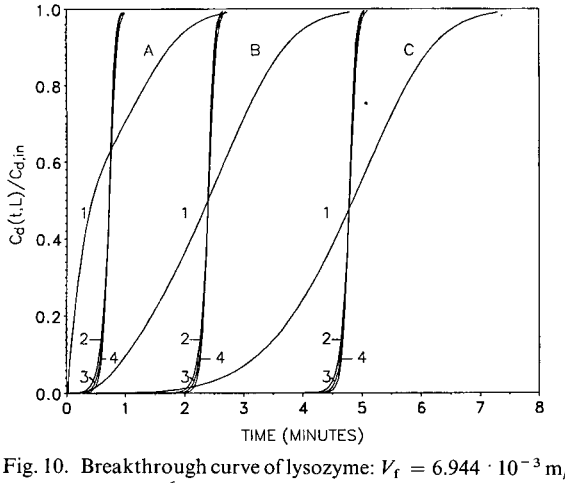

Fig. 10. Breakthrough curve of lysozyme: $V_f = 6.944 \cdot 10^{-3}$ m/s; $z_0 = 16.120 \cdot 10^{-6}$ m. Column lengths: (A) 0.03; (B) 0.1; (C) 0.2 m. For all column lengths: (1) $v_p = 0$; (2) $v_p = 0.02V_f$; (3) $v_p = 0.03V_f$; (4) $v_p = 0.05V_f$.

from the perfusive particles are very much steeper than those obtained from the purely diffusive particles. Further, the times at which breakthrough begins are significantly larger in the columns with perfusive particles, especially in the case where the larger particles are employed.

In Figs. 8 and 9, the lysozyme breakthrough curves are presented for different column lengths and particle sizes when $V_f = 5.556 \cdot 10^{-3}$ m/s. For the smaller particles (Fig. 8) the qualitative behavior is similar to that in Fig. 6, but for the larger particles (Fig. 9) the lysozyme breakthrough curves obtained from the purely diffusive particles are much more disperse than those in Fig. 7, and there is a significant difference in the shape of the breakthrough curves for the column length $L = 0.03$ m. It is also observed in Figs. 8 and 9 that the breakthrough curves obtained from the columns with perfusive particles are very steep; the significant increase in the column fluid superficial velocity, V_f, had no significant effect on the shape of the breakthrough curves obtained from the columns with perfusive particles. Further, the results in Figs. 8 and 9 show that the increased value of V_f affected, for a given column length, the time at which breakthrough begins (compare Figs. 6 and 8 and Figs. 7 and 9). By comparing the results for the perfusive particles in Figs. 6 and 7 and in Figs. 8 and 9, it is found that the time at which breakthrough begins, for a given column length, is larger when the smaller particles are used.

In Fig. 10, the lysozyme breakthrough curves are shown when $V_f = 6.944 \cdot 10^{-3}$ m/s and $z_0 = 16.120 \cdot 10^{-6}$ m. By comparing the results in Figs. 9 and 10, it can be observed again that the columns with perfusive particles provide very steep breakthrough curves. The data in Figs. 6–10 also show that as the intraparticle velocity, v_p, is increased (for the values of the superficial velocity considered in Figs. 6–10), the time at which breakthrough begins, for a given column length, is increased.

An analysis of the dynamic behavior of the two different adsorption systems in Table I indicated that the differences in the dynamic behavior (Figs. 1–10) of β-galactosidase and lysozyme depend significantly on (i) the differences in the values of k_1, the value of k_1 characterizing the formation of the adsorbate–ligand complex ($k_1 = 2.35 \cdot 10^{-2}$ for β-galactosidase and 4.108 for lysozyme), and (ii) the differences in the values of the effective pore diffusivities of β-galactosidase and lysozyme ($D_p = 6.9 \cdot 10^{-12}$ for β-galactosidase and $17.885 \cdot 10^{-12}$ for lysozyme). The ratio of the k_1 value of the lysozyme–anti-lysozyme system to that of the β-galactosidase–anti-β-galactosidase system is $1.748 \cdot 10^2$, and the ratio of the D_p value of lysozyme to that of β-galactosidase is 2.592. The analysis has indicated that, although the equilibrium adsorption constant of the β-galactosidase–anti-β-galactosidase system is significantly larger than that of the lysozyme–anti-lysozyme system (see Table I), the breakthrough curves of lysozyme obtained from the columns with perfusive particles are much steeper than the corresponding breakthrough curves of β-galactosidase, because the values of k_1 and D_p of the lysozyme–anti-lysozyme system are significantly larger than those of the β-galactosidase–anti-β-galactosidase system.

In Fig. 11, the concentration profiles of lysozyme in the pore fluid and in the adsorbed phase of a single particle of slab geometry are shown. This particle is located within the column at a position $x = 6.6645 \cdot 10^{-5}$ m from the column entrance, and the concentration profiles are shown for time $t = 0.05$ min. It can be clearly observed that for the purely diffusive

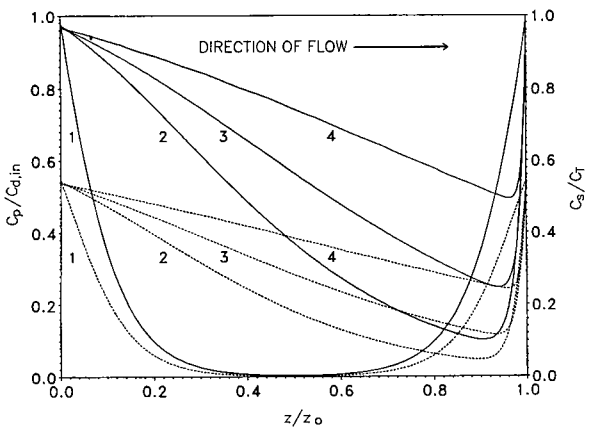

Fig. 11. Dimensionless concentration profiles of lysozyme in the pore fluid and in the adsorbed phase of the porous adsorbent particle at time $t = 0.05$ min and at position $x = 6.6645 \cdot 10^{-5}$ m in the column. $V_f = 2.778 \cdot 10^{-3}$ m/s; $z_0 = 16.120 \cdot 10^{-6}$ m; column length, $L = 0.03$ m. The data for the solid curves represent $C_p/C_{d,in}$ *versus* z/z_0. The data for the broken curves represent C_s/C_T *versus* z/z_0. For the solid and broken curves the intraparticle fluid velocities are (1) $v_p = 0$; (2) $v_p = 0.02V_f$; (3) $v_p = 0.03V_f$; (4) $v_p = 0.05V_f$.

particle ($v_p = 0$) the concentration of lysozyme in the pore fluid and in the adsorbed phase is about equal to zero in a significant portion of the particle; further, the concentration profiles of the purely diffusive particle are symmetrical, as expected, and the point of symmetry is located at the center of the particle where $z/z_0 = 0.5$. For the perfusive particle ($v_p > 0$), it is observed that the concentrations of lysozyme in the pore fluid and in the adsorbed phase are non-zero at every point in the particle, and this makes the average concentration of lysozyme in the pore fluid and in the adsorbed phase of the perfusive particle higher than that in the pore fluid and in the adsorbed phase of the purely diffusive particle. Further, the results in Fig. 11 show that as the intraparticle velocity, v_p, increases, the concentration minimum in the pore fluid and the concentration minimum in the adsorbed phase move downstream while the overall lysozyme content of the particle increases.

Certain interesting aspects of column performance could be studied by examining some characteristic pieces of information of the dynamic behavior of a given column. When the value of C_p in the equilibrium isotherm expression is equal to the inlet concentration of the adsorbate, $C_{d,in}$, in the column, then the equilibrium isotherm expression would provide the equilibrium value for the concentration of the adsorbate in the adsorbed phase, C_s, for the given value of $C_{d,in}$. Then, by knowing the total amount of the adsorbent particles in a given column, one can calculate the equilibrium amount of adsorbate that could be adsorbed in the column for the given inlet concentration $C_{d,in}$. Hence one possible measure for evaluating the performance of a given column [it should be noted that adsorption in a column is a dynamic (non-steady-state) operation], could be the ratio of the amount of adsorbate that has been adsorbed in the particles of the column after a certain time of operation to the amount of adsorbate that could be adsorbed in the particles of the column at equilibrium. This ratio is called here relative adsorptivity; the percentage of relative adsorptivity is obtained by multiplying the relative adsorptivity by 100.

It is thought that a plot of the percentage of relative adsorptivity *versus* time could provide useful information for evaluating column performance. If, for example, a high value for the percentage of relative adsorptivity may be obtained in a shorter time, then this could imply that in a given overall operational time a larger number of adsorption cycles could be realized. Another possible measure for evaluating the performance of a given column is to examine the variation in the value of the percentage of relative adsorptivity when the percentage of breakthrough varies; the percentage of breakthrough is obtained by multiplying the dimensionless ratio $C_d(t,L)/C_{d,in}$ (see Figs. 1–10) by 100. If, for instance, a high value of the percentage of relative adsorptivity may be obtained at a low value of the

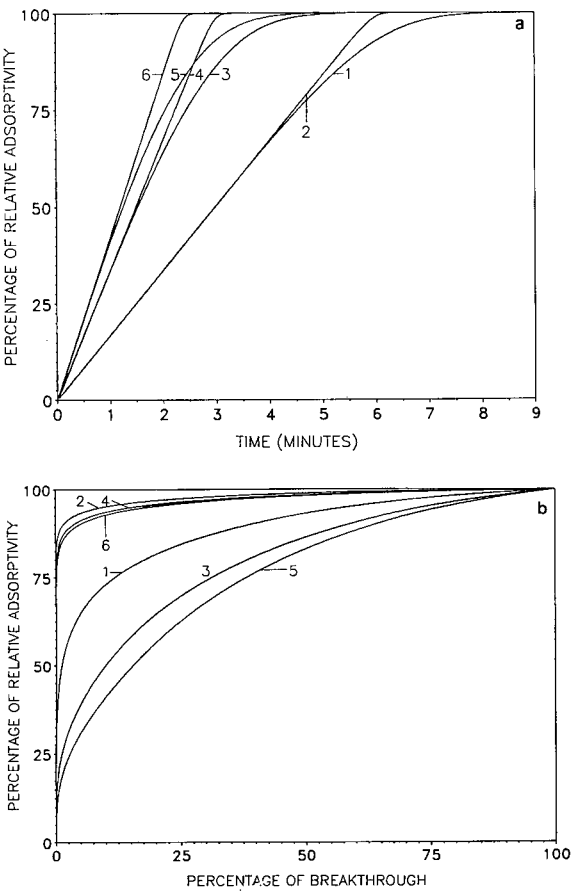

Fig. 12. Percentage of relative adsorptivity *versus* (a) time and (b) percentage of relative adsorptivity *versus* percentage of breakthrough for the lysozyme–monoclonal anti-lysozyme adsorption system. In both instances $L = 0.1$ m; $z_0 = 16.120 \cdot 10^{-6}$ m; (1) $V_f = 2.778 \cdot 10^{-3}$ m/s, $v_p = 0$; (2) $V_f = 2.778 \cdot 10^{-3}$ m/s, $v_p = 0.02V_f$; (3) $V_f = 5.556 \cdot 10^{-3}$ m/s, $v_p = 0$; (4) $V_f = 5.556 \cdot 10^{-3}$ m/s, $v_p = 0.02V_f$; (5) $V_f = 6.944 \cdot 10^{-3}$ m/s; $v_p = 0$; (6) $V_f = 6.944 \cdot 10^{-3}$ m/s, $v_p = 0.02V_f$.

percentage of breakthrough, then this could indicate that the adsorption capacity of the particles may have been utilized effectively and the total amount of adsorbate that left the column (before the introduction of column switch) may be not large.

It is thought that a plot of the percentage relative adsorptivity *versus* the percentage of breakthrough could provide useful information for evaluating column performance. In Fig. 12a the percentage of relative adsorptivity for lysozyme is plotted *versus* time and in Fig. 12b it is plotted *versus* the percentage of breakthrough, for a column length of 0.1 m and for different superficial and intraparticle velocities.

The results in Fig. 12a indicate that, for a given time, the highest value of the percentage of relative adsorptivity is obtained when perfusive particles are employed and the superficial velocity has its highest value. Also, for a given time and a given superficial velocity, the perfusive particles provide a higher value of the percentage of relative adsorptivity; further, the differences in the values of the percentage of relative adsorptivity obtained from the purely diffusive and perfusive particles increase when the superficial velocity increases, as well as when the time increases.

The results in Fig. 12b indicate that for a given percentage of breakthrough, the perfusive particles provide a higher value of the percentage of relative adsorptivity. It is also observed that, for a given percentage of breakthrough, the value of the percentage of relative adsorptivity increases as the superficial velocity decreases; the effect of the superficial velocity on the percentage of relative adsorptivity is significantly smaller when perfusive particles are used and practical values for the percentage of breakthrough are considered.

The information in Fig. 12a and b may also be used as follows: for a selected percentage of breakthrough, the value of the percentage of relative adsorptivity is obtained from the appropriate curve in Fig. 12b; this value is then utilized with the appropriate curve in Fig. 12a to obtain the time at which the selected percentage breakthrough will occur. From the above discussion, it is suggested that by examining the kind of information shown in Fig. 12a and b, one could develop operating conditions (after appropriate optimization) that could provide the desired column performance.

Another aspect of the perfusive particles that is examined in this work is the effect of the variation of C_T on column performance. If, for example, one could develop a purely diffusive particle whose pore-size distribution could provide an accessible active surface whose area is larger than that of the perfusive particle, when both the purely diffusive and perfusive particles have the same kind of active surface and the same particle size, then this could suggest that the value of C_T in the purely diffusive particle may be larger than the value of C_T in the perfusive particle. Further, the pore-size distribution of the perfusive particle, the lengths of the throughpores and the distances between the throughpores may result in an effective pore diffusivity for the adsorbate in the perfusive particle that has a higher value than the effective pore diffusivity of the adsorbate in the purely diffusive particle.

It was considered worth examining the effects that the variation of C_T and D_p may have on the dynamic behavior of a column system. In Figs. 13a and 14a, the percentage of relative adsorptivity is plotted *versus* time for the adsorption systems in Table I and for different values of C_T, D_p and v_p. In Figs. 13b and 14b, the percentage of relative adsorptivity is plotted *versus* the percentage of breakthrough for the same adsorption systems and values of C_T, D_p and v_p, as in Figs. 13a and 14a.

The results in Fig. 13a and b indicate that for the β-galactosidase–anti-β-galactosidase system, an increase of 10% in the value of D_p does not appear to have a significant effect on column behavior; the results in Fig. 13b indicate that an increase in the value of D_p by 10% has a small influence on the behavior of the column having purely diffusive particles whereas the effect on the column involving perfusive particles appears to be insignificant. When the value of C_T is reduced by 10%, the results in Fig. 13a and b indicate that the reduction in the C_T value may have a considerable effect on the behavior of a column having purely diffusive or perfusive particles. A comparison of the results expressed by curves 1 and 6 and by curves 3 and 8 in Fig. 13b indicates that the value of the percentage of relative adsorptivity obtained from the perfusive particles, for a given practical value of the percentage of breakthrough, is higher than that obtained from the purely diffusive particles, although the value of C_T of the purely diffusive particles is taken to be 10%

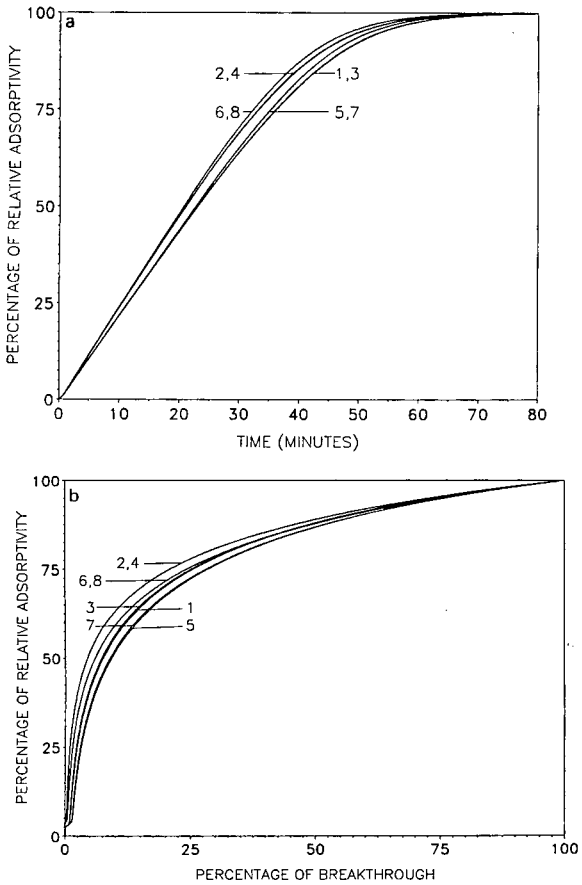

Fig. 13. Percentage of relative adsorptivity *versus* (a) time and (b) percentage of breakthrough for the β-galactosidase–monoclonal anti-β-galactosidase adsorption system. In both instances L = 0.5 m; $z_0 = 16.120 \cdot 10^{-6}$ m; $V_f = 2.778 \cdot 10^{-3}$ m/s; (1) C_T = 2.2 kg/m^3, $D_p = 6.9 \cdot 10^{-12}$ m^2/s, $v_p = 0$; (2) C_T = 2.2 kg/m^3, D_p = $6.9 \cdot 10^{-12}$ m^2/s, $v_p = 0.02V_f$; (3) C_T = 2.2 kg/m^3, D_p = 1.1 · $(6.9 \cdot 10^{-12})$ m^2/s, $v_p = 0$; (4) C_T = 2.2 kg/m^3, D_p = 1.1 · $(6.9 \cdot 10^{-12})$ m^2/s, $v_p = 0.02V_f$; (5) $C_T = 0.9 \cdot (2.2)$ kg/m^3, D_p = $6.9 \cdot 10^{-12}$ m^2/s, $v_p = 0$; (6) $C_T = 0.9 \cdot (2.2)$ kg/m^3, $D_p = 6.9 \cdot 10^{-12}$ m^2/s, $v_p = 0.02V_f$; (7) $C_T = 0.9 \cdot (2.2)$ kg/m^3, D_p = 1.1 · $(6.9 \cdot 10^{-12})$ m^2/s, $v_p = 0$; (8) $C_T = 0.9 \cdot (2.2)$ kg/m^3, D_p = 1.1 · $(6.9 \cdot 10^{-12})$ m^2/s, $v_p = 0.02V_f$.

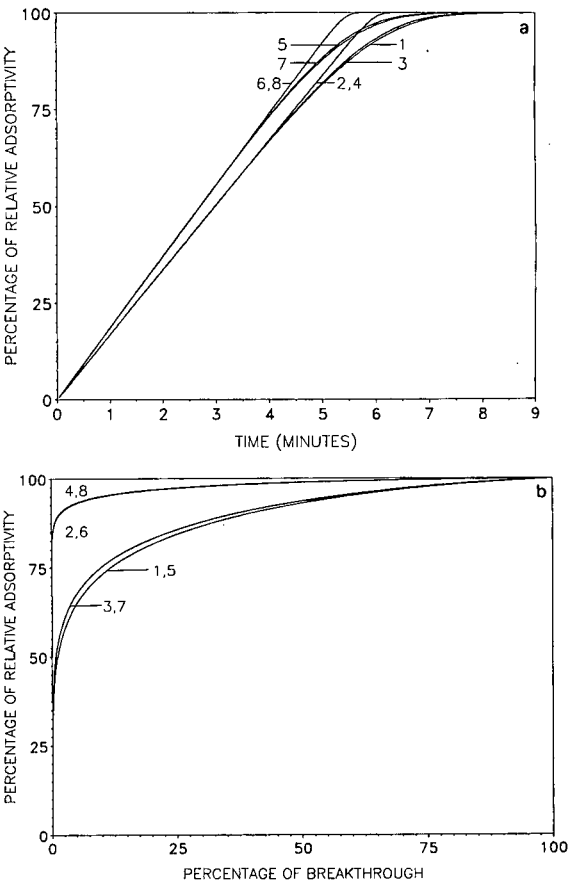

Fig. 14. Percentage of relative adsorptivity *versus* (a) time and (b) percentage of breakthrough for the lysozyme–monoclonal anti-lysozyme adsorption system. In both instances L = 0.1 m; $z_0 = 16.120 \cdot 10^{-6}$ m; $V_f = 2.778 \cdot 10^{-3}$ m/s; (1) C_T = 2.2 kg/m^3, $D_p = 17.885 \cdot 10^{-12}$ m^2/s, $v_p = 0$; (2) C_T = 2.2 kg/m^3, D_p = $17.885 \cdot 10^{-12}$ m^2/s, $v_p = 0.02V_f$; (3) C_T = 2.2 kg/m^3, D_p = 1.1 · $(17.885 \cdot 10^{-12})$ m^2/s, $v_p = 0$; (4) C_T = 2.2 kg/m^3, D_p = 1.1 · $(17.885 \cdot 10^{-12})$ m^2/s, $v_p = 0.02V_f$; (5) $C_T = 0.9 \cdot (2.2)$ kg/m^3, D_p = 17.885 · 10^{-12} m^2/s, $v_p = 0$; (6) $C_T = 0.9 \cdot (2.2)$ kg/m^3, D_p = 17.885 · 10^{-12} m^2/s, $v_p = 0.02V_f$; (7) $C_T = 0.9 \cdot (2.2)$ kg/m^3, D_p = 1.1 · $(17.885 \cdot 10^{-12})$ m^2/s, $v_p = 0$; (8) $C_T = 0.9 \cdot (2.2)$ kg/m^3, D_p = 1.1 · $(17.885 \cdot 10^{-12})$ m^2/s, $v_p = 0.02V_f$.

larger than the C_T value of the perfusive particles.

The results in Fig. 14a indicate that for the lysozyme–anti-lysozyme system, an increase of 10% in the value of D_p does not appear to have a significant effect on column behavior; an increase in the value of D_p by 10% has a small influence on the behavior of the column having purely diffusive particles, and this appears to occur only at longer times of operation. When the value of C_T is reduced by 10%, the results in Fig. 14a indicate that the reduction in the C_T value may have a considerable effect on the dynamic behavior of a column having purely diffusive or perfusive particles. The data in Fig. 14b suggest that for practical values of the percentage of breakthrough, an increase in the value of D_p by 10% has some effect on the value of relative

adsorptivity obtained from the columns having purely diffusive particles, whereas it has an insignificant effect on the value of the percentage of relative adsorptivity obtained from the columns with perfusive particles. In Fig. 14b, it is also observed that the effect of the reduced value of C_T on the percentage of relative adsorptivity, for a given practical value of the percentage of breakthrough, is not significant for this adsorption system. A comparison of the results in Fig. 14b indicates that the value of the percentage of relative adsorptivity obtained from the perfusive particles is higher than that obtained from the purely diffusive particles, even when the value of C_T of the perfusive particles is 10% smaller than the C_T value of the purely diffusive particles.

It is worth mentioning again here that the dynamics of the interaction kinetics of the lysozyme–anti-lysozyme adsorption system are faster than those of the β-galactosidase–anti-β-galactosidase adsorption system, and that the effective pore diffusivity of lysozyme is higher than that of β-galactosidase; these differences were found to be responsible for the differences observed in the dynamic behavior of these systems. It should be noted that by combining and examining (as discussed above for Fig. 12a and b) the kind of information shown in Fig. 13a and b or in Fig. 14a and b, one could develop operating conditions (by varying, for example, the values of V_f, v_p and L, and performing appropriate system optimization) that could provide the desired column performance under conditions of variation (or uncertainty) in the values of C_T and D_p.

In Figs. 15 and 16, the breakthrough curves of lysozyme when the interaction of lysozyme with immobilized monoclonal anti-lysozyme is taken to be infinitely fast (eqn. 25), are shown for different particle sizes and intraparticle velocities. It can be observed (as was the case when the results in Figs. 6 and 7 were compared) that the effect of particle size on the breakthrough curve of lysozyme obtained from purely diffusive particles is very significant, whereas the magnitude of the effect is considerably smaller when perfusive particles are employed in the column. The breakthrough curves obtained from the perfusive particles are very steep and, for a given particle size, the time at which breakthrough begins is increased as the intraparticle velocity, v_p, increases. Further, for a given intraparticle velocity,

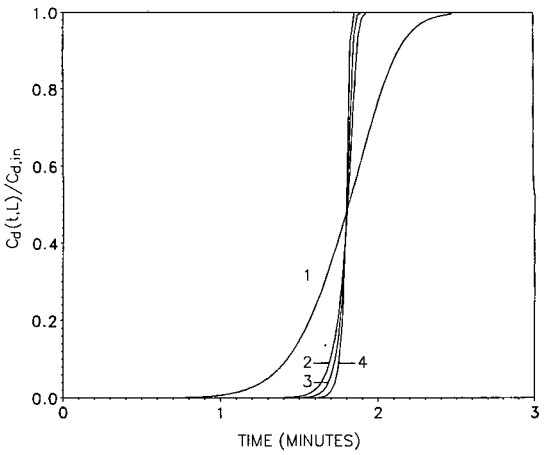

Fig. 15. Breakthrough curve of lysozyme when the dynamics of the interaction kinetics of the adsorption step are taken to be infinitely fast. $L = 0.03$ m; $z_0 = 8.060 \cdot 10^{-6}$ m; $V_f = 2.778 \cdot 10^{-3}$ m/s; (1) $v_p = 0$; (2) $v_p = 0.02V_f$; (3) $v_p = 0.03V_f$; (4) $v_p = 0.05V_f$.

v_p, the time at which breakthrough begins is increased as the particle size decreases.

In Fig. 17a, the percentage of relative adsorptivity is plotted *versus* time for the lysozyme–anti-lysozyme system, when the interaction kinetics between the adsorbate and ligand do not occur infinitely fast (system in Fig. 7), and when the interaction kinetics

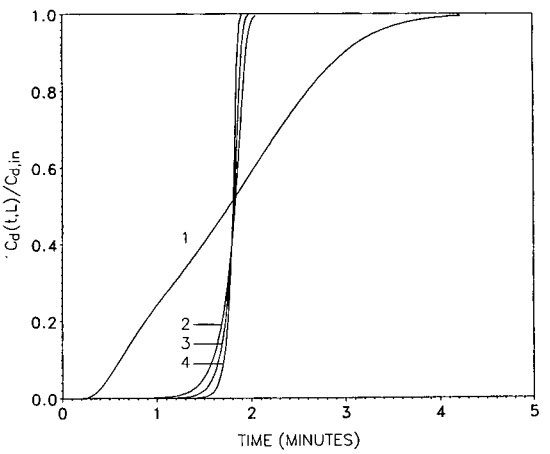

Fig. 16. Breakthrough curve of lysozyme when the dynamics of the interaction kinetics of the adsorption step are taken to be infinitely fast. $L = 0.03$ m; $z_0 = 16.120 \cdot 10^{-6}$ m; $V_f = 2.778 \cdot 10^{-3}$ m/s; (1) $v_p = 0$; (2) $v_p = 0.02V_f$; (3) $v_p = 0.03V_f$; (4) $v_p = 0.05V_f$.

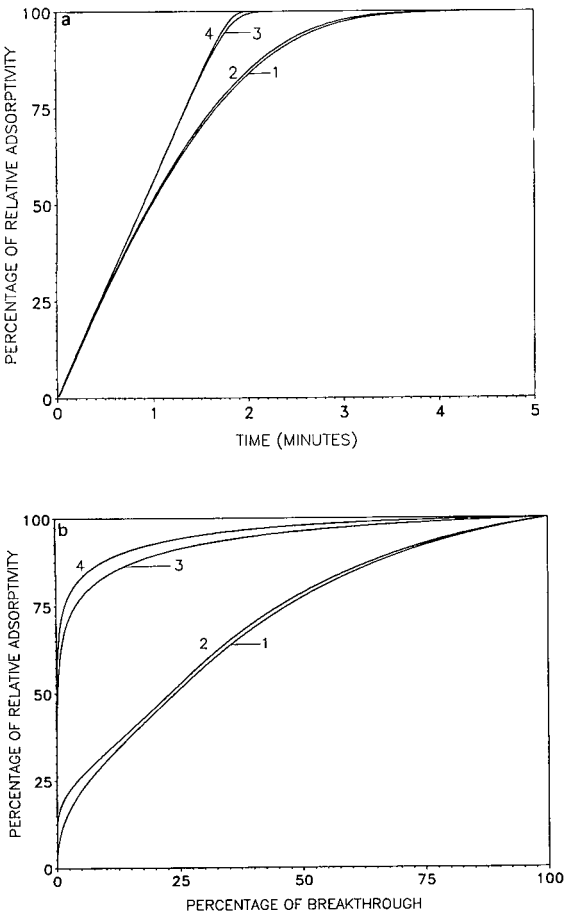

Fig. 17. Percentage of relative adsorptivity *versus* (a) time and (b) percentage of breakthrough for the lysozyme–monoclonal anti-lysozyme system when the dynamics of the interaction kinetics of the adsorption step are as follows: case I = finite (relatively fast) and case II = infinitely fast. $L = 0.03$ m; $z_0 = 16.120 \cdot 10^{-6}$ m; $V_f = 2.778 \cdot 10^{-3}$ m/s; (1) case I, $\nu_p = 0$; (2) case II, $\nu_p = 0$; (3) case I, $\nu_p = 0.02V_f$; (4) case II, $\nu_p = 0.02V_f$.

are taken to occur infinitely fast (system in Fig. 16); for the same adsorption system and conditions, the percentage of relative adsorptivity is plotted *versus* the percentage of breakthrough in Fig. 17b.

The results in Fig. 17a clearly show that, for a given time, the perfusive particles provide a higher percentage of relative adsorptivity than the percentage of relative adsorptivity obtained from the purely diffusive particles. However, for a given time and for the same value of ν_p, the data in Fig. 17a indicate that the differences in the values of the percentage of relative adsorptivity obtained from finite and infinitely fast interaction kinetics are small; it should be noted that the implications of the influence of ν_p and of the kinetics of interaction on column performance should be analyzed by considering simultaneously (by combining) the information obtained from Fig. 17a and b, as discussed earlier.

The results in Fig. 17b clearly show that, for a given percentage of breakthrough, the perfusive particles provide a higher percentage of relative adsorptivity than the percentage of relative adsorptivity obtained from the purely diffusive particles; however, the data in Fig. 17b indicate that for a given practical value of the percentage of breakthrough, the differences in the values of the percentage of relative adsorptivity obtained from finite and infinitely fast interaction kinetics are larger for the system involving perfusive particles. This latter result and the results obtained from the analysis of the data in Figs. 1–14 suggest that for adsorption systems having relatively fast or infinitely fast interaction kinetics, the use of perfusive particles could have the potential to provide improved column performance.

CONCLUSIONS

A mathematical model of perfusion chromatography has been constructed for column systems. The theoretical expression of the model could describe single- and multi-component adsorption in perfusive ($\nu_p > 0$) particles, and also in purely diffusive ($\nu_p = 0$) particles. The equations of the model for the adsorbent particles include the intraparticle mass transfer mechanisms of convection (intraparticle fluid flow) and diffusion, and the mass transfer step involving the interaction between the adsorbate molecules and the active sites on the surface of the porous adsorbent particles. The continuity expression for the fluid flowing stream in the column includes the mechanism of axial dispersion.

The perfusion chromatographic model was solved and used to study the dynamic behavior of column systems having perfusive or purely diffusive adsorbent particles of slab geometry. Two different adsorption systems were examined: one system considers the adsorption of β-galactosidase on immobilized monoclonal anti-β-galactosidase, and the other system involves the adsorption of lysozyme on

immobilized monoclonal anti-lysozyme. The values of the rate constants that characterize the dynamics of the interaction kinetics of the adsorption step are significantly different for these two adsorption systems. Whereas the dynamics of the interaction mechanisms for these two different adsorption systems are finite, a third case was also examined where the dynamics of the interaction mechanisms were considered to be infinitely fast. The dynamic behavior of column systems (frontal analysis studies) was examined for different column lengths (L), particle sizes (z_0), column fluid superficial velocities (V_f) and intraparticle fluid velocities (v_p), and for different values of the effective pore diffusivity (D_p) and of the parameter C_T that represents the highest concentration that the adsorbate could have in the adsorbed phase [the value of the parameter C_T could increase (decrease) if the total concentration of accessible active sites on the surface of the particles could increase (decrease)].

The results indicate that when the dynamics of the interaction kinetics of the adsorption step are relatively not fast and the column fluid superficial velocity is low, then the breakthrough curves obtained from column systems having perfusive particles are not significantly different from the breakthrough curves obtained from columns having purely diffusive particles; when the column fluid superficial velocity is high, then the breakthrough curves obtained from the columns involving perfusive particles are different from those obtained from columns with purely diffusive particles, and their differences become larger as the particle size increases.

When the dynamics of the interaction kinetics of the adsorption step are relatively fast or infinitely fast, the results show that the breakthrough curves obtained from column systems having perfusive particles are very steep, and the shape of the breakthrough curves was found (for the system conditions studied in this work) not to be significantly affected when the particle size (z_0) and the column fluid superficial velocity (V_f) were increased; on the contrary, the shape of the breakthrough curves obtained from column systems involving purely diffusive particles was found to be influenced significantly when the particle size and the column fluid superficial velocity were increased. Further, the steepness of the breakthrough curves obtained from columns having perfusive particles and the time at which breakthrough begins were found to increase with increasing intraparticle fluid velocity in the systems studied in this work. When the value of C_T of the perfusive particles was reduced by 10% relative to that of the purely diffusive particles, it was found that (for the systems examined here) the columns with the perfusive particles provided a higher percentage of relative adsorptivity than that obtained from the columns with the purely diffusive particles.

In conclusion, the results obtained from the systems studied in this work suggest that for adsorption systems having relatively fast or infinitely fast interaction kinetics (that is, the dynamics of the interaction step between the adsorbate molecules and the active sites are relatively fast or infinitely fast), the use of perfusive particles could have the potential to provide improved column performance.

ACKNOWLEDGEMENTS

The authors gratefully acknowledge support of this work by Monsanto and the NATO Scientific Affairs Division under Grant No. 880770.

SYMBOLS

A	molecule of adsorbate (expression 22)
AS	adsorbate–active site complex (expression 22)
C_d	concentration of adsorbate (single-component system) in the flowing fluid stream of the column, kg/m^3
C_{di}	concentration of component i (multicomponent system) in the flowing fluid stream of the column, kg/m^3
$C_{d,in}$	concentration of adsorbate (single-component system) at $x < 0$ when $D_L \neq 0$, or at $x = 0$ when $D_L = 0$, kg/m^3
$C_{di,in}$	concentration of component i (multicomponent system) at $x < 0$ when $D_{Li} \neq 0$, or at $x = 0$ when $D_{Li} = 0$, kg/m^3
C_p	concentration of adsorbate (single-component system) in pore fluid, kg/m^3
$\mathbf{C}_p$	vector of concentration variables defined after eqn. 9

C_{pi} concentration of component i (multi-component system) in pore fluid, kg/m^3

$\bar{C}_{psi}$ concentration variable defined in eqn. 16

C_s concentration of adsorbate (single-component system) in adsorbed phase, kg/m^3 particle

$\mathbf{C}_s$ vector of concentration variables defined after eqn. 9

C_{si} concentration of component i (multi-component system) in adsorbed phase, kg/m^3 particle

C_T maximum equilibrium concentration of adsorbate (single-component system) in adsorbed phase when all accessible active sites are utilized (eqn. 24), kg/m^3 particle

D_L axial dispersion coefficient of adsorbate (single-component system), m^2/s

D_{Li} axial dispersion coefficient of component i (multi-component system), m^2/s

D_p effective pore diffusion coefficient of adsorbate (single-component system), m^2/s

$\mathbf{D}_p$ effective pore diffusivity matrix (multi-component system)

D_{pij} effective pore diffusion coefficients of multi-component system (terms of the effective pore diffusivity matrix), m^2/s

$\mathbf{D}_s$ surface diffusivity matrix (multi-component system)

D_s surface diffusion coefficient of adsorbate (single-component system), m^2/s

D_{sij} surface diffusion coefficients of multi-component system (terms of the surface diffusivity matrix), m^2/s

dV volume differential in eqns. 16 and 19

$f_i(\mathbf{C}_p, \mathbf{C}_s, \mathbf{k})$ functional form defined after eqn. 9

$g_i(\mathbf{C}_p, \mathbf{K})$ functional form defined after eqn. 11

K equilibrium adsorption constant of adsorbate (single-component system), $K = k_1/k_2$, m^3/kg

$\mathbf{K}$ vector of equilibrium adsorption constants defined after eqn. 11

$\mathbf{k}$ vector of adsorption rate constants defined after eqn. 9

K_p permeability of the porous adsorbent particle (eqn. 20), m^2

k_1 adsorption rate constant in eqn. 23, m^3/kg · s

k_2 adsorption rate constant in eqn. 23, s^{-1}

l total number of components adsorbed by specific and non-specific adsorption (multi-component system)

L column length, m

n total number of components in multi-component system

r radial distance in adsorbent particle of spherical geometry, m

r_0 radius of spherical adsorbent particle, m

S active site (expression 22)

T temperature, K

t time, s

V_f column fluid superficial velocity, m/s

v_p intraparticle fluid velocity (intraparticle convective velocity), m/s

V_{pv} volume of adsorbent particle, m^3

x axial distance, m

z space coordinate of adsorbent particle of slab geometry, m

z_0 length (size) of adsorbent particle of slab geometry, m

Greek letters

α_1 constant in eqn. 20

α_2 constant in eqn. 20

ε void fraction in column

ε_p void fraction in porous adsorbent particle

REFERENCES

1 N. B. Afeyan, N. F. Gordon, I. Mazsaroff, L. Varady, S. P. Fulton, Y. B. Yang and F. E. Regnier, *J. Chromatogr.*, 519 (1990) 1.

2 J. H. Petropoulos, J. K. Petrou and A. I. Liapis, *Ind. Eng. Chem. Res.*, 30 (1991) 1281.

3 J. H. Petropoulos, A. I. Liapis, N. P. Kolliopoulos, J. K. Petrou and N. K. Kanellopoulos, *Bioseparation*, 1 (1990) 69.

4 A. I. Liapis and D. W. T. Rippin, *Chem. Eng. Sci.*, 32 (1977) 619.

5 A. I. Liapis and D. W. T. Rippin, *Chem. Eng. Sci.*, 33 (1978) 593.

6 M. Balzli, A. I. Liapis, and D. W. T. Rippin, *Trans. Inst. Chem. Eng.*, 56 (1978) 145.

7 A. I. Liapis and D. W. T. Rippin, *AIChE J.*, 25 (1979) 455.

8 A. I. Liapis and R. J. Litchfield, *Chem. Eng. Sci.*, 35 (1980) 2366.

9 D. M. Ruthven, *Principles of Adsorption and Adsorption Processes*, Wiley, New York, 1984.

10 B. H. Arve and A. I. Liapis, *AIChE J.*, 33 (1987) 179.

11 D. M. Ruthven, in A. I. Liapis (Editor), *Fundamentals of Adsorption*, Engineering Foundation, New York, 1987, pp. 29–49.

12 B. H. Arve and A. I. Liapis, *Biotechnol. Bioeng.*, 32 (1988) 616.
13 A. I. Liapis, *J. Biotechnol.*, 11 (1989) 143.
14 P. C. Wankat, *Rate-Controlled Separations*, Elsevier Applied Science Publ., Barking, 1990.
15 A. I. Liapis, *Sep. Purif. Methods*, 19 (1990) 133.
16 M. A. McCoy and A. I. Liapis, *J. Chromatogr.*, 548 (1991) 25.
17 F. H. Arnold, H. W. Blanch and C. R. Wilke, *Chem. Eng. J.*, 30 (1985) B9.
18 J. H. Harwell, A. I. Liapis, R. J. Litchfield and D. T. Hanson, *Chem. Eng. Sci.*, 35 (1980) 2287.
19 C. J. Geankoplis, *Transport Processes and Unit Operations*, Allyn & Bacon, Boston, 2nd ed., 1983.
20 F. H. Arnold, H. W. Blanch and C. R. Wilke, *Chem. Eng. J.*, 30 (1985) B25.
21 W. Norde, *Adv. Colloid Interface Sci.*, 25 (1986) 267.
22 A. I. Liapis, in A. B. Mersmann and S. E. Scholl (Editors), *Fundamentals of Adsorption*, Engineering Foundation, New York, 1990, pp. 25–61.
23 A. I. Liapis, A. B. Anspach, M. E. Findley, J. Davies, M. T. W. Hearn and K. K. Unger, *Biotechnol. Bioeng.*, 34 (1989) 467.
24 H. L. Toor and K. R. Arnold, *Ind. Eng. Chem., Fundam.*, 4 (1965) 363.
25 A. I. Liapis and R. J. Litchfield, *Trans. Inst. Chem. Eng.*, 59 (1981) 122.
26 I. Lundstrom, B. Ivarsson, U. Jonsson and H. Elwing, in W. J. Feast and H. S. Munro (Editors), *Polymer Surfaces and Interfaces*, Wiley, New York, 1987, pp. 201–230.
27 R. L. Beissinger and E. F. Leonard, *J. Colloid Interface Sci.*, 85 (1982) 521.
28 A. L. Myers, in A. I. Liapis (Editor), *Fundamentals of Adsorption*, Engineering Foundation, New York, 1987, pp. 3–25.
29 E. C. Moreno, M. Kresak, J. J. Kane and D. I. Hay, *Langmuir*, 3 (1987) 511.
30 D. P. Valenzuela and A. L. Meyers, *Adsorption Equilibrium Data Handbook*, Prentice Hall, Englewood Cliffs, NJ, 1989.
31 O. Talu and I. Zweibel, *AIChE J.*, 32 (1986) 1263.
32 C. M. Shu, S. Kulvaranon, M. E. Findley and A. I. Liapis, *Sep. Technol.*, 1 (1990) 18.
33 B. H. Arve, *Ph.D. Dissertation*, Department of Chemical Engineering, University of Missouri–Rolla, Rolla, MO, 1986.
34 M. A. McCoy, *Report Number 5*, Department of Chemical Engineering, University of Missouri-Rolla, Rolla, MO, 1991.
35 R. B. Bird, W. E. Stewart and E. N. Lightfoot, *Transport Phenomena*, Wiley, New York, 1960.
36 J. Villadsen and M. L. Michelsen, *Solution of Differential Equation Models by Polynomial Approximation*, Prentice-Hall, Englewood Cliffs, NJ, 1978.
37 C. D. Holland and A. I. Liapis, *Computer Methods for Solving Dynamic Separation Problems*, McGraw-Hill, New York, 1983.
38 T. Wicks, *Scientific Computing and Analysis Library Report*, SCA-LR-52, Boeing Computer Services, Seattle, WA, 1988.
39 M. A. McCoy, B. J. Hearn and A. I. Liapis, *Chem. Eng. Commun.*, 108 (1991) 225.

Journal of Chromatography, 599 (1992) 105–111
Elsevier Science Publishers B.V., Amsterdam

CHROMSYMP. 2549

Isolation of *Der pI*, the *Dermatophagoides pteronyssinus* major mite allergen, from a crude mite culture extract, purification by ion-chromatography, and comparison between the material obtained and a cDNA-coded *Der pI*

J.-P. Dandeu*, J. Rabillon, M. Lux and B. David

Unité d'Immuno-Allergie, Institut Pasteur, Paris (France)

J.-L. Guillaume and L. Camoin

Immuno-Pharmacologie, CNRS SDI-6231, CHU Cochin, Paris (France)

ABSTRACT

A high degree of purity is a prerequisite for an allergen preparation to be suitable for clinical diagnosis and therapy. A pure allergen can easily be obtained from a crude mite culture extact by using an immunosorbent prepared with highly specific monoclonal antibodies or from a cDNA-coded material. However, up to now none of these methods has been performed on a process scale. Here large-scale purification is defined as a process in which a crude *Dermatophagoides pteronyssinus* mite culture extract is essentially fractionated by acetone and ammonium sulphate precipitations followed by anion-exchange high-performance liquid chromatography. A high yield of a very pure *Der pI* allergen is obtained during the first isocratic run, as shown by sodium dodecylsulphate–polyacrylamide gel electrophoresis, capillary electrophoresis, chromatofocusing and a two site monoclonal antibody enzyme-linked immunosorbent assay. Microsequencing revealed that the 25-residue sequence obtained is entirely in agreement with the sequence derived from the cDNA of *Der pI*.

INTRODUCTION

The major allergen from *Dermatophagoides pteronyssinus* mite was first isolated about 10 years ago [1–3] and was shown to have common epitopes with the corresponding major allergen of the *Dermatophagoides farinae* mite [4], a second species of the same arthropod family. Both allergens were isolated by several authors but *Der pI* (named p1, Ag 7 or Ag 42 before standardization [5]) was more purified in particular by Chapman and Platts-Mills [1] from *D. pteronyssinus* mite culture and *Der fI* (named Ag 11, Ag 21, Ag 6 before standardization [5]) by Dandeu *et al.* [6] from a *D. farinae* mite culture.

Both *Der pI* and *Der fI* were stated to be single peptides with some traces of carbohydrates. The binding of these to the protein moiety was not fully demonstrated. Similarity between its inferred amino acid sequence and the group of cysteine proteases appeared from the sequence of the mRNA [7,8] and secondly of the cDNA [9] coding for *Der pI*. Here we confirm these observations, as our results essentially do not differ from those of the above-mentioned experiments, at least for the amino acid sequence of the 25-residue N-terminal peptide of *Der pI*, biochemically prepared from a crude mite culture extract.

EXPERIMENTAL

Dp 80d

A partially purified extract was prepared from

0021-9673/92/$05.00

the crude mite culture extract obtained according to the method described previously in detail [10] by exhaustive dialysis against water [6]. When the absorbance of the dialysate reached zero, the resulting brownish solution was named Dp 80d.

The A 60 fraction

A very enriched *Der pI* fraction was obtained at 60% ammonium sulphate saturation as described previously [6] for *D. farinae*. The precipitate was dissolved in water, exhaustively dialysed against water and lyophilized.

Anion-exchange chromatography

Preliminary experiments showed that all of the allergenic components of A 60 were negatively charged [4], so an anion exchanger was used to separate them. A Mono Q HR 10/10 column (Pharmacia, Uppsala, Sweden) controlled by a fast protein liquid chromatographic (FPLC) system (Pharmacia) was equilibrated with 0.02 *M* Tris–HCl buffer (pH 8.60).

A 200-mg sample of A 60 dissolved in the same buffer was loaded on to the column. Stepwise elution was performed: first an isocratic run with the equilibration buffer was carried out at 1 ml/min followed by a second and third steps with the same buffer containing 1 *M* and 2 *M* NaCl, respectively, at 3 ml/min. The absorbance was monitored at 280 nm. Thereafter the column was re-equilibrated and used again.

Two-site monoclonal antibody enzyme-linked immunosorbent assay (Mab ELISA)

The identity and degree of purity of the *Der pI* allergen obtained by the process described above were controlled by a two-site Mab ELISA using anti-*Der pI* (5H8) monoclonal antibodies and anti-*Der pI* (4C1) biotinylated monoclonal antibodies from Charlottesville University, VA, USA), Martin Chapman Laboratory, according to the method described by Luczynska *et al.* [11].

A CEB immunoplate (Centre Européen de Biotechnologie, France) was coated with 1 μg per well of Mab 5H8 (anti-*Der pI*, 10 mg/ml) in 0.1 *M* sodium hydrogencarbonate buffer (pH 9.6) overnight at 4°C. The plate was then washed twice with phosphate-buffered saline (PBS) containing 1% of Tween 20 (pH 7.4) and treated for 1 h with 100 μl per well of the same solution containing 1% of bovine serum albumine.

The wells were incubated for 1 h at room temperature with 100 μl of diluted fractions (from 10^{-2} to 10^{-7}) using double dilutions of a reference antigen, *Der pI* International Standard Dp 82518, to make a calibration graph (from 250 to 3.9 ng).

After washing five times, the wells were incubated for 1 h at room temperature with 100 μl of a 1:1000 dilution of biotinylated Mab 4Cl (anti-*Der pI*, 10 mg/ml). The plate was then washed five more times and the wells were incubated for 30 min with 1:1000 streptavidin–peroxidase (Sigma, St. Louis, MO, USA) (0.25 mg of protein was dissolved in 1 ml of distilled water). Finally, the assays were developed by adding 100 μl per well of 1 m*M* ABTS [2,2'-azino di(3-ethylbenzthiazoline-6-sulphonic acid)] and 5% hydrogen peroxide in 70 m*M* citrate–phosphate buffer (pH 4.2) (Sigma). The reaction was stopped after 10 min by adding 100 μl per well of 2 m*M* sodium azide solution. Absorbance was monitored at 414 nm in an ELISA microplate reader.

Capillary electrophoresis

This was performed in an HPE TM 100 system (Bio-Rad, France) at 8 kV/cm for 8 s on a coated HPE capillary cartridge (50 cm × 50 μm I.D.). from Bio-Rad. A 0.1 *M* phosphate buffer (pH 2.5) from Bio-Rad was used. Absorbance was monitored at 214 nm.

Chromatofocusing

A Mono P column of the HR 5/20 type (Pharmacia) was used after being equilibrated with 0.025 *M* Tris buffer (pH 8). The protein of interest was dissolved in the same buffer and loaded on to the column. A linear concentration gradient was applied, between 0 and 100% of Servalytes 2–4 at 40% (Serva, Heidelberg, Germany) diluted with water to 0.2% and adjusted to pH 3 with HCl. The pH gradient was recorded using a pH monitor (Pharmacia). Absorbance was monitored at 280 nm.

Sodium dodecyl sulphate–polyacrylamide gel electrophoresis (SDS-PAGE)

Analyses were performed using homogeneous 15% gel on a Hoefner apparatus. Before electrophoresis samples were treated with SDS or with SDS and dithiotreitol (50 m*M*) as reducer. After

electrophoresis Coomassie Brilliant Blue staining was used.

Amino acid analysis

The amino acid compositions were determined with a Beckman Model 7300 amino acid analyser after acidic hydrolysis performed in the vapour phase with 6 *M* HCl containing 0.1% of phenol for 24 h at 110°C *in vacuo*, according to Moore and Stein [12].

Reversed-phase high-performance liquid chromatography (RP-HPLC)

RP-HPLC purification of the allergenic fraction was performed on a Brownlee Labs. Aquapore butyl column (220 mm × 2.1 mm I.D.), using a linear gradient of acetonitrile in water, containing 0.1% of TFA, from 31 to 50% acetonitrile in 60 min at 200 μl/min. The process was controlled by an HPLC system (Pharmacia–LKB). Absorption was monitored at 214 nm.

Protein sequencing and amino acid sequence homology determination

Proteins were sequenced on a Model 470 gas-phase protein sequencer (applied Biosystems, France). Phenylthiohydantoin (PTH) derivatives of amino acids were separated and identified by on-line RP-HPLC with an RP-18 column (Brownlee Labs). Biobrene (Applied Biosystems) was added to prevent wash-out and to improve the initial yields [13].

RESULTS

Dp 80d

Both *D. pteronyssinus* and *D. farinae* mite culture were generally performed on a human danders and yeast extract-supplemented medium. Extraction with an aqueous medium and acetone treatment were first described by Guibert and Causse-Combes [10] and led to a material we named Dp 80 (or Df 80), which was exhaustively dialysed against distilled water in order to eliminate the low-molecular mass molecules, and named "partially purified extract" Dp 80d or Df 80d [4].

Dp A 60

A major allergen-enriched fraction, either *Der pI* or *Der fI* was obtained by ammonium sulphate precipitation at 60% saturation, as was previously described for *Der fI* [6]. Dp A 60 is a very enriched *Der pI* fraction, as shown by two-site Mab ELISA, which indicated a concentration of at least 78% of *Der pI* when compared with the International Standard, as a solution at 2.3 mg/ml contains 1.8 mg/ml of *Der pI*. Therefore, further purification was necessary and the following process was applied.

Anion-exchange chromatography

Using anion-exchange chromatography performed on microbeads of a strong anion exchanger, Mono Q, we were able to purify *Der pI* in a single step. A 200-mg sample of the Dp A 60 fraction was dissolved in and dialysed against solution A, 0.02 *M* Tris–HCl buffer (pH 8.6), and loaded on to the Mono Q HR 10/10 column which had previously been equilibrated with the same buffer.

During the first, isocratic run, with solution A only one peak of non-adsorbed material was eluted. The material strongly bound to the support was desorbed by adding solution B diluted 1:2 with solution A [solution B = 0.02 *M* HCl buffer (pH 8.6) containing 2 *M* NaCl]. Finally, in order to desorb more strongly bound material essentially composed of brownish pigments, the column was washed with 100% solution B.

The elution profile obtained is shown in Fig. 1.

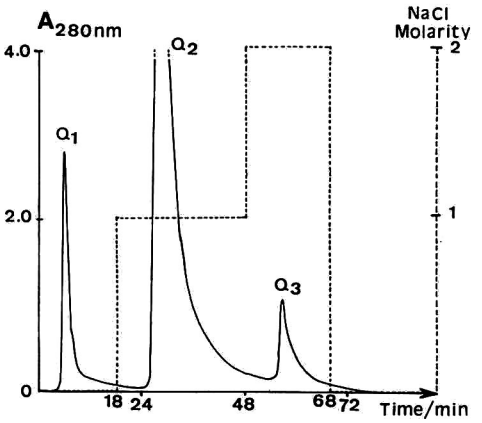

Fig. 1. Chromatogram of Dp 80d on a Mono Q HR 10/10 column equilibrated with 0.02 *M* Tris–HCl buffer (pH 8.6) (solution A). Elution was carried out with 1 *M* NaCl in 0.02 *M* Tris–HCl buffer (pH 8.6) (50% solution B), flow-rate 1 ml/min, followed by 2 *M* NaCl in 0.02 *M* NaCl in 0.02 *M* Tris–HCl buffer (pH 8.6) (100% solution B). Flow-rate, 3 ml/min. UV detection at 280 nm.

The three fractions obtained by this procedure were named Q1, Q2 and Q3 and were tested for their *Der pI* content by the two-site Mab ELISA. Only Q1 contained a significant amount of *Der pI*, *i.e.*, 100%.

The Q1 fraction was analysed using SDS-PAGE, both before and after a reduction treatment with dithiothreitol. In the former instance three bands were observed, with molecular masses (M_r) 25 000, 15 500 and 14 500. In the latter instance only two bands were observed, with M_r 15 000 and 13 500 (Fig. 2).

Only one major peak was found to occur in capillary electrophoresis (Fig. 3). Chromatofocusing (Fig. 4) indicated a p*I* of *ca.* 7.85. Both of these experiments indicated a great homogeneity for the Q1 fraction.

Table I shows the amino acid composition of Q1 in comparison with that found for a cDNA-coded *Der pI* prepared by other workers [7–9]. Significant differences appear for some amino acid residues: in our *Der pI* preparation there is twice as much proline whereas isoleucine, histidine and arginine are present at a concentration half of those determined for the cDNA preparation. There is four times less tyrosine and about five times more lysine.

Der pI purified as described above was submitted to Edman degradation for N-terminal sequence analysis. However, owing to the high background,

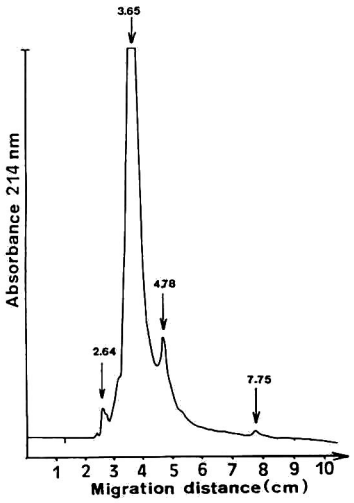

Fig. 3. Electropherogram obtained by capillary electrophoresis as described in the text.

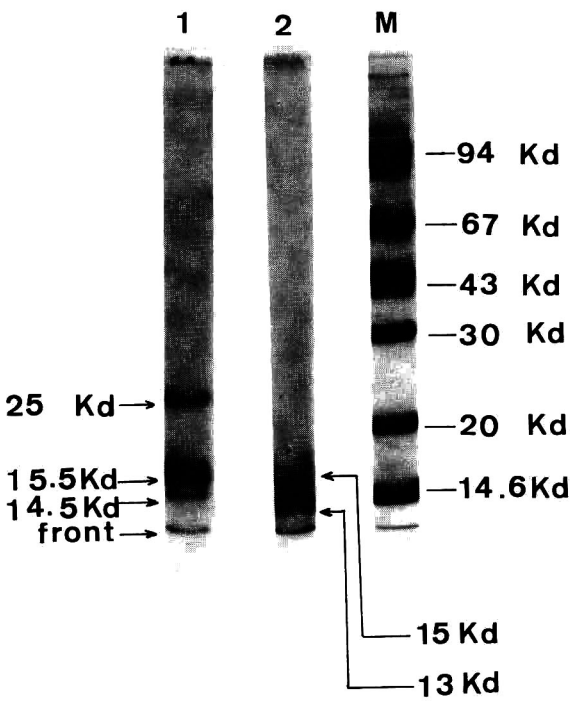

Fig. 2. SDS-PAGE performed in a homogeneous 15% gel. A 1-μl sample of either dithiothreitol-treated or untreated Q1 fraction, corresponding to 10 μg dry weight, was deposited. The gel was stained with Coomassie Brilliant Blue. M = protein markers of known molecular mass. 1 = Native *Der pI* (Q1); 2 = *Der pI* (Q1) treated with dithiothreitol. Kd = kilodaltons.

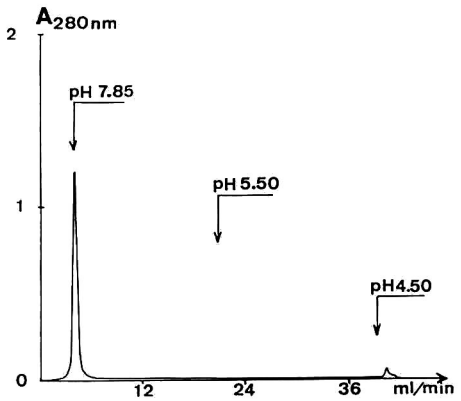

Fig. 4. Chromatofocusing with a Mono P HR 5/20 column equilibrated with 0.025 *M* Tris–HCl buffer (pH 8.00). An 8.5-mg amount of *Der pI* (Q1) was loaded on the column. Elution was performed at a flow-rate of 1.0 ml/min with a Servalytes 2–4 solution at 0.2% adjusted to pH 3.00. The pH gradient was recorded using a pH monitor.

TABLE I

AMINO ACID COMPOSITION

Amino acid	Theoretical (mol%)[a]	*Der pI* (mol%)
Asx	13.4	9.5
Thr	3.7	5.3
Ser	5.1	6.8
Glx	11.6	18.0
Pro	4.2	9.8
Gly	7.8	8.9
Ala	9.2	8.1
Cys	3.7	3.4
Val	5.5	5.4
Ile	7.8	3.6
Leu	4.2	5.6
Met	1.8	1.1
Tyr	8.3	2.0
Phe	1.8	2.2
His	3.2	1.9
Lys	0.9	4.6
Arg	7.8	3.8
Total	100.0	100.0
Trp	—[b]	—[b]

[a] From the cDNA sequence [8].
[b] Not determined.

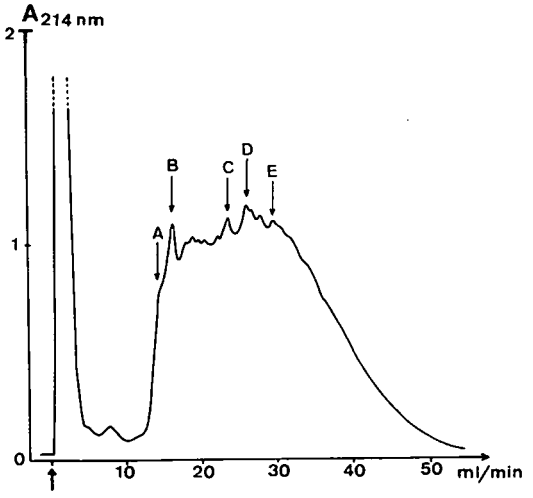

Fig. 5. RP-HPLC purification of the allergenic fraction Q1 performed on an Aquapore butyl column (220 mm × 2.1 mm I.D.) as described in the text.

the first residues were not identified. To overcome this problem, the Q1 fraction was further purified by RP-HPLC to remove contaminating products unrevealed by other analyses. Their presence, however, seems not to influence the allergenic and antigenic activity. The chromatographic data (Fig. 5) showed a sharp peak of non-adsorbed material, only detectable at 214 nm, and major broad overlapping peaks which were collected individually, denoted A, B, C, D and E, respectively and reseparated to homogeneity. Several of these peaks were sequenced for N-terminal analysis. This failed to show differences among the N-terminal residues, suggesting heterogeneity elsewhere in the molecule.

The common 25-residue sequence obtained is shown in Table II. An extent of 52% of homology were found with two cysteine proteases and almost 100% with the cDNA-coded *Der pI* (Table II).

DISCUSSION

Advances in biotechnology have permitted the synthesis and recovery of the specific DNA coding for a given protein and the cloning of it in certain microorganisms. Unfortunately, the protein of interest, although the majority component, is produced together with natural proteins from which it has to be isolated.

A cDNA clone coding for the major house dust *D. pteronyssinus* mite allergen *Der pI* was isolated from a lambda gt 11 library [14]. It produces a fusion protein which reacts with rabbit immunoglobulin G (IgG) antibodies raised against *Der pI* but does not react with human IgE antibodies present in sera from mite-sensitized patients, or at least only very weakly [15]. Moreover, the amount of soluble fusion protein in the bacterial lysate is very low and so far the biochemical preparation of a pure and highly allergenic *Der pI* from mite culture extract remains the only scale process available.

Either from a bacterial lysate or from a mite culture extract, separation and purification of such a biopolymer is performed using liquid chromatography.

Because no two proteins are alike, methods which give satisfactory results with some proteins cannot be used with others. Nevertheless, anion or cathion exchangers are generally effective with most proteins. This was illustrated by the purification of two other important allergens. The cat major allergen, *Fel dI* was isolated and purified from a house dust extract, a very complex mixture of organic and

TABLE II

Der pI HOMOLOGIES (N-TERMINUS): N-TERMINUS COMPARISON

Cysteinyl protease (23)						I	N	G	K	A	T	A	L	A	N	L	R	K	S	R					
						:	:	:		:		:				:	:			:					
cDNA-coded *Der pI* (8)	T	N	A	C	S	I	N	G	N	A	P	A	E	I	D	L	R	Q	M	R	T	V	T	P	I
	:	:	:		:	:	:	:	:	:	:	:	:	:	:	:	:	:	:	:	:	:	:	:	:
Biochemicaly purified *Der pI*	T	N	A	?	S	I	N	G	N	A	P	A	E	I	D	L	R	Q	M	R	T	V	T	P	I
											:			:	:		:					:	:	:	:
Cysteine proteinase 2 precursor (22)											P	K	S	I	D	W	R	T	K	N	A	V	T	P	I

inorganic molecules, using anion-exchange chromatography followed by copper chelate chromatography [16]. Cat serum albumin (CSA), a very potent allergen, was isolated and purified using a similar procedure applied to a cat sera pool [17].

Here we have reported the large-scale preparation of a highly pure *Der pI* using a very simple chromatographic process. This process essentially consists of anion-exchange chromatography on a Mono Q column applied to an ammonium sulphate fraction obtained from a partially purified mite culture extract. The protein of interest is eluted during the first isocratic part of the run. All the contaminants remain strongly bound to the support.

We used an original two-site monoclonal antibody assay described by Luczynska *et al.* [11] to evaluate the concentration and allergenic activity of the *Der pI* allergen, whatever its origin. Monoclonal antibodies significantly improved the standardization of most clinically relevant allergens.

Several techniques for determining the composition and activity of allergens are available. This essentially depends on the specific IgE-containing human sera pool or on the patient populations tested, *e.g.*, radio-allergo-sorbent test (RAST) or crossed radio-immunoelectrophoresis (CRIE). With monoclonal antibodies, as a consequence of their high specificity and homogeneity, a very effective method has been developed in which epitope recognition is the main factor in allergen identification. A prerequisite is the identity between epitopes recognized by human IgE antibodies and these monoclonal antibodies. This has been particularly well reviewed by Diener and Jäger [18]. Two-site immunoassays seem to be the method of choice. Hence we used this assay in comparison with an international standard of the allergen studied and the corresponding monoclonal antibodies [11].

This approach allowed a high degree of allergenic activity for the *Der pI* allergen we isolated and purified to be demonstrated. Moreover, this was confirmed using a histamine release experiment where this pure allergen was tested on basophilic cells from mite-sensitized human patients (results not shown) [19].

In order to assess the real homogeneity of this *Der pI* preparation we performed SDS-PAGE. Here the major component had $M_r \approx 25\,000$, a result very close to that reported by other workers [1,8]. Two other components with M_r 15 500 and 14 500 are also present and probably result from denaturation or degradation. These two lower-M_r peptides can be obtained from the major component by a reducing treatment of the S–S bonds.

These results lead to the suggestion that *Der pI* could consist of two peptides probably held together by one or several disulphide bridges. *Der pI* in the Q1 fraction appears highly homogeneous in capillary electrophoresis, the most critical method of analysis currently available. The relative heterogeneity observed in RP-HPLC may reflect C-terminal variations of the protein (length or amino acid content, a conclusion supported by the results of the amino acid analysis), but may also result from glycosylation of *Der pI*. Although a potential glycosylation site is present in its sequence, no significant amount of saccharides has been found. On chromatofocusing it also appears homogeneous and has a $pI \approx 7.85$, which differs from the $pI \approx 6.6$ mentioned by other workers [1], but this may be explained by the above remarks.

On the other hand, at the level of the 1–25 N-

terminal peptide sequence no differences appear when compared with the same peptide of the cDNA-coded *Der pI*.

As noted above, the cDNA-coded *Der pI* only reacts with rabbit IgG antibodies while its allergenicity was shown to be poor when tested with human specific IgE [15]. The same authors [20] isolated a cDNA coding for the second major allergen from *D. pteronyssinus* mite, *Der pII*, which expressed a high allergenic activity. It should also be noted that Tovey *et al.* [21] cloned and sequenced a cDNA-coded recombinant house dust mite protein that binds human IgE, but it was not identified.

The allergenicity of *Der pI* could be highly dependent on its tertiary structure, which is probably not very well conserved in the cloning process. Post-translational modifications constitute an unpredictable group of changes that can lead to a post-synthetic active or inactive protein. The nature of these changes can be determined by protein sequencing without anticipating their influence on the secondary and tertiary structures. Tertiary structure has the most important function both in the antigenicity and in the allergenicity of a protein. It is also well known that a change of only one amino acid residue in the active site of an enzyme can have a dramatic effect [22]. It should be noted that the catalytic site is particularly conserved in cysteine proteases of highly divergent organisms [23] and this is very important when considering amino acid sequence homology, which has been recognized for *Der pI* with several cysteine proteases. A 25% homology was noted on comparing the sequence of the *Der pI* cDNA clone and its inferred amino acid sequence with those of proteins already analysed [8]. We confirmed this homology on the basis of the 1–25 N-terminal peptide sequence, *i.e.*, 52% homology with the cysteine proteinase 2 precursor (E.C. 7.4.22–.) from *Dictyostelium discoideum* (slime mould) [24] and the cysteinyl protease from *Asclepia syriaca* L. (milkweed) (E.C. 3.4.22.7) [25]. These results do not allow any conclusions to be drawn concerning the role or the origin of the *Der pI* protein.

The availability of large amounts of pure allergen will allow further studies of these points and also of hypersensitization, hyposensitization or tolerance induction in animals for a better understanding of these phenomena in humans.

ACKNOWLEDGEMENTS

Monoclonal antibodies against *Der pI* were kindly provided by M. D. Chapman and T. A. E. Platts-Mills of Charlottesville University, Charlottesville, VA, USA.

REFERENCES

1 M. D. Chapman and T. A. E. Platts-Mills, *J. Immunol.*, 125 (1980) 87.
2 S. Krilis, B. A. Baldo and A. Basten, *J. Allergy Clin. Immunol.*, 74 (1984) 142.
3 P. Lind and H. Löwenstein, *Scand. J. Immunol.*, 17 (1983) 263.
4 J. Le Mao, J.-P. Dandeu, J. Rabillon, M. Lux and B. David, *J. Allergy Clin. Immunol.*, 71 (1983) 588.
5 D. G. Marsh, *Bull. WHO*, 64 (1986) 767.
6 J. P. Dandeu, J. Le Mao, M. Lux, J. Rabillon and B. David, *Immunology*, 46 (1982) 107.
7 G. A. Stewart and W. R. Thomas, *Int. Arch. Allergy Appl. Immunol.*, 83 (1987) 384.
8 K. Y. Chua, G. A. Stewart, W. R. Thomas, R. J. Simpson, R. J. Dilworth, T. M. Plozza and K. J. Turner, *J. Exp. Med.*, 167 (1988) 175.
9 G. A. Stewart, W. R. Thomson, K. Y. Chua, and H. M. Geysen, *Adv. Biosci.*, 74 (1989) 297.
10 L. Guibert and R. Causse-Combes, *Ann. Inst. Pasteur*, 108 (1965) 579.
11 C. M. Luczynska, L. K. Arruda, T. A. E. Platts-Mills, J. D. Miller, M. Lopez and M. D. Chapman, *J. Immunol. Methods*, 118 (1989) 227.
12 S. Moore and W. H. Stein, *J. Biol. Chem.*, 176 (1948) 367.
13 G. E. Tarr, J. F. Beecher, M. Bell and D. McKean, *Anal. Biochem.*, 84 (1978) 622.
14 T. V. Huynh, R. A. Young and R. W. Davis, in D. M. Glover (Editor), *DNA Cloning, Vol. 1, a Practical Approach*, IRL Press, Oxford, Washington, 1985, pp. 48–78.
15 W. R. Thomas, G. A. Stewart, R. J. Simpson, K. Y. Chua, T. M. Plozza, R. J. Dilworth, A. Nisbet and K. J. Turner, *Int. Arch. Allergy Appl. Immunol.*, 85 (1988) 127.
16 J.-P. Dandeu, J. Rabillon, M.-J. Beltrand, M. Lux, R. Duval and B. David, *J. Chromatogr.*, 512 (1990) 177.
17 J.-P. Dandeu, J. Rabillon, J.-L. Guillaume, L. Camoin, M. Lux and B. David, *J. Chromatogr.*, 539 (1991) 475.
18 C. Diener and L. Jäger, *Res. Trends, ACI News*, 1 No. 6 (1989) 180.
19 A. Weyer, personal communication.
20 K. Y. Chua, C. R. Doyle, R. J. Simpson, K. J. Turner, G. A. Stewart and W. R. Thomas, *Int. Arch. Allergy Appl. Immunol.* 91 (1990) 118.
21 E. R. Tovey, M. C. Johnson, A. L. Roche, G. S. Cobon and B. A. Baldo, *J. Exp. Med.*, 170 (1989) 1457.
22 J. F. Bazan and R. J. Fletterick, *Proc. Natl. Acad. Sci. U.S.A.*, 85 (1988) 7872.
23 A. N. Eakin, J. N. Higaki, J. H. McKerrow and C. S. Craik, *Nature (London)*, 342 (1989) 132.
24 C. J. Pears, H. M. Mahbuni and J. G. Williams, *Nucleic Acids Res.*, 13 (1985) 8853.
25 L. A. Allison, M. Moyle, M. Shales and C. J. Ingles, *Cell*, 48 (1985) 599.

Journal of Chromatography, 599 (1992) 113–118
Elsevier Science Publishers B.V., Amsterdam

CHROMSYMP. 2536

High-performance liquid chromatographic separation of detritylated oligonucleotides on highly cross-linked poly-(styrene–divinylbenzene) particles

Christian G. Huber

Institute of Radiochemistry, Leopold-Franzens University, A-6020 Innsbruck (Austria)

Peter J. Oefner and Günther K. Bonn*

Department of Analytical Chemistry, Johannes-Kepler University, A-4040 Linz (Austria)

ABSTRACT

Detritylated oligonucleotides were separated by reversed-phase high-performance liquid chromatography on highly cross-linked polystyrene-based particles having a mean particle diameter of 2.3 μm. The addition of poly(vinyl alcohol) during polymerization, which resulted in the presence of hydroxyl groups on the surface of the poly(styrene–divinylbenzene) beads, was necessary to obtain baseline resolution of phosphorylated oligodeoxyadenylic acids with a chain length of up to 30 bases. The impact of temperature was investigated and optimum resolution was achieved at 40°C. At pH 7.0, the retention times of oligonucleotides were found to depend on the ratio of bases and to increase in the order of C < G < A < T. Under the same conditions, it was possible to separate phosphorylated from dephosphorylated oligonucleotides, the former being eluted earlier. Recoveries ranged from 92 to 100%.

INTRODUCTION

Because of the increasing need for linkers, primers and probes in molecular biology, the demand for single-stranded oligonucleotides has grown rapidly over the past few years. Since the introduction of phosphoramidite chemistry [1], it has been possible to prepare them fairly easily in a short time by using an automated synthesizer. However, the samples synthesized usually contain many impurities together with the target oligonucleotides and hence purification is essential. Polyacrylamide gel electrophoresis [2] and conventional liquid chromatography [3] are mainly employed for this purpose, but they are time consuming and laborious. Therefore, it has been attempted to apply high-performance liquid chromatography (HPLC), in particular reversed-phase [4–6] and ion-exchange modes [7–9]. In reversed-phase HPLC separations, advantage is taken of the hydrophobic 5′-protecting group used during solid-phase synthesis, namely the dimethoxytrityl group, to resolve the desired product from 5′-hydroxylated failure sequences. This approach, however, requires the subsequent hydrolysis and extraction of the purified oligonucleotides before their use in molecular biological experiments. Ion-exchange chromatography, on the other hand, offers high resolution of oligonucleotides which have been already detritylated on the synthesizer, but requires subsequent desalting. Therefore, an optimum chromatographic purification protocol should employ a stationary phase that allows the separation of detritylated oligonucleotides using volatile buffer systems which can be readily evaporated.

Based on the recent demonstration that reversed-phase chromatography on highly cross-linked poly-(styrene–divinylbenzene) (PS–DVB) particles is very effective for the rapid analysis of proteins with

0021-9673/92/$05.00

high resolution [10], we have now investigated the applicability of PS–DVB for the separation of detritylated oligonucleotides.

EXPERIMENTAL

Instrumentation

The HPLC system consisted of two pumps (Model 114M, Beckman, Berkeley, CA, USA), a dynamic gradient mixer (Model 340, Beckman), a gradient controller (Model 421, Beckman), a sample injection valve (Model 7125, Rheodyne, Cotati, CA, USA) with a 20-μl sample loop, a variable-wavelength UV monitor (Model 484, Waters, Milford, MA, USA), a column oven (Model CTO-2A, Shimadzu, Kyoto, Japan) and an integrator (Model C-R6A, Shimadzu).

Chemicals

Styrene, divinylbenzene (DVB) and poly(vinyl alcohol) (PVA) were purchased from Riedel-de Haën (Seelze, FRG). HPLC gradient-grade acetonitrile and methanol were obtained from Merck (Darmstadt, Germany). Buffers were prepared using a stock solution of 2 *M* HPLC-grade triethylammonium acetate (TEAA) (Applied Biosystems, San Jose, CA, USA) and high-purity water (NANOpure; Barnstead, Newton, MA, USA).

Oligonucleotides

Standards of dephosphorylated oligodeoxyadenylic acids [$d(A)_{12}$, $d(A)_{12-18}$], phosphorylated oligodeoxyadenylic acids [$pd(A)_{12}$, $pd(A)_{14}$, $pd(A)_{16}$, $pd(A)_{12-18}$, $pd(A)_{19-24}$, $pd(A)_{25-30}$], phosphorylated oligodeoxycytidylic acids [$pd(C)_{12-18}$], phosphorylated oligodeoxyguanylic acids [$pd(G)_{12-18}$] and phosphorylated oligodeoxythymidylic acids [$pd(T)_{12-18}$] were purchased from Pharmacia (Uppsala, Sweden). Using phosphoramidite chemistry, the oligonucleotides listed in Table I were synthesized on a DNA synthesizer (Model 381-A, Applied Biosystems). Subsequently, they were purified by means of oligonucleotide purification cartridges (Applied Biosystems).

Column

For a 50 × 4.6 mm I.D. column, 1.1 g of the highly cross-linked PS–DVB particles [60% (v/v) DVB], which had been prepared by a two-step microsuspension method either in the absence or in the presence of 0.1% (w/v) PVA [11], were suspended in dioxane. The slurry was then sonicated and packed into the column at a pressure of 70 MPa with the use of an air-driven pump (Model Maximator MSF 111, Ammann Technik, Kölliken, Switzerland) and methanol as the driving solvent. Thereafter, methanol was replaced with water at the same inlet pressure.

Chromatographic conditions

Gradient profiles used for reversed-phase separations are given on each chromatogram. Isocratic runs at appropriate concentrations of organic solvent were made to determine the number of theoretical plates and resolution. The aqueous buffer was 0.1 *M* TEAA (pH 7.0) throughout. In order to keep the concentration of TEAA constant and not to be affected by volume contraction during mixing of organic solvents with water, the mobile phase was prepared as follows: for a 10% solution of acetonitrile in 0.1 *M* TEAA, 50 ml of the 2 M TEAA stock solution were added to 100 ml of acetonitrile in a 1000-ml volumetric flask and the final volume was made up to 1000 ml by the addition of water.

RESULTS AND DISCUSSION

Fig. 1 shows a scanning electron micrograph of the stationary phase particles made of a highly cross-linked styrene–divinylbenzene copolymer. Be-

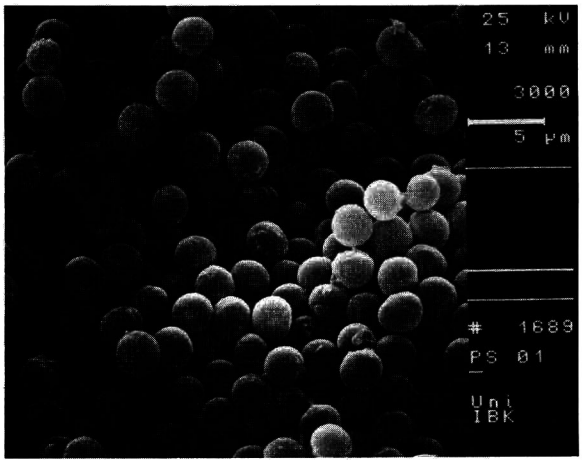

Fig. 1. Scanning electron micrograph of the cross-linked poly(styrene–divinylbenzene) particles used.

cause of their uniform size, no sieving of the beads was required. The mean size and the specific surface area of the particles as assessed by mercury porosimetry were 2.3 μm and 1.3 m^2/g, respectively. No significant differences in size and surface area could be discerned between particles polymerized either in the absence or in the presence of PVA. Moreover, no pores larger than 30 Å could be detected. The advantage of a highly cross-linked PS–DVB adsorbent is that the totally organic polymer is operable over a wide pH range, typically 1–13, without any damage occurring to the packing. This results in a long column lifetime and allows the regeneration of a deteriorated column with aqueous sodium hydroxide, which is of great advantage in the analysis of biopolymers.

The chromatographic performance of PS–DVB batches polymerized without or with PVA is shown in Fig. 2a and b, respectively. It is evident that the addition of PVA during polymerization results in superior resolution of phosphorylated oligodeoxycytidylic and oligodeoxythymidylic acids 12–18 nucleotides in length. PVA was used as a stabilizer during the polymerization step and it is known to be incorporated into the surface of PS beads [12]. Moreover, it has been demonstrated [13] that the adsorption of PVA at a polystyrene–latex surface yields layers of controlled thickness, thus creating both a more homogeneous and also, owing to the presence of hydroxyl groups, a less hydrophobic surface in comparison with PVA-free beads. Hence, the addition of PVA during polymerization led to both shorter retention times and enhanced resolution owing to improved mass transfer.

The effect of temperature on the separation of phosphorylated oligodeoxyadenylic acids 14 and 16 bases in length was studied under isocratic conditions. Optimum resolution (R_s = 5.8) was obtained at column temperature of 30–40°C. This is also reflected in the number of theoretical plates, which was about $2 \cdot 10^4$ m at 40°C with acetonitrile as organic modifier and which declined thereafter to $1 \cdot 10^4$/m at 60°C (Fig. 3). With methanol, the maximum resolution was observed at 22°C (R_s = 5.7) and the number of theoretical plates decreased steadily from $17 \cdot 10^3$ to $3 \cdot 10^3$/m at 22 and 60°C, respectively (Fig. 3). All subsequent separations were carried out with acetonitrile at 40°C because the time of analysis is shorter and the formation of secondary structures due to either self-complemen-

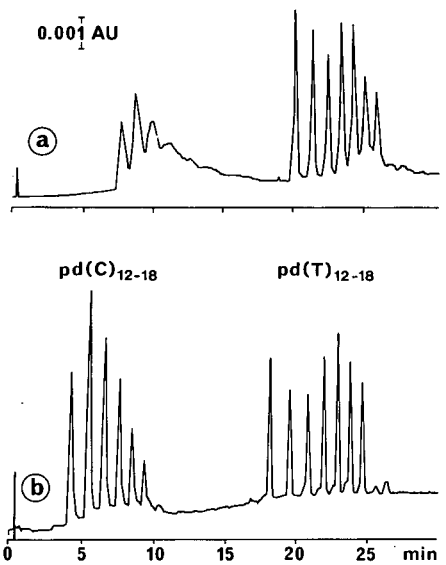

Fig. 2. Comparison of two batches of PS–DVB particles polymerized either (a) without or (b) with PVA. Column, PS–DVB (2.3 μm, 50 × 4.6 mm I.D.); eluents, (A) 0.1 *M* TEAA (pH 7.0) and (B) 0.1 *M* TEAA–acetonitrile (75:25), linear gradient from 10 to 50% B in 40 min; flow-rate, 1 ml/min; temperature, 40°C; detection, UV, 254 nm; sample, 0.5 μg each of $pd(C)_{12-18}$ and $pd(T)_{12-18}$.

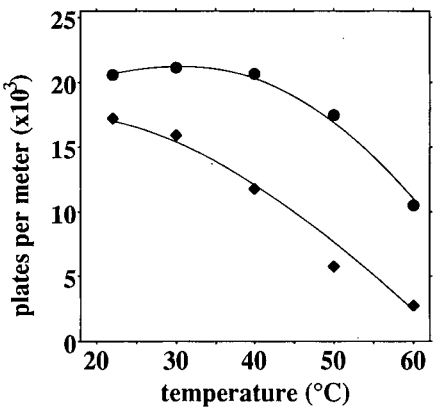

Fig. 3. Number of theoretical plates as a function of temperature under isocratic conditions. Column, PS–DVB–PVA (2.3 μm, 50 × 4.6 mm I.D.); eluents, (●) 0.1 *M* TEAA (pH 7.0)–acetonitrile (95.3:4.7) and (◆) 0.1 *M* TEAA (pH 7.0)–methanol (86.8:13.2); flow-rate, 1 ml/min; detection, UV, 254 nm; sample, 0.165 μg of $pd(A)_{14}$.

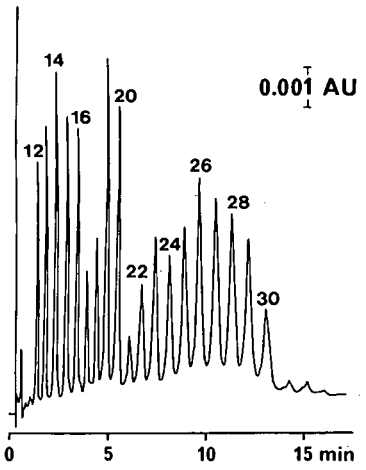

Fig. 4. Chromatogram of a mixture of oligodeoxyadenylic acids, $pd(A)_{12-30}$. Column, PS–DVB–PVA (2.3 μm, 50 × 4.6 mm I.D.); eluents, (A) 0.1 *M* TEAA (pH 7.0) and (B) 0.1 *M* TEAA–acetonitrile (90:10), linear gradient from 48 to 60% B in 3 min, followed by a 20-min linear gradient from 60 to 80% B; flow-rate, 1 ml/min; temperature, 40°C, sample size, 1.125 μg.

tarity or a high G content of the oligonucleotides [14] is reduced.

Using a 3-min linear gradient from 4.8 to 6.0% acetonitrile followed by a 20-min linear gradient from 6.0 to 8.0% acetonitrile, a ladder of phosphorylated oligodeoxyadenylic acids ranging from 12 to 30 nucleotides in length could be resolved completely in less than 13 min (Fig. 4). Subsequently, the efficiency of PS–DVB–PVA particles in separating failure sequences from the desired heterooligonucleotide was evaluated. As shown in Fig. 5, a detri-

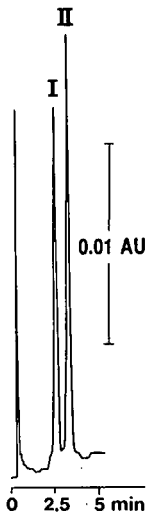

Fig. 5. Chromatogram of two detritylated heterooligonucleotides differing in length by one nucleotide. Column, PS–DVB–PVA (2.3 μm, 50 × 4.6 mm ID.); eluents, (A) 0.1 *M* TEAA (pH 7.0) and (B) 0.1 *M* TEAA–acetonitrile (90:10), linear gradient from 60 to 80% B in 5 min; flow-rate, 1 ml/min; temperature, 40°C; detection, UV, 254 nm; sample size, (I) 0.29 μg and (II) 0.31 μg. For peak identification, see Table I.

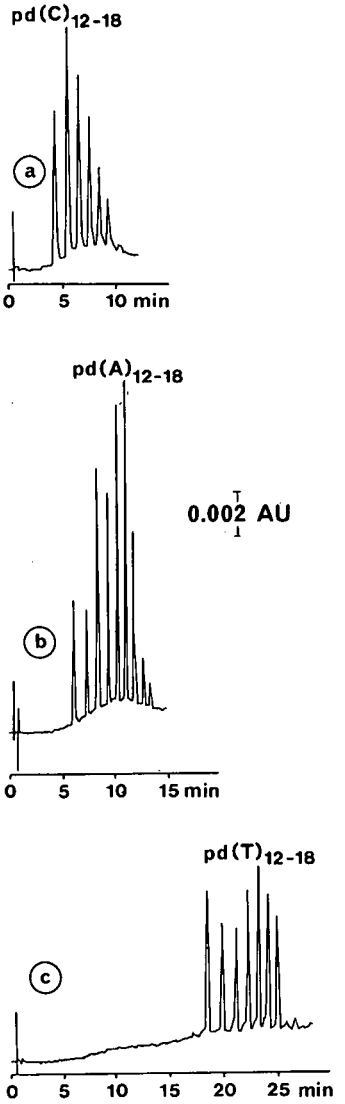

Fig. 6. Retention behaviour of various phosphorylated homooligonucleotides. Column, PS–DVB–PVA (2.3 μm, 50 × 4.6 mm I.D.); eluents, (A) 0.1 *M* TEAA (pH 7.0), and (B) 0.1 *M* TEAA–acetonitrile (75:25), linear gradient from 10 to 50% B in 40 min; flow-rate, 1 ml/min; temperature, 40°C; detection, UV, 254 nm; samples, (a) $pd(C)_{12-18}$, (b) $pd(A)_{12-18}$ and (c) $pd(T)_{12-18}$, 0.5 μg each.

TABLE I

SEQUENCES OF THE OLIGONUCLEOTIDES ANALYSED

Peak	Sequence (5'–3')	Length	C (%)	G (%)	A (%)	T (%)	k'^a
I	GCTCAGTGTAGCCCAGGAT	19	26.2	31.6	21.1	21.1	17.22
II	TGCTCAGTGTAGCCCAGGAT	20	25.0	30.0	20.0	25.0	18.39
III	CATGGGAGGGTTAGATAG	18	5.6	44.4	27.8	22.2	16.16
IV	AGTAGGTGGAAGATTCAG	18	5.6	38.9	33.3	22.2	17.37
V	GTGCTCAGTGTAGCCCAGGATC	22	27.3	31.8	18.2	22.7	18.52
VI	GTGCTCAGTGTAGCCCAGGATG	22	22.7	36.4	18.2	22.7	18.69
VII	GTGCTCAGTGTAGCCCAGGATA	22	22.7	31.8	22.7	22.7	19.08
VIII	GTGCTCAGTGTAGCCCAGGATT	22	22.7	31.8	18.2	27.3	19.39

[a] Capacity factors were determined using a linear gradient of 3% to 10% acetonitrile in 0.1 *M* TEAA in 10 min; flow-rate 1 ml/min; see Fig. 5.

tylated 20-mer oligonucleotide could be separated sucessfully from a detritylated 19-mer oligomer.

Reversed-phase chromatographic separations of oligonucleotides have been found to depend significantly on base composition [15,16]. As can be seen in Fig. 6, the retention times of homooligonucleotides increased in the order C < A < T. Owing to their tendency to fold back and to form aggregates, oligodeoxyguanylic acids (n = 12–18) could not be separated successfully even under strongly denaturing conditions such as 2-min heating at 80°C in the presence of 2 *M* NaOH or 80% formamide, but were eluted as a single broad peak.

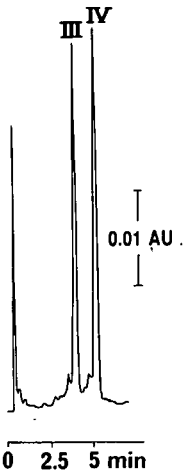

Fig. 7. Effect of base composition on the separation of two heterooligonucleotides of the same chain length. Column, PS–DVB–PVA (2.3 μm, 50 × 4.6 mm I.D.); eluents, (A) 0.1 *M* TEAA (pH 7.0) and (B) 0.1 *M* TEAA–acetonitrile (90:10), linear gradient from 65 to 80% B in 2 min; flow-rate, 1 ml/min; temperature, 40°C; detection, UV, 254 nm; sample size, 0.28 μg each. For peak identification, see Table I.

Based on this characteristic behaviour of reversed-phase chromatography, even isomeric oligonucleotides which differ only in respect of their base composition can be resolved. The sole difference between the two oligonucleotides separated in Fig. 7 is the replacement of one residue of adenine with a residue of guanine. As guanine is less retained than adenine, the oligonucleotide with the higher content of guanine is eluted earlier. In addition to base composition, the sequence of bases may also affect their retention behaviour on PS–DVB–PVA. This is corroborated by the k' values given in Table I. Whereas the exchange of the last base at the 3'-end does exert a small effect on the k' values of the oligonucleotides V–VIII in the order C < G < A < T, the far greater difference in k' values observed between the oligonucleotides III and IV is due to the presence of a cluster of six guanine bases in the former, which influences the retention behaviour far more than just the exchange of a single base.

For certain experiments in molecular biology, such as *in situ* hybridization, it is necessary to radiolabel oligonucleotides with [^{32}P]ATP. In order to avoid competitive hybridization of unlabelled probes to the DNA template, purification of the radiolabelled oligonucleotide is required [17]. As can be seen in Fig. 8, reversed-phase chromatography on PS–DVB–PVA particles permits the separation of a dephosphorylated from a phosphorylated 12-mer oligodeoxyadenylic acid. According to the sup-

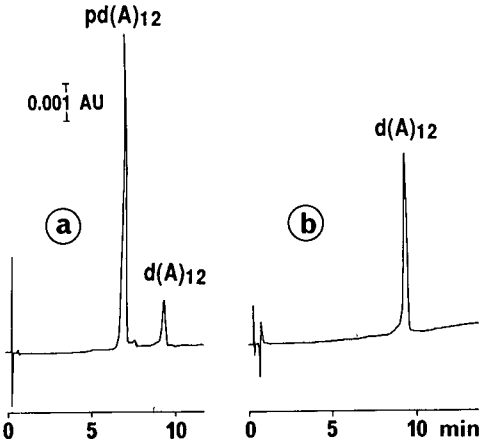

Fig. 8. Chromatograms of commercial preparations of (a) dephosphorylated and (b) phosphorylated 12-mer oligodeoxyadenylic acids. Column, PS–DVB–PVA (2.3 μm, 50 × 4.6 mm I.D.); eluents (A) 0.1 *M* TEAA (pH 7.0) and (B) 0.1 *M* TEAA–acetonitrile (90:10), linear gradient from 30 to 75% B in 20 min; flow-rate, 1 ml/min; temperature, 40°C; detection, UV, 254 nm; sample size, 0.25 μg each.

plier, phosphorylated oligodeoxyadenylic acids are prepared first in the dephosphorylated form using phosphoramidite chemistry and, following purification, they are submitted to phosphorylation by polynucleotide kinase. From Fig. 8a, it can be seen clearly that the phosphorylated product contains non-phosphorylated parent material (Fig. 8b). Recoveries of different non-phosphorylated and phosphorylated oligonucleotides were in the range 92–100% (Table II).

TABLE II

RECOVERIES OF OLIGONUCLEOTIDES

Oligonucleotide	Amount injected (μg)	Recovery (%)
$d(A)_{12}$	0.75	98.7
II[a]	0.31	100.3
VII[a]	0.34	92.7
$pd(A)_{12}$	0.75	93.3
$pd(A)_{16}$	0.50	92.8
$pd(T)_{16}$	0.13	91.8

[a] For sequence, see Table I.

CONCLUSIONS

Detritylated oligonucleotides up to 30 nucleotides in length have been resolved within a few minutes on PS–DVB–PVA particles. Further, phosphorylated probes have been separated successfully from their non-phosphorylated analogues. The recoveries being excellent, HPLC on PS–DVB–PVA particles may prove a valuable tool in the purification of oligonucleotides, because they can be used in subsequent molecular biological experiments such as polymerase chain reaction and *in situ* hybridization without any further pretreatment after evaporation of the eluent.

ACKNOWLEDGEMENTS

This work was supported in part by the Ministry of Science, Vienna, Austria (G.Z. 49.685/3-II/A/4/90) and grants from the Austrian National Bank (Nos. 3533 and 4776).

REFERENCES

1 M. E. Scott, *Am. Biotechnol. Lab.*, 3 (1985) 20.
2 R. Frank, D. Miller and G. Wolff, *Nucleic. Acids Res.*, 9 (1981) 4967.
3 L. J. McBridge and C. McCollum, *BioTechniques*, 6 (1988) 362.
4 S. Ikuta, R. Chattopadhyaya and R. E. Dickerson, *Anal. Chem.* 56 (1984) 2253.
5 H. Moriyama and Y. Kato, *J. Chromatogr.*, 445 (1988) 225.
6 T. L. Hill and J. W. Mayhew, *J. Chromatogr.*, 512 (1990) 415.
7 J. D. Pearson and F. E. Regnier, *J. Chromatogr.*, 255 (1983) 137.
8 Y. Kato, T. Kitamura, A. Mitsui, Y. Yamasaki, T. Hashimoto, T. Murotsu, S. Fukushige and K. Matsubara, *J. Chromatogr.*, 447 (1988) 212.
9 R. Bischoff and L. W. McLaughlin, *J. Chromatogr.*, 296 (1984) 329.
10 Y. Maa and C. Horváth, *J. Chromatogr.*, 445 (1988) 71.
11 S. Wongyai, J. M. Varga and G. K. Bonn, *J. Chromatogr.*, 536 (1991) 155.
12 J. R. Miller, D. G. Smith, W. E. Marr and T. R. E. Kressmann, *J. Chem. Soc.*, (1963) 218.
13 S. Chibowski, *J. Colloid Interface Sci.*, 134 (1990) 174.
14 R. T. Pon, N. Usman, M. J. Damha and K. K. Ogilvie, *Nucleic Acids Res.*, 14 (1986) 6453.
15 W. Haupt and A. Pingoud, *J. Chromatogr.*, 260 (1983) 419.
16 C. R. Becker, J. W. Efcavitch, C. R. Heiner, N. F. Kaiser, *J. Chromatogr.*, 326 (1985) 293.
17 A. M. Delort, R. Derbyshire, A. M. Duplaa, A. Guy, D. Molko and R. Teoule, *J. Chromatogr.*, 283 (1984) 462.

Journal of Chromatography, 599 (1992) 119–130
Elsevier Science Publishers B.V., Amsterdam

CHROMSYMP. 2507

Application of capillary reversed-phase high-performance liquid chromatography to high-sensitivity protein sequence analysis

Robert L. Moritz and Richard J. Simpson*

*Joint Protein Structure Laboratory, *Ludwig Institute for Cancer Research (Melbourne Branch), and The Walter and Eliza Hall Institute of Medical Research, P.O. Royal Melbourne Hospital, Parkville, Victoria 3050 (Australia)*

ABSTRACT

A continuous gradient elution method for capillary column (<0.32 mm I.D.) liquid chromatography was developed. Gradient eluent from a microbore liquid chromatograph was split ahead of the injector so that an accurate percentage (2–3%) of the mobile phase delivered by the pump flowed through the capillary column. The outlet of the column was connected to a length of 0.075 mm I.D. fused-silica capillary tubing which, in turn, was connected to a 6-mm optical path length longitudinal capillary flow cell. Fused-silica capillary columns of 0.32 mm I.D. were slurry-packed efficiently with 7-μm spherical, 300 Å pore size, C_8 bonded-phase particles, and evaluated in terms of their ability to resolve mixtures of proteins, peptides or phenylthiohydantoin (PTH)-amino acid derivatives. The gradient elution profiles agreed with those obtained using microbore (<2.1 mm I.D.) and larger bore columns. The minimum detectable amounts for proteins and PTH-amino acids on 0.32 mm I.D. capillary columns were 50 pg and 25 fmol, respectively. At a flow-rate of 3.6 μl/min, proteins and peptides were recovered from the capillary columns in volumes of about 2–8 μl. The use of a multiple-wavelength, forward-optics detector for identifying tryptophan- and tyrosine-containing peptides is discussed.

INTRODUCTION

Microbore column liquid chromatography [1–4], combined with high-sensitivity protein sequence analysis [5], has become a routine procedure in the primary structure determination of low-abundance proteins and peptides [6–10]. Although commercially available protein sequencers are capable of yielding amino acid sequence information from 10–20 pmol of starting material [5], it is recognized that the rate-limiting step in obtaining such data resides in the ability to manipulate (*e.g.*, concentrate, buffer exchange, reduce and alkylate, remove detergents, etc.) low-microgram amounts of proteins and peptides [6,11,12].

During the past 7 years, we have been involved in the development and application of microbore column liquid chromatographic techniques that are compatible with high-sensitivity microsequencing methodologies [6–10,12]. Compared with their conventional column counterparts (4.6 mm I.D.), microbore columns (1–2.1 mm I.D.) offer enhanced mass sensitivity (5–20-fold) and decreased peak volumes (40–60 μl) without any striking diminuition of resolution [7,13–15]. Microbore column liquid chromatography is now widely used for peptide mapping with proteases [6–10,12,16], complete protein structure determinations [17–19] and the isolation of proteins form acrylamide gel electroeluates [20] and detergent mixtures [16]. More recently, microbore chromatography has been used in combination with mass spectrometry [21–25] (for reviews, see refs. 12, 26 and 27).

The potential for further miniaturization of liquid chromatography has been known for a long time [1,28]. Of the various ways of reducing column dimensions, first pioneered by Ishii *et al.* [1], slurry-packed fused-silica tubing (0.2–0.35 mm I.D.) [28–30] appears to be promising. Whereas the initial protein separation studies using capillary liquid

0021-9673/92/$05.00

chromatography were based on reversed-phase principles [1,28–32], other stationary phase materials with additional selectivities (*e.g.*, size-exclusion chromatography [32,33], chromatofocusing [34], affinity chromatography using chitosan beads [35], normal-phase chromatography [36]) have been used for capillary columns.

Other significant instrumental improvements in capillary chromatography include accurate and precise management of low flow-rates (< 5 μl/min) using microsyringe-type pumps [37] and stream-splitting devices [38], continuous [39] or stepwise gradient elutions [40] and "on-column" UV [41] and fluorescence [42], "in-column" fluorescence [43] and axial beam–longitudinal UV capillary flow cells [44].

Although the advantages of miniaturized columns are obvious [45], progress with this technology has been restricted by the availability of packed capillary columns and instrumentation designed to facilitate the operation of such columns.

In this paper we describe the design of a liquid chromatographic system allowing gradient elution from reversed-phase capillary (0.32 mm I.D.) columns, a procedure for slurry packing fused-silica capillary columns and the application of this technology to high-sensitivity protein separations and microsequencing.

EXPERIMENTAL

Chemicals

Recombinant murine interleukin-6 (mIL-6) was produced by overexpression in *Escherichia coli* and purified as described previously [46]. Chick egg lysozyme, bovine serum albumin, ribonuclease A, myoglobin, carbonic anhydrase and ovalbumin were purchased from Sigma (St. Louis, MO, USA). *Staphyloccocus aureus* V8 protease was obtained from Miles Scientific (Naperville, IL, USA).

High-performance liquid chromatographic (HPLC)-grade organic solvents were purchased from Mallinckrodt (Melbourne, Australia) and trifluoroacetic acid (Sequenal grade) from Pierce (Rockford, IL, USA). High-purity, deionized water was obtained from a tandem Milli-R015 and Milli-Q system (Millipore, Bedford, MA, USA). Ammonium hydrogencarbonate (AnalaR grade) was purchased from BDH (Poole, UK).

Conventional HPLC

The chromatographic equipment employed consisted of a Hewlett-Packard (Waldbronn, Germany) liquid chromatograph (HP 1090A), equipped with an autosampler and diode-array detector (HP 1040A). Spectral and chromatographic data were stored on electronic disk, using a Hewlett-packard HP-85 computer and a Model 9153C disk drive. Manual injections were performed with a Rheodyne (Cotati, CA, USA) Model 7125 injector, equipped with a 2-ml injection loop, installed in the column oven compartment. An Applied Biosystems (Foster City, CA, USA) liquid chromatograph (Model 120A), equipped with a Rheodyne Model 8125 injector installed in the column oven compartment, was also used.

Capillary HPLC

A schematic diagram of the two capillary HPLC systems used is shown in Fig. 1.

System 1. The solvent delivery for this system was supplied by an Applied Biosystems Model 120A liquid chromatograph. Accurate low flow-rates (2–5 μl/min) through the capillary columns and reproducible gradient formation were achieved with a preinjection solvent split that diverted most of the solvent flow through *ca.* 100 cm of 0.10 mm I.D. × 0.26 mm O.D. fused-silica tubing (SGE, Melbourne, Australia) at an Upchurch (Oak Harbor, WA, USA) 1/16-in. tee (P/N U-428). Capillary columns were direclty connected to a Rheodyne Model 8125 injector fitted with 0.5–5-μl injection loops. The flow through the column could be adjusted to 3–5 μl/min by the splitter from a pump flow-rate of 100–200 μl/min. With this split-flow approach, frequent monitoring of the actual flow through the capillary column is necessary. This is readily achieved by applying a 10-μl chromatographic syringe (Microliter 700 Series; Hamilton, Reno, NV, USA) to the effluent and accurately timing the advancing meniscus with a stop-watch. For detection, the conventional flow cell was replaced with a 6-mm optical path length U-shaped longitudinal capillary flow cell (LC Packings, Amsterdam, Netherlands).

System 2. The solvent delivery system was a Hewlett-Packard HP1090A liquid chromatograph. Accurate solvent delivery rates and gradient formation were achieved as described for system 1. Capillary columns were directly connected to a Rheodyne

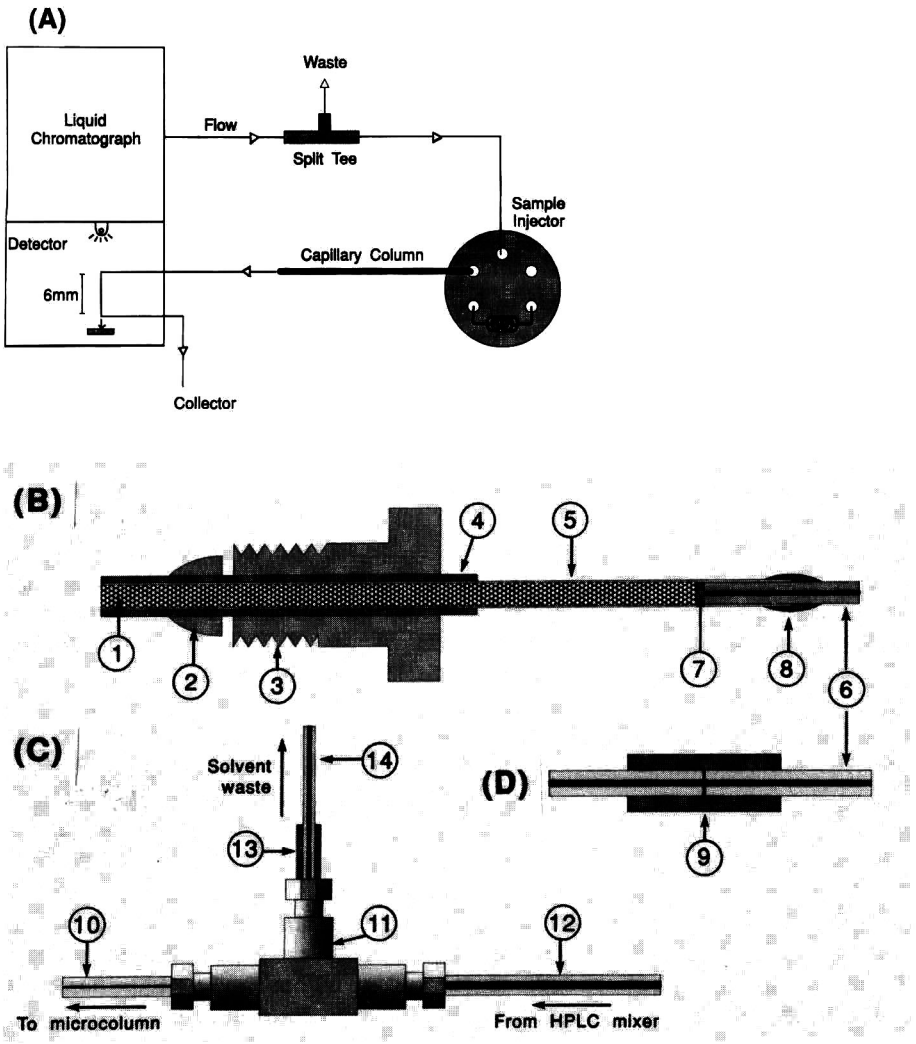

Fig. 1. Schematic diagram of the gradient capillary HPLC system. (A) System 1 consisted of an Applied Biosystems Model 120A liquid chromatograph and system 2 of a Hewlett-Packard Model 1090A liquid chromatograph equipped with a Spectra-Physics Spectra Focus multiple-wavelength detector. Further details are given under Experimental. (B) Capillary column. (C) Split-flow device. (D) Zero-dead-volume tubing union. 1 = Chromatographic stationary phase; 2 = standard 1.59-mm (1/16-in.) stainless-steel ferrule; 3 = standard 1.59-mm (1/16-in.) stainless-steel male nut; 4 = PTFE tubing, 1.59 mm (1/16-in.) O.D. × 0.5 mm I.D. (Beckman, Melbourne, Australia); 5 = polyimide-coated fused-silica 0.42 mm O.D. × 0.32 mm I.D capillary tubing; 6 = polyimide-coated fused-silica 0.275 mm O.D. × 0.075 mm I.D capillary tubing; 7 = hydrophilic poly(vinylidine difluoride) frit, 0.32 mm diameter, 0.45 μm pore size; 8 = epoxy resin; 9 = PTFE tubing, 20 mm × 1.59 mm (1/16-in.) O.D. × 0.25 mm I.D; 10 = Polysil tubing, 1.59 mm (1/16-in.) O.D. × 0.05 mm I.D (SGE); 11 = standard stainless-steel tee, 1.59 mm (1/16-in.), with 0.5-mm flow ports; 12 = PEEK tubing 1.59 mm (1/16-in.), O.D. × 0.178 mm I.D (Upchurch); 13 = PTFE tubing, 1.59 mm (1/16-in.) O.D. × 0.25 mm I.D; 14 = polyimide-coated fused-silica 0.26 mm O.D. × 0.1 mm I.D capillary tubing (SGE).

Model 7520 injector fitted with 0.2–1.0 μl internal sample rotors. A U-shaped longitudinal capillary flow cell (6 mm path length, illuminated volume *ca.* 26.5 nl) installed in a conventional Spectra-Physics forward-optics scanning detector flow cell holder (LC Packings) was used for eluate detection. Data collected were either sent to a strip-chart recorder via the single wavelength mode or collected on an

IBM PS/2 computer (Model P70 386) with Spectra Focus software installed and operated in the multiple-wavelength mode (195–340 nm, 5-nm intervals).

Column supports

The following packing materials were used: (a) Brownlee RP-300 C_8 (particle diameter 7 μm, dimethyloctylsilica, pore size 300 Å, packed into 30 × 4.6 mm I.D., 100 × 2.1 mm I.D. and 30 × 2.1 mm I.D. cartridges), obtained from Applied Biosystems; Brownlee RP-300 C_8 packed into a 50 × 0.32 mm I.D. glass-lined column was provided by LC Packings; (b) Applied Biosystems PTH-C_{18} packed into a 150 × 0.32 mm I.D. glass-lined column was supplied by LC Packings; and (c) Brownlee RP-300 C_8 packing in-house into fused-silica capillary tubing as decribed below.

Fused-silica capillary column construction. Microcolumns of 0.32 mm I.D. were constructed in the following manner. A 20-mm length of 0.420 mm O.D. × 0.320 mm I.D. polyimide-coated fused-silica tubing (Polymicro, Phoenix, AZ, USA) was used as a disc cutter to fabricate internal column frits from 0.45-μm porosity hydrophilic poly(vinylidine difluoride) (PVDF) (Millipore, Bedford, MA, USA). Using a length of 0.275 mm O.D. × 0.075 mm I.D. polyimide-coated fused silica, the frit was inserted into a 60-mm length of polyimide-coated fused silica (Polymicro) to a depth of 5 mm. A small bead of epoxy resin (E-Pox-E Glue, Loctite, Knoxfield, Victoria, Australia) (the resin was precured by stirring whilst applying heat with a heat gun until a tacky consistency was achieved) was then applied to the join and gentle heating was continued until the epoxy resin had fully cured. Proper precuring of epoxy glue is important to ensure that it does not run up the capillary and thereby block the frit [47].

Once the PVDF frit had been positioned in the fused-silica capillary column, a slurry-packing procedure was employed to pack the column. The slurry reservoir consisted of an empty 50 × 2 mm I.D. stainless-steel glass-lined tube (SGE) with standard 1/4-in. column end-fittings (Alltech, Deerfield, IL, USA) that had 0.5 mm I.D. holes as flow-through ports. The fused-silica capillary column was connected to the standard 1/4-in. column end-fitting, either by Minitight fittings (Upchurch, Part No. F-218) or by a PTFE tubing sleeve (see Fig. 1B). Brownlee RP-300 C_8 dimethyloctylsilica (600 mg) was obtained by unpacking a 30 × 4.6 mm I.D. cartridge (Applied Biosystems, P/N 0711-0055). A slurry of this material in *n*-propanol (20 mg in 500 μl) was sonicated for 15 min in a 1.5-ml polypropylene tube. Before packing, the capillary column was filled with packing solvent (*n*-propanol) using a column-packing pump (Shandon, Runcorn, UK) at a pressure of 100 bar. This step prefilled the column with packing solvent and also allowed the system to be checked for leaks. The slurry reservoir was then emptied and quickly replaced with 200 μl of the prepared packing–slurry mixture. The column was packed at a constant pressure of 100 bar for 16 h and then conditioned with 50% (v/v) aqueous methanol for a further 4 h at the same pressure. The capillary column was then carefully dismantled and plugged by inserting the bottom end into a silicone-rubber septum and placing a closed-off 1/16-in. stainless-steel zero-dead-volume union (Swagelock, Solon, OH, USA) on the top of the column. The column efficency was tested using a series of standard proteins (ribonuclease A, lysozyme, bovine serum albumin, myoglobin, carbonic anhydrase and ovalbumin).

Peptide mapping

Recombinant mIL-6 (120 μg) in 200 μl of 1% (w/v) ammonium hydrogencarbonate containing 0.01% (w/v) Tween 20 was digested with *Staphylococcus aureus* V8 protease at an enzyme-to-substrate mass ratio of 1:20 at 37°C for 18 h.

Protein determination

Lysozyme was dissolved in 1 ml of water and the protein concentration was accurately determined by measuring the absorbance at 281.5-nm using an $A^{1\%}_{281.5\ nm}$ value of 26.4 [48].

Peptide synthesis

Peptides were synthesized on an Applied Biosystems peptide synthesizer (Model 430A) using 2-(1*H*-benzotriazol-1-yl)-1,1,3,3-tetramethyluronium tetrafluoroborate (TBTU) for the coupling of Boc-amino acids as described elsewhere [49].

RESULTS AND DISCUSSION

Capillary column performance

For the efficient operation of capillary columns ($\leqslant$0.3 mm I.D.), both the flow-rate and detector volumes have to be substantially reduced compared with microbore and large-bore liquid chromatography. The capillary liquid chromatographic system used in this study was designed to achieve accurate low-flow-rate (3–5 μl/min) and to minimize the extra column volume (see Fig. 1). Whereas the detector was the same as that used for the operation of the 2.1 and 4.6 mm I.D. columns (either a Spectra-Physics Spectra Focus Detector System (Part No. SF102-0122) or an Applied Biosystems Model 120A detector), the 4.5-μl standard flow cell in both of these detectors was replaced with a longitudinal 0.075 mm I.D. fused-silica capillary flow cell (LC Packings). The path length of this U-shaped axial-beam capillary flow cell is 6 mm and the illuminated volume is 26.5 nl.

The accuracy of the flow-rate, under gradient elution conditions, over six consecutive chromatographic runs (calculated from the variance in retention time for lysozyme) was $\pm$0.26%. For protein and peptide separations, prolonged capillary column usage (*e.g.*, 20–30 consecutive chromatographic runs) often resulted in a 25% reduction in the flow-rate (*i.e.*, form 4 to 3 μl/min). This was presumably due to "dirty" samples which caused partial column/frit blockage and, in the first instance, could be readily corrected by increasing the total flow-rate of the liquid chromatograph (say, from 200 to 266 μl/min). With prolonged usage, this problem was corrected by either replacing the top column frit (for the commercial glass-lined stainless-steel columns) or by cutting 2 mm off the top of the column (for the fused-silica tube columns that we packed).

In PTH-amino acid separations, the samples were much "cleaner" and the potential problem of frit plugging was less pronounced, thereby extending the column lifetime.

Mass sensitivty achieved with capillary columns

It is established that to operate microbore columns (1–2 mm I.D.) at linear flow velocities equivalent to those used with larger bore columns ($\geqslant$4.6 mm I.D.), the flow-rate must be decreased in proportion to the square of the reduction in column inside diameter. Provided that the microbore columns are packed with similar efficiency to that of largerbore columns, and are not overloaded, their sample peak volumes will be proportionally decreased in comparison with those from larger bore columns [3,4].

The advantages of narrow-bore and capillary columns with respect to enhanced sensitivity of protein detection and reduced peak volumes are shown in Fig. 2. All columns were packed with the same support (Brownlee RP-300) and operated at equivalent linear flow velocities. A comparison of the 4.6 and 2.1 mm I.D. columns revealed that a fivefold increase in sensitivity of protein detection was achieved by using the 2.1 mm I.D. column. As the extra-column volumes and detector cell geometry (Hewlett-Packard Model 1090A diode-array cell, 6 mm path length, 4.5 μl volume) were identical for the operation of both the 2.1 and 4.6 mm I.D. col-

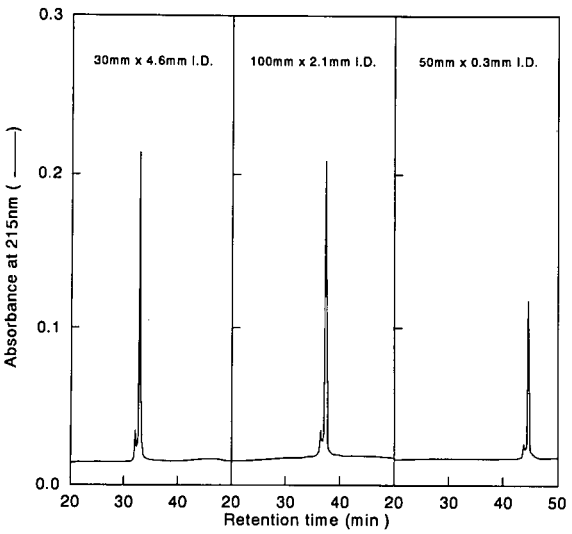

Fig. 2. Effect of column side diameter and flow-rate on detector sensitivity. Column support, Brownlee RP-300 C_8 (7-μm dimethyloctylsilica, pore size 300 Å, 30 × 4.6 mm I.D. and 100 × 2.1 mm I.D., Applied Biosystems, and 50 × 0.32 mm I.D. packed in-house; see Experimental); linear 60-min gradient from 0 to 100% B, where eluent A is 0.1% (v/v) trifluoroacetic acid and eluent B is acetonitrile–water (60:40) containing 0.1% (v/v) trifluoroacetic acid; column temperature, 45°C; detection, 215 nm; flow-rates, 1 ml/min, 200 μl/min and 4 μl/min for 4.6, 2.1 and 0.32 mm I.D. columns, respectively. Sample, lysozyme (4.6 mm I.D. column: 10 μg; 2.1 mm I.D. column: 2 μg; 0.3 mm I.D. column: 0.04 μg).

umns, such an increase in mass sensitivity is expected. The small variance in retention times between the two columns is due to the variation in column length and to the precolumn instrumental dead volume (about 300 μl) for the instrument used in this experiment (Hewlett-Packard Model 1090A liquid chromatograph).

When the 0.32 mm I.D. capillary column was compared with 2.1 and 4.6 mm I.D. columns, 25- and 125-fold increases in sensitivity of protein detection were achieved, respectively (Fig. 2). The constant peak band widths, as a function of time, for the three columns shown in Fig. 2 indicated that comparable column efficiencies can be achieved with capillary liquid chromatography compared with conventional liquid chromatography. Peak recovery volumes for the 0.3, 2.1 and 4.6 mm I.D. columns were 2.5, 133.5 and 660 μl, respectively.

Linearity of detector response

The linearity of the output response of the Applied Biosystems Model 120A detector, fitted with a 6-mm longitudinal capillary flow cell, was examined using various concentrations of ribonuclease A. For this experiment, ribonuclease A (2.0 mg/ml) was dissolved in acetonitrile–water (40:60) containing 0.1% (v/v) trifluoroacetic acid. This stock solution was serially diluted to the required concentrations and 200-μl aliquots were injected directly into the capillary flow cell and the absorbance at 215 nm

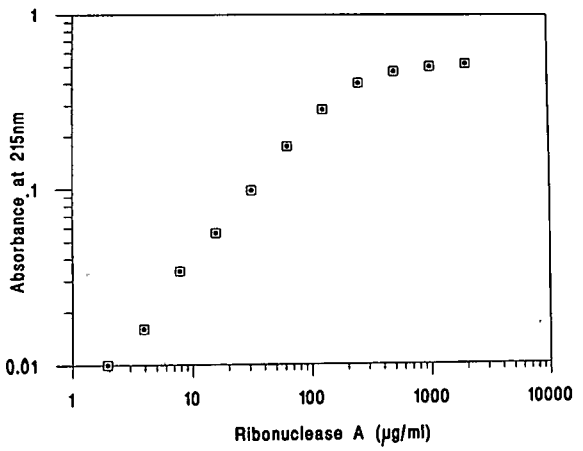

Fig. 3. Linearity of detector response for ribonuclease A injected direclty into the longitudinal capillary flow cell. Calibration graph presented in log–log format.

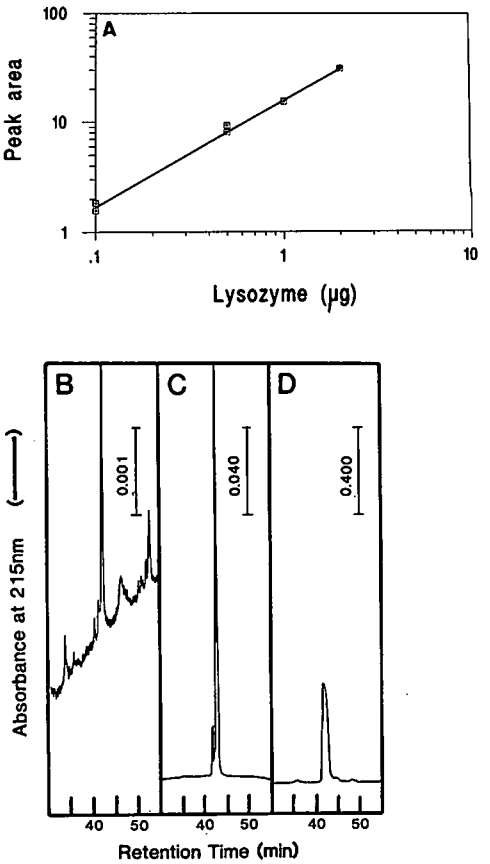

Fig. 4. Linearity of detector response for lysozyme chromatographed on a 50 × 0.32 mm I.D. Brownlee RP-300 column (LC Packings). The liquid chromatograph system 1 described under Experimental was used. Elution conditions as for the 0.32 mm I.D. column in Fig. 2. Progressively larger amounts of lysozyme were chromatographed in duplicate and average peak-area values (arbitrary units) at each concentration were plotted (A). Representatives chromatograms for (B) 500 pg, (C) 100 ng and (D) 2 μg of lysozyme are shown so that the practical limits of sensitivity can be assessed.

was measured. It can be seen in Fig. 3 that the output signal of the detector appears to be linear up to about 0.5 absorbance; this corresponds to a protein concentration of about 125 μg/ml.

To determine the extent to which the detector deviates from linearity, the data in Fig. 3, up to and including absorbance values for protein concentrations of 125 μg/ml, were fitted to the equation $y = Ac^r$ reported by Scott [50], where y is the detector response, c is the solute concentration, A is a con-

stant and r is the response index. For ribonuclease A in Fig. 3, r = 0.86 and the correlation coefficient for the curve is 1.00. Although this value of r indicates that the detector deviates slightly from true linearity (according to Scott, [50], true linearity can only be assumed for values $0.98 \geqslant r \geqslant 1.02$), calibration graphs can still be used with reasonable accuracy.

The linearity of the detector response using our packed 0.32 mm I.D. capillary column, operated under gradient conditions at a flow-rate of 5 μl/min, was investigated using the liquid chromatograph configuration described for system I (see Experimental). The linearity of the detector was determined by plotting the peak area (arbitrary units) against the amount (micrograms) of lysozyme injected on to the column. Fig. 4 shows that the dynamic linear range of the 6-mm longitudinal capillary flow cells for lysozyme extends to 2 μg. Representative chromatograms for lysozyme in the range 500–2000 ng are shown in Fig. 4B–D. For the 6-mm pathlength capillary flow cell and the equipment used for generating low solvent delivery rates (3–5 μl/min) (see system 1 in Fig. 1 and Experimental), it appears that the detection limits are 50–100 pg. We estimate that the minimum detectable amount (MDA) of lysozyme at 215 nm, using the capillary liquid chromatography described, which produces a peak that is twice the baseline noise (signal-to-noise ratio = 2) is *ca.* 50 pg (3.6 fmol). The MDA for ribonuclease A at 215 nm was estimated to be *ca.* 100 pg (7.3 fmol).

Resolution of proteins

Fig. 5 illustrates the separation efficiency that can be achieved for proteins on a reversed-phase capillary column. This chromatogram was obtained with a 50 × 0.32 mm I.D. RP-300 column, packed by us (see Experimental). Using gradient elution between 0.1% (v/v) aqueous trifluoroacetic acid and acetonitrile–0.1% (v/v) aqueous trifluoroacetic (60:40) at a flow-rate of 3.6 μl/min, the resolution of this set of proteins (Fig. 5) is as good as that obtained on microbore and largerbore columns packed with the same support. For the 0.32 mm I.D. columns, proteins were recovered in peak volumes of 2–8 μl, which are small enough to allow efficient interfacing with electrospray mass spectrometry [47,51].

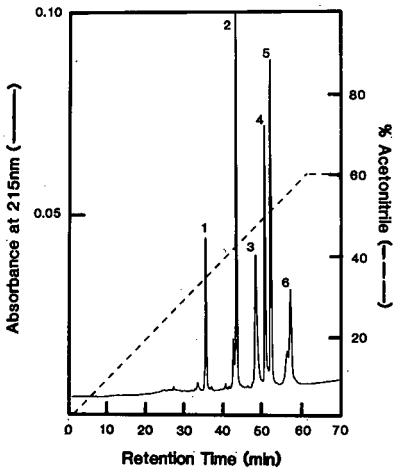

Fig. 5. Separation of protein standards on a Brownlee RP-300 column (50 × 0.32 mm I.D.). This column was slurry-packed in-house as described under Experimental. The column was developed with a linear 60-min gradient from 0 to 100% B, where solvent A was 0.1% (v/v) trifluoroacetic acid and solvent B was acetonitrile–water (60:40) containing 0.1% (v/v) trifluoroacetic acid. Column temperature, 45°C. Flow-rate, 3.6 μl/min. Protein standards: 1 = ribonuclease A; 2 = lysozyme; 3 = bovine serum albumin; 4 = carbonic anhydrase; 5 = myoglobin; 6 = ovalbumin. Sample load, 50 ng in 0.5 μl of water.

Load capacity

The effect of the mass of lysozyme on peak width for a representative 50 × 0.32 mm I.D. Brownlee RP-300 column is shown in Fig. 6. For protein loads of 50–500 ng there was very little variation in band width (measured by the peak width half-height) or band shape. With amounts of protein in excess of 1 μg the band width increased significantly (Fig. 6) and the band profile became distorted (see Fig. 4D), in a similar manner to that described by Snyder *et al.* [52]. Hence it appears that the optimum working range for a column of this dimension is <1 μg and that beyond this, mass overload and detector saturation (see Fig. 3) conditions are encountered.

Peptide mapping

Peptide mapping by reversed-phase liquid chromatography is an extremely powerful technique that is now widely applied in the structural analysis of proteins. Some important applications include the localization of post-translational modifications in proteins (*e.g.*, deamidation, oxidation, glycosyla-

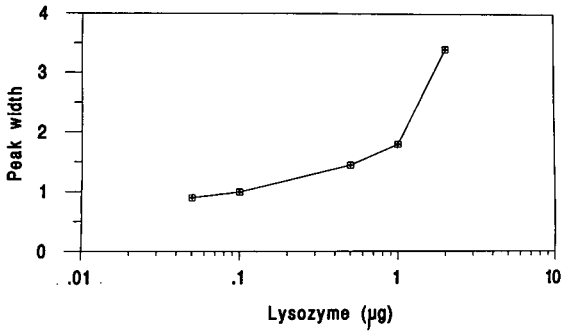

Fig. 6. Effect of protein load on peak width of eluted lysozyme for a 50 × 0.32 mm I.D. column (Brownlee RP-300). Values are averages of two experiments. Chromatographic conditions in Fig. 5. Peak widths (mm) were measured at half-height.

tion, phosphorylation, sulphation, methylation, blocked N-terminus, truncated N- and C-termini), the localization of disulphide bonds in proteins, the identification of genetic variants and the analysis of purity and quality control of genetically engineered protein products. The power of this technology is considerably enhanced when it is integrated with classical biochemical techniques such as the Edman degradation procedure [53] and mass spectrometric analysis (21,22,25,28,51,54,55], which allow amino acid sequence and accurate molecular weight determinations, respectively. This latter information is crucial for establishing the nature of post-translational modifications, many of which are critical to the biological activity of a molecule. Such modifications are not revealed by DNA sequences obtained from gene cloning experiments.

An example of a high-sensitivity peptide map obtained with capillary liquid chromatography is given in Fig. 7. Recombinant mIL-6 (200 ng) was digested with *S. aureus* V8 protease and the resultant digest chromatographed on 0.32 mm I.D. capillary columns, packed by us (Fig. 7A) or obtained commercially (LC Packings) (Fig. 7B), using a trifluoroacetic acid–acetonitrile gradient elution system. Fig. 7. indicates that the chromatographic efficiency of our packed column (A) compares favourably with that of a commercial capillary column (B), and both with that of a commercial microbore (2.1 mm I.D.) column (C). All three columns were packed with the same support (Brownlee RP-300). The flow-rates for the capillary columns (A and B) were

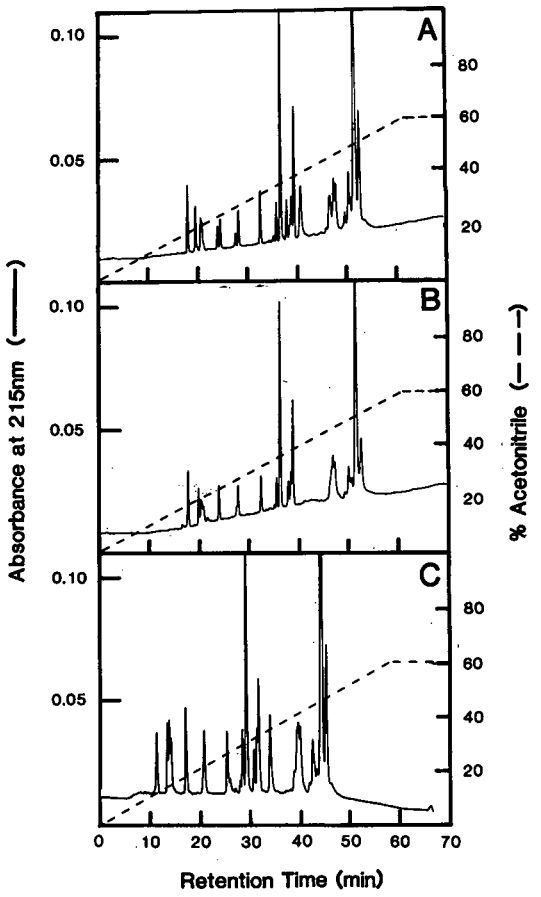

Fig. 7. High-sensitivity peptide mapping of recombinant mIL-6 using 0.32 mm I.D. reversed-phase capillary columns. Support, Brownlee RP-300 (7-μm dimethyloctyl silica, pore size 300 Å). Elution conditions were as in Fig. 5. (A) 50 × 0.32 mm I.D. fused-silica column packed in-house (see Experimetnal); (B) 50 × 0.32 mm I.D. glass-lined column packed by LC Packings; (C) 30 × 2.1 mm I.D. cartridge (Applied Biosystems). Sample load (A and B) 200 ng of digest, 10 pmol; (C) 5 μg of digest, 250 pmol. Flow-rate: 0.32 mm I.D. columns (A and B), 3.6 μl/min; 2.1 mm I.D. column (C), 178 μl/min.

3.6 μl/min whereas that for the microbore column (C) was 178 μl/min. Average peak volumes of 2–8 μl were obtained for the capillary columns (A and B) compared with 100–300 μl for the microbore column (C).

The sensitivity of peptide mapping on 0.32 mm I.D. capillary columns, demonstrated in Fig. 7, where 200 ng (*ca.* 10 pmol) of mIL-6 digest was chromatographed, is ideally suited to the peptide mapping of proteins resolved by two-dimensional

gel electrophoresis (2-DE). We have reported elsewhere [56,57] that protein spots from six to eight identical 2-DE gels can be readily revealed by high-resolution dynamic imaging [58] and the recovered from the gel by passive elution. For peptide mapping, protein (1–2 μg) can be recovered from the eluate, free of gel-related contaminants, by desalting using either reversed-phase or "inverse-gradient" reversed-phase liquid chromatography [59–62].

Multiple-wavelength detection

A multiple-wavelength spectrophotometric absorbance monitor (Spectra-Physics, Spectra Focus) was adapted for use in the capillary liquid chromatography system shown in Fig. 1. The geometry of this monitor, based on a rapidly moving grating, uses a forward-optics system [63].

We were interested in establishing whether this multiple-wavelength detector, fitted with a 6-mm optical path length capillary flow cell, would be useful for monitoring the absorbance of the column eluate at 195 nm rather than at 215 nm. This interest was based on the finding by Rosenheck and Doty [64] that the maximum UV absorption for polypeptides occurs at *ca.* 195 nm. Fig. 8 shows the peptide map for an *S. aureus* V8 digest of mIL-6. Two observations were made: first, the detector signal for peptides was 2–6 times higher at 195 nm than 215 nm (compare peaks 1 and 2), and second, the noise in the baseline at 195 nm is only twice that observed at 215 nm (see insets E and F in Fig. 8B).

In order to determine whether the multiple-wavelength detector would be useful for identifying aromatic amino acid-containing peptides, two synthet-

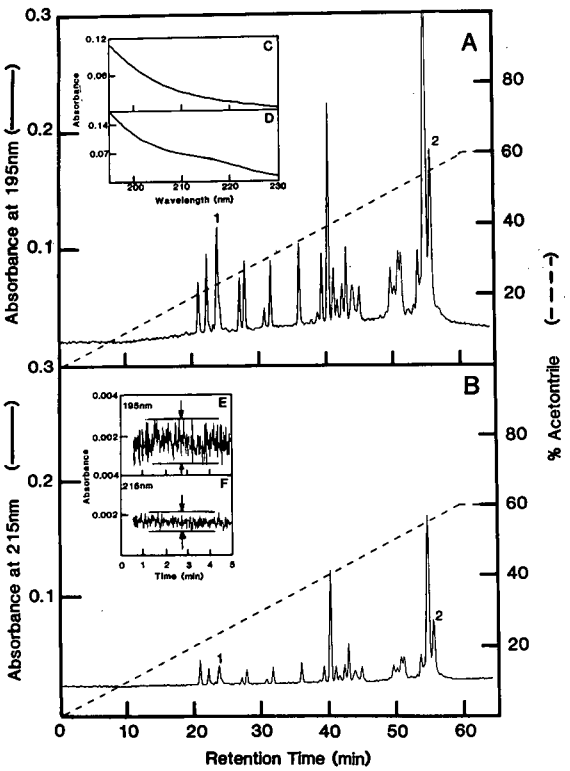

Fig. 8. Multiple-wavelength detector performance. Sample: *S. aureus* V8 protease digest of mIL-6 (200 ng). Column: 100 × 0.32 mm I.D. Brownlee RP-300 packed in-house (see Experimental) and operated as described in Fig. 5. Detector: Spectra-Physics Spectra Focus fitted with a 6-mm optical path length longitudinal capillary flow cell (LC Packings). (A and B) detection at 195 and 215 nm, respectively; (C and D) spectral analysis of peaks 1 and 2, respectively; (E and F) baseline noise at 195 and 215 nm, respectively.

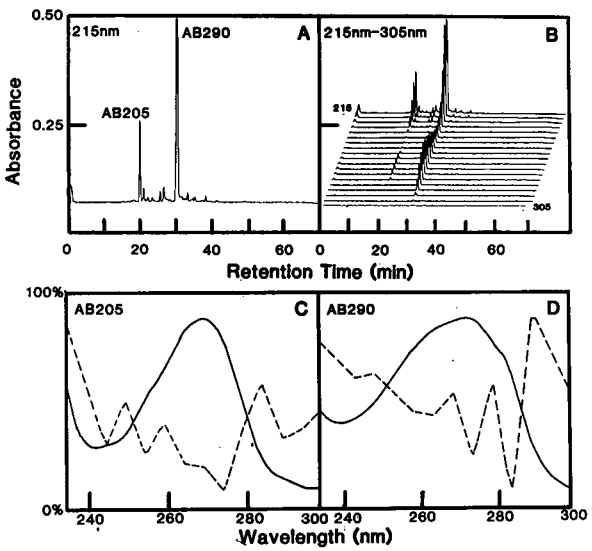

Fig. 9. Spectral analysis of aromatic amino acid-containing synthetic peptides chromatographed by reversed-phase capillary liquid chromatography. Spectral data were obtained using a multiple-wavelength detector (Spectra-Physics) fitted with a 6-mm optical path length longitudinal capillary flow cell (LC Packings). Chromatographic conditions as in Fig. 8. (A) 0.32 mm I.D. capillary column profile of synthetic peptides AB205 (SRDMYMESEGGDGY) and AB290 (DLAWWELR); (B) multiple signal plot of data shown in A; (C and D) zero-order (solid lines) and second-order derivative spectra (dashed lines) of synthetic peptides AB205 and AB290, respectively. Sample load, 250 ng.

ic peptides were chromatographed by reversed-phase capillary liquid chromatography (Fig. 9A): peptide AB205 (SRDMYMESEGGDGY), a tyrosine-containing fourteen-residue synthetic peptide, and peptide AB290 (DLAWWELR), a tryptophan-containing eight-residue peptide. A multiple signal plot of the data shown in Fig. 9A is given in Fig. 9B. Inspection of these spectra reveals major absorption peaks in the range 270–290 nm which are indicative of the aromatic amino acids tyrosine and tryptophan.

Analysis of the spectra by second-order derivative spectroscopy reveals characteristic minima at 287 ± 5 nm for AB290 and 277 ± 5 nm for AB205 (Fig. 9C and D). Previously, it has been shown [65–67] that minima at 290 ± 2 nm) and 278 ± 2 nm are characteristic of tryptophan residues, while a single minimum at 280 ± 2 nm is characteristic of tyrosine residues.

High-sensitivity phenylthiohydantoin-amino acid analysis

With the introduction of the gas-phase sequencer in 1981 [5], N-terminal amino acid sequence analysis of proteins and peptides can now be routinely performed on as little as 10 pmol of material. Since this development in sequencing technology. There has been a concerted research effort in many protein chemistry laboratories towards increasing the sensitivity of amino acid sequence analysis even further [68–71].

The development of more sensitive sequence analysis methods can be realized in two ways: one is to explore new Edman-type reagents and the other to increase the sensitivity for detection of the PTH-amino acids. New Edman-type reagents that have been investigated include 4-N,N-dimethylamino-azobenzene 4′-isothiocyanate (DABITC) [69,72], fluorescein isothiocyanate (FITC) [69,73] and more recently dansylamino-PITC (dimethylaminonapthylsulphonylamino phenylisothiocyanate) [69–70, 74]. In the last instance, dansylamino-PTH-amino acid detection is possible at the 200-fmol level by reversed-phase HPLC [68]. A number of other Edman-type coupling reagents for N-terminal sequence analysis have been documented (for a review, see ref. 75); however, these reagents have not yet gained general applicability owing to problems such as poor coupling yields and serious side-reactions. Another exciting prospect for increasing the sensitivity of the Edman degradation procedure was reported by Tsugita and co-workers [71,76]. Using conventional Edman degradation chemistry, the phenylthiocarbonyl (PTC)-protein is cleaved with trifluoroacetic acid and the resulting anilinothiazolinone derivative, rather than being converted to the stable UV-detectable PTH derivative, is sensitized by reaction with the fluorescent reagent 4-aminofluorescein. The amino acid derivatives sensitized with 4-aminofluorescein were separated by reversed-phase HPLC at 0.1–0.2-pmol levels [71,76].

We report here a method for increasing the sensitivity of detection of PTH-amino acids that relies on the use of reversed-phase capillary liquid chromatography. Fig. 10 illustrates the separation efficiency for PTH-amino acids that can be achieved by capillary liquid chromatography. The chromatogram was obtained with a 150 × 0.32 mm I.D. column packed with Applied Biosystems PTH-C_{18} support (LC Packings). The resolution in Fig. 10 is very similar to that achieved with a commercial 220

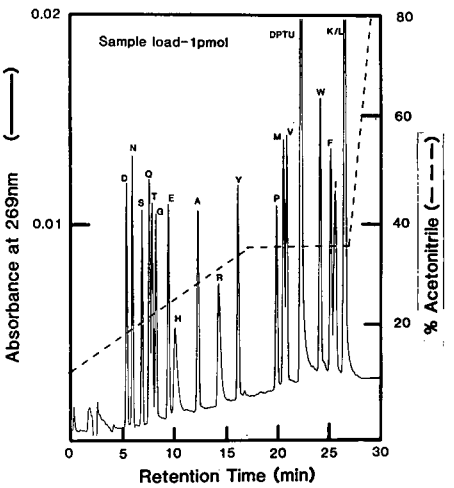

Fig. 10. Separation of phenylthiohydantoin-amino acids by reversed-phase capillary liquid chromatography. Column, 150 × 0.32 mm I.D. Applied Biosystems PTH-C_{18} (packed by LC Packings). Solvent A, 8.3 m*M* sodium acetate–5% (v/v) tetrahydrofuran (pH 4.1); solvent B, acetonitrile. Column temperature, 55°C. Flow-rate, 5 μl/min. Sample load: mixture of 1 pmol each of PTH-amino acids in 0.5 μl of 2% (v/v) aqueous acetonitrile. Capillary liquid chromatography configuration, system 1 (see Fig. 1 and Experimental). PTH-amino acid notation is shown using the one-letter code for amino acids; DPTU, diphenylthiourea.

× 2.1 mm I.D. cartridge obtained from Applied Biosystems (Foster City, CA, USA) [56]; however, the sensitivity of detection of PTH-amino acids using the 0.32 mm I.D. capillary column is, conservatively, 25 times higher (25 fmol) than that achievable with the 2.1 mm I.D. column.

The enhanced mass sensitivity of PTH-amino acid analysis by capillary liquid chromatography, like capillary electrophoresis (data not shown), offers great potential for low-femtomole protein sequence analysis. The obvious drawback for interfacing capillary liquid chromatography with existing sequencer hardware is the problem of sample volume limitations. Given that low concentrations of organic solvent are required to solubilize all of the PTH derivatives, this restricts the volume that can be applied to a capillary column (*ca.* $\leqslant 1$ μl). The technical challenge for the future is to design miniaturized sequencer hardware that allows accurate, reproducible sub-microlitre solvent deliveries that will permit its interfacing with capillary column ($\leqslant 0.5$ mm I.D.) liquid chromatography.

ACKNOWLEDGEMENTS

We thank P. Sacchetta (Merck, Australia) for the use of a Spectra-Physics Spectra Focus detector, Dr. J.-P. Chervet for the use of a longtitudinal capillary flow cell designed for use in the Spectra-Physics detector and Dr. A. W. Burgess for critical reading of the manuscript.

REFERENCES

1 D. Ishii, K. Asai, K. Hibi, T. Jonokuchi and M. Nagaya, *J. Chromatogr.*, 144 (1977) 157–168.
2 R. P. W. Scott and P. Kucera, *J. Chromatogr.*, 185 (1979) 27–41.
3 R. P. W. Scott and P. Kucera, *J. Chromatogr.*, 169 (1979) 51–72.
4 M. V. Novotny and D. Ishii (Editors), *Microcolumn Separations: Columns, Instrumentation and Ancillary Techniques (Journal of Chromatography Library*, Vol. 30), Elsevier, Amsterdam, 1985.
5 R. M. Hewick, M. W. Hunkapiller, L. E. Hood and W. J. Dreyer, *J. Biol. Chem.*, 256 (1981) 7990–7997.
6 B. Grego, I. R. Van Driel, P. A. Stearne, J. W. Goding, E. C. Nice and R. J. Simpson, *Eur. J. Biochem.*, 148 (1985) 485–491.
7 R. J. Simpson and E. C. Nice, in K. A. Walsh (Editor), *Methods in Protein Sequence Analysis, 1986*, Humana Press, Clifton, NJ, 1987, pp. 213–228.
8 B. Grego, I. R. Van Driel, J. W. Goding, E. C. Nice and R. J. Simpson, *Int. J. Pept. Protein Res.*, 27 (1986) 201–207.
9 R. J. Simpson, G. S. Begg, G. E. Reid, M. R. Rubira, L. D. Ward and R. L. Moritz, in B. Wittmann-Liebold (Editor), *Methods in Protein Sequence Analysis, Berlin, 1988*, Springer, New York, 1989, pp. 256–263.
10 R. J. Simpson, R. L. Moritz, G. E. Reid and L. D. Ward, in H. Jörnvall, J.-O. Hoog and A.-M. Gustavsson (Editors), *Methods in Protein Sequence Analysis*, Birkhäuser, Basle, 1991, pp. 67–78.
11 F. S. Esch, *Anal. Biochem.*, 136 (1984) 39–47.
12 R. J. Simpson, R. L. Moritz, G. S. Begg, M. R. Ribira and E. C. Nice, *Anal. Biochem.*, 177 (1989) 221–236.
13 E. C. Nice, C. J. Lloyd and A. W. Burgess, *J. Chromatogr.*, 296 (1984) 153–170.
14 E. C. Nice, B. Greco and R. J. Simpson, *Biochem. Int.*, 11 (1985) 187–195.
15 E. C. Nice and R. J. Simpson, *J. Pharm. Biomed. Anal.*, 7 (1989) 1039–1053.
16 R. J. Simpson, L. D. Ward, G. E. Reid, M. P. Batterham and R. L. Moritz, *J. Chromatogr.*, 476 (1989) 345–361.
17 R. J. Simpson, R. L. Moritz, R. M. Rubira and J. Van Snick, *Eur. J. Biochem.*, 176 (1988) 187–197.
18 R. J. Simpson, J. A. Smith, R. L. Moritz, M. J. O'Hare, P. S. Rudland, J. R. Morrison, C. J. Lloyd, B. Grego, A. W. Burgess and E. C. Nice, *Eur. J. Biochem.*, 153 (1985) 629–637.
19 R. J. Simpson, R. L. Moritz, M. R. Rubira, J. J. Gorman and J. Van Snick, *Eur. J. Biochem.*, 183 (1989) 715–722.
20 R. J. Simpson, R. L. Moritz, E. C. Nice and B. Grego, *Eur. J. Biochem.*, 165 (1987) 21–29.
21 T. Covey, B. Shushan, R. Bonner, W. Schroder and F. Hucho, in H. Jörnvall, J.-O. Hoog and A.-M. Gustavsson (Editors), *Methods in Protein Sequence Analysis*, Birkhäuser, Basle, 1991, pp. 249–256.
22 J. E. Coutant, T.-M. Chen and B. L. Ackermann, *J. Chromatogr.*, 529 (1990) 265–275.
23 R. M. Caprioli, W. T. Moore, B. DaGue and M. Martin, *J. Chromatogr.*, 443 (1988) 355–362.
24 R. M. Caprioli, B. B. DaGue and K. Wilson, *J. Chromatogr. Sci.*, 26 (1988) 640–644.
25 R. M. Caprioli, B. DaGue, T. Fan and W. T. Moore, *Biochem. Biophys. Res. Commun.*, 146 (1987) 291–299.
26 R. J. Simpson and E. C. Nice, in *The Use of HPLC in Receptor Biochemistry*, Alan R. Liss, New York, 1989, pp. 221–244.
27 M. Novotny, *J. Microcol. Sep.*, 2 (1990) 7–20.
28 F. Yang, *J. Chromatogr.*, 236 (1982) 265–277.
29 J. C. Gluckman, A. Hirose, V. L. McGuffin and M. Novotny, *Chromatographia*, 17 (1983) 303–309.
30 Y. Hirata and K. Jinno, *J. High Resolut. Chromatogr. Chromatogr. Commun.*, 6 (1983) 196–199.
31 C. Borra, S. M. Han and M. Novotny, *J. Chromatogr.*, 385 (1987) 75–85.
32 C. L. Flurer, C. Borra, F. Andreolini and M. Novotny, *J. Chromatogr.*, 448 (1988) 73–86.
33 A. Hirose and D. Ishii, *J. Chromatogr.*, 411 (1987) 221–227.
34 A. Hirose and D. Ishii, *J. Chromatogr.*, 438 (1988) 15–22.
35 K. Jinno and K. Takayama, *J. Microcol. Sep.* 1 (1989) 195–199.

36 F. Andreolini, C. Borra and M. Novotny, *Anal. Biochem.*, 59 (1987) 2428–2432.
37 Y. Ito, T. Takeuchi, D. Ishii, M. Goto and T. Mizuno, *J. Chromatogr.*, 358 (1986) 201–207.
38 J. Frenz, J. Bourell and W. S. Hancock, *J. Chromatogr.*, 512 (1990) 299–314.
39 T. Takeuchi and D. Ishii, *J. Chromatogr.*, 253 (1982) 41–47.
40 J. F. Banks and M. Novotny, *J. Microcol. Sep.*, 2 (1990) 84–87.
41 F. Yang, *J. High Resolut. Chromatogr. Chromatogr. Commun.*, 4 (1981) 83–00.
42 E. J. Cuthrei and J. W. Jorgenson, *Anal. Chem.*, 56 (1984) 483–486.
43 M. Verzele and C. Dewaele, *J. Chromatogr.*, 395 (1987) 85–89.
44 J. P. Chervet, M. Ursem, J. P. Salzmann and R. W. Vannort, *J. High Resolut. Chromatogr.*, 12 (1989) 278–281.
45 M. Verzele, C. Dewaele and M. de Weerdt, *LC · GC*, 6 (1988) 966–974.
46 R. J. Simpson, R. L. Moritz, E. Van Roost and J. Van Snick, *Biochem. Biophys. Res. Commun.*, 157 (1988) 364–372.
47 D. C. Shelly, J. C. Gluckman and M. V. Novotny, *Anal. Chem.*, 56 (1984) 2990–2992.
48 K. C. Aune and C. Tanford, *Biochemistry*, 8 (1969) 4579–4585.
49 G. E. Reid and R. J. Simpson, *Anal. Biochem.*, 200 (1992) 301–309.
50 R. P. W. Scott, *Liquid Chromatography Detectors, Part I*, Elsevier, Amsterdam, 1977.
51 D. F. Hunt, J. Shabanowitz, M. A. Mosely, A. L. McCormack, H. Michel, P. A. Martino, K. B. Tomer and J. W. Jorgenson, in H. Jornvall, J.-O. Hoog and A.-M. Gustavsson (Editors), *Methods in Protein Sequence Analysis*, Birkhäuser, Basle, 1991, pp. 257–266.
52 L. R. Snyder, G. B. Cox anbd P. E. Antle, *J. Chromatogr.*, 444 (1988) 303–324.
53 P. Edman and G. S. Begg, *Eur. J. Biochem.*, 1 (1967) 80–91.
54 W. J. Henzel, J. H. Bourell and J. T. Stults, *Anal. Biochem.*, 187 (1990) 228–233.
55 D. M. Desiderio, *Mass Spectrometry of Peptides*, CRC Press, Boca Raton, FL, 1991.
56 R. L. Moritz, L. D. Ward and R. J. Simpson, in R. Angeletti-Hogue (Editor), *Techniques in Protein Chemistry III*, Academic Press, New York, in press.
57 L. D. Ward, J. Hong, R. H. Whitehead and R. J. Simpson, *Electrophoresis*, 11 (1990) 883–891.
58 L. D. Ward and R. J. Simpson, *Pept. Res.*, 4 (1991) 187–193.
59 R. J. Simpson, R. L. Moritz, E. C. Nice and B. Grego, *Eur. J. Biochem.*, 165 (1987) 21–29.
60 R. J. Simpson and R. L. Moritz, *J. Chromatogr.*, 474 (1989) 418–423.
61 R. J. Simpson, L. D. Ward, M. P. Batterham and R. L. Moritz, *J. Chromatogr.*, 476 (1989) 345–361.
62 R. J. Simpson, and R. L. Moritz, in R. S. Hodges and C. T. Mant (Editors), *HPLC of Peptides and Proteins: Separation, Analysis, and Conformation*, CRC Press, Boca Raton, FL, 1991, pp. 399–408.
63 D. R. Carver, S. R. Weinberger and L. Housek, *Am. Lab.*, 19 (1987) 64–71.
64 K. Rosenheck and P. Doty, *Proc. Natl. Acad. Sci. U.S.A.*, 47 (1961) 1775–1785.
65 B. Grego, E. C. Nice and R. J. Simpson, *J. Chromatogr.*, 352 (1986) 359–368.
66 B. Grego, I. Van Driel, J. W. Goding, E. C. Nice and R. J. Simpson, *Int. J. Pept. Protein Res.*, 27 (1986) 201–207.
67 A. F. Fell, *Trends Anal. Chem.*, 2 (1983) 63–66.
68 J. Salnikow, Z. Palacz and B. Wittmann-Liebold, in K. A. Walsh (Editor), *Methods in Protein Sequence Analysis, 1986*, Humana Press, Cliffon, NJ, 1987, pp. 247–260.
69 H. Hirano and B. Wittman-Liebold, in B. Wittman-Liebold (Editor), *Methods in Protein Sequence Analysis*, Springer, Berlin, 1989, pp. 42–59.
70 S.-W. Jin, S.-Z. Xu, X.-L. Zhang and T.-B. Tang, in B. Wittman-Liebold (Editor), *Methods in Protein Sequence Analysis*, Springer, Berlin, 1989, pp. 35–41.
71 A. Tsugita and M. Kamo, in H. Jörnvall, J.-O. Hoog and A.-M. Gustavsson (Editors), *Methods in Protein Sequence Analysis*, Birkhäuser, Basle, 1991, pp. 123–132.
72 J. Y. Chang, *Biochim. Biophys. Acta*, 578 (1979) 188–195.
73 K. Muramoto, Y. Kano, Y. Tanoka, R. Kozeki, Y. Ohashi, N. Tshuchida and N. Yamamoto, *Agric. Biol. Chem.*, 42 (1978) 1559–1563.
74 S.-W. Jin, G.-X. Chen, Z. Palacz and B. Wittmann-Liebold, *FEBS Lett.*, 198 (1986) 150–154.
75 R. F. Doolittle, in M. Elizinga (Editor), *Methods in Protein Sequence Analysis*, Humana Press, Clifton, NJ, 1982, pp. 1–24.
76 A. Tsugita, I. Arai, M. Kamo and C. S. Jones, *J. Biochem.*, 103 (1988) 399–410.

Journal of Chromatography, 599 (1992) 131–136
Elsevier Science Publishers B.V., Amsterdam

CHROMSYMP. 2555

Characterization of hydrophobic interaction and hydrophobic interaction chromatography media by multivariate analysis

Per Kårsnäs* and Tua Lindblom

Pharmacia BioProcess Technology AB, S-751 82 Uppsala (Sweden)

ABSTRACT

Mapping of the selectivity of different hydrophobic interaction chromatography (HIC) media was performed using principal component analysis. The elution positions of proteins in a descending salt gradient were determined for a selection of commercially available and experimental gels. Data regarding the proteins obtained from the literature, such as hydrophobicity indices, polar/non-polar volume ratio and charge, were compared with the elution positions. Principal component analysis revealed that the media could be divided into several groups. The map also showed that the different hydrophobicity indices could be related to the different retention patterns of the media groups. Some media were selecting mainly according to protein hydrophobicity as expressed by the fraction of hydrophobic amino acids, and their mechanism of interaction was insensitive to protein charge. On other media the charge on the protein, or rather the lack of charge, was the most important factor. The results suggest that HIC in many cases works by a combination of two different mechanisms, thus explaining the irregular behaviour which is so often experienced when using HIC media. Principal component analysis and other multivariate techniques were found to be valuable tools in the process of understanding and optimizing hydrophobic or salt-promoted interaction chromatography.

INTRODUCTION

Hydrophobic interaction chromatography (HIC) is a separation technique that is widely used in bioscience and biotechnology. Sometimes, users find that the behaviour of proteins on HIC media is unpredictable. Generally, it is difficult to identify the characteristics of a protein, *e.g.* its hydrophobicity index, that will predict its interaction with a HIC matrix, in the way that the isoelectric point is used in the case of ion-exchange chromatography.

Our study began with the aim of empirically characterizing hydrophobic matrices by determining the elution positions of a set of test proteins in two different standard gradients. In this way we anticipated obtaining a map of the differences in the elution selectivity of the tested media. Later we found it a natural approach to process the generated information by multivariate analysis, a tool that we had started to investigate and use in other contexts. This then permitted us to directly compare other protein data, such as hydrophobicity indices (HIs), hydrophilicity coefficients, polar/non-polar volume ratio and charge, with the chromatographic data.

EXPERIMENTAL

Materials

The experiments were performed using fast protein liquid chromatography (Pharmacia LKB Biotechnology, Uppsala, Sweden). A bed height of 10 cm was packed in HR 10/10 columns (Pharmacia). The proteins were divided into two separate sample mixtures: 1, myoglobin, β-lactoglobulin and α-lactalbumin; 2, cytochrome c, ribonuclease, lysozyme and α-chymotrypsinogen A (all chemicals from Sigma). The protein concentrations were 1 mg/ml (β-lactoglobulin 2 mg/ml) and the sample volume 1 ml. Two gradients with different starting conditions

0021-9673/92/$05.00

TABLE I

INVESTIGATED HIC MEDIA

Agarose–hexane (AgHex)	Phenyl Sepharose 6 FF (low sub) (PheFFLs)
Butyl Sepharose 4B (But4B)	Phenyl Sepharose 6 FF (high sub) (PheFFhs)
Butyl Sepharose 4 FF (ButFF)[a]	Neopentyl HP (Nphp)[b]
Octyl Sepharose CL-4B (OctC14B)	Thio ether Sepharose 6 FF (TEFF)[b]
Octyl Sepharose 6 FF (OctFF)[a]	Hexyl mercaptane 6 FF (HexMFF)[b]
Phenyl Sepharose CL-4B (Phe4B)	Pyridine sulphate 6 FF (PySFF)[c]
Phenyl Sepharose HP (PheHP)	

[a] Only available as custom designed medium from Pharmacia.
[b] Experimental gels. Not commercially available.
[c] To be launched.

were used for every protein. The proteins were dissolved in the starting buffer, 100 m*M* sodium phosphate pH 7.0 containing 1 *M* or 1.5 *M* ammonium sulphate. The final buffer was 100 m*M* sodium phosphate, pH 7.0. The gradient volume was ten column volumes, the linear flow-rate 40 cm/h for Sepharose 4B and Sepharose CL-4B matrices, and 75 cm/h for Sepharose FF matrices.

Media

The tested media are listed in Table I. Seven of them are commercially available, two at present only in bulk as custom-designed media from Pharmacia. One medium, pyridine sulphate Sepharose FF, is to be launched, and three media are not commercially available and were tested to increase the base of the characterization (Table I).

Collection of data

Two elution positions of the seven proteins, one for each gradient, were determined for every chromatographic medium. The void volume was subtracted. The values of five different. hydrophobicity (or hydrophilicity) indices, the polar/non-polar volume ratio (*p*) [1] and charge [1] completed the variables. The HIs were: the non-polar side chain frequency (NPS) [1], hydrophilicity according to Hopp and Woods [2], and hydrophobicity according to Janin [3], Kyte and Dolittle [4] and Rose *et al.* [5]. The data are summarized in Table II.

Multivariate an analysis

General description [6]. Any data table built up of x rows and y columns can be represented by y vectors in an x-dimensional space. Such a vector graphically carries exactly the same information as the table. If, for example, $x = 3$ and $y = 3$, the resulting three-dimensional diagram is easy to interpret. On the other hand, it is very difficult to imagine the nineteen vectors (variables) in the fourteen-dimensional space (experiments, objects) which is the result of this investigation. Mathematically, however, the passage from three to four dimensions and more is trivial.

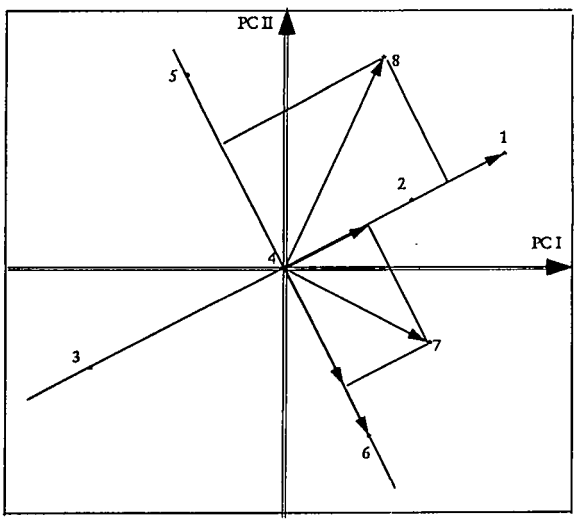

Fig. 1. Interpretation of a principal component projection of variables. Consider point 1 to correspond to a dependent variable. Variable 2 is covariate and 3 varies inversely to 1. Points 4, 5 and 6 vary independently of 1. If 6 is considered a second dependent variable, an increase in variable 7 will increase the values of both 1 and 6, while an increase in 8 will increase 1 and decrease 6. For further details see the text.

In multivariate analysis interpretation of the information in the data set is made possible by projections of the multidimensional space on to planes. The planes which retain most of the available information can be determined by principal component analysis (PCA). The first principal component (PC I) is the direction in the multidimensional space in which the sum of the lengths of the projections of all the vectors is the highest. The length of the projection of a variable vector on a PC is called "loading". The second PC is the direction in which the sum of projections is the next highest, and moreover it has to be perpendicular to the first PC. In the same way more PCs can be calculated. The later principal components carry less and less information, and in practice it is often found that from the fourth PC onwards only noise is expressed. If the number of PCs equals the number of dimensions in the experimental space, the only result of the operation is a transformation of the axes in the space. Very often, in practice, the plane spanned by the first and second PGs carries more than 75% of the

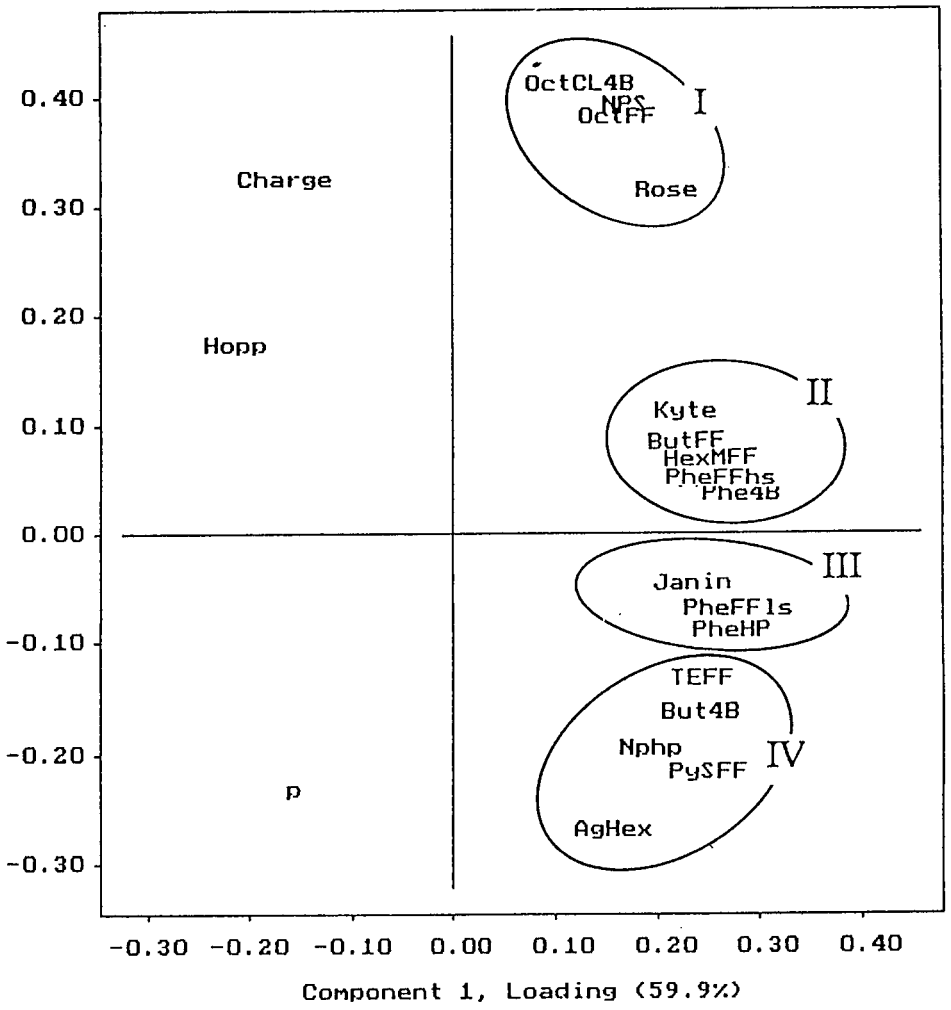

Fig. 2. Principal component map of the selectivity of HIC media (loadings). A classification of the media into different groups is indicated. Some media (I) retard proteins mainly depending on their content of hydrophobic amino acids, some (IV) in inverse proportion to charge and some (II, III) by a combination of the two. The existence of at least two different interaction mechanisms is visualized. The covaration of the media groups with the different indices is clearly vizualized.

TABLE II

EXPERIMENTAL DATA

Objects: proteins at two different starting conditions. Variables: retention times on the different media, hydrophobicity indices (Rose, Kyte and Janin), hydrophilicity coefficients (p and Hoppe) and charge. Proteins that stick to the column at the final gradient conditions were given the retention time 100. A variation of this figure from 80 to 200 did not significantly change the results.

Protein[a]	Medium																		
	AgHex	ButFF	OctCL4B	OctFF	PheHP	Phe4B	PheFFls	PheFFhs	Nphp	TEFF	HexMFF	PySFF	NPS	p	charge	Rose	Kyte	Janin	Hopp
Cyt c	1	0	1	1	0	1	0	0	0	0	0	0	27	112	34	0.54	−0.92	−0.33	0.38
Cyt c	1	1	1	2	1	2	1	2	0	0	1	1	27	112	34	0.54	−0.92	−0.33	0.38
Myoglobin	1	1	100	100	2	12	2	14	0	0	1	2	32	112	34	0.64	−0.40	−0.10	0.14
Myoglobin	2	2	100	100	24	26	11	11	1	1	9	6	32	112	34	0.64	−0.40	−0.10	0.14
RNAse	1	18	5	1	6	7	5	31	0	0	7	5	23	173	24	0.48	−0.67	−0.12	0.09
RNAse	14	19	12	12	26	18	13	26	2	0	8	17	23	173	24	0.48	−0.67	−0.12	0.09
Lysozyme	1	18	19	28	27	39	25	53	0	6	9	31	26	118	14	0.64	−0.48	0.00	−0.04
Lysozyme	14	41	33	49	49	52	41	65	6	17	31	45	26	118	14	0.64	−0.48	0.00	−0.04
β-Lac	1	45	100	100	16	47	21	61	0	0	26	2	37	96	28	0.70	−0.16	−0.06	0.11
β-Lac	6	62	100	100	41	57	38	66	1	8	53	20	37	96	28	0.70	−0.16	−0.06	0.11
α-Lac	1	78	100	100	49	47	31	81	0	6	26	28	34	111	28	0.71	−0.46	−0.06	0.10
α-Lac	13	81	100	100	64	61	45	81	9	22	53	43	34	111	28	0.71	−0.46	−0.06	0.10
α-Chy	1	46	26	43	55	56	39	71	0	6	18	48	33	83	15	0.64	0.05	0.12	−0.26
α-Chy	14	60	40	59	68	65	53	77	18	17	42	60	33	83	15	0.64	0.05	0.12	−0.26

[a] Cyt c = Cytochrome c; β-Lac = β-lactoglobulin; α-Chy = α-chymotrypsinogen A.

information of the entire multidimensional space.

It is also possible to let the variable vectors form the space and the object vectors be expressed in this space. In this case the projections are called scores. A PC plane in this space will express the quality of the experimental design, *e.g.* whether or not the space is properly spanned by the values of experimental parameters.

Interpretation of PC projections. In Fig. 1 is shown an example of a PC projection plane. If point 1 corresponds to a dependent variable, the direction from the point through the origin is of great interest. The independent variable 2 is pointing in the same direction, which means that increasing the value of the corresponding parameter will also increase the value of parameter 1. Variable 3 points in the opposite direction and an increase in the value of this parameter will decrease the value of 1! Parameter 4, which is situated near the origin, does not have any influence at all. It can be varied freely or, for example, if the set-up is a quality control, it does not have to be measured at all. If the scales of the two PC axes are the same, any parameter on a line through the origin perpendicular to the direction of 1 will have no influence on 1.

Analysis of HIC data. A protein combined with

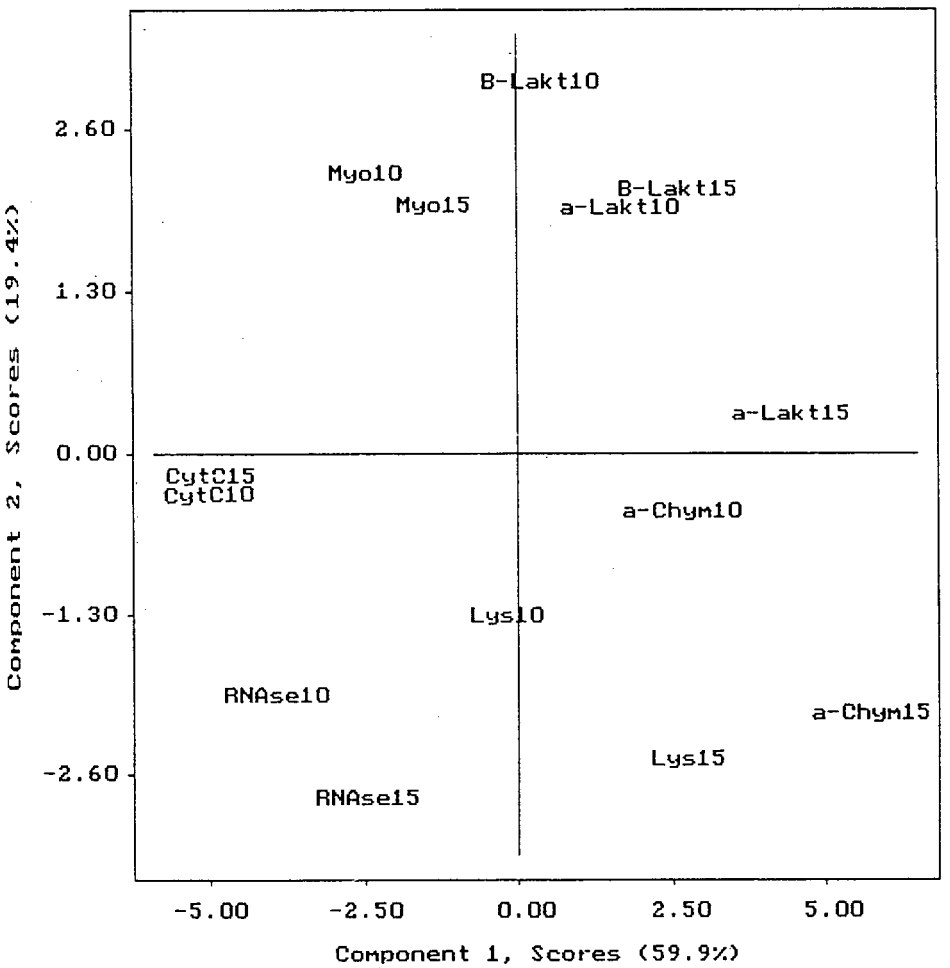

Fig. 3. Principal component projection (score projection) of the proteins with the initial concentration of ammonium sulphate at which they were run (1 *M* ammonium chloride designated "10", etc.). The diagram shows that the objects span the experimental space evenly, thus expressing high reliability of the variable projection.

one starting concentration of the gradient was considered an object (experiment). Thus, every protein gave rise to two objects. The values of the corresponding elution positions and also the values of the hydrophobicity (hydrophilicity) indices (Rose, Kyte, Janin, Hoppe), the polar/non-polar ratio (p) and the charge on the test proteins were variables. The resulting table was fed into SIRIUS (Pattern Recognition Systems, Bergen, Norway), a computer program for multivariate calculations. The data set was centered and the variable values standardized by dividing by the standard deviation. Three PCs were calculated.

RESULTS AND DISCUSSION

The loading plane formed by PC I and PC II was found to carry 80% of the information in the data set. The resulting diagram (Fig. 2) reveals that the media can be divided into several groups or classes depending on their elution selectivity pattern. Moreover the different HIs were shown to be covariate with different classes of gels. The variation in the retention on the octyl gels of group I is covariate with the NPS values [1] of the proteins and also with the HI as defined by Rose *et al.* [5]. Since this variation is nearly perpendicular to the charge, the difference in the charge on the proteins is of less importance for the binding to octyl gels. The media in group IV retard the proteins more the less their charge, because the corresponding vectors are in the opposite direction. The NPS value is of less importance for this interaction. The two groups mentioned clearly point towards the existence of two separate mechanisms of HIC, one related to the fraction of hydrophobic amino acids of a protein and one inversely related to protein charge. One way of interpreting this is that the first type of interaction occurs some distance inside the molecule while the second interaction only occurs with hydrophobic structures at the surface where the interaction will be increased by the absence of charges in the vicinity.

Thus most media of phenyl and butyl type work according to a mixed mode where both hydrophobicity and lack of charge simultaneously play a role. Of course, this may explain the sometimes unpredictible behaviour of HIC media. It is interesting that the HIs defined by Kyte and Dolittle [4] and Janin [3] correlate well with the retention on group II and group III media, respectively. Obviously they express hydrophobicity in a more functional way than NPS, which is just describing the fraction of hydrophobic amino acids without taking any account of whether or not they are exposed on the surface of the protein. Further experiments with other proteins have to be performed to verify which of the indices is best able to predict how proteins will interact with the different types of media. The score projection (Fig. 3) shows that the chosen proteins span the experimental space in a proper way.

There are other possible ways of using a PCA map of the kind presented here. By running the test proteins on other HIC media in the same way it is possible to classify these and to find possible substitutes for a certain medium. Very often we have found that, for example, the butyl media made by one manufacturere have selectivities more similar to the phenyl media of another. The reason for this is probably differences in the type of base matrix, coupling chemistry and spacers.

If a certain protein is run on a sufficient number ($\geqslant 5$) of the media in the map it is possible to classify it as similar to one of the proteins tested here. Successful separation of the test protein will then also be valid for the unknown protein. To establish this as a successful optimization method, further work is required.

ACKNOWLEDGEMENT

The authors are indepted to Dr. Rolf Hjort, Pharmacia BioProcess Technology AB, for help with the calculation of hydrophobicity coefficients.

REFERENCES

1 C. C. Biglow, *J. Theor. Biol.*, 16 (1967) 187.
2 T. P. Hopp and K. R. Woods, *Proc. Natl. Acad. Sci. USA*, 78 (1981) 3824.
3 J. Janin, *Nature*, 277 (1979) 491.
4 J. Kyte and R. F. Dolittle, *J. Mol. Biol.*, 157 (1982) 105.
5 G. D. Rose, L. M. Gierasch and J. A. Smith, *Adv. Protein Chem.*, 37 (1985) 1.
6 S. Wold, C. Albano, W. J. Dunn III, U. Edlund, K. Esbensen, P. Geladi, S. Hellberg, E. Johansson, W. Lindberg and H. Sjöström, in B. R. Kowalski (Editor), *Chemometrics: Mathematics and Statistics in Chemistry*, Reidel, Dordrecht, 1984, Ch. 1, p. 1.

Journal of Chromatography, 599 (1992) 137–140
Elsevier Science Publishers B.V., Amsterdam

CHROMSYMP. 2548

Monitoring the accumulation of nucleoside triphosphates by high-performance liquid chromatography

Probir K. Dutta*

Viscotek, 1032 Russell Drive, Porter, TX 77365 (USA)

Mark Shanley and Gerard A. O'Donovan

Department of Biological Sciences, University of North Texas, Denton, TX 76203 (USA)

ABSTRACT

An anion-exchange high-performance liquid chromatographic method was developed to examine the effect of uracil starvation on purine and pyrimidine metabolism. The isolation, separation and determination of adenosine triphosphate (ATP) and guanosine triphosphate (GTP) from a mutant strain of *Escherichia coli* in a single run is described. The separation was performed using a Waters Radial-PAK Partisil SAX cartridge. The experimental procedure included the preparation of a neutralized Freon–amine extract and injection of 100 μl of it into the column. The results showed the accumulation of ATP and GTP under uracil starvation.

INTRODUCTION

Purine and pyrimidine nucleotides are important compounds for the syntheses of all macromolecules in living cells [1,2]. Dynamic changes and adjustments in intracellular nucleotides evoke metabolic reorientation of essential metabolites, alter the genetic expression of the genome and induce changes in macromolecular syntheses.

The pyrimidine biosynthetic pathway is universal and is obligately required for the balanced synthesis of nucleotide precursors of RNA and DNA [2]. The occurrence of bacterial mutants with an absolute requirement for pyrimidines shows that an alternative to the *de novo* pathway for the generation of pyrimidine nucleotides must exist. The fact that uracil, cytosine, uridine, cytidine, deoxyuridine and deoxycytidine satisfy the pyrimidine requirement of such mutants [3–5] further indicates that considerable interconversions may occur among the compounds. Accordingly, isotope studies show that any of the above mentioned pyrimidine compounds are equally effective as precursors for all the pyrimidine moieties of RNA and DNA [6–8].

Measurement of endogenous nucleotides has been revolutionized by the development of three different methods, based on high-performance liquid chromatography (HPLC): anion-exchange [9,10], reversed-phase [11] and ion-pair reversed-phase [12–14] chromatography. In our laboratory [10,14], the analysis of ribonucleotides was accomplished in the gradient anion-exchange HPLC mode in a single run. This method affords the detection of changes in the levels of low concentrations of nucleoside triphosphates in bacteria.

In this work we re-examined the effect of uracil starvation on purine and pyrimidine metabolism and developed a scheme for the efficient production of adenosine and guanosine nucleotides and their analogues using specially constructed mutant strains of bacteria.

EXPERIMENTAL

Chemicals and reagents

Nucleotides, trichloroacetic acid (TCA) and tri-*n*-octylamine were obtained from Sigma (St. Louis, MO, USA), 1,1,2-trichloro-1,2,2-trifluoroethane

0021-9673/92/$05.00

(Freon) and monobasic ammonium phosphate from Mallinckrodt (Paris, KY, USA) and potassium chloride from Eastman Kodak (Rochester, NY, USA). All other chemicals were of analytical-reagent grade and were purchased from Fisher Scientific (Fairlawn, NJ, USA).

Bacterial strains

A mutant strain of *Escherichia coli* K12 having a genotype of pyrBI argG argI (designated here as TB2) was used.

Growth conditions

All cultures were grown at 37°C in a Lab Room Controlled Environmental Room (Lab-Line, Melrose Park, IL, USA) in M9 medium containing 0.2% glucose + 20% casamino acids + uracil (50 μg/ml). Liquid cultures were incubated in Klett erlenmeyer flasks (Kontes, Vineland, NJ, USA) in a G10 gyratory shaker (New Brunswick, Edison, NJ, USA) set at 120 rpm. The turbidity was measured every 20 min with a photoelectric Klett Summerson colorimeter using a No. 54 green filter and recorded as Klett units (KU), where 1 KU = $1 \cdot 10^7$ cells/ml. Volumes of 50 ml of bacterial cultures at different stages of the exponential phase were harvested, the actual KU recorded and then spun at 12 000 *g* at 4°C for 2 min. The supernatant was decanted and the cell pellet was used for nucleotide extraction.

The culture was not allowed to grow once the cells had reached a density of 85 KU. A 200-ml sample of this culture was then centrifuged and washed and the pellet was resuspended in 200 ml of the same medium without uracil. The cells at this stage showed a density of 25 KU. The cells were shaken for 1 h before harvesting in the same manner as before.

Extraction of ribonucleotides

A 1-ml volume of ice-cold 6% (w/v) TCA was added to the cell pellet and thoroughly mixed for 2 min in a vortex mixer. The mixture was allowed to stand at 4°C for 30 min before further centrifugation at 12 000 *g* for 10 min. The clear supernatant was then neutralized with an equal volume of ice-cold Freon–amine [15] solution (0.7 *M* tri-*n*-octylamine in Freon 113, 1.06 ml of amine per 5 ml of Freon). The Freon-amine mixture was agitated on a vortex mixer for 2 min and then allowed to separate while standing at 4°C for 10 min. The top aqueous layer, which contained the ribonucleotide pool extract, was filtered through a 0.45-μm ACRO LC3A filter (Gelman, Ann Arbor, MI, USA) and kept frozen at −20°C until used.

Chromatographic apparatus and conditions

The HPLC equipment (Waters, Milford, MA, USA) consisted of two Model 510 pumps, a Model 680 automated gradient controller, a U6K injector and a Model 481 LC spectrophotometer. Ribonucleotides were detected by monitoring the column effluent at 254 nm with the sensitivity fixed at 0.05 V aufs. Separations were performed on an anion-exchange Waters Radial-PAK Partisil SAX cartridge (10 cm × 0.8 cm I.D.) inside a Waters Radial Compression Z-module system.

Nucleotide samples (100 μl) obtained from bacteria were injected into the column. A linear gradient [10] of eluent A, 7 m*M* $NH_4H_2PO_4$ (pH 3.8), to eluent B, 250 m*M* $NH_4H_2PO_4$ (pH 4.5) containing 500 m*M* potassium chloride, was applied for 20 min followed by an isocratic period of 10 min with eluent B. The flow-rate was maintained at 4.5 ml/min and all analyses were performed at ambient temperature. Peaks were integrated either manually on a Cole-Palmer (Chicago, IL, USA) strip-chart recorder or a Waters 740 Data Module.

Individual components of the ribonucleotide pool mixture were identified on the basis of their retention times in comparison with standards and by injecting known internal standards. The recoveries of ribonucleotides from solutions of ribonucleotide standards were determined by measuring peak heights before and after the extraction procedures. The recoveries of added NTP (mean of three experiments ± standard error of the mean) were UTP 97 ± 5.1, CTP 88 ± 1.5, ATP 98 ± 4.1 and GTP 96 ± 2.3%.

Calculation

The concentration of the sample was calculated by comparing its peak height with the standard, for which the concentration was known (1 m*M*). Values in micromoles per gram dry weight for all nucleotides were calculated as described previously [10].

RESULTS AND DISCUSSION

The ATP and GTP levels of the culture were monitored during initial growth in M9 + uracil + casamino acid medium by HPLC. Fig. 1a shows a typical profile of the nucleotides from *E. coli* strain TB2. The range of buffer pH in this study was 3.8–4.5. It was observed that the resolution of the nucleoside triphosphates was very sensitive to the pH of the high-phosphate buffer B. The levels of ATP and GTP continued to accumulate, reaching a maximum when the cells reached a density of 75 KU after 265 min. Cells were grown to various densities from 60 to 100 KU. The precipitous increase in ATP concentration occurred to the greatest extent when uracil was removed from strain TB2 at 75 KU. At this stage, the cells were harvested, centrifuged, washed and resuspended in a medium without uracil.

The bacterial suspension at this stage contained $2.5 \cdot 10^8$ cells/ml. The cells were allowed to grow for 1 h, at which time a density of $3.0 \cdot 10^8$ cells/ml was attained. When the ATP and GTP pools were measured for this uracil-less culture, a six-fold increase was noted in comparison with cells having the same density during initial growth in the presence of uracil (Fig. 1b and Table I). The ATP and GTP levels started to decrease after reaching their peak as growth continued in the absence of uracil in the medium.

The massive elevation and accumulation of ATP and GTP (at molar concentrations) under uracil starvation are noteworthy. Nucleoside triphosphates increase specifically whenever cells are subjected to stress. The older literature [16] leaves no doubt that purines regulate pyrimidine synthesis but that pyrimidines do not regulate the synthesis of purines. The only logical interpretation can be offered in terms of the old concept wherein the ATP concentration is taken as the key mediator in metabolic control [17]. As can be seen in Pyr$^-$ mytant, uracil is an absolute requirement for the ultimate production of UTP and CTP to be used for the synthesis of RNA. When uracil is removed, RNA synthesis stops, RNA is degraded and nucleotides accumulate. Thus, the cell starts to produce and accumulate massive amounts of ATP and GTP. If this were a wild-type cell (*i.e.*, Pyr$^+$), all four nucleoside triphosphates would accumulate. However, as strain TB2 is a uracil-requiring mutant, then UTP and CTP do not accumulate. Further, as RNA is not produced, vital ATP- and GTP-requiring steps

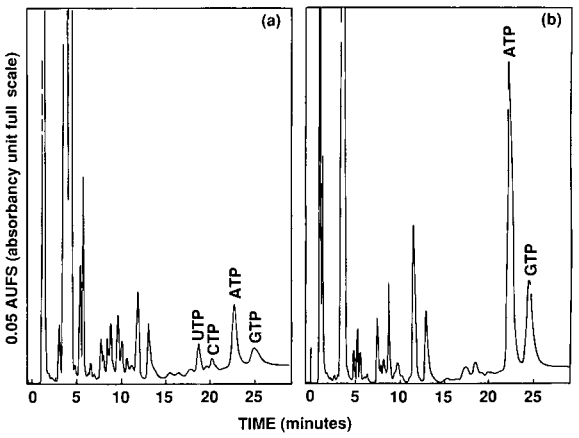

Fig. 1. Elution profiles of ribonucleoside mono-, di- and triphosphates from *E. coli* strain TB2. (a) Grown in M9 medium containing 0.2% (w/v) glucose + 0.4% (w/v) casamino acids and uracil (50 μg/ml). (b) Cells were grown in uracil as in (a) to 75 KU/ml, and were then harvested, washed and resuspended at 25 KU/ml in the same medium without uracil. They were starved of uracil for 1 h.

TABLE I

ACCUMULATION OF ATP AND GTP LEVELS UNDER VARIOUS GROWTH CONDITIONS

Growth conditions	Actual KU	ATP (μmol/g dry weight)	GTP (μmol/g dry weight)
M9 + uracil + casamino acids	30	1.92	0.74
M9 + casamino acids[a]	30	11.61	4.49
M9 + uracil + casamino acids	75	5.79	2.03

[a] Cells were starved of uracil at this stage.

in protein biosynthesis no longer occur such that they do not require ATP and GTP. Hence cellular ATP and GTP might accumulate. Taken together, this massive accumulation of ATP and GTP is a logical extension of the uracil starvation.

To our knowledge, this study is the first to provide a new direction for the manufacture of adenosine and guanosine nucleotides industrially. Kawamoto *et al.* [18] were able to show that a uracil-requiring mutant of *Arthrobacter paraffineus* accumulated orotic acid and orotidine when grown on *n*-paraffins as a sole carbon source. A decoyinine-resistant mutant [19,20] of *Bacillus ammoniagenes* was used to show the direct production of 5'-guanine nucleotides from a carbohydrate by mixed cultivation of 5'-XMP-accumulating strain and 5'-XMP-converting mutant. However, no study so far has shown that an extensive accumulation of ATP and GTP can occur in a uracil-requiring strain. Although this technique of producing ATP and GTP certainly shows great promise for the future, similar work should be conducted on industrial strains such as those of *B. ammoniagenes* and *Corynebacterium glutamicum* using large-scale fermentation for industrial adaptation.

In conclusion, this study has shown that it is possible to develop an ion-exchange HPLC method for monitoring nucleoside triphosphate levels in bacteria. The rapid information that can be deduced from these high-resolution separations is invaluable in the characterization and quality control of the nucleoside triphosphate-derived products. Finally, this technique puts forward the concept of using mutant strains of bacteria in the field of biotechnology.

REFERENCES

1 A. G. Moat and H. Friedman, *Bacteriol. Rev.*, 24 (1960) 339.
2 G. A. O'Donovan and J. Neuhard, *Bacteriol. Rev.*, 34 (1970) 278.
3 J. C. Gerhard, *Curr. Top. Cell. Regul.*, 2 (1970) 275.
4 S. S. Cohen, *Cold Spring Harbor Symp. Quant. Biol.*, 18 (1953) 221.
5 A. M. Moore and J. B. Boylen, *Arch. Biochem. Biophys.*, 54 (1955) 312.
6 E. T. Bolton, *Proc. Natl. Acad. Sci. U.S.A.*, 40 (1954) 764.
7 E. T. Bolton and A. M. Reynard *Biochim. Biophys. Acta*, 13 (1954) 381.
8 L. Siminovitch and A. F. Graham, *Can. J. Microbiol.*, 1 (1955) 721.
9 A. L. Poglotti and D. V. Santi, *Anal. Biochem.*, 126 (1982) 335.
10 P. K. Dutta and G. A. O'Donovan, *J. Chromatogr.*, 385 (1987) 119.
11 R. A. Cunha, A. M. Sebastiao and J. A. Ribiero, *Chromatographia*, 28 (1989) 610.
12 V. Stocchi, L. Cucchiarini, F. Canestari, M. P. Piacentini and G. Fornaini, *Anal. Biochem.*, 167 (1987) 181.
13 T. Ryll and R. Wagner, *J. Chromatogr.*, 570 (1991) 77.
14 G. A. O'Donovan, S. Herlick, D. E. Beck and P. K. Dutta, *Arch. Microbiol.*, 153 (1989) 19.
15 J. X. Khym, *Clin. Chem.*, 21 (1975) 1245.
16 *Purine and Pyrimidine Metabolism* (*Ciba Foundation Symposium*, No. 48), Elsevier, New York, 1977.
17 D. E. Atkinson, *Cellular Energy Metabolism and its Regulation*, Academic Press, New York, 1977.
18 I. Kawamoto, T. Nara, M. Misawa and S. Kinoshita, *Agric. Biol. Chem.*, 34 (1970) 1142.
19 A. Furuya, S. Abe and S. Kinoshita, *Biotechnol. Bioeng.*, 13 (1971) 229.
20 A. Furuya, R. Okachi, K. Takayami and S. Abe, *Biotechnol. Bioeng.*, 15 (1973) 795.

Journal of Chromatography, 599 (1992) 141–155
Elsevier Science Publishers B.V., Amsterdam

CHROMSYMP. 2519

Characterization of the heterogeneity of polyethylene glycol-modified superoxide dismutase by chromatographic and electrophoretic techniques

Jeffrey Snider, Christopher Neville, Lung-Chi Yuan and John Bullock*

Sterling Drug, Inc., 9 Great Valley Parkway, Malvern, PA 19355 (USA)

ABSTRACT

Covalent attachment of polyethylene glycol (PEG) chains to the enzyme Cu,Zn-superoxide dismutase (SOD) produces a heterogeneous mixture of modified protein species. The heterogeneity of the product (PEG–SOD) derives from a variable stoichiometric combination of PEG with individual SOD molecules in addition to the polydispersity of the PEG reagent. Characterization of PEG–SOD presents significant challenges due in part to this heterogeneity in addition to the hybrid nature of the modified enzyme. The application of classical methods of protein characterization is not always successful for these PEG–proteins requiring the development of alternative or modified procedures. A series of chromatographic techniques including reversed-phase, ion-exchange, size-exclusion, and hydrophobic interaction high-performance liquid chromatography along with electrophoretic techniques including isoelectric focusing, sodium dodecyl sulfate–polyacrylamide gel electrophoresis, and capillary zone electrophoresis have been developed for assessing the degree of heterogeneity of PEG–SOD samples which encompass a range of different stoichiometries. Examples will be given demonstrating the application of these techniques to characterize PEG–SOD samples of different composition produced during the course of the reaction between SOD and an activated PEG reagent.

INTRODUCTION

With the emergence of biotechnology there has been a substantial increase in the investigation of proteinaceous materials as therapeutic agents. While these materials typically possess high specificity and activity, formulating and delivering such pharmaceuticals presents significant problems. An additional problem is the potential immunogenicity of these products, which is especially relevant to the use of exogenous proteins. Covalent attachment of polyethylene glycol (PEG) chains to potential therapeutic proteins has shown promise for increasing *in vitro* stability, *in vivo* half-life, and protein solubility as well as decreasing immunogenicity [1,2]. Several examples exist demonstrating the advantages of this process for improving one or more of these properties for proteins including Cu,Zn-superoxide dismutase (SOD) [3], catalase [4], adenosine deaminase (ADA) [5], asparaginase [6], interleukin-2 (IL-2) [7] and streptokinase [8], among others.

The process of attaching PEG to the protein is typically achieved by making one of several different types of activated PEG reagents [1,2,9,10] react with accessible primary amine (primarily lysine) residues on the protein, although other amino acid residues have also been targeted [11]. Since a typical protein will possess a number of such groups, each having different reactivities and degrees of accessibility, the resulting product contains a family of species which is characterized by a distribution in both the number and position of attachment of the PEG groups. Another factor complicating this situation is the inherent polydispersity which is typical of a polymer such as PEG (nominal molecular weight of 5000 for this study).

Since the properties of the PEG–protein product may depend on its composition, it is important to be able to characterize this heterogeneity in order to

0021-9673/92/$05.00

assure product consistency. For SOD, which has 20 possible PEG attachment sites per dimer, the theoretical maximum number of species produced on reaction with PEG is approximately 20^{20}. This theoretical maximum does not include the polydispersity of the PEG reagent which will be superimposed over the site attachment heterogeneity. The actual number of different PEG–SOD species will be less than the theoretical maximum since not all lysines will typically be derivatized and reaction conditions can be optimized to exercise some control over the product composition. Still, it is clear that the product will be quite heterogeneous and it is not practical to try to separate all possible species. Instead, the goal is to establish a separation pattern which can serve as a type of fingerprint which can be used to distinguish between samples of different composition and degrees of heterogeneity.

The characterization of PEG–proteins has been addressed by several investigators with varying degrees of success [12–14]. In most cases this involved the application of classical protein characterization methods which generally did not have the necessary degree of resolution to address this heterogeneity issue. McGoff *et al.* [13] provided a fairly comprehensive evaluation of PEG–SOD using standard protein methods. Except for sodium dodecyl sulfate–polyacrylamide gel electrophoresis (SDS-PAGE) and to a lesser extent isoelectric focusing (IEF), the authors found these classical techniques to be inadequate in characterizing product heterogeneity. Recently, Cunico *et al.* [15] presented a new procedure involving charge-reversal capillary zone electrophoresis (CZE) for separating components of some model PEG-proteins. Depending on the length of the PEG chain, these authors were able to separate up to four components. Emerging technologies such as high-molecular-weight mass spectrometry using an electrospray interface have also shown some promise for characterizing PEG–proteins [16].

For the current study, the reaction of SOD with an activated succinyl succinate ester of PEG (see Fig. 1) was evaluated at different time points during the course of the reaction using chromatographic and electrophoretic techniques. Emphasis was placed on the ability of these methods to characterize the distribution of modified species in the product at the different stages of the reaction. In several

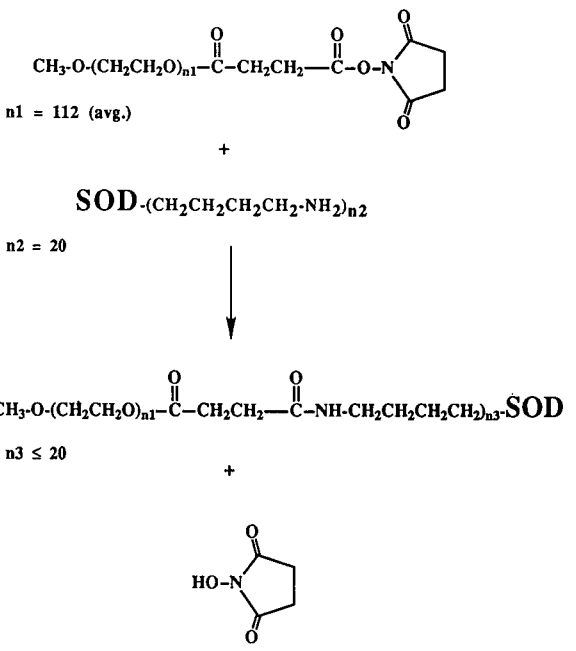

Fig. 1. Reaction used to prepare PEG–SOD.

cases, where classical methods were found to be inadequate, new approaches or modified procedures were developed enabling the separation of several fractions representing different degrees of PEG modification. The identification of the specific lysine residues on SOD which reacted with the activated PEG reagent is beyond the scope of this paper, although others have addressed the site attachment distribution as a function of the total number of modified lysine residues [16,17].

EXPERIMENTAL

Chemicals

Bovine erythrocyte SOD was from DDI Pharmaceuticals (Mountain View, CA, USA). PEG–SOD and the succinyl succinate ester of PEG (PEG-SS) were prepared in our laboratory. Glycine and ammonium sulfate were obtained from Bio-Rad (Richmond, CA, USA). Acrylamide, N,N-methylenebisacrylamide, Coomassie blue G-250, ammonium persulfate, molecular weight and isoelectric focusing markers and Ampholine mixtures pH 4.0–6.5 and 2.5–4.0 were purchased from Pharmacia LKB (Piscataway, NJ, USA). Histidine hydrochloride

was obtained from Fluka Biochemika (Buchs, Switzerland). Urea and SDS were purchased from J. T. Baker (Phillipsburg, NJ, USA). Fluorescamine was obtained from Pierce (Rockford, IL, USA). All other reagents, solvents and buffers were of the highest quality available.

Preparation of PEG-SOD

The temperature for the synthesis of PEG–SOD was held constant at 30°C using a Multitemp II thermostatic circulator (Pharmacia LKB). To 100 ml of a 5.1-mg/ml solution of SOD (0.016 mmol) in a pH 7.80, 0.1 *F* sodium phosphate buffer, was added 1.70 g (0.327 mmol) of PEG-SS while stirring at high speed to affect rapid dissolution. The stir rate was reduced and the reaction pH was held constant at pH 7.80 using a Mettler Model DL25 titrator operated in the pH-stat mode by the addition of 0.5 *F* NaOH.

Chromatographic equipment

For the determination of the average extent of modification of SOD, a high-performance liquid chromatographic (HPLC) system consisting of a Waters (Waters, Millipore, Milford, MA, USA) WISP Model 712 autoinjector, a Waters Model 600E system controller and pump and an ABI (Foster City, CA, USA) Model 980 fluorescence detector was used. The high-performance size-exclusion chromatographic (HPSEC) system for the evaluation of the heterogeneity of PEG-SOD consisted of a Waters WISP Model 712 autoinjector, a Waters Model 590 pump, and an ABI Model 757 detector. Chromatographic data obtained from the Waters HPLC systems were collected and processed by the PENelson Access*Chrom Model 6000 data system (Cupertino, CA, USA) on a VAX computer. High-performance hydrophobic interaction chromatographic (HPHIC) reversed-phase (RP) HPLC and high-performance ion-exchange chromatographic (HPIEC) analyses were performed using a Hewlett-Packard (Avondale, PA, USA) 1090 diode-array HPLC system equipped with a HP chromatography data station.

Determination of the extent of modification of SOD

The average degree of modification of SOD was evaluated by determining the number of unreacted lysines remaining on SOD using fluorescamine derivatization. At appropriate time intervals during the synthesis of PEG–SOD, 100-μl aliquots of the reaction mixture were removed and immediately quenched with excess glycine (5.00 ml of a 0.235-mg/ml glycine solution). The fluorescamine derivative was prepared by mixing 250 μl of the quenched sample with 250 μl of a pH 9.0, 0.2 *F* H_3BO_3 buffer. Then, while vortexing this mixture, 500 μl of a 3.0 mg/ml fluorescamine solution was added in a drop-wise fashion. Separation of the SOD/PEG–SOD fluorescamine derivatives from lower-molecular-weight interfering substances (*i.e.* < 1000 dalton, including glycine) was performed on a 300 × 7.8 mm Bio-Gel 20 XL chromatographic column (Bio-Rad) using a mobile phase consisting of acetonitrile–0.15 *F* H_3BO_3, 0.2 *F* NaCl buffer pH 9.0 (20:80, v/v), containing 0.28% (w/v) SDS. All peaks were eluted from the column at a flow-rate of 1.0 ml/min and detection was accomplished using a fluorescence detector with an excitation wavelength at 390 nm and a 480 nm emission cut-off filter. A 20-μl injection volume was used. Further details of this method may be found elsewhere [18].

Additional quantities of the reaction mixture were removed at the 0, 1, 4 and 50 min time points for evaluation by chromatographic and electrophoretic methods. For each of these samples the reaction was quenched in excess glycine as stated above and the resulting PEG–SOD product concentrated to approximately 2.5 mg/ml using a Centriprep ultrafiltration tube having a 10 000 molecular weight cut-off filter (Amicon, W. R. Grace & Co., Beverly, MA, USA) to remove some of the lower-molecular-weight substances.

HPSEC. Separations were performed on a 300 × 7.8 mm Progel-TSK G3000SWXL column (Supelco, Bellefonte, PA, USA) using a mobile phase consisting of methanol–pH 6.8, 0.1 *F* NaH_2PO_4, 0.2 *F* NaCl buffer (45:55, v/v). A 1.0-ml/min flow-rate, a 20-μl injection volume, and UV detection at 214 nm were used.

HPIEC. Cation-exchange separations were performed on a 35 × 4.6 mm TosoHaas SP-NPR column using a gradient mobile phase consisting of (A) pH 2.6, 0.02 *F* sodium phosphate; (B) pH 2.6, 0.02 *F* sodium phosphate, 1 *F* NaCl. The gradient was varied linearly from 0–100% B over 15 min at a flow-rate of 1.0 ml/min. The column was cooled to 10°C using the thermostatic circulator. An injection vol-

ume of 20 μl and UV detection at 220 nm were used.

RP-HPLC. Reversed-phase separations were performed on a 35 × 4.6 mm TosoHaas C18-NPR column using a gradient mobile phase consisting of (A) pH 7.0, 0.02 *F* sodium phosphate; (B) isopropanol. The gradient was varied as specified in the appropriate figures. A 1.0-ml/min. flow-rate, a 10-μl injection volume (5 μg), and UV detection at 214 nm were used.

HPHIC. Hydrophobic interaction separations were performed on a 35 × 4.6 mm TosoHaas butyl-NPR column using a gradient mobile phase consisting of (A) pH 7.0, 2 *F* ammonium sulfate, 0.1 *F* sodium phosphate; (B) pH 7.0, 0.1 *F* sodium phosphate. The gradient was varied linearly from 10–80% B over 40 min at a flow-rate of 1.0 ml/min. An injection volume of 10 μl (5 μg), and UV detection at 214 nm were used.

SDS-PAGE. Separations were performed on a Pharmacia Phast System using a precast 0.45 mm PhastGel, gradient 8–25, at a uniform temperature of 15°C. The system was programmed to apply a maximum of 3.0 W, 250 V, and 10 mA for a 70-volthour time period. Gels were stained in Coomassie Blue G-250 stain in the leuco form [19] overnight and were then washed in water for 4 h.

IEF. Analyses were performed on a horizontal LKB Multiphor II electrophoresis unit connected to a LKB Multitemp II thermostatic circulator and a Macrodrive 5000 power supply. Separations were performed using an in-house prepared 188 × 115 × 1 mm, 4% T, 6% C polyacrylamide gel[a] containing 9 *M* urea and 2.0% pH 4.0–6.5 Ampholine. The anode wick was soaked in 2% pH 2.5–4.0 Ampholine and the cathode wick was soaked in pH 7.0, 0.2 *F* histidine. The electrophoretic system was programmed to apply a maximum of 8 W, 1000 V and 15 mA for 90 min which was then increased to 16 W, 1420 V and 15 mA for an additional 90 min. The temperature was uniformly maintained at 17°C. The resulting gel was stained in Coomassie blue G-250 stain in the leuco form as stated above.

CZE. Two systems were used. System A was a Beckman PACE 2000. System B was a laboratory-built modular system consisting of a Bertan Model 230 30-kV power supply, platinum wire electrodes, and a Linear Model 204 UV detector (Reno, NV, USA). Fused-silica capillary tubing for all work (50 μm I.D. × 357 μm O.D.) was from Polymicro Technologies (Phoenix, AZ, USA). Capillaries were washed with 1 *F* NaOH for 30 min, water for 5 min and equilibrated with operating buffer for 20 min. Data for all experiments was collected using PE-Nelson Access★Chrom software at a sampling rate of 3 Hz.

RESULTS AND DISCUSSION

The extent of derivatization of the lysines on SOD during the course of the reaction with the activated ester of PEG was determined using the method described in the Experimental section. Further details of this method can be found elsewhere [18]. The graph in Fig. 2 depicts the time course of the reaction where the *y*-axis represents the percentage of lysines on SOD (20 per SOD dimer) derivatized with PEG.

HPSEC

Since each PEG chain that is attached to SOD will contribute on average 5000 dalton to the total mass of the modified protein (16% of the native protein weight), HPSEC is a natural choice for trying to separate different species. Fig. 3 shows a series of HPSEC chromatograms of the four different samples of modified SOD (0, 5, 19, and 37% mod-

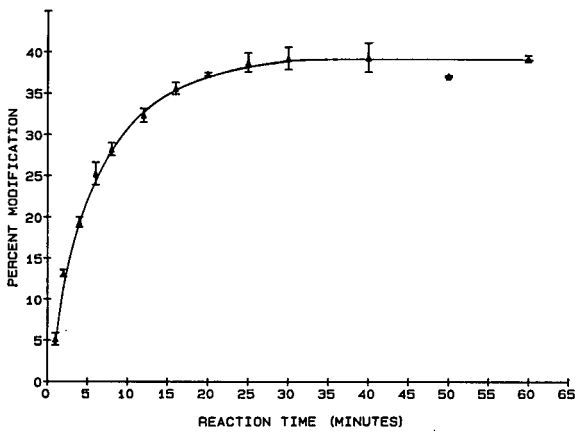

Fig. 2. Curve depicting the cumulative percent modification of lysines on SOD during the course of the reaction used to prepare PEG–SOD.

[a] T = [g acrylamide + g N,N′-methylenebisacrylamide (Bis)]/100 ml solution; C = g Bis/% T.

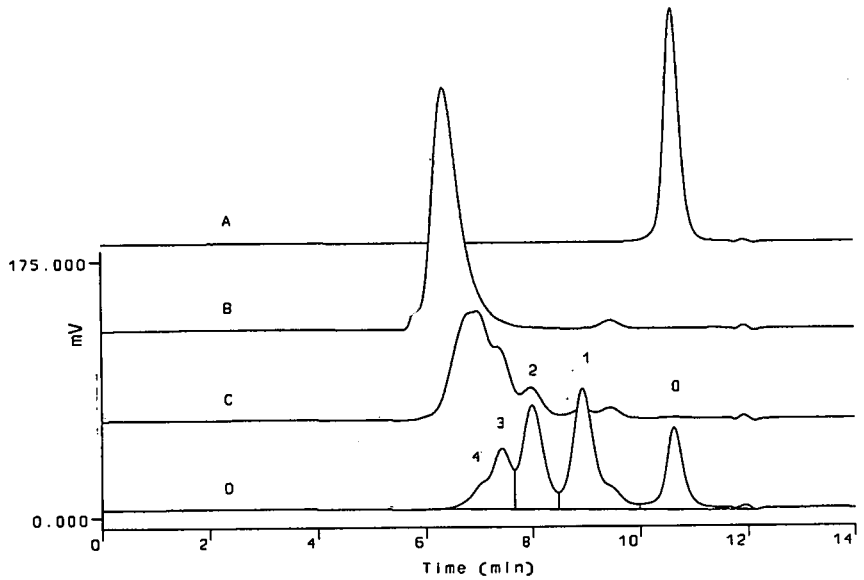

Fig. 3. HPSEC chromatograms of (A) unmodified SOD, (B) 50-min PEG–SOD sample, (C) 4-min PEG–SOD sample and (D) 1-min PEG–SOD sample. Numbers over the peaks refer to the predicted number of PEG chains per SOD dimer.

ified). The unmodified SOD elutes at 10.7 min. The peak at 9.5 min is due to residual PEG reagent. The next peak at about 9 min is assigned to a mono-PEG–SOD species followed at successively shorter elution times by the di-, tri- and tetraPEG–SOD species. The exact identity of these peaks has not been independently confirmed but is based on their relative positions in the chromatogram in addition to the known average degree of modification of the protein determined using the method described in the experimental section. After four PEGs per SOD dimer the resolution drops off dramatically. This fact is not unexpected based on the hybrid nature of the modified enzyme (globular protein core with a shell of random coil polymers). With the addition of successive PEG chains to the protein, the relative difference in molecular size between individual species drops off considerably correlating to lower chromatographic resolution.

HPIEC

In addition to a change in the mass of the protein on addition of PEG chains to SOD, there is also a change in total protein charge due to the conversion of the effected lysine residues to amides. Therefore, it would be expected that HPIEC should be able to discriminate among the different PEG–SOD species. In fact, we have found, as have others [10,13,14], that HPIEC of PEG–proteins is difficult. This is apparently due to the PEG chains sterically interfering with the interaction of charged residues on the protein with the ion-exchange support or a shielding of protein charge by PEG [13].

A further complicating factor, which is generic to all modes of HPLC analysis of PEG–proteins, is their significant hydrodynamic size. Due to the random coil nature of PEG compared to the globular folded structure of the protein, the effective hydrodynamic size of PEG–SOD (in relation to protein standards) is found to be several times larger than the native protein (data not shown). The larger size of PEG–SOD results in slower diffusion kinetics through traditional porous supports correlating into poorer resolution. To circumvent these problems, a different strategy for analyzing PEG–SOD was used. This involved the use of a non-porous support in combination with a low pH eluent. Non-porous supports provide for better mass transfer kinetics for large molecules [20]. The low pH eluent maximizes the net positive charge on the modified protein enabling retention on a cation exchanger.

Fig. 4 shows a series of HPIEC chromatograms obtained on the different PEG–SOD samples. The complexity of these chromatograms is in stark con-

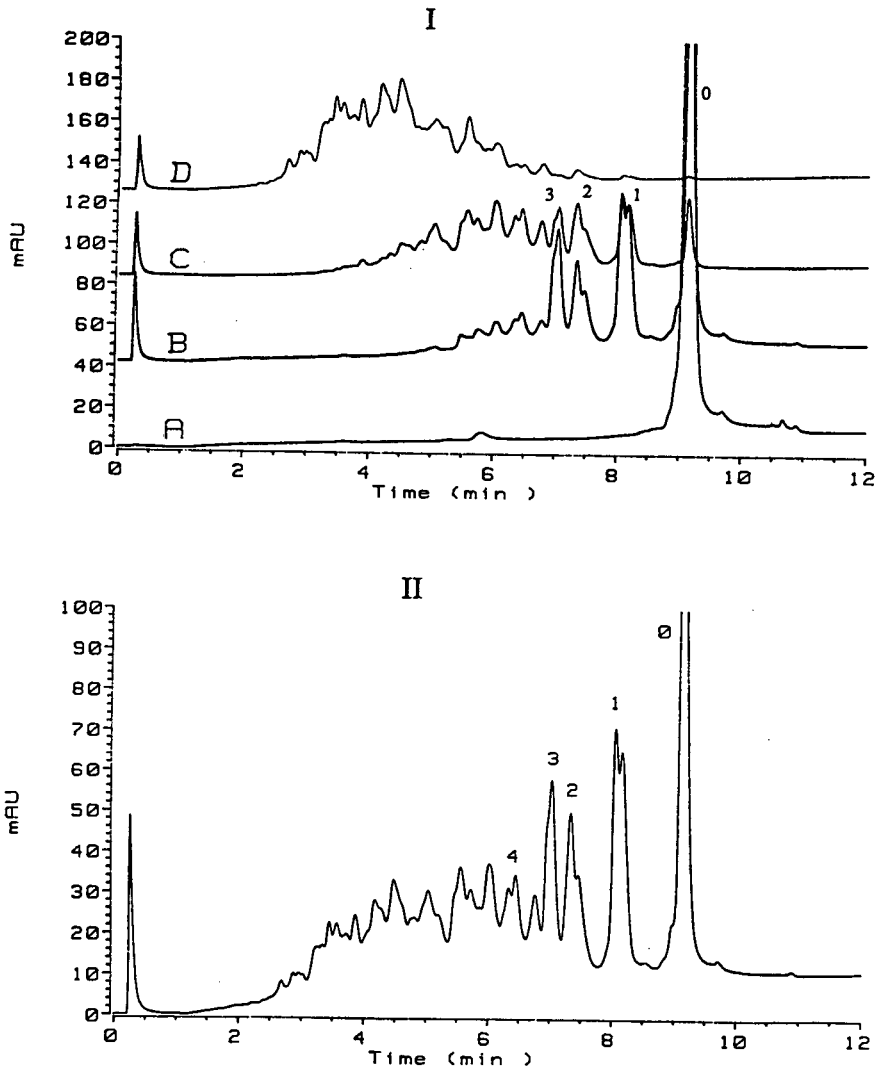

Fig. 4. HPIEC chromatograms of PEG–SOD samples. (I): Chromatograms of (A) unmodified SOD, (B) 1-min PEG–SOD sample, (C) 4-min PEG–SOD sample and (D) 50-min PEG–SOD sample. (II): HPIEC chromatograms of a mixture of the samples in (I). Numbers over peaks refer to the predicted number of PEG chains per SOD dimer.

trast to those obtained by HPSEC and they begin to depict the heterogeneity of the samples. A series of experiments was run to demonstrate that these peaks represent real components of the sample rather than artifacts produced during the chromatographic process. Close examination of these chromatograms reveals a pattern in which peaks can be grouped into subsets which are interpreted to represent mono-, di-, tri-, etc. PEG–SOD species. The multiple bands within each subset would then represent the isomers differing in the sites of attachment and/or length of the PEG chains. The chromatographic profiles of these samples reflect the trend that would be expected based on the known average degree of modification of the samples. That is, the higher the degree of modification, the shorter the retention time and the greater the number of possible species. This leads to more complex chromatograms with decreasing definition between the major fractions.

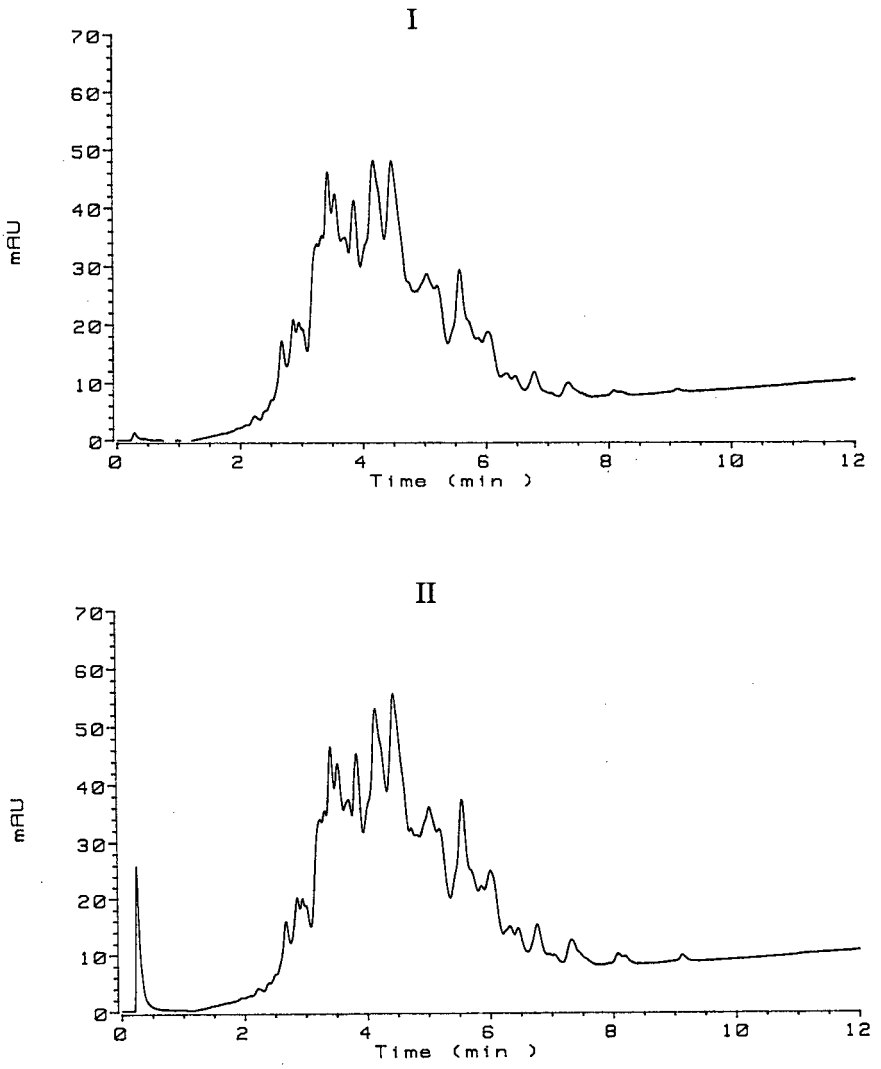

Fig. 5. HPIEC chromatograms of two different samples of PEG–SOD; (I) production scale sample, (II) small lab scale sample.

The potential utility of this technique is demonstrated in Fig. 5 which shows a comparison of two chromatograms of different samples of PEG–SOD prepared using the same reaction conditions but at different times and on different scales (small lab scale *versus* a larger production scale). The peak patterns are identical, indicating that the chromatograms can serve as a type of fingerprint to establish product consistency from lot to lot. It should be noted that chromatography of these same samples on a traditional large-pore support of the same chemistry resulted in very little resolution of individual peaks as shown in Fig. 6, clearly demonstrating the advantages of non-porous supports for PEG-proteins.

RP-HPLC

Although PEG is generally considered a hydrophilic polymer, under RP-HPLC conditions the effect of the addition of PEG to a protein is to increase its hydrophobicity and thus, its retention time relative to the unmodified protein. As was the case for HPIEC, a new approach was used to analyze PEG–SOD by RP-HPLC. This entailed the use

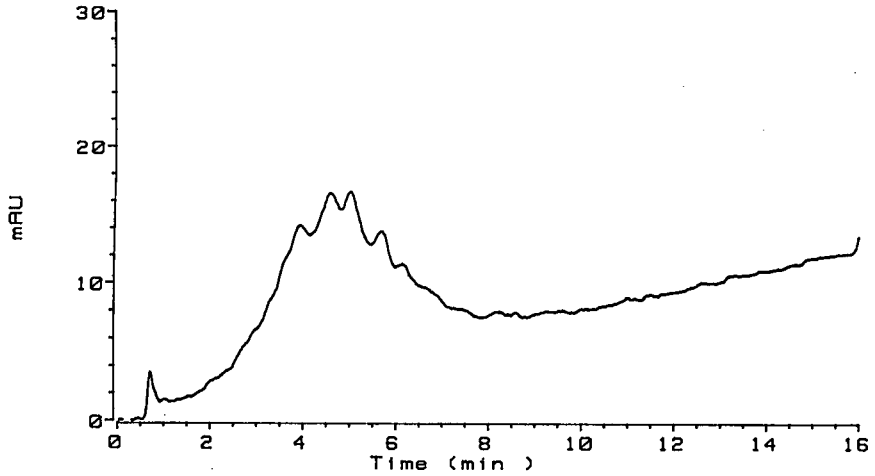

Fig. 6. HPIEC chromatogram of 50-min PEG–SOD reaction product obtained on a traditional porous support. Chromatography was performed using an Ultropak 75 × 7.5 mm TSK SP-5PW (LKB Pharmacia) at a flow-rate of 3.0 ml/min at 10°C with a 15-min linear gradient from 0–100% B; mobile phase A = pH 2.6, 0.02 *F* sodium phosphate; mobile phase B = pH 2.6, 0.02 *F* sodium phosphate, 1 *F* sodium chloride. The injection volume was 20 μl and detection was accomplished at 220 nm.

of a non-porous RP-HPLC support in conjunction with a non-denaturing mobile phase at pH 7. Fig. 7 contains chromatograms of the different PEG–SOD samples obtained using an isopropanol gradient at pH 7.0. These conditions were optimized so that unmodified SOD was not retained and, therefore, retention is due solely to the attached PEG chains. Under these conditions, the first group of peaks that elutes is expected to be the monoPEG–SOD species followed in order by the di-, tri-, etc. species.

As was the case with HPIEC, the chromatograms appear to be composed of a series of major peaks each of which displays some fine structure. The interpretation of these chromatograms is the same as for the corresponding HPIEC data.

A further insight into the high degree of heterogeneity possible with PEG–SOD is shown in Fig. 8. This figure represents chromatograms of the same two samples of PEG-SOD as depicted in Fig. 5. These RP-HPLC chromatograms were obtained using the same conditions used in Fig. 7 but with a shallower gradient profile. Again, the profiles of these samples were found to be nearly identical.

HPHIC

Since HPHIC relies on the same type of forces (partitioning into a hydrophobic phase) encountered in RP-HPLC, except in a diminished capacity, it would be expected that the two methods would produce similar results. As was the case for HPIEC and RP-HPLC, a non-porous support was used along with a traditional inverse ammonium sulfate gradient. The chromatograms in Fig. 9 show peak profiles for these samples that are very similar to the corresponding RP-HPLC chromatograms. A notable difference is the absence of fine structure in the major peak fractions which results in a clearer discrimination between adjacent peaks in the HPHIC chromatograms. A speculative explanation for this difference between the two techniques is that HPHIC responds more to the bulk properties of the molecule such as solubility which are determined more by the total number of attached PEG chains and less by the positioning of these chains along the polypeptide chain. RP-HPLC, on the other hand, is more of a surface interaction technique. Therefore, the positioning and size of the PEG chains on SOD exert more influence on the separation process resulting in more separation of these isoforms.

SDS-PAGE

The results of SDS-PAGE analysis of the PEG–SOD samples are shown in Fig. 10. Samples were heated with SDS and 2-mercaptoethanol to break the SOD dimer into its subunits and reduce the di-

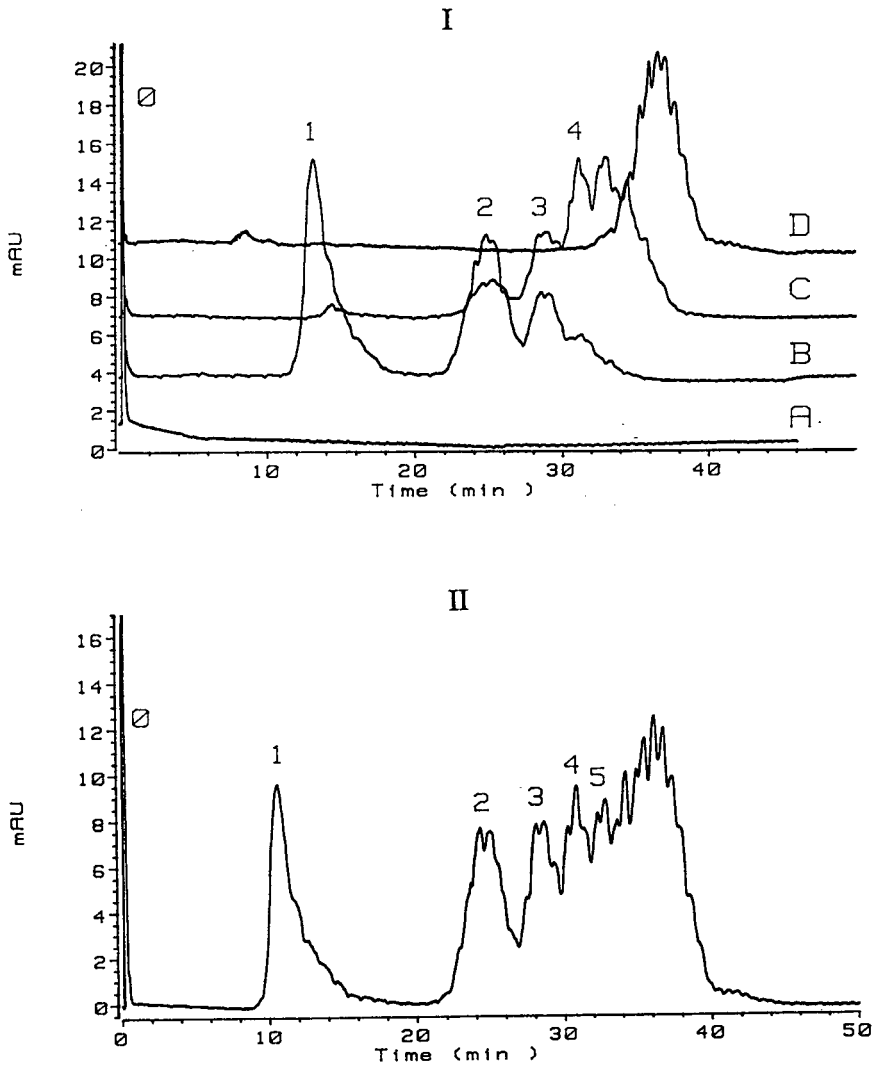

Fig. 7. RP-HPLC chromatograms of different samples of PEG–SOD using the following gradient profile: 5–7% B in 5 min and then 7–16% B in 45 min. Refer to the Experimental section for the remaining chromatographic conditions. (I): Chromatograms of (A) unmodified SOD, (B) 1-min PEG–SOD sample, (C) 4-min PEG–SOD sample and (D) 50-min PEG–SOD sample. (II): Chromatogram of a mixture of the samples in (I). Numbers over the peaks refer to the predicted number of PEG chains per SOD dimer.

sulfide linkages. Because of the high solubility of PEG–proteins even after fixing with trichloroacetic acid, detection of the separated protein bands was problematic due to loss of sample during the washing step. Therefore, Coomassie blue G-250 stain prepared in the leuco form was used so that the fixing and staining of the protein could be performed in a single step. Band assignments for the samples are given in the figure. The separation of bands is quite good up to four PEGs per SOD monomer, although the calculated molecular weights based on the protein standard calibration are not in good agreement with theory. This may be due to the difference between the binding of SDS to PEG (on the PEG–SOD) and SOD which is explained further under the CZE section below. Another problem with this technique is that it is unknown how the PEG will effect the staining procedure and, there-

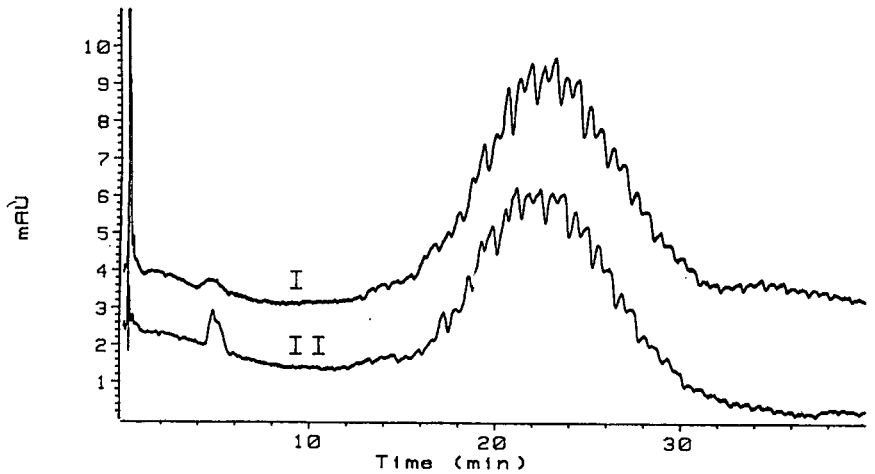

Fig. 8. RP-HPLC chromatograms of the two samples of PEG–SOD depicted in Fig. 5. Chromatograms obtained using the following gradient profile: 5–11.5% B in 5 min and then 11.5–14.9% in B in 40 min. Refer to the Experimental section for the remaining chromatographic conditions.

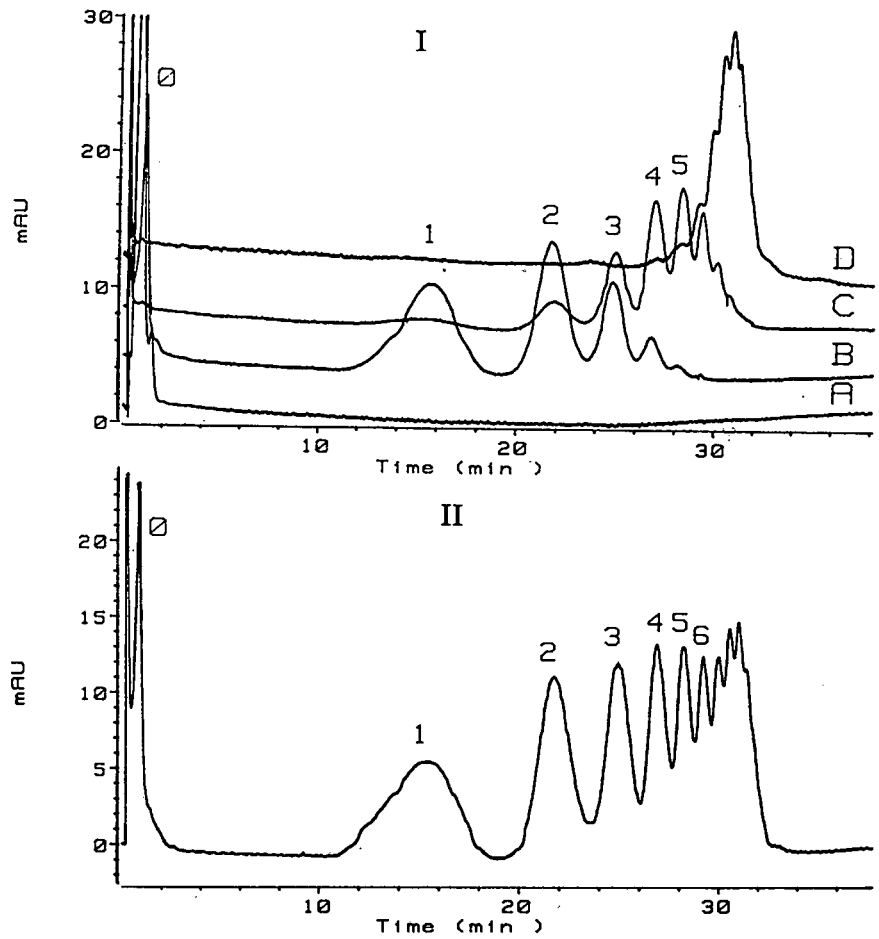

Fig. 9. HPHIC chromatograms of different samples of PEG–SOD. (I): Chromatograms of (A) unmodified SOD, (B) 1-min PEG–SOD sample, (C) 4-min PEG–SOD sample and (D) 50-min PEG–SOD sample. (II): Chromatogram of a mixture of the samples in (I). Numbers over the peaks refer to the predicted number of PEG chains per SOD dimer.

Fig. 10. SDS-PAGE analysis of different samples of PEG–SOD. Lanes: 1 and 7 = molecular weight (Mw) markers; 2 = production scale sample of PEG–SOD; 3 = 50-min PEG–SOD; 4 = 4-min PEG–SOD; 5 = 1-min PEG–SOD; 6 = unmodified SOD.

fore, the quantitative aspects of this method are in some doubt.

IEF

The results of IEF analysis of the PEG-SOD samples are shown in Fig. 11. SOD and two other bands, believed to be the mono- and diPEG–SOD species, are separated from the rest of the reaction mixture. However, the resolution of the remaining PEG–SOD species drops off dramatically as the degree of PEG modification of SOD increases. The pore size of the gel is not suspected of causing this loss of resolution since agarose gels, which typically contain much larger pore sizes than can be obtained using polyacrylamide gels, provided similar results. More likely, the addition of more than 3–4 PEG units shield the charge on the protein thereby masking charge differences observed for the highly PEG modified compounds.

Two bands were observed in the laboratory-scale preparation samples that were not observed in the larger, production-scale preparations of PEG–SOD. The p*I* values of these extra bands are 4.4 and 4.6. Preliminary evidence suggests these extra bands are due to the residual PEG reagents in the PEG–SOD samples.

Other investigators have reported that native SOD is not homogeneous, citing the appearance of several bands using disc gel electrophoresis and/or IEF [21,22]. The SOD sample used for the present study was determined to contain a few minor components as evidenced by SDS-PAGE, IEF and CZE; however, the levels of these components were quite low in comparison with the major SOD component. Therefore, to demonstrate the homogeneity of the native SOD used in the PEG–SOD reaction and to confirm that the appearance of additional bands/peaks in the PEG–SOD samples were due to the formation of different PEG–SOD species as opposed to other variants of native SOD, SOD controls were run with each analytical technique. In each case, only minor secondary components, if any, were observed for the SOD controls.

CZE

Given the high resolving power that has been demonstrated in several instances for the CZE analysis of proteins, it was expected that this technique would be ideally suited to the analysis of a complex material such as PEG–SOD. In fact, the characterization of PEG–SOD is somewhat analogous to the characterization of the heterogeneity of glycoproteins which have been successfully analyzed by CZE [24,25]. However, the initial results did not meet expectations. Fig. 12 shows a series of free solution CZE electropherograms obtained on the different samples of PEG–SOD used in this work. The use of a high pH buffer (10.1) along with an electroosmotic flow rate modifier (1,3-diaminopropane) was required to achieve separation of individual species. Again, the breadth of the PEG–SOD peaks, which is in stark contrast to the sharp peak for unmodified SOD, is believed to be due to the wide distribution

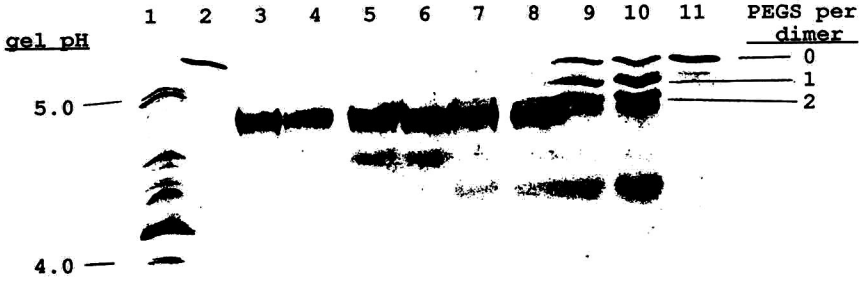

Fig. 11. IEF analysis of different samples of PEG–SOD. Lanes: 1 = p*I* markers; 2 and 11 = unmodified SOD; 3 and 4 = production-scale samples of PEG–SOD; 5 and 6 = 50-min PEG–SOD; 7 and 8 = 4-min PEG–SOD; 9 and 10 = 1-min PEG–SOD.

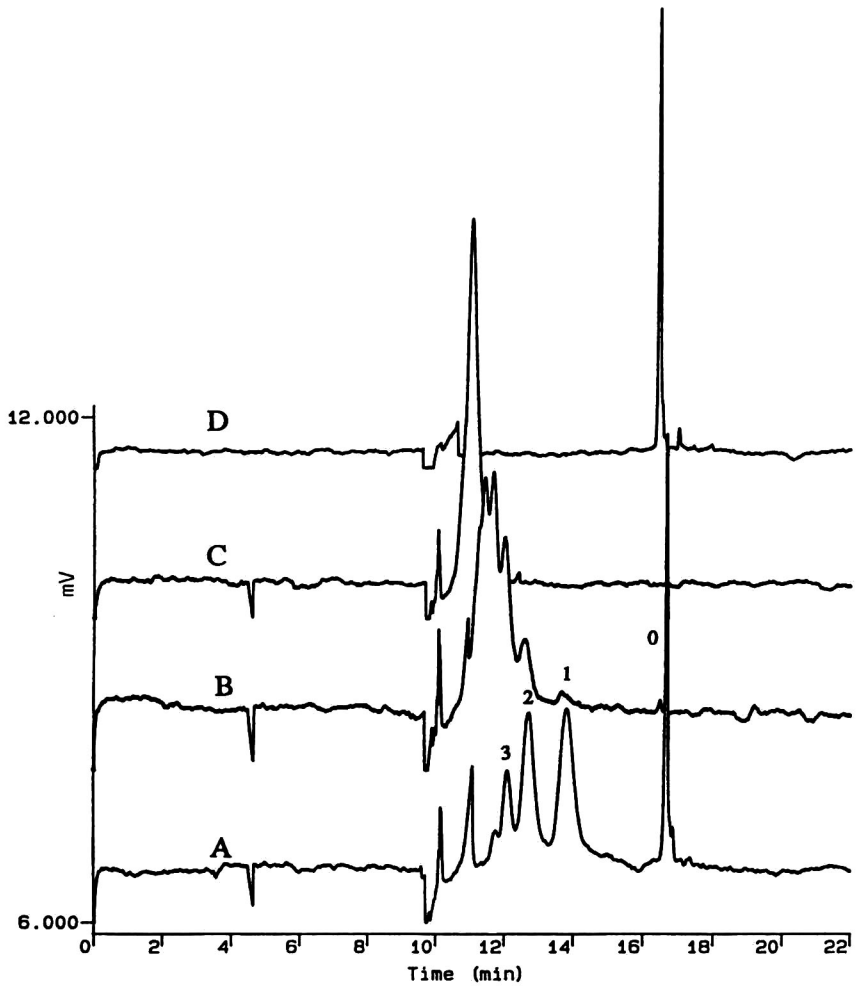

Fig. 12. Free solution CZE analyses of different PEG–SOD samples. (A) 1-min sample, (B) 4-min sample, (C) 50-min sample and (D) unmodified SOD. Data collected using CZE system B. Capillary: 100 cm × 50 μm I.D. (Separation distance 70 cm). Buffer: 15 m*M* boric acid, 15 m*M* 1,3-diaminopropane, 10 m*M* NaCl, pH 10.1. 30 kV, 8-s hydrodynamic injection at a height of 7 cm (2 mg/ml), detection at 200 nm. Numbers over the peaks refer to the predicted number of PEG chains per SOD dimer.

of species possible for a given stoichiometric combination of PEG with SOD. However, the resolution achieved here could not match that achieved by the chromatographic methods.

Fig. 13 contains a series of electropherograms obtained on these same samples using a buffer containing SDS. The use of SDS results in a significant increase in resolution for the lower percent modified SOD samples. This is not believed to be a micellar separation mechanism since these modified proteins are believed to be too large to partition into an SDS micelle. Instead, the enhancement in resolution is thought to be due to a difference in the binding of SDS among the various PEG modified SOD species. That is, the PEG binds to a greater extent than does the polypeptide chain of PEG–SOD. This would explain the reversal in migration order witnessed here compared to results obtained in the absence of SDS. A strong association of SDS with PEG type polymers (*ca.* 1.6 g SDS/g PEG) has been documented elsewhere [23].

The generally lower-than-expected degree of resolution of PEG–SOD by free solution CZE prompted investigation of alternative ways to ana-

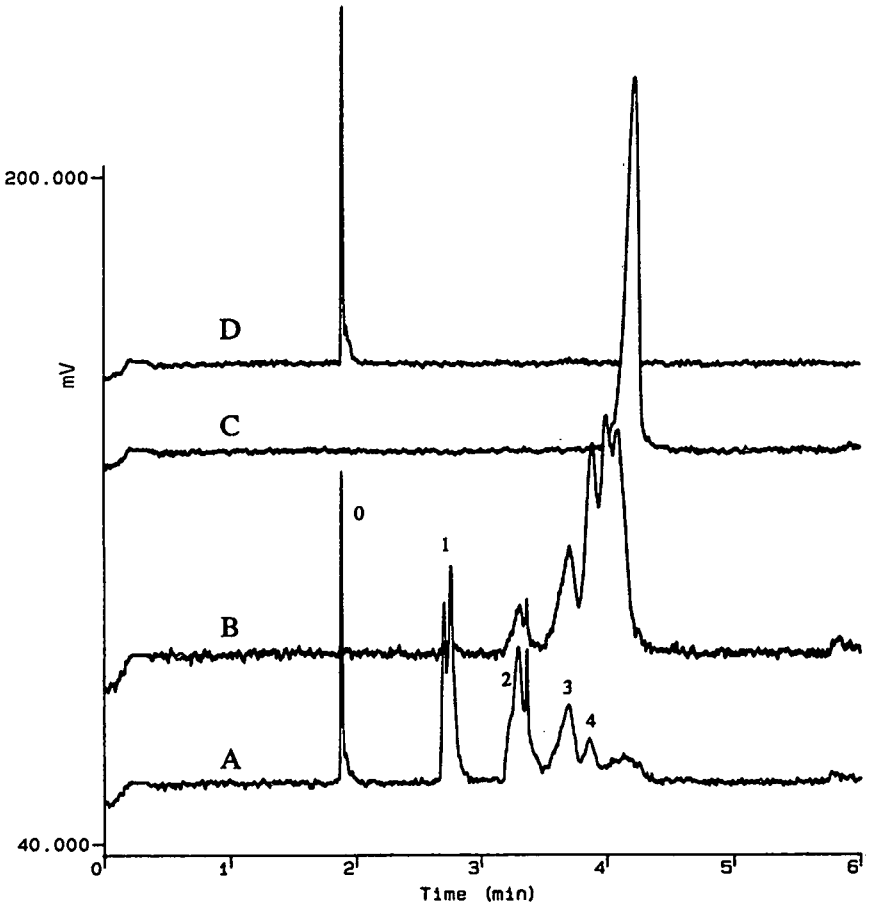

Fig. 13. CZE analyses of different PEG–SOD samples in the presence of SDS. (A) 1-min sample, (B) 4-min sample, (C) 50-min sample and (D) unmodified SOD. Numbers over peaks represent the predicted number of PEG chains per SOD dimer. Data collected on CZE system A. Capillary: 47 cm × 50 μm (separation distance 40 cm). Buffer: 20 m*M* boric acid, 50 m*M* SDS pH 9.3. 30 kV, 1-s pressure injections (1 mg/ml) with detection at 200 nm.

lyze the samples. It is possible that the PEG groups are masking charge differences in the samples or it could be that the high degree of heterogeneity in both the mass and charge of the product results in a broad distribution of closely eluting incompletely resolved peaks. In order to simplify this problem, an attempt was made to remove the PEG from the PEG–SOD by hydrolysis prior to analysis by CZE. In this way the material would retain its charge differences (*i.e.* PEG modified lysines remain amidated while the mass differences in the species would be nearly eliminated. Fig. 14 shows electropherograms of the samples of PEG–SOD after treatment with a borate buffer at pH 10.3. A SOD control was treated in the same way to demonstrate that there would be no significant change to the polypeptide chain. Significantly better resolution of individual species is achieved upon removal of the PEG groups. The peak at 8.4 min in the 1- and 4-min PEG–SOD samples is due to glycine succinate formed by hydrolysis of the quenched PEG reagent.

A close examination of these electropherograms shows that the later eluting peaks (higher degree of modification) seem to display anomalously high peak broadening (assuming diffusion limited peak broadening). Apparently, this broadening reflects a degree of heterogeneity that still exists for a given stoichiometric combination of PEG with SOD.

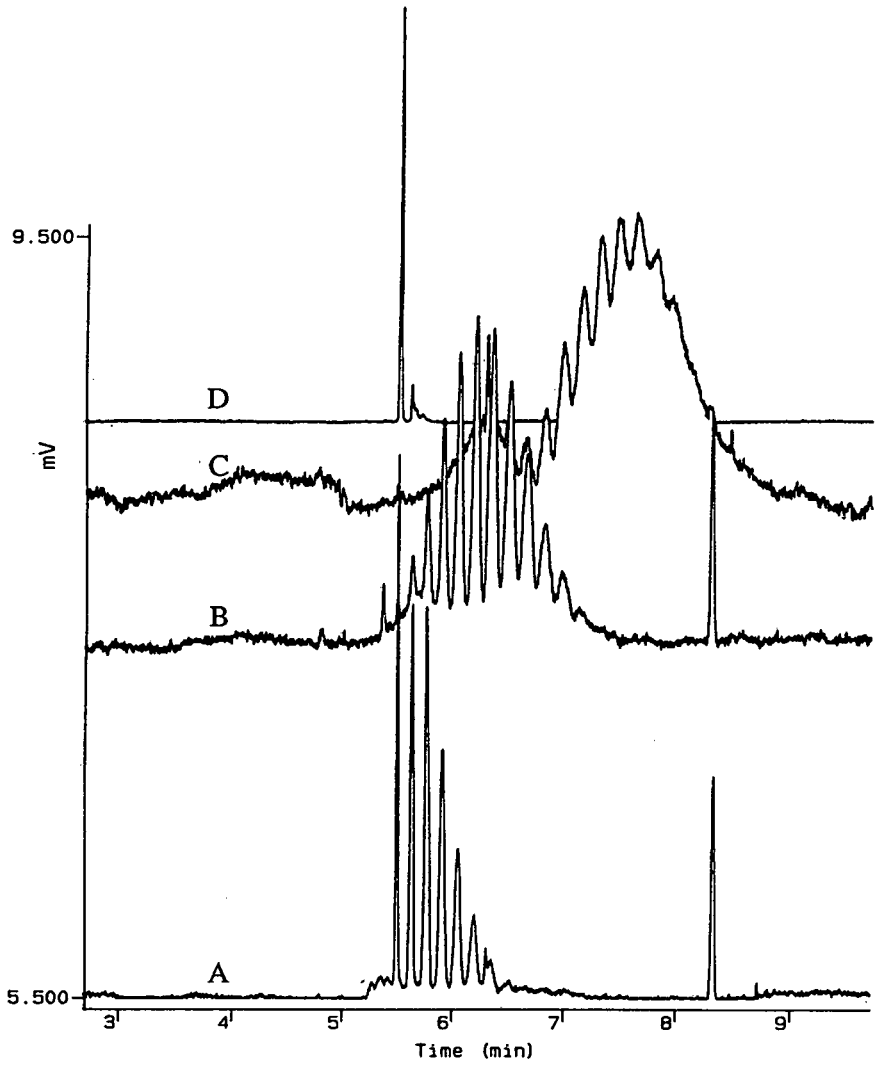

Fig. 14. Free solution CZE analyses of different PEG–SOD samples after removal of the PEG chains. (A) 1-min PEG–SOD sample, (B) 4-min PEG–SOD sample, (C) 50-min PEG–SOD sample and (D) SOD control. Data collected using CZE system B. Capillary: 85 cm long × 50 μm I.D. (separation distance 70 cm). Buffer: 50 m*M* boric acid, pH 9.0 with NaOH. 30 kV, 40–10-s hydrodynamic injections at a height of 7 cm (1 mg/ml), detection at 200 nm.

This is not unexpected since the lysines on SOD will have slightly different pK_a values depending on their position along the polypeptide backbone as well as their local environment and so are not all equivalent. The higher the nominal degree of modification the larger is the number of possible combinations of modified lysines which correlates into broader peaks.

CONCLUSIONS

Modification of proteins by covalent attachment of PEG chains produces a complex product which displays heterogeneity in both the size and charge of the resulting species. A series of chromatographic and electrophoretic techniques have been developed which have shown the ability to separate and quan-

titate individual species. These methods should have utility in characterizing the reaction of PEG with SOD under different conditions as well as serving as a qualitative tool for verifying the consistency of the product from lot-to-lot.

REFERENCES

1 Y. Inada, A. Matsushima, Y. Kodera and H. Nishimura, *J. Bioact. Compatible Polym.*, 5 (1990) 343.
2 A. Abuchowski and F. F. Davis, in I. S. Holcenberg and J. Roberts (Editors), *Enzymes as Drugs*, Wiley-Interscience, New York, 1981, pp. 367–383.
3 P. S. Pyatak, A. Abuchowski and F. F. Davis, *Res. Commun. Chem. Pathol. Pharmacol.*, 29 (1980) 113.
4 A. Abuchowski, J. R. McCoy, N. C. Pakzuk, T. VanEs and F. F. Davis, *J. Biol. Chem.*, 252 (1977) 3582.
5 S. Davis, A. Abuchowski, Y. K. Park and F. F. Davis, *Clin. Exp. Immunol.*, 46 (1981) 649.
6 A. Abuchowski, G. M. Kazo, C. R. Verhoest, T. VanEs, D. Kafkewitz, M. L. Nucci, A. T. Viau and F. F. Davis, *Cancer Biochem. Biophys.*, 7 (1984) 175.
7 N. V. Katre, M. J. Knauf and W. L. Laird, *Proc. Natl. Acad. Sci. U.S.A.*, 84 (1987) 1487.
8 S. Rajagopalan, S. L. Gonias and S. U. Pizzo, *J. Clin Invest.*, 75 (1985) 413.
9 A. Abuchowski and F. F. Davis, *Biochim. Biophys. Acta*, 578 (1979) 41.
10 P. Wirth, J. Souppe, D. Tritsch and J. F. Biellmann, *Bioorganic Chem.*, 19 (1991) 133.
11 R. J. Goodson and N. V. Katre, *Bio/Technology*, 8 (1990) 343.
12 F. M. Veronese, P. Caliceti, A. Pastorino, O. Schiauon, L. Sartore, L. Banci and L. M. Scolaro, *J. Controlled Release*, 10 (1989) 145.
13 P. McGoff, A. C. Baziotis and R. Maskiewicz, *Chem. Pharm. Bull.*, 36 (1988) 3079.
14 R. Somak. M. G. P. Saifer and L. D. Williams, *Free Radical Res. Commun.*, 12–13 (1991) 553.
15 R. L. Cunico, V. Gruhn, L. Kresin and J. E. Wiktorowicz, *J. Chromatogr.*, 559 (1991) 467.
16 M. M. Vestling, C. M. Murphy, M. Kelly, C. Fenselau, J. Dedinas, M. S. Doleman, P. B. Harrsch, R. Kutny, D. L. Ladd and M. A. Olsen, in R. H. Angeletti (Editor), *Techniques in Protein Chemistry III*, Academic Press, San Diego, CA, 1992, pp. 477–485.
17 M. S. Doleman, C. W. Emery, R. Kutny, M. Rogers and S. Kelly, presented at the *5th Symposium of the Protein Society, Baltimore, MD, June 22–26, 1991.*
18 C. J. Neville, J. L. Snider, J. Bullock and L. C. Yuan, presented at the *American Association Of Pharmaceutical Scientists' Sixth Annual Meeting, Washington, DC, November 17–21, 1991.*
19 A. T. Andrews, in A. R. Peacocke and W. F. Harrington (Editors), *Electrophoresis: Theory, Techniques and Biochemical and Clinical Applications*, Oxford University Press, New York, 1987 pp. 25–37.
20 Y. F. Maa and Cs. Horváth, *J. Chromatogr.*, 445 (1988) 71.
21 S. Yano, *Arch. Biochem. Biophys.*, 279 (1990) 60.
22 D. P. Malinowski and I. Fridovich, *Biochemistry*, 18 (1979) 237.
23 E. A. Lissi and E. Abuin, *J. Colloid Interface Sci.*, 105 (1985) 1.
24 A. D. Tran, S. Park, P. J. Lisi, O. T. Huynh, R. R. Ryall and P. A. Lane, *J. Chromatogr.*, 542 (1991) 459.
25 S.-L. Wu, G. Teshima, J. Cacia and W. S. Hancock, *J. Chromatogr.*, 516 (1990) 115.

Journal of Chromatography, 599 (1992) 157–162
Elsevier Science Publishers B.V., Amsterdam

CHROMSYMP. 2535

Comparison of detergents for extraction and ion-exchange high-performance liquid chromatography of Sendai virus membrane proteins

G. W. Welling*, Y. Hiemstra and M. Feijlbrief

Laboratorium voor Medische Microbiologie, Rijksuniversiteit Groningen, Oostersingel 59, 9713 EZ Groningen (Netherlands)

C. Örvell

Department of Virology, Karolinska Institute, School of Medicine and Department of Virology, National Bacteriological Laboratory, S-10521 Stockholm 1 (Sweden)

J. van Ede and S. Welling-Wester

Laboratorium voor Medische Microbiologie, Rijksuniversiteit Groningen, Oostersingel 59, 9713 EZ Groningen (Netherlands)

ABSTRACT

The integral membrane proteins of Sendai virus, haemagglutinin–neuraminidase (HN) and fusion protein (F) were extracted from purified virions with a non-ionic and two zwitterionic detergents, *i.e.*, pentaethylene glycol monolauryl ether ($C_{12}E_5$), lauryldimethylamine oxide (LDAO) and dodecyldimethylammoniopropane-1-sulphonate (SB12), respectively. The extracts were subjected to ion-exchange high-performance liquid chromatography (HPIEC) using 0.1% of the detergent in the eluent on four different columns (MA7Q, Zorbax BioSeries SAX, Mono Q and PL-SAX) with a quaternary amine as interacting ligand and with different pore sizes: non-porous and 30, 80 nm and 400 nm, respectively. The relative recoveries of protein were similar for all the columns. The highest recovery of HN and F protein and the best separation were obtained with $C_{12}E_5$. Analysis of HPIEC fractions with monoclonal antibodies directed against conformational epitopes showed that $C_{12}E_5$ had less effect on the conformation than the other two detergents.

INTRODUCTION

When the conformation of an integral membrane protein has to be retained, purification by ion-exchange high-performance liquid chromatography (HPIEC) in the presence of a detergent (surfactant) is particularly suitable as the elution conditions are generally mild [1–3]. Detergent extraction is often the first step in the purification of an integral membrane protein. Detergents are lipid-like substances and they possess a hydrophilic head and a hydrophobic tail and are able to compete with the lipids in a bilayer. They are also more hydrophilic than the lipids. As a consequence, detergent–protein complexes are soluble in aqueous solutions and the detergent molecules, in mimicking the lipid molecules, help to maintain the native configuration of the membrane proteins during a purification procedure. Extraction can be achieved with a wide variety of detergents [4–8], but in order to preserve biological activity non-ionic or zwitterionic detergents are used. We have used the integral membrane proteins of Sendai virus as a model mixture for the development of methodologies for purification of membrane proteins using different detergents and different modes of high-performance liquid chromatography (HPLC) [9–18]. The two integral membrane proteins of Sendai virus are the haemaggluti-

0021-9673/92/$05.00

nin–neuraminidase protein HN (relative molecular mass, M_r = 68 000) and the fusion protein F (M_r = 65 000). Both proteins are present in detergent extracts in multimeric forms [19]. Dimeric HN (HN_2) and tetrameric HN and F (HN_4, F_4) are observed in addition to truncated forms of HN due to proteolytic degradation.

In an earlier study different polyethylene glycol alkyl ethers were investigated [17]. In this study one non-ionic and two zwitterionic detergents, *i.e.*, pentaethylene glycol monolauryl ether ($C_{12}E_5$) [17], lauryldimethylamine oxide (LDAO) [20] and N-dodecyl-N,N-dimethylammonio-3-propanesulphonate (SB12) [8], respectively, were used for extraction and as additive to the eluents for HPIEC. In addition, the effect on the immunological activity was studied. As the extracts contain relatively large multimeric forms of the Sendai proteins [19], separation and recovery may be adversely affected by the pore size of the column matrix. Therefore, we subjected these proteins to chromatography on four columns (MA7Q, Zorbax BioSeries SAX, Mono Q and PL-SAX) with a quaternay amine as interacting ligand and with different pore sizes: non-porous and 30, 80 and 400 nm, respectively.

EXPERIMENTAL

Detergent extraction of Sendai virus

Sendai virus was grown in 10-day-old embryonated chicken eggs. Allantoic fluid was harvested after incubation at 37°C for 3 days. Cell debris was removed by low-speed centrifugation (2000 *g*, 10 min, 5°C) and virus particles were obtained from the supernatant by centrifugation for 1 h at 70 000 *g* at 5°C. Virus was resuspended in 10 m*M* Tris–HCl (pH 7.2), supplemented with 10% sucrose and stored at −80°C. The amount of protein was determined [21]. Sendai virions were extracted with three detergents with the same hydrophobic tail (C_{12}) (see Fig. 1), *i.e.*, pentaethylene glycol monolauryl ether ($C_{12}E_5$) (Kwant-Hoog Vacolie Recycling and Synthesis, Bedum, Netherlands), lauryldimethylamine oxide (LDAO; N,N-dimethyldodecylamine-N-oxide) (Fluka, Buchs, Switzerland) and N-dodecyl-N,N-dimethyl-3-ammoniopropane-1-sulphonate (SB12) (Serva, Heidelberg, Germany). A Sendai virus suspension containing 40 mg of protein was pelleted and resuspended in 1 ml of 10 m*M* Tris–HCl (pH 7.2). The same volume of buffer containing 4% (w/w) of the detergent was added, resulting in a final detergent concentration of 2%. After incubation for 20 min at room temperature, the suspension was centrifuged for 1 h at 70 000 *g* at 5°C. The supernatant contains the HN and F proteins and was stored at −80°C.

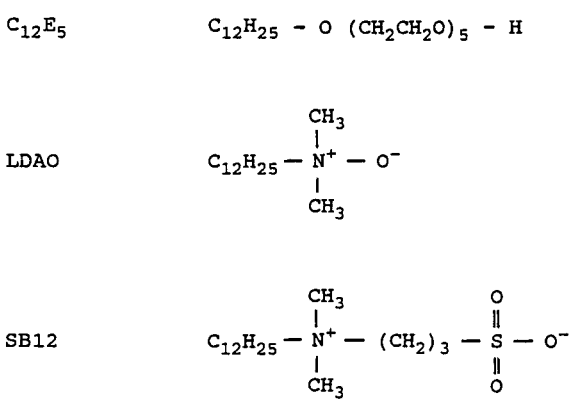

Fig. 1. Structural formula of $C_{12}E_5$, LDAO and SB12.

Ion-exchange and size-exclusion HPLC

Chromatography was performed with a system consisting of an LKB 2150 pump (Pharmacia–LKB, Uppsala, Sweden), a Rheodyne Model 7125 injector (Inacom, Veenendaal, Netherlands) and a Waters Model 441 detector (Millipore–Waters, Etten-Leur, Netherlands). Anion-exchange HPLC was performed with an MA7Q (50 mm × 7.8 mm I.D.) column (Bio-Rad Labs., Richmond, CA, USA) consisting of non-porous polymeric particles with a particle size of 7 μm, a Zorbax BioSeries SAX (80 mm × 6.2 mm I.D.) column (DuPont, Wilmington, DE, USA) consisting of zirconium oxide-stabilized silica with a particle size of 6 μm and a pore size of 30 nm, a Mono Q HR 5/5 (50 mm × 5 mm I.D.) column (Pharmacia–LKB) consisting of polymer beads with a particle size of 10 μm and pores of 80 nm and a PL-SAX 4000 Å (50 mm × 4.6 mm I.D.) column (Polymer Labs. Church Stretton, UK) consisting of polymer beads with a particle size of 8 μm and pores of 400 nm. To determine a gradient time suitable for all four columns, 730–1000 μg of a $C_{12}E_5$ extract of Sendai virus membrane proteins were subjected to HPIEC. After isocratic elution for 10 min, retained proteins were eluted with a linear 6-, 12- and 24-min gradient

from 20 m*M* Tris–HCl (pH 7.8) containing 0.1% $C_{10}E_{5-9}$ (decylPEG-300) [18] to 0.5 *M* sodium chloride in the same buffer. In subsequent experiments, using a gradient time of 12 min, the eluent contained 0.1% of the detergent used for extraction. In that case, 440–510 μg of Sendai virus proteins were subjected to HPIEC.

The amount of protein in the extracts and fractions after HPIEC was determined by size-exclusion HPLC (HPSEC). A Polyol Si500 (100 nm × 4.6 mm I.D.) column (Serva) with 5-μm particles and a pore size of 50 nm was used for HPSEC. To a volume of 100 μl of extract or HPIEC fraction (freeze-dried and after dialysis dissolved in 500 μl of water) sodium dodecyl sulphate (SDS) was added to a final concentration of 4%. After heating for 3 min in a bath of boiling water, 10 μl of the fractions were subjected to HPSEC. The proteins were eluted with 50 m*M* sodium phosphate (pH 6.5) containing 0.1% SDS at a flow-rate of 0.8 ml/min. The absorbance was monitored at 280 nm. The amount of HN and F protein was then calculated from the peak height. Similarly treated bovine serum albumin was used as a standard. Relative recoveries of total protein after HPIEC were calculated from the area of the peaks at 280 nm.

SDS–polyacrylamide gel electrophoresis (PAGE)

Samples of the HPIEC fractions were analysed by SDS-PAGE [22] on 12% gels under non-reducing conditions. After electrophoresis, the gels were fixed and silver-stained as described [23].

Enzyme-linked immunosorbent assay (ELISA)

Selected HPIEC fractions containing predominantly F or HN protein were analysed with the conformation-dependent monoclonal antibodies (mAbs) HN 851 and F 1.216. The properties of these mAbs have been described [16,24]. ELISA trays were coated with 100 μl of twofold dilutions of fractions diluted in coating buffer, consisting of 50 m*M* sodium carbonate (pH 9.6) supplemented with 0.6 *M* NaCl. The starting dilution contained 10 μg protein/ml as determined by HPSEC. After coating overnight at 4°C, the ELISA was performed as described earlier [17]. The absorbance at 492 nm (A_{492}) was measured in a microplate photometer. Absorbances below 0.2 were considered as negative. The amount of protein (ng) giving an absorbance value of 1.2 was recorded. This amount is inversely related to the immunological activity of the protein.

RESULTS AND DISCUSSION

It has been shown that zwitterionic detergents are useful in retaining the biological activity of integral membrane proteins [8]. Two series of such detergents with varying lengths of hydrophobic tails are commercially available, the alkylamine oxides [20] and the alkylammoniopropanesulphonates [8]. We decided to compare the C_{12} variant of these detergents (LDAO and SB12, respectively) with the non-ionic C_{12} oxyethylene ether ($C_{12}E_5$) with which the highest yields of protein were obtained after extraction of purified Sendai virions [17]. Extraction was performed at a final detergent concentration of 2%, which is well above the critical micellar concentration (CMC) (Table I). Extraction of Sendai virions with $C_{12}E_5$, LDAO and SB12 resulted in 204, 189 and 110 μg of protein per 100 μl of extract, respectively. These extracts were compared by HPIEC on four different columns. However, prior to this comparison a suitable gradient time for all four columns was selected by subjecting a Sendai virus $C_{12}E_5$ extract to HPIEC using gradient times of 6, 12 and 24 min after isocratic elution for 10 min. The elution patterns with a gradient time of 12 min are shown in Fig. 2. Non-proteinaceous material and the HN proteins are eluted first, followed by a broad peak containing the F protein (indicated with an asterisk). Despite the differences in column volume, 2.4, 2.4, 1.0 and 0.8 ml of the MA7Q, Zorbax SAX, Mono Q and PL-SAX columns, respectively, the elution patterns with respect to the separation between the first peaks (containing non-proteinaceous material and HN proteins) and the F peak were similar using gradient times of 6, 12 and 24 min, except for a gradient time of 6 min with the Zorbax

TABLE I

CRITICAL MICELLAR CONCENTRATIONS (%)

Detergent	0–0.05 *M* Cl^-	0.2 *M* Cl^-	Ref.
$C_{12}E_5$	0.020		17
LDAO	0.048	0.034	20
SB12	0.144	0.047	8

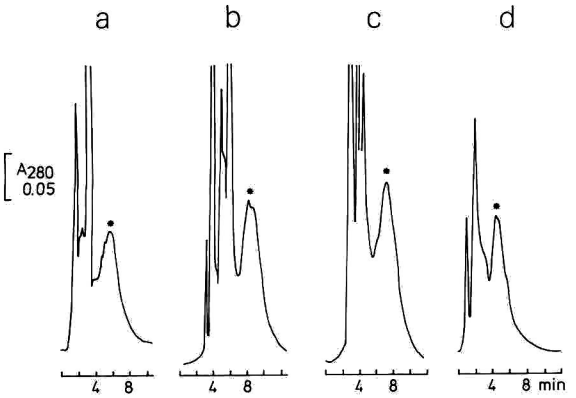

Fig. 2. Anion-exchange HPLC of a $C_{12}E_5$ extract of Sendai virus membrane proteins on four different columns: (a) MA7Q (non-porous), (b) Zorbax BioSeries SAX (30-nm pores), (c) Mono Q (80-nm pores) and (d) PL-SAX (400 nm-pores). Conditions: linear A–B gradient (0 to 0.5 *M* NaCl in 12 min), following 10-min isocratic elution with buffer A, where buffer A is 20 m*M* Tris–HCl (pH 7.8) containing 0.1% $C_{10}E_{5-9}$ and buffer B is buffer A containing 0.5 *M* NaCl; flow-rate, 1 ml/min; absorbance monitored at 280 nm. The amounts of protein applied to columns a, b, c and d were 790, 1000, 980 and 730 μg, respectively. Peak * = fusion protein (F).

SAX column, which resulted in less separation between these peaks. Therefore, a gradient time of 12 min was chosen for further experiments.

Amounts of Sendai virus membrane proteins ranging from 440 to 510 μg were subjected to HPIEC on the four columns. When a detergent is applied as additive to an elution buffer, it is most satisfactorily used at concentration above the CMC [25]. We used a concentration of 0.1% of the detergents in the eluent. Very shortly after starting the gradient, this is above the CMC (see Table I). The elution patterns obtained with the PL-SAX column together with the SDS-PAGE analysis are given as an example (Fig. 3). The most satisfactory separations with all columns were obtained when $C_{12}E_5$ was used for extraction and as an additive to the elution buffer. With SB12 less separation between HN and F protein was obtained and with LDAO hardly any separation was found. The corresponding SDS gels (Fig. 3) also indicate that the highest resolution is obtained with $C_{12}E_5$. This can also be judged from HPSEC analysis of selected HPIEC fractions. In Fig. 3a, b and c, the HN/F ratio was 4.8, 2.0 and 3.3 in fractions 2 plus 3, 2 and 2, respectively. For fractions 6, 6 and 4 in Fig. 3a, b and c the HN/F ratio was 0.35, 0.81 and 0.85, respectively.

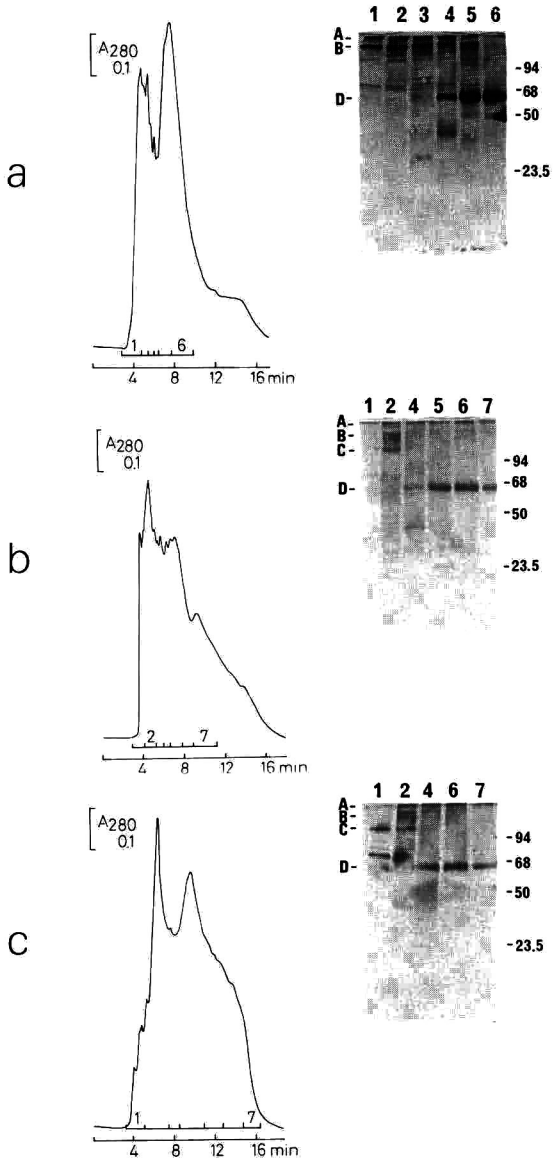

Fig. 3. Anion-exchange HPLC of (a) $C_{12}E_5$, (b) LDAO and (c) SB12 extract of Sendai virus membrane proteins on a PL-SAX column. Elution conditions: linear A–B gradient (0 to 0.5 *M* NaCl in 12 min), following 10-min isocratic elution with buffer A, where buffer A is 20 m*M* Tris–HCl (pH 7.8) containing 0.1% of the detergent used for extraction and buffer B is buffer A containing 0.5 *M* NaCl; flow-rate, 1 ml/min; absorbance monitored at 280 nm. Fractions were collected as indicated and analysed by SDS-PAGE (12% gel) under non-reducing conditions. The sample of reference proteins contained mercaptoethanol, which occasionally affected Sendai proteins in other lanes [*e.g.*] lane 6 in (a)]. Polypeptides were revealed by silver staining. A, B, C and D are the tetrameric, dimeric and truncated forms of HN protein and F protein, respectively. The molecular masses ($\times 10^{-3}$) of reference proteins are given on the right.

TABLE II

RELATIVE RECOVERIES (%) OF PROTEIN FROM THE PEAK AREA AT 280 nm AFTER HPIEC OF SENDAI VIRUS EXTRACTED WITH DIFFERENT DETERGENTS

The highest yield was taken as 100%.

Detergent	Column			
	MA7Q	Zorbax SAX	Mono Q	PL-SAX
C12E5	100	72	98	82
LDAO	88	93	99	100
SB12	90	100	89	93

An interesting difference is that the HN protein is fragmented to greater extent when SB12 and LDAO are used (Fig. 3b and c, fraction 2). Large amounts of the tetrameric and dimeric form of HN are only present when $C_{12}E_5$ is used. Absolute recoveries were higher than 70% and the relative recoveries of total protein are listed in Table II.

None of the columns showed always the highest recovery, regardless of which detergent was used in the eluent. For example, the MA7Q column showed a 100% relative recovery when $C_{12}E_5$ was used and the PL-SAX column showed a relative recovery of 100% when LDAO was used. The average relative recoveries obtained with the three detergents for the four columns were similar and ranged from 88 to 95%. It has been argued that increasing the pore size may improve intraparticle mobile phase mass transfer for large macromolecules [26]. Another solution would be to use a non-porous matrix [27]. Our results do not indicate that the pore size of the matrix is of paramount importance for the separation. One reason may be that relatively small amounts of protein were used consisting of a mixture of differently sized macromolecules. The detergent extract may contain monomeric, dimeric and tetrameric forms of the integral membrane proteins of Sendai virus in addition to aggregated forms. In addition, proteolytically degraded smaller forms may be present. The capacity of the columns will probably be sufficient to accommodate the relatively small amounts of large proteins and aggregated forms on the outside of the column particles resulting in similar performances of all four columns.

Another matter of concern may be the effect of the detergent on the conformation of the membrane proteins during chromatography. This was measured in an ELISA with mAbs directed against conformation-dependent epitopes of HN and F protein. ELISA plates were coated with serial dilutions of the HPLC fractions. The detergent concentration in the fractions which gave an A_{492} of 1.2 was *ca.* 0.0005%. This concentration did not interfere with the coating procedure. Only detergent concentrations higher than 0.015%, 0.020% and 0.025% for $C_{12}E_5$, SB12 and LDAO, respectively, disturbed the coating of HN and F protein. The structural intactness of HN and F protein is expressed as the amount of protein needed to obtain an A_{492} of 1.2. For F protein from the different fractions the amount varies from 3.2 to 7.2 ng (Table III). This shows that the F protein is not affected by HPIEC in the presence of the three detergents, as the amount of F protein necessary for an A_{492} of 1.2 in detergent extracts (the starting material for HPIEC) ranges from 2 to 7 ng [17]. For the HN protein present in the HPIEC fractions, the amount required to obtain an A_{492} of 1.2 varies from 3.5 to 28.6 ng (Table III). This is slightly more than the amount of 4–11 ng of HN protein that is required to obtain an A_{492} of 1.2 for HN protein from detergent extracts [17]. In contrast, more than 1000 ng of HN were required to obtain an A_{492} of 1.2 when HN was denaturated by boiling in 4% SDS [17]. This means that the F protein is not affected by the

TABLE III

IMMUNOLOGICAL REACTIVITY OF HN AND F PROTEIN AFTER HPIEC IN THE PRESENCE OF DIFFERENT DETERGENTS

Immunological activity is expressed as the amount (ng) of HN or F protein needed to give an A_{492} of 1.2.

Column	Detergent					
	$C_{12}E_5$		LDAO		SB12	
	HN	F	HN	F	HN	F
MA7Q	6.6	2.5	13.6	7.2	28.6	3.6
Zorbax SAX	3.9	2.3	27.0	3.4	12.0	3.6
Mono Q	3.5	2.7	12.8	6.9	15.9	3.5
PL-SAX	3.7	2.8	15.5	6.3	15.5	4.4
Average	4.4	2.6	17.2	6.0	18.0	3.8

three detergents used in this study, and that the HN protein is slightly affected when LDAO and SB12 are used as additives to the eluent, independent of the column used for HPIEC. With $C_{12}E_5$ in the eluent neither the HN nor the F protein is affected.

CONCLUSIONS

The results show that the non-ionic detergent $C_{12}E_5$ is more suitable for extraction, chromatography and preservation of conformation of Sendai virus integral membrane proteins than the two zwitterionic detergents SB12 and LDAO. The resolution in HPIEC largely depended on the detergent used for extraction and used as additive in the elution buffer.

ACKNOWLEDGEMENTS

We thank Mr. J. J. van Dijk, Bio-Rad, Veenendaal, Netherlands, for the MA7Q column, Dr. A. Dams, DuPont, 's-Hertogenbosch, Netherlands, for the Zorbax BioSeries SAX column, Dr. L. L. Lloyd, Polymer Labs. Church Stretton, UK for the PL-Sax 400 Å column, Serva, Heidelberg, Germany, for the Polyol Si500 column and Mr. B. Kwant, Bedum, Netherlands, for the non-ionic detergent $C_{12}E_5$.

REFERENCES

1 G. W. Welling, R. van der Zee and S. Welling-Wester, *J. Chromatogr.*, 418 (1987) 223.
2 G. W. Welling and S. Welling-Wester, In C.T. Mant and R. S. Hodges (Editors), *High-Performance Liquid Chromatography of Peptides and Proteins: Separation, Analysis, and Conformation*, CRC Press, Boca Raton, FL, 1991, p. 223.
3 M. Rögner, *J. Chromatogr.*, 512 (1990) 219.
4 A. Helenius and K. Simons, *Biochim. Biophys. Acta*, 415 (1975) 29.
5 C. Tanford and J. A. Reynolds, *Biochim. Biophys. Acta*, 457 (1976) 133.
6 A. Helenius, D. R. McCaslin, E. Fries and C. Tanford, *Methods Enzymol.*, 56 (1979) 734.
7 L. M. Hjelmeland and A. Crambach, *Methods Enzymol.*, 104 (1984) 305.
8 A. Gonenne and R. Ernst, *Anal. Biochem.*, 87 (1987) 28.
9 G. W. Welling, G. Groen and S. Welling-Wester, *J. Chromatogr.*, 266 (1983) 629.
10 R. van der Zee, S. Welling-Wester and G. W. Welling, *J. Chromatogr.*, 266 (1983) 577.
11 G. W. Welling, J. R. J. Nijmeijer, R. van der Zee, G. Groen, J. B. Wilterdink and S. Welling-Wester, *J. Chromatogr.*, 297 (1984) 101.
12 G. W. Welling, G. Groen, K. Slopsema and S. Welling-Wester, *J. Chromatogr.*, 326 (1985) 173.
13 G. W. Welling, K. Slopsema and S. Welling-Wester, *J. Chromatogr.*, 359 (1986) 307.
14 G. W. Welling, K. Slopsema and S. Welling-Wester, *J. Chromatogr.*, 397 (1987) 165.
15 G. W. Welling, B. Kazemier and S. Welling-Wester, *Chromatographia*, 24 (1987) 790.
16 S. Welling-Wester, B. Kazemier, C. Örvell and G. W. Welling, *J. Chromatogr.*, 443 (1988) 255.
17 J. van Ede, J. R. J. Nijmeijer, S. Welling-Wester, C. Örvell and G. W. Welling, *J. Chromatogr.*, 476 (1989) 319.
18 S. Welling-Wester, R. M. Haring, H. Laurens, C. Örvell and G. W. Welling, *J. Chromatogr.*, 476 (1989) 477.
19 O. Sechoy, J. R. Phillipot and A. Bienvenue, *J. Biol. Chem.*, 262 (1987) 11519.
20 K. W. Hermann, *J. Phys. Chem.*, 66 (1962) 295.
21 O. H. Lowry, N. J. Rosebrough, A. L. Farr and R. J. Randall, *J. Biol. Chem.*, 193 (1951) 265.
22 U. K. Laemmli, *Nature (London)*, 227 (1970) 680.
23 W. Wray, T. Boulikas, V. P. Wray and R. Hancock, *Anal. Biochem.*, 118 (1981) 197.
24 C. Örvell and M. Grandien, *J. Immunol.*, 129 (1982) 2779.
25 Y. Kato. T. Kitamura, K. Nakamura, A. Mitsui, Y. Yamasaki and T. Hashimoto, *J. Chromatogr.*, 391 (1987) 395.
26 L. L. Lloyd and F. P. Warner, *J. Chromatogr.*, 512 (1990) 365.
27 J. K. Duncan, A. J. C. Chen and C. J. Siebert, *J. Chromatogr.*, 397 (1987) 3.

Journal of Chromatography, 599 (1992) 163–170
Elsevier Science Publishers B.V., Amsterdam

CHROMSYMP. 2564

High-performance liquid chromatography of amino acids, peptides and proteins

CXX☆. Evaluation of bandwidth behaviour of proteins chromatographed on tentacle-type anion exchangers

F. W. Fang, M. I. Aguilar and M. T. W. Hearn*

Department of Biochemistry and Centre for Bioprocess Technology, Monash University, Clayton, Victoria 3168 (Australia)

ABSTRACT

The dynamic behaviour of several proteins chromatographed on the Fractogel-TMAE and LiChrospher-TMAE tentacle-type anion exchangers was investigated through the analysis of experimental bandwidth data. Results were analysed by comparison of experimental data with bandwidths calculated on the basis of the protein assuming a rigid globular structure with a uniform interactive surface using the general plate height theory. The influence of the displacer salts NaCl and KBr and different mobile phase pH conditions (pH 5.5, 6.5, 7.5 and 9.6) on solute bandwidths were investigated. Very similar bandwidth dependencies were observed for all proteins separated on the Fractogel-TMAE sorbent with both displacer salt systems used. However, there was a marked difference in the bandwidth behaviour on the LiChrospher-TMAE sorbent with the two displacer salts. Furthermore, changes in the mobile phase pH resulted in significant differences in the dependence of the bandwidth ratios on both the gradient time and the type of displacer salt.

INTRODUCTION

High-performance ion-exchange liquid chromatography (HPIEC) is now used extensively for the high-resolution analysis and purification of peptides, proteins and polynucleotides [1]. Recently, a new class of ion-exchange sorbents for biochromatography has been introduced, namely the tentacle-type ion exchangers [2,3]. These chromatographic sorbents are characterised by coulombic ligands composed of linear polyelectrolyte chains of average length between 20–50 monomer units graft-polymerised to the hydroxyl groups of a hydrophilic support material. In a previous study [4], we investigated the comparative retention behaviour of proteins separated by strong anion-exchange liquid chromatography on the tentacle sorbents. While some proteins exhibited retention properties which were comparable to that observed with conventional high-performance ion exchangers, other proteins showed significantly different retention properties. In the present study the evaluation of these tentacle-type ion exchangers is continued through analysis of the bandwidth behaviour of several proteins separated by strong anion-exchange chromatography.

EXPERIMENTAL

Chemicals and reagents

Bovine erythrocyte carbonic anhydrase, whale sperm myoglobin (type III), hen egg white lysozyme (grade 1), bovine ribonuclease A (type IIIA), bovine insulin, piperazine, bis-tris, triethanolamine were all purchased from Sigma (St. Louis, MO, USA). The recombinant porcine growth hormone was available in highly purified form from associated studies in this laboratory. Sodium chloride, potassium bromide, hydrochloric acid and hydrobromic acid

☆ For Part CXIX, see ref. 23.

0021-9673/92/$05.00

(AnalaR grade) were obtained from BDH (Port Fairy, Australia).

Quartz distilled water was further purified on a Milli-Q system (Millipore, Bedford, MA, USA). Buffers were adjusted to the respective pH using either hydrochloric acid or hydrobromic acid.

Apparatus

All chromatographic studies were carried out with either a Pharmacia (Uppsala, Sweden) fast protein liquid chromatographic (FPLC) system, as previously described [5,6] or a Beckman System Gold liquid chromatograph. The Fractogel EMD TMAE-650 (Fractogel-TMAE, particle diameter d_p = 25–40 μm, pore size = 650 Å) and the LiChrospher 1000 TMAE (LiChrospher-TMAE, d_p = 5 μm, pore size = 1000 Å) sorbents were obtained as prepacked columns (150 × 10 mm I.D. and 50 × 10 mm I.D., respectively) from E. Merck (Darmstadt, Germany). Samples were injected using glass syringes (Scientific Glass Engineering, Ringwood, Australia), at protein concentrations of 5 mg/ml, typically as 10–100-μl injections. The protein solutions were prepared in mobile phase A and prefiltered through 0.22-μm filters.

Chromatographic procedures

The preparation of eluents and procedures for acquisition of gradient elution data has been described previously [5,6]. Gradient bandwidth parameters ($\sigma_{v,calc}$, $\sigma_{v,exp}/\sigma_{v,calc}$, G, C, D_m and N) were calculated using the Sigma program written in this laboratory in Basic language for IBM AT computers as previously described [6].

RESULTS AND DISCUSSION

Theoretical background

The analysis of the chromatographic performance of proteins separated by interactive modes of chromatography is usually carried out in terms of the evaluation of retention behaviour employing various descriptive, theoretical models. For example, the application of two empirical approaches, namely the stoichiometric displacement model [5,7] and the linear solvent strength (LSS) model [5,8] have considerably increased our understanding of the factors controlling protein retention. While these approaches provide significant information on the physical parameters, *e.g.*, flow-rate, particle size, ligand density, etc., that control the interaction between the stationary phase surface and the protein surface, limited information is derived on the kinetic or mechanistic aspects of the separation. The use of retention parameters derived from the LSS model can be combined with the general plate height theory to provide a method for predicting solute bandwidths so that overall chromatographic resolution can be evaluated and optimized [6,9,10]. A number of studies have adopted this approach for the analysis of retention data derived under reversed-phase [11–15] and ion-exchange conditions [6,10]. It is generally found with small peptides and some proteins that high correlations exist between the experimentally and theoretically derived bandwidths using these procedures [6,10,11]. However significant deviations occur for polypeptides and proteins undergoing secondary equilibria such as conformational rearrangement or aggregation [6,9,15]. In particular, it has been shown in some HPIEC systems that the nature of the displacer salt can exert significant effects on the experimental bandwidths [6]. Previous studies [6,9,10] on protein bandbroadening behaviour in HPIEC have focussed on ion-exchange sorbents derived from mono-layer or cross-linked polymer layer ligand systems. Under conditions of regular retention behaviour, *i.e.*, in the absence of secondary equilibria such as conformational or aggregational effects, excellent correlations between the LSS predictions and experimental peak widths have been documented with these sorbents. The question arises whether sorbents involving the tentacle-type ligand structures also follow similar bandbroadening trends. Recent studies with non-porous sorbents have shown [3] that the adsorption behaviour of tentacle-based HPIEC sorbents is fundamentally different when compared to polyethyleneimine (PEI)-based (HPIEC) sorbents. These studies demonstrated that the tentacle-based sorbents are characterised by Hill-type isotherms with pseudo-Gaussian distribution of binding sites, *i.e.*, a type I isothermal surface according to the classification of Gregg and Sing [16].

In the present study the experimental bandwidths of proteins separated on the tentacle-type strong anion-exchangers has been evaluated to assess the utility of the LSS approach with this class of sorbents. According to the LSS concepts [8,10],

under ideal HPIEC conditions of gradient elution, the relationship between peak width, represented by $4\sigma_v$, can be expressed as

$$\sigma_{v,calc} = [(\bar{k}/2 + 1)]GV_m N^{-1/2} \quad (1)$$

where $\bar{k}$ is the median capacity factor of the solute, V_m is the column void volume, N is the plate number and G is the band compression factor which arises from the increase in solvent strength across the solute zone as the gradient developes along the column. The parameter G is given by the expression

$$G^2 = [1 + 2.3b + 1/3(2.3b)^2]/(1 + 2.3b)^2 \quad (2)$$

where b is the gradient steepness parameter. Under normal operating conditions, N can be approximated by

$$N = D_m t_0/Cd_p^2 \quad (3)$$

where d_p is the particle diameter and t_0 is the column deadtime. The diffusion coefficient D_m of the solute in the mobile phase can be expressed in terms of the solute molecular weight, MW, by

$$D_m = 8.34 \cdot 10^{-10}\, T/\eta(MW)^{1/3} \quad (4)$$

where T is the absolute temperature and η is the eluent viscosity. The Knox equation parameter, C, can be estimated from

$$C = \frac{[(1 - x + \bar{k})/(1 + \bar{k})]^2}{15\rho^* a' + 15\rho^* b'\,\bar{k} - 19.2\rho^* x} \quad (5)$$

where x is the interstitial column fraction assumed to be 0.62 for a well-packed column, a' is 1.1 and b' is the surface diffusion parameter which from previous studies is assumed to be equal to 0.72. The restricted diffusion parameter ρ^* was calculated according to the Renkin relationship

$$\rho^* = 1 - 2.104\rho + 2.09\rho^3 - 0.95\rho^5 \quad (6)$$

where ρ is equal to the ratio of the solute diameter to the sorbent pore diameter. The linear logarithmic relationship found between ρ^* and solute molecular weight for the two tentacle-type columns was

$$\log \rho^* = 0.19 - \log MW \quad (7)$$

According to the stoichiometric displacement model, the elution of a protein from a charged surface is accompanied by the adsorption of a stoichiometric amount of displacer counter-ion. As a result, retention properties should be independent of the chemical nature of the displacer co-ion and should only reflect the relative affinity of the counter-ion for the anion-exchange sorbent. In order to utilise these theoretical procedures, the requirement exists that defined values of the particle diameter and pore diameter are available so that the parameters N, C and ρ can be computed according to eqns. 3–6. The use of eqns. 1–7 also assumes that the solute migrates as a unique, conformationally rigid molecule and that the diffusional properties are independent of the nature of the displacing species. However, it is well established that peptides and proteins can undergo conformational and other secondary equilibria in solution and at the surface of chromatographic sorbents [17,18]. If these equilibria do not occur or are extremely rapid compared to the chromatographic separation time, then the ratio between the experimentally observed bandwidth, $\sigma_{v,exp}$, and the bandwidth determined by eqn. 1 should approach unity. However, if these conformational processes occur with similar time scales as the chromatographic retention times, the resulting changes in the diffusional and interactive properties of the solute will lead to a pattern of migration which is more complex than anticipated by conventional plate height theory. In these cases, the ratio, $\sigma_{v,exp}/\sigma_{v,calc}$, will become significantly greater than unity and can be anticipated to show, for example, non-linear dependencies with regard to system residence and gradient steepness.

The influence of NaCl and KBr on protein band-broadening

In the present study, the effect of systematic changes in the displacer salt concentration on the bandwidth behaviour of protein solutes has been investigated under conditions of varied gradient time and constant flow-rate. The proteins listed in Table I were eluted from either the Fractogel-TMAE or the LiChrospher-TMAE strong anion-exchange columns by salt gradients (0–300 mM) varying in time from 20 to 120 min at a constant flow-rate of 1 ml/min. Theoretical bandwidths were calculated according to eqn. 1 and were then compared to the corresponding experimental bandwidths and plotted as a function of the reciprocal of the gradient steepness parameter, b.

Fig. 1 shows plots of the relative $\sigma_{v,exp}/\sigma_{v,calc}$ ratio as a function of $1/b$ for several proteins separated on

TABLE I

PHYSICAL PROPERTIES OF PROTEINS

Protein (source)	Abbreviation	p*I*	MW	D_m (10^{-7} cm^2/s)
Ovalbumin (hen egg white)	OV	4.70	43 000	7.09
Insulin (bovine pancreas)	INS	5.32	5700	13.91
Carbonic anhydrase (bovine erythrocytes)	CA	5.89	30 000	8.00
Growth hormone (porcine recombinant)	GH	6.70	22 100	8.86
Myoglobin (sperm whale muscle)	MYO	7.68	17 500	9.57
Ribonuclease A (bovine pancreas)	RIB	9.60	12 640	10.70
Lysozyme (hen egg white)	LYS	11.00	14 300	10.24

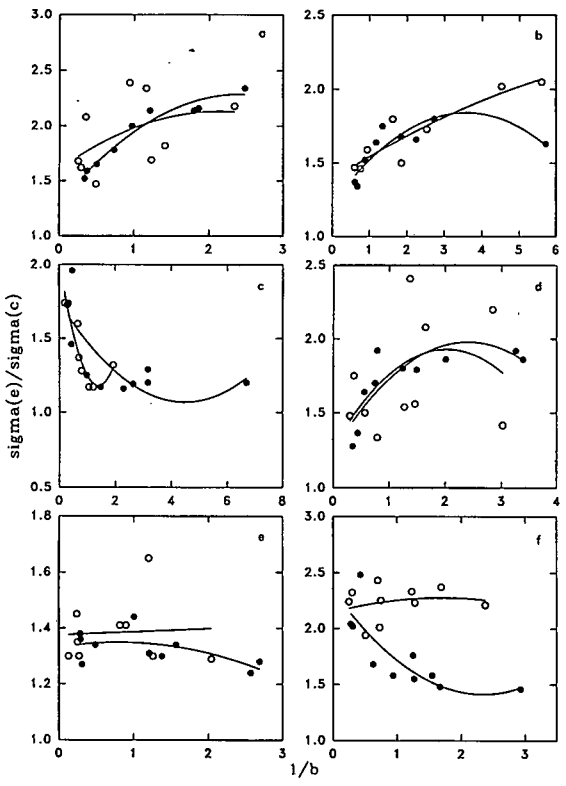

Fig. 1. The influence of displacer salt on the dependence of $\sigma_{v,exp}/\sigma_{v,calc}$ [sigma (e)/sigma (c)] *versus* $1/b$ for several proteins separated on the Fractogel-TMAE sorbent. ○ = NaCl; ● = KBr. Proteins used are (a) OV, (b) INS, (c) CA, (d) GH, (e) MYO and (f) RIB. Data were acquired under conditions of varied gradient time at a flow-rate of 1 ml/min and pH 9.6 as described in the Experimental section and $\sigma_{v,calc}$ was calculated using eqn. 1. All data points were fitted according to a second order regression and fell within 95% confidence limits. See Table I for abbreviations for protein solutes.

the Fractogel-TMAE column with NaCl and KBr as the displacer salt and the mobile phase pH equal to 9.6. It is evident that there is a significant variation in the dependencies of the bandwidth ratio on the residence time with the proteins studied. For OV, INS and GH the bandwidth ratios increase with increasing $1/b$ values for both NaCl and KBr. For CA and MYO the bandwidth ratios approach unity for both displacer salts, while for RIB there is a significant difference in the bandwidth ratio with the two salts. When eluted by steep gradients, protein solutes have reduced column residence times and their elution behaviour is influenced predominantly by mobile phase parameters. The initial decrease in the solute bandwidth ratio at low $1/b$ values seen, for example, with CA with both displacer salts at $1/b < 1$ has been referred to as the "*J*-effect" [8,11]. With $1/b$ values $\ll 1$, this effect results in almost stepwise elution with very pronounced changes in bandwidth dependencies. Moreover, the results of the present study suggest that variations occur in the kinetics of the adsorption process with different proteins on the Fractogel-TMAE tentacle support. In particular, the data indicate that time-dependent exposure of some proteins to the charged TMAE tentacle surfaces and different salt species may strongly influence their interactive and/or diffusional properties, particularly when $1/b$ values are >2.

Fig. 2 shows the corresponding bandwidth plots for the separation of proteins on the LiChrospher-TMAE sorbent with NaCl and KBr as the displacer salts. Comparison of the dependence of the bandwidth ratio on $1/b$ for individual proteins reveals that the influence of the displacer salt on the

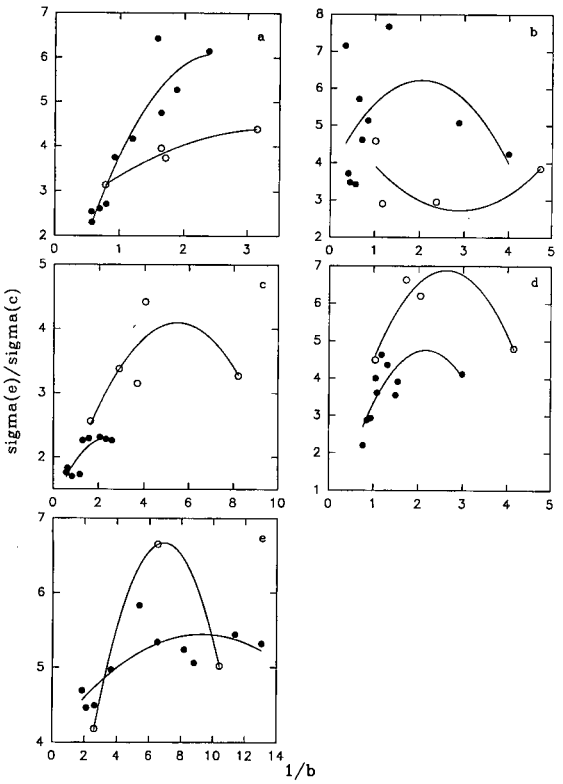

Fig. 2. The influence of displacer salt on the dependence of $\sigma_{v,exp}/\sigma_{v,calc}$ *versus* $1/b$ for several proteins separated on the LiChrospher-TMAE sorbent. ○ = NaCl; ● = KBr. Proteins used are (a) OV, (b) INS, (c) GH, (d) RIB and (e) LYS. See Fig. 1 for other details.

bandwidths is more evident with the LiChrospher-TMAE sorbents than the Fractogel-TMAE sorbent. The bandwidth ratios for OV and INS were larger for KBr than for NaCl. At longer residence times, a number of smaller peaks were resolved from the main OV peak. This phenomenon, which has been observed previously [19], has been attributed to the presence of structural and/or conformational variants of this protein that influence the experimentally observed bandwidth. For GH and RIB larger bandwidth ratios were observed with NaCl compared to KBr. Similar variations in the bandwidth behaviour of proteins separated with different displacer salts on HPIEC sorbents have also been observed, including for example, the conventional Mono-Q strong anion-exchange material [6]. These effects can, in part, be attributed to the kosmotropic or chaotropic properties of various salts which, depending on their concentration, can significantly alter the ion- and ligand-interaction as well as the diffusional properties of proteins in ion-exchange systems. In the case of the tentacle-type sorbents, the specific electrolyte nature of the displacer salt may also influence the dynamic structure of the tentacular surface. While these new phases were designed to specifically interact with a protein in a flexible manner in order to give rise to improved resolution, the interactive process will be extremely sensitive to factors which influence the structure of the ligands as well as the protein solute. Additional evidence for the changes in the dynamic structure and the intercalation of the tentacle polyelectrolyte chains has been provided by the studies on the temperature dependence of protein adsorption with these sorbents [3].

The influence of pH on retention and bandwidth behaviour

Protein retention in HPIEC arises from electrostatic interactions between the protein surface and charged groups immobilized on a stationary phase. According to the net-charge concept, a protein will be retained on an anion-exchange resin when the pH of the eluent is above the p*I* of the protein. However, there are numerous examples [7,9,19–21] where proteins are retained under eluent pH conditions where according to their p*I*, they should be repelled from the stationary phase surface. Nevertheless, the retention of proteins in HPIEC is intimately affected by the pH of the mobile phase. The influence of pH on both the retention and bandwidth properties of the proteins listed in Table I was therefore assessed on the LiChrospher-TMAE sorbent. The retention data were evaluated according to the dependencey of $\log \bar{k}$ on $\log 1/\bar{c}$ according to relationship derived from the LSS model as follows

$$\log \bar{k} = \log K + Z_c \log 1/\bar{c} \quad (8)$$

where $\bar{k}$ is the median capacity factor of the solute and $\bar{c}$ is the corresponding median salt concentration. The value of the parameter Z_c is taken as a measure of the average number of charges located in the contact area established betweeen the protein and the sorbent surface. Tables II and III summarise the results of this evaluation with different mobile phase pHs for both NaCl and KBr respectively. Values of $\log K_c$ were determined by extrapolation

TABLE II

INFLUENCE OF pH ON RETENTION PARAMETERS FOR PROTEINS CHROMATOGRAPHED WITH NaCl

– = Not retained.

Protein	pH 9.6		pH 7.5		pH 6.5		pH 5.5	
	Z_c	log K_c	Z_c	log K_c	Z_c	log K_c	Z_c	log K_c
OV	2.3	11.7	4.4	22.8	2.6	13.4	–	–
INS	1.4	7.2	1.7	8.6	1.4	7.7	–	–
CA	–	–	–	–	–	–	–	–
GH	0.7	3.3	0.7	3.4	–	–	–	–
MYO	–	–	–	–	–	–	–	–
RIB	0.7	2.1	–	–	–	–	–	–
LYS	4.9	24.3	–	–	–	–	–	–

of the log $\bar{k}$ *versus* log $1/\bar{c}$ plots to the limit case of $\bar{c} \rightarrow 10^{-6}$ *M*. Log K_c values also provide an indication of the influence of experimental conditions on the affinities of protein solutes for the sorbent. It is evident from these data that protein retention generally decreases with decreasing pH while none of the test proteins were retained at pH 5.5. This finding with the LiChrospher-TMAE sorbent is in contrast to the results obtained for the isocratic elution of these proteins under similar salt and pH conditions on the Mono-Q sorbent where both OV and CA exhibited significant retention. Additional results which are not anticipated by the net-charge theory were also observed. These included the non-retention of CA and MYO at pH 9.6 as previously noted, and the observation that OV is not retained with mobile phases of pH 5.5 which is still 0.8 pH units above the protein p*I*. These results thus confirm and extend the findings of our previous study [4] on the retention behaviour of proteins on the tentacle-type sorbents which suggested that the density and/or the accessibility of the coulombic binding sites on the silica based material differ from that on the Mono-Q type materials.

Fig. 3 shows the plots of the bandwidth ratio *versus* $1/b$ for OV and INS at pH 7.5 and 6.5 with NaCl and KBr as the displacer salt. For OV, the magnitude of the bandwidth ratio generally increases with decreasing pH with NaCl as the displacing salt, while the opposite effect is observed with KBr. For INS, while similar bandwidth ratio dependencies were observed with both NaCl and KBr at pH 6.5, there were large differences in the relative bandwidth ratio at the higher mobile phase

TABLE III

INFLUENCE OF pH ON RETENTION PARAMETERS FOR PROTEINS CHROMATOGRAPHED WITH KBr

– = Not retained.

Protein	pH 9.6		pH 7.5		pH 6.5		pH 5.5	
	Z_c	log K_c	Z_c	log K_c	Z_c	log K_c	Z_c	log K_c
OV	1.6	7.2	2.5	13.1	2.7	14.0	–	–
INS	1.6	6.5	1.2	6.2	1.1	5.8	–	–
CA	–	–	–	–	–	–	–	–
GH	0.7	2.8	–	–	–	–	–	–
MYO	–	–	–	–	–	–	–	–
RIB	0.4	1.7	–	–	–	–	–	–
LYS	1.9	10.1	–	–	–	–	–	–

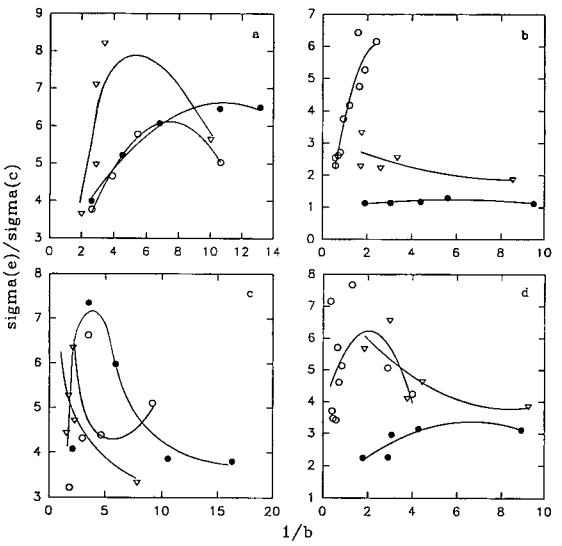

Fig. 3. The influence of mobile phase pH on the dependence of $\sigma_{v,exp}/\sigma_{v,calc}$ *versus* $1/b$ for OV with (a) NaCl and (b) KBr, and INS with (c) NaCl and (d) KBr. ○ = pH 9.6; ● = pH 7.5; ▽ = pH 6.5. See Fig. 1 for other details.

pH values. These results demonstrate that, as the ionisation state of the protein solute is systematically altered through variation of the eluent pH, there is a strong dependence of the kinetic properties of the protein solute on the gradient time and the nature of the displacer salt. Furthermore, the eluent pH can also be anticipated to influence the dynamic structure of the tentacle ligands which will inturn affect the retention and bandwidth behaviour. As a consequence of the nature of the Ce^{4+}-initiated linear graft polymerisation used to prepare the tentacle sorbents, a gradient of tentacles of different monomer lengths may form with porous support materials due to steric restrictions. This effect, coupled with electrostatic repulsion of the positively charged ligands within the pore chambers, could result in the solute experiencing the influence of unmodified sites on the surface of the support matrix. In these circumstances, and particularly with silica based sorbents, the retention and bandwidth behaviour of a protein at different mobile phase pH values would be anticipated not to follow an anion-exchange mode of elution.

CONCLUSIONS

This study has shown that the bandbroadening behaviour of proteins separated on the tentacle-type anion-exchange sorbents is dependent on the nature of the displacer salt, the mobile phase pH and the gradient time. Differences in the bandwidth dependencies for each of the proteins studied also implicate a role for the charge anisotropy of the protein surface structure rather than net charge *per se* in the kinetics of the interactive process. Such effects are consistent with current concepts for the kinetics of molecular docking. Moreover, the experimental data indicate that it cannot be assumed that globular proteins will migrate with these tentacle sorbents as conformationally rigid species with their size and diffusivity predicted solely on the basis of bulk calculations. Rather the results suggest a dynamic interplay between the flexible tentacle ligand and the protein solute under the experimental conditions, a chromatographic behaviour which is somewhat analogous to clathrin-binding phenomena observed with biological membranes [22]. As a result, it can be anticipated that tentacle sorbents of different ligand type should exhibit principally different types of adsorption kinetics depending on the chemical nature of the ligand and the surface properties of the sorbent. This hypothesis is currently being tested with tentacle ligands of different monomer size and chemical composition.

ACKNOWLEDGEMENTS

These investigations were supported by a grant from the Australian Research Council. Assistance with provision of prepacked columns from E. Merck is also acknowledged.

REFERENCES

1 M. T. W. Hearn (Editor), *HPLC of Proteins, Peptides and Polynucleotides —Contemporary Topics and Applications*, VCH, New York, 1991.
2 W. Muller, *J. Chromatogr.*, 510 (1990) 133.
3 R. Janzen, K. K. Unger, W. Muller and M. T. W. Hearn, *J. Chromatogr.*, 522 (1990) 77.
4 M. T. W. Hearn, A. N. Hodder, F. W. Fang and M. I. Aguilar, *J. Chromatogr.*, 458 (1988) 27.
5 A. N. Hodder, M. I. Aguilar and M. T. W. Hearn, *J. Chromatogr.*, 476 (1989) 391.

6 A. N. Hodder, M. I. Aguilar and M. T. W. Hearn, *J. Chromatogr.*, 512.(1990) 41.
7 W. Kopaciewicz, M. R. Rounds, J. Fausnaugh and F. E. Regnier, *J. Chromatogr.*, 266 (1983) 3.
8 L. R. Snyder, in Cs. Horváth (Editor), *High-Performance Liquid Chromatography —Advances and Perspectives*, Vol. 1, Academic Press, New York, 1980, p. 208.
9 M. T. W. Hearn, A. N. Hodder and M. I. Aguilar, *J. Chromatogr.*, 458 (1988) 27.
10 R. W. Stout, S. I. Sivakoff, R. D. Ricker and L. R. Snyder, *J. Chromatogr.*, 353 (1986) 439.
11 M. A. Stadalius, H. S. Gold and L. R. Snyder, *J. Chromatogr.*, 327 (1985) 27.
12 M. A. Stadalius, B. F. D. Ghrist and L. R. Snyder, *J. Chromatogr.*, 387 (1987) 21.
13 M. T. W. Hearn and M. I. Aguilar, *J. Chromatogr.*, 359 (1986) 31.
14 M. T. W. Hearn and M. I. Aguilar, *J. Chromatogr.*, 392 (1987) 33.
15 M. T. W. Hearn and M. I. Aguilar, *J. Chromatogr.*, 397 (1987) 47.
16 S. J. Gregg and K. S. W. Sing, *Adsorption, Surface Area and Porosity*, Academic Press, London, 1982.
17 A. W. Purcell, M. I. Aguilar and M. T. W. Hearn, *J. Chromatogr.*, 593 (1992) 103
18 S. Lin and B. Karger, *J. Chromatogr.*, 499 (1990) 89.
19 A. N. Hodder, M. I. Aguilar and M. T. W. Hearn, *J. Chromatogr.*, 506 (1990) 17.
20 W. Kopaciewicz and F. E. Regnier, *Anal. Biochem.*, 133 (1983) 251.
21 M. T. W. Hearn, A. N. Hodder, P. G. Stanton and M. I. Aguilar, *Chromatographia*, 24 (1987) 769.
22 J. E. Rothman and S. L. Schmid, *Cell*, 46 (1986) 5.
23 M. T. W. Hearn, *Anal. Sci.*, 7 (1991) 1519–1523.

Journal of Chromatography, 599 (1992) 171–177
Elsevier Science Publishers B.V., Amsterdam

CHROMSYMP. 2534

High-performance liquid chromatography of amino acids, peptides and proteins

CXXI.* 8-Hydroxyquinoline–metal chelate chromatographic support: an additional mode of selectivity in immobilized-metal affinity chromatography

M. Zachariou and M. T. W. Hearn*

Department of Biochemistry and Centre for Bioprocess Technology, Monash University, Clayton, Victoria 3168 (Australia)

ABSTRACT

In our associated studies, the binding of proteins in immobilized-metal affinity chromatography has been shown to be independent of surface-exposed histidines and aromatic amino acid residues, when hard metals are used. The present investigation documents the behaviour of iminodiacetic acid (IDA) and 8-hydroxyquinoline (8-HQ) immobilized on Sepharose CL-4B and chelated with detergent (Brij-35), at pH 7.0. The 8-HQ gel had a higher capacity for tuna heart cytochrome *c* (THCC) when Fe^{3+} was immobilized than when Al^{3+} or Yb^{3+} was used, whilst 8-HQ-Cu^{2+} and 8-HQ-Ca^{2+} did not bind this protein. The equivalent IDA chelates showed no binding of the protein. The THCC was recovered from the 8-HQ-Fe^{3+}, -Yb^{3+} and -Al^{3+} supports upon elution with high concentrations of phosphate, glutamate or malonic acids, suggesting that acidic amino acid residues were involved in the binding. Application of molecular graphics procedures reveals that the 8-HQ-metal^{3+} chelate represents a new class of coordination geometry for binding to proteins, and hence offers an additional mode of selectivity in immobilized-metal affinity chromatographic separations.

INTRODUCTION

Immobilized metal affinity chromatography (IMAC) has been a relatively recent addition to the many modes of protein chromatography. Its high degree of specificity, as was first suggested by Everson and Parker for metalloproteins [1] and significantly advanced by Porath *et al.* [2], Sulkowski [3] and other investigators with globular proteins [4–7], has seen this technique become one of the more popular chromatographic modes.

Borderline type metals, as defined by Pearson [8], such as Cu^{2+}, Ni^{2+}, Zn^{2+} and Co^{2+}, have been the most commonly used in IMAC for protein purification. Their preference for nitrogen-containing amino acid side chains has been exploited by many workers [9–11]. The outcome has been the observation that when these metals are used, histidine is the primary putative electron donor, and hence represents an important interactive amino acid, accessible on the surface of proteins. Tryptophan and cysteine play a secondary role in the protein binding, depending on the presence of histidine [12]. Although most amino acids are able to interact individually with immobilized metal chelating systems [11], most do not seem to do so when exposed on the surface of a protein. This degree of specificity for histidine, by borderline metals, has been recently highlighted by the cloning of protein products with polyhistidine tails for later purification using

* For part CXX, see ref. 41.

0021-9673/92/$05.00

IMAC [13], the resolution of similar peptides varying by none, one, two, and three histidines [14], and the use of IMAC as a facile probe for the detection of histidine residues on proteins [15].

Using species variants of cytochrome *c* as model proteins, Hemdan *et al.* [15] were able to differentiate between cytochrome *c* variants containing none, one and two histidine residues on an iminodiacetic acid (IDA)-Cu^{2+} column. These investigators did not observe any binding of tuna heart cytochrome *c* (THCC) when this protein was loaded in phosphate buffer at high ionic strength. The THCC does not have any exposed histidine, tryptophan or cysteine residues.

Hard metals have not been extensively studied in IMAC. Fe^{3+} and Ca^{2+} have received some attention [16–18] whilst the use of hard metals such as the lanthanides and aluminium have rarely been reported [19,20]. It has emerged that hard metal IMAC differs somewhat from conventional IMAC in that a number of different modes of interactions are involved, including composite electrostatic and coordination type bonding. Sulkowski [17] has suggested that electrostatic interactions are more evident for basic proteins in hard metal IMAC. Ramadan and Porath [21] indicated that aspartate and glutamate showed a higher affinity for Fe^{3+} than did other amino acids, including histidine and tryptophan. Cysteine had the highest affinity for Fe^{3+} of all the common protein amino acids. However, Fe^{3+} has also shown a high degree of affinity toward phosphoproteins and glycoproteins [17,22, 23].

In the present investigation, THCC was chosen as a model protein for the study of its interaction with the hard metals, Fe^{3+}, Al^{3+}, Yb^{3+}, Ca^{2+} and Cu^{2+} as a borderline metal ion control. THCC has a large number of surface exposed aspartic and glutamic acid residues [24] and we sought to exploit the preference of hard metals for oxygen rich groups. These metals were immobilized on covalently bound IDA and 8-hydroxyquinoline (8-HQ) chromatographic supports (Fig. 1). The former chelating support has been extensively used in IMAC and behaves as a tridentate chelator [3]. To our knowledge the 8-HQ ligand has only been used once before, with Zn^{2+} as the immobilized metal, for the isolation of metalloproteins [1], although it has been well characterized on silica supports [25,26]

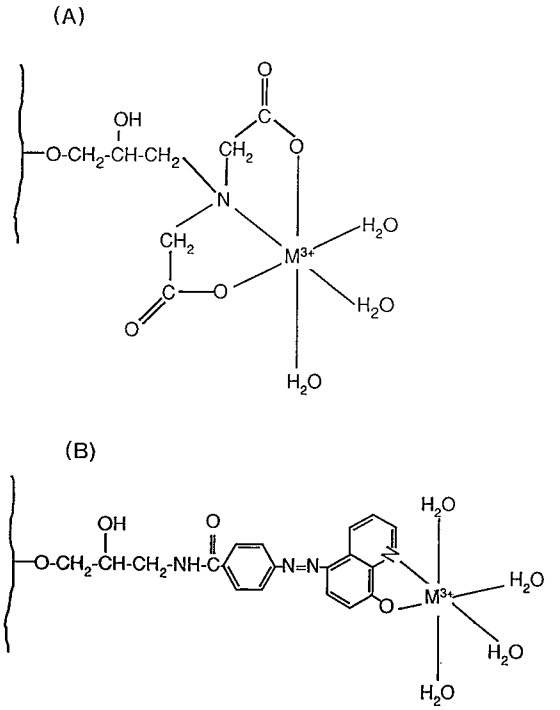

Fig. 1. Diagrammatic representation of the immobilized tridentate chelating agent IDA (A) and the bidentate chelating agent 8-HQ (B) on Sepharose-CL-4B. M = Metal.

and methacrylate supports [27,28], where it has been used extensively for the chromatography of metal ions [29]. Studies on the chromatography of metal ions on immobilized 8-HQ, in a variety of conditions has shown good selectivity for the metals used in the present work [30–32]. The 8-HQ ligand is a bidentate chelating agent but its rigid structure attributes it with higher stability constants for the hard metals compared to IDA [33]. This property is advantageous in protein chromatography since it allows an extra site on the metal, and thus enables an additional mode of selectivity to be achieved. Because of the high value of the stability constants metal leakage is minimized and thus the effective capacity of the immobilized metal complex for the protein is increased.

We report for the first time the use of hard metals immobilized on 8-HQ-Sepharose CL-4B for the isolation of proteins. The use of this adsorbent enables the isolation of THCC using IMAC methods which hitherto have not been applicable to this protein. Furthermore, the results indicate that binding of

THCC and other cytochromes *c* to hard metals, immobilized on 8-HQ-Sepharose CL-4B, is independent of histidine, tryptophan, and cysteine residues in the protein. Application of the 8-HQ ligand thus introduces an additional mode of selectivity in IMAC separations.

EXPERIMENTAL

Materials

Metal salts and 8-HQ were purchased from Aldrich (Milwaukee, WI, USA). THCC type XI, and iminodiacetic acid were purchased from Sigma (St. Louis, MO, USA). Sepharose CL-4B was purchased from Pharmacia (Uppsala, Sweden). All other reagents were of analytical-grade purity and Milli-Q water was used for all preparations. All glassware was extensively washed with dilute nitric acid before use.

Immobilization of chelating agents

The 8-HQ-Sepharose-CL-4B was prepared by modification of the procedure by Hill [34]. In brief, 50 g of Sepharose-CL-4B were epoxy activated using 10 ml of epichlorohydrin in 25 ml of 2 *M* NaOH and 94 mg of $NaBH_4$. The reaction mixture was gently stirred for 15 h at room temperature and then washed under suction with 20 volumes of Milli-Q water. After washing, 1.5 volumes of 25% (v/v) ammonia solution were added to the suctioned dry gel and incubated in a shaking water bath at 40°C, for 1.5 h. The aminated gel was subsequently washed with 10 volumes of Milli-Q water, before passage via acetone, into a neat chloroform solvent using 5 volumes of 20% (v/v) solvent increments. The aminated gel in neat chloroform, was benzoylated with 5 g of *p*-nitrobenzoyl chloride and 5 ml of triethylamine. This mixture was incubated at 50°C for 48 h in a shaking water bath. The gel was extracted out of the chloroform via acetone and into Milli-Q water using 5 volumes of 20% (v/v) solvent decrements. The gel was checked for free amines using the trinitrobenzene sulphonic acid test [34]. If free amines were observed, the incubation was continued. The gel was then placed into a 100 ml solution of 5% (w/v) sodium dithionite, to reduce the $-NO_2$ groups to $-NH_2$, and incubated at 45°C, for approximately 15 h in a shaking water bath. The gel was then washed with 20 volumes of Milli-Q water and incubated at 0–4°C, for 30 min with 100 ml of 2% (w/v) sodium nitrite in 10 m*M* HCl whilst gently stirring. At this stage the gel turned yellow indicating that the diazo bond had formed. The gel was then washed with 10 volumes of cold Milli-Q water and passaged into neat ethanol solution using 5 volumes of 20% (v/v) increments of solvent. The final mixture contained the gel in 100 ml of neat ethanol and 2% (w/v) 8-HQ. The mixture was gently stirred for 3 h at room temperature. After the incubation, the gel had turned a deep, "fire red" colour, indicating that the 8-HQ was immobilized. The gel was then suspended in a final 20% (v/v) ethanol solution where it was stored at 4°C until used for chromatography. Nitrogen analysis done by Dairy Technical Services (Melbourne, Australia), revealed that a substitution of $518 \cdot 10^{-6}$ mol of 8-HQ/g dry gel was obtained.

IDA-Sepharose-CL-4B was prepared without deviation by the method of Porath and Olin [35]. Nitrogen analysis by Dairy Technical Services, revealed $500 \cdot 10^{-6}$ mol of IDA/g dry gel.

Loading of metals

Various studies have shown that metal nitrates or sulphates were preferred over the less dissociating chloride equivalents [36], so as to avoid the immobilization of metal chloride species. The chelate gels, prepared as described above, were incubated at room temperature with either 10 m*M* ferric nitrate or aluminium nitrate, or 50 m*M* calcium nitrate, copper nitrate or ytterbium sulphate, in the presence of 0.1 *M* KNO_3, whilst stirring under reduced pressure (*ca.* 20 mmHg) for 30 minutes to ensure the gel pores were filled with liquid. The lower concentration of metal was used for iron and aluminium to minimize the formation of hydrolytic species which develop more readily with these metals.

The gel was then incubated with 50 m*M* acetic acid and 0.1 *M* KNO_3 pH 4.0 in ratio of 1:10, for 10 min under vacuum to remove any lossely bound ions.

Chromatography

The metal-bound gel was then washed with the equilibration buffer, 20 m*M* imidazole in 0.5 *M* NaCl and 0.005% (v/v) Brij-35 pH 7.0, and incubated in this buffer, under vacuum for 30 min. The

equilibrated gel was then packed into 20-ml Bio-Rad econocolumns.

THCC was resuspended in equilibrating buffer to a concentration of 1 mg/ml. Aliquots of 0.2 ml were loaded on to the metal columns and washed with 5 ml of equilibration buffer. The breakthrough/wash volume was collected and labelled the non-adsorbed fraction. Then 5 ml of elution buffer, either 20 m*M* imidazole and 0.16 *M* K_2HPO_4 and 0.005% (v/v) Brij-35, pH 7.0 (buffer A), 20 m*M* imidazole and 0.16 *M* malonic acid and 0.005% (v/v) Brij-35, pH 7.0 (buffer B), or 20 m*M* imidazole, 0.16 *M* sodium glutamate, 0.34 *M* NaCl and 0.005% Brij-35 pH 7.0 (buffer C), were then loaded onto the columns. This volume was collected and labelled the eluted fraction.

Quantitation of THCC was achieved by analytical high-performance liquid chromatography (HPLC) of the appropriate sample down a J. T. Baker C_{18} or C_8 reversed-phase column (250 × 4.6 mm I.D., 5 μm) using a 1 ml/min flow-rate and a linear gradient of 0.1% (v/v) trifluoroacetic acid to 0.09% (v/v) trifluoroacetic acid and 50% (v/v) acetonitrile over 30 min. The HPLC system used was a Hewlett-Packard HP 1090. The peak area was monitored using a diode array detector set at 215 nm and 400 mm. The sample areas were compared to those of an accurately weighed sample of THCC standard. The lower sensitivity level of this method was 75 ng.

Computer analysis of crystallographic structure

The Insight II programme from Biosym (San Diego, CA, USA) was used on an Iris molecular graphics terminal to determine the space filling model and the ribbon format model of THCC. The programme used crystallographic coordinates from the Brookhaven Data Bank for THCC (1CYT).

RESULTS

Binding behaviour of THCC on immobilized 8-HQ and IDA chelated with metal

Results are shown in Table I for the binding and elution behaviour of THCC on the tridentate IDA support chelated with Cu^{2+}, Ca^{2+}, Yb^{3+}, Fe^{3+} and Al^{3+}. THCC did not bind to any of the immobilized metals with the IDA support with the equilibration conditions used. There was no suggestion of detectable non-specific binding on this support as is indicated by the total recovery of THCC in all the non-adsorbed fractions.

TABLE I

BINDING BEHAVIOUR OF THCC ON IMMOBILIZED 8-HQ AND IDA CHELATED WITH METAL

THCC was resuspended in the equilibration buffer, 20 m*M* imidazole–HCl in 0.5 *M* NaCl and 0.005% (v/v) Brij-35 pH 7 before loading on to the 8-HQ and IDA supports as described under *Chromatography* in the Experimental section. THCC was quantitated as described under *Chromatography* in the Experimental section.

IMAC gels	Protein non-adsorbed (%)	IMAC gels	Protein non-adsorbed (%)
IDA-Cu^{2+}	>99	8-HQ-Cu^{2+}	88
IDA-Ca^{2+}	>99	8-HQ-Ca^{2+}	88
IDA-Yb^{3+}	>99	8-HQ-Yb^{3+}	60
IDA-Fe^{3+}	>99	8-HQ-Fe^{3+}	<1
IDA-Al^{3+}	>99	8-HQ-Al^{3+}	80
IDA-Blank	>99	8-HQ-Blank	85

Results are also shown in Table I for the binding behaviour of THCC on the bidentate 8-HQ support chelated with Cu^{2+}, Ca^{2+}, Yb^{3+}, Fe^{3+} and Al^{3+}. In this case, THCC bound to metal in the following quantitative order; $Fe^{3+} > Yb^{3+} > Al^{3+} > Ca^{2+}$, Cu^{2+}. Interestingly, up to 15% of THCC bound to the naked 8-HQ-Cl-4B support even though Brij-35 was included. More Brij-35 was not added so as to avoid exceeding the critical micelle concentration of this detergent. THCC binding to Cu^{2+} or Ca^{2+} immobilized to 8-HQ affinity gels was about the same as for the blank 8-HQ gel and thus these IMAC sorbents were considered not to have bound THCC specifically.

Elution behaviour of THCC on immobilized 8-HQ chelated with metal

Elution of the THCC from immobilized Fe^{3+}, Yb^{3+} and Al^{3+} was attempted with glutamic acid, malonic acid and phosphate (Table II). Glutamic acid and phosphate eluted approximately the same amount of bound THCC for the three metals tested. Not all the THCC however, could be accounted for in the eluted fractions. For example, only 70% of THCC could be accounted for in the case of Yb^{3+}, allowing for the 15% of THCC bound non-specifi-

TABLE II

ELUTION BEHAVIOUR OF THCC ON IMMOBILIZED 8-HQ CHELATED WITH METAL

Binding conditions for THCC on the 8-HQ metal support was as described for Table I. Elution of THCC was either by 20 m*M* imidazole and 0.16 *M* K_2HPO_4 and 0.005% (v/v) Brij-35 pH 7 (buffer A), 20 m*M* imidazole and 0.16 *M* malonic acid and 0.005% Brij-35 pH 7 (buffer B), or 20 m*M* imidazole, 0.16 *M* sodium glutamate, 0.34 *M* NaCl and 0.005% (v/v) Brij-35 pH 7 (buffer C). THCC was quantitated as described under *Chromatography* in the Experimental section.

IMAC gels	Percentage of bound protein eluted		
	Buffer A	Buffer B	Buffer C
8-HQ-Yb^{3+}	58	35	52
8-HQ-Fe^{3+}	31	9	35
8-HQ-Al^{3+}	13	<1	15

cally. In the case of immobilized Al^{3+}, nearly 70% of bound THCC could not be eluted. Malonic acid appears to be an even less effective eluting agent than does glutamic acid or phosphate. A pattern for recovery of THCC also emerges from these results. Recovery of THCC is greatest for Yb^{3+} followed by Fe^{3+} and then Al^{3+}, independent of elution conditions.

Computer analysis of THCC

Examination of the molecular surface of THCC on the Iris revealed the accessible amino acid residues that could donate electrons and hence afford binding to the immobilized metals. The amino acids were 3 aspartates, 5 glutamates, 2 asparagines, 4 glutamines and 16 lysines. The lysine residues are probably not involved since their ε-amino groups are still fully protonated at pH 7.0 and, with the exception of Cu^{2+}, the other metals being hard Lewis acids, would not have any strong affinity for amino acid side chain groups, especially in the presence of a large molar excess of imidazole. The amino acids that are therefore likely to bind and are accessible to solvents as suggested by the Insight II programme and the available literature [37], are aspartate 50, aspartate 62, aspartate 2, aspartate 93, glutamate 44, glutamate 69, glutamate 66, glutamate 21, and glutamate 90. Fig. 2 shows the ribbon form of THCC, with glutamate 69 and 66, and aspartate 62, in close proximity to each other, and at

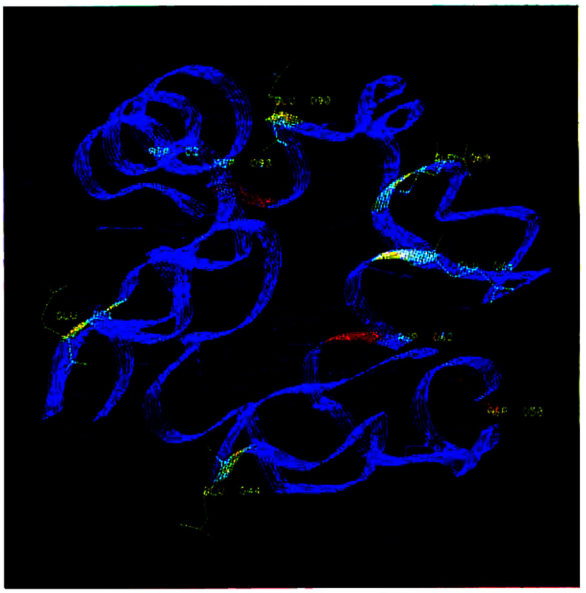

Fig. 2. Ribbon print of THCC depicting the surface accessible glutamate (yellow shade) and aspartate (red shade) residues on the bends of helices reproduced from the Insight II programme.

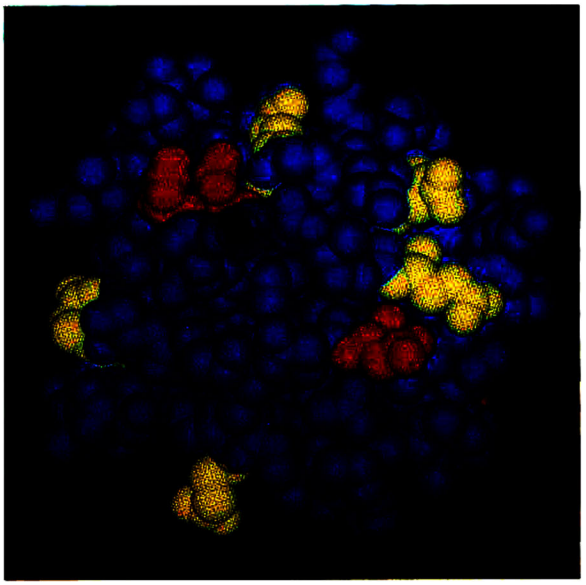

Fig. 3. Space filling model of THCC depicting the surface exposed glutamates (yellow) and aspartates (red) residues grouped into two clusters. THCC in this figure is in the same orientation as that depicted in the ribbon form of Fig. 2.

bends of a helix. Furthermore, aspartate 2 and 93, and glutamate 90 also appear to form a negatively charged cluster. Glutamate 21, and 44 and aspartate 50 all appear solvent accessible but with no vicinal negatively charged groups. The two negatively charged clusters are well separated form each other as is shown in the space filling diagram of Fig. 3.

DISCUSSION

Since the inception of using immobilized metals in IMAC for the isolation of proteins, most of the work has used borderline type Lewis metals, immobilized to the tridentate chelating agent IDA. Other chelating agents that have been immobilized for use in IMAC, include ethylenediaminetetraacetic acid [38], tris(carboxymethyl)ethylenediamine (TED) [35], the carboxymethylated agents [18,13,39] and the monohydroxamate agent [21]. With the exception of the latter ligand structure, all the above chelating agents are tri-, tetra- and pentadentate. As documented here, we have successfully expanded this range by using a bidentate ligand, namely 8-HQ, used for the first time in IMAC of proteins in combination with hard metal ions. In view of the current interest in exploiting the specificity of IMAC as a probe to study the surfaces of proteins, we have also examined the possibility of amino acids in a tertiary protein context, other than histidine, tryptophan and cysteine that may also have an affinity for metals. Using THCC which does not have any of these amino acids on its surface, in association with hard metals immobilized on 8-HQ-Sepharose CL-4B, we have shown that binding of proteins in IMAC, can be independent of histidine, tryptophan and cysteine.

Hemdan *et al.* [15] were unable to isolate THCC on an IDA-Cu^{2+} IMAC column at pH 7.0 using a phosphate buffer, even though THCC has 16 lysines which are solvent accessible. These workers attributed this to a lack of histidines on the surface of the protein. Our results indicate however, that a change from phosphate to an imidazole buffer at pH 7.0 still did not ellicit any binding of THCC to the IDA-Cu^{2+} or 8-HQ-Cu^{2+} sorbents. This observation is consistent with the view that borderline metals, such as Cu^{2+} have a low preference for oxygen-rich groups. Furthermore, it can be concluded that Cu^{2+} has no (or very low) affinity for any other exposed electron-donating groups on THCC eventhough this M^{2+} ion has had an extra coordination site made available by its immobilization on to 8-HQ-Sepharose Cl-4B.

By immobilizing hard metals on 8-HQ-Sepharose CL-4B we were able to retain and subsequently elute THCC. These results can be explained by the extra metal coordination site made available by their immobilization on the bidentate 8-HQ. IDA-Ca^{2+} and 8-HQ-Ca^{2+} did not bind any THCC, eventhough it is considered a hard metal. Further work is currently being done to extend these observations.

Our results suggest that specific THCC binding on 8-HQ immobilized metals is through aspartic and/or glutamic acid residues rather than nitrogen rich groups such as lysines or hydrophobic residues. The behaviour of horse heart and dog heart cytochrome *c* (two variants with surface histidine residues and with similar surface distribution of lysines and hydrophobic amino acid residues) with hard metals immobilized on IDA and 8-HQ in the presence of imidazole buffer further support these findings [40].

The bound THCC could be recovered in varying yield form the metal supports without changing the ionic strength or the pH of the elution buffer from that of the gel equilibration buffer. Of the eluents examined (Table II), malonic acid was the least effective in eluting THCC from the immobilized metals. This observation can be explained by the low affinity of metal ions for malonic acid relative to glutamate and phosphate [33]. The THCC that was not recovered using these elution conditions may represent cytochrome molecules which are bound at higher affinity sites involving clusters of aspartate and glutamate residues as shown in Figs. 2 and 3. In conjunction with this, the heterogenous nature of the spacer arm and ligand may also be contributing to the lack of total THCC recovery. Our proposal that aspartate and glutamate are directly responsible for the binding of THCC to hard metals immobilized on 8-HQ sorbents is the subject of further investigation.

The preliminary results presented in this paper introduce an additional mode of bidentate interaction in IMAC. Furthermore, these data suggest that the use of hard metal ions in IMAC may have important attributes for the study of the surface interactions and properties of proteins.

ACKNOWLEDGEMENTS

These investigations were supported by the Australian Research Council. We are grateful to Dr. Irene Cosic for her help with the Insight II programme. We also thank Dr. Ivan Traverso, Dr. Mibel Aguilar and Jeff Davies for their helpful discussions.

REFERENCES

1 R. J. Everson and H. E. Parker, *Bioinorg. Chem.*, 4 (1974) 15.
2 K. Porath, J. Carlsson, I. Olsson and G. Belfrage, *Nature (London)*, 258 (1975) 598.
3 E. Sulkowski, *Trends Biotechnol.*, 3 (1985) 1.
4 F. H. Arnold, *Bio/Technol.*, 9 (1991) 151.
5 L. Kagedal, in J.-C. Janson and L. Ryden (Editors), *Protein Purification*, VCH, Weinheim, 1989, p. 227.
6 A. J. Fatiadi, *CRC Crit. Rev. Anal. Chem.*, 18 (1987) 1.
7 B. Lonnerdal and C. L. Keen, *J. Appl. Biochem.*, 4 (1982) 203.
8 R. G. Pearson, *Coordin. Chem. Rev.*, 100 (1990) 403.
9 S. A. Margolis, A. J. Fariadi, L. Alexander and J. J. Edwards, *Anal. Biochem.*, 183 (1989) 108.
10 T.-T. Yip, Y. Nakagawa and J. Porath, *Anal. Biochem.*, 183 (1989) 108.
11 E. S. Hemdan and J. Porath, *J. Chromatogr.*, 323 (1985) 255.
12 E. Sulkowski, *BioEssays*, 10 (1989) 169.
13 E. Hochuli, W. Bannwarth, H. Dobeli, R. Gentz and D. Stuber, *Bio/Technol.*, 6 (1988) 1321.
14 T. W. Hutchens and T.-T. Yip, *J. Chromatogr.*, 500 (1990) 531.
15 E. S. Hemdan, Y. Zhao, E. Sulkowski and J. Porath, *Proc. Natl. Acad. Sci. U.S.A.*, 86 (1989) 1811.
16 Z. Kucerova, *J. Chromatogr.*, 489 (1989) 390.
17 E. Sulkowski, *Macromol. Chem. Macromol. Symp.*, 17 (1988) 335.
18 T. Mantovaara, *The Use of Calcium(II) and Cobalt(II) as Adsorbents in Immobilized Metal Affinity Chromatography; Ph.D. Thesis*, University of Uppsala, Uppsala, 1990.
19 M. A. Vijayalakshmi, *Affinity Chromatography and Biological Recognition*, Academic Press, New York, 1983, p.269.
20 J. Porath, B. Olin and N. Granstrand, *Arch. Biochem. Biophys.*, 225 (1983) 543.
21 N. Ramadan and J. Porath, *J. Chromatogr.*, 321 (1985) 93.
22 L. Andersson and J. Porath, *Anal. Biochem.*, 154 (1986) 250.
23 B. H. Chung and F. H. Arnold, *Biotechnol Let.*, 13 (1991) 615.
24 T. Takano, O. B. Kallai, R. Swanson and R. E. Dickerson, *J. Biol. Chem.*, 248 (1973) 5234.
25 C. Fulcher, M. A. Crowell, R. Bayliss, K. B. Holland and J. R. Jezorek, *Anal. Chim. Acta*, 129 (1981) 29.
26 J. R. Jezorek, C. Fulcher, M. A. Crowell, R. Bayliss, B. Greenwood and J. Lyon, *Anal. Chim. Acta*, 131 (1981) 223.
27 K. Janak and J. Janak, *Collect. Czech. Chem. Commun.*, 48 (1981) 2352.
28 Z. Slovac and J. Toman, *Z. Anal. Chem.*, 278 (1976) 115.
29 O. Abollino, E. Mentasti, V. Porta and C. Sarzanini, *Ann. Chim.*, 80 (1990) 1.
30 K. Isshiki, F. Tsuji, T. Kuwamoto and E. Nakayama, *Anal. Chem.*, 59 (1987) 2491.
31 J. R. Jezorek and H. Freiser, *Anal. Chem.*, 51 (1979) 366.
32 G. J. Shahwan and J. R. Jezorek, *J. Chromatogr.*, 256 (1983) 39.
33 L. G. Sillen and A. E. Martell, *Stability Constants, Supplement No. 1 (Special Publication* No. 25), Chemical Society, London, 1971.
34 J. M. Hill, *J. Chromatogr.*, 76 (1973) 455.
35 J. Porath and B. Olin, *Biochemistry*, 22 (1983) 1621.
36 G. H. Khoe, P. L. Brown, R. N. Sylva and R. G. Robins, *J. Chem. Soc. Dalt. Trans*, (1986) 1901.
37 W. Kabasch and C. Saunders, *Biopolymers*, 22 (1983) 2577.
38 Y. Moroux, E. Boschetti, R. Barot-Ciobaru, J. L. Plasat and J. M. Egly, *Affinity Chromatography and Biological Recognition*, Academic Press, New York, 1983, p. 275.
39 E. Sulkowski and J. Porath, *9th International Symposium on Affinity Chromatography and Biological Recognition, Yokohama, September 1991*, Abstracts, p. 54.
40 M. Zachariou and M. T. W. Hearn, in preparation.
41 F. W. Fang, M. I. Aguilar and M. T. Hearn, *J. Chromatogr.*, 599 (1992) 163.

Journal of Chromatography, 599 (1992) 179–184
Elsevier Science Publishers B.V., Amsterdam

CHROMSYMP. 2515

Peptide maps of five human pepsin isoenzymes and other aspartic proteinases

A. T. Jones* and N. B. Roberts

Department of Clinical Chemistry, Royal Liverpool University Hospital, Duncan Building, Prescot Street, Liverpool L7 8XW (UK)

ABSTRACT

Peptide maps of five individual human pepsins were developed using reversed-phase high-performance liquid chromatography after protein digestion with either *Staphylococcus aureus* proteinase (V8) or α-chymotrypsin. Human pepsins 3a, 3b and 3c produced almost identical peptide maps suggestive of proteins with very similar amino acid sequences. The map for human pepsin 1 was similar to pepsin 3b (the most predominant human pepsin) but less than half the expected amount of each equivalent peptide fragment was generated, indicating that the actual mass of digested protein used was less than the dry weight measurement would suggest, probably as a result of carbohydrate attached to pepsin 1. Comparison of human pepsin 3b maps with other aspartic proteinases confirmed a significant homology with swine pepsine A but not with endothiapepsin. The α-chymotrypsin digests compared with V8 gave more complex peptide maps as a result of its broader bond cleavage specificities.

INTRODUCTION

The separation and purification of five proteolytically active human pepsins (1, 3a, 3b, 3c and 5, where 5 is equivalent to gastricsin, using the pepsin classification based on mobility on agar gel electrophoresis [1]) has been reported previously [2]. Keen *et al.* [3] subsequently sequenced up to 37 N-terminal amino acids for five human pepsins and indicated no differences between pepsin 1, 3a, 3b and 3c. Pepsin 5 was clearly different and was identified as gastricsin. Athauda *et al.* [4] confirmed these findings by analysis of the N-terminal sequences of human pepsinogens. However, little information is available on the complete primary sequence of these individual human pepsins from protein analysis, and particularly pepsin 1, the ulcer-associated pepsin [5].

Human pepsin gene studies have been able to identify three pepsin (3) genes which were found to differ in up to only four amino acids, and one gastricsin gene [6–7], but there is no information from human pepsin gene studies on the amino acid sequence of pepsin 1.

Enzymic cleavage and reversed-phase high-performance liquid chromatography (HPLC) peptide mapping are well established techniques for preliminary studies of protein structures. The predicted amino acid sequence of three human pepsins from gene analysis [6] shows only three arginine residues located predominantly at the C-terminus and no lysine residues. The use of trypsin for pepsin digestion was therefore unsuitable. Glutamic acid residues, however, are distributed throughout the pepsin sequence (fourteen in pepsin 3) and cleavage at these residues would theoretically produce up to fifteen fragments. The proteinase V8 from *Staphylococcus aureus* can be specifically used for cleavage at glutamic acid residues [8]. We have therefore investigated the development of peptide map profiles using reversed-phase HPLC after V8 cleavage of the individual pepsins to highlight possible differences in their protein structures. Of particular interest was the degree of peptide map analogy between human pepsin 1 and the major isoenzyme 3b. Other aspartic proteinases with established amino acid sequences were investigated to identify any similar peptide fragments and thus sequence similarities with the human pepsins. Peptide maps developed after digestion with α-chymotrypsin (having a

0021-9673/92/$05.00

broader bond cleavage specificity) were also studied as a further comparison.

EXPERIMENTAL

Chemicals

Urea (molecular biology reagent), dithiothreitol (DTT), iodoacetamide (IAA), swine pepsin A, bovine pancreas α-chymotrypsin and *Staphylococcus aureus* V8 proteinase (V8) were obtained from Sigma (Poole, UK). Ammonium hydrogencarbonate and ammonium acetate (AnalaR grade) were obtained from British Drug Houses (Poole, UK), trifluoroacetic acid from Pierce and Warriner (Chester, UK) and acetonitrile (HPLC grade S) from Rathburn Chemicals (Walkerburn, UK). Human pepsins were prepared according to the method of Peek and Roberts [2], then dialysed against 1 mmol/l hydrochloric acid and dried by freeze-drying. Endothiapepsin from the fungus *Endothia parasiticia* was obtained from Dr. J. Cooper, Department of Crystallography, Birkbeck College, University of London.

Staphylococcus aureus proteinase (V8) digests

Aspartic proteinases were digested with V8 using modifications of the established methods of Drapeau [9] and Stone *et al.* [10]. An aliquot, 500 μg, of dry enzyme was dissolved in 500 μl of 0.1 mol/l ammonium acetate containing 8 mol/l urea, 50 μl of 45 mmol/l DTT were added and the mixture was incubated at 50°C for 15 min. After cooling to room temperature, 50 μl of 100 mmol/l IAA were added and the solution was incubated at 20–25°C for 10 min. Water (1.4 ml) was added, followed by 16.5 μl of 1 mg/ml V8 (1:33 enzyme: substrate ratio). The digest (final pH 6.21) was incubated at 37°C for 8 h. All reactions were stopped by either freezing to −20°C or immediate chromatography. The following enzymes were digested with V8: swine pepsin A, endothiapepsin, human pepsins 1, 3a, 3b, 3c and human gastricsin.

α-Chymotrypsin digests

Chymotrypsin digests of the same proteins were performed according to the method of Stone *et al.* [10]. The method was similar to that described for V8 digests except that ammonium acetate was replaced with 0.4 mol/l ammonium hydrogencarbonate and the digests (final pH 8.34) were terminated after 24 h.

Reversed-phase HPLC

Peptides, after V8 and chymotrypsin digestion, were separated on an Exsil 300Å C_{18} (5 μm) reversed-phase column (15 × 0.46 cm I.D.) (Jones Chromatography, Hengoed, UK). Peptides were detected at 220 nm (SM 3000 UV detector; LDC, Stone, UK). Binary linear gradients were developed on a low-pressure tertiary mixing pump (Model CM 4000; LDC). Chromatograms were recorded on a CI 4000 computing integrator (LDC).

RESULTS

V8 digests

The V8 maps for the human pepsins 1, 3c, 3b, 3a and gastricsin are shown in Fig. 1a–g and the elution times of the major peptide fragments are summarized in Table I. The peptide profiles for pepsins

TABLE I

COMPARISON OF PEPTIDE RETENTION TIMES IN REVERSED-PHASE HPLC AFTER V8 DIGESTS OF FIVE INDIVIDUAL HUMAN PEPSINS AND SWINE PEPSIN A

Human pepsins 3c, 3b, 3a, 1, gastricsin (GTN) and swine pepsin A (SPA) were the individual enzymes used. Dashes indicate the absence of a peak.

Retention time (min)					
3c	3b	3a	1	GTN	SPA
–	–	–	–	–	22.1
–	–	–	–	24.4	–
–	–	–	–	24.8	–
–	–	26-7	–	–	–
28.3	28.6	–	28.9	–	–
–	–	30.7	–	–	–
33.0	33.2	33.5	33.2	–	–
34.0	34.4	34.3	34.2	34.8	–
35.0	35.4	35.3	35.5	36.1	–
36.7	37.1	37.0	37.0	36.9	37.0
39.3	40.0	40.0	39.6	39.8	39.6
–	41.2	–	41.8	–	41.8
–	–	–	–	–	43.6
57.3	58.3	58.5	57.0	57.1	58.6
59.4	59.1	59.6	58.1	59.1	60.3
62.1	61.8	62.2	62.0	–	62.3
–	–	–	–	74.0	–

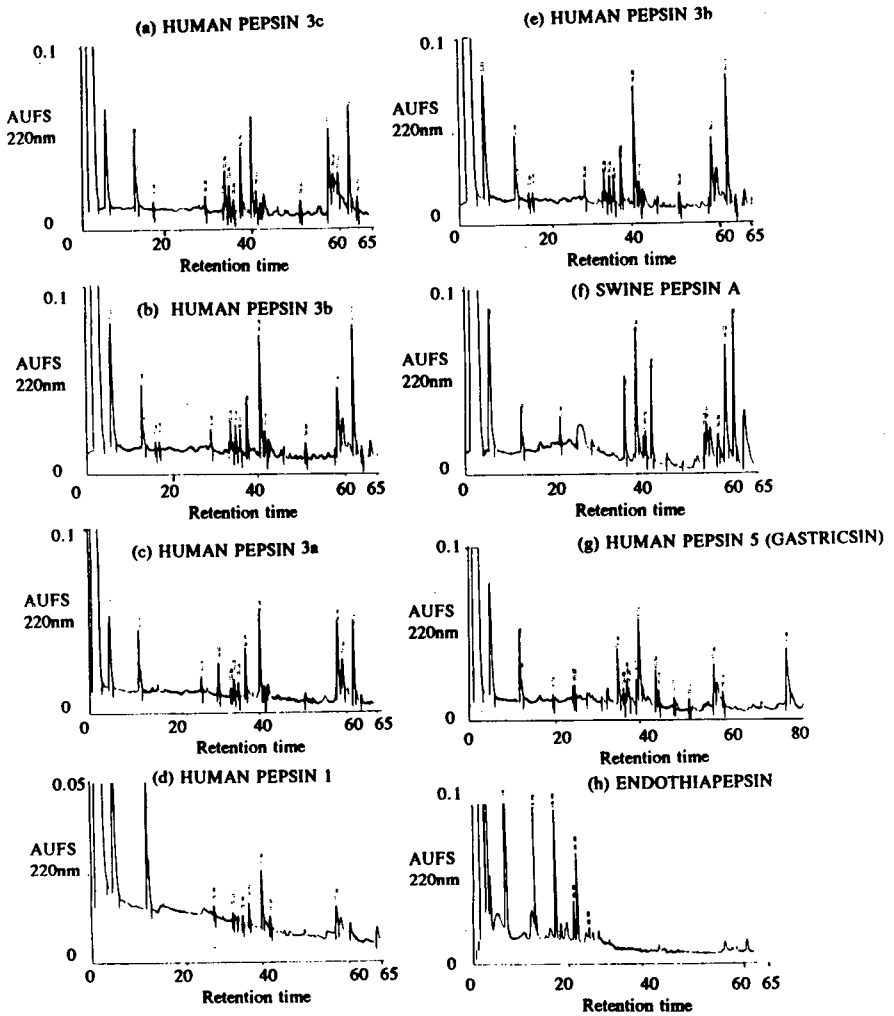

Fig. 1. Peptide maps after V8 digestion of five human pepsins, swine pepsin A and endothiapepsin, separated by reversed-phase HPLC. Injection volume, 350-μl (corresponding to 87 μg of digested protein); flow-rate, 1.5 ml/min; operating back-pressure, 1400–2000 psi (9653–13 870 kPa). Solvent A = trifluoroacetic acid–water (0.1:99.9, v/v); solvent B = solvent A–acetonitrile (40:60, v/v). Linear gradient: 100% A for 5 min, 0–30% B over 20 min and 30–80% B generated over 50 min. AUFS = Absorbance units full-scale; retention times in minutes.

3a, 3b and 3c were very similar although 3a produced specific peptides eluting at 26.7 and 30.7 min and none at 28 min. The pepsin 1 map (Fig. 1d) was also very similar to that of human pepsin 3b although the relative amount of the peptide eluting at 62 min was markedly reduced, as was the overall amount of eluting material (the AUFS scale was set at 0.05 for pepsin 1 compared with 0.1 for the other pepsins).

The human gastricsin and swine pepsin A maps showed a number of peptide similarities compared with the other human pepsin maps. The peptide map for endothiapepsin (Fig. 1h), however, was different, with all the major peptide eluting before 22 min.

Chymotrypsin digests

Chymotryptic maps (Fig. 2a–d) confirmed the marked similarities between human pepsins 1, 3c, 3b and 3a. For pepsin 1, however, the fragment at

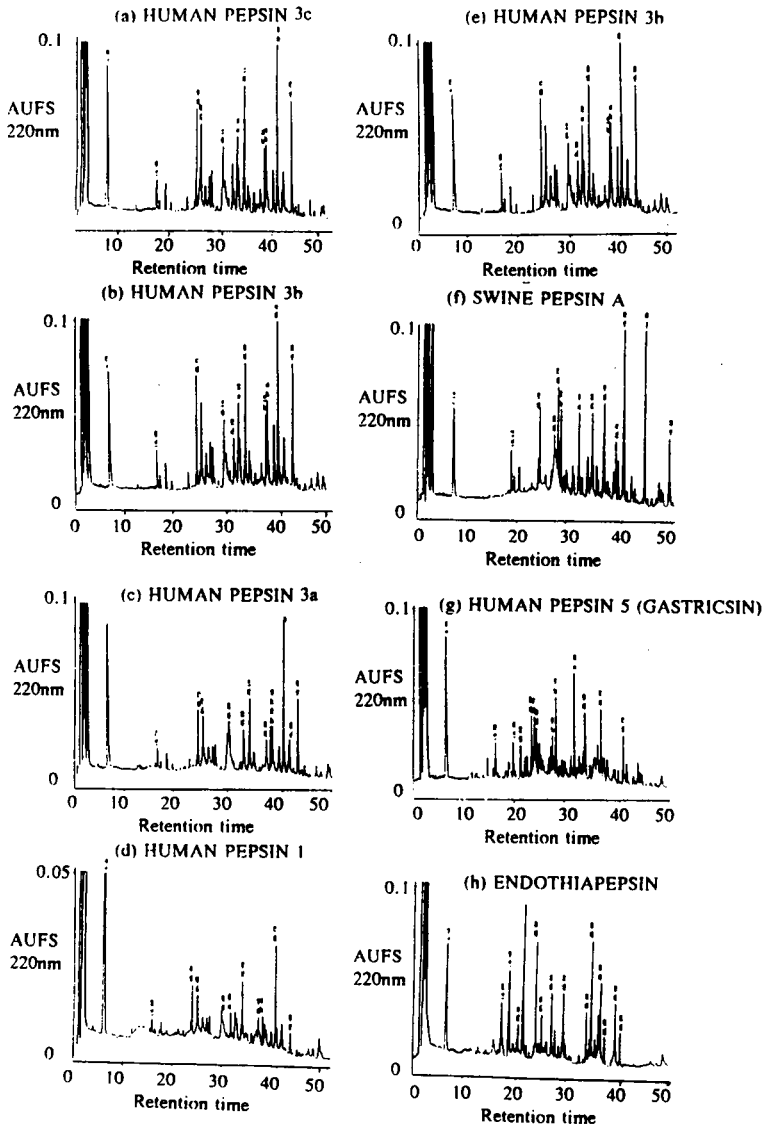

Fig. 2. Peptide maps after chymotrypsin digestion of five human pepsins, swine pepsin A and endothiapepsin, separated by reversed-phase HPLC. Injection volume, 250 μl (corresponding to 63 μg of digested protein); flow-rate, 1.5 ml/min; operating back-pressure, 1400–2000 psi (9653–13 780 kPa). Solvents A and B as in Fig. 1. Linear gradient: 100% A for 5 min, 0–75% B generated over 45 min. AUFS = Absorbance units full-scale; retention times in minutes.

42.6 min was significantly reduced compared with 3b, as was the overall amount of peptides. The human gastricsin map (Fig. 2g) gave a different profile in comparison with the other human pepsins.

Swine pepsin A (Fig. 2f) showed a similar overall profile to human pepsin 3b but with distinct fragments eluting at 26–28, 34, 44 and 49 min. The map for endothiapepsin had a significant proportion of early-eluting peptides, although some peptides eluted at similar times to the other pepsins, *viz.*, 23–25, 33 and 40 min.

The early-eluted peaks (Figs. 1 and 2) were associated with buffer, urea and IAA (0–4 min) and DTT (6–7 min). Protein blank experiments showed

a V8-related self-cleavage fragment eluting between 11 and 14 min (Fig. 1), but no other peaks were produced.

DISCUSSION

We have developed enzyme digest procedures using V8 and chymotrypsin, and reversed-phase HPLC peptide maps to investigate the similarities in amino acid structures between five human pepsins and other aspartic proteinases, namely swine pepsin A and endothiapepsin.

A relatively low proteolytic activity of V8 was observed when digests were performed in 0.1 *M* ammonium hydrogencarbonate (pH 8.1), a commonly used buffer [11], but was much improved when replaced with 0.1 *M* ammonium acetate (pH 6.2). A buffer-related susceptibility to bond cleavage has been described previously for this enzyme [12]. The HPLC gradient was extended for the V8 maps to improve the separation for subsequent peptide collection, human pepsin amino acid sequence analysis and confirmation of the site(s) of bond cleavage by V8. The maps after chymotrypsin digestion were more complex, as expected, as this enzyme is able to hydrolyse several types of peptide bonds, thus generating many more peptides *i.e.*, about 30 fragments. Hitherto very few if any detailed studies have been made on human pepsins using these procedures, but differences in the N-terminal sequences of two human pepsinogens PGA-3 and PGA-5 were identified using peptide mapping after cleavage with endoproteinase Lys-C [13].

The marked similarities in the V8 and chymotrypsin maps of human pepsins 1, 3a, 3b and 3c in this study suggest a high degree of amino acid homology in these proteins. The human pepsin 3c and 3b maps are in fact almost indistinguishable, which suggests that they correspond to PGA-3 and PGA-5, respectively, which from gene structural analysis [6] were found to differ in only one substitution (valine–leucine) at residue 77 on pepsinogen or residue 29 on pepsin. Pepsin 3a, which showed some differences from the 3b map, could then correspond to PGA-4, which Evers *et al.* [6] found differed by three amino acid residues.

The V8 map for pepsin 1 was very similar to that for pepsins 3b and 3c in terms of the number and retention times of peptides separated in reversed-phase HPLC (Table I), which suggests that pepsin 1 has a similar primary structure to pepsins 3b and 3c. However, less than half the amount of each equivalent peptide (in terms of comparative peak areas) was formed, implying that the actual weight of pepsin 1 used was less than the dry weight would suggest, probably as a result of carbohydrate attached to pepsin 1 [14]. Peptide sequence studies should clarify whether human pepsins 3b and 1 have the same primary structure and therefore that some post-translational modification (*i.e.*, incorporation of carbohydrate) has occurred in pepsin 1, thus modifying its enzymic properties [15].

The peptide maps also confirm the high degree of amino homology (89%) [16] between swine pepsin A and human pepsins, and lower homology (52%) between human gastricsin and human pepsins [7]. The endothiapepsin maps do not share any peptide similarities to the pepsin maps, which confirms little sequence homology [17].

ACKNOWLEDGEMENTS

The authors would like to acknowledge the financial support of the Science and Engineering Research Council UK to A.T.J., Professor T. L. Blundell of Birkbeck College, University of London, for making that possible and Professor A. Shenkin, in whose department the work was carried out.

REFERENCES

1 D. J. Etherington and W. H. Taylor, *Nature (London)*, 216 (1967) 279.
2 K. Peek and N. B. Roberts, *J. Chromatogr.*, 476 (1989) 291.
3 J. N. Keen, J. B. C. Findlay, K. Peek, N. B. Roberts and W. H. Taylor, *Clin. Sci.*, 77, Suppl. 22 (1989) 94.
4 S. B. P. Athauda, M. Tanji, T. Kageyama and K. Takahashi, *J. Biochem.*, 106 (1989) 920.
5 W. H. Taylor, *Nature (London)*, 227 (1970) 76.
6 M. P. J. Evers, B. Zelle, J. P. Bebelman, *Genomics*, 4 (1989) 232.
7 G. Pals, T. Azuma, T. K. Mohandas, G. I. Bell, J. Bacon, I. M. Samloff, D. A. Walz, P. J. Barr and T. Taggarrt, *Genomics*, 4 (1989) 137.
8 J. Houmard and G. R. Drapeau, *Proc. Natl. Acad. Sci. U.S.A.*, 69 (1972) 3506.
9 G. R. Drapeau, *Methods Enzymol.*, 47 (1977) 189.
10 K. L. Stone, M. B. LoPresti, J. M. Crawford, R. DeAngelis and K. Williams, in P. T. Matsudaira (Editor) *A Practical Guide to Protein and Peptide Purification for Microsequencing*, Academic Press, New York, 1987, pp. 31–47.

11 A. Aitken, M. J. Geisow, J. B. C. Findlay, C. Holmes and A. Yarwood, in J. B. C. Findlay and M. J. Geisow (Editors), *Protein Sequencing, a Practical Approach*, IRL Press, Oxford, 1989, pp. 43–68.
12 G. R. Drapeau, Y. Boily and J. Houmard, *J. Biol. Chem.*, 247 (1972) 6720.
13 R. A. Bank, B. C. Crusius, T. Zwiers, S. G. M. Meuwissen, F. Arwert and J. C. Pronk, *FEBS Lett.*, 238 (1988) 105.
14 J. P. Pearson, A. Allen, N. B. Roberts and W. H. Taylor, *Clin. Sci.*, 72, Suppl. 16 (1987) 33.
15 J. P. Pearson, R. Ward, A. Allen, N. B. Roberts and W. H. Taylor, *Gut*, 27 (1986) 243.
16 B. Foltmann, *Essays Biochem.*, 53 (1981) 52.
17 T. L. Blundell, A. Jenkins, B. T. Sewell, L. H. Pearl, J. B. Cooper, I. J. Tickle, B. Veerapandian and S. P. Wood, *J. Mol. Biol.*, 211 (1990) 919.

Journal of Chromatography, 599 (1992) 185–194
Elsevier Science Publishers B.V., Amsterdam

CHROMSYMP. 2516

High-performance hydrophobic interaction chromatography as a tool for protein refolding

Xindu Geng* and Xiaoqing Chang

Laboratory of Modern Separation Science, Department of Chemistry, Northwest University, Xi'an 710069 (China)

ABSTRACT

A method for the refolding of previously unfolded proteins with a concentrated solution of denaturing agent is presented, involving the use of high-performance hydrophobic interaction chromatography (HPHIC) to separate the denaturing agent completely from the unfolded protein and to provide a suitable environment for its refolding. The retention, peak shape and peak height in HPHIC and size-exclusion chromatography, UV spectra, circular dichroic spectra and bioactivity were used to test the possibility and the completeness of the protein refolding. The proposed method permits the extracted solution from *Escherichia coli* cells to be injected directly into the HPHIC column and, at the same time, the refolding and purification of the proteins to be effected. The renaturation and purification of recombinant human interferon – γ from *E. coli* cells is one example of the application of the method in biotechnology.

INTRODUCTION

About 20 years ago, Anfinsen [1] reported the significant discovery of the spontaneous refolding of ribonuclease as it moves into aqueous solution from 8.0 mol/l urea solution containing β-mercaptoethanol in which ribonuclease had been reduced and denatured to its unfolded state. Since then many workers have studied protein refolding in two steps: first to make the protein unfold and then to make it refold [2]. Therefore, means of making the protein refolding and obtaining information about its refolding and renaturation are of significant interest [3].

Many kinds of therapeutic proteins can be produced from recombinant DNA technology either in the plant or in the laboratory. A new and convenient technique for extraction these therapeutic products from the bacterium *Escherichia coli* is to use a denaturing agent in a suitable concentration [4]. In some instances 7.0 mol/l guanidine hydrochloride (GuaHCl) or 8.0 mol/l urea solution is needed to extract very strong hydrophobic proteins in the unfolded state. Therefore, to achieve protein refolding completely from a concentrated solution of denaturing agent is vital not only for theoretical studies in molecular biology, but also for lowering the cost of these therapeutic proteins in industry. However, the refolding is usually not complete and this seriously influences the output and benefit of therapeutic proteins in industry.

According to Anfinsen [1], the three-dimensional structure of a protein molecule is based on its primary structure, *i.e.*, the sequence of amino acid residues. If the denaturing agent is removed from its mother solution containing the denatured protein, the hydrophobic environment of water or a dilute aqueous solution of salt of suitable viscosity, ionic strength, etc., will make the denatured protein refold spontaneously to its thermodynamically stable state so as to be identical with its native form, even if this refolding process takes place very slowly. High-performance hydrophobic interaction chromatography (HPHIC) is a powerful tool for the separation and purification of biopolymers [5] and may satisfy these conditions during gradient elution with a mobile phase consisting of both a concentrated salt solution and water. In previous work [6] we used HPHIC for the renaturation and separation of recombinant human interferon-γ (rIFN-γ)

0021-9673/92/$05.00

and obtained good results in terms of the completeness of its refolding and purification, with the simple operation.

In this work, we investigated the refolding of protein only unfolded with a denaturing agent and studied the possibility of protein refolding using HPHIC; the mechanism was not considered. Measurements of both the conformational changes of protein molecules, including UV spectrophotometry, circulair dichroism (CD) and size-exclusion chromatography (SEC), and its bioactivity were used to test the possibility and the completeness of the refolding of a denatured protein. An example of the renaturation and purification of a therapeutic protein *E. coli* cell in biotechnology is presented.

EXPERIMENTAL

Equipment

An LC-9A liquid chromatograph (Shimadzu, Kyoto, Japan) was used, consiting of two pumps (LC-6A), a variable-wavelength UV–visible detector (SPD-6AV), a column oven (CTO-4A) and a recorder (R-112). Stainless-steel columns (100–150 × 4.0 mm I.D. and 250 × 7.9 mm I.D.) were used. The size-exclusion column (diol 150) was bought from Shimadzu. The HPHIC packings (XDF-GM, silica linked to ligands consiting of a polyethylene glycol chain and with a hydrophobic end-group) used were made and packed in our laboratory. Equipment for optical measurement consisted of a Jasco J-20c automatic recording spectropolarimeter (Japan Spectroscopic), a UV–VIS spectrophotometer (Perkin-Elmer) and a dual- wavelength thin-layer chromatographic scanner (CS-930, Shimadzu). Equipment for studying the cytopathic effect (CPE) inhibition for rIFN-γ included a carbondioxide incubator (Sheldon Manufacturing), an inverted microscope (Chongqing Optical Instrument Factory) and a super clean bench.

Chemicals

Egg white lysozyme (LYS), ribonuclease (RNase) and bovine serum albumin (BSA) were purchased from the Institute of Biochemicals (Shanghai, China) and α-amylase (α-AMY, *Bacillus anthracis*, type II A) from Sigma (St. Louis, MO, USA). Other chemicals were of analytical-reagent grade. Water was re-distilled (quartz).

Mobile phase

HPHIC eluent consisted of solution A, 3.0 mol/l ammonium sulphate–0.020 mol/l potassium dihydrogenphosphate (pH 7.0), and solution B, 0.020 mol/l potassium dihydrogenphosphate (pH 7.0). The SEC eluent was 0.020 mol/l Tris–0.10 mol/l sodium chloride (pH 8.0).

The reagents used for the CPE inhibition assay of rIFN-γ were of analytical-reagent grade. The cells and virus used for the CPE inhibition assay of rIFN-γ were WISH cell and VSV virus. The medium used for assay was Eagle's–BSA (90:10) containing 250 U/ml of penicillin and 250 U/ml of streptomycin (pH 7.2–7.4, adjusted with sodium hydrogencarbonate).

Protein refolding with HPHIC

A denatured protein solution in 7.0 mol/l GuaHCl or 8.0 mol/l urea was injected directly into the HPHIC column (150 × 4.0 mm I.D.), which had already been equilibrated with eluent A. A 20-min linear gradient with a flow-rate of 1.0 ml/min from 100% eluent A to 100% eluent B and followed by a 10-min delay was applied. The collected fractions were then tested for the completeness of refolding of protein.

CPE inhibition assay of rIFN-γ [7]

The procedure is as follows.

(1) Seed cells: add 100 μl of medium containing suspended cells (600 000 cells/ml) to each well in a 96-well culture plate. Incubate the cells at 37°C for 24 h to obtain a monolayer.

(2) Incubate the cells with dilutions of rIFN-γ. Remove the growth medium and add rIFN-γ dilution (in the medium) to monolayers at 100 μl per well. Incubate the cells at 37°C for 24 h.

(3) Infect the cells with virus. Remove the rIFN-γ dilutions, then add VSV virus (100–400$TCID_{50}$, one $TCID_{50}$ equals 50% of tissue culture infective dose) at 100 μl per well. The viruses are diluted in medium. Incubate at 37°C for 24 h.

(4) Measure the viral effect. When CPE appears more than 75% destroyed in IFN-free wells, score an estimate of CPE by microscopic observation of each infected culture.

(5) Calculate the rIFN-γ titres by the Reed–Muehch method.

RESULTS AND DISCUSSION

Although it was about 60 years ago when Wu and Yang [8], Anson and Mirsky [9] and Northrop [10] defined the "native structure" for a protein not only by the activity, but also by some physical characteristics and chemical properties, this may still be valid today. The bioactivity of a protein and its molecular conformational changes are simply connected with each other. Four proteins, RNase, LYS, α-AMY and BSA, were selected as the representatives of three types of proteins. The first two have a low molecular mass (less than 20 000), the third has an irreversible process for thermal denaturation and the fourth one has a higher molecular mass (67 000). The renaturation and purification of rIFN-γ from *E. coli* cells was selected as a representative application in biotechnology. The results were very successful.

Retention and refolding with HPHIC

According to the stoichiometric displacement model for retention (SDM-R) of solute [11], Kunitani *et al.* [12] reported that the changes in the molecular conformation of protein in reversed-phase liquid chromatography (RPLC) necessarily cause changes in the contact surface area between the stationary phase and protein molecules, and so do both its Z value (the number of displacing agent molecules required to displace a protein from ligand) and retention. Karger and co-workers also confirmed this point in both RPLC [13] and HPHIC [14,15]. We also tested their conclusion again using both HIC and RPLC [16]. Benedek *et al.* [13] also reported that the changes in the peak height of native and unfolded protein indicate the changes in its molecular conformation in RPLC if the unfolded protein has only one kind of conformation. Hence the changes in either the retention or the peak height of a protein may be considered as important parameters for the characterization of conformational changes of protein molecules.

Fig. 1 shows four chromatograms of BSA and LYS in their native forms and refolded from their unfolded state. Fig. 1a and c represent the refolded and the native BSA, respectively, and Fig.b and d represent the refolded and the native LYS, respectively. The chromatographic profiles of the two native proteins and the corresponding profiles of the refolded proteins are the same in terms of retention, peak shape and peak height. This is very unusual, because LYS is a relatively small enzyme and has a molecular mass of 14 600, but BSA is a three times larger protein than LYS. From the traditional point of view, the BSA refolding should be much more difficult than the LYS refolding. The results in Fig. 1 show that HPHIC may have a special function for protein refolding.

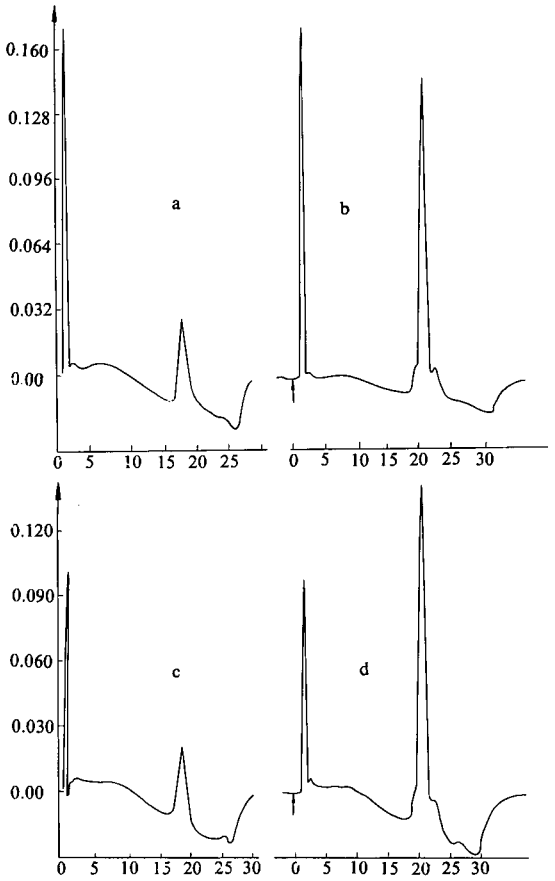

Fig. 1. Comparison of results of HPHIC between native and refolding proteins. Linear gradient elution from 100% solution A [3.0 mol/l ammonium sulphate–0.020 mol/l potassium dihydrogenphosphate (pH 7.0)] to 100% solution B [0.020 mol/l potassium dihydrogenphosphate (pH 7.0) at a flow-rate of 1.0 ml/min for 20 min with a delay for 10 min. Chart paper speed, 2.5 mm/min; detection wavelength, 280 nm, 0.64 a.u.f.s. Peks: a and c = native and refolded BSA, respectively; b and d = native and refolded LYS, respectively. y-axis: Absorbance at 280 nm; x-axis: time in min.

If the three parameters for a chromatogram can

be used to characterize the native, unfolded or refolded state of a protein, we may conclude that the two kinds of proteins unfolded with 7.0 mol/l GuaHCl can really be refolded using HPHIC. The reasons why this occurs need to be considered.

Factors affecting protein refolding with HPHIC

It is very difficult to answer the above question exactly, but it would be useful to consider a few possible answers. We first used SEC to examine the possibility and the completeness of the refolding of an unfolded protein in the same way as that with HPHIC, in order to find out the reason why HPHIC does it so well. Because an ideal SEC column should never display any interactions between the stationary phase and a protein molecule, even if the protein molecule has polar groups and electrostatic charge, the retention of a protein on an SEC column depends only on the size and shape of the protein molecules [17]. For the same protein, changes in its retention would indicate conformational changes if the same column and the same mobile phase are used. GuaHCl or urea should be removed during the SEC process and therefore, if the protein refolds in this instance, it is due only to the removal of the denaturing agent. Hence SEC should be a means of investigating the reasons for the change in molecular conformation of proteins.

Fig. 2 shows the comparative size-exclusion chromatograms of the three types of protein, LYS, RNase and BSA, where the sample solutions were injected in both (a) the native and (b) unfolded forms. Peaks 1, 2 and 3 represent BSA, RNase and LYS, respectively. BSA, RNase and LYS have different chromatographic profiles, retentions, peak heights and peak shapes in the two instances. The difference between the two retention times for LYS in Fig. 2a and b is more than 2 min. Based on the facts that the retentions of BSA and RNase in Fig. 2a and b are the same, but their peak shapes are different, we cannot conclude that refolding of either BSA or RNase with SEC would be possible or complete. Comparing Figs. 1 and 2, we know that the protein refolding cannot be accomplished only by removing the denaturing agent by SEC, or at least not in a short time. Although the compositions of the mobile phases for HPHIC and SEC are different, the latter may be more in favour of protein refolding. Hence we may conclude that the reason

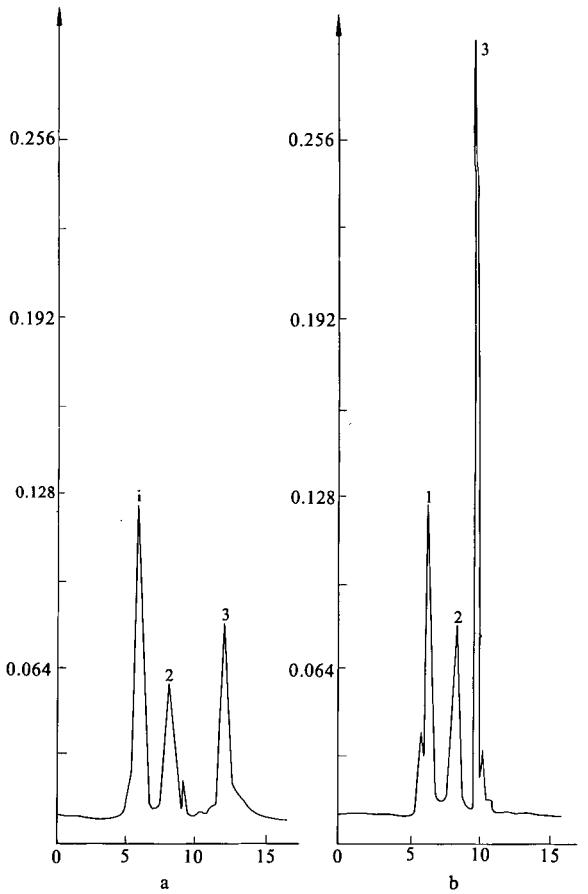

Fig. 2. Comparison of results of SEC between native and unfolding proteins. Column, Shimadzu diol 150 (250 × 7.9 mm I.D.); mobile phase, 0.020 mol/l Tris–0.10 mol/l NaCl (pH 7.0); Flow-rate 1.0 ml/min; chart paper speed, 2.5 mm/min; detection wavelength, 280 nm; 0.32 a.u.f.s. Proteins: 1, BSA; 2, RNase; 3, LYS. (a) Native proteins; (b) unfolded proteins. Axes as in Fig. 1.

for refolding with HPHIC is not or not only due to the removal of denaturing agent during the chromatographic process.

We need a full understanding of the mechanism of retention of proteins in HPHIC. In other words, we must know how protein molecules bind to and desorb from an HPHIC column and also what happens during this whole adsorption–desorption process. Based on the SDM-R of proteins HPHIC [18], we also need to know the contributions of the contact surface and the continuous conformational change of a protein during its refolding. The hydro-

phobicity of a salt solution of high concentration is high enough to push the protein molecules into contact with the surface of the HPHIC stationary phase, and to be adsorbed by it. Because HPHIC offers a higher hydrophobicity on this surface than that in the mobile phase, more hydrophobic amino acid residues in the protein molecule would face the surface of the stationary phase whereas more hydrophilic amino acid residues would face to the mobile phase. In this case, in the specific contact region, the hydrophobic forces make part of the unfolded protein molecules form a local configuration. The local configuration of the unfolded protein molecule may become a potential "seed" to continue its folding when it leaves the surface and passes into the mobile phase which has less hydrophobicity than that previously, as the hydrophobicity in the mobile phase changes continuously during gradient elution. Which part of a given unfolded protein molecule will contact the surface of the stationary phase? It really depends on both its primary structure, *i.e.*, its amino acid sequence, and the nature of HPHIC. Fausnaugh-Pollitt *et al.* [19] concluded that chromatographic retention in HPHIC is determined by amino acids on a single surface of the protein opposite to its catalytic left. A reasonable assumption is that an unfolded protein molecule makes contact in HPHIC also with the same region and it becomes a "seed" to continue refolding until complete refolding of this protein molecule has occurred. However, for any single unfolded protein molecule, it may contact the hydrophobic surface of the stationary phase with an incorrect hydrophobic part of the molecule because of the effect of Brownian motion. If this happens, the "wrong seed" or "ill-seed" may also grow. However, it is short-lived, because it is thermodynamically unstable and it tends to adopt a stable state, or any stable kind of intermediate configuration. Therefore, the above elucidation of the exact refolding of an unfolded protein molecule is only in terms of statistics. In addition, the continuous changes in the hydrophobicity and water concentration, and also the viscosity of the eluent during gradient elution in HPHIC, may provide a suitable environment for refolding of a given protein. Hence the hydrophobic surface of an HPHIC stationary phase and a mobile phase with a variable composition may not only provide energy to effect refolding but may also provide a infinite chance for unfolded protein molecules to find their right "seed" and their thermodynamically stable state. Consequently, it accelerates the refolding process.

Application and limitations of protein refolding with HPHIC

If the above explanation of the reasons for protein refolding with HPHIC is reasonable, it seems that HPHIC can effect the refolding of any kind of

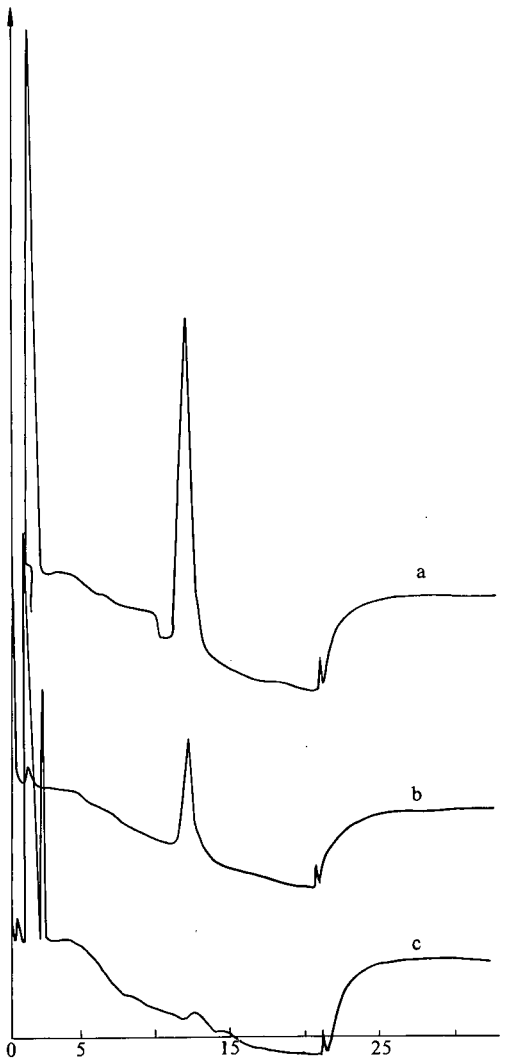

Fig. 3. Comparison of results of HPHIC of α-amylase: (a) native (b) unfolded with GuaHCl; (c) unfolded by boiling for 15 min. Chromatographic conditions as in Fig. 1. Time scale in min.

unfolded protein, such as thermal, acid or base, and even biological denaturation. However, Fig. 3 shows a comparison of α-amylase refolding chromatograms for three cases. Fig. 3a, b and c represent the native α-amylase, the unfolded α-amylase with 7.0 mol/l GuaHCl and the unfolded α-amylase after boiling for 15 min, respectively. The chromatographic conditions were as in Fig. 1. Although the retentions and shapes are identical for each peak, the peak heights are different. After boiling for 15 min, α-amylase aggregated and became a suspension, therefore, the height of peak c is the smallest of the three, but we do not know the reason why peak c has the characteristics of native α-amylase or where it comes from. It may come from either incomplete unfolding of α-amylase during boiling or from incomplete refolding with HPHIC. Anyhow, peak b shows incomplete refolding of α-amylase unfolded with 7.0 mol/l GuaHCl and we do not understand the exact reason. Fig. 3. demonstrates that HPHIC is not a universal method for refolding of every kind of protein from their unfolded states by any kind of denaturing method, even with GuaHCl. Nevertheless, we cannot draw the conclusion from Fig. 3 that HPHIC may effect refolding only of some proteins and not of other unfolded proteins either with a denaturing agent or in other ways. However, we used only one kind of mobile phase and chromatographic conditions to do the refolding of four kinds of proteins after having them unfolded in two ways. The composition hydrophobicity, pH, ionic strength, viscosity and temperature should be optimized for each protein to make complete refolding of the proteins possible, but this is beyond the scope of this paper.

UV spectra

UV spectrophotometry is one of the most important tools for investigating the changes in the molecular conformation and refolding of proteins [2].

Without injecting a sample, we ran the same gradient elution and collected the eluate in the same time interval as if the unfolded standard RNase had been injected. The collected eluate was divided into two parts: the first was used as the solvent for standard RNase and the second was used as the blank solution for UV spectral measurement of the refolded RNase. Also, a suitable standard RNase was dissolved in 7.0 mol/l GuaHCl and its UV spectrum was compared with that of the refolded RNase.

Fig. 4 shows a comparison of the UV spectra of RNase of (a), the native form, (c) the unfolded form, denatured with 7.0 mol/l GuaHCl, and (b) the refolded form after HPHIC of the unfolded RNase. The maximum absorption wavelength (202.5 nm) in (a) and (b) are the same, but are different from that in (c). The intensity in (b) is slightly lower than that in (a) probably because its mass recovery is not 100%. Anyhow, the refolding of unfolded RNase with 7.0 mol/l GuaHCl appears to be almost complete. The measurement of UV spectra is as usually reliable as the wavelength is longer than 200 nm [20]. Therefore, the shift of the maximum absorption wavelength towards the UV re-

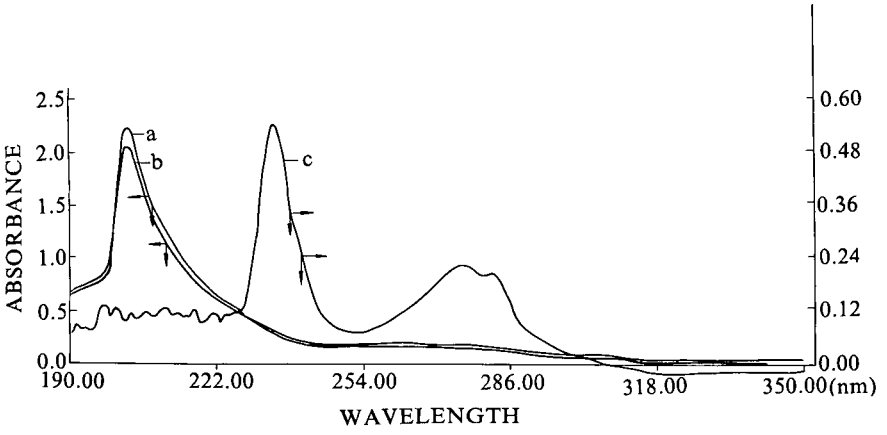

Fig. 4. Comparison of UV spectra of (a) native RNase, (b) refolded RNase and (c) RNase unfolded with 7.0 mol/l GuaHCl. Concentration of RNase: (a) and (b) 0.083 mg/ml for left-hand scale; (c) 0.50 mg/ml for right-hand scale.

gion can be attributed completely to changes in the molecular conformation of the RNase, as the sample and blank solutions had the same composition except for the proteins in the sample in (a) and (b). We obtained similar results in corresponding experiments for LYS and BSA which had been unfolded with both 7.0 mol/l GuaHCl and 8.0 mol/l urea.

Circular dichroic spectra

When a protein unfolds, the UV spectrum shows changes in the aromatic amino acids (tyrosine, tryptophan, phenylalanine) on exposure to the solvent, while CD spectra can denote changes in secondary structures (α-helices, β-pleated sheet and antiparallel β-sheet) of the unfolded protein, *i.e.*, CD spectra give some information concerning the global transition of a protein. Hence CD is also a very important method for investigating the variation of the molecular conformation of a protein.

Fig. 5 shows a comparison of the CD profile of the native (solid line) and the refolded (dotted line) RNase which has been unfolded with 7.0 mol/l GuaHCl and then refolded with HPHIC. The two CD spectra are identical in terms of their maximum absorption wavelength, absorption intensity and spectroscopic profile, although we did not calculate the changes in ellipticity. The composition of the solution containing native RNase is identical with that of the refolded RNase, hence Fig. 5 again indicates that HPHIC may effect refolding of unfolded RNase.

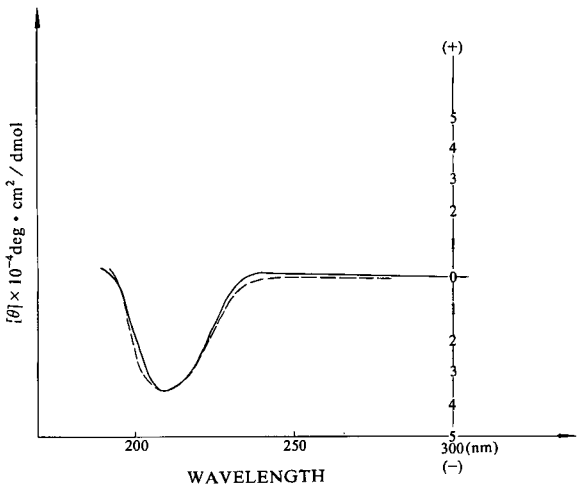

Fig. 5. CD spectra of (solid-line) native and (dashed line) refolded RNase.

Applications of protein refolding with HPHIC in biotechnology

An important factor complicating the recovery of rIFN-γ from *E. coli* is its interacellular location. An alternative to the commonly used method of releasing it by mechanical disruption is to permeate chemically the cells with a concentrated denaturing agent. These methods have several undesirable properties, *e.g.*, the extensive fragmentation of the cells makes the subsequent centrifugation difficult and nearly all of the soluble cellular proteins are released, resulting in difficulties in downstream production in industry.

However, GuaHCl can make the cell permeable to proteins without causing extensive breakage of the cell and can dissolve protein from *E. coli* membrane fragments [4]. The cell membrane acts as a molecular sieve which retards RNA and most of the DNA inside the cells. Hence it is possible to simplify the technology for the purification of therapeutic proteins in biotechnology. However, it is then necessary to separate GuaHCl from rIFN-γ. Several means can be used to effect renaturation of therapeutic protein, *e.g.*, common dialysis, dilution with an approprite aqueous solution to adjust hydrophobicity, viscosity and ionic strength or the removal of sodium dodecyl sulphate (SDS) with mild neutral detergents [21], but only low recoveries of bioactivity are normally obtained.

Fig. 6 shows the chromatogram of the solution of rIFN-γ extracted with 7.0 mol/l GuaHCl from *E. coli* cells. This extracted solution was injected directly into the HPHIC column (250 × 7.9 mm I.D.). The shaded areas show the recovery of the bioactivity of rIFN-γ. The major peak in Fig. 6 is rIFN-γ containing some impurities. Its retention time is about 33 min. Because rIFN-γ easily forms inclusion bodies, it is very difficult to dissolve it with the usual media, and hence to measure its real native bioactivity. Therefore, we have to make a comparision with the bioactivity of rIFN-γ in the sample before injection into the HPHIC column. The average bioactivity recovery of the renaturated rIFN-γ with HPHIC is about 280%. This is due to the comparison of the recovery of the bioactivity of rIFN-γ between the dilution method mentioned

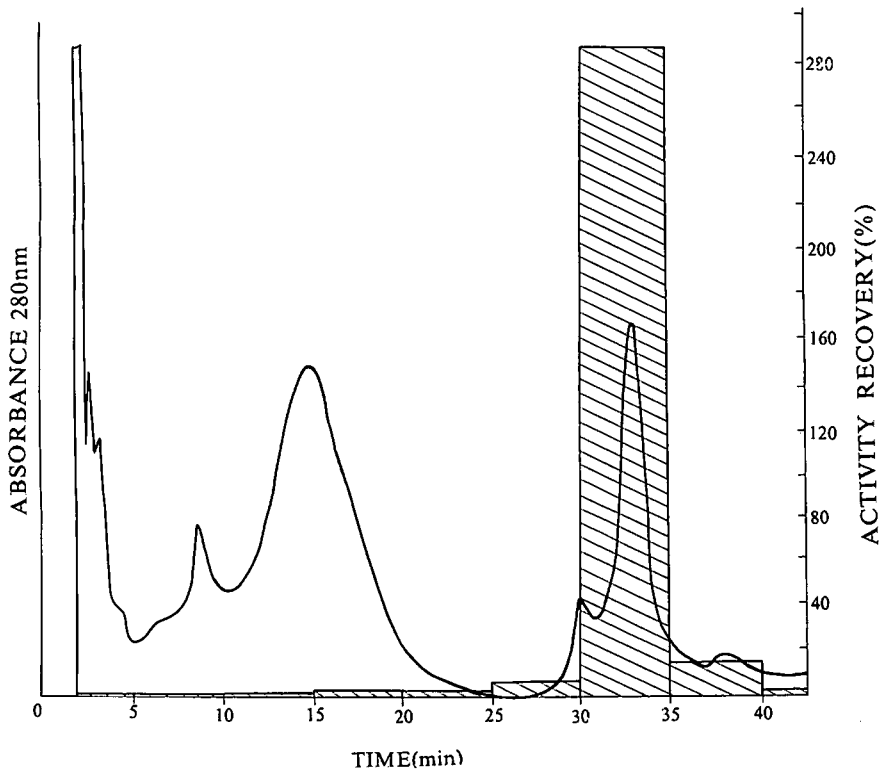

Fig. 6. HPHIC of rIFN-γ solution extracted from *E. coli* cells. Chromatographic conditions as in Fig. 1. Sample size, 1.0 ml; flow-rate, 2.0 ml/min. The shaded areas represent the bioactivity recovery in collections in every 5 min (right-hand scale).

above and the HPHIC refolding method in this work, because the CPE inhibition assay, in fact, makes many folds during dilution of the original extracted solution. For this sample, it was eluted up to 2000–4000 fold. The concentration of GuaHCl in this instance is so low that its influence on bioactivity may be ignored. However, it is still necessary to check further the bioactivity recovery with other methods [22].

Fig. 7 shows the results of SDS–polyacrylamide gel electrophoresis (PAGE). The right lane is the original extracted solution form *E. coli* cells and the left lane shows the major peak containing rIFN-γ in Fig. 6 using standard protein. The molecular mass of protein in the main spot is calculated to be about 17 000 (data not shown), as expected for rIFN-γ. The purity of refolded rIFN-γ is about 85% as determined by dual-wavelength thin-layer chromatographic scanner (not shown). We also did refolding and purification of an extracted solution of interleukin-2 and recombinant human interferon-β from *E. coli* cells using the same chromatographic conditions as in Fig. 6, and obtained a positive result, *i.e.*, their unfolded forms can be refolded and purified. However, the results are not comparable to those for rIFN-γ.

The bioactivity recovery of rIFN-γ refolded with HPHIC is so high that it is difficult to explain it only by removing GuaHCl from the purification system. As was pointed out above, the HPHIC system provides desirable conditions which can be further optimized for rIFN-γ refolding. rIFN-γ is a small protein with a molecular mass of less than 20 000, it is a very strong hydrophobic protein without any disulphide bond. The refolding of rIFN-γ should be much easier than that of other proteins, even small proteins, such as LYS and RNase.

Both Figs. 6 and 7 show that HPHIC is a powerful tool not only for protein refolding but also for the separation and purification of proteins.

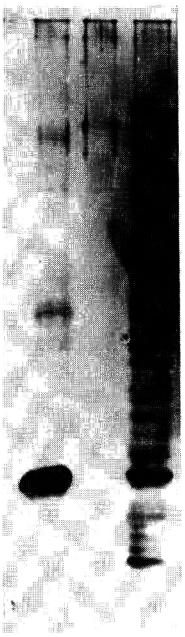

Fig. 7. SDS-PAGE of rIFN-γ. The large spot in the left-hand lane denotes the SDS-PAGE of the purified rIFN-γ from the peak at 33 min in Fig. 6. The right-hand lane represents the SDS-PAGE of the original solution extracted from *E. coli* cells with 7.0 mol/l GuaHCl.

CONCLUSIONS

HPHIC can be used to accomplish the refolding of a protein unfolded by a concentrated solution of denaturing agent, such as 7.0 mol/l GuaHCl and 8.0 mol/l urea solution. For some protein the refolding may be complete.

The reason for the protein refolding with HPHIC may be partially due to the completely removal of denaturing agent and to the establishment of a suitable environment in which its hydrophobicity, viscosity, ionic strength, etc., can be ajusted by gradient elution. The contact surface region between the surface of the HPHIC matrix with a suitable hydrophobicity and the hydrophobic part of the whole unfolded protein molecule may play the most important role in starting the protein refolding, apart from a contribution of the mobile phase to the spontaneous refolding of unfolded protein.

This method of protein refolding with HPHIC can be used for the renaturation of some therapeutic proteins extracted from *E. coli* in the biotechnological industry, whereby these proteins can be separated and purified.

ACKNOWLEDGEMENTS

The authors are obliged to Mr. Jianhua Chang and Mrs. Jianning Yin of this laboratory for making the HPHIC packings and assaying the bioactivity of rIFN-γ, respectively, and to Associate Professor Jing Hu of the Lanzhou Institute of Chemical Physics, Chinese Academy of Science, for providing CD spectra. The authors also thank Professor Kuitang Tong of Shanghai Institute of Biological Products and Associate Professor Zhiqing Zhang of the National Laboratory of Molecular Virology and Genetic Engineering Institute of Virology, Chinese Academy of Preventive Medicine, for providing a crude solution of rIFN-γ extracted from *E. coli*. This project was supported by the National Natural Science Foundation of China.

REFERENCES

1 C. B. Anfinsen, *Science (Washington, D.C.)*, 181 (1973) 223.
2 C. Ghelis and J. Yon, *Protein Folding*, Academic Press, New York, 1982.
3 R. L. Baldwin, *Annu. Rev. Biochem.*, 44 (1975) 453.
4 D. J. Hettwer and H. Y. Wang, in J. A. Asenjo and J. Hong (Editors), *Separation, Recovery, and Purification in Biotechnology (ACS Symposium Series, No. 314)*, American Chemical Society, Washington, DC, 1986, p. 2.
5 J. Chang and X.-D. Geng, *Xibei Daxue Xuebao X'ian*, 4 (1989) 103.
6 X.-D. Geng, W. Feng, J. Chang, X. Chang, F. Ma, J. Yin, H. Li and L. Bian, *Gaojishu Tongxun*, 7 (1991) 1.
7 P. C. Familletti, S. Rubinstein and S. Pestka, *Methods Enzymol.*, 78 (1981) 387.
8 H. Wu and E.-F. Yang, *Chin. J. Physiol.*, 5 (1931) 301.
9 M. L. Anson and A. E. Mirsky, *J. Gen. Physiol.*, 17 (1934) 393.
10 J. H. Northrop, *J. Gen. Physiol.*, 16 (1932) 333.
11 X.-D. Geng and F. E. Regnier, *J. Chromatogr.*, 296 (1984) 15.
12 M. Kunitani, D. Johnson and L. R. Snyder, *J. Chromatogr.*, 371 (1986), 313.
13 K. Benedek, S. Dong and B. L. Karger, *J. Chromatogr.*, 317 (1984) 227.
14 S.-L. Wu, K. Benedek and B. L. Karger, *J. Chromatogr.*, 539 (1986) 3.
15 S.-L. Wu, A. Figueroa and B. L. Karger, *J. Chromatogr.*, 371 (1986) 3.
16 J. Chang, W. Feng and X.-D. Geng, *Chromatographia*, (1991) submitted for publication.
17 R. L. T. Corbett and R. S. Roche, *Biochemistry*, 23 (1984) 1888.

18 X.-D. Geng, L. Guo and J. Chang, *J. Chromatogr.*, 507 (1990) 1.
19 J. Fausnaugh-Pollitt, G. Thevenon, L. Janis and F. E. Regnier, *J. Chromatogr.*, 443 (1988) 221.
20 Y.-Z. Chen, *Organic Analysis*, High Education Publishers, Beijing, 1983.
21 S. Hjertén, M. Sparrman and J.-L. Liao, *Biochim. Biophys. Acta*, 939 (1988) 476.
22 S. H. E. Kaufmann, E. Hug, U. Väth and G. D. Libero, *Eur. J. Immunol.*, 17 (1987) 237.

Journal of Chromatography, 599 (1992) 195–203
Elsevier Science Publishers B.V., Amsterdam

CHROMSYMP. 2527

Influence of operating parameters on the preparative gradient elution chromatography of insulins

Geoffrey B. Cox

Prochrom Inc., 5622 West 73rd Street, Indianapolis, IN 46278 (USA)

ABSTRACT

The mass-overloaded separation of bovine and porcine insulins has been studied in the reversed-phase gradient elution mode. Strong solute–solute displacement effects have been found, which are related to the efficiency of the column used. Low flow-rates and small particle diameters maximise the displacements, as well as improve the resolution between the parent insulin and its desamido contaminant. The gradient slope did not substantially affect the separation between the parent insulins, but, due to the relative "S" values of the solutes, an increase in gradient slope improved the separation of the parent insulin from its desamido compound. An optimum pore size of 150 Å was found for the insulins. Experiments to optimise the loadability were not carried out, but a recovery of 90% at a purity of 99.5% was obtained with a loading of 12 mg/g of porcine insulin.

INTRODUCTION

The isolation of peptides and proteins by preparative reversed-phase chromatography is becoming a preferred route toward their purification. During the past two years, studies of solute–solute interactions in the mass-overloaded separations of proteins have demonstrated that strong displacements can occur between the components of the samples. The separation of cytochrome *c* from lysozyme or RNAse [1] by preparative gradient elution chromatography has been shown to be characterised by strong solute–solute displacements. The question of the occurrence of such strong displacements between more closely related proteins was not addressed. Although displacements during the elution chromatography of proteins are not well known, several separations of proteins by displacement chromatography have been reported. Papers by Huang and Horváth [2] and by Subramanian *et al.* [3] have demonstrated that very strong displacements can be seen under the right conditions. In many of these cases, the structural difference between the proteins is marked, and it is not clear if very closely related proteins would demonstrate the same effects.

Vigh *et al.* [4] have described the displacement chromatography of bovine and porcine insulins. These have very similar structures and appear to be more difficult to separate, at least under the reversed-phase conditions reported. The yields and purity of materials isolated from these experiments were rather poor, and displacement trains were not apparently well established. It is not clear if the problem lay in the choice of cetrimide as a displacer, poor isotherms or too high a load and insufficient column length.

The elution chromatography of insulins is well documented, and reversed-phase preparative liquid chromatography has been carried out on a number of insulin variants [5,6]. Probably the most important of these is the production-scale purification of biosynthetic human insulin for use in the treatment of diabetes mellitus [7]. This reversed-phase purification was carried out on a large scale using high-efficiency columns, showing approximately 40 000 plates/m. The purity of the insulin was raised from 83 to 98.6% with a recovery of 82% at a sample loading of 21 mg insulin/g of packing material. It was not explicitly shown that displacement effects occurred. From inspection of the analytical chromatograms, however, one can deduce that they

0021-9673/92/$05.00

were probably important since the impurities eluted very closely to the major peak and would otherwise have been engulfed by it at the loads described.

The work reported in this paper was carried out to study the effects of operating conditions — gradient slope and initial composition, flow-rate, particle size, pore diameter, etc. — on the interactions between solutes which are structurally similar. The same insulin variants, bovine and porcine insulins, were chosen for this work as had been used in the earlier displacement work. This choice reflected the availability of standard materials rather than a conscious attempt to compare the techniques of gradient elution and displacement chromatography. Nevertheless, it was felt that the results may be relevant to the continuing discussions upon the relative merits of the techniques.

EXPERIMENTAL

Equipment

A HP1090 L liquid chromatograph (Hewlett-Packard, Avondale, PA, USA), fitted with a preparative autoinjector and a diode array detector was used for this work. Data storage and processing were performed using a HP 3365 Chem Station data system.

Chromatography

Columns. Kromasil 100 10 C_8 and 150 10 C_8 columns (Eka Nobel, Surte, Sweden, 10 μm, 100 and 150 Å pore size respectively), 25 cm × 4.6 mm I.D. and a range of Matrex 250 Å C_8 columns (Amicon, Danvers, MA, USA), of 6.5, 20 and 50 μm particle size, 10 cm × 4.6 mm I.D. were obtained from the manufacturer. Zorbax® PRO-10 Protein Plus (DuPont, Wilmington, DE, USA; 10 μm, 300 Å pore size) and Poroquartz 200 C_{18} (10 μm, 200 Å pore diameter) (Moscow Institute of National Economy, Centre of Applied Liquid Chromatography, Moscow, USSR) were packed into columns (15 cm and 25 cm × 4.6 mm I.D., respectively) by a downward slurry technique.

Chemicals and mobile phases. Acetonitrile was obtained in HPLC grade from EM Science (Gibbstown, NJ, USA). Trifluoroacetic acid (TFA) was obtained from J. T. Baker (Phillipsburg, NJ, USA). Protein standards were from Sigma (St. Louis, MO, USA). HPLC-grade water was prepared with a Nanopure unit (Barnstead/Thermolyne, Dubuque, IA, USA).

Analysis of fractions. Because the deamidation of insulins is promoted by low pH, the fractions from the preparative separations were either collected into a pH 7 buffer or (more usually) were stored at 4°C between collection and analysis. No evidence for the decomposition of insulins in the fractions was found.

RESULTS AND DISCUSSION

The structures of bovine and porcine insulins are closely similar and the chromatographic separation of these compounds is expected to be difficult. A conventional acetonitrile–0.1% trifluoroactic acid gradient was used throughout, since it was known that such a solvent system would allow the elution of the insulins and also the dissolution of the samples to the concentrations required for the study. A low-pH solvent was used, despite the possibility of deamidation of the insulins, because the value of the isoelectric point of insulin (p$I \approx 5.5$) means that operation at a significantly higher pH would limit the solubility. During this study, no attempt was made to optimise the mobile phase components. The reason for this was because a difficult separation was required for the study; too high a selectivity would negate part of the reason for carrying out the work.

Preparative gradient design

In order to design the gradient to effect the separation, it was desirable to determine the basic gradient parameters. These are the slope of a plot of log capacity factor *vs.* solvent composition (S) and the capacity factor of the solutes in water (k'_w) [8]. From these data, it is possible to calculate the retention time of the solutes using any other gradient profile. A commercial software package (DryLab G; LC Resources, Lafayette, CA, USA) was used for the calculations.

Measurements of retention times of the solutes were made on Zorbax Pro-10 Protein Plus under the conditions described in Table I. The S and log k'_w values determined are also shown in that Table. The predictions from the software suggested that an isocratic composition of 30% would give a good resolution of the components. This was refined ex-

TABLE I

GRADIENT PARAMETERS FOR BOVINE AND PORCINE INSULINS

Experimental conditions: column, Zorbax Pro-10 Protein Plus, 25 cm × 4.6 mm I.D.; gradient, 10 to 60% acetonitrile in 0.1% aqueous TFA; gradient duration: (a) 30 min, (b) 90 min; flow-rate, 1.0 ml/min; detection wavelength, 230 nm; sample, 10 μl of 1 mg/ml solution of bovine and porcine insulins in 10% aqueous acetonitrile containing 0.1% TFA.

Solute	S	Log k'_w
Bovine insulin	14.9	5.31
Porcine insulin	15.23	5.48
Desamidoporcine	14.92	5.45

perimentally to 29%, and a gradient from 27 to 31% acetonitrile was selected. Following the recommendations arising from an earlier study of the separation of proteins by preparative reversed-phase chromatography [9], the sample was loaded at a low solvent strength to avoid the problem of displacement of acetonitrile by the proteins during their adsorption and the consequent elution of part of the sample. A steep gradient from the 10% loading composition to the initial composition of the elution gradient was used. Because the resolution at 1 ml/min was small, the chromatography was performed at 0.5 ml/min, which was seen to improve the separation by reduction of the band width of the insulins by increasing the column efficiency.

Effect of gradient slope

Preparative separations of the insulins were performed both isocratically at 29% acetonitrile and by gradient, from 27 to 31% acetonitrile in 28 min, using the Pro-10 Protein Plus column under conditions shown in Table II. A sample load of 2.5 mg of a 1:1 mixture of the insulins was introduced at 10% acetonitrile in the mobile phase. This was increased over 10 min (later work showed that a step gradient was just as effective) to the desired elution composition. Fractions were collected through the peak envelopes and these were subsequently analysed for content of the components of the mixture. Fig. 1 shows the gradient elution chromatogram together with the distribution through the peak of the individual components, reconstructed from the results

TABLE II

RECOVERIES OF BOVINE AND PORCINE INSULINS

(a) Isocratic conditions: loading, 2 min at 10% acetonitrile in 0.1% aqueous TFA; gradient to starting conditions; 10 to 90% acetonitrile in 0.1% aqueous TFA over 10 min; separation conditions, isocratic, 29% acetonitrile in 0.1% aqueous TFA; flow-rate, 0.5 ml/min; detection wavelengths, 230 and 290 nm; sample, 250 μl of a solution 5 mg/ml of each of bovine and porcine insulin. (b) Gradient conditions: gradient to starting conditions, 10 to 27% acetonitrile in 0.1% aqueous TFA over 10 min; separation conditions; 27 to 31% acetonitrile in 0.1% aqueous TFA over 28 min; other conditions as (a).

Conditions	Ratio	Bovine		Porcine	
		Purity (%)	Recovery (%)	Purity (%)	Recovery (%)
b	1:1	100	91	99.5	83
a	1:1	100	95	99.5	82
b	1:9	100	61	99.5	90
b	9:1	100	98	100	96

of analysis of the fractions. Fig. 2 shows similar data from the isocratic experiment. In both chromatograms, the trailing edge of the bovine insulin peak does not follow the same profile as that of the porcine insulin. The tail shows a distinct break at the point at which the porcine insulin starts to elute, and rapidly falls to the baseline. If this displacement were not observed, the bovine insulin would tail to

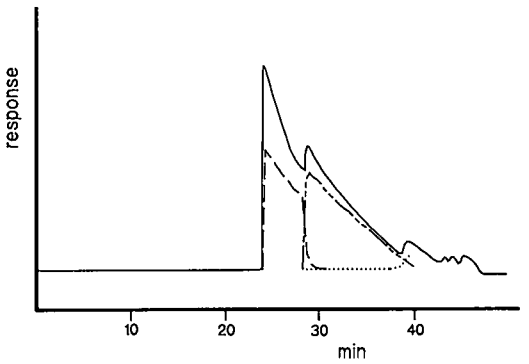

Fig. 1. Gradient chromatogram of a 1:1 mixture of bovine and porcine insulins, 2.5 mg total load. Solid line: chromatogram. Dashed line: bovine insulin; dashed/dotted line: porcine insulin; dotted line: desamidoporcine insulin. Conditions as Table II, conditions b.

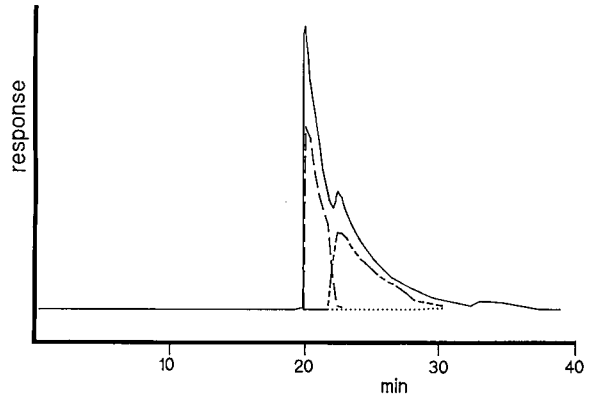

Fig. 2. Isocratic chromatogram of a 1:1 mixture of bovine and porcine insulins, 2.5 mg total load. Key as Fig. 1. Conditions as Table II, conditions a.

the retention time of an analytical scale load and would substantially contaminate the porcine insulin. At the same time, of course, it would itself be substantially contaminated by the porcine insulin with which it was co-eluting, In the isocratic separation, where the tail of the porcine insulin peak is extremely long, the extent of peak overlap would be very great. The displacements are similar to those seen in the preparative separations of other proteins [1,9] and mean that the purity and recovery of the components are higher than would at first be expected.

Combinations of the collected fractions were calculated which gave a product with a purity of at least 99.5%. The recoveries of the insulins were determined for these combinations. These are shown in Table II, along with data calculated from similar gradient runs using the same total load but 1:9 and 9:1 mixtures of the two insulins. Chromatograms arising from these last two experiments are shown in Fig. 3, along with the distribution of each component through the main peak envelope, derived again from the results of the analysis of the fractions collected during the experiment. These show the same strong displacements as seen in the 1:1 mixtures, and also demonstrate the absence of any "tag-along" effect between the insulins.

There was little difference between the recoveries of the isocratic and gradient experiments. This is consistent with both theory [10] and results reported earlier [9]. The results for the experiments using 1:9 and 9:1 mixtures were at variance with results of

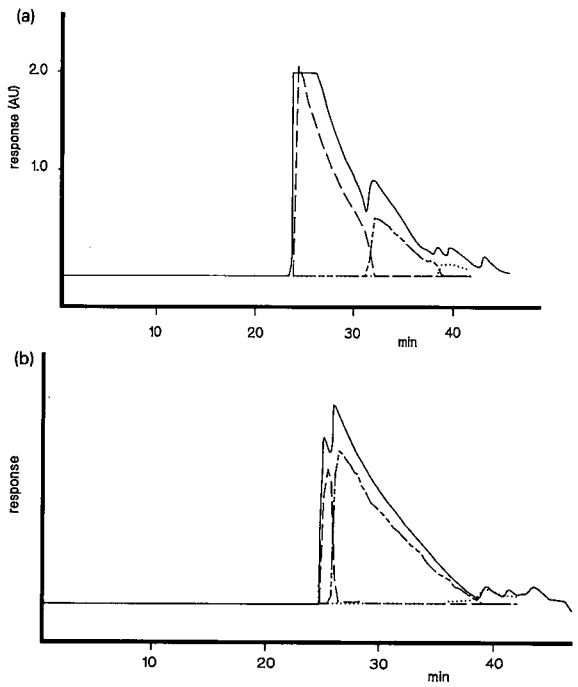

Fig. 3. Gradient chromatograms of 9:1 and 1:9 mixtures of bovine and porcine insulins, 2.5 mg total load. Gradient conditions as Fig. 1. (a) Bovine–porcine insulins (9:1) gradient chromatogram; (b) bovine–porcine insulins (1:9) gradient chromatogram; key as Fig. 1.

computer simulations in isocratic chromatography [11], where the displacement effects gave a better recovery of the first eluted component when it was present at lower concentration. This is because there is no tag-along effect between the bovine and porcine insulins; the displacements maintain the separation between them. Inspection of the two chromatograms reveals that the zones of overlap between the peaks are similar for the 1:9 and 9:1 mixtures. When the bovine insulin is the minor component, the overlap with the high concentration front of the porcine insulin peak means that it is substantally contaminated with the later eluting component. When the porcine insulin is the minor component, it interacts only with the low-concentration tail of the bovine insulin, is thus less contaminated and the recovery is higher.

The influence of gradient slope on separations using higher sample loads was also investigated. This work was performed on a smaller column, 10 cm × 4.6 mm I.D. packed with 6.5-μm C_8 particles of

250-Å pore diameter, and with twice the load used earlier. Allowing for the higher surface area of the smaller pore, irregular packing material, this increased the effective load on the column by a factor of around 4. The increase in load was expected to have a deleterious effect upon the recovery at a given purity of insulin. In addition, this separation was performed using a mixture of less pure insulin standards which contained appreciable quantities of both of the desamido compounds.

Two gradient experiments were carried out, using 10- and 30-min gradient times respectively, as detailed in Table III. Fractions were collected through the main peak envelopes and were analysed using the same column, but under isocratic conditions (30% acetonitrile) which allowed a good resolution of all of the components. The results of this analysis are shown in Fig. 4, which shows the profiles of the individual components through the peak envelopes for the two gradients. Table III also shows the purity and recoveries achieved under these conditions. Despite the higher load, the recovery of product at high purity remained acceptable, especially for the earlier eluted bovine insulin. Interestingly, the separation with the steeper gradient gives better recoveries than the other. This can be understood by reference to the S values of the insulin *versus* its desamido impurity. Earlier work has suggested that the separations of proteins are dependent not only upon the gradient parameters but also upon their S values [1]. When the S values of two components are equal, the separation should be independent of the gradient slope. When they are unequal, the effects of the slope will depend upon which component has the greater value of S. If the first eluting component has the greater S value, a steeper gradient will improve the separation, since the components elute at a higher effective solvent strength. This is the case here, in that the desamido impurities have lower S values than the parent compounds (experiments not reported here indicate that the desamido bovine insulin has a lower S value than its parent). Thus, the separation of both the bovine and porcine insulins from their desamido impurities will be improved by the steeper gradient. It might be expected that the separation between the desamido bovine insulin and the porcine insulin would be degraded at the higher gradient slope; this separation is probably maintained because of the displacement effects.

TABLE III

EFFECT OF GRADIENT SLOPE ON RECOVERIES OF BOVINE AND PORCINE INSULINS

Column, Matrex 250 C_8 (6.5 μm), 10 cm × 4.6 mm I.D.; loading, 2 min at 10% acetonitrile in 0.1% aqueous TFA; gradient, step to 29% acetonitrile, 29 to 33 % acetonitrile in 0.1% aqueous TFA; gradient durations, 10 and 30 min; flow-rate, 1 ml/min; sample, 250 μl of 10 mg/ml of each of bovine and porcine insulins in 0.1% aqueous TFA containing 10% acetonitrile.

Gradient run time (min)	Bovine		Porcine	
	Purity (%)	Recovery (%)	Purity (%)	Recovery (%)
10	100	83.5	100	58.4
	93.3	98.5		
	78.8	100		
30	100	67.4	100	18.9
	87.8	98.5	97.6	67.5
	64.4	100	97.0	76.0
			91.8	81.5

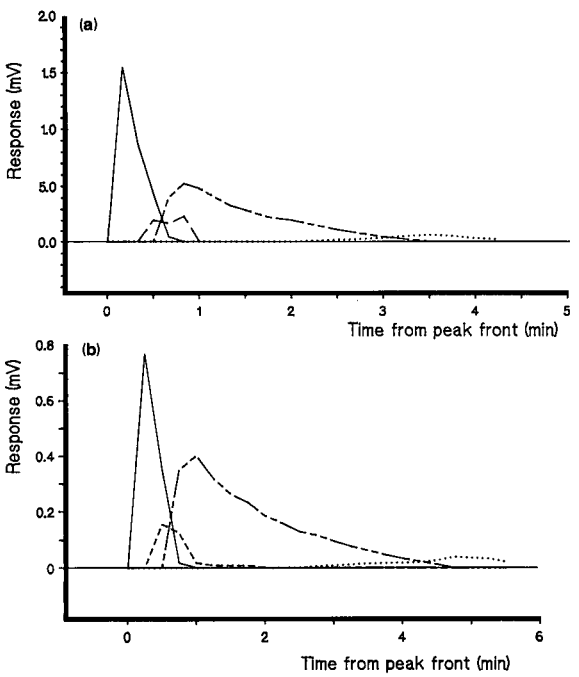

Fig. 4. Influence of gradient slope on the separation of bovine and porcine insulins, load: 2.5 mg each. Reconstructed chromatograms from fraction analysis; (a) Conditions as Table III, conditions a; (b) as (a) but final gradient duration was 30 min. Column: 10 × 0.46 cm I.D. Matrex 250 C_8, 6.5 μm. —— = Bovine insulin; – — = desamido bovine insulin; — – – – = porcine insulin; ···· = desamido porcine insulin.

Effect of flow-rate

The column efficiency in the chromatography of proteins is strongly influenced by the flow-rate in the system due to the very low values of the diffusion coefficients of these large molecules. The separation of porcine insulin from its desamido impurity was studied at two disparate flow-rates in order to investigate the effects of changes in efficiency. In order to maintain all other parameters constant, the gradient slopes in terms of % change per ml were maintained constant between the two runs whilst the flow-rates were changed from 1 ml/min to 0.1/min. Other conditions are described in Table IV. Fig. 5 shows the chromatograms, reconstructed from analysis of fractions taken through the peak envelope. The improvement in the separation caused by operation at the low flow-rate is clear. The front-running impurity has a much narrower band width at the low flow-rate, reflecting the narrower displacement zone at the higher column efficiency. In addition, the separation between the main peak and that of the desamido insulin is also improved at the lower flow-rate. When the separation is performed at 1 ml/min, there appears to be a pronounced "tag-along effect" of the desamido compound. Reduction of the flow-rate (and the consequent increase in efficiency) reduces this quite

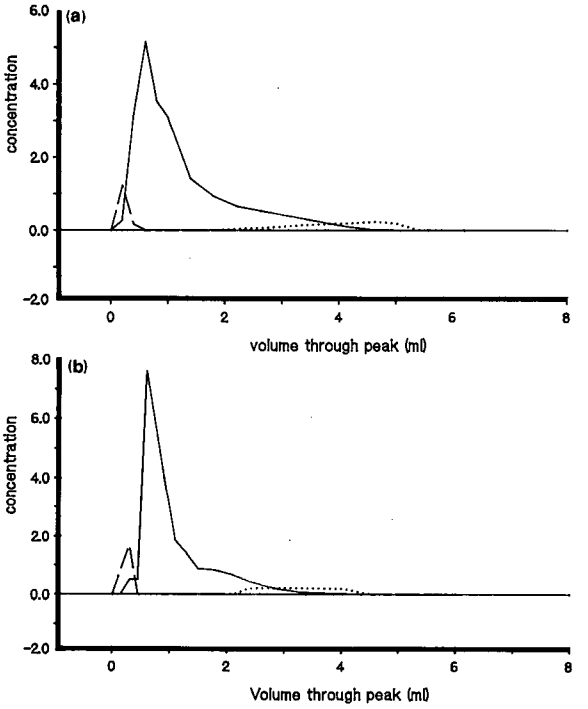

Fig. 5. Influence of flow-rate upon the purification of porcine insulin. Sample load 30 mg. Flow-rates: (a) 1 ml/min; (b) flow-rate: 0.1 ml/min. Other conditions as in Table IV. – – – = Unknown impurity; —— = porcine insulin; ····· = desamido porcine insulin. y-Axis: arbitrary units related to peak areas.

TABLE IV

RECOVERIES OF PORCINE INSULIN AT 1 AND 0.1 ml/min

Column, Kromasil 100 C_8, 25 cm × 4.6 mm I.D.; loading, 2 min at 5% acetonitrile in 0.1% aqueous TFA; gradient, step to 27% acetonitrile; 27 to 37% acetonitrile in (a) 15 min and (b) 150 min; flow-rate, (a) 1 ml/min and (b) 0.1 ml/min; sample, 30 mg of porcine insulin in 3 ml of 5% acetonitrile in 0.1% aqueous TFA.

Flow-rate (ml/min)	Purity (%)	Recovery (%)
1.0	99.95	63.0
	99.3	72.5
	98.7	80.4
	97.9	86.8
	96.7	91.9
	95.0	95.6
	93.2	97.9
0.1	100	88.8
	97.9	92.8
	93.7	96.9

dramatically. It is, therefore, important to operate the system at high efficiency if high recoveries are desired; this is often the case for recombinant proteins which typically have a very high value. High-efficiency operation usually translates to the use of low flow-rates because of the low diffusion rates of proteins. In such cases the production rate can be maximised by the use of small particles since at low flow-rates the operating pressure is usually low. With smaller particle diameters, the minimum in the Knox plot (of reduced plate height *vs.* reduced flow velocity) occurs at higher absolute velocities and the slope of the curve is generally less steep, allowing higher flow-rates.

The sample load in these experiments was 30 mg. The recovery and purity of a number of combinations of the fractions collected were calculated from both experiments. These results are shown in Table IV. The improved recovery of the run at 0.1 ml/min is seen clearly for the highest purity fractions. As the purity of the combined fractions is diminished,

there comes a point where the recovery from the experiment carried out with low flow-rate is less than that at faster flow. This is presumably because of the higher concentration of the impurity bands obtained at the lower flow-rate. The recovery from the combinations of fractions which yield products at 99.5% purity can be estimated to be 90% for the run at 0.1 ml/min and 70% for that at 1 ml/min flow-rate. This does not, of course, mean that the best flow-rate for the purification is 0.1 ml/min. The optimum flow-rate in preparative chromatography is a complex function of chromatographic parameters [purity, recovery, load and production rate (itself a function of flow-rate)], and economic factors (the cost of the starting material, the value of the product and the operating costs) [12]. Because the latter parameters are undefined in this example, the optimum flow-rate cannot be calculated.

It is interesting to compare these results for porcine insulin with those reported for the displacement chromatography of bovine insulin [4]. Because of the close similarity in structures, it is expected that there will be very little difference in the chromatographic behaviour of these two compounds and that comparison of the two experiments will be valid. Analysis of the displacement chromatographic data indicated that only one of the reported separations, carried out at a flow-rate of 0.1 ml/min with a load of 140 mg of bovine insulin on a column of dimensions 25 cm × 4.6 mm I.D., gave product pure enough for the comparison to be made. In this case, a purity of 98% was obtained with a recovery of 20%. Thus, in the 18.3 h of the experiment (110 ml at a flow-rate of 0.1 ml/min) a total of 28 mg at 98% purity could be collected. The purification of porcine insulin by gradient elution with the flow-rate of 0.1 ml/min was complete in 4 h and 10 min. In this time, a product of 98% purity could be isolated in 92.5% recovery, *i.e.* 27.8 mg. At the higher flow-rate (and a run time of 25 min), the recovery was less, but still 25.5 mg of porcine insulin at 98% purity could be isolated — a production rate 40 times higher than observed in the displacement separation. Because of the low recovery of high-purity material, it appears that the displacement separations reported may be more useful for an initial purification of crude material rather than a final preparation of high-purity product.

Effect of pore size

The pore diameter necessary for the effective chromatography of proteins has received some attention. For analytical separations, products with pore diameters of 300 Å are commonly available. More recently, it has been shown that the optimum pore diameter for preparative loading is smaller than this value, although this work was carried out statically and did not measure the dynamic effects [13].

The effect of pore diameter was studied using three packings of differing pore size. Two of these were spherical with pore diameters of 100 and 150 Å, respectively. The other was irregular, of 200 Å pore diameter. This last packing had a C_{18} bonded phase rather than the C_8 of the other phase. This was expected to reduce the effective pore size and surface area a little. The influence of pore size was studied by introduction of a given load upon the column and measurement of the change in retention time and the increase in band width over those observed for an analytical load. The theoretical plate height for a band is made up of contributions due to the band spreading from the column (small sample, *i.e.* kinetic effects) and the mass overload (thermodynamic effects) [14]. Since the band widths are proportional to the square roots of the individual plate height contributions, the mass overload band width is obtained by subtraction of the square of the analytical band width from that of the total band width and taking the square root of the result.

Both the change in retention at a given mass load and the mass overload band width are dependent upon the accessible surface area. This is a function of both the absolute surface area of the packing material and the pore diameter. Large molecules are excluded from the smaller pores of the packing and so only a certain percentage of the surface area is available for adsorption. When the surface area is high (and the pores therefore have small diameter), a relatively low percentage of the area is accessible. With increasing pore diameters, a greater percentage of the surface area is available, but the absolute area of the particle is reduced. Eventually, all of the surface is available as the pore becomes large compared with the molecules, but the surface area is reduced so much by the increase in pore size that very little solute can be adsorbed. Thus, for any molecular size there is an optimum combination of

pore size and surface area which allows a maximum loading.

The band width of a solute due to mass overload effects in gradient elution has been demonstrated to be approximately proportional to the square root of the mass load [13]. In order to ensure that the band widths measured in different columns would be related only to the different physical parameters of the particles within them, this relation was checked for porcine insulin. A graph plotting the logarithm of the mass-overload band width against the logarithm of the load was seen to be linear, with a slope of 0.53, very close to that reported earlier.

The changes in band widths and retention times due to mass overload caused by the injection of 2.5 mg of porcine insulin in the three columns are shown in Table V along with the experimental conditions. The minimum values occur for the 150-Å packing material, and this pore size is taken to be close to the optimum for this separation. In addition, the band width for an analytical load was found to be smallest for the 150-Å pore diameter packing. This is expected if the rate of mass transfer in and out of the pores is higher than for the 100-Å packing. The larger analytical band width for the 200-Å packing can be ascribed to its irregular particle shape; the effective particle size is probably larger than that of the spherical materials.

Effect of particle size

The effects of column efficiency upon the separation have been touched upon throughout this paper. Chromatography of the insulins was studied on columns with different particle sizes in order better to quantify the effects. It is known that for other protein separations the displacement effects are dependent upon particle size (*i.e.*, column efficiency) [15]. For the example of cytochrome *c* and lysozyme, the maximum recovery was obtained only with a column efficiency above 1500 plates (for the protein). This was obtained in a 10-cm column packed with 15-μm particles. Since the selectivity for these proteins was high, it was expected that the minimum efficiency for the more difficult separation of insulins would be higher.

Columns 10 cm in length, packed with C_8 bonded-phase particles of 250 Å pore diameter and of 6.5, 20 and 50 μm, respectively, were used for the study. Sample loads of 10 mg of a 1:1 mixture of bovine and porcine insulins were used. The same gradient and flow-rate were used for all three columns, shown in Table VI. Fractions were collected through the peaks and were subsequently analysed. The purity and recoveries of combinations of fractions were calculated. These values are shown in Table VI. The recovery is markedly reduced as particle size is increased. With a particle diameter of 20 μm, the displacements are substantially degraded and for the 50-μm packing they are to all practical purposes eliminated. Extrapolation of the data suggests strongly that an acceptable recovery (85 to 90% at 99.5% purity) will be obtained only with particles of less than around 10 μm in the 10-cm columns used.

In order to obtain acceptable yields and purity it is clearly necessary to perform the separation with a high value of efficiency. This does not, of course, have to be achieved with particles as small as those used here; a column 20 to 50 cm long, packed with 13-μm particles would give almost the same separation as the 10-cm column packed with the 6.5-μm medium. Care must be taken if larger particles are used, because the large particle diameter means that the reduced plate height is also larger at constant flow-rate and either the flow-rate (and hence the production rate) must be decreased or disproportionately longer beds must be employed. When the separation is to be carried out at a large scale, the availability (and cost) of long columns has to be taken into account; in such cases, packing materials with small particle diameters become an essential part of the separation requirement [7].

TABLE V

COMPARISON OF COLUMN PACKINGS UNDER 2.5 mg LOAD

Column, 25 cm × 4.6 mm I.D.; gradient, as Table IV, conditions a; sample, 2.5 mg porcine insulin in 250 μl of 5% acetonitrile in 0.1% aqueous TFA.

Packing material	Retention change (min)	Overload bandwidth (min)	Analytical bandwidth (min)
Kromasil 100	1.65	1.97	0.31
Kromasil 150	1.62	1.86	0.27
Poroquartz 200	1.66	1.89	0.39

TABLE VI

EFFECT OF PARTICLE SIZE ON PURITY AND RECOVERY

Column, Matrex 250 C_8, 10 cm × 4.6 mm, I.D.; gradient, as Table III, except that the step from 10 to 29% was made over a period of 10 min; other conditions as Table III.

Particle size (μm)	Bovine		Porcine	
	Purity (%)	Recovery (%)	Purity (%)	Recovery (%)
6.5	100	95.9	100	55.6
			99.5	75.3
			99.0	84.7
20	100	61.3	100	12.3
	99.6	76.1	98.6	31.4
	98.7	87.3	96.9	56.2
	96.3	95.4	96.0	66.3
	89.7	98.6	89.3	84.4
			88.7	94.1
50	97.1	10.4	100	18.0
	94.8	37.1	96.0	31.7
	90.3	58.8	90.2	50.8
	86.0	73.5	88.0	58.3
	81.6	83.0		

CONCLUSIONS

Solute–solute displacements between the insulins were found under both gradient and isocratic conditions. Tag-along effects were not seen for the insulins, but were observed between an insulin and the corresponding desamido impurity. This implies that solute–solute displacements probably occur in the majority of preparative protein separations. The gradient slope was demonstrated to have relatively small effects upon the separation between the major components, but did affect the separation between the insulin and its desamido modification.

The influence of particle diameter upon the separation was profound. Reduction in column efficiency by increase in the particle diameter of the packing eliminated the effects of the displacements. This had a major impact upon the purity and recovery of the components and demonstrated that high-efficiency operation is vital where solute–solute displacements are important to the purification.

The most important effect of flow-rate upon the chromatography of insulins was seen in the separation of the "tagged-along" desamidoinsulin, where a low flow rate — *i.e.* a high efficiency — improved the resolution between this and the main component.

The effects of pore diameter upon the loadability indicated that a pore diameter of approximately 150 Å was optimal for the preparative chromatography of insulins.

REFERENCES

1 L. R. Snyder, J. W. Dolan and G. B. Cox, *J. Chromatogr.*, 484 (1989) 437.
2 J.-X. Huang and Cs. Horváth, *J. Chromatogr.*, 406 (1987) 285.
3 G. Subramanian, M. W. Phillips and S. M. Cramer, *J. Chromatogr.*, 439 (1988) 341.
4 Gy. Vigh, Z. Varga-Puchony, G. Szepesi and M. Gazdag, *J. Chromatogr.*, 386 (1987) 353.
5 B. H. Frank, M. J. Beckage and K. A. Willey, *J. Chromatogr.*, 266 (1983) 239.
6 A. U. Parman and J. M. Rideout, *J. Chromatogr.*, 256 (1983) 283.
7 E. P. Kroeff, R. A. Owens, E. L. Campbell, R. D. Johnson and H. I. Marks, *J. Chromatogr.*, 461 (1989) 45.
8 M. A. Quarry, R. L. Grob and L. R. Snyder, *Anal. Chem.*, 58 (1986) 907.
9 G. B. Cox and L. R. Snyder, *J. Chromatogr.*, 590 (1992) 17.
10 G. B. Cox, P. E. Antle and L. R. Snyder, *J. Chromatogr.*, 444 (1988) 325.
11 G. Guiochon and S. Ghodbane, *J. Phys. Chem.*, 92 (1988) 3682.
12 R. M. Nicoud and H. Colin, *LC·GC*, 8 (1991) 24.
13 G. B. Box, L. R. Snyder and J. W. Dolan, *J. Chromatogr.*, 484 (1989) 409.
14 J. H. Knox and H. M. Pyper, *J. Chromatogr.*, 363 (1986) 1.
15 G. B. Cox, in preparation.

Journal of Chromatography, 599 (1992) 205–209
Elsevier Science Publishers B.V., Amsterdam

CHROMSYMP. 2528

Determination of molecular mass distributions of whey protein hydrolysates by high-performance size-exclusion chromatography

Servaas Visser*, Charles J. Slangen and Arjan J. P. M. Robben

Department of Biophysical Chemistry, Netherlands Institute for Dairy Research (NIZO), P.O. Box 20, 6710 BA Ede (Netherlands)

ABSTRACT

Two high-performance size-exclusion chromatographic columns (Superose-12 HR 10/30 and Superdex-75 HR 10/30) were compared for their use in the determination of the molecular mass (M_r) distribution of whey protein hydrolysates. For calibration 21 reference compounds of known M_r (ranging from 500 to 68 000) were used by applying two procedures for least-squares curve fitting. Based on the calibration graphs constructed, three apparent-M_r regions were arbitrarily assigned: M_r(app) <5000, 5000–10 000 and $>10\,000$. Different results for the M_r distributions of the whey protein hydrolysates were obtained with the two columns. This was mainly due to a difference in peak resolution, which was better for the Superdex-75 column in the M_r region relevant for the major whey proteins and their hydrolysates. The results were also dependent on the mode of calibration curve fitting used.

INTRODUCTION

To characterize protein hydrolysates for functional or nutritional (dietetic) purposes, it is often desirable to obtain an impression of the molecular mass (M_r) distribution or average peptide chain length of the constituents in the mixtures. For food applications this criterion is connected with the ability of the constituent peptides to be absorbed in the digestive tract, or with the destruction of antigenic determinants during the hydrolytic degradation of food proteins responsible for allergenic reactions [1–4].

Size-exclusion chromatography, particularly when applied in the high-performance mode (HPSEC), is an attractive procedure for investigating peptide profiles in protein hydrolysates if at the same time the molecular size or approximate M_r distribution therein has to be determined. The accuracy of such a method largely depends on the calibration graph constructed for a series of standards of known M_r; these substances should normally have, as far as possible, the same molecular shape and density as the peptides in the hydrolysate under investigation. Hence, the number and diversity of reference compounds should be large enough to compensate for possible deviations of individual standards from the calibration graph and to allow such a graph to be generally applicable to the characterization of different kinds of hydrolysates.

Some years ago, an HPSEC procedure was applied to the determination of M_r distributions in several sources of plant protein hydrolysates [5]; in that study use was made of a silica-based column packing chemically modified with a glycerylpropylsilyl coating (SynChrom). More recently, two HPSEC columns, the silica-based Protein Pack 125 (Waters Assoc.) and the agarose-type Superose-12 HR 10/30 (Pharmacia/LKB), were tested for their applicability in M_r distribution studies of milk protein hydrolysates [6]. Systematically different M_r values were found with these two columns, which was ascribed to hydrophobic interactions between the solute and the gel matrix.

For the investigation of whey protein hydrolysates, we compared the Superose-12 HR 10/30 column with the recently introduced Superdex-75 HR 10/30 column (Pharmacia/LKB). The gel material

0021-9673/92/$05.00

in either column consists of highly cross-linked agarose beads of average size 13 μm, but with the Superdex-75 having dextran chains (covalently) bound to the agarose. Further, we applied two approaches for least-squares fitting in the construction of calibration graphs.

EXPERIMENTAL

Materials

The standards (see Table I) were of analytical-reagent grade. Whey protein hydrolysates were prepared from whey protein concentrate using food-grade enzymes. In the two examples given the degree of hydrolysis, as determined by the pH-stat method [2], was about 14%.

Analysis

The liquid chromatographic equipment consisted of a Waters M 510 pump, a Gilson Model 231/401 automatic sample injector and a Waters Model 481 UV detector operating at 220 nm (0.2 a.u.f.s.). The equipment was linked to a Waters Maxima 820 data acquisition and processing system. Both columns investigated had identical dimensions (300 × 10 mm I.D.).

The sample and elution buffer consisted of 125 m*M* potassium phosphate–125 m*M* sodium sulphate (pH 6.65). Elution was performed at ambient temperature and at a flow-rate of 0.4 ml min^{-1}. The concentrations of standard solutions ranged from 0.05 to 0.2 mg ml^{-1}; the sample load was 50 μl. In some experiments urea was included in the sample solution at a concentration of 6 *M* (pH 6.65). As urea did not have any influence on the elution patterns of the standards and hydrolysates investigated, further separations were carried out without the use of urea. The system pressure was 100 p.s.i.

Based on the calibration graphs constructed, three apparent-M_r regions were arbitrarily assigned: M_r(app) < 5000, 5000–10 000 and > 10 000.

Least-squares fitting was done using Fig. P software (Biosoft, Cambridge, UK).

TABLE I

MOLECULAR MASSES (M_r) AND ELUTION VOLUMES (V_e) OF THE STANDARDS USED FOR THE CONSTRUCTION OF CALIBRATION GRAPHS

Standard	M_r	V_e [a] (ml)	V_e [b,c] (ml)
Serum albumin	68 000	12.56	9.01
Ovalbumin	43 000	13.45	10.07
β-Lactoglobulin A	36 000	13.95	11.22
Carbonic anhydrase	29 000	14.19	11.25
Chymotrypsinogen A	25 000	14.47	11.59
Soybean trypsin inhibitor	21 000	14.81	12.03
α-Lactalbumin	14 400	14.90	12.61
Lysozyme	14 400	15.74	14.01
Cytochrome *c*	12 500	14.55	12.54
Aprotinin	6512	15.65	14.33
Insulin	5734	17.68	16.39
Insulin B-chain (oxidized)	3496	18.92	17.55
α_{s1}-Casein (f1–23)	2764	16.25	14.98
Insulin A-chain (oxidized)	2532	17.11	15.75
β-Casein (f193–209)	1880	17.90	16.85
Bacitracin	1423	18.91	18.33
Vitamin B_{12}	1355	19.91	19.30
Angiotensin (f2–8, 2-Leu)	888	20.91	20.51
β-Casein (f60–66)	790	20.46	19.99
β-Casein (f60–64)	580	20.92	20.57
β-Casein (f60–63)	523	21.57	21.27

[a] Superose-12 HR 10/30 column.
[b] Superdex-75 HR 10/30 column.
[c] Relative standard deviation = 0.5% (n = 13).

RESULTS AND DISCUSSION

The relationship between molecular size [M_r(app)] and elution volume can be expressed by an exponential function, as represented by Fig. 1 for the 21 standards listed in Table I. The shape of the curve obtained by this "exponential" fitting procedure is largely determined by the experimental data for the higher-M_r compounds (left parts of the curves in Fig. 1). Modern computer facilities allow the easy construction of such exponential calibration graphs and the calculation of M_r(app) values of unknown compounds from such graphs by using the appropriate equations. In Fig. 2 the exponential calibration graphs of Fig. 1 are shown on a logarithmic scale for the Superose-12 and Superdex-75 columns (dashed lines) and compared with the corresponding graphs obtained by the commonly used "logarithmic" procedure (solid lines representing log M_r *vs.* elution volume). Theoretically, for ideally behaving standards, the "exponential" and "logarithmic" procedures should lead to the same results. In the (normal) case of non-ideal behaviour, the logarithmic graph should actually be constructed

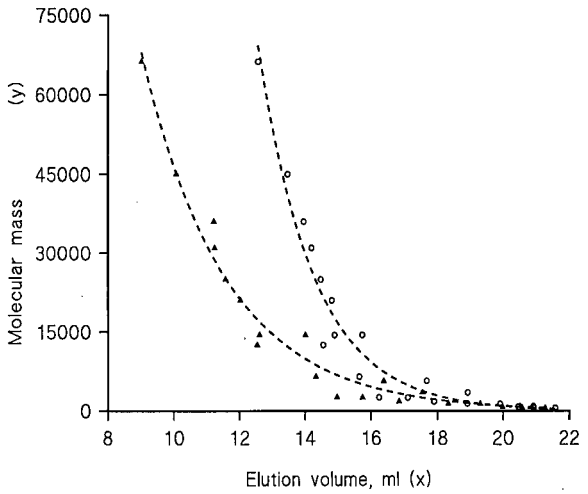

Fig. 1. Exponential curves representing the relationship between molecular mass and elution volume for the 21 standards listed in Table I. (○) Superose-12 HR 10/30; equation: $y = 1.056 \cdot 10^8 \cdot e^{-0.233x}$. (▲) Superdex-75 HR 10/30; equation: $y = 2.194 \cdot 10^6 \cdot e^{-0.154x}$.

by including weighting factors to account for the above-mentioned relative importance of the standards of higher M_r. The fact that such weighting factors are unknown forms an argument for the application of the more direct "exponential" curve-fitting procedure.

As seen in Fig. 2, the calibration graphs constructed for the two columns are significantly different, irrespective of the fitting procedure used.

Applying both curve-fitting procedures we made comparative M_r distribution estimates for several whey protein hydrolysates. Fig. 3 shows a typical example of the separation of one hydrolysate on each of the two columns under the same experimental conditions. In terms of peak resolution in

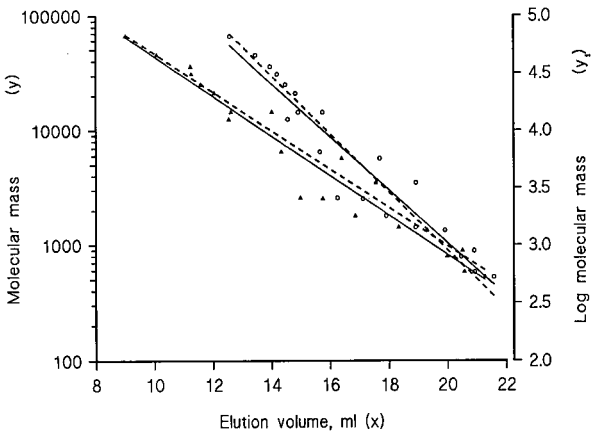

Fig. 2. Linear presentation of the relationship between molecular mass (logarithmic scale) and elution volume for the 21 standards listed in Table I. ○- - -○ = Superose-12 HR 10/30; ▲- - -▲ = Superdex-75 HR 10/30; for the equations of the graphs in their non-linear forms, see the legend of Fig. 1. Comparison with graphs representing log(molecular mass) *vs.* elution volume relationships. ○——○ = Superose-12 HR 10/30; equation: $y_1 = -0.093x + 7.647$. ▲——▲ = Superdex-75 HR 10/30; equation: $y_1 = -0.069x + 6.367$.

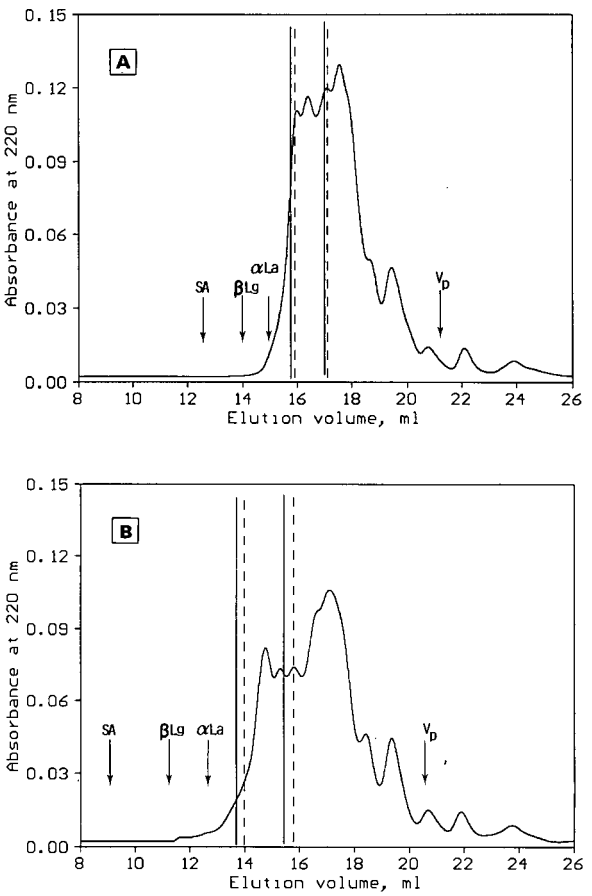

Fig. 3. Peptide profiles of a whey protein hydrolysate (WPH 1 in Table II) fractionated on (A) the Superose-12 HR 10/30 column and (B) the Superdex-75 HR 10/30 column. Positions of the intact whey proteins serum albumin (SA), β-lactoglobulin (βLg) and α-lactalbumin (αLa) and of the column's permeation volume (V_p) are indicated. Vertical lines represent M_r 5000 and 10 000 mass limits as derived from the calibration graphs obtained by "exponential" (dashed lines) and by "logarithmic" (solid lines) curve fitting.

TABLE II

MOLECULAR MASS (M_r) DISTRIBUTION (% OF TOTAL PEAK AREA) OF TWO WHEY PROTEIN HYDROLYSATES, WPH 1 AND WPH 2, AS DETERMINED WITH THE TWO COLUMNS AND BY APPLYING THE EXPONENTIAL AND LOGARITHMIC MODE OF CALIBRATION CURVE FITTING

Sample	Apparent M_r region[a]	Superose-12		Apparent M_r region[a]	Superdex-75	
		Exponential	Logarithmic		Exponential	Logarithmic
WPH 1	a	12	9	a	8	6
	b	29	33	b	25	21
	c	59	59	c	67	73
WPH 2	a	22	18	a	18	16
	b	27	30	b	23	21
	c	52	51	c	59	63

[a] (a) M_r(app) > 10 000; (b) 5000 < M_r(app) < 10 000; (c) M_r(app) < 5000.

the M_r region relevant for the major whey proteins (α-lactalbumin and β-lactoglobulin) and their hydrolysates, the Superdex-75 column is better; this is in line with its recommended M_r fractionation range for globular proteins (3000–70 000) as compared with that of the Superose-12 column (1000–300 000). From Fig. 3 it is also apparent that M_r regions as derived from the two curve-fitting procedures are slightly different (*cf.*, the vertical lines representing the M_r 5000 and 10 000 limits). Consequently, M_r distribution determinations based on these two methods lead to systematic differences in the results (Table II); however, such differences are not necessarily always of practical importance.

By using an elution buffer of elevated ionic strength we have as far as possible circumvented non-size-exclusion effects caused by electrostatic solute–matrix interactions. However, as can be seen for instance in Fig. 3, adsorption effects (probably hydrophobic) could not be fully eliminated. A possible remedy for this could be the inclusion of an organic solvent in the elution buffer or elution under denaturing conditions [5,7–10]. However, such procedures are not always satisfactory; also, the presence of (high concentrations of) denaturing agent, or impurities therein, may interfere with detection at low wavelengths (especially relevant to non-aromatic peptides).

The quantitative aspects of the present calculations are based on the determination of peak areas obtained by absorbance measurements at 220 nm. It should be realized that this method does not take account of differences in absorptivities between the various constituents of the hydrolysates (a drawback which would also have been encountered with detection at any other wavelength). At 220 nm a general underestimation of the low-M_r compounds (peptides and amino acids) can be expected in M_r distribution estimates of this kind. An alternative could be refractive index detection, which, however, has a lower intrinsic sensitivity than detection at 220 nm; moreover, when applied in combination with an elevated ionic strength of the eluent, baseline drift is observed [11].

CONCLUSIONS

In the determination of M_r distributions of whey protein hydrolysates, the Superdex-75 HR 10/30 column shows better resolution than the Superose-12 HR 10/30 column. Generally, by applying the HPSEC procedure, only apparent values for M_r distributions can be expected, which are dependent on the nature of the column and on the mode of calibration curve fitting used. In principle, the "exponential" fitting procedure is better than the commonly used "logarithmic" method in which no weighting factors are employed.

The HPSEC method for M_r distribution determination has its limitations as long as spectrophotometric detection is applied. Nevertheless, the method can be used for comparative purposes.

REFERENCES

1 R. J. Knights, in F. Lifshitz (Editor), *Nutrition for Special Needs in Infancy (Protein Hydrolysates)*, Marcel Dekker, New York, Basle, 1985, Ch. 8, pp. 105–115.
2 J. Adler-Nissen, *Enzymic Hydrolysis of Food Proteins*, Elsevier Applied Science Publ., Barking, New York, 1986.
3 H. Otani, X. Y. Dong and A. Hosono, *Milchwissenschaft*, 45 (1990) 217–220.
4 S. L. Turgeon and S. F. Gauthier, *J. Food Sci.*, 55 (1990) 106–110, 157.
5 H. G. Barth, *Anal. Biochem.*, 124 (1982) 191–200.
6 D. Baylocq, C. Majcherczyk and F. Pellerin, *Analusis*, 17 (1989) 335–340.
7 N. Ui, *J. Chromatogr.*, 215 (1981) 289–294.
8 R. C. Montelaro, M. West and C. J. Issel, *Anal. Biochem.*, 114 (1981) 398–406.
9 W. O. Richter, B. Jacob and P. Schwandt, *Anal. Biochem.*, 133 (1983) 288–291.
10 K. Konishi, in H. Parvez, Y. Kato and S. Parvez (Editors), *Progress in HPLC (Gel Permeation and Ionic Exchange Chromatography of Proteins and Peptides)*, Vol. 1, VNU Science Press, Utrecht, 1985, pp. 43–57.
11 C. Olieman, personal communication.

Journal of Chromatography, 599 (1992) 211–225
Elsevier Science Publishers B.V., Amsterdam

CHROMSYMP. 2553

Prediction of peptide retention time in reversed-phase high-performance liquid chromatography

Claire Chabanet

Station de Biométrie, INRA, 78352 Jouy-en-Josas (France)

Mireille Yvon*

Station de Recherches Laitières, INRA, 78352 Jouy-en-Josas (France)

ABSTRACT

Peptide retention in reversed-phase chromatography depends mainly on the amino acid composition of peptides and can therefore be predicted by summing the relative hydrophobic contributions of each constitutive amino acid residue. The prediction is correct for small peptides but overestimates the retention times of peptides larger than 10–15 residues. A new prediction model is proposed in which the contribution to peptide retention of each amino acid residue is not a constant but a decreasing function of peptide length. From the retention times of 104 peptides, the parameters of decreasing functions were estimated by a non-linear multiple regression analysis. The contribution to peptide retention of charged, polar and non-polar residues appears to be differently affected by peptide length. The secondary structure of most peptides during reversed-phase high-performance liquid chromatography could be responsible for this. The high correlation between the predicted and observed retention times of peptides which were not used to establish the model indicates a good predictive accuracy of the new model.

INTRODUCTION

Several workers [1–3] have reported the advantages of predicting the retention of peptides of known composition in reversed-phase high-performance liquid chromatography (RP-HPLC). Briefly, a knowledge of the retention times of given peptides would simplify their chromatographic separation and purification from complex mixtures. In addition, it would allow one to predict the solubility of peptides in precipitating agents such as trichloroacetic acid or sulphosalicylic acid solutions, as this solubility has been found to be highly correlated with the peptide retention time in RP-HPLC [4]. For preparative applications, such precipitation techniques would allow a first mixture separation before the use of RP-HPLC as the final step of the isolation procedure.

It is now recognized that the retention times of small peptides can generally be predicted by summing the relative hydrophobic contributions of each constitutive amino acid residue. Therefore, retention coefficients for amino acid residues have been determined for different chromatographic systems (mobile phase, stationary phase, pH) using either the retention times of a wide range of peptides of varied composition and length [1,5–10] or the retention time of a synthetic octapeptide model in which two residues were successively substituted by each of the 20 amino acids found in proteins [2].

The retention times of peptides larger than 10–15 residues are less than that predicted by summing the retention coefficients of each constitutive amino acid residue. Several researchers [3,11] have reported an exponential relationship between the observed retention times and the peptide length for a series of peptide polymers. Moreover, Mant *et al.* [3] demonstrated that this exponential relationship varied from one series of peptide polymers to another, depending on their hydrophobicity. They therefore

0021-9673/92/$05.00

introduced a correction factor for peptide retention time prediction, taking into account the hydrophobicity and the length of the peptide [3,12]. Recently, the same group [13] added to their prediction method a further correction factor, to predict the retention behaviour of amphipathic α-helices during reversed-phase chromatography.

Assuming that this chromatographic behaviour for large peptides could be due to a decrease in the accessibility of certain residues or to a removal of certain residues from contact with the stationary phase, we attempted to establish and to test a new model, in which the contribution of each amino acid residue to peptide retention times would not be a constant value but a decreasing function of peptide length, depending on the non-polar, polar or charged nature of the residues.

EXPERIMENTAL

Materials

HPLC-grade acetonitrile was obtained from Baker (Deventer, Netherlands) and trifluoroacetic acid (TFA) from Pierce (Rockford, IL, USA). Water was purified by passage through a Milli-Q water purification system (Millipore, Bedford, MA, USA).

Most of the peptides were obtained by enzymatic (tryptic, chymotryptic, pepsic, plasmic) degradation of milk proteins (α_{s1}-casein, α_{s2}-casein, β-casein, κ-casein, β-lactoglobulin, lactoperoxidase) as described previously [4,14–16]. Other peptides were purchased from Sigma (St. Louis, MO, USA). The origin of the peptides is noted in the tables.

Apparatus

The HPLC instrument consisted of two M510 pumps, a Wisp 710B injector and a Lambda Max M481 spectrophotometer (Waters Assoc., Milford, MA, USA). The system was coupled to a computer equipped with Baseline 810 software (Waters Assoc.).

Chromatographic measurements

Chromatographic measurements were made at room temperature using a Waters μBondapack C_{18} (10 μm) column (250 × 4.6 mm I.D.).

Linear elution was carried out with 0.11% TFA in water and 0.1% TFA in acetonitrile–water (60:40) over a gradient slope of 1.2% acetonitrile/min at a flow-rate of 1 ml/min. The elution was monitored by measuring the absorption at 220 nm.

The retention time was expressed as the acetonitrile concentration in the solvent at the elution time. This was calculated by subtracting the gradient elapsed time from the peak elution time and then multiplying by the percentage of acetonitrile per minute in the linear gradient. The gradient elapsed time (t_g) was previously defined by Guo *et al.* [2] as the time for the gradient to reach the detector from the proportioning valve via the pump, injection system and column. This value was measured as described previously [2].

Establishment of the model

Retention times of the small peptides were recorded and fitted to the linear relationship

$$T_{\mathrm{ret}_i} = \sum_{j=1}^{19} n_{ij} a_j + b_0 + \varepsilon_i \qquad (1)$$

where

n_{ij} = number of amino acid residues j in peptide i;
a_j = retention coefficient for residue j;
b_0 = retention coefficient for α-NH_2 and α-COOH terminal functions;
ε_i = independent errors which are assumed to be normally distributed, with the same variance.

In order to simulate a decrease in the contribution of residues in larger peptides, we considered a new model in which the contribution of each residue to peptide retention time (A_j) is a decreasing function of peptide length (l_i). The decreasing function was chosen to have a slope equal to zero when $l_i = 0$, an inflection point and a lower asymptote:

$$T_{\mathrm{ret}_i} = \sum_{j=1}^{19} n_{ij} A_j(l_i) + b_0 + \varepsilon_i \qquad (2)$$

where

$A_j(l) = (a_j - I_j)\mathrm{e}^{-b_j l^2} + I_j$
$I_j = a_j/k_j$

In small peptides the contribution of each residue (A_j) is close to a_j (the retention coefficient for residue j). In very long peptides this contribution is I_j (lower asymptote) which, is proportional to a_j ($I_j = a_j/k_j$).

The b_j parameter of the function sets the curve slope.

From this general model, two sub-models were considered. In the first, assuming that the peptide chain length effects may be the same on all residues, we imposed k_j and b_j to be similar for all residues. In the second, we assumed the decrease in the contribution of residues to be dependent on the amino acid residue considered. This model thus consisted of nineteen functions and each of them contained three parameters, a_j, b_j and k_j. Therefore, 58 ($19 \times 3 + b_0$) parameters had to be estimated. It was impossible to estimate as many parameters from the 104 observed data. In order to decrease the number of parameters, three groups of amino acid residues were formed: Gly, Ala, Val, Met, Ile, Leu, Phe, Trp were considered as non-polar residues, Asp, Asn, Thr, Ser, Glu, Gln, Pro, Tyr, His as polar residues and Lys and Arg as charged residues. Based on the accessibility of residues in proteins [17,18], the same k_j was imposed for all residues in the same group (which means that the same proportion of the residues surface area was assumed to be accessible in proteins) and for each group the decreasing function $A_j(l_i)$ was supposed to have the same shape (same b_j).

Therefore, the retention times of the total peptides were recorded and fitted to eqn. 2 where:

in model 1:

$$A_j(l) = (a_j - I_j)e^{-bl^2} + I_j \quad \text{for all residues}$$
$$I_j = a_j/k$$

and in model 2:

$$A_j(l) = (a_j - I_j)e^{-b_1 l^2} + I_j \quad \text{for non-polar residues}$$
$$I_j = a_j/k_1$$

$$A_j(l) = (a_j - I_j)e^{-b_2 l^2} + I_j \quad \text{for polar residues}$$
$$I_j = a_j/k_2$$

$$A_j(l) = (a_j - I_j)e^{-b_3 l^2} + I_j \quad \text{for charged residues}$$
$$I_j = a_j/k_3$$

A non-linear multiple regression analysis was done to estimate $a_j(19)$, b_0, b, k of the first model and $a_j(19)$, b_0, b_1, b_2, b_3, k_1, k_2, k_3 of the second model using the maximum-likelihood method and the statistical package "NL" [19].

RESULTS AND DISCUSSION

Retention behaviour of peptides

The retention times of 104 peptides tested are listed in Table I. We used peptides of different length and composition so that all residues often enough appear to permit an accurate determination of their contribution to peptide retention time according to the peptide length.

TABLE I

OBSERVED AND PREDICTED RETENTION TIMES OF PEPTIDES USED TO ESTABLISH THE MODEL

The retention times were predicted using eqn. 2 with the parameter values in Table II.

Peptide	Sequence	No. of residues	t_R observed [CH_3CN (%)]	t_R predicted [CH_3CN(%)]	
				Model 1	Model 2
1[a]	Y	1	0.2	0.6	0.9
2[a]	F	1	2.1	4.7	3.4
3[a]	W	1	7.3	6.4	5.4
4[a]	FA	2	2.5	4.1	3.1
5[a]	YA	2	0.2	0	0.4
6[a]	FG	2	2.9	4.8	3.9
7[a]	FY	2	8.4	8.7	9.3
8[a]	LV	2	3.0	4.5	3.8
9[a]	SY	2	1.3	1.3	1.8
10[a]	YV	2	2.8	2.7	3.2
11[a]	WG	2	6.2	6.4	5.8
12[a]	LL	2	8.5	8.4	7.7
13[a]	LY	2	5.8	6.5	7.2
14[a]	HF	2	3.8	3.3	2.2

(*Continued on p. 214*)

TABLE I (*continued*)

Peptide	Sequence	No. of residues	t_R observed [CH_3CN (%)]	t_R predicted [CH_3CN(%)]	
				Model 1	Model 2
15[a]	MP	2	6.5	3.9	3.7
16[a]	LP	2	4.9	4.7	4.7
17[a]	LF	2	12.1	10.6	9.8
18[a]	TL	2	1.7	2.8	1.9
19[a]	WA	2	5.6	5.7	5.1
20[a]	LM	2	4.8	7.6	6.7
21[a]	LW	2	13.8	12.2	11.8
22[a]	WE	2	5.2	6.9	6.3
23[a]	WGG	3	5.0	6.5	6.3
24[a]	YVG	3	6.4	2.7	3.5
25[a]	YYL	3	14.2	10.5	12.6
26[a]	IPI	3	10.8	9.7	9.7
27[a]	FGG	3	2.3	4.8	4.3
28[a]	MLF	3	18.8	15.5	15.2
29[a]	MLG	3	4.7	7.6	7.2
30[a]	LLL	3	17.0	14.1	14.0
31[a]	EPM	3	3.4	4.4	4.5
32	LRF	3	13.9	11.3	10.8
33	YQL	3	9.4	6.8	7.9
34	RFF	3	14.3	13.5	12.9
35[a]	FGFG	4	14.7	15.5	12.7
36	LQSW	4	12.0	12.9	13.5
37	FRQF	4	12.4	13.6	13.7
38	RQFY	4	9.6	9.7	10.6
39	HIQK	4	0.9	0.4	0.2
40	HPIK	4	1.8	2.3	2.4
41[a]	YGGFL	5	17.8	15.7	15.4
42	LHSMK	5	4.7	6.1	6.2
43	RLKKY	5	5.3	6.0	6.7
44[a]	WHWLQL	6	27.4	25.6	27.4
45	VNELSK	6	4.4	5.8	5.6
46	EAMAPK	6	2.2	2.5	2.8
47	EMPFPK	6	12.5	13.6	14.2
48	TTMPLW	6	22.1	19.2	20.0
49[a]	MEHFRWG	7	18.4	18.4	19.4
50[a]	YPFPGPI	7	21.6	19.7	20.3
51	VLPVPQK	7	9.8	10.2	11.0
52	DMPIQAF	7	17.8	14.4	16.7
53	GPFPIIV	7	24.3	20.8	21.6
54	AVPYPQR	7	7.3	7.1	7.7
55	EDVPSER	7	3.9	2.7	3.0
56	EKVNELSK	8	5.9	5.4	5.3
57	DAYPSGAW	8	13.0	10.7	11.4
58	KKYKVPQL	8	14.0	8.5	9.2
59	YVPLGTQY	8	13.6	14.2	14.4
60	VAPFPQVF	8	21.3	19.2	20.2
61	LGYLEQLL	8	22.3	23.1	24.2
62	EGIHAQQK	8	3.2	0.5	1.5
63	YYVPLGTQY	9	15.7	17.5	16.6
64[a]	PHPFHFFVYK	10	22.3	24.6	25.1
65	QLDAYPSGAW	10	15.3	15.6	16.0

TABLE I (*continued*)

Peptide	Sequence	No. of residues	t_R observed [CH_3CN (%)]	t_R predicted [CH_3CN(%)]	
				Model 1	Model 2
66	YLGYLEQLLR	10	27.7	26.3	26.4
67	QLDAYPSGAWY	10	16.6	18.6	17.9
68	SLSQSKVLPVPE	12	14.7	12.8	15.1
69	FFVAPFPQVFGK	12	29.8	30.4	31.3
70	QLDAYPSGAWYY	12	18.3	21.4	19.5
71	QFYQLDAYPSGAW	13	23.8	24.2	23.3
72	RPKHPIKHQGLPQE	14	9.0	9.6	9.9
73	VPQLEIVPNSAEER	14	15.4	15.4	14.4
74	AVPYPQRDMPIQAF	14	18.8	20.2	19.3
75	HQGLPQEVLNENLLR	15	20.8	20.5	20.8
76	YYVPLGTQYTDAPSF	15	20.3	22.2	19.0
77	FQSEEQQQTEDELQDK	16	8.1	8.9	9.4
78	YKVPQLEIVPNSAEER	16	17.7	16.8	15.1
79	YQEPVLGPVRGPFPIIV	17	28.9	29.3	28.4
80	LYQEPVLGPVRGPFPIIV	18	29.7	32.2	31.7
81	LLYQEPVLGPVRGPFPIIV	19	31.2	34.8	34.6
82	LTLTDVENLHLPLPLLQSW	19	32.0	35.7	36.3
83	EPMIGVNQELAYFYPELFR	19	30.7	34.1	32.6
84	RPKHPIKHQGLPQEVLNENL	20	18.8	17.6	17.8
85	SDIPNPIGSENSEKTTMPLW	20	22.6	24.3	22.7
86	RPKHPIKHQGLPQEVLNENLLRF	23	25.9	23.8	24.6
87	RPKHPIKHQGLPQEVLNENLLRFF	24	27.6	27.2	27.9
88	TDAPSFSDIPNPIGSENSEKTTMPLW	26	23.9	23.9	23.0
89	SLSQSKVLPVPQKAVPYPQRDMPIQA	26	19.2	19.6	20.7
90	SLSQSKVLPVPQKAVPYPQRDMPIQAF	27	22.8	22.8	23.8
91	SLSQSKVLPVPQKAVPYPQRDMPIQAFL	28	26.1	24.7	25.7
92	SLPQNIPPLTQTPVVVPPFLQPEVMGVSK	29	30.0	26.9	27.0
93	YYVPLGTQYTDAPSFSDIPNPIGSENSEK	29	23.1	20.9	21.4
94	YPVEPFTESQSLTLTDVENLHLPLPLPLLQSW	30	34.9	32.3	31.7
95	YVPLGTQYTDAPSFSDIPNPIGSENSEKTTMPLW	34	25.7	25.4	25.8
96	YYVPLGTQYTDAPSFSDIPNPIGSENSEKTTMPLW	35	28.8	26.3	27.1
97	LQPEVMGVSKVKEAMAPKHKEMPFPKYPVQPFTESQS	37	21.4	20.1	20.8
98	KVPQLEIVPNSAEERLHSMKEGIHAQQKEPMIGVNQEL	38	19.9	18.7	18.4
99	KVPQLEIVPNSAEERLHSMKEGIHAQQKEPMIG VNQELAYF	41	21.6	21.8	21.2
100	KVPQLEIVPNSAEERLHSMKEGIHAQQKEPMIGVN QELAYFYPELF	46	28.4	27.6	26.6
101	QFYQLDAYPSGAWYYVPLGTQYTDAPSFSDIPNPI GSENSEK	42	28.5	26.7	29.5
102	IHPFAQTQSLVYPFPGPIPNSLPQNIPPLTQTPVVVPPFLQ PEVMGVSK	49	32.7	35.2	34.8
103	YPVEPFTESQSLTLTDVENLHLPLPLLQSWMHQPHQPL PPTVMFPPQSVLSLSQSK	56	37.6	40.3	37.9
104	MAIPPKKNQDKTEIPTINTIASGEPTSTPTIEAVESTVAT LEASPEVIESPPEINTVQVTSTAV	64	25.4	25.4	26.6

[a] Peptides purchased from Sigma. The other peptides were obtained by enzymatic degradation of α_{s1}-, β- and κ-caseins [4].

Calculation of retention parameters

The retention coefficients for amino acid residues (a_j) were first determined from retention times of small peptides containing either up to ten residues (67 peptides) or up to seven residues (55 peptides) using the linear eqn. 1. Retention coefficients could not be calculated from retention times of peptides smaller than six residues because some residues did not appear. The correlation between observed and predicted retention times was much better with the retention times calculated by summing the coefficients determined with peptides containing up to seven residues. Moreover, all but two coefficients were estimated with a better precision although the sample was smaller. These results indicate that the linear model is no longer satisfactory for peptides containing more than seven residues. The same observation was previously made by Mant *et al.* [3], who reported observed retention times less than those expected from the sum of the retention coefficients of each constitutive residue for some ten-residue peptides.

From the retention times of all peptides and using the new model 1 of retention time prediction (eqn. 2), the 22 parameters ($19a_j + b_0 + b + k$) of the function were determined simultaneously. Using model 2 it was impossible to estimate all the parameters of the function together and therefore some parameters had to be set. Because only two residues are charged and their retention coefficients are small, we chose to set a parameter for this group. Taking into account that about 50% of their surface area remains accessible in proteins [17], I_j for charged residues was set to $a_j/2$ and the other parameters were calculated. The k_1 and k_2 values were calculated to be 4.9 and 2.9, respectively. I_j was thus approximated and set to $a_j/5$ for non-polar, $a_j/3$ for polar and $a_j/2$ for charged residues and the other parameters, $a_j(19)$, b_1, b_2 and b_3, were re-calculated. It was found that b_3 was not significantly different from zero and the sub-model with $b_3 = 0$ was accepted using the likelihood ratio test. This indicated that the contribution of a charged residue to the peptide retention time was not significantly dependent on the peptide length. Hence the contribution to the peptide retention time of charged residues [$A_j(l)$] was set equal to a_j and $k_3 = 2$ had no meaning.

The calculated parameters of both models and the retention coefficients determined with the linear model and the small peptides are listed in Table II.

Comparison and validity of the two new models

As neither model 1 or 2 was a sub-model of the other, they could not be compared by the likelihood ratio test and therefore four criteria were used to compare and to evaluate them.

(1) Comparison of the calculated retention coefficients for amino acid residues (a_j) with those determined with small peptides. The retention coefficients (a_j) calculated with both new models were well related with those determined with the linear model and the small peptides ($\leqslant 7$ residues) (Fig. 1). However, the sum of squares of differences between the calculated coefficients was the least with the second model (13.46 against 14.6). The a_j values determined with the second model are slightly higher than those obtained with the first model, especially for polar residues, whereas the b_0 value was much smaller.

(2) Relationship between predicted and observed retention times. The retention times calculated with both new models were plotted against the observed retention times for the 104 peptides used to establish the model (Fig. 2). A high correlation was observed in both instances; the coefficients were 0.98 and 0.99 for models 1 and 2, respectively.

(3) The likelihood. The parameters of both models were calculated by using the maximum likelihood method. For a similar number of calculated parameters (degrees of freedom = 89) the likelihood was higher for model 2 [-2 log (likelihood) = 433 and 460.7 for models 2 and 1, respectively].

(4) Structure of reduced residuals. The reduced residuals (difference between observed and calculated retention times of peptide i divided by the estimated standard error) must be randomly distributed around zero.

With both models the plot of reduced residuals *versus* calculated retention time did not have any structure but a structure was observed in the plot of reduced residuals *versus* peptide length with the first model (Fig. 3).

With this first model, depending on the peptide chain length, the predicted retention time was either underestimated (for peptides containing between four and ten residues and those containing over twenty residues) or overestimated (for very short

TABLE II

RETENTION COEFFICIENTS OF AMINO ACID RESIDUES (a_j) AND PARAMETERS OF THE FUNCTION $A_j(l)$

The retention coefficients [CH_3CN (%)] were predicted either (1) from retention times of small peptides ($\leqslant 7$ residues) and from eqn. 1, or (2) from retention times of all peptides and from eqn. 2 with model 1 or (3) from retention times of all peptides and from eqn. 2 with model 2. The numbers in parentheses represent the number of amino acids used for each calculation and S.E. is the estimated standard error.

Amino acid residue and parameter		Retention coefficient					
		1		2		3	
		a_j	S.E.	a_j	S.E.	a_j	S.E.
	Trp	10.24	0.56 (11)	9.81	0.65 (25)	10.64	0.59 (25)
	Phe	8.81	0.43 (22)	8.15	0.39 (64)	8.65	0.35 (64)
	Leu	6.91	0.33 (27)	5.93	0.30 (134)	6.51	0.29 (134)
	Tyr	5.45	0.45 (16)	4.10	0.38 (71)	6.16	0.49 (71)
	Ile	6.16	0.52 (11)	5.50	0.53 (63)	5.90	0.46 (63)
	Met	5.15	0.58 (11)	5.13	0.67 (35)	5.54	0.60 (35)
	Pro	2.39	0.36 (21)	2.26	0.38 (178)	3.58	0.41 (178)
	Val	2.55	0.57 (9)	2.03	0.51 (91)	2.56	0.43 (91)
	Ser	0.58	0.77 (5)	0.64	0.52 (85)	1.14	0.65 (85)
	Gln	−0.41	0.64 (8)	0.30	0.43 (102)	1.11	0.50 (102)
	Arg	0.74	0.60 (9)	0.84	0.63 (30)	1.06	0.44 (30)
	Glu	0.24	0.56 (12)	0.56	0.40 (94)	1.03	0.48 (94)
	Asn	−1.10	1.14 (2)	1.02	0.79 (43)	1.03	0.97 (43)
	Thr	0.73	0.69 (3)	0.31	0.47 (55)	0.65	0.50 (55)
	Gly	−0.05	0.37 (15)	0.12	0.41 (63)	0.50	0.36 (63)
	Asp	1.30	1.25 (2)	−0.40	0.97 (32)	0.31	1.21 (32)
	Lys	−1.35	0.41 (18)	−0.55	0.39 (70)	−0.18	0.26 (70)
	Ala	−0.39	0.55 (7)	−0.61	0.46 (57)	−0.27	0.42 (57)
	His	−0.96	0.69 (6)	−1.35	0.60 (31)	−1.24	0.74 (31)
α-Amino + α-COOH	b_0	−4.66	0.49 (55)	−3.45	0.55 (104)	−5.25	0.48 (104)
	b_1	–	–	0.0019	0.0001	0.0017	0.0001
	b_2	–	–	0.0019	0.0001	0.0136	0.0028
	b_3	–	–	0.0019	0.0001	0	
	k_1	–	–	3.11	0.13	5	
	k_2	–	–	3.11	0.13	3	
	k_3	–	–	3.11	0.13	2	

peptides with less than three residues and those containing between ten and twenty residues). Such a structure did not exist with the second model.

All the criteria and especially the structure of reduced residuals *versus* peptide length indicate that the second model was slightly better than the first. Consequently, the peptide retention time prediction was improved by considering three groups of amino acid residues with their contributions following different functions of peptide length. However, from these data, the first model cannot be ruled out categorically.

On the other hand, in the second model three groups of amino acids may not be enough and the amino acids distribution in the different groups may not be accurately chosen, but we would need much more data to be able to estimate the b_j *and* k_j parameters for each residue.

Contribution of residues to peptide retention times as a function of peptide length $A_j(l)$

Model 1. With this model, the contribution of all residues to peptide retention times followed the same relationship:

$$A_j(l) = (a_j - I_j)e^{-0.0019l^2} + I_j$$
$$I_j = a_j/3.11$$

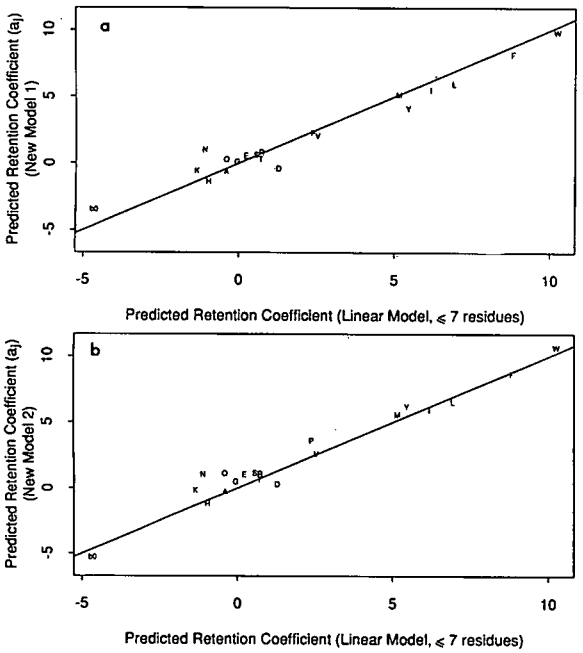

Fig. 1. Comparison of the sets of predicted retention coefficients for amino acid residues (Table I). (a) Relationship between the set determined with all peptides and model 1, and that determined with eqn. 1 and small peptides ($\leqslant 7$ residues). (b) Relationship between the set determined with all peptides and model 2, and that determined with eqn. 1 and small peptides ($\leqslant 7$ residues).

(Fig. 4a). It mainly decreased when the peptide length increased from 7 to about 30 residues.

Model 2. The contribution of non-polar residues to peptide retention times followed the relationship

$$A_j(l) = (a_j - I_j)e^{-0.0017l^2} + I_j$$
$$I_j = a_j/5$$

(Fig. 4b), that of polar residues the relationship

$$A_j(l) = (a_j - I_j)e^{-0.014l^2} + I_j$$
$$I_j = a_j/3$$

(Fig. 4c) and that of charged residues

$$A_j(l) = a_j$$

(Fig. 4d).

The contribution of the residues to peptide retention time decreased rapidly when the peptide length increased, especially for polar residues. In a pentapeptide the contribution of polar residues would be lower than in a dipeptide. These results could explain why the retention coefficients for polar

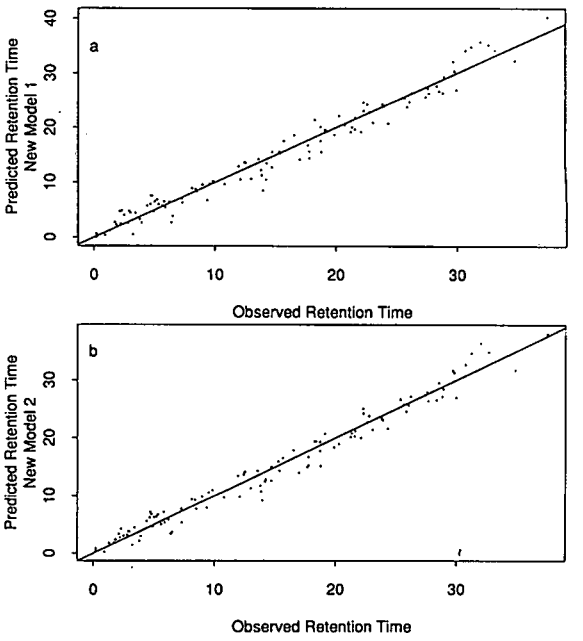

Fig. 2. Relationship between observed retention times of peptides used to establish the model and their predicted retention times (Table I) using (a) model 1 and (b) model 2. The correlation coefficients are 0.98 and 0.99, respectively.

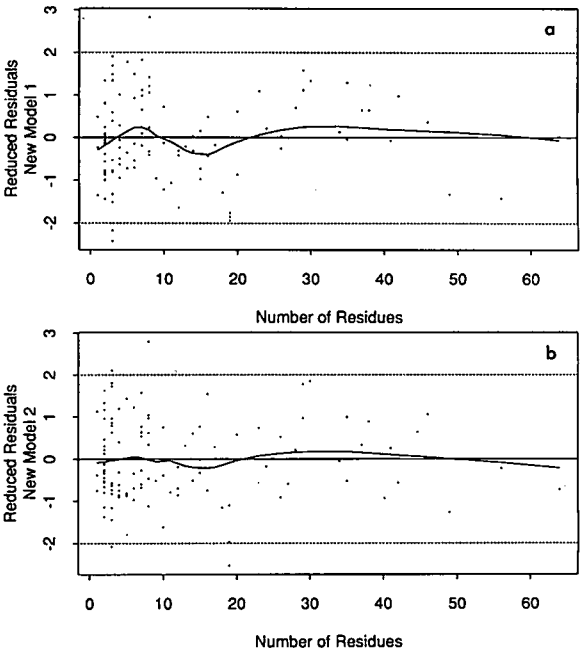

Fig. 3. Plots of the reduced residuals (difference between the observed and predicted retention times divided by the estimated standard error) *versus* peptide length, (a) with model 1 and (b) with model 2.

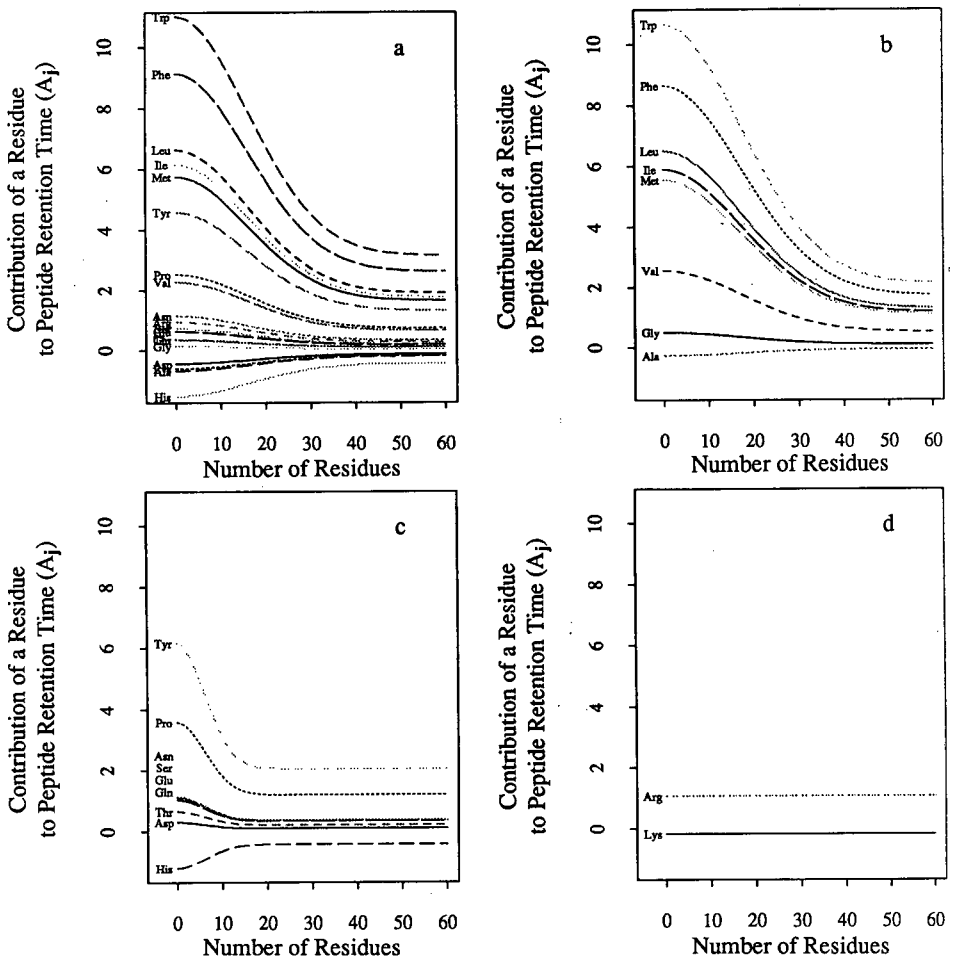

Fig. 4. Plots of predicted residue contribution (A_j) *versus* peptide length (l). (a) In model 1, for all residues the relationship is

$$A_j(l) = \left(a_j - \frac{a_j}{3.11}\right)e^{-0.0019l^2} + \frac{a_j}{3.11}$$

(b) In model 2, for non-polar residues the relationship is

$$A_j(l) = \left(a_j - \frac{a_j}{5}\right)e^{-0.0017l^2} + \frac{a_j}{5}$$

(c) In model 2, for polar residues the relationship is

$$A_j(l) = \left(a_j - \frac{a_j}{3}\right)e^{-0.014l^2} + \frac{a_j}{3}$$

(d) In model 2, for charged residues the relationship is

$$A_j(l) = a_j$$

residues predicted with the linear model from small peptides (less than seven residues) were slightly smaller than the a_j of the new model 2 (Fig. 1).

Our a_j values were compared with retention constants determined by other workers using chromatographic conditions close to ours (C_{18} column and aqueous TFA as the mobile phase and acetonitrile as the mobile phase modifier in a linear gradient elution system). With the weighted fit retention constants determined by Sasagawa *et al.* [1] (Fig. 5), the correlations were good (0.93 and 0.94 for models 1 and 2, respectively) and were better than that found with the non-weighted constants. The retention constants obtained using weighted analysis probably reflect more realistic constants than those obtained using non-weighted analysis because information on the conformation of large peptides was incorporated in the analysis.

The correlation between the a_j values of model 2 and the retention coefficients determined by Guo *et al.* [2] was poor. But as they used an octapeptide

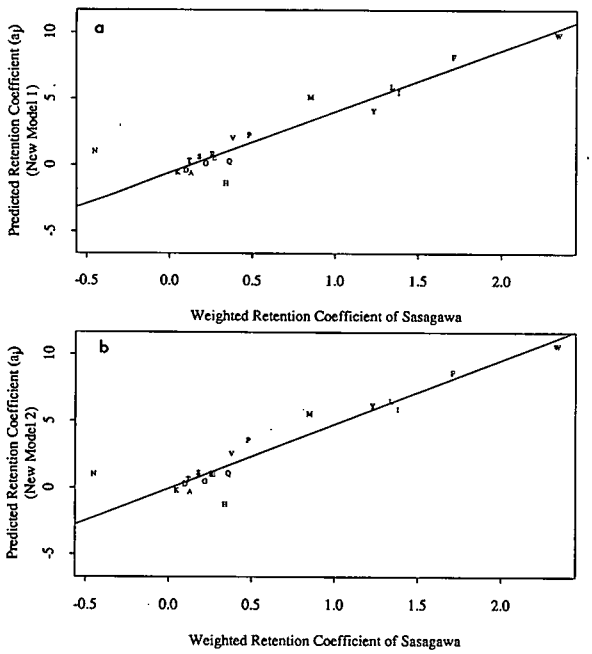

Fig. 5. Relationship between Sasagawa *et al.*'s retention constants for amino acid residues calculated by weighted curve fitting [1] and our retention coefficients (a_j) predicted by (a) model 1 (correlation coefficient 0.93) and (b) model 2 (correlation coefficient 0.94).

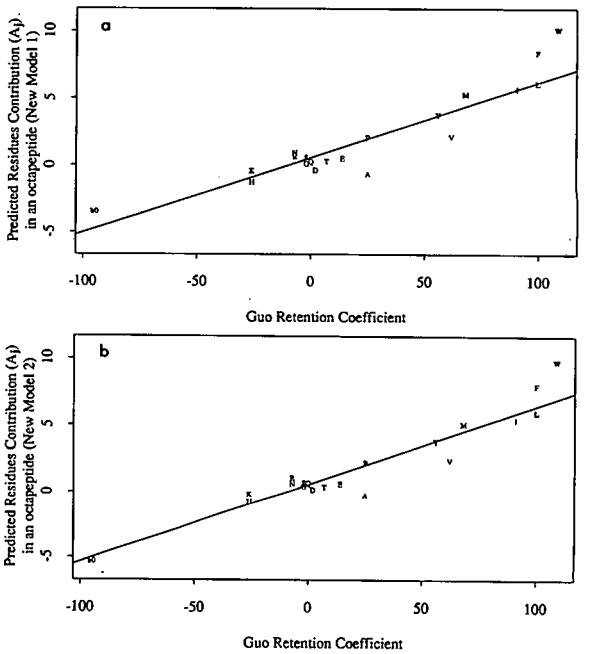

Fig. 6. Relationship between Guo *et al.*'s retention constants for amino acid residues obtained from synthetic octapeptides [2] and our values of residue contributions (A_j) in an eight-residue peptide. (These contributions were calculated with the equations in Fig. 4.)

model for the determination, their retention coefficients were compared with our predicted residues contributions in an eight-residue peptide (Fig. 6). These residue contributions were calculated using the functions $A_j(l)$ established for the three groups of amino acid residues with $l = 8$. The correlation was good (0.94) even though slight differences were found for four non-polar residues (Ala, Val, Phe and Trp). Similar discrepancies were observed with model 1 with the correlation being slightly lower (0.93). These differences might be due to the different column packing material used (we used μBondapack C_{18} instead of Synchropack C_{18}), especially for Ala and Val, as the constants determined by Sasagawa *et al.* [1], who used a μBondapack column, were similar to ours. Another possible explanation is that we imposed a similar function $A_j(l)$ for all non-polar residues and this function could be slightly different for each of them.

The calculated retention coefficient for His agreed with that calculated from the linear model and with

Guo *et al.*'s and Sasagawa *et al.*'s constants, although it was considered as a polar residue, whereas it could have been considered as a charged residue under our chromatographic conditions.

In the first model we assumed that whatever the peptide chain length, every residue contributed equally to the overall peptide hydrophobicity. Hence this model looks like the prediction method developed by Mant and co-workers [3,12] and suggested that the main peptide length effect is due to a decrease in the proportion of the peptide which binds to the stationary phase at any time and that there is no specific portion of the polypeptide chain interacting with the stationary phase. However, the structure of reduced residuals *versus* peptide length suggested that this model had a "bias", which means that, depending on the peptide length, the predicted retention time was either underestimated or overestimated. Although the interpretation of this feature is not easy, we can suggest an explanation. With this model, most of the a_j values were slightly lower than those obtained with the small peptides and with the second model. Therefore, generally, peptide retention was underestimated except for peptides containing between 7 and 25 residues. For these peptides the overestimation was probably due to an overestimation of the proportion of polar residues contributing to peptide retention (Fig. 4a and c). This high proportion was related to the low b value (model 1), which was due to the constraint $b_1 = b_2 = b_3$, and hence it seems that the peptide length affected the contributions of polar and non-polar residues differently.

In the second model, we assumed the effect of the peptide length on the contribution of residues to the peptide retention times to be dependent on the nature of the amino acid residues. This could be due to conformational constraints which removed certain residues from contact with the stationary phase or which led to a decrease in the accessibility of residues.

The b_j parameter of the function $A_j(l)$ sets the curve slope. The calculated b value for polar residues (b_2) was significantly higher than that for non-polar residues (b_1) as the sub-model with $b_1 = b_2$ (and with $k_1 = 5, k_2 = 3, k_3 = 2$) was rejected using the likelihood ratio test. The curve patterns (Fig. 4b and c) indicate that the decrease in the contribution of polar residues occurred mainly when the peptide length increased from 2 to 20 residues and thus could be due to the secondary structure, whereas the contribution of non-polar residues mainly decreased when the peptide length increased from 10 to 60 residues.

An explanation for the decrease in the contribution of polar residues to the peptide retention time during the formation of the secondary structure was proposed by Zhou *et al.* [13]. They showed that the formation of an amphipathic α-helix results in a preferred binding domain which is non-polar. Hence the polar residues which are not in the preferred binding domain would contribute less to peptide retention. For a peptide series having an α-helical structure with hydrophobic residues almost equally distributed on both sides of the helix, only a slight discrepancy between the observed and predicted [13] peptide retention time was observed. We cannot say that all peptides used in our study can form an amphipathic α-helix, but as the hydrophobicity of the column can induce secondary structures, most of them could adopt a structure (helical or other) on binding, leading to a preferred binding domain which would be the most non-polar but would not include all the non-polar residues. This could explain why the decrease in the non-polar residue contribution was lower than that of polar residues during the formation of the secondary structure.

With this model, the calculated residue contribution in a very large peptide (I_j) was in good agreement with the accessibility of residues in proteins determined by Chotia [17]: for non-polar residues, the average proportion of the residue surface area that remains accessible in proteins is 15.6%, for polar residues it is 33% and for charged residues 50%. This seems to indicate that the accessibility of residues in large peptides during RP-HPLC was close to that observed in proteins. However, imposing the k_j value to be similar for all residues ($k_1 = k_2 = k_3$), but $b_1 \neq b_2 \neq b_3$, led to a model almost as good as the previous one, without a structure of reduced residuals. In this model the k_j value was calculated between k_1 and k_2 values (4.05) and b_j and a_j values very close to those determined with the previous model ($b_1 = 0.0016, b_2 = 0.0130$ and b_3 close to 0). Moreover, as it has been demonstrated that RP-HPLC is a strong denaturant of tertiary and quaternary structures [11] of proteins and polypeptides, it is extremely difficult to argue

TABLE III

COMPARISON OF PREDICTED AND OBSERVED RETENTION TIMES OF 47 PEPTIDES NOT USED TO ESTABLISH THE MODEL

Retention times were predicted using eqn. 2 and model 2 with the parameter values in Table II (3).

Peptide	Sequence	No. of residues	t_R predicted [CH_3CN(%)]	t_R observed [CH_3CN(%)]	Error [CH_3CN(%)]
1[a]	VP	2	0.8	1.1	−0.3
2[a]	VW	2	7.9	8.9	−1.0
3[a]	GF	2	3.9	3.3	0.6
4[a]	FR	2	4.4	1.6	2.8
5[a]	GW	2	5.8	6.8	−1.0
6[a]	YL	2	7.2	6.1	1.1
7[a]	VA	2	−3.0	0	–
8[a]	KY	2	0.5	0.1	0.4
9[a]	VY	2	3.2	2.1	1.1
10[a]	GR	2	−3.7	0	–
11[a]	VS	2	−1.6	0	–
12[a]	GY	2	1.2	0.5	0.7
13[a]	VD	2	−2.4	0	–
14[a]	GWG	3	6.3	5.8	0.5
15[a]	VGG	3	−1.7	0	–
16[a]	GFG	3	4.3	3.0	1.3
17[a]	EVF	3	6.8	8.6	−1.8
18[a]	GHG	3	−5.4	0	–
19[a]	ETY	3	2.0	2.7	−0.7
20[a]	GPGG	4	−0.7	0	–
21[a]	PFGK	4	6.6	4.1	2.5
22[a]	MRFA	4	9.5	9.8	−0.3
23	SLLFM	5	22.0	20.0	2.0
24	VAGTWY	6	12.6	14.3	−1.7
25	ALPMHIR	7	14.0	13.0	1.0
26	TKIPAVFK	8	12.5	14.8	−2.3
27[a]	RGFFYTPKA	9	17.2	16.4	0.8
28[a]	RPPGFSPFR	9	19.5	16.3	3.2
29[a]	DRVYIHPFHL	10	20.4	20.9	−0.5
30	VLVLDTDYKK	10	14.1	13.9	0.2
31	TKVIPYVRYL	10	19.4	20.9	−1.5
32[a]	RPKPQQFFGLM	11	25.5	22.4	3.1
33[a]	ELYENKPRRPYIL	13	20.9	19.3	1.6
34	TPEVDDEALEKFDK	14	11.1	16.3	−5.2
35	IVGYLDEEGVLDQNR	15	18.6	16.1	2.5
36	WLPAEYEDGLALPFGWTQR	19	33.6	28.1	5.5
37	AMKPWIQPKTKVIPYVRYL	19	28.8	23.6	5.2
38	SLAMAASDISLLDAQSAPLR	20	21.2	23.7	−2.5
39	VYVEELKPTPEGDLEILLQK	20	23.9	25.4	−1.5
40	DLYKTPDNIDIWIGGNAEPM	20	25.5	23.4	2.1
41	KNTMEHVSSSEESIISQETYKQEK	24	11.1	14.4	−3.3
42	EQINAVTSFLDASLVYGSEPSLASR	25	21.5	29.3	−7.8
43	TVYQHQKAMKPWIQPKTKVIPYVRYL	26	25.3	22.6	2.7
44[a]	HSQGTFTSDYSKYLDSRRAQDFVQWLMNT	29	23.9	22.0	1.9
45	QKWIPPYQGYRNSVDPRISNVFTFAFRFGHM	31	32.3	30.1	2.2
46	NAVPITPTLNREQLSTSEENSKKTVDMESTEVFTKK	36	15.4	17.4	−2.0
47	KTKLTEEEKNRLNFLKKISQRYQKFALPQYLKTVYQH QKAMKPWIQPKTKVIPYVRYL	58	35.5	29.6	5.9

[a] Peptides purchased from Sigma. The other peptides were obtained by enzymatic or chemical (CNBr) degradation of α_{S2}-casein [14], β-lactoglobulin [15] and lactoperoxidase [16].

that the tertiary structure of peptides explains our results concerning both the I_j values and the decrease in the contribution of non-polar amino acid residues when the peptide length increases from 10 to 60 residues.

Accuracy of peptide retention prediction

The value of a predictive method must be assessed by its accuracy in predicting the retention times of peptides that were not used to determine the model. Therefore, model 2 was applied to predict the retention times of 47 peptides (Table III). These peptides were of various origins and their length varied from 2 to 58 residues. They were chromatographed under the conditions used to establish the model. As expected, several peptides predicted to have negative retention times had an observed retention time of zero. The predicted retention times were plotted against the observed retention times (Fig. 7). The relationship was linear with a correlation coefficient of 0.97.

We also used our model for predicting the retention times of peptides tested under chromatographic conditions close to ours (same stationary and mobile phases) by Sasagawa *et al.* [1] (Table IV). The correlation between their observed retention times and our predicted retention times for 71 peptides was 0.93 (Fig. 8). We only tested 71 peptides out of the 100 used by Sasagawa *et al.* because the others contained aminoethylcysteine, carboxymethylcysteine and trimethyllysine residues, for which we had not calculated the retention coefficients.

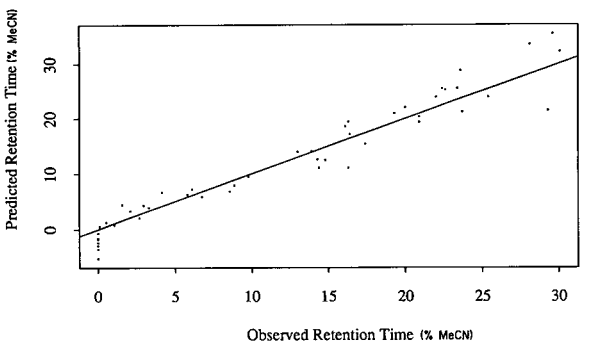

Fig. 7. Relationship between observed retention times for 48 peptides which were not used to establish the model (Table III) and their predicted retention times using the new model. The correlation coefficient is 0.97. MeCN = Acetonitrile.

The observed and predicted retention times were in good agreement except for 8 or 9 out of the 118 peptides tested (47 + 71). As these peptides (Nos. 34, 36, 37, 42 and 47 in Table III and Nos. 40, 46, 63 and 70 in Table IV) have different lengths (7, 8, 14, 19, 20, 25, 58 and 93 residues), the discrepancies observed might be due to sequence specific conformations or to nearest neighbour effects as defined by Mant *et al.* [3]. Nevertheless the new model permits a good prediction of peptide retention times.

In this empirical study, from the retention times of a large number of peptides of various lengths and compositions and mainly coming from milk proteins, we calculated the average contribution to the peptide retention time of each amino acid residue according to the peptide length. From the results, it seems that an almost similar proportion of polar and non-polar residues contributes to the peptide retention of small peptides (<5 residues). In the same way, a similar proportion of polar and non-polar residues contributes to the peptide retention of large peptides (>25 residues). However, for peptides containing between 7 and 25 residues, the proportion of non-polar residues contributing to the peptide retention is higher than that of the polar residues (1.5–2-fold higher). Such a feature may be due to the secondary structure of most peptides during RP-HPLC which leads to a most hydrophobic preferred binding domain, as shown previously by Zhou *et al.* [13] for peptides with an amphipathic α-helix structure.

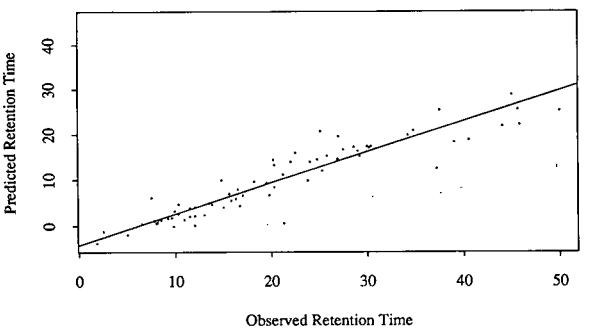

Fig. 8. Comparison of retention times observed by Sasagawa *et al.* [1] for 71 peptides (2–93 residues) with predicted retention times using our new model (eqn. 2). The chromatographic conditions used by Sasagawa *et al.* were close to ours: Waters μBondapack C_{18} column (300 × 4.0 mm I.D.), gradient from 0.1% aqueous TFA to 0.07% TFA in acetonitrile at 1% acetonitrile/min and flow-rate 2 ml/min.

TABLE IV

COMPARISON OF DATA FROM LITERATURE WITH PREDICTED RETENTION TIMES

Data were taken from Sasagawa *et al.* [1]. Retention times were predicted using eqn. 2 and model 2 with the parameter values in Table II (3).

Peptide	Sequence	No. of residues	Retention time	
			Observed	Predicted
1	GGG	3	1.8	−3.8
2	PG	2	2.5	−1.3
3	TEEQ	4	5.0	−1.9
4	MTAK	4	6.5	0.3
5	MAR	3	7.8	0.5
6	YK	2	8.0	0.6
7	TPGSR	5	8.1	1.2
8	KYE	3	8.2	1.2
9	GY	2	8.5	1.2
10	TEAEMK	6	9.2	1.6
11	EY	2	9.6	1.7
12	HLK	3	9.8	−0.1
13	FK	2	9.9	3.2
14	IRE	3	10.3	2.6
15	PL	2	10.3	4.7
16	IAE	3	10.9	1.3
17	GF	2	11.5	3.9
18	KMKDTDSEEE	10	11.5	2.0
19	AFR	3	12.0	4.1
20	DIAAK	5	12.0	0
21	QIAE	4	12.0	2.1
22	ASEDLK	6	13.0	2.3
23	EAFR	4	13.5	4.9
24	FDR	3	13.8	4.6
25	VFDKDGNGY	9	14.8	9.9
26	FKE	3	15.0	4.1
27	KVFGR	5	15.6	7.0
28	SLGQNPTEAE	10	15.8	5.5
29	GW	2	16.3	5.8
30	MIRE	4	16.5	7.9
31	SHPETLEK	8	16.7	4.3
32	HGLDNYR	7	17.0	6.6
33	LFK	3	18.2	9.5
34	IAEFK	5	19.5	9.2
35	ADIDGDGQVNYEE	13	19.8	6.6
36	VFDKDGNGYI	10	20.2	14.4
37	ISAAELR	7	20.3	8.4
38	FESNFNTQATNR	12	20.3	13.2
39	ELGTVMR	7	21.2	11.1
40	GHHEAELK	8	21.3	0.5
41	LQDMINE	7	22.0	13.9
42	FVQMMTAK	8	22.5	15.9
43	QIAEFK	6	23.8	9.8
44	RSLGQNPTEAELQDM	15	24.0	13.9
45	MIREADIDGDGQVNYEE	17	24.8	14.4
46	FLTMMAR	7	25.1	20.6
47	VDADGNGTIDFPE	13	25.3	12.0
48	LGTVMRSLGQNPTEAE	16	25.8	15.2
49	NTDGSTDYGILQINSR	15	26.9	14.5

TABLE IV (*continued*)

Peptide	Sequence	No. of residues	Retention time	
			Observed	Predicted
50	VEADVAGHGQDILIR	15	26.9	14.3
51	FLTMMARKMKDTDSEEE	17	27.0	19.5
52	VFDKDGNGYISAAELR	16	27.5	16.6
53	AFRVFDKDGNGYISAAE	17	28.6	17.1
54	VFDKDGNGYISAAEL	15	29.0	16.3
55	IREADIDGDGQVNYEEFVQM	20	29.2	15.2
56	EAFSLFDKDGDGTITTK	17	30.0	17.3
57	ALELFR	6	30.2	17.0
58	AFSLFDKDGDGTITTKE	17	30.4	17.3
59	NKALELFRKDIAAKYKELGYQG	22	34.2	19.8
60	PGYPGVYTEVSYHVDWIK	18	34.8	20.8
61	EADIDGDGQVNYEEFVQMMTAK	22	37.2	17.5
62	INEVDADGNGTIDFPEFLTM	20	37.5	25.3
63	IILHENFDYDLLDNDISLLK	20	38.5	35.7
64	ASSTNLKDILADLIPKEQARIKTFRQQHGNTVVGQITVDM	39	39.0	18.2
65	HGVTVLTALGAILK	14	40.5	18.7
66	SLGQNPTEAELQDMINEVDADGNGTIDFPEFLTM	34	44.0	21.8
67	YLEFISEAIIHVLHSR	16	45.0	28.7
68	VLSEGEWQLVLHVWAKVEADVAGHGQDILIRLFKSHPETLEKFDRFK HLKTEAEM	55	45.6	25.5
69	SLGQNPTEAELQDMINEVDADGNGTIDFPEFLTMMAR	37	45.8	22.1
70	FKEAFSLFDKDGDGTITTKELGTVMRSLGQNPTEAELQDMINEVDAD GNGTIDFPEFLTMMARKMKDTDSEEEIREAFRVFDKDGNGYISAAE	93	48.9	44.6
71	KASEDLKKHGVTVLTALGAILKKKGHHEAELKPLAQSHATKHKIPIK YLEFISEAIIHVLHSRHPGNFGADAQGAM	85	50.0	25.2

REFERENCES

1 T. Sasagawa, T. Okuyama and D. C. Teller, *J. Chromatogr.*, 240 (1982) 329.
2 D. Guo, C. T. Mant, A. K. Taneja, J. M. R. Parker and R. S. Hodges, *J. Chromatogr.*, 359 (1986) 499.
3 C. T. Mant, T. W. L. Burke, J. A. Black and R. S. Hodges, *J. Chromatogr.*, 458 (1988) 193.
4 M. Yvon, C. Chabanet and J. P. Pélissier, *Int. J. Pept. Protein Res.*, 34 (1989) 166.
5 J. L. Meek, *Proc. Natl. Acad. Sci. U.S.A.*, 77 (1980) 1632.
6 J. L. Meek and Z. L. Rossetti, *J. Chromatogr.*, 211 (1981) 15.
7 S. J. Su, B. Grego, B. Niven and M. T. W. Hearn, *J. Liq. Chromatogr.*, 4 (1981) 1745.
8 K. J. Wilson, A. Honegger, R. P. Stötzel and G. J. Hughes, *Biochem. J.*, 199 (1981) 31.
9 C. A. Browne, H. P. J. Bennett and S. Solomon, *Anal. Biochem.*, 124 (1982) 201.
10 T. Sasagawa, L. H. Ericsson, D. C. Teller, K. Titani and K. A. Walsh, *J. Chromatogr.*, 307 (1984) 29.
11 S. Y. M. Law, A. K. Taneja and R. S. Hodges, *J. Chromatogr.*, 317 (1984) 129.
12 C. T. Mant, N. E. Zhou and R. S. Hodges, *J. Chromatogr.*, 476 (1989) 363.
13 N. E. Zhou, C. T. Mant and R. S. Hodges, *Pept. Res.*, 3 (1990) 8.
14 D. Le Bars and J. C. Gripon, *J. Dairy Res.*, 56 (1989) 817.
15 M. Dalgalarrondo, J. M. Chobert, E. Dufour, C. Bertrandharb, J. P. Dumont and T. Haertle, *Milchwissenschaft*, 45 (1990) 212.
16 M. M. Cals, P. Mailliart, G. Brignon, P. Anglade and B. Ribadeau-Dumas, *Eur. J. Biochem.*, 198 (1991) 733.
17 C. Chotia, *J. Mol. Biol.*, 105 (1976) 1.
18 J. Janin, *Nature (London)*, 277 (1979) 491.
19 S. Huet and A. Messean, in F. De Antoni, N. Lauro and A. Rizzi (Editors), *Proceedings in Computational Statistics*, Physica Verlag, Heidelberg, Vienna, 1986, p. 326.

Journal of Chromatography, 599 (1992) 227–237
Elsevier Science Publishers B.V., Amsterdam

CHROMSYMP. 2556

Synthesis and evaluation of epoxy polymer coatings for the analysis of proteins by capillary zone electrophoresis

John K. Towns, Jianmin Bao and Fred E. Regnier*

Department of Chemistry, Purdue University, West Lafayette, IN 47907 (USA)

ABSTRACT

This paper reports a diol-epoxy coating process to deactivate the inner surface of fused-silica capillaries for use in capillary zone electrophoresis. The most effective coating consists of an epoxy polymer covalently bonded to the silica surface through glycerylpropyl silane which eliminates a number of the negatively charged silanol groups. The epoxy polymer phase also further masks residual surface silanols and sterically limits interaction of proteins with the inorganic surface of the capillary.

Application of the coating was a multi-step process. In the inital step, glycidylpropyltrimethoxy silane was used to derivatize the surface of fused-silica capillaries. This was followed by deposition at the capillary wall of a film of multifunctional oxirane. Polymerization was achieved by either boron trifluoride or tertiary amine. These coatings were of sufficient thickness and hydrophilicity to reduce protein adsorption but still allow sufficient electroosmotic pumping to carry both positive and negative species past the detector. The coatings provided capillaries with lifetimes exceeding 120 h. Proteins were resolved quickly and efficiently with high recovery of both cationic and anionic species between pH 5 to 10.

INTRODUCTION

Dissipation of joule heat has been a major problem in electrophoresis for almost half a century. By carrying out electrophoretic separations in fused-silica capillaries this problem has now been substantially diminished [1]. Unfortunately, surface silanol groups in these high-surface-area systems have a large impact on electrophoretic separations. It has been seen that electroendosmosis is a major, if not the dominant, contributor to solute mobility above pH 4 in native fused-silica capillaries. This is due to the ionization of surface silanol groups [2–5]. Solute adsorption onto these surface silanols is a second major problem, particularly in the case of cationic species such as basic proteins [6]. Adsorption of charged species can change the properties of the wall and cause multiple problems, among these being broad asymmetrical peaks, poor efficiency, altered electroosmotic flow [EOF], reduced protein recovery, and poor reproducibility.

Many strategies have been examined to reduce the problem of protein adsorption. These include the use of high-pH buffers [7–9], low-pH buffers [10,11], amine additives [7,12], high concentrations of salt [13,14], zwitterionic buffers [15], additives to the sample [16] and surface coatings [6,11,14,17–24]. Each of these strategies have had varying degrees of success in reducing protein adsorption. Using coatings to reduce protein adsorption has the advantage that limits do not have to be placed on the sample and separation buffers in terms of salt concentrations, additives to compete for surface sites, and high or low pH. Manipulation of buffers has limitations such as the generation of heat, detector incompatibility, limited pH range, reduced sensitivity, denaturation of proteins, and decreased elution time reproducibility.

Although derivatization of capillary walls with simple organosilanes [11,17,19] greatly reduces surface silanol effects, silane derivatives leach from the capillary and performance deteriorates rapidly. Another approach is to apply a methylcellulose coating [21] to the capillary wall. This coating has been reported to totally control electro-endosmosis and apparently the protein adsorption problem. The

0021-9673/92/$05.00

disadvantage of this coating is that cationic and anionic species will be swept in opposite directions along the capillary axis. Two runs must be made and the polarity of the capillary reversed to analyze both the anionic and cationic compouds of a mixture. A third approach is to use non-ionic surfactants adsorbed to the surface of an octadecyl silane-derivatized capillary to control the adsorption problem [6]. The advantage of this solution is that the coating prevents protein adsorption while still allowing sufficient electroendosmosis to sweep both anionic and cationic species past a single detector. The disadvantage is that non-ionic surfactant must be used in the buffers to replace surfactant that leaves from the hydrophobic surface of capillaries during operation. Samples collected from capillaries will be contaminated with surfactant.

One of the first attempts to coat the inside of a capillary for the separation of proteins was by Jorgenson and Lukacs [17,24]. They followed the coating procedure of Chang *et al.* [25] for the preparation of high-performance liquid chromatography packing materials. The coating process involves the bonding of glycol groups to the surface of fused silica from an aqueous phase. They found that this coating was successful in reducing protein adsorption but had a lifetime of only a few days and exhibited separation efficiencies far below that predicted by theory. It was suggested that sample overloading was the most serious source of zone broadening for proteins. Bruin *et al.* [20] also analyzed the epoxy-diol type coating but carried out the derivatization in organic solvent instead of water. Below, pH 5, this coating produced broader peaks than those of a polyethylene glycol coating tested previously [19]. This was attributed to weak adsorption of the proteins to residual surface silanols. Above pH 5, peak shapes were very broad due to either strong interaction of the proteins with the residual silanols or possibly with the epoxy-diol layer.

This research examines the utility of cross-linking covalently bonded diol coatings with oxiranes [ethylene glycol diglycidyl ether (EGDE) and glycidol] in an attempt to extend the lifetime and pH range of diol based coated capillaries. The objective was to produce a thicker, more stable coating that would further mask silanol groups at the capillary wall. Further objectives were to reduce protein adsorption, extend the pH range of operation, increase resolution, and extend the lifetime of the capillaries. It was anticipated that this coating would also reduce the EOF due to a more complete masking of the silanol groups on the capillary.

EXPERIMENTAL

Apparatus

Capillary electrophoresis was performed on a laboratory-designed instrument which has been previously described [18]. Polyimide-coated fused-silica capillaries (Polymicro Technologies, Phoenix, USA, AZ) of 75 μm I.D. $\times$ 360 μm O.D. were used to prepare the capillaries. Capillaries were 60–100 cm long with separation length of 40 to 85 cm. Detection was achieved with a variable-wavelength UV absorbance detector (Model V4; Isco, Lincoln, NE, USA). When two detectors were employed, another Isco Model V4 UV detecor or UV-8 (Bioanalytical Systems, West Lafayette, IN, USA) was used. Protein elution was monitored at 200 nm when a single detector was used or 214 nm when double detectors were employed. The neutral marker mesityl oxide was detected at either 254 or 214 nm. Linear 2000 (Reno, NV, USA) strip chart recorders were used.

Reagents

Protein samples were purchased from Sigma (St. Louis, MO, USA). γ-Glycidoxy-propyltrimethoxy silane (Gox), EGDE, glycidol, 1,4-diazabicyclo[2.2.2]octane (DABCO), boron trifluoride etherate, mesityl oxide, toluene, triethylamine and methylene chloride were purchased from Aldrich (Milwaukee, WI, USA) as were buffer reagents. Electrophoresis buffers were prepared from laboratory-filtered (0.2 μm) double-distilled water.

Electrophoresis

Protein solutions of 1.0 mg/ml were introduced into the capillary by syphoning for a fixed time (1 to 3) at a fixed height (10–15 cm). Mesityl oxide was used as the neutral marker. Several buffer solutions were used to operate capillaries over the pH range of 3 to 11: 0.01 *M* acetate from pH 3 to 5, 0.01 *M* phosphate at pH 6 and 7, 0.01 *M* 4-(2-hydroxyethyl)-1-piperazineethanesulfonic acid (HEPES) at pH 8, 0.01 *M* tris(hydroxymethyl)aminomethane (Trizma) at pH 9, and 0.01 *M* diaminopropane at pH 10

and 11. Salt was added to each buffer to give comparable ionic strengths and currents. During electrophoresis, current through the capillary never exceed 50 μA with all analyses being run at ambient temperature without temperature control. Between analyses, the capillary was flushed with doubled-distilled water and separation buffer for 1 min.

Preparation of capillaries ***I–VI***

Pretreatment of capillaries ***I.*** Capillaries were first treated with 1.0 *M* NaOH for 15 min followed by 15 min of washing with deionized water. Residual water was evaporated from the capillaries by connecting them to a gas chromatography oven at 100 °C for 2 h under a nitrogen pressure of 400 kPa. This uncoated capillary will be designated as **I**.

Preparation of 3-glycidoxy-propyltrimethoxy silane (GOX) ***II.*** The pretreated capillary **I** was filled with GOX containing 5% methylene chloride by aspiration with a syringe. The capillary was placed in an oil bath at 90°C for 3 h with fresh solution being pulled through the capillary every 15 min. After the 3-h silylation, the capillary was removed from the bath, wiped clean of oil, and residual GOX removed by pushing nitrogen through the capillary. The capillary was washed with several capillary volumes of methanol followed by a 10-min wash with filtered (0.2 μm), double-deionized water.

Preparation of the cross-linked ethylene glycol diglycidyl ether (EGDE) phase ***III.*** A fim of EGDE was deposited onto a 2-m section of the oxirane-derivatized capillary **II** by aspirating a volume of reagent sufficient to fill a 10 cm length of column into the capillary. Three different solutions were evaluated: 1% and 10% EGDE in methylene chloride, and 100% EGDE. The bolus of reagent was pushed through the capillary in a gas chromatography oven with nitrogen at 400 kPa. Nitrogen flow through the capillary was continued for 30 min to drive off the methylene chloride. Catalyst in the form of boron trifluoride vapor from an etherate solution was then sent through the capillary in a stream of nitrogen to cross-link the oxiranes. Catalyst was delivered from a 3-ml vial containing 1 ml BF_3 etherate that was capped with a rubber septum. The capillary was connected to this vessel by insertion through the septum. Careful attention was placed on making sure that the capillary cleared the BF_3 etherate solution by one half inch so that no liquid enters the capillary. A second capillary was connected to the nitrogen line and pushed through the rubber septum to the bottom of the vial so that nitrogen bubbled through the BF_3 etherate. The gaseous catalyst stream was forced through the capillary with nitrogen for 1 h at a rate of 2 ml/min. The coated capillary was cured in a gas chromatography oven for 2 h at 100°C under nitrogen pressure of 400 kPa.

Preparation of glycidol derivatized phase ***IV.*** A 2-m section of previously coated capillary **III** was further derivatized by depositing 10% glycidol in methylene chloride in a volume sufficient to form a 10-cm bolus. After excess glycidol was pushed out of the capillary, polymerization was catalyzed in the same fashion as described above for the phase **III**.

Esterification of the phase ***IV*** *coating* ***V.*** A 2-m section of phase **IV** coated capillary was further derivatized by sending diazomethane through the capillary in diethyl ether to methylate possible carboxyl groups generated in the previous coating steps. The diazomethane was generated by placing approximately 1 g of N-nitrosomethylurea in a polished round-bottom flask containing 50 ml each of diethyl ether and a 50% KOH solution. At the interface, the N-nitrosomethylurea is converted into diazomethane which extracts into the ether phase giving a yellow color. Diazomethane in diethyl ether was aspirated through the capillary for 10 min at 0.25 ml/min. The capillary was then washed with diethyl ether, water and running buffer.

Preparation of the base-catalyzed diol-EGDE cross-linked phase ***VI.*** A solution of 0.5% DABCO in CH_2Cl_2 was aspirated into a capillary with the diol-bonded phase **II** and allowed to ion-pair with residual silanol groups in the capillary for 5 min before removal with pressurized nitrogen. A 10% solution of EGDE was forced into the column and allowed to react for 30 min at room temperature before heating to 120°C and continuing the reaction for another 30 min. Non-bound monomer was pushed out of the column with pressurized nitrogen and the column washed with methanol. Heavier

coatings were obtained by repeating the cross-linking reaction with EGDE for an additional 3 h followed by a 12-h treatment at 120°C. Removal of non-bound material and washing was as described above.

Determination of protein recovery

Protein recovery was determined with a dual detector system as previously described [6]. Placing detectors at 20 cm and 70 cm from the capillary inlet allowed protein recovery to be measured over the 50 cm section of capillary between the detectors. Recovery was determined using 10 ng of protein and a non-adsorbed internal standard. Detectors were switched from front to back to accommodate for differences in detector response. Percent recoveries were determined by subtracting peak areas from each detector after taking into account differences in detector response.

RESULTS AND DISCUSSION

Reactions in the epoxy coating process are shown schematically in Fig. 1. It should be noted that the structures in this scheme do not represent the exact structure of the coating. GOX was coupled to sur-

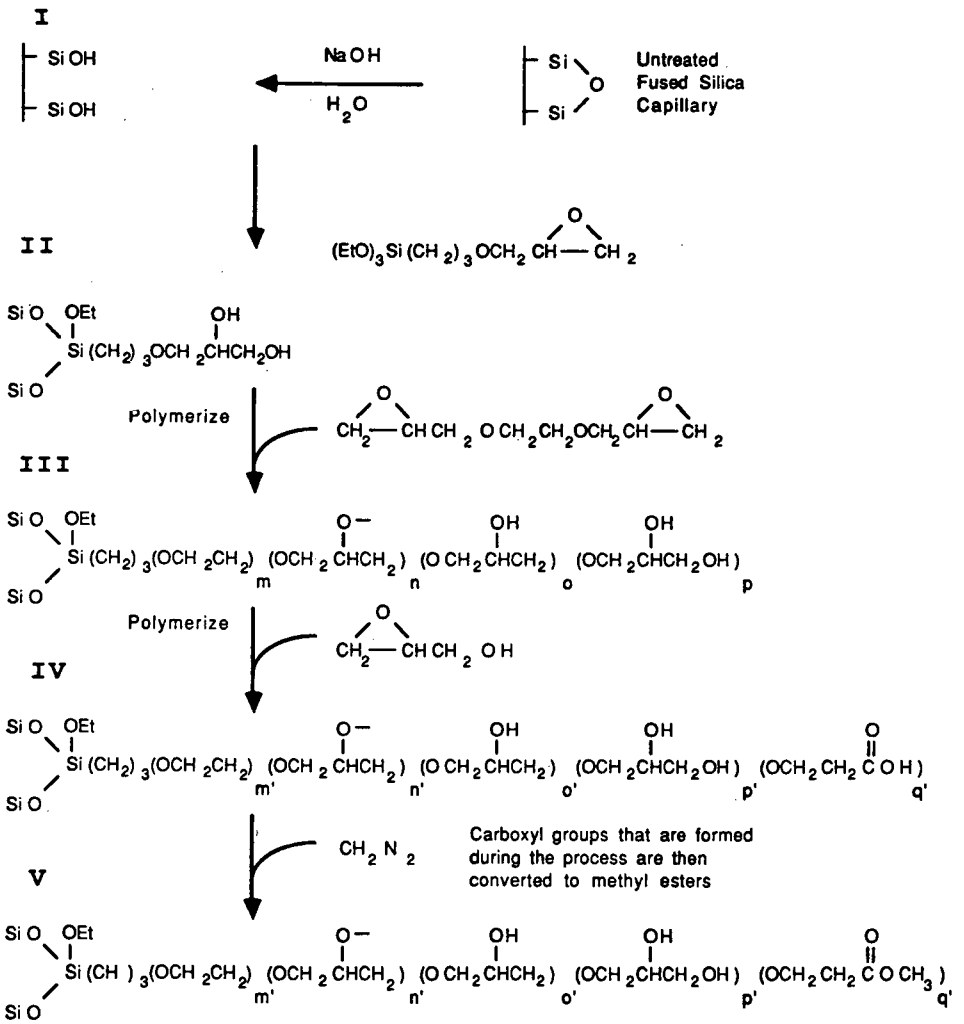

Fig. 1. Typical reaction scheme for the multi-step process used in the preparation of the diol-based expoxide coating. Et = Ethyl.

face silanols by the elimination of methanol in the first step. Since polymerization may occur with trimethoxy silanes, silane monomer solution was continuously pumped through capillaries to minimize polymerization. After the reaction was finished, excess GOX was washed from the capillary and the epoxy group at the capillary surface used in a second binding reaction. Copolymerization of EGDE and surface epoxy groups were used in the second step to form a highly crosslinked surface layer. Multifunctional oxiranes, such as EGDE, have been shown previously to produce highly cross-linked structures in preparing chromatographic media [16]. The resulting epoxy polymer has only C–O, C–C and C–H bonds and is stable in both acid and base. In addition, the high content of ether and hydroxyl groups in the polymer produced capillaries with very hydrophilic walls.

Evaluation of acid-catalyzed epoxy-based coatings

Fig. 2 shows the corresponding peak shape for each step of the acid-catalyzed coating process (pretreated uncoated capillary **I** with coated capillaries **II–V**). Separations were carried out with 0.01 *M* phosphate buffer (pH 7.0) using a 80 cm × 75 μm capillary (65 cm to detector) at 300 V/cm. Capillaries were evaluated in terms of EOF, peak efficiency, lysozyme recovery, peak skew and capillary lifetimes for each stage of the coating process (Table I).

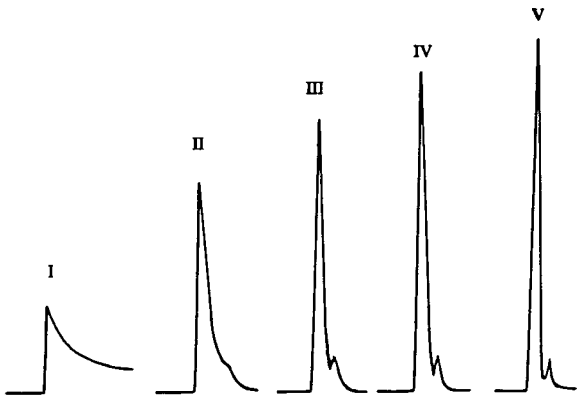

Fig. 2. Peak shape and migration times for lysozyme and a neutral marker (mesityl oxide) for each step of the acid-catalyzed epoxy coating process. Conditions: 0.01 *M* phosphate, pH 7.0, detection at 200 nm, 100 cm × 75 μm capillary (85 cm to detector), 28 kV, 30 μA.

The first three 10-ng injections of lysozyme were completely adsorbed to the wall before reaching the detector. The fourth injection, shown at the far left in Fig. 2 reached the detector but the peak tailed badly and eluted much later than expected. The long elution time of this positively charged protein (p*I* 11) is the result of adsorption to the capillary wall. Following lysozyme adsorption, the negative charge on the wall is reduced, modifying the double layer and significantly lowering EOF.

The first coating stage involved the bonding of glycidoxy-propylsilyl to the capillary wall. Silylation was achieved from both aqueous and non-aqueous solutions [17,20]. It was found that silylation in 5% methylene chloride gave improved results compared to an aqueous solution in terms of reduced EOF, increased efficiency, increased peak symmetry and improved resolution. In addition to reducing the concentration of negatively charged silanol groups, silylation also moves the plane of shear some distance from the wall by lowering the charge potential. These two effects cause a two-fold reduction in EOF compared to the uncoated capillary. Lysozyme in a 50-cm section of capillary increased to 80% with the diol coating **II**. This is a 15-fold increase in recovery relative to an uncoated capillary of the same length. Although the diol coating substantially improved performance compared to uncoated capillaries, plate efficiency is far below that predicted by theory and much less than has been observed with other coatings using similar conditions [6,18]. The diol coating **II** also suffers from severe peak tailing, lower protein recovery and shorter column lifetimes compared to results that have been reported by others [6,11,14,18,21,22].

With the objective of further masking the negatively charged wall and extending the lifetimes of the capillary, the diol coating **II** was cross-linked with EGDE to form the second stage of coating. The BF_3-catalyzed polymerization of the dioxirane monomers onto the diol ligand produced a very hydrophilic coating (**III**). These highly active monomers react rapidly with hydroxyl groups on the diol ligand and with each other to form a stabile coating. This coating further masks charges on the capillary wall.

To optimize concentration film deposition on the diol coating **II**, 1%, 10%, and pure EGDE were

TABLE I

SEPARATION PARAMETERS FOR EPOXY-COATED CAPILLARIES

EOF = Electroosmotic flow (0.01 *M* phosphate buffer, pH 7.0); plate number $N = 5.54 (t_c/w_{1/2})^2$ for lysozyme on a 100 cm × 75 μm capillary (where t_c = retention time and $w_{1/2}$ is peak width at half height); recovery is for lysozyme (p*I* 11.3) at pH 7.0 taken over a 50-cm section of capillary; peak skew = ratio of *a*/*b* at 10% peak height [18]; life time is the time required to deviate 10% from original electroosmotic flow.

Capillary	EOF (10^8 m^2/V s)	Efficiency	Recovery (%)	Peak skew	Life time (h)
Untreated					
I	5.62	–	0	–	–
Diol					
II	2.98	35 000	80	0.33	20
Acid catalyzed					
III	1.49	80 000	85	0.80	50
IV	0.92	85 000	87	0.90	60
V	0.67	92 000	90	0.93	>150
Base catalyzed					
VI	1.30	85 000	85	0.83	>100

evaluated. Table II shows the performance parameters for the three concentrations examined. The 10% EGDE solution was found to give the best results in terms of efficiency, lifetime, peak skew and lysozyme recovery while giving the lowest EOF and was used for the remainder of the study. This coating **III** showed increased efficiency, lower EOF, better resolution, reduced peak skew and a 5% increase in lysozyme protein recovery up to 85%. Lifetime of the capillary was also increased beyond the few days of the diol coating. This coating, however, still gives efficiencies less than expected and further masking was needed to increased separation performance.

To create a thicker hydrophilic coating, glycidol was bonded to phase **III**, resulting in a highly branched matrix. This coating **IV** showed further improvement in separation performance with respect to increased percent recovery, improved peak symmetry, and a more complete masking of the silanol groups as indicated by the further reduction in electro-osmotic flow. However, there was little improvement in efficiency.

A problem with both the **III** and **IV** coating is that EOF gradually increases. It is unacceptable for the elution time of solutes to change in this manner. This problem is attributed to the formation of aldehyde groups during the BF_3-catalyzed cross-linking step. Over time, these groups oxidize to carboxyl groups and increase the negative charge at the capillary walls. This results in increased EOF and a reduction in the separation performance of the capil-

TABLE II

EFFECT OF PERCENT EDGE IN METHYLENE CHLORIDE ON SEPARATION PARAMETERS FOR ACID-CATALYZED DIOL-EDGE COATING **III**

See Table I for definitions.

Coating (%)	EOF (10^8 m^2/V s)	Efficiency	Recovery (%)	Peak skew	Life time (h)
1%	2.78	41 000	82	0.68	30
10%	1.49	80 000	85	0.80	50
100%	2.92	45 000	81	0.72	35

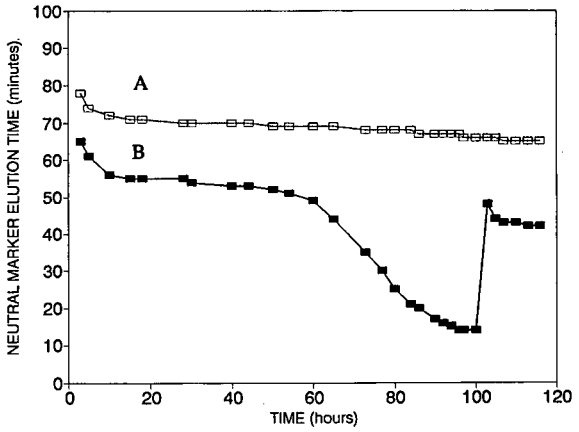

Fig. 3. Plot of neutral marker elution time *vs.* electrophoretic running time for (A) phase **V** coated capillary and (B) phase **IV** coated capillary treated after 100 h with diazomethane. Conditions as in Fig. 2 with the exception of detection at 254 nm.

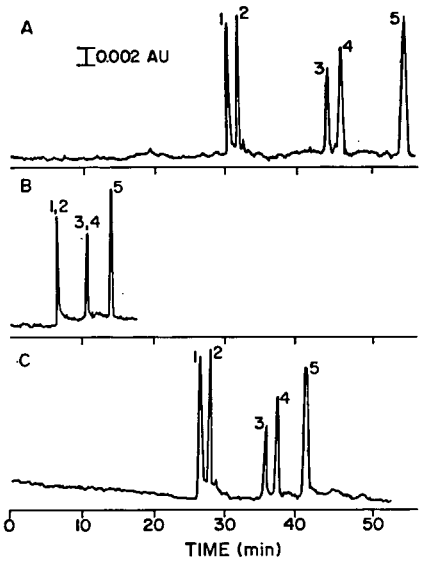

Fig. 4. Separation of five basic proteins on a phase **IV** coated capillary at (A) 5 h, (B) 100 h, and (C) after treatment with diazomethane. Peaks: 1 = lysozyme; 2 = cytochrome *c*; 3 = ribonuclease A; 4 = chymotrypsinogen; 5 = myoglobin. Conditions as in Fig. 2.

lary. This problem was alleviated by converting these acid groups to esters. Diazomethane was used for esterification because it is easily introduced into the capillaries.

The effect of the diazomethane treatment on neutral marker elution time (a measure of EOF) is shown in Fig. 3 for two coated capillaries. Line A shows the elution times of the neutral marker *vs.* electrophoretic running time for an **IV** coated capillary treated with diazomethane. This capillary exhibited long term stability past the 120-h, mark (run over a two week period). Diazomethane treatment further decreased EOF by methylation of carboxyl groups formed in the initial cross-linking steps. Line B shows the elution time of a neutral marker *vs.* electrophoretic running time for the phase **IV** coated capillary. After approximately 60 h EOF increases drastically, presumably due to the formation of negatively charged carboxyl groups in the coating surface. This was confirmed by esterification of the capillary with diazomethane. EOF was restored to a value comparable to that of the phase **V** coating. Fig. 4 shows the electropherograms of five basic proteins run on the phase **IV** capillary at the 5-h mark, the 100-h mark, and then after treatment with diazomethane. The electropherograms show the influence of the oxidation and removal of carboxyl groups on EOF.

Although phase **V** gives good results in terms of peak efficiency, lysozyme recovery and peak shape, there are still some drawbacks with this coating. Delivery of the catalyst into the capillary in the gas phase apparently limits the length of capillary that can be prepared during the cross-linking step. Capillary lengths above 3 m gave wide fluctuation in segment to segment reproducibility. The capillary end nearest the point of catalyst entry is exposed to too much catalyst. This appears to cause excess formation of aldehydes which are subsequently oxidized to carboxyl groups that increased the EOF. In contrast, the exit of the capillary was not exposed to enough catalyst and perhaps did not cross-link sufficiently. The mid-section of the capillary was suitable. This means that only there middle 3 m of a 10-m capillary would be coated properly. Another problem is the need to esterify the phase **IV** coating. Along with the time needed for this extra step, diazomethane is carcinogenic and explosive.

Evaluation of base-catalyzed epoxy-diol phase ***VI***

The problems associated with the acid catalyst were circumvented by the use of a base catalyst for polymerization. Using DABCO, the catalyst is sent

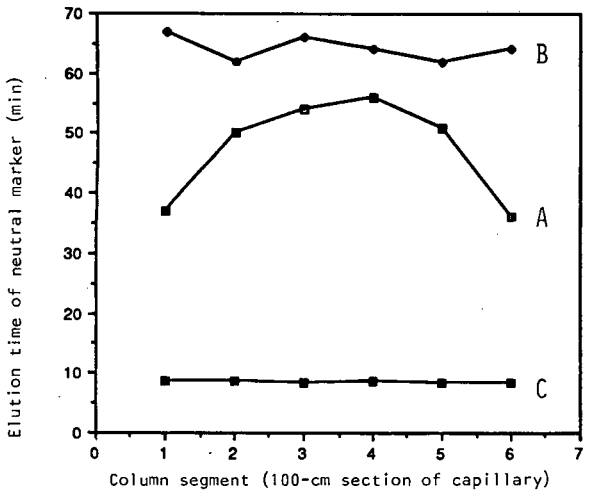

Fig. 5. Neutral marker elution time as a function of meter long sections of a 6-m length of coated capillary for (A) acid-catalyzed coating **IV**, (B) base-catalyzed coating **VI** and (C) uncoated capillary. Conditions as in Fig. 3.

through the capillary in solution, rather than the gaseous form. This allows capillaries of longer length to be coated without the adverse effects associated with the gaseous catalysis. Fig. 5 shows the difference in neutral marker elution time for both acid- and base-catalyzed epoxy-diol coated capillaries as a function of position in a 6-m capillary. The elution times of an uncoated capillary is shown for comparison. The curvature seen for the acid-catalyzed coating is indicative of sections over-exposed and under-exposed to catalyst. This is not the case with the base catalyzed process where all sections are evenly exposed to the catalyst. The percent difference of the first section to middle section of capillary for the acid and base catalyzed procedures are 36% and 3%, respectively.

An unusual feature of this base catalyzed coating process was that the DABCO catalyst and oxirane monomer were added sequentially. This was done because the capillary was positively charged after the coating process when they were added together. It is thought this is because the amine catalyst is incorporated into the coating. The success of sequential addition is attributed to the fact that residual silanols on the capillary will ion-pair with DABCO catalyst and retain a small amount of the amine even after displacement of the catalyst solution from the capillary. This small amount of catalyst is apparently sufficient to cross-link the multifunctional oxirane monomer. Catalyst concentration is important. When more than 1% DABCO was used, the coating was cationic and a negative EOF was detected at pH 7. This is because the extra amine ion-paired on the surface will be protonized and form positive charges on the surface. These positive charges will induce a negative layer in the buffer solution and reverse the zeta potential at the capillary wall and cause the EOF to move in the opposite direction. Although DABCO catalyst might be incorporated into the polymer in the sequential addition process, it probably is masked by the anionic silanol groups and the coating.

Capillaries coated with the hydrophilic epoxy layer (**VI**) give good separation of the positively charged protein test mixture (Fig. 6) previously run on the acid-catalyzed coating (**V**). The separation is comparable to coating **V**, but required fewer synthetic steps and much longer lengths of capillary could be coated. As was the case with the acid catalysis, coating **VI** maintains sufficient EOF at pH 7 to sweep both anionic and cationic species past the detector as seen in the separation of trypsinogen, myoglobin, conalbumin, carbonic anhydrase and α-amylase (Fig. 7). It was seen that less band broad-

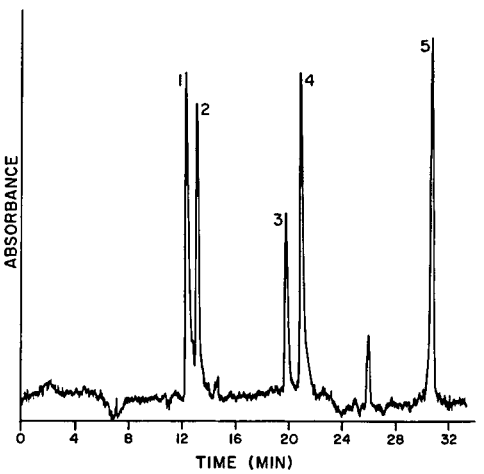

Fig. 6. Capillary electrophoretic separation of five basic model proteins on a base-catalyzed coated capillary (**VI**). Peaks: 1 = lysozyme; 2 = cytochrome *c*; 3 = ribonuclease A; 4 = chymotrypsinogen; 5 = myoglobin. Conditions: 85 cm × 50 μm I.D. (65 cm separation length); 0.01 *M* phosphate buffer, pH 7.0; 300 V/cm, 17 μA.

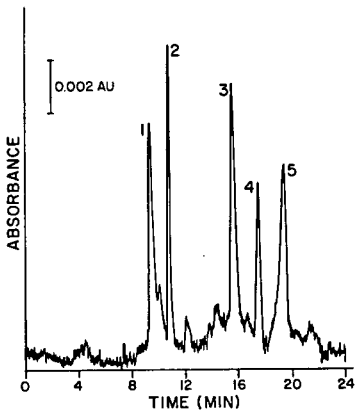

Fig. 7. Capillary electrophoretic separation of near neutral proteins on a base-catalyzed diol-epoxide coated capillary (**VI**). Peaks: 1 = trypsinogen; 2 = myoglobin; 3 = conalbumin; 4 = carbonic anhydrase; 5 = amylase. Conditions as in Fig. 6 with the exception of a shorter capillary (60 cm with a 42 cm separation length).

ening was experienced with positive proteins (pI>7) than that with negative proteins (pI>7). This has been attributed to the fact that positive proteins move in the direction of EOF whereas negative proteins migrated against the flow [6].

The utility of this coating in electrophoretic mobility studies was examined as a function of pH. It is well known that the net charge of a protein at a specific pH determines its migration rate under an applied electrical field. In general, positive charge on a protein will decrease as pH increases. Thus, lower electrophoretic mobility is expected at higher pH. This means that resolution will be difficult when EOF is large [6,18]. Fig. 8 shows that EOF is low and does not vary widely as a function of pH with the coated phase **VI** capillary. A pH *vs.* electrophoretic mobility map (Fig. 9) shows that there is a pH optimum for separating any set of proteins. It was easy to see from these electropherograms that, in contrast to uncoated capillaries, sharp peaks were obtained for all separations. This is a major advantage of this coating over uncoated capillaries where proteins can only be separated at either high pH (such as pH 9 or above) or low pH (such as pH 2).

A comparison of the base-catalyzed coating and acid-catalyzed coatings at neutral pH showed the former to be more stable coating in terms of run-to-run and day-to-day relative standard deviations (R.S.D.) and more reproducible in terms of segment

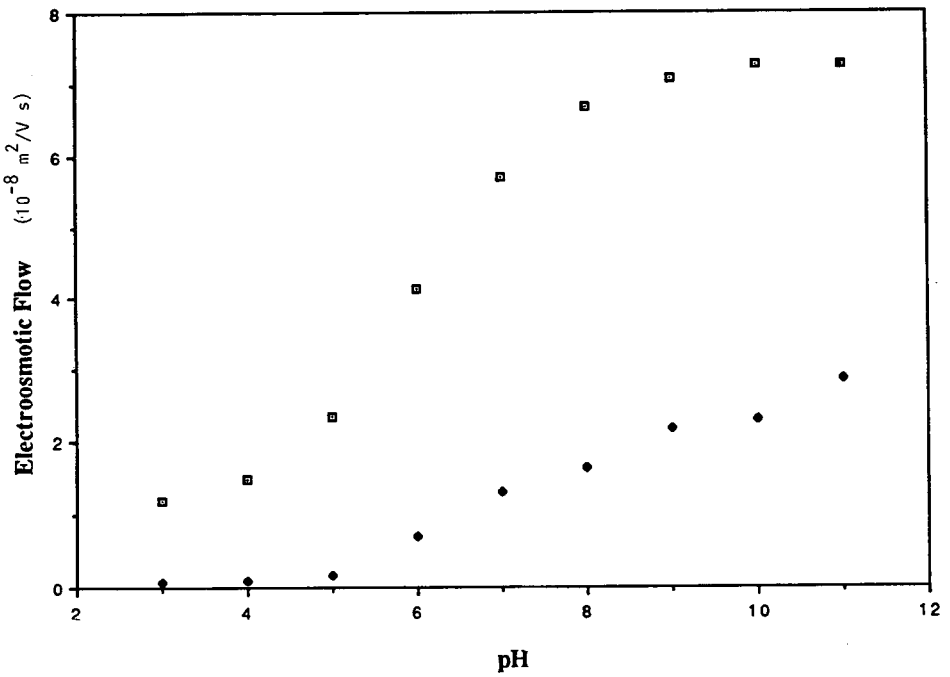

Fig. 8. Dependence of EOF on pH for (□) uncoated and (◆) base-catalyzed diol-epoxide (**VI**) coated capillaries.

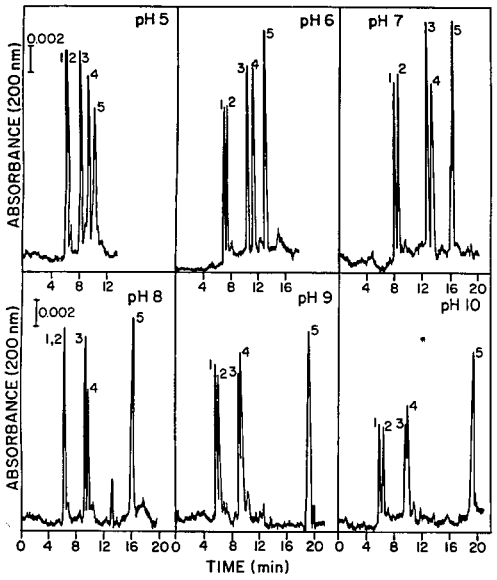

Fig. 9. Separation of five basic proteins at pH values ranging from 5 to 10 on a base-catalyzed coated (**VI**) capillary. Peaks: 1 = lysozyme; 2 = cytochrome *c*; 3 = ribonuclease; 4 = chymotrypsinogen; 5 = myoglobin. Capillary: 65 cm × 50 μm I.D. (40 cm separation length).

to segment R.S.D. values (Table III). The larger value for the segment-to-segment R.S.D. value of the acid-catalyzed coatings is again attributed to the uneven exposure of the gaseous catalyst as compared to the solution application with the base-catalyzed coating. The base-catalyzed coating process has the additional advantage of only two steps as compared to the four with the acid-catalyzed process.

The stability of the coatings was also examined under alkaline pH conditions (pH 10.0). The stability of the coatings at elevated pH were found to increase as subsequent layers of coating were applied (coated capillaries **II–V**). This extension in capillary lifetimes at high pH is presumably due to increased shielding of the siloxane bond from the alkaline buffer. The acid-(**V**) and base-(**VI**) catalyzed coatings gave similar stability results deviating 10% from their initial EOF values after 5 days (50 h, total running time). This deterioration over time is characteristic of organosilane coatings which are removed from the surface of the capillary under alkaline conditions. The increased cross-linking, however, was able to extend the lifetimes of these capillaries approximately 10-fold compared to that of the simple organosilane coating.

TABLE III

ACID-CATALYZED COATING (**IV**) *vs.* BASE-CATALYZED COATING (**VI**) NEUTRAL MARKER ELUTION TIME REPRODUCIBILITY

	Relative standard deviation (%)	
	Acid catalyzed	Base catalyzed
Run-to-run ($n=6$)	3.1	2.0
Day-to-day ($n=5$)	3.5	2.8
Segment-to-segment ($n=6$) (sections of same capillary)	18.3	3.2

CONCLUSIONS

Epoxy polymer layers bonded to the fused-silica capillary produce a hydrophilic coating that greatly reduces protein adsorption. These coated capillaries give high efficiency, symmetrical peaks and high protein recovery. Column lifetime exceed 150 h without significant loss in resolution or change in elution time. Base catalysis was most effective in producing stable, reproducible epoxy polymer-coated surfaces that can be used over a wide pH range with wide variation in EOF and still allow sufficient EOF for both negative and positive species under the same conditions.

The separations presented here demonstrate the applicability of covalently bonded phases in the separation of proteins by capillary zone electrophoresis. One of the most attractive features of capillary zone electrophoresis is the short times required both in terms of the separation and the time required to equilibrate the system when buffer pH is switched. The time that must be taken to bond coatings to the capillary wall are far outweighed by added freedom that is allowed with the separation buffer. This becomes increasingly important for example when coupling capillary electrophoresis to mass spectrometry where limited buffer compatibility is a major concern.

REFERENCES

1 J. W. Jorgenson and K. D. Lukacs, *Anal. Chem.*, 53 (1981) 1298.
2 T. Tsuda, K. Nomura and G. Nakagawa, *J. Chromatogr.*, 264 (1983) 385.

3 C. F. Simpson and K. D. Altria, *Anal. Proc.*, 23 (1986) 453.
4 C. S. Lee, W. C. Blanchard, and C. T. Wu, *Anal. Chem.*, 62 (1990) 1550.
5 W. J. Lambert and D. L. Middleton, *Anal. Chem.*, 62 (1990) 1585.
6 J. K. Towns and F. E. Regnier, *Anal. Chem.*, 63 (1991) 1126.
7 H. H. Lauer and D. McManigill, *Anal. Chem.*, 58 (1986) 166.
8 Y. Walbroehl and J. W. Jorgenson, *J. Microcolumn Sep.*, 1 (1989) 41.
9 M. Zhu, R. Rodriquez, D. Hansen and T. Wehr, *J. Chromatogr.*, 516 (1990) 123.
10 J. C. Grossman, H. H. Colburn, R. G. Lauer, R. M. Nielsen, G. S. Riggen, E. C. Rickard and G. S. Sittampalam, *Anal. Chem.*, 61 (1989) 1186.
11 R. M. McCormick, *Anal. Chem.*, 60 (1988) 2322.
12 R. G. Nielsen, G. S. Sittampalam and E. C. Rickard, *Anal. Biochem.*, 177 (1989) 20.
13 J. S. Green and J. W. Jorgenson,, *J. Chromatogr.*, 478 (1989) 63.
14 S. A. Swedberg, *Anal. Biochem.*, 185 (1990) 51.
15 M. M. Bushey and J. W. Jorgenson, *J. Chromatogr.*, 480 (1989) 301.
16 M. J. Gordon, K-J. Lee, A. A. Arras ans R. N. Zare, *Anal. Chem.*, 63 (1991) 69.
17 J. Jorgenson and K. D. Lukacs, *Science (Washington, D.C.)*, 222 (1983) 266.
18 J. K. Towns and F. E. Regnier, *J. Chromatogr.*, 516 (1990) 69.
19 G. J. M. Bruin, J. P. Chang, R. H. Kuhlman, K. Zegers, J. C. Kraak and H. Poppe, *J. Chromatogr.*, 471 (1989) 429.
20 G. J. M. Bruin, R. Huisden, J. C. Kraak and H. Poppe, *J. Chromatogr.*, 480 (1989) 339.
21 S. Hjertén, *J. Chromatogr.*, 347 (1985) 191.
22 K. A. Cobb, V. Dolnik and M. Novotny, *Anal. Chem.*, 62 (1990) 2478.
23 M. A. Mosely, L. J. Deterding, K. B. Tumer and J. W. Jorgenson, *Anal. Chem.*, 63 (1991) 109.
24 J. W. Jorgenson, *Trends Anal. Chem.*, 3 (1984) 51.
25 S. H. Chang, K. M. Gooding and F. E. Regnier, *J. Chromatogr.*, 120 (1976) 321.

Journal of Chromatography, 599 (1992) 239–253
Elsevier Science Publishers B.V., Amsterdam

CHROMSYMP. 2526

Schemes for efficient protein purification on a family of polymeric ion exchangers in glass columns

Dorothy J. Phillips*, Paul J. Cheli, Donna M. Dion, Holly L. Hodgdon☆, Arthur M. Pomfret and Brian R. San Souci

Millipore Corporation Waters Division, 34 Maple Street, Milford, MA 01757 (USA)

ABSTRACT

The Protein-Pak HR series is a family of anion (DEAE and Q) and cation (SP and CM) exchange packings for protein and nucleic acid purifications. The characteristics of the weak anion-(DEAE) and the strong cation-(SP) series were reported in an earlier paper. The weak cation (CM) and strong anion (Q) series are new members of the Protein-Pak HR family. All four ion exchangers are available in 8-, 15- and 40-μm particle sizes. In this study we demonstrated that the 15- and 40-μm bulk packings are suited for the early states of large scale-protein purifications. The Protein-Pak 8HR series of pre-packed Advanced Purification (AP) glass columns with 8-μm particles gave the high resolution required in the latter stages of the purification or analysis. These packings were used in the AP-1 (100 mm × 10 mm) glass columns to demonstrate their performance at several flow-rates (0.5–4 ml/min), sample loads and pH values. Both CM and Q 8HR packings were shown to have good recovery of both protein mass and biological activity. Protein mixtures used to evaluate these packing materials included those of mouse serum, egg white, and papain. The Protein-Pak HR series has also been shown to be stable to operation at 4°C and to regeneration (sodium hydroxide and acetic acid) which is important for use of these packings in a purification scheme.

INTRODUCTION

The efficiency of large-scale protein purifications is becoming more important as the new therapeutic proteins move from research to manufacturing. The purification of proteins from crude mixtures normally consist of three stages: the preliminary or initial isolation stage, the purification stage and the final polishing stage [1]. The purification stage often requires at least four steps involving two or more chromatographic modes. The two most frequently used modes are ion-exchange and affinity chromatography [2]. Naveh and Siegel [3] explained that the scheme for large-scale purification of therapeutic monoclonal antibodies requires a combination of chromatographic steps to remove all contaminants, each being resolved under different conditions or on different principles. The choice of certain chromatographic techniques is dictated by several parameters: (1) sample volume; (2) protein concentration and viscosity of the sample; (3) the desired degree of purity of the protein product; (4) the presence and level of contaminants such as nucleic acids, pyrogens and proteolytic enzymes; and (5) the ease with which different packings can be regenerated or washed free of contaminants and denatured proteins. The ability to regenerate a chromatographic material and the purchase price sets the material cost of a given purification step [1]. Burnouf [4] stressed that the scheme for an industrial purification process must yield a safe and efficient product and provide the highest possible purity and yield at the lowest cost.

The purification scheme frequently begins with the use of an open column containing an inexpensive soft gel and ends with the use of high-resolution liquid chromatographic separations. The low cost and ability to regenerate the softer gels have made them attractive for the early purification step. These

☆ Present address: Cambridge Biotech, 365 Plantation Street, Worcester, MA, USA.

0021-9673/92/$05.00

early hydrophilic ion exchangers which were first developed in the 1950s are still used today [5]. However, the swelling and shrinking properties of the soft gels make them tedious to use. The long time period required to complete the chromatography has the potential to give low recoveries (often due to proteolytic digestion).

A solution to these problems is the use of hard hydrophilic packings for ion-exchange chromatography which are either cross-linked agarose gels or hydrophilic vinyl polymers [6,7]. These ion exchangers are normally rugged materials (chemically and physically stable) that are available in bulk. The large-particle ($\geqslant 15$ μm), rigid-polymeric packings are applicable in the initial steps of the purification scheme; in many cases they can be regenerated like the softer gels. However, these materials allow rapid throughput because the flow-rate limit is orders of magnitude higher than for soft gels. The significant reduction in time and improvements in recoveries over the soft gels often outweigh the increase in packing material cost. The higher resolving power of the rigid packings than the softer gel leads to higher degrees of purification in the early stages. This also reduces the number of steps required for purification which gives an additional improvement in mass recovery and reduction in process cost.

The latter stage of the purification uses the smaller particle size packings ($\leqslant 10$ μm) which are now available as both polymeric and silica-based materials. Therefore, it is possible to have a cost-effective purification scheme which uses high-performance liquid chromatography (HPLC) throughout the process.

The Protein-Pak HR family of anion and cation exchangers discussed in this report are useful throughout the purification scheme. The family includes 15- and 40-μm bulk packings for concentrating the sample and separating the desired protein in the early stages of purification. The Protein-Pak HR family also includes 8-μm materials in prepacked glass columns for the high resolution required in the final stages of the purification. The Protein-Pak HR series are rigid, spherical, porous hydrophilic, polymeric methacrylate gels. The particles have 1000 Å pores which allow proteins up to 10^6 molecular weight to penetrate and interact with the functional groups. The strong anion-exchange (Q) packings have quaternary methylamine functional groups. The weak cation-exchange (CM) packings have carboxymethyl functional groups. This paper discusses the characteristics of and utility for the Protein-Pak Q HR and CM HR series ion-exchange packings for protein purification and analysis. The characteristics and performance of the Protein-Pak DEAE HR and SP HR series have been reported previously [8].

EXPERIMENTAL

The Protein-Pak HR materials were characterized by a standard procedure for protein resolution, mass recovery and protein binding capacity [8]. The protein resolution was also determined at different flow-rates and over a range of protein loads. The Protein-Pak HR materials were packed in Waters Advanced Purification glass columns (AP-1) with dimensions of 100 mm × 10 mm.

All proteins and buffer salts were from Sigma (St. Louis, MO, USA). Acetone was the marker for measuring the column plate counts or efficiencies. The biological activity of glucose-6-phosphate dehydrogenase was measured with the assay kit 345-B from Sigma.

These studies used three different solvent delivery systems, including the Waters 600E multisolvent delivery system, the 650 Advance Protein Purification (APP) System and the 625 non-metallic LC System. The other components of the HPLC systems were either the Model 490 programmable multiwavelength detector or 484 tunable absorbance Detector, the 712 WISP automatic sample injector and a Wescan conductivity meter. A Foxy fraction collector was connected to the Model 650 APP system. A Waters Model 845 computer controlled the HPLC systems and contained the System Suitability software to analyze the data.

The eluents used for the protein resolution, capacity, flow-rate, sample load, and mass recovery studies on Protein-Pak Q HR packings were 20 m*M* Tris–HCl (pH 8.2, eluent A) and 20 m*M* Tris–HCl (pH 8.2) with 1 *M* sodium chloride (eluent B). The proteins in the standard mixture were carbonic anhydrase, human transferrin, ovalbumin and soybean trypsin inhibitor with adenosine as the void volume marker. The isoelectric points and molecular weights are in Table I. The gradient for protein

TABLE I

PROTEINS USED TO EVALUATE THE PERFORMANCE OF ION-EXCHANGE COLUMNS

Protein	Molecular weight	Isoelectric point	Concentration (%, based on mg/ml)
Protein-Pak Q HR series protein mixture			
Adenosine	267		0.3
Carbonic anhydrase	28 000	7.3	12.5
Human transferrin	77 000	6.0–6.5	31.1
Ovalbumin	44 500	4.7	25.0
Soybean trypsin inhibitor	21 500	4.5	31.1
Protein-Pak CM HR series protein mixture			
Myoglobin	17 500	7.0	8.0
Ribonuclease A	13 500	8.8	33.0
Chymotrypsinogen A	25 000	9.0	17.0
Cytochrome *c*	12 400	9.4	25.0
Lysozyme	14 400	11.0	17.0

resolution was 0–25% eluent B at flow-rates of 0.5, 1.0, 1.56, 2 and 4 ml/min. The gradient duration was adjusted at each flow rate to cover 7.8 column volumes.

The protein resolution on Protein-Pak Q 8HR was also evaluated at pH 6.0 using 20 m*M* piperazine and 20 m*M* piperazine with 1 *M* sodium chloride. The standard mixture in Table I was used.

The Protein-Pak CM HR packings were evaluated with 20 m*M* sodium phosphate (pH 7.0) (eluent A) and 20 m*M* sodium phosphate (pH 7.0) with 1 *M* sodium chloride (eluent B). The eluents were used for sample load, recovery of mass and biological acitivity (pH 6.0) studies. The proteins in the standard mixture were myoglobin, ribonuclease A, chymotrypsinogen A, cytochrome *c* and lysozyme. The isoelectric points and molecular weights are in Table I.

The protein resolution as a function of load was determined on both the Protein-Pak Q and CM 8 HR AP-1 glass columns. The Waters Model 490 programmable multiwavelength detector was modified with a prep cell in order to detect the large protein loads. The 2-ml injection loop was put in the Waters Model 712 WISP automatic sample injector to accomodate the large sample volumes. The sample (mixture in Table I) was applied to the Protein-Pak CM 8HR AP-1 glass column at five protein loads. Injection volumes ranged from 10 to 1600 μl for 0.2-, 2-, 8-, 20- and 32-mg protein loads. The gradient was 0–50% eluent B in 20 min. A mixture of conalbumin (29.8%), cytochrome *c* (0.8%), ovalbumin (39.6%) and soybean trypsin inhibitor (29.8%) was injected on the Protein-Pak Q 8HR AP-1 glass column. The sample loads were 0.53, 5.3, 26, 53, and 106 mg of total protein. The gradient was 0–25% buffer B in 18 min.

Tables II and III list the proteins for the mass recovery studies performed on the Protein-Pak Q and CM 8HR columns, respectively. The protein load for both columns was 150 μg per injection. The proteins were eluted from the CM 8HR column using a steep linear gradient from 0 to 100% eluent B (20 m*M* sodium phosphate buffer, pH 7.0, with 1 *m* sodium chloride) in 2 min at 1 ml/min.The mass recovery was done at both pH 7.0 (20 m*M* sodium phosphate) and pH 8.2 (20 m*M* Tris–HCl) on the Protein-Pak Q 8HR column. The gradient was 0–50% eluent B (each eluent A with 1 *M* sodium chloride) in two min at 1 ml/min. The mass recoveries for these proteins were determined from the ratio of peak areas with and without the column in line.

The protein-binding capacities of the packings were determined by pumping the appropriate protein solution into the column until breakthrough occurred. The columns (75 mm × 8 mm steel column) were then flushed with an eluent A until the absorbance at 280 nm decreased below 0.02 absorbance units. The bound protein eluted with an eluent B and the amount was determined based on

TABLE II

MASS RECOVERY OF VARIOUS PROTEINS USING PROTEIN-PAK Q 8HR

Conditions: eluent A, 20 m*M* Tris–HCl, pH 8.2; eluent B, eluent A + 1 *M* sodium chloride; injection volume, 20 μl in eluent A (150 μg); flow-rate, 1 ml/min; gradient, 0–50% B in 2 min.

Proteins, 150 μg (0.03% of capacity)	Molecular weight	Isoelectric point	Recovery (%)
Bovine serum albumin	67 500	4.9	84
Carbonic anhydrase	28 000	7.3	92
Conalbumin	76 600	6.8	82
Cytochrome *c*	12 400	9.4	86
Ferritin	445 000	3	91[a]
Human transferrin	77 000	6.0–6.5	84
Goat immunoglobulin G	155 000	6.0–7.0	90
β-Lactoglobulin A	35 000	5.1	70
Ovalbumin	44 500	4.7	87
Soybeen trypsin inhibitor	21 500	4.5	87

[a] Ferritin: eluent A, 20 m*M* sodium phosphate, pH 7.0; eluent B, eluent A + 1 *M* sodium chloride.

its extinction coefficient. Bovine serum albumin (4 mg/ml, extinction coefficient equal to 0.65 absorbance units per mg/ml) was used to measure the capacity of the strong anion exchanger. The capacity study for the Protein-Pak CM 8HR column employed cytochrome *c* (4 mg/ml, extinction coefficient of 1.9); eluents A and B were 25 m*M* 2-(N-morpholino)ethanesulfonic acid (MES) (pH 5.0) and 25 m*M* MES (pH 5.0) with 1 *M* sodium chloride, respectively.

The chicken egg white was separated from the yolk, diluted (1:4 with eluent A) and then filtered (0.45-μm Millex Filter, Millipore) prior to analysis. The diluted egg white (100 μl) was applied to the Protein-Pak CM 8HR AP-1 glass column at pH 6.0. The most retained peak (containing lysozyme) was collected in five 1-ml fractions and assayed for activity. A commercial preparation of lysozyme was also analyzed on the CM 8HR column and checked for biological acitivity after chromatography. The

TABLE III

MASS RECOVERY OF VARIOUS PROTEINS USING PROTEIN-PAK CM 8HR

Conditions: eluent A, 20 m*M* sodium phosphate, pH 7.0; eluent B, eluent A + 1 *M* sodium chloride; injection volume, 15 μl in eluent A (150 μg); flow-rate, 1 ml/min; gradient, 0–100% B in 2 min.

Proteins, 150 μg (0.08% of capacity)	Molecular weight	Isoelectric point	Recovery (%)
Chymotrypsin	21 600	8.8	94
Chymotrypsinogen A	25 000	9	92
Cytochrome *c*	12 400	9.4	98
Hemoglobin	64 500	7	73
Immunoglobulin G	155 000	6.0–7.0	92
β-Lactoglobulin A	35 000	5.1	89
Lysozyme	14 400	11	92
Myoglobin	17 500	7	89
Ovalbumin	44 500	4.7	88
Soybean trypsin inhibitor	21 500	4.5	91

enzyme assay was discussed previously [8].

Glucose-6-phosphate dehydrogenase (G6-PDH) was isolated from yeast enzyme concentrate (2 mg) using the Protein-Pak Q 8HR AP-1 glass column. The mobile phases were 20 m*M* Tris acetate, pH 8.0 (eluent A) and eluent A with 0.5 *M* sodium acetate (eluent B). Ten fractions (2 min each or 3.12 ml) were collected and assayed for protein concentration and G6-PDH activity. The fractions were collected based on the retention time of a commercial preparation of G6-PDH. The crude yeast enzyme concentrate was also checked for G6-PDH activity. The G6-PDH assays was discussed in an earlier publication [8]. The assay used to measure the protein concentrations was also reported earlier [8].

Regeneration

The Protein-Pak Q and CM 8HR AP-1 glass columns were regenerated by washing with (four column volumes each) water, 0.1 *M* sodium hydroxide, water, 30% acetic acid, water, and finally 1 *M* sodium chloride. The washings were carried out at 0.5 ml/min on both columns. The resolution of the standard protein mixture (Table I) was determined before and after the regeneration.

Natural mixtures

Egg white (prepared above) and mouse serum were applied to the Protein-Pak Q 8HR column. The separation of mouse serum and egg white proteins was done at pH 8.2 using the Tris–HCl buffers mentioned above.

Papain from papaya latex was analyzed on the Protein-Pak CM 8HR column using the sodium phosphate buffers at pH 7.0.

RESULTS AND DISCUSSION

The column backpressure was monitored to determine the flow-rate range over which the packing can be used. The pressure across the packed bed is proportional to the inverse square of the mean particle size. Therefore, the backpressure is expected to decrease with an increase in particle size. The pressure across the Protein-Pak Q 8HR AP-1 glass column was 2.6–4.8-fold greater than that of the 15HR column between 0.5 and 2.0 ml/min (for example, at 2 ml/min, 260 p.s.i. *versus* 100 p.s.i.). The 15HR column and the 40HR column differed the most in pressure at 4 ml/min where the latter column was 4-fold lower in pressure (292 p.s.i. *versus* 72 p.s.i.). The Protein-Pak CM HR AP-1 glass columns also showed a decrease in pressure across the packed bed as particle size increased. At 4 ml/min the pressures were 338, 116 and 100 p.s.i. for the 8, 15 and 40 HR AP-1 glass columns, respectively.

The protein resolutions of the standard mixture in Table I by the Protein-Pak Q HR series are shown in Figs. 1–3. The proteins are baseline resolved on each packing. The difference in the 8-μm and 15-μm packings in Figs. 1 and 2 is noted by the higher resolution on the smaller particle packing. The 40-μm packing in Fig. 3 gave much broader peaks as expected and as supported by its lower efficiency than the 8HR AP-1 column (1000 *versus* 4000 plates at 1 ml/min). The retention times of the proteins are slightly less on the 40HR column because a lower dead volume solvent delivery system (Model 625) was used for its analysis. The Q 8HR and 15HR packings were analysed on the larger delay volume system (Model 600E).

The selectivities were constant (within the error limits of the measurement) with an increase in particle size for both the anion- and cation-exchange columns. Therefore, a separation can be scaled-up to larger columns using either the same packing or one with a greater particle size.

The 40HR bulk packings are applicable at the early purification stage where rapid throughput of large sample volumes may be required. The selectivity (α) did not change significantly with an increase in flow-rate. As an example, the change in the selectivity with flow-rate is presented in Fig. 4 for Protein-Pak Q 40HR packing. The peak widths do change with flow-rate as expected which leads to a decrease in resolution. At the early stages of purification throughput is more important than high resolution.

Ion-exchange packings separate proteins based on both their isoelectric point and surface charge (Z value) [9,10]. The strength of the electrostatic interaction between the packing and the protein determines its retention on the column. Therefore, the proteins in the standard mixtures interacted with the CM and Q packings to various degrees resulting in their separation. Since a wide range of molecular weight and isoelectric point proteins are separated on both the Q and CM HR packings, they should

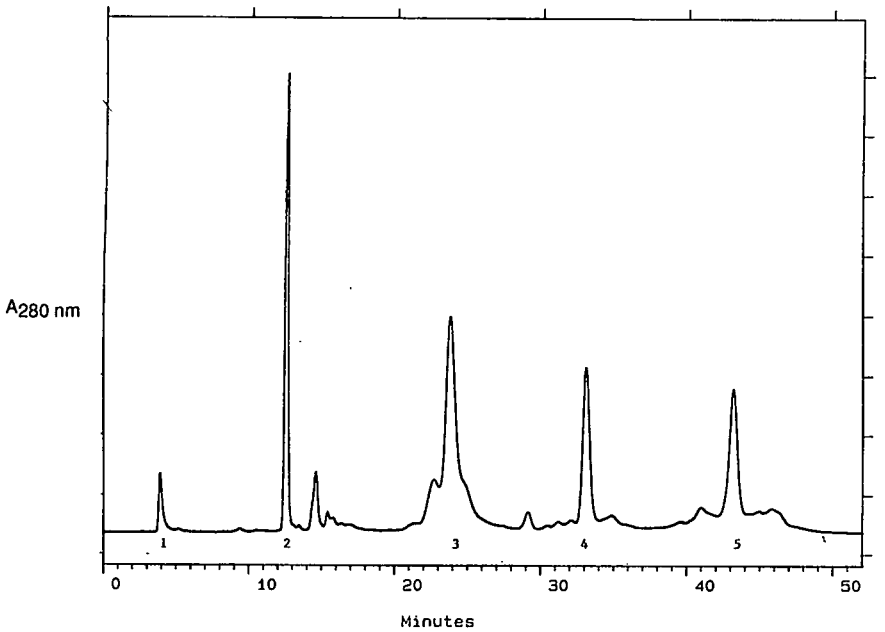

Fig. 1. Protein resolution on Protein-Pak Q 8HR anion-exchange column. Column, AP-1 (100 mm × 10 mm) glass column; eluent A, 20 m*M* Tris–HCl (pH 8.2); eluent B, eluent A + 1 *M* sodium chloride; flow-rate, 1 ml/min; detector, 280 nm; gradient, 0–25% eluent B over 38 min; sample load, 0.5 mg protein; system, Model 600E multisolvent delivery system. Peaks: 1 = adenosine; 2 = carbonic anhydrase; 3 = human transferrin; 4 = ovalbumin; 5 = soybean trypsin inhibitor.

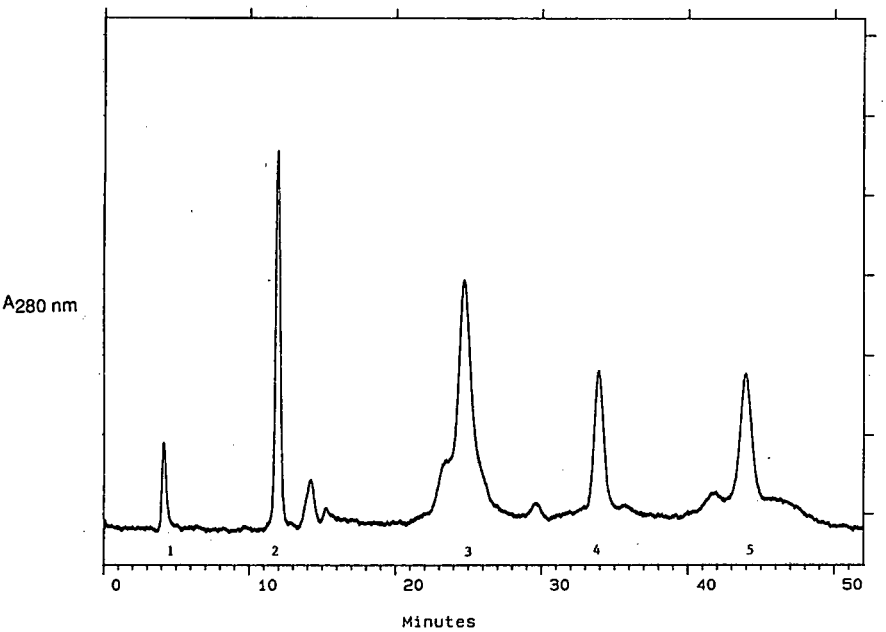

Fig. 2. Protein resolution on Protein-Pak Q 15HR anion-exchange column. For conditions see Fig. 1.

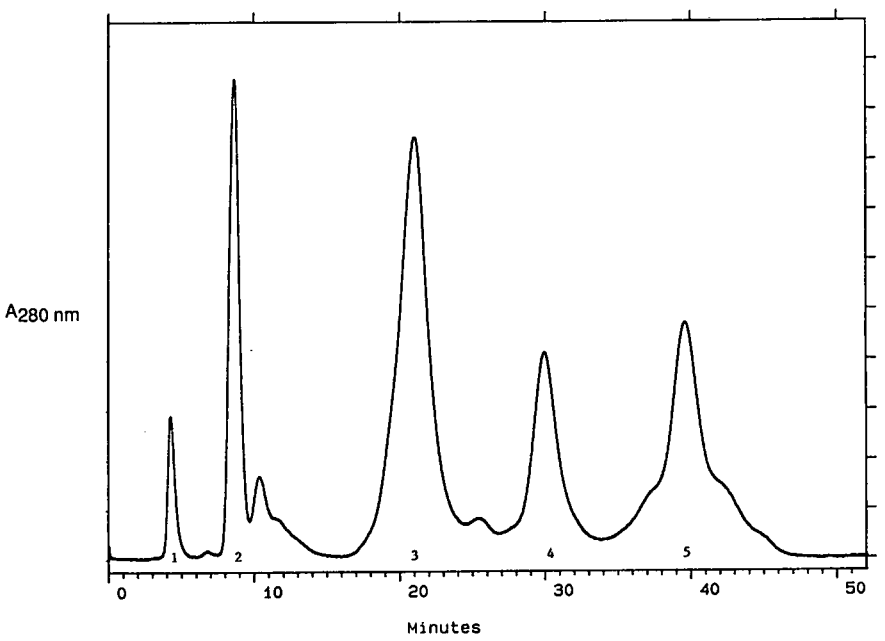

Fig. 3. Protein resolution on Protein-Pak Q 40HR anion-exchange column. System: Model 625 non-metallic LC. For all other conditions see Fig. 1.

be applicable for the purification of many different proteins.

The separation of the desired protein can be optimized by changing the operating pH. The operating pH may also be determined by the pH range where the biological acitivity is maintained. Therefore, it is important to show that a given packing is operational over a pH range. A protein mixture was well resolved on the Protein-Pak Q HR column at both pH 8.2 and pH 6.0 when comparing the upper (A) and lower chromatogram (B) in Fig. 5. The major difference is that carbonic anhydrase is not retained at pH 6.0 since its isoelectric point is pH 7.0. In anion-exchange chromatography a protein is normally retained if the operating pH is above its isoelectric point [9]. As discussed earlier, the number and the distribution of charges on the protein surface also impacts upon its retention [9].

Another property of ion-exchange packings which determines their applicability for purification is the protein-binding capacity. The capacity is influenced by the physical properties of the given protein, pH, buffer strength and buffer type [1]. The flow-rate was shown not to have an effect on the protein-binding capacity in the normal operating range. The capacity of the Protein-Pak Q and CM HR series are given in Table IV. The capacity of the Protein-Pak Q 8HR AP-1 column (510 mg BSA) is competitive with that of other commercial materials. For instance, the 1-ml Pharmacia Mono Q column has a capacity of 100 mg BSA and the Toso-Haas Progel-TSK DEAE 5PW column (75 mm × 7.8 mm) has a capacity of 272 mg BSA. The capacity is consistent across particle size for both CM and Q HR packings which facilitates scale-up.

Most ion-exchange columns give good protein resolution up to at least 5% and sometimes as high as 20% of absolute protein binding capacity. The upper level (20%) is referred to as the dynamic capacity and represents the amount of protein that can be adsorbed and desorbed rapidly (about 30 s) [1]. The amount of protein loaded on the column also impacts upon the resolution. Most preparative chromatography conditions will set the loading level at the dynamic capacity.

Fig. 6 illustrates chromatography at three loads on the Protein-Pak Q 8HR AP-1 column. The three levels represent 0.1% (0.53 mg), 5% (26 mg) and 20% (106 mg) of capacity (capacity data in Table IV), respectively. The selectivity between conalbu-

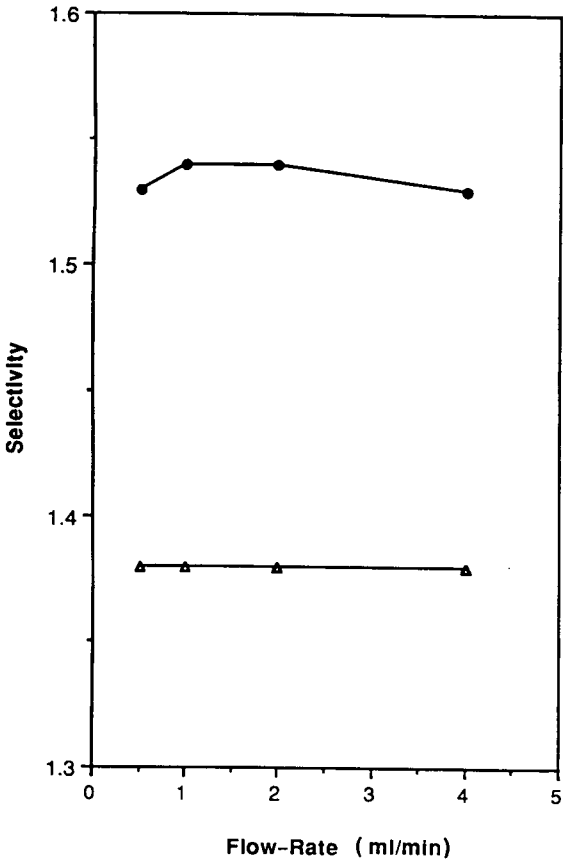

Fig. 4. Flow-rate *versus* selectivity on Protein-Pak Q 40HR column. Flow-rates, 0.5, 1, 2 and 4 ml/min; gradient, 0–25% eluent B. For all other conditions see Fig. 1. Selectity (α): ● = ovalbumin–human transferrin; △ = soybean trypsin inhibitor–ovalbumin.

min and ovalbumin did not change as the protein load increased; however, both proteins eluted slightly earlier at the highest loading. The shift in ovalbumin did cause an increase in the selectivity (1.03 at 5% *vs.* 1.24 at 20%) between this protein and soybean trypsin inhibitor. The minor component eluting with the soybean trypsin inhibitor became more pronounced at the high load.

Fig. 7 presents the effect of sample load on the Protein-Pak CM 8HR column. Chromatography is shown at 0.10% (0.2 mg), and 20% (32 mg) of capacity. The five proteins are still baseline resolved at 5% of capacity which is desired (data not shown). The proteins are separated at 20% loading but there is a noticeable decrease in resolution. The decrease in resolution between neighboring proteins was due more to the increases in peak widths than to changes in selectivity. For example, the width of both ribonuclease A and chymotrypsinogen A increased three-fold between the highest and lowest load but the selectivity changed by only 9%. The Protein-Pak Q and CM 8HR columns can definitely be used up to 5% of capacity for protein resolution and in most cases at loads equivalent to the dynamic capacity.

The Protein-Pak HR series of packings contain a hydrophilic polymeric material with 1000-Å pores which allows a wide range of proteins to be recovered at high yield. Excellent protein recoveries have been reported for the strong cation- (SP 8HR) and weak anion- (DEAE 8HR) exchange packings [8]. Tables II and III give the mass recoveries for various proteins on Protein-Pak Q 8HR and CM 8HR, respectively. The proteins cover a wide range of molecular weights and isoelectric points. The recoveries on the Protein-Pak Q 8HR were greater than 80% for all proteins except β-lactoglobulin A. β-Lactoglobulin A is very strongly retained on an anion exchanger due to the available surface charges. This strong retention by the anion exchanger probably leads to some irreversible binding, especially at the low load (150 μg) used in this study. The recovery of β-lactoglobulin was not improved by changing the operating conditions to pH 7.0. The mass recovery of ferritin ws significantly greater at pH 7.0 than at pH 8.2 (91% *versus* 57%). The low isoelectric point of ferritin (pI 3) and its high molecular weight may have contributed to its low recovery at the higher pH. Several of the other proteins also gave higher recoveries at pH 7.0 than at pH 8.2 (for example, conalbumin, 104%, bovine serum albumin, 113%). When the operating pH is closer to the isoelectric point of a protein its net charge is less and consequently it may bind less strongly to the ion-exchange packings [11].

The mass recoveries of 10 proteins on Protein-Pak CM were greater than or equal to 88%. The eleventh protein analyzed, hemoglobin, was recovered at 73%. Hemoglobin recoveries were lower than those of the other proteins on Protein-Pak SP 8HR (84%) and SP 5PW (65%) [8]. The possible reasons given for the low recovery of hemoglobin on the SP cation exchange packings were the dependence of recovery on the gradient steepness and

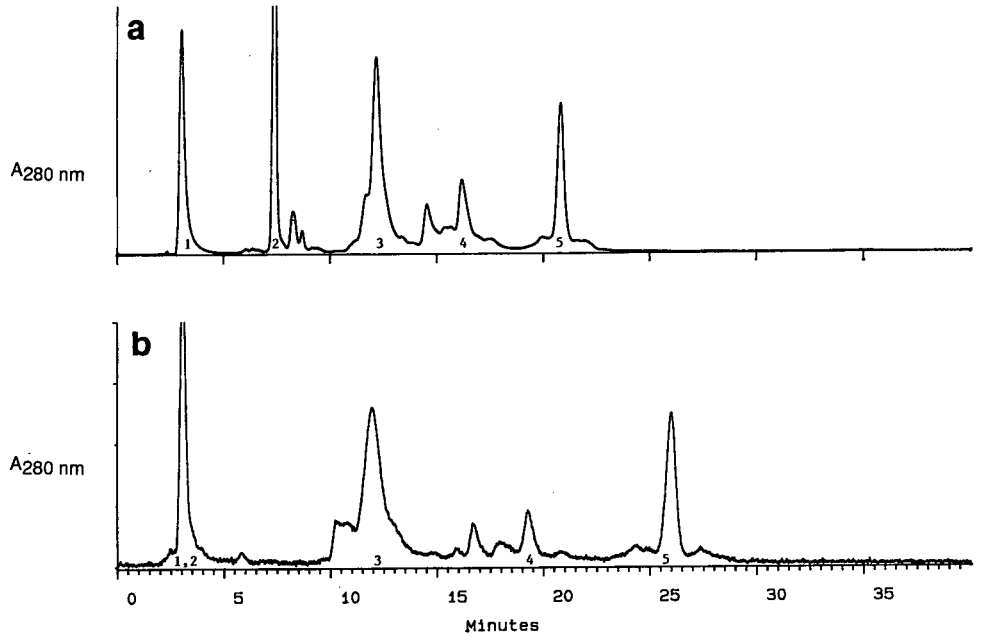

Fig. 5. Protein resolution *versus* pH on Protein-Pak Q 8HR column. Flow-rate, 2 ml/min; gradient, 0–40% eluent B in 40 min. (a) injection volume, 200 μl (1 mg); for all other conditions see Fig. 1; (b) eluent A, 20 m*M* piperazine–HCl, pH 6.0; eluent B: eluent A + 0.5 *M* sodium chloride; injection volume, 90 μl (0.43 mg). For identity of peaks see Fig. 1.

the pH. In addition, it was suggested that since hemoglobin consists of four subunits it may be difficult to recover as an intact protein [8].

The large-scale processes used in manufacturing must be able to give good recovery of both mass applied and the biological activity. An increase in specific acitivity should occur at each purification step. Protein purification by ion-exchange chromatography in contrast to reversed-phase seldom causes loss of biological activity. However, conformational changes during ion-exchange chromatography which result in loss of mass (irreversible binding) or biological activity have been addressed [12,13]. These conformational changes occur due to either protein–protein or protein–surface interactions during adsorption and desorption. If the pro-

TABLE IV

PROTEIN-BINDING CAPACITY OF THE PROTEIN-PAK HR SERIES PACKINGS

Conditions: Anion: eluent A, 20 m*M* Tris–HCl, pH 8.2; eluent B, eluent A + 1 *M* sodium chloride; sample, bovine serum albumin (BSA) in eluent A; cation: eluent A, 25 m*M* MES, pH 5.0; Eluent B, eluent A + 1 *M* sodium chloride; sample, cytochrome *c*; column, AP-1 (100 mm × 10 mm) glass column.

Capacity	Anion exchangers: Protein-Pak Q			Cation exchangers: Protein-Pak CM		
	8HR	15HR	40HR	8HR	15HR	40HR
BSA (mg/ml)	65	75	74			
BSA (mg/column)	510	590	581			
Cytochrome *c* (mg/ml)				23	25	32
Cytochrome *c* (mg/column)				181	196	250

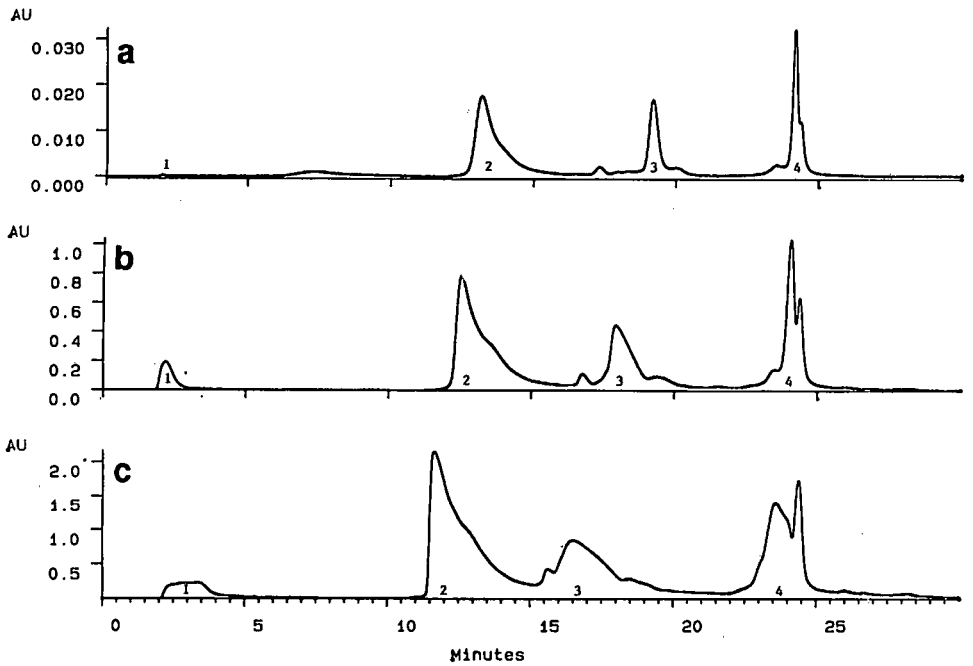

Fig. 6. Protein load study on Protein-Pak Q 8HR column. Gradient, 0–25% eluent B in 18 min; for all other conditions see Fig. 2. Peaks: 1 = cytochrome *c*; 2 = conalbumin; 3 = ovalbumin; 4 = soybean trypsin inhibitor; sample loads, (a) 0.53 mg; (b) 26 mg; (c) 106 mg.

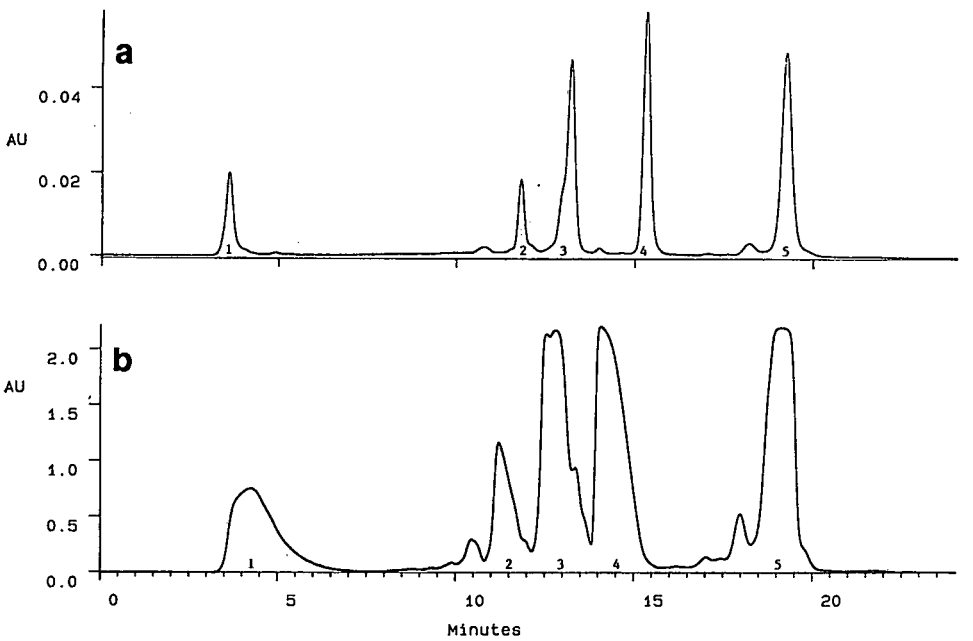

Fig. 7. Protein load study on Protein-Pak CM 8HR column. Column, AP-1 (100 mm × 10 mm) glass column; eluent A, 20 m*M* sodium phosphate at pH 7.0; eluent B, eluent A + 1 *M* sodium chloride; flow-rate, 1.56 ml/min; gradient, 0–50% eluent B in 20 min; system: Model 625 non-metallic LC. Peaks: 1 = myoglobin; 2 = ribonuclease A; 3 = chymotrypsinogen; 4 = cytochrome *c*; 5 = lysozyme. (a) Injection volume, 10 μl (0.2 mg); (b) injection volume, 1600 μl (32 mg).

tein conformation changes during the adsorption/desorption process, then intermediates can form which bind irreversibly or become biologically inactive. Biologically active lysozyme and glucose-6-phosphate dehydrogenase were purified on Protein-Pak 8HR AP-1 glass columns as shown in Table V and Figs. 8 and 9. There was no evidence that irreversible intermediates formed or the presence of any problems associated with protein-surface interactions.

The lysozyme peak was isolated from chicken egg white at pH 6.0 on the Protein-Pak CM 8HR AP-1 column. The biological activity was found in fraction 4 (25–26 min). The retention times for the lysozyme isolated from egg white and that of a commercial lysozyme preparation were the same, as shown in Fig. 8. Both lysozyme peaks contained biological activity.

TABLE V

PURIFICATION OF BIOLOGICALLY ACTIVE PROTEINS

Conditions: Protein-Pak Q 8HR: eluent A, 20 m*M* Tris acetate, pH 8.0; eluent B, eluent A + 0.5 *M* sodium acetate; sample, yeast enzyme concentrate, 200 μl (10 ml/ml) ref. Fig. 9. Protein-Pak CM 8HR: eluent A, 20 m*M* sodium phosphate, pH 6.0, eluent B, eluent A + 1 *M* sodium chloride; sample, chicken egg white; ref. Fig. 8.

Column	Q 8HR
Protein	Glucose-6-phosphate dehydrogenase from yeast enzyme concentrate (YEC)
Mass applied (mg)	2
Fractions 19–23 (38–46 min)	
Mass (mg)	0.075
Units	10.4
Specific activity (units/mg)	138
Crude specific activity (units/mg)	7.9
Purification factor	18
Column	**CM 8HR**
Protein	Lysozyme from chicken egg white
Amount applied (1:4 dilution) (μl)	100
Fraction 4 (25–26 min)	
Mass in lysozyme peak (μg)	27
Mass in enzyme reaction (μg)	2.7
Units	40
Specific acitivity (units/mg)	14 814
Commerical enzyme	
Mass in enzyme reaction (μg)	4
Units	18
Specific acitivity (units/mg)	4500
Ratio laboratory: commercial preparation	3.3

Glucose-6-phosphate dehydrogenase was isolated from yeast enzyme concentrate on the Protein-Pak Q 8HR column with a 18-fold purification. The specific activity for G6-PDH increased from 7.9 units/mg in the crude mixture to 138 units/mg for material collected from the column. The shaded area in Fig. 9 shows that G6-PDH was one of the more retained yeast enzymes and composed about 4% of the total sample mass. The broad area with biological activity may be related to the many variants of G6-PDH (a tetrameric enzyme with molecular weight between 206 000 and 240 000).

Stability

The use of the ion-exchange columns for large-scale purification processes is affected by the stability of the columns to regeneration, and temperature. The ability to regenerate a packing is critical to its utilization in the early stage with crude mixtures. The lifetime of the column can be extended by regeneration. The Protein-Pak Q 8HR and CM 8HR AP-1 glass columns withstood regeneration with 0.1 *M* sodium hydroxide followed by 30% acetic acid. In most cases the columns were regenerated by washing with four column volumes of each eluent as determined by testing the standard protein mixtures. There were no changes in backpressures nor in protein resolution after regeneration. The backpressures of the Q 8HR column were 250 p.s.i. before and 180 p.s.i. after regeneration at 1 ml/min. It is interesting to note that the Protein-Pak HR columns can withstand washing with 50% aqueous ethanol to remove lipids.

The ability to perform a gradient analysis at 4°C is important for enzymes that may decrease in activity when purified at room temperature. The Protein-Pak Q 8HR AP-1 column could be operated up to 1.5 ml/min at 4°C without the backpressure exceeding the recommended 500 p.s.i. The pressure was 180 p.s.i. at room temperature and 330 p.s.i. at 4°C (1 ml/min flow-rate). The backpressure decreased by about 50 p.s.i. when the column was switched to a high-salt buffer. The larger particle

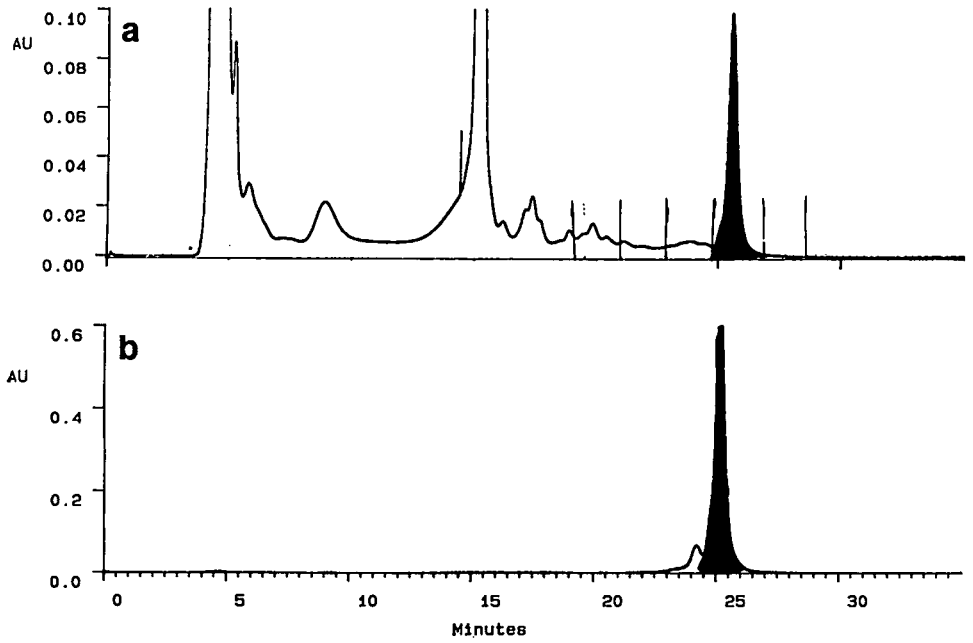

Fig. 8. Purification of egg white lysozyme on Protein-Pak CM 8HR. Column, AP-1 glass column (100 mm × 10 mm); eluent A, 20 m*M* sodium phosphate, pH 6.0; eluent B, eluent A + 1 *M* sodium chloride; flow-rate, 1 ml/min; gradient, 0–50% buffer B in 15 min, hold for 15 min. (a) Lysozyme from egg white; injection volume, 100 μl of 1:4 dilution with eluent A; (b) commercial lysozyme, injection volume, 100 μl (0.5 mg). Shaded peak areas contain lysozyme activity.

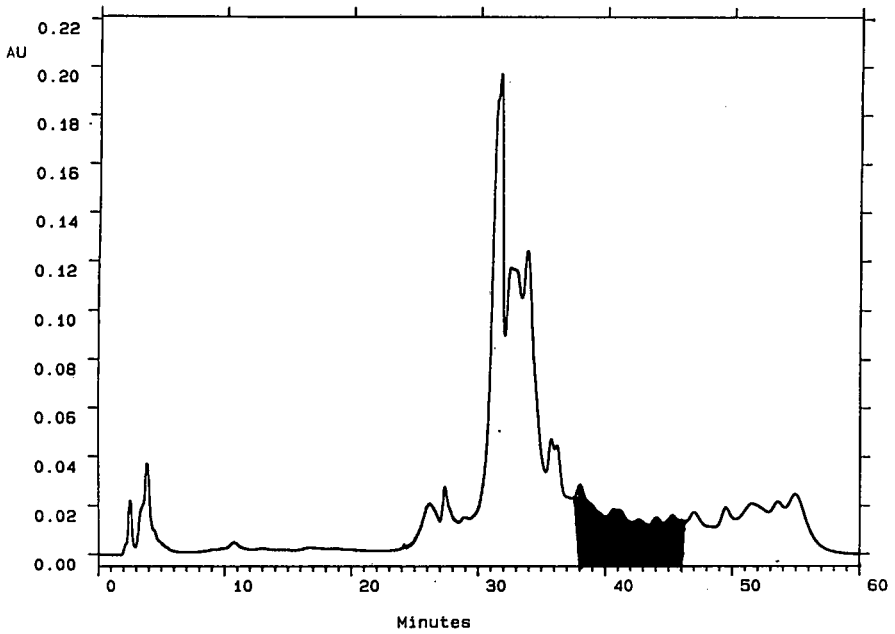

Fig. 9. Purification of glucose-6-phosphate dehydrogenase on Protein-Pak Q 8HR. Column, AP-1 (100 mm × 10 mm) glass column; eluent A, 20 m*M* Tris acetate at pH 8.0; eluent B, eluent A + 0.5 *M* sodium acetate; flow-rate, 1.56 ml/min; detector, 280 nm; gradient, 17 min hold, 0–100% eluent B over 30 min; sample load, 200 μl (2 mg) yeast enzyme concentrate in eluent A. Shaded area contains enzyme activity.

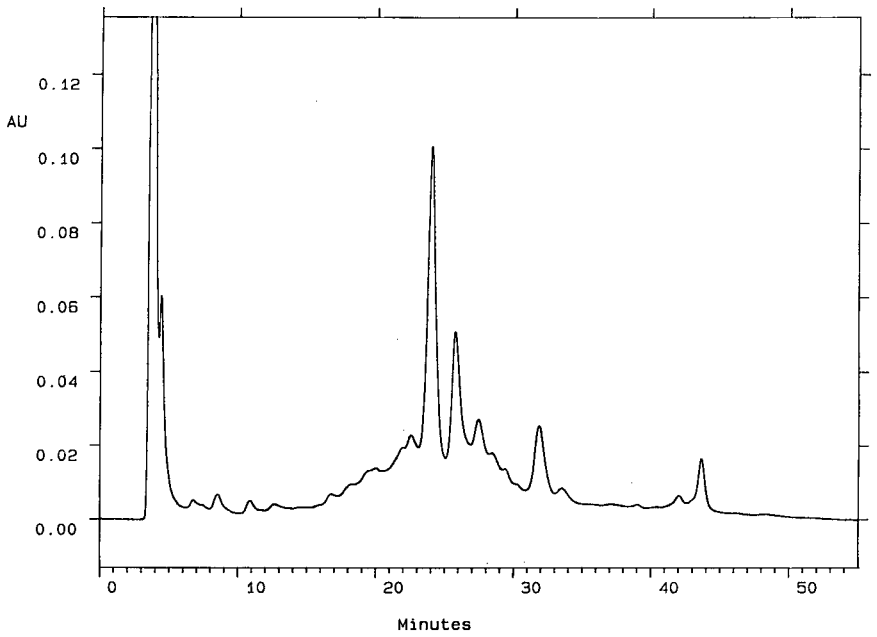

Fig. 10. Chromatogram of papain on Protein-Pak CM 8HR. Injection volume, 200 μl (400 μg) papain from Papaya latex; for all other conditions see Fig. 7.

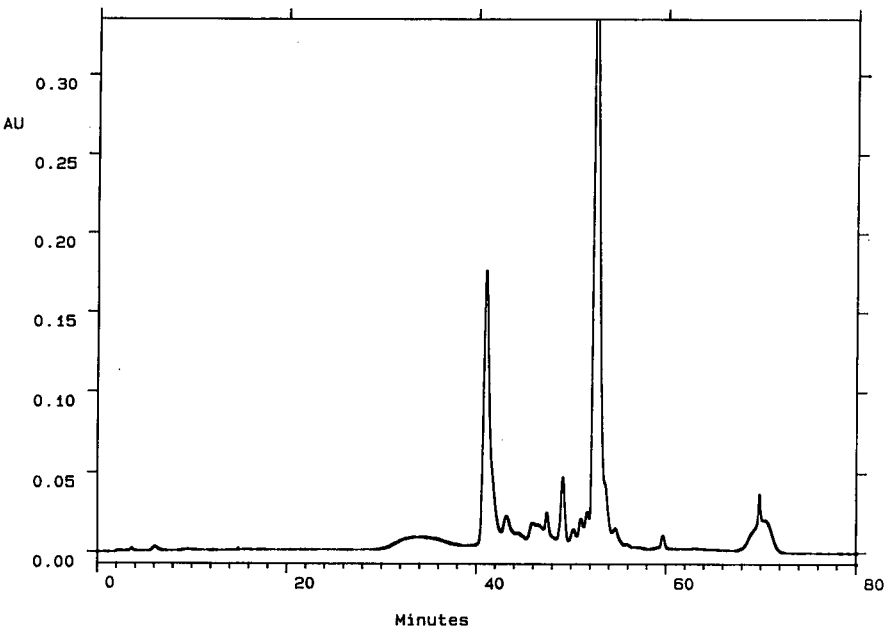

Fig. 11. Chromatogram of egg white proteins on Protein-Pak Q 8HR column. Flow-rate, 1.56 ml/min; gradient, 22 min in eluent A then 0–25% eluent B in 40 min; injection volume, 100 μl of chicken egg white diluted 1:4 with eluent A. For all other conditions see Fig. 1.

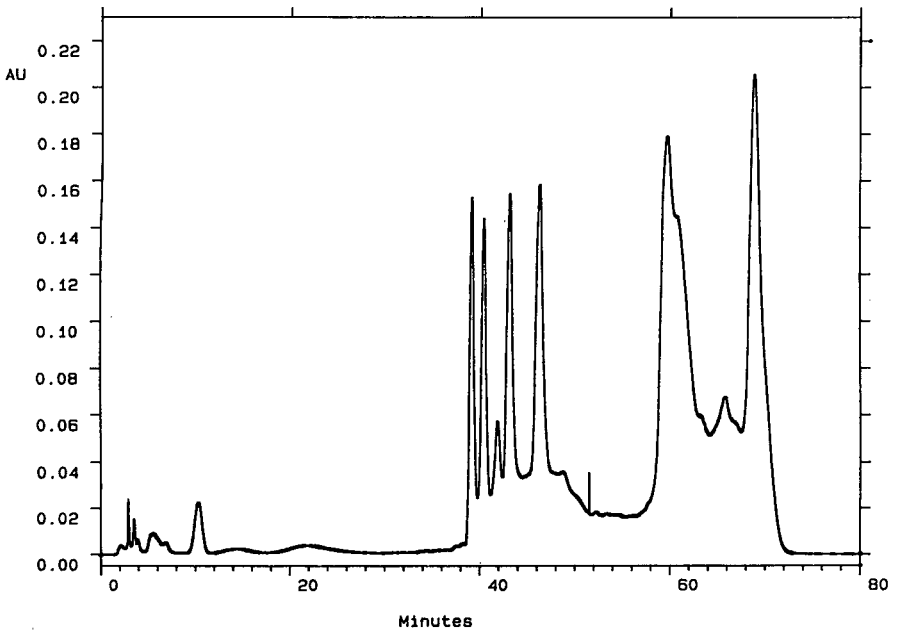

Fig. 12. Chromatogram of mouse serum proteins on Protein-Pak Q 8HR. Flow-rate, 1.56 ml/min; gradient, 22 min in eluent A then 0–25% eluent B in 40 min; injection volume, 75 μl of mouse serum. For all other conditions see Fig. 1.

packings (15 and 40HR) should operate in the cold without difficulty since the backpressure will be lower for these materials than the 8HR packing as discussed earlier.

Natural protein mixtures

The industrial processes require the separation of crude mixtures of proteins with a variety of different properties. The Protein-Pak HR series performed well for separating natural protein mixtures. Fig. 10 shows the separation of papain on the Protein-Pak CM 8HR column which is competitive with that shown in the product bulletin for another commercial CM column [14]. The egg white proteins were resolved on Protein-Pak CM 8HR column as shown in Fig. 8a; ovalbumin is not retained. Conalbumin appears at about 15 min and lysozyme is the most retained peak.

The Protein-Pak Q 8HR column was used to separate the proteins in egg white and mouse serum at pH 8.2. Both mixtures contain acidic proteins (isoelectric point less than 7.0) which are separated on the anion-exchange column as shown in Figs. 11 and 12. The two retained peaks in Fig. 11 are probably conalbumin and ovalbumin. Some of the proteins in mouse serum in Fig. 12 which are retained and separated are albumin, transferrin and immunoglobulins.

CONCLUSIONS

The Protein-Pak HR ion-exchange series meets the challenges of industrial large-scale purification schemes. The Protein-Pak HR series packings can be used at any stage since they (1) perform well at fast flow-rates for rapid throughput, (2) have competitive protein-binding capacities, (3) are usable at low temperatures (4°C) and (4) can be regenerated. The Protein-Pak 8HR series should work well in a protein purification scheme. Proteins were recovered from the 8HR packing in high yield and with retention of biological activity. The Protein-Pak HR packings also performed well at loads equivalent to dynamic capacity; the amount of crude material applied in preparative chromatography is often about 20% (dynamic capacity) or greater of the absolute capacity. The packings can be used for the separation of crude mixtures such as mouse serum

and egg white. Since both anion and cation materials are available which operate over a wide pH range the Protein-Pak HR series should be included in the purification scheme for many therapeutic proteins.

REFERENCES

1 B. Ersson, L. Rydén and J.-C. Janson, in J. C. Janson and L. Rydén (Editors), *Protein Purification: Principles, High Resolution Methods, and Applications*, VCH, Weinheim, 1989, Ch. 1.
2 J. Bonnerjea, S. Oh, M. Hoare and P. Dunhill, *Biotechnology*, 4 (1986) 954.
3 D. Naveh and R. C. Siegel, *Bioseparation*, 1 (1991) 351.
4 T. Burnouf, *Bioseparation*, 1 (1991) 383.
5 H. A. Sober and E. A. Peterson, *J. Am. Chem. Soc.*, 78 (1956) 751.
6 J. Porath, J. C. Janson and T. Laas, *J. Chromatogr.*, 60 (1971) 167.
7 Y. Kato, K. Nakamura and T. Hashimoto, *J. Chromatogr.*, 245 (1982) 193.
8 D. Dion, K. O'Connor, D. Phillips, G. Vella and W. Warren, *J. Chromatogr.*, 535 (1990) 127.
9 W. Kopaciewicz, M. A. Rounds, J. Fausnaugh and F. E. Regnier, *J. Chromatogr.*, 266 (1983) 3.
10 M. A. Rounds and F. E. Regnier, *J. Chromatogr.*, 283 (1984) 37.
11 E. Karlsson, L. Rydén and J. Brewer, in J. C. Janson and L. Rydén (Editors), *Protein Purification: Principles, High Resolution Methods, and Applications*, VCH, Weinheim, 1989, Ch. 4.
12 A. Sadana and R. Raju, *Bioseparation*, 1 (1990) 119.
13 E. S. Parente and D. B. Wetlaufer, *J. Chromatogr.*, 314 (1984) 337.
14 *Product Bulletin for TSK-Gel IEC Series*, TosoHaas, Philadelphia, PA, 1989, p. 5.

Journal of Chromatography, 599 (1992) 255–265
Elsevier Science Publishers B.V., Amsterdam

CHROMSYMP. 2554

Study of the adsorption of self-associating proteins on an anion exchanger

Application to the chromatography of β-lactoglobulin B

Ramona Lemque, Alain Jaulmes, Bernard Sébille and Claire Vidal-Madjar*

Laboratoire de Physico-Chimie des Biopolymères, CNRS UM 27, Université Paris XII, B.P. 28, 94320 Thiais (France)

Piotr Cysewski

Akademia Medyczna w Bydgoszczy, Zaklad Chemii Fizycznej, M. Sklodowskiej-Curie 9, 85-094 Bydgoszcz (Poland)

ABSTRACT

The stoichiometric displacement model (SDM) for the adsorption of proteins on an ion exchanger was extended to describe the adsorption of self-associated molecules. The model based on the mass-balance equations assumes a monomer–dimer equilibrium with a rapid interconversion rate. The role of protein self-association in solution and in the adsorbed state is discussed in terms of adsorption isotherm shapes and of zonal elution chromatographic behaviours. The influence of the parameter Z, defined as the ratio of the protein valency to the displacing counter-ion valency, is demonstrated. The model was applied to analyse the zonal elution behaviour of β-lactoglobulin B (β-lact B) on a polymeric anion-exchange stationary phase. The influence of the counter-ion valency was studied by adding NaCl or Na_2SO_4 to the eluent. The adsorption isotherm of β-lact B on the anion exchanger was determined at pH 7.5 from the non-linear zonal elution profiles observed with increasing sample size. Various aspects of the adsorption behaviour of β-lact B, such as positive cooperativity, were deduced from the isotherm shape and the corresponding Scatchard plot. The column capacity, the association constant in solution and the parameter defining the association in the adsorbed phase were determined from the best fit of the theoretical model to the experimental profiles. In agreement with the model, these parameters can be used to describe the experiments performed with a monovalent or a divalent counter ion. It is shown that protein–protein interactions exist in the adsorbed state and lead to an increase in the protein self-association.

INTRODUCTION

Anion-exchange chromatography is routinely used for the separations of acidic proteins [1]. The process results from the interaction between the protein and the ion exchanger and is described by the stoichiometric displacement model (SDM). It relates the retention volume at low concentration to the displacing salt concentration [2,3]. On the basis of this simple equilibrium model, the adsorption isotherm expression can be derived from the mass balance equations [4,5]. In a previous study [6], we used this SDM adsorption isotherm model to simulate the non-linear chromatographic behaviour of proteins in the isocratic and gradient zonal elution mode.

It has been shown, however, that the SDM model is only a rough representation of the adsorption behaviour of proteins. Several other mechanisms may interfere, such as the hydrophobic interactions [7] or those more complex than the simple electrostatic interactions based on a Coulomb law [8,9]. Another limitation is that the isotherm expression based on the SDM model cannot be applied to predict the elution behaviour of self-associating proteins.

0021-9673/92/$05.00

Milk proteins are often separated using anion-exchange chromatography [10,11] and it is important to understand better the adsorption behaviours of these proteins on ion exchangers. Some whey proteins, such as the β-lactoglobulins (β-lact) A and B, undergo self-associations, which occur in three separate pH ranges [12]. At pH 3.5 and below and at pH 7.5 and above, the monomer is in rapid equilibrium with its dimer. The tendency for dissociation at pH 7.5 and 20°C is in the order A > B. For the pH region 3.5–5.4, β-lact A forms higher order aggregates beyond the dimer such as octamers. In the same pH range, the B variant can form mixed tetramers with the A variant, but B by itself only octamerizes very weakly.

Size-exclusion chromatography has been widely used to study protein self-associations. Quantitative analysis in these experiments is based on a linear partition isotherm model for each of the eluted species. The analytical model [13] for interpreting the frontal elution experiments assumes that the equilibrium between the interacting macromolecules is reached. Numerical simulations are needed to analyse the zonal elution experiments [14,15]. Several algorithms were described that assume rapid [16] or slow kinetic exchanges [17] between the interacting macromolecules.

The frontal elution behaviour of self-associating proteins was studied in subunit-exchange affinity chromatography by Chiancone and co-workers [18–20]. The experiments were analysed on the basis of an equilibrium isotherm expression describing the adsorption behaviour of a self-associating protein on a support where the monomer is immobilized. This experimental approach was applied to extract selectively β-lact A and B from whey [21].

Protein aggregation of β-lact A has been widely studied by Karger and co-workers [22–24] in hydrophobic interaction chromatography. At 4°C, pH 4.5 and high ammonium sulphate concentrations, the chromatograms revealed three peaks which were identified as tetramer, octamer and dodecamer species [22]. These stoichiometries were confirmed in a separate study by on-line low-angle laser light scattering [25]. The study at pH 4.5 of the adsorption isotherm of β-lact A on a methyl ether bonded phase by frontal analysis yielded an S-shape isotherm and the adsorption–desorption isotherms revealed hysteresis loops [23,24]. The role of association on the shape of the adsorption isotherm was demonstrated by Blanco *et al.* [23] and an adsorption isotherm expression is given, valid in the region of low protein concentration, where a linear Henry law can be applied to describe the adsorption behaviour of each individual macromolecule.

A model for protein aggregation was developed by Whitley *et al.* [26] on the basis of a multicomponent Langmuir isotherm accounting for axial dispersion, film mass transfer and intraparticle diffusion. The kinetic interconversion rate for a dimerized system was considered. It was shown that, with a slow reaction rate, the monomer and dimer forms are eluted as two separated species. When the reaction rate increases the chromatogram goes from two well resolved peaks to one broad peak. The model was applied to simulate, in the low concentration range, the elution profile of self-associating proteins and it agrees well with the experiments of Karger and Blanco [27].

Although the effect of association on the frontal elution behaviour of proteins has been widely studied, there are few examples showing the corresponding zonal elution behaviour in mass overload conditions. The importance of the adsorption isotherm model on the shape of the peak resulting from a pulse injection is already well known [28]. Numerical simulations have been used to predict elution profiles in non-linear zonal elution in ion-exchange chromatography [6,29–33]. The models, however, are generally based on a Langmuir [29–31] or a bi-Langmuir type of isotherm [32,33].

Recently, we applied the rigorous SDM adsorption isotherm expression to simulate the peak profiles of bovine serum albumin (BSA) eluted from an anion-exchange column [6], packed with silica coated with a copolymer of polyvinylpyrrolidone (PVP) and polyvinylimidazole (PVI). The elution behaviour of the protein at column saturation was well predicted. This work is a continuation of the previous one and we shall consider the adsorption of a self-associating protein, β-lact B, on the same anion exchanger.

The aim of this work was to study the non-linear zonal elution behaviour of β-lact B on an anion-exchange support. At pH 7.5 where the experiments were performed, one can assume a monomer–dimer equilibrium. The SDM model for ion-exchange adsorption was extended to describe the adsorption

behaviour of proteins with a rapid monomer–dimer kinetic exchange.

THEORY

Ion-exchange isotherm for a monomer–dimer equilibrium

Let us assume that solute P^{m-} and counter ions A^{n-} are in equilibrium with the dimer P_2^{2m-} and an anion exchanger X^+. The equilibria involved may be described by the following equations:

(a) For the liquid phase:

$$2P^{m-} \rightleftharpoons P_2^{2m-} \tag{1}$$

(b) For the exchange between P^{m-} and A^{n-}:

$$nP^{m-} + mX_nA \rightleftharpoons nX_mP + mA^{n-} \tag{2}$$

(c) For the exchange between P_2^{2m-} and A^{n-}:

$$nP_2^{2m-} + 2mX_nA \rightleftharpoons nX_{2m}P_2 + 2mA^{n-} \tag{3}$$

This set of equilibria is ruled by the following three equations:

$$\frac{[P_2^{2m-}]}{[P^{m-}]^2} = K_a \tag{4}$$

$$\frac{[A^{n-}]^Z \{X_mP\}}{\{X_nA\}^Z [P^{m-}]} = K_1 \tag{5}$$

$$\frac{[A^{n-}]^{2Z} \{X_{2m}P_2\}}{\{X_nA\}^{2Z} [P_2^{2m-}]} = K_2 \tag{6}$$

where $Z = m/n$. The brackets [ ] are used for molar concentrations in the mobile phase; the braces { } are used for molar pseudo-concentrations in the exchanger, *i.e.*, the amount of fixed anion per units of a reference volume V', which may be the volume of the mobile phase V_0 accessible to the protein.

The material balance gives for the global molar concentration C in moiety P

$$C = [P^{m-}] + 2[P_2^{2m-}] \tag{7}$$

and for the total amount Q_x of X^+ in the exchanger

$$\frac{Q_x}{V'} = n\{X_nA\} + m\{X_mP\} + 2m\{X_{2m}P_2\} \tag{8}$$

where the counter-ion concentration is assumed to be in large excess compared with that of the protein. The total amount Q of moieties P fixed on the exchanger is

$$\frac{Q}{V'} = \{X_mP\} + 2\{X_{2m}P_2\} \tag{9}$$

Using eqns. 7–9 enables $\{X_nA\}$ to be expressed as a function of Q:

$$\{X_nA\} = \frac{(Q_x - mQ)}{nV'} \tag{10}$$

Using the expressions for $\{X_mP\}$ and $\{X_{2m}P_2\}$ in eqns. 5 and 6 gives for Q

$$\frac{Q}{V'} = K_1 x + 2K_a K_2 x^2 \tag{11}$$

where

$$x = \left(\frac{\{X_nA\}}{[A^{n-}]}\right)^Z \cdot [P^{m-}] \tag{12}$$

The positive root of eqn. 11 can be written in the form

$$x = \frac{2Q/(K_1V')}{1 + \left(1 + \frac{8K_aK_2}{K_1^2V'} \cdot Q\right)^{\frac{1}{2}}} \tag{13}$$

The expression of the relationship between the concentration of the protein in solution, C, and the amount adsorbed, Q, is described by the following set of equations:

$$x = \frac{2Q}{K_1V'\left[1 + \left(1 + 8 \cdot \frac{K_aK_2}{V'K_1^2} \cdot Q\right)^{\frac{1}{2}}\right]} \tag{14}$$

$$[P^{m-}] = x\left(\frac{nV'[A^{n-}]}{Q_x - mQ}\right)^Z \tag{15}$$

$$C = [P^{m-}] + 2K_a[P^{m-}]^2 \tag{16}$$

One often uses the experimentally measurable quantity k', called the limit capacity factor:

$$k' = \frac{1}{V_0}\left(\frac{dQ}{dC}\right)_{C=0} \tag{17}$$

A more proper way of calculating it is given by the expression:

$$k' = \frac{1}{V_0\left(\frac{dC}{dp}\right)_{p=0}\left(\frac{dp}{dQ}\right)_{Q=0}} \tag{18}$$

where $p = [P^{m-}]$. The intermediate expressions are

$$\left(\frac{dp}{dQ}\right)_{Q=0} = \left(\frac{nV'[A^{n-}]}{Q_x}\right)^Z \left(\frac{dx}{dQ}\right)_{Q=0} \tag{19}$$

Since $(dx/dQ)_{Q=0} = 1/K_1V'$ and $(dC/dp)_{p=0} = 1$, we obtain finally for k'

$$k' = K_1 \cdot \frac{V'}{V_0}\left(\frac{Q_x}{n[A^{n-}]V'}\right)^z \tag{20}$$

The equilibrium isotherm as a function of k' reduces to

$$[P^{m-}] = \frac{2Q}{k'V_0}\left(1 - \frac{mQ}{Q_x}\right)^{-z}\cdot\left[1 + \left(1 + 8\cdot\frac{K_aK_2}{V'K_1^2}\cdot Q\right)^{\frac{1}{2}}\right]^{-1}$$

$$C = [P^{m-}] + 2K_a[P^{m-}]^2 \tag{21}$$

This set of equations describing the equilibrium isotherm can be conveniently written as a function of the protein "surface coverage", $\theta = mQ/Q_x$, and in terms of reduced variables:

$$p' = [P^{m-}]\cdot\frac{mV_0}{Q_x} = \frac{2\theta}{k'}(1-\theta)^{-z}[1 + (1 + 8\cdot K'_a\theta)^{\frac{1}{2}}]^{-1} \tag{22}$$

$$C\cdot\frac{mV_0}{Q_x} = p' + 2K'_ap'^2$$

where

$$K'_a = K_a\cdot\frac{Q_x}{mV_0} \text{ and } \beta = \frac{K_2V_0}{K_1^2V'}$$

Influence of the parameters on the shape of the adsorption isotherm

With given values of k', Z and β, Fig. 1a shows the influence of the parameter K'_a on the shape of the adsorption isotherm. Reduced coordinates were used for the graph and the surface coverage θ was plotted as a function of the total amount of protein in solution (CV_0), divided by the maximum amount that can be adsorbed (Q_x/m). For non-zero values of the association constant in solution, K_a, an S-shape is observed. The corresponding Scatchard plot (Fig. 1b) presents a maximum, which indicates a positive cooperativity.

When $K_a = 0$ (dashed line), the adsorption isotherm is that of the SDM model and the resulting Scatchard plot is a non-linear decreasing function. The observation of this hyperbolic-shaped diagram often suggests a heterogeneous nature of the adsorbent surface. As already emphasized, this conclusion is wrong with an ion exchanger if $Z \neq 1$. For comparison, a Langmuir-type isotherm ($Z = 1$, dotted line) and the corresponding linear Scatchard plot are also shown.

The influence of the parameter β on the shape of the equilibrium isotherm is shown in Fig. 2 for given k', Z and β values. The parameter β characterizes the role of the support in the protein aggregation process. Combining eqns. 5 and 6 leads to another expression for β:

$$\beta = \frac{K_2V_0}{K_1^2V'} = \frac{\{X_{2m}P_2\}}{\{X_mP_2\}}\cdot\frac{V_0}{K_aV'} \tag{23}$$

Therefore, β is proportional to the degree of association induced by the support relative to that in solution, the ratio $\{X_{2m}P_2\}/\{X_mP\}$ being considered as a pseudo-association constant for the adsorbed species in the reference volume V'. The protein self-association is increased with increasing β values (Fig. 2a) and larger amounts of protein are ad-

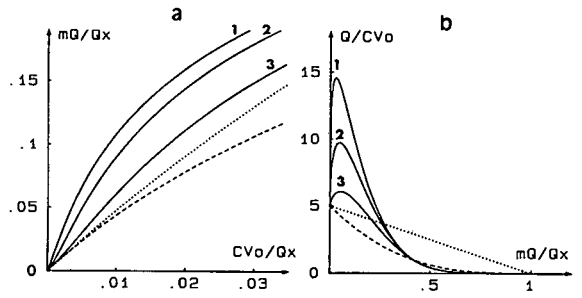

Fig. 1. Influence of the association constant on the shape of the adsorption isotherm of a self-associating protein. (a) Isotherm in reduced coordinates; (b) Scatchard plot. $k' = 5$; $K'_a = K_aQ_x/mV_0$; $Z = 3$. Solid lines, $Z = 3$, (1) $K'_a = 1000$, (2) $K'_a = 100$, (3) $K'_a = 10$; dashed lines, $Z = 3$, $K'_a = 0$; dotted lines, $Z = 1$, $K'_a = 0$.

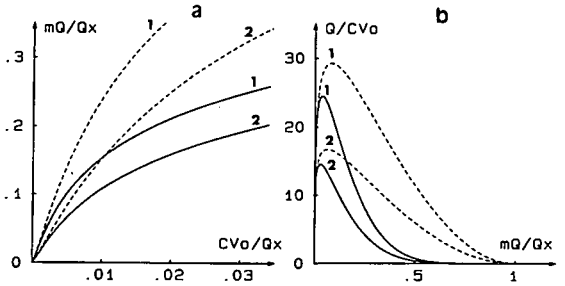

Fig. 2. Influence of the self-association in the adsorbed phase on the shape of the adsorption isotherm of a self-associating protein. (a) Isotherm in reduced coordinates; (b) Scatchard plot. $k' = 5$; $K'_a = 1000$; (1) $\beta = 2$; (2) $\beta = 1$. Solid lines, $Z = 3$; dashed lines, $Z = 1$.

sorbed. Similarly, the Scatchard plot indicates an increased cooperativity, with a higher maximum. The influence of β on the shape of the isotherm differs from that of K'_a in the high concentration range: an increase in β leads to a more convex shape for the decreasing part of the Scatchard plot, while the apparent saturation level is increased.

Fig. 2 shows the isotherm generated with the same parameters (dotted line), except that $Z = 1$. Previously [6], we studied the effect of increasing the ratio Z on the adsorption behaviour of non-associating proteins on an ion exchanger. It was shown that a lower apparent saturation level is reached for larger Z values. This is true also for a self-associating protein as shown in Fig. 2, where the isotherms with $Z = 3$ (solid line) and $Z = 1$ (dotted line) are compared.

Numerical simulations

On the basis of the isotherm model developed for the adsorption on an ion-exchange support of self-associating proteins undergoing a monomer–dimer equilibrium (eqn. 21), we used the numerical simulation methods to generate the theoretical zonal elution profiles.

The numerical method used to solve differential equations describing the propagation of the solute through the column has already been explained [6]. The method ensures mass conservation all through the simulated chromatographic process. The column is divided into an arbitrary number of discrete slices in which the equilibrium is assumed to be reached. The thickness of the slices was chosen so as to give a numerical dispersion equal to the "plate height" of the elution peaks [28].

The parameters defining the equilibrium isotherm are V_0, k', Q_x, m, Z, K_a and β (eqns. 21 and 23). The parameters m and Z can be determined experimentally from independent measurements according to the SDM model: one studies the variation of the retention volume of the solute *versus* the displacing salt concentration, measured at infinite dilution. The parameters k', Q_x, K_a and β are to be optimized by curve fitting of the theoretical model to the experimental profiles observed in mass overload conditions, for various amounts of protein injected.

The influence of the parameters K'_a and β on peak shapes was studied for a retention capacity factor k' equal to 5 (Fig. 3). The elution profiles are given in

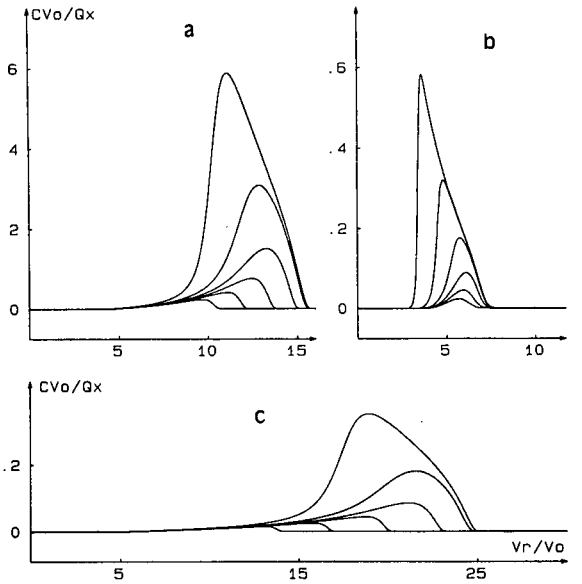

Fig. 3. Chromatographic simulations in isocratic elution on the basis of the isotherms in Figs. 1 and 2. $k' = 5$; $K'_a = K_a Q_x / m V_0$; $Z = 3$. (a) $K'_a = 1000, \beta = 1$; (b) $K'_a = 10, \beta = 1$; (c) $K'_a = 1000$, $\beta = 2$.

reduced coordinates and were simulated on the basis of the isotherms of Figs. 1 and 2. The influence of the association constant is illustrated in Fig. 3a and b, where the profiles are generated for two different values of the association constant, given in reduced units ($K'_a = 1000$ and $K'_a = 10$), but the same β parameter ($\beta = 1$). In agreement with the diagram in Fig. 1, the isotherm with a more convex shape leads to more diffuse fronting peaks, while a shock is observed at the end of the peak. An increase in β, while keeping K'_a constant (Fig. 3a and b), results in an increase in the front tailing at low concentrations and a marked second shock at the peak end.

EXPERIMENTAL

Equipment

Isocratic elution chromatography was conducted on a system consisting of a pump (HPLC PUMP 420; Kontron Instruments, Zürich, Switzerland) and a variable-wavelength UV detector (Spectra-100, Spectra-Physics, San Jose, CA, USA) operating at 280 nm. A sample injector (Model 7125; Rheodyne, Berkeley, CA, USA) with a 0.02-ml loop was used for injecting proteins in the low chromato-

graphic concentration range and a 0.5-ml loop was used for mass-overload experiments. The absorbance output was connected to a digital voltmeter (Model 3497; Hewlett-Packard, Palo Alto, CA, USA). The data stored on floppy disk were processed with a personal computer (Compaq Deskpro, Model 386/20e) equipped with an arithmetic co-processor.

The column packing was the anion exchanger LiChrospher silica (particle size 10 μm and pore diameter 300 Å) (Merck, Darmstadt, Germany) coated with the copolymer PVP–PVI (75:25), cross-linked with butane-1,4-diol diglycidyl ether and prepared as described by Sébille and co-workers [34,35]. The ion-exchange capacity per unit volume was 0.15 mequiv./ml as determined by frontal analysis [6]. The chromatographic column (100 × 4.6 mm I.D.) was slurry-packed under pressure. The temperature of the column was regulated at 25°C by a thermostated water-bath.

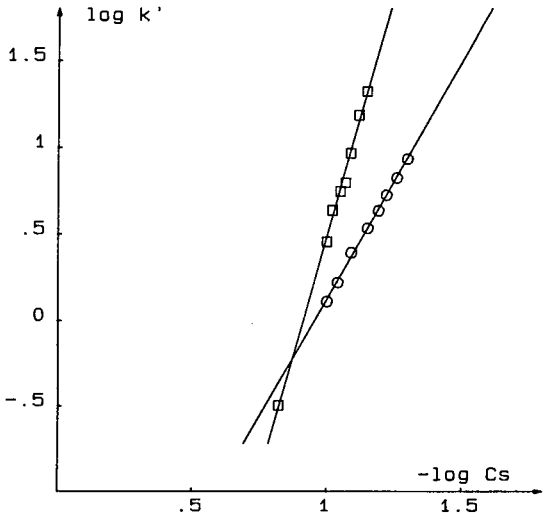

Fig. 4. Dependence of log k' on log(salt concentration) for β-lact B on an anion exchanger, PVP–PVI on silica. Flow-rate, 1 ml/min; temperature, 25°C; eluent, 0.020 *M* Tris buffer (pH 7.5). □ = NaCl; ○ = Na_2SO_4.

Chemicals

Bovine β-lact B was purchased from Sigma (St. Louis, MO, USA). The Tris buffer was obtained from Aldrich-Chemie (Steinheim, Germany).

Procedures

For isocratic elution, the eluent was 20 m*M* Tris buffer (pH 7.5) and the ionic strength was imposed by a monovalent salt (NaCl) or a divalent salt (Na_2SO_4). The protein solutions were prepared in the same eluent. The mobile phase volume accessible to the protein, V_0, was measured from the elution volume of α-chymotrypsinogen A, a protein that is not retained by the anion exchanger.

RESULTS

Retention studies of β-lactoglobulin B at infinite dilution

The value of Z was determined from the retention studies of the protein at infinite dilution according to the SDM model. The capacity factor k' corresponding to zero sample size is related to the displacing counter-ion concentration (A^{n-}) according to the equation

$$\log k' = a - Z\log(A^{n-}) \quad (24)$$

Fig. 4 illustrates the variations of k' with the concentration of two different displacing counter anions, Cl^- and SO_4^{2-}. This was achieved in the isocratic elution mode by adding various concentrations of NaCl and Na_2SO_4 to the eluent and measuring the retention times at the peak maximum, extrapolated to zero sample size. The Z value is 5.7 ± 0.3 with NaCl as the displacing salt and 2.7 ± 0.1 with Na_2SO_4. These values were calculated by a linear regression analysis and the errors are given for a 95% confidence interval. Within experimental errors, the result is in agreement with theory, *i.e.*, Z measured in the presence of a monovalent displacing ion is twice as large as that measured with a divalent ion. The value of the effective charge of the protein, m, is close to 6, a value selected for curve-fitting simulations, with $Z = 6$ when NaCl is used as the displacing salt and $Z = 3$ with Na_2SO_4.

Zonal elution profiles in the isocratic mode

Fig. 5a and b illustrate the elution peaks of β-lact B observed for increasing sample sizes with Na_2SO_4 and NaCl as the displacing salt, respectively (dashed lines). These experiments were performed in the range of low concentrations for the output signal, by using a 20-μl sample loop. The salt concentrations were chosen so as to obtain comparable k' values. Nevertheless, this was only partially achieved be-

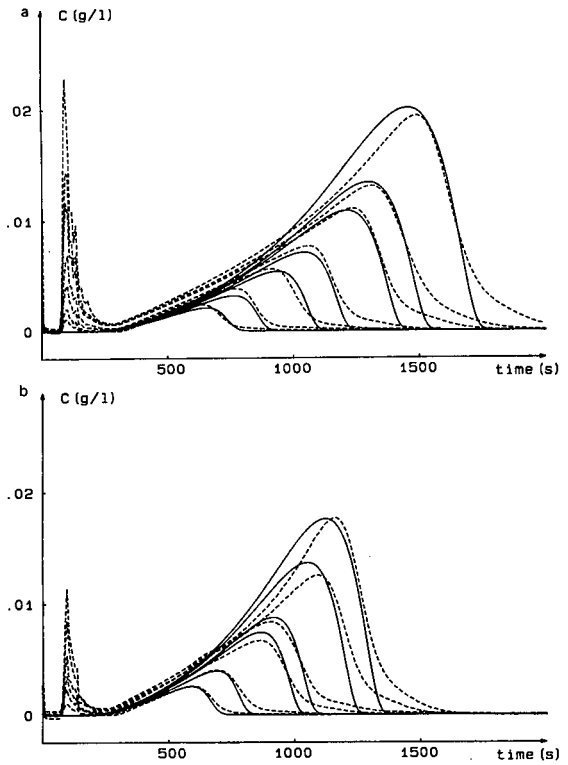

Fig. 5. Experimental and simulated elution profiles of β-lact B eluted from an anion-exchange support for small sample sizes. Sample loop, 0.020 ml; flow-rate, 1 ml/min; V_0 = 1.2 ml; column length, 10 cm; temperature, 25°C; eluent, 0.020 *M* Tris buffer (pH 7.5). Dashed lines, experiment; solid lines = theoretical model with Q_x, K_a and β parameters from Table I. (a) k' = 4, 0.035 *M* Na_2SO_4, sample size 0.005–0.2 mg; (b) k' = 3.6, 0.075 *M* NaCl, sample size 0.005–0.15 mg.

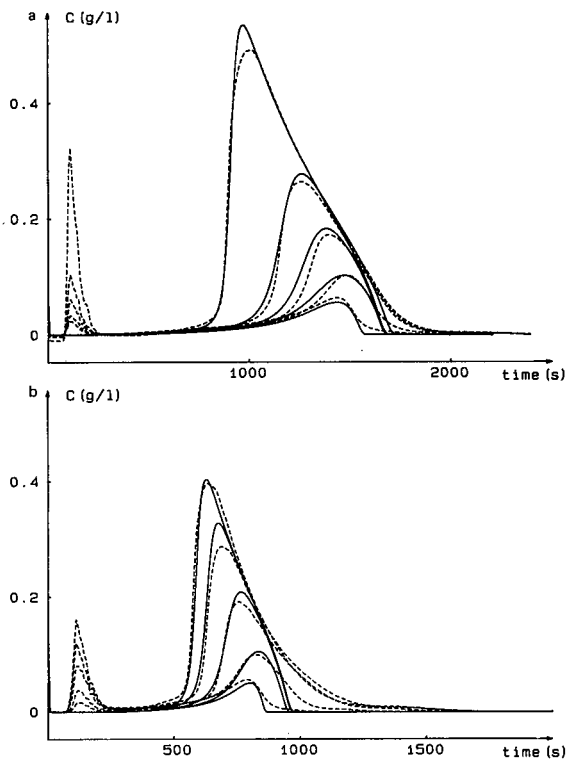

Fig. 6. Experimental and simulated elution profiles of β-lact B eluted from an anion-exchange support for large sample size. Sample loop, 0.5 ml; flow-rate, 1 ml/min; V_0 = 1.2 ml; column length, 10 cm; temperature, 25°C; eluent, 0.020 *M* Tris buffer (pH 7.5). Dashed lines, experimental values; solid lines, best fit of the simulated peak. (a) k' = 3.6, 0.045 *M* Na_2SO_4, sample size, 0.05–5 mg; (b) k' = 2.56, 0.085 *M* NaCl, sample size, 0.05–4 mg.

cause of the large retention time differences observed with small variations of the displacing salt concentration (eqn. 24).

When increasing amounts of β-lact B are injected into the column, the elution peaks begin to deviate from the original symmetric shape by exhibiting a diffuse front. This front tailing is enhanced and the retention time at peak maximum increases. This behaviour reveals a convave adsorption isotherm in the lower protein concentration range.

When increased mass overload conditions, Fig. 6a and b show that the chromatographic behaviour of β-lact B is totally modified. Larger amounts of protein were injected with a 0.5-ml sample loop, 40 times as large as that used in the experiments in Fig. 2. The diffuse front disappears, but a tailing at the rear edge of the peak is observed for large sample sizes and the retention time at the peak maximum decreases with increasing amounts of protein injected.

Curve fitting of theoretical peak profiles to experiments

The profiles for β-lact B observed with increasing sample sizes can be predicted by numerical simulations based on the isotherm model developed for the adsorption on an ion exchanger of a protein undergoing a monomer–dimer equilibrium. The parameters of the adsorption isotherm (eqn. 21) can be determined from the best fit of the theoretical peaks

TABLE I

ISOTHERM PARAMETERS OF β-LACTOGLOBULIN B IN MASS OVERLOAD CONDITIONS

Sample loop: 0.5 ml.

Salt	k'	Z	Q_x/m (mg)	K_a (l/mol)	β
Na_2SO_4 (45 mM)	3.6	3	150	$3.7 \cdot 10^5$	1.6
NaCl (85 mM)	2.7	6	150	$3.7 \cdot 10^5$	1.6

to the experimental ones obtained for large amounts injected (Fig. 6). This was achieved by fixing the three parameters measured at infinite dilution (k', Z, m) and determining Q_x, K_a and β from the least-squares fit of the theoretical profiles to the experimental values (full and dashed lines, respectively, in Fig. 6).

In Table I are listed the parameters of the isotherm determined from the best fit of the model to the experimental profiles observed in isocratic elution when a monovalent or a divalent counter ion is added to the eluent. The concentration of the displacing salt was selected so as to obtain reasonable k' values for performing the experiments. Fig. 7 shows the corresponding adsorption isotherm, in the presence of sodium sulphate (solid line, $Z = 3$). In agreement with the model, the parameters determined for large amounts injected (Table I) predict well the experiments in Fig. 5 performed at a different displacing salt concentration.

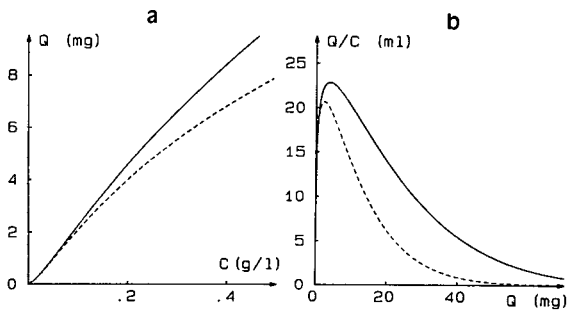

Fig. 7. Equilibrium isotherm of β-lact B adsorbed on the PVP–PVI anion-exchange support. (a) Adsorption isotherm; (b) Scatchard plot. Solid lines, model corresponding to the experiments in Fig. 6a, with $k' = 3.6$, $m = 6$, $Z = 3$, $Q_x = 900$ mg, $K_a = 3.7 \cdot 10^5$ l/mol, $\beta = 1.6$; dashed lines, model with the same parameters, except $m = Z = 6$.

DISCUSSION

The adsorption isotherm on an ion exchanger accounting for solute self-association exhibits an inflection point, with a concave shape towards the abscissa axis in the low concentration range and a convex shape near saturation (Fig. 7). This determines the increase in the retention volumes in the low sample size range and generates a rear shock with a shape more or less dispersed according to diffusion effects or slow mass-transfer kinetics. For larger amounts injected, a second shock appears at the front of the peak.

It is only possible to observe a tailing front in the low sample size range. This effect may not be noticed if large sample loops are employed with heavily loaded columns. For example, in work outlining the advantages of using displacement chromatography [11] for separating β-lact A and B on an anion exchanger, a tailing at the rear edge of the peaks is observed in isocratic elution, probably because of the large sample loop used and therefore the large sample sizes injected.

Simulations of the experimental profiles based on the isotherm assuming a monomer–dimer equilibrium describe well the elution profiles observed in mass-overload conditions. The same association constants K_a and the same maximum loading capacity for the protein are found with monovalent and the divalent counter ions. This result is in good agreement with theory and demonstrates the validity of the isotherm model that assumes protein self-association for describing the elution behaviour of β-lact B on the anion-exchanger support.

The maximum loading capacity of protein is $Q_x/m = 150$ mg, but as with the SDM model without association, an apparent saturation is reached for a smaller amount adsorbed (Fig. 7a). Comparison with the equilibrium isotherm (dashed line) generated with the same values of k' and Q_x/m, but with $Z = 6$ (monovalent displacing ion), indicates that the apparent saturation capacity decreases with increasing Z.

Fig. 7b presents the corresponding Scatchard plots. The S-shaped isotherm induces a positive cooperativity that indicates protein self-association. When there is no association, as previously shown for BSA adsorbed on the same anion exchanger [6], the isotherm has a convex shape and the correspond-

ing Scatchard plot deviates from linearity, indicating that the equilibrium isotherm is not of the Langmuir type. The plot has a hyperbolic shape located lower than the straight line generated with a Langmuirian isotherm ($Z = 1$).

The best fit of the theoretical model to the experimental peaks yields an association constant of $3.7 \cdot 10^5$ l/mol, which is of the same order as that measured in solution. The dimer–monomer equilibrium constant in solution of β-lact B near neutral pH was measured by several methods. The values of association constant obtained at 20°C and pH 7–7.5 by sedimentation equilibrium [36] and light-scattering measurements [37] are $1.26 \cdot 10^5$ and $1.42 \cdot 10^5$ l/mol, respectively.

The difference between the constant determined in this work and that reported in the literature may be due to the different experimental conditions used in this work (higher ionic strength of the solvent). Other reasons are inherent to the theoretical model applied, which is based on simplifying assumptions.

In agreement with the model, the constant K_a and the ratio β are the same with both displacing salts. The parameter β is characteristic of the degree of association of the protein by the support compared with that in solution (eqn. 23). Its value, larger than 1, shows that the adsorption process on the ion exchanger increases the protein self-association. However, the self-association constant of the protein in the adsorbed phase cannot be determined from the β value: this parameter is a function of the reference volume used to define the concentrations of the adsorbed species. When dealing with porous materials, V' may be the pore volume accessible to the protein.

The adsorption isotherm model (eqn. 21) is based on several assumptions and probably the equilibrium constant for associations in solution has to be considered as an apparent value. The model assumes that the charge number of the monomer remains unchanged after association. In fact, the association may mask some charges of the protein and therefore reduce the number of charges of the subunit when associated. Further, the model assumes that the surfaces available for adsorption of the monomer and dimer are equal. This may not be the case, as the Stokes radius of the monomer (2.0 nm) is significantly lower than that of the dimer (2.68 nm) [38].

On the other hand, the desorption step might be slower owing to slow mass exchange with the support. Probably slow mass-transfer kinetics from the bulk phase to the support are the main contribution to the overall kinetics. They are the main source of band broadening for proteins when eluted in isocratic elution [35]. This effect may be accounted for in peak simulations by using a global dispersive term [28].

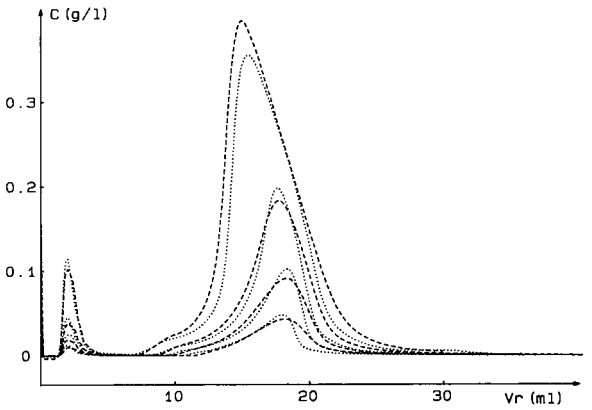

Fig. 8. Study at different flow-rates. Comparison of the experimental profiles of β-lact B eluted from a PVP–PVI anion-exchange column. Sample loop, 0.5 ml; sample size, 0.05–2.5 mg; column length, 10 cm; $V_0 = 1.2$ ml; temperature, 25°C; eluent, 0.020 M Tris buffer (pH 7.5), 0.04 M Na_2SO_4. Dotted lines, 0.5 ml/min; dashed lines, 1.5 ml/min.

Another limitation of the model is that it neglects the kinetic effects due to the slow dimer–monomer exchange: it assumes that the equilibrium is reached for the protein association. Kinetic effects can be revealed by performing the isocratic elution of β-lact B under mass-overload conditions at various flow-rates. The corresponding chromatograms are shown in Fig. 8, where peak profiles are given as a function of the retention volumes for two flow-rates.

For a given mass injected, the general peak shapes observed at 0.5 and 1.5 ml/min are almost the same, except for the diffusive part. This diffusion and also peak tailing become more important with increasing flow-rate. This observation qualitatively shows that kinetic effects are not negligible and do have an influence on peak shapes.

These effects may be due to the slow kinetics of the dimerization of the β-lact B. Indeed, in this study, the rate of the monomer–dimer interconversion during the reversible association has been assumed to be so high that the association equilibrium is

established almost instantaneously. In previous studies of the dimerization of β-lact B near neutral pH, the equilibrium was found to be established immediately on mixing the solution [37,38].

It is difficult to evaluate the relative contribution between mass-transfer kinetics and the slow monomer–dimer kinetic exchanges. Moreover, the chromatograms in Fig. 8 show that the profiles at the two different flow-rates superimpose well enough to be described by a single theoretical profile assuming instantaneous chemical equilibrium.

CONCLUSIONS

This study has shown that the rigourous adsorption isotherm derived from the SDM could be extended to establish the adsorption isotherm expression of self-associating proteins in ion-exchange chromatography. The comparison of the elution profiles predicted on the basis of the SDM theory and the experimental profiles provided information on the nature of the adsorption process on ion exchangers. Using the appropriate parameters derived from the numerical simulations, it has been demonstrated that the β-lact B isotherm is S-shaped and the protein displays a positive cooperativity on adsorption on the ion-exchange surface as indicated by the corresponding Scatchard plot. These results described well the adsorption behaviour of a protein undergoing monomer–dimer equilibrium and predicted well the zonal elution behavior of β-lact B at pH 7.5.

As was shown in the previous work on the adsorption isotherm of a non-associating protein (BSA) in anion-exchange chromatography [6], the non-linear effects in zonal elution due to column overloading could be reduced by using a counter ion with higher valency.

These results indicate that protein aggregation and the value of the ratio Z play a significant role in protein adsorption isotherms in ion-exchange chromatography and should be considered for optimizing protein separations on a preparative scale.

REFERENCES

1 H. G. Barth, W. E. Baker, C. H. Lochmüller, R. E. Majors and F. E. Regnier, *Anal. Chem.*, 60 (1988) 387R.
2 W. Kopaciewicz, M. A. Rounds, J. Fausnaugh and F. E. Regnier, *J. Chromatogr.*, 266 (1983) 3.
3 M. A. Rounds and F. E. Regnier, *J. Chromatogr.*, 283 (1984) 37.
4 A. Velayudhan and Cs. Horváth, *J. Chromatogr.*, 367 (1986) 160.
5 R. D. Whitley, R. Wachter, F. Liu and N. H. L. Wang, *J. Chromatogr.*, 465 (1989) 137.
6 P. Cysewski, A. Jaulmes, R. Lemque, B. Sébille, C. Vidal-Madjar, *J. Chromatogr.*, 548 (1991) 61.
7 W. R. Melander, Z. El Rassi and Cs. Horváth, *J. Chromatogr.*, 469 (1989) 3.
8 M. T. W. Hearn, A. N. Hodder and M. I. Aguilar, *J. Chromatogr.*, 443 (1987) 97.
9 M. T. W. Hearn, A. N. Hodder and M. I. Aguilar, *J. Chromatogr.*, 458 (1988) 45.
10 J. S. Swan, M. Azadpur, A. J. Bharucha and M. A. Krafczyk, *J. Liq. Chromatogr..*, 11 (1988) 3385.
11 A. W. Liao, Z. El Rassi, D. M. LeMaster and Cs. Horváth, *Chromatographia*, 24 (1987) 881.
12 H. A. McKenzie, in H. A. McKenzie (Editor), *Milk Proteins: Chemistry and Molecular Biology*, Vol. II, Academic Press, New York, 1970, p. 304.
13 G. K. Ackers and T. E. Thompson, *Proc. Natl. Acad. Sci. U.S.A.*, 53 (1965) 342.
14 J. P. Mahieu, B. Sébille, C. T. Craescu, M.-D. Rhoda and Y. Beuzard, *J. Chromatogr.*, 327 (1985) 813.
15 V. Baudin-Chich, M. Marden and H. Wajcman, *J. Chromatogr.*, 437 (1988) 193.
16 F. J. Stevens and M. Schiffer, *Biochem. J.*, 195 (1981) 213.
17 F. J. Stevens, *Biophys. J.*, 55 (1989) 1155.
18 E. Chiancone, M. Gattoni and E. Antonini, in I. M. Chaiken, M. Wilchek and I. Parikh (Editors), *Affinity Chromatography and Biological Recognition*, Academic Press, Orlando, FL, 1983, p. 103.
19 E. Chiancone and D. Winzor, *Anal. Biochem.*, 158 (1986) 211.
20 E. Chiancone and M. Gattoni, *Methods Enzymol.*, 135 (1987) 487.
21 E. Chiancone and M. Gattoni, *J. Chromatogr.*, 539 (1991) 455.
22 N. Grinberg, R. Blanco, D. M. Yarmush and B. L. Karger, *Anal. Chem.*, 61 (1989) 514.
23 R. Blanco, A. Arai, N. Grinberg, D. M. Yarmush and B. L. Karger, *J. Chromatogr.*, 482 (1989) 1.
24 S. Lin, R. Blanco and B. L. Karger, *J. Chromatogr.*, 557 (1991) 369.
25 I. S. Krull, R. Mhatre and H. H. Stuting, *Trends Anal. Chem.*, 8 (1989) 260.
26 R. D. Whitley, K. E. Van Cott, J. A. Berninger, N. H. L. Wang, *AIChE J.*, 37 (1991) 555.
27 B. L. Karger and R. Blanco, *Talanta*, 36 (1989) 243.
28 G. Guiochon and A. Katti, *Chromatographia*, 24 (1987) 165.
29 R. D. Whitley, J. M. Brown, N. P. Karajgikar and N. H. L. Wang, *J. Chromatogr.*, 483 (1989) 263.
30 F. D. Antia and Cs. Horváth, *J. Chromatogr.*, 484 (1989) 1.
31 L. R. Snyder, G. B. Cox and P. E. Antle, *J. Chromatogr.*, 444 (1988) 303.
32 G. B. Cox, P. E. Antle and L. R. Snyder, *J. Chromatogr.*, 444 (1988) 325.
33 J. X. Huang, J. Schudèl and G. Guiochon, *J. Chromatogr.*, 504 (1990) 335.

34 B. Sébille, J. Piquion and B. Boussouira, *Eur. Pat. Appl.*, EP225829 (1987).
35 R. Lemque, C. Vidal-Madjar, M. Racine, J. Piquion and B. Sébille, *J. Chromatogr.*, 553 (1991) 165.
36 H. A. McKenzie and W. H. Sawyer, *Nature (London)*, 214 (1967) 1101.
37 C. Georges, S. Guinand and J. Tonnelat, *Biochim. Biophys. Acta*, 59 (1962) 737.
38 H. E. Swaisgood, in P. F. Fox (Editor), *Developments in Dairy Chemistry—1: Proteins* Applied Science, Barking, 1982, p. 46.

Journal of Chromatography, 599 (1992) 267–272
Elsevier Science Publishers B.V., Amsterdam

CHROMSYMP. 2552

Purification and quantification of recombinant Epstein–Barr viral glycoproteins gp350/220 from Chinese hamster ovary cells

Martin Hessing*, Harm B. van Schijndel and Wout M. J. van Grunsven

Biotechnological Research Unit, Organon Teknika, Boseind 15, 5280 AB Boxtel (Netherlands)

Hans Wolf

Max von Pettenkofer Institute, Munich (Germany)

Jaap M. Middeldorp

Biotechnological Research Unit, Organon Teknika, Boseind 15, 5280 AB Boxtel (Netherlands)

ABSTRACT

Truncated Epstein–Barr virus (EBV) membrane antigen gp350/220 (EBV-MA) lacking the membrane anchor was expressed and secreted into the medium of recombinant Chinese hamster ovary cells that had been cultured in Plasmapur hollow-fibre modules using defined serum-free medium. The EBV-MA in the medium was concentrated by 70% (w/v) ammonium sulphate precipitation and subsequently purified by immunoaffinity chromatography using an anti-EBV-MA (EBV.0T6) monoclonal antibody (mAb) column. Adsorbed antigen was eluted with 3 *M* $MgCl_2$ in phosphate-buffered saline, concentrated by Mono Q anion-exchange chromatography and analysed by sodium dodecyl sulphate–polyacrylamide gel electrophoresis, silver staining and Western blotting using EBV-positive serum and anti-EBV-MA specific mAbs. Monospecific polyclonal rabbit antibodies against the purified EBV-MA were raised and purified by protein G affinity chromatography. For the measurement of EBV-MA antigen levels a sandwich enzyme-linked immunosorbent assay using rabbit polyclonal antibodies and a horseradish peroxidase-conjugated anti-MA mAb was developed having a detection level of 10 ng/ml.

INTRODUCTION

The Epstein–Barr virus (EBV) is a human lymphotropic and immunomodulating herpes virus which causes infectious mononucleosis upon primary infection in adults [1]. In addition, EBV is associated with a number of other human malignancies, *e.g.*, nasopharyngeal carcinoma and Burkitt's lymphoma. Another result of primary infection is the presence in serum of antibodies to a number of EBV antigens, some of which are maintained at constant levels throughout life. One possibility for affecting the course of the various EBV-associated diseases is vaccination. At the moment the target antigen for the development of an EBV vaccine is the EBV membrane antigen (EBV-MA) gp350/220 complex [2–4], which is found both on the envelopes of viral particles [5] and on the surface of EBV producer cells. In addition, EBV-MA may be a useful antigen in diagnostic assays.

EBV-MA consists of the glycoproteins gp350 and gp220 that are encoded by the same gene, which has been mapped to the BamHI L DNA fragment of the B95-8 genome [6]. The mRNA of gp220 arises by internal splicing of the mRNA of gp350 in such a manner that the same open reading frame (BLLF1) is maintained [6]. EBV-MA is important for virion binding to human B lymphocytes via its specific in-

0021-9673/92/$05.00

teraction with the complement receptor 2 (CR2) [7] and is also an efficient activator of the alternative pathway of complement [8]. The gp350 primary sequence consists of 907 amino acids and includes 36 potential signals for N-linked glycosylation, a single hydrophobic transmembrane domain and a short C-terminal domain. More than half of the relative molecular mass (M_r) is contributed by glycosyl residues. EBV-MA is synthesized in the endoplasmic reticulum, undergoes rapid cotranslational N-linked glycosylation and is transported to the Golgi, where high-mannose N-linked oligosaccharides are trimmed and complex N- and O-linked oligosaccharides are added [9–13].

Several monoclonal antibodies (mAbs) against EBV-MA have been prepared and it has been reported by different groups that such antibodies mediate virus neutralization, antibody-dependent cellular cytotoxicity, complement-dependent cytotoxicity and inhibition of virus release [14–18]. It should be emphasized that the different epitopes of the EBV-MA complex play variable roles in virus neutralization, virus binding to target cell receptors and virus penetration [19]. Recent data suggest that only one epitope, located in the N-terminal region of EBV-MA, is involved in EBV neutralization and binding to target cell receptors [9,20].

Production of native EBV-MA for vaccination or diagnostic purposes is hampered by the lack of a suitable high-level expression system [3,4]. Recombinant EBV-MA has been produced in bacteria [21], yeast [22], mouse L cells [29], rat pituitary GH3 cells [23], Vero cells [23] and Chinese hamster ovary (CHO) cells [24] and has been expressed via different viral vectors [3,25,26]. Although cell-specific post-translational modifications critically influence the antigenic presentation of EBV-MA, all mammalian cell-derived versions of EBV-MA were found capable of inducing EBV-specific neutralizing antibodies [2]. As expressing levels of recombinant EBV-MA were low, suggesting that the protein is toxic for eukaryotic cells, truncated forms of EBV-MA lacking the membrane anchor have been expressed [2,27,28]. Truncated EBV-MA was secreted into the medium of transformed cells in culture. Determination of truncated EBV-MA secretion was difficult and for CHO cells has been estimated from Coomassie Brilliant Blue-stained gels to be in the range 1–10 μg per 10^6 cells per day [28].

In this paper we describe the culturing and purification of recombinant truncated EBV-MA from CHO cells [28] by mAb-based affinity chromatography and the subsequent development of an enzyme-linked immunosorbent assay (ELISA) procedure for the measurement of EBV-MA antigen levels.

EXPERIMENTAL

Materials

Protein G-Sepharose FF, a Mono Q column and cyanogenbromide-activated Sepharose were obtained from Pharmacia LKB Biotechnology (Uppsala, Sweden). Prestained molecular mass markers and N,N'-diallyltartardiamide (DATD) were obtained from Bio-Rad Labs. (Richmond, CA, USA). All culture plastics were obtained from Costar (Badhoevedorp, Netherlands). Culture media were based on HAM's F12–Dulbecco's modified Eagle's medium (DMEM) (1:1) from Gibco (Paisley, UK) and were occasionally supplemented with 10% foetal calf serum (Bocknek, Canada). Plasmapur hollow-fibre modules and bovine serum albumin (BSA) were from Organon Teknika (Boxtel, Netherlands). Horseradish peroxidase (HRP) was purchased from Sigma (St. Louis, MO, USA). All other chemicals were of the highest grade available.

Antibodies

Polyclonal antibodies against EBV-MA were obtained from rabbits by multiple subcutaneous injections of 0.2 mg of purified EBV-MA in Freund's complete adjuvant and after 2, 4 and 6 weeks they were boosted with the same amount of antigen in incomplete adjuvant. Anti-EBV-MA specific mAbs (EBV.OT2, -3, -6 and -7) were prepared as will be described elsewhere. MAb EBV.OT1C was generously provided by Dr. D. Thorley-Lawson. Hybridomas were cultured in serum-free medium using Plasmapur hollow-fibre bioreactors [29]. Supernatants from the extra-capillary compartment were harvested, centrifuged, divided into aliquots and stored at −20°C. The total mouse immunoglobulin G (IgG) concentration in samples of hybridoma cultures was determined using the Sol Particle Immunoassay [30]. IgGs were isolated on protein G-Sepharose FF according to the instructions of the manufacturer. The concentration of the purified monoclonal antibodies was determined by measur-

ing the absorbance at 280 nm using a molar absorptivity (1%, 1 cm) of 14.3 [31].

Human sera

EBV-seropositive sera were obtained from healthy laboratory volunteers and commercial blood donor populations. Sera from acutely infected patients were provided by Dr. G. Weers-Pothof (Department of Medical Microbiology, University Hospital, Nijmegen, Netherlands).

Purification of EBV-MA

Culturing of CHO cells secreting truncated EBV-MA was performed in roller bottles under methotrexate selection [28]. When the cells were in the logarithmic phase they were inoculated in the extra-capillary compartment of hollow-fibre bioreactors and cultured without methotrexate essentially as described above for the hybridomas [29].

The EBV-MA in the extra-capillary harvest fluid of the CHO cells was precipitated with 70% (w/v) ammonium sulphate and dissolved in phosphate-buffered saline (PBS) (pH 7.4) and dialysed against the same buffer. Then EBV-MA was purified by monoclonal anti-EBV-MA antibody affinity chromatography. For this mAb EBV.OT6 was coupled to cyanogen bromide-activated Sepharose 4B (10 mg/ml) according to the manufacturer's instructions, and the gel was packed into a column (15 × 1 cm I.D.). EBV-MA-containing dialysate was passed through a Millex-HA 0.22-μm filter (Millipore) and subsequently applied to the column, which had been equilibrated in PBS (pH 7.4) (10 ml/h). After extensive washing with the equilibration buffer, adsorbed EBV-MA was eluted with 3 *M* $MgCl_2$ in PBS (pH 7.4). The eluted protein fractions were pooled and dialysed against 50 m*M* Tris–HCl–50 m*M* NaCl (pH 7.4). Concentration of EBV-MA and removal of traces of IgG leakage from the affinity matrix was performed with Mono Q anion-exchange chromatography using fast protein liquid chromatographic (FPLC) equipment (Pharmacia) with a linear gradient of NaCl (50–500 m*M* NaCl, 20 ml) with a flow-rate of 60 ml/h and a fraction size of 1 ml. Protein concentrations were determined by the bicinchoninic acid (BCA) protein assay (Pierce, Rockford, IL, USA) using BSA as reference.

Electrophoretic and immunochemical techniques

Sodium dodecyl sulphate–polyacrylamide gel electrophoresis (SDS-PAGE) was performed under non-reducing and reducing conditions on 6% slab gels with DATD as cross-linker using the Mini-Protean II system (Bio-Rad Labs.) or on 4–15% gradient gels using the Phast system (Pharmacia) essentially according to Laemmli [32]. After electrophoresis, proteins were transferred to Immobilon membranes (Millipore) essentially as described [33]. The membranes were blocked with 5% (v/v) horse serum, 4% (w/v) non-fat dry milk [34] in PBS, incubated with monoclonal or polyclonal antibodies against EBV-MA and visualized with peroxidase-conjugated antiserum using 4-chloro-1-naphthol as substrate.

The gels were stained with Coomassie Brilliant Blue R-250 or with an ammonical silver staining procedure essentially according to Morrisey [35]. Reduction was performed by incubating the samples for 5 min at 90°C with 5% (v/v) 2-mercaptoethanol–10 m*M* Tris–HCl–2% (w/v) SDS–0.01% (w/v) bromophenol blue–10% (v/v) glycerol (pH 6.8).

ELISA for the measurement of EBV-MA

A two-stage ELISA was developed using polyclonal anti-EBV-MA IgG and an HRP-conjugated anti-EBV-MA mAb. Purified polyclonal anti-EBV-MA antibodies (5 μg/ml, 50 m*M* $NaHCO_3$, pH 9.6) were coated overnight on 96-well microtitre plates (Greiner) at 4°C. After removal of unbound EBV-MA antibodies by washing with PBS–Tween-20, the plates were blocked with 3% (w/v) BSA in PBS for 30 min and subsequently incubated with dilutions of purified EBV-MA [in 5% (v/v) normal goat serum–0.05% (v/v) Tween-20 in PBS] at room temperature for 2 h. After washing, HRP-conjugated mAb (EBV.OT6) was applied and incubated for 1 h. Bound conjugated antibody was developed for peroxidase activity using the substrate 3,3′, 5,5′-tetramethylbenzidine. The absorbance at 450 nm was read against a blank using an Anthos 2001 reader. MAb EBV.OT6 was conjugated with HRP (Type VI) (Sigma) by periodate oxidation.

RESULTS

Characterization of monoclonal antibodies against EBV-MA

For the development of an EBV-MA specific immunoaffinity purification process, five mouse mAbs against EBV-MA were obtained and characterized by Western blotting and ELISA. The mAbs EBV.OT1C and EBV.OT6 demonstrated a strong positive reactivity with EBV-MA in ELISA (Fig. 1), whereas the mAb's EBV.OT 2, 3 and 7 showed minor reactivity. As only mAb EBV.OT6 was reactive in Western blotting (Fig. 2), this mAb was selected for purification purposes.

Purification of EBV-MA

Recombinant truncated EBV-MA secreting CHO cells were cultured in Plasmapur hollow-fibre modules using defined serum-free medium. Fig. 3 shows a Western blot analysis of supernatants derived from the cell line at several days of culture using an anti-EBV positive human serum. Owing to extensive glycosylation EBV-MA appears as diffuse bands.

The EBV-MA was purified from the medium of CHO cells by ammonium sulphate precipitation, monoclonal anti-EBV-MA antibody affinity and Mono Q anion-exchange chromatography (not shown), and subsequently analysed by SDS-PAGE and Western blotting. The purified EBV-MA demonstrated a characteristic doublet of gp350 and gp220 on a silver-stained SDS–polyacrylamide (PAA) slab gel and was devoid of low-M_r contaminants (Fig. 4a). Reduced and non-reduced purified EBV-MA showed similar electrophoretic mobilities (not shown). Fig. 4b shows the positive reactivity of the purified EBV-MA with the HRP-labelled anti-

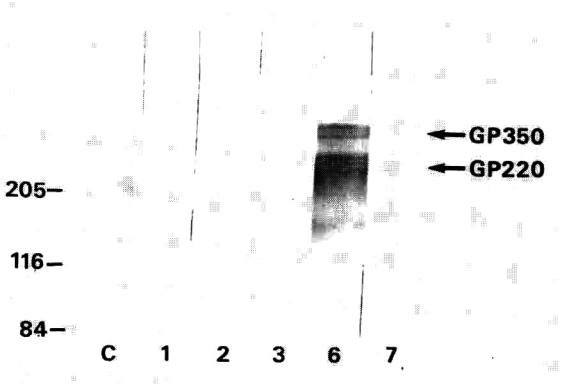

Fig. 2. Western blot analysis of the reactivity of different anti-EBV-MA mAbs with recombinant EBV-MA. EBV-MA was subjected to 6% SDS-PAGE and the gels were transferred to Immobilon membranes. The membranes were incubated with the mAbs and visualized with peroxidase-conjugated antiserum. M_r standards (kilodaltons) and a positive control (C) with EBV-positive human serum are included.

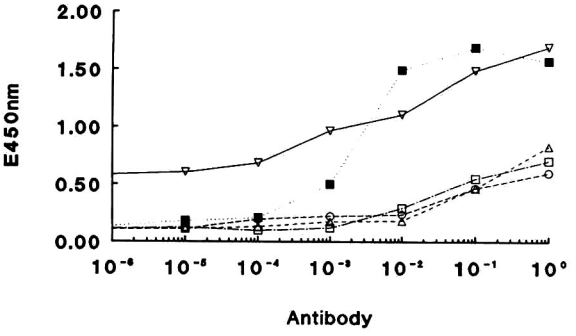

Fig. 1. Reactivity of mAbs with recombinant truncated EBV-MA. The binding activities of (▽) mAb EBV.OT1C, (△) -2, (○) -3, (■) -6 and (□) -7 to recombinant EBV-MA were determined by ELISA. Microtitre wells were coated with 1:100 dilutions of ammonium sulphate-concentrated EBV-MA preparations and incubated with various concentrations of each mAb. Bound antibody was detected with peroxidase-conjugated sheep anti-mouse IgG and 3,3′,5,5′-tetramethylbenzidine.

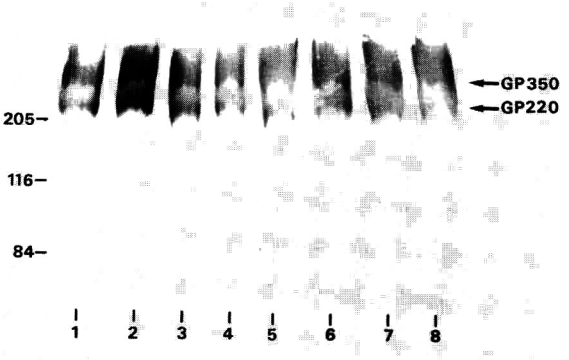

Fig. 3. Western blot analysis of culture supernatants from CHO cells secreting truncated EBV-MA [28]. Culture supernatants from subsequent passages were run on a 6% SDS-PAA gel and transferred to Immobilon membranes. The membranes were developed with a 1:1000 dilution of an anti-EBV positive human serum and HRP-labelled anti-human antiserum.

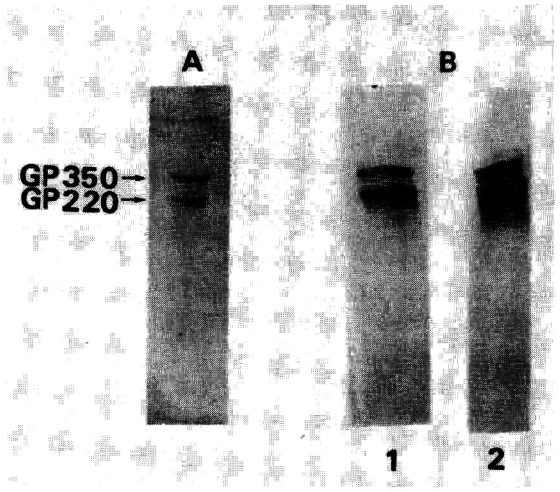

Fig. 4. SDS-PAGE of immunopurified recombinant EBV-MA visualized by (A) silver staining and (B) immunoblotting. Reduced EBV-MA was subjected to 6% SDS-PAGE and the gels were stained with silver or transferred to Immobilon membranes. The membranes were incubated with the mAb EBV.OT6 (lane 1) or human serum (lane 2) and visualized with peroxidase-conjugated antiserum. M_r standards are indicated (kilodalton).

EBV-MA mAb EBV.OT6 and an EBV-positive human serum in Western blotting analysis.

ELISA for EBV-MA

A two-stage EBV-MA ELISA was developed using immunopurified polyclonal anti-EBV-MA IgG, coated to 96-well microtitre plates, in the solid phase and peroxidase-conjugated monoclonal anti-EBV-MA IgG in the liquid phase. Fig. 5 shows a representative dose–response curve for the EBV-MA ELISA. A significant difference in absorbance as compared with buffer alone corresponded to a detection limit of about 10 ng/ml.

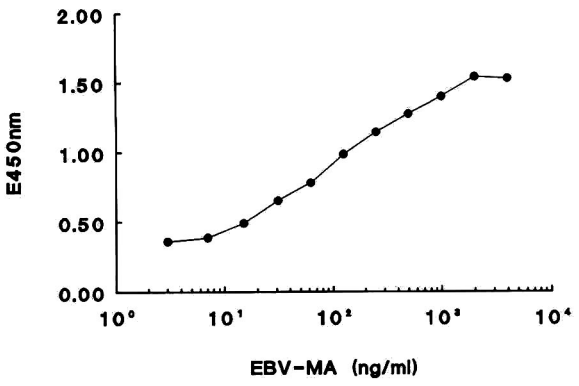

Fig. 5. Dose–response curve of serially diluted EBV-MA in ELISA.

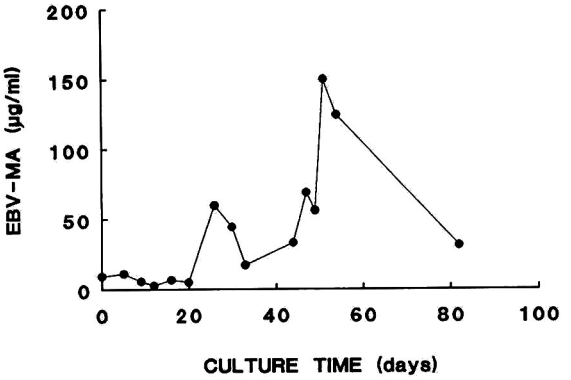

Fig. 6. Long-term cultivation of CHO cells secreting truncated EBV-MA in hollow-fibre modules. Monitoring of EBV-MA production was performed during the culture period as measured by ELISA.

The EBV-MA production during the cell culture period of the CHO cells was monitored by this procedure, as shown in Fig. 6. Starting at day 0 a concentration of 9.3 µg/ml of EBV-MA (in roller bottle culture) was obtained. The concentration of EBV-MA in the medium of the hollow-fibre modules increased slowly up to 20 days, followed by a period of decline. This decline was caused by the change of the culture in the extra-capillary compartment to a serum-free medium. Subsequently, a period of exponential increase of EBV-MA production was observed that reached its maximum (150 µg/ml) at day 50 which was followed by a period of decline until the end of the culture.

DISCUSSION

Truncated recombinant EBV-MA derived from CHO cells was purified by ammonium sulphate precipitation and anti-EBV-MA mAb affinity and anion exchange chromatography. Both gp350 and gp220 species were obtained, which is in agreement with previously reported results [24,28]. The observed M_r values suggest a close to natural glycosylation, which is relevant for vaccination purposes [2–4]. However, the nature of the N- and O-linked

oligosaccharides attached to the recombinant EBV-MA remains to be characterized. The recombinant CHO cell line showed stable production characteristics over several weeks under serum-free culture conditions without methotrexate selection. No dramatic changes were observed in either production level (about 75 μg/ml per day) or the nature of the protein species produced. Hence the procedure described in this paper allows for the development of a simple, efficient and economical system for the large-scale production of EBV-MA.

The purified EBV-MA may be used for a possible EBV subunit vaccine or could be used as antigen for early diagnosis, thereby providing an efficient approach to the control of EBV-related diseases. The EBV-MA itself can be used for immunological studies or used in ELISAs for determining antibody to EBV-MA or used in receptor binding studies [7]. In this study, we developed a monoclonal antibody-based ELISA for the determination of EBV-MA in cell culture. The assay was sensitive, accurate and specific with a limit of detection of EBV-MA antigen of about 10 ng/ml. This assay may be generally useful in the determination of EBV-MA derived from natural or recombinant sources.

REFERENCES

1 K. Nilsson, G. Klein, W. Henle and G. Henle, *Int. J. Cancer*, 8 (1971) 443–450.
2 E. A. Emini, W. A. Schleif, M. C. Armstrong, M. Silberklang, L. D. Schlutz, D. Lehman, R. Z. Maigetter, L. F. Qualtiere, G. R. Pearson and R. W. Ellis, *Virology*, 166 (1988) 387–393.
3 A. J. Morgan, M. Mackett, S. Finerty, J. R. Arrand, F. Scullion and M. A. Epstain, *J. Med. Virol.*, 25 (1988) 189–195.
4 A. J. Morgan, A. C. Allison, S. Finerty, N. E. Byars and M. A. Epstein, *J. Med. Virol.*, 29 (1989) 74–78.
5 G. R. Pearson and L. F. Qualtiere, *J. Virol.*, 28 (1978) 344–351.
6 M. Hummel, D. A. Thorley-Lawson and E. Kieff, *J. Virol.*, 49 (1984) 413–417.
7 J. Tanner, J. Weis, D. Fearon, Y. Whang and E. Kieff, *Cell*, 50 (1987) 203–213.
8 C. Mold, B. M. Bradt, G. R. Nemerow and N. R. Cooper, *J. Immunol.*, 140 (1988) 3867–3874.
9 G. R. Nemerow, R. A. Houghten, M. D. Moore and N. R. Cooper, *Cell*, 56 (1989) 369–377.
10 C. M. Edson and D. A. Thorley-Lawson, *J. Virol.*, 46 (1983) 547–556.
11 F. Serafini-Cessi, N. Malagolini, M. Nanni, F. Dallolio, G. Campadelli-Fiume, J. Tanner and E. Kieff, *Virology*, 170 (1989) 1–10.
12 B. C. Strnad, M. R. Adams and H. Rabin, *Virology*, 127 (1983) 168–176.
13 J. Tanner, Y. Whang, J. Sample, A. Sears and E. Kieff, *J. Virol.*, 62 (1988) 4452–4464.
14 G. Hoffman, S. Lazarowitz and S. D. Hayward, *Proc. Natl. Acad. Sci. U.S.A.*, 77 (1980) 2979–2983.
15 L. F. Qualtiere, R. Chase, B. Vroman and G. R. Pearson, *Proc. Natl. Acad. Sci. U.S.A.*, 79 (1982) 616–620.
16 L. F. Qualtierre, J. F. Decoteau and M. H. Nasr-El-Din, *J. Gen. Virol.*, 68 (1987) 535–543.
17 D. A. Thorley-Lawson and K. Geillinger, *Proc. Natl. Acad. Sci. U.S.A.*, 77 (1980) 5307–5311.
18 T. Sairenji, P. S. Reisert and R. C. Spiro, *J. Exp. Med.*, 161 (1985) 1097–1111.
19 M. A. Epstein, B. J. Randle and S. Finerty, *Clin. Exp. Immunol.*, 63 (1986) 485–490.
20 R. Stocco, G. Sauvageau, I. Stefanescu and J. Menezes, *Intervirology*, 31 (1990) 295–300.
21 C. Beisel, J. Tanner, T. Matsuo, D. Thorley-Lawson, F. Kezdy and E. Kieff, *J. Virol.*, 54 (1985) 665–674.
22 L. D. Schultz, J. Tanner, K. Hofmann, K. J. Emini, J. H. Condra, R. E. Jones, E. Kieff and R. W. Ellis, *Gene*, 54 (1987) 113–123.
23 Y. Whang, M. Silberkalng, A. Morgan, S. Munski, A. Lenny and E. Kieff, *J. Virol.*, 61 (1987) 1796–1807.
24 M. Motz, G. Deby, W. Jilg and H. Wolf, *Gene*, 44 (1986) 353–359.
25 R. S. Lowe, P. M. Keller, B. J. Keeck, A. J. Davidson, Y. Whang, A. J. Morgan, E. Kieff and R. W. Ellis, *Proc. Natl. Acad. Sci. U.S.A.*, 84 (1987) 3896–3900.
26 M. Mackett and J. R. Arrand, *EMBO J.*, 4 (1985) 3229–3234.
27 M. Conway, A. Morgan and M. Mackett, *J. Gen. Virol.*, 70 (1989) 729–734.
28 M. Motz, G. Deby and H. Wolf, *Gene*, 58 (1987) 149–154.
29 O. T. Schonherr, P. T. J. A. van Gelder, P. J. van Hees, A. M. J. M. van Os and H. W. M. Roelofs, *Dev. Biol. Stand.*, 66 (1987) 211–220.
30 J. H. W. Leuvering, B. C. Goverde, P. J. H. M. Thal and A. H. W. M. Schuurs, *J. Immunol. Methods*, 60 (1983) 9–23.
31 J. R. Little and H. Donahue, *Methods Immunol. Immunochem.*, 2 (1968) 343–368.
32 U. K. Laemmli, *Nature (London)*, 227 (1970) 680–685.
33 H. Towbin, Th. Staehelin and J. Gordon, *Proc. Natl. Acad. Sci. U.S.A.*, 76 (1979) 4350–4354.
34 D. A. Johnson, J. W. Gautsch, J. R. Sportman and J. H. Elder, *Gene Anal. Tech.*, 1 (1984) 3–8.
35 J. H. Morrisey, *Anal. Biochem.*, 117 (1981) 307–310.

Author Index

PUBLICATION SCHEDULE FOR 1992

Journal of Chromatography and *Journal of Chromatography, Biomedical Applications*

MONTH	O 1991–F 1992	M	A	M	J	
Journal of Chromatography	Vols. 585–593	594/1 + 2 595/1 + 2	596/1 596/2 597/1 + 2	598/1 598/2 599/1 + 2 600/1 600/2	602/1 + 2	The publication schedule for further issues will be published later.
Cumulative Indexes, Vols. 551–600						
Bibliography Section		610/1			610/2	
Biomedical Applications	Vols. 573 and 574	575/1 575/2	576/1	576/2 577/1	577/2	

INFORMATION FOR AUTHORS

(Detailed *Instructions to Authors* were published in Vol. 558, pp. 469–472. A free reprint can be obtained by application to the publisher, Elsevier Science Publishers B.V., P.O. Box 330, 1000 AH Amsterdam, The Netherlands.)

Types of Contributions. The following types of papers are published in the *Journal of Chromatography* and the section on *Biomedical Applications:* Regular research papers (Full-length papers), Review articles and Short Communications. Short Communications are usually descriptions of short investigations, or they can report minor technical improvements of previously published procedures; they reflect the same quality of research as Full-length papers, but should preferably not exceed five printed pages. For Review articles, see inside front cover under Submission of Papers.

Submission. Every paper must be accompanied by a letter from the senior author, stating that he/she is submitting the paper for publication in the *Journal of Chromatography*.

Manuscripts. Manuscripts should be typed in double spacing on consecutively numbered pages of uniform size. The manuscript should be preceded by a sheet of manuscript paper carrying the title of the paper and the name and full postal address of the person to whom the proofs are to be sent. As a rule, papers should be divided into sections, headed by a caption (*e.g.*, Abstract, Introduction, Experimental, Results, Discussion, etc.). All illustrations, photographs, tables, etc., should be on separate sheets.

Introduction. Every paper must have a concise introduction mentioning what has been done before on the topic described, and stating clearly what is new in the paper now submitted.

Abstract. All articles should have an abstract of 50–100 words which clearly and briefly indicates what is new, different and significant.

Illustrations. The figures should be submitted in a form suitable for reproduction, drawn in Indian ink on drawing or tracing paper. Each illustration should have a legend, all the *legends* being typed (with double spacing) together on a *separate sheet.* If structures are given in the text, the original drawings should be supplied. Coloured illustrations are reproduced at the author's expense, the cost being determined by the number of pages and by the number of colours needed. The written permission of the author and publisher must be obtained for the use of any figure already published. Its source must be indicated in the legend.

References. References should be numbered in the order in which they are cited in the text, and listed in numerical sequence on a separate sheet at the end of the article. Please check a recent issue for the layout of the reference list. Abbreviations for the titles of journals should follow the system used by *Chemical Abstracts.* Articles not yet published should be given as "in press" (journal should be specified), "submitted for publication" (journal should be specified), "in preparation" or "personal communication".

Dispatch. Before sending the manuscript to the Editor please check that the envelope contains four copies of the paper complete with references, legends and figures. One of the sets of figures must be the originals suitable for direct reproduction. Please also ensure that permission to publish has been obtained from your institute.

Proofs. One set of proofs will be sent to the author to be carefully checked for printer's errors. Corrections must be restricted to instances in which the proof is at variance with the manuscript. "Extra corrections" will be inserted at the author's expense.

Reprints. Fifty reprints of Full-length papers and Short Communications will be supplied free of charge. Additional reprints can be ordered by the authors. An order form containing price quotations will be sent to the authors together with the proofs of their article.

Advertisements. The Editors of the journal accept no responsibility for the contents of the advertisements. Advertisement rates are available on request. Advertising orders and enquiries can be sent to the Advertising Manager, Elsevier Science Publishers B.V., Advertising Department, P.O. Box 211, 1000 AE Amsterdam, Netherlands; courier shipments to: Van de Sande Bakhuyzenstraat 4, 1061 AG Amsterdam, Netherlands; Tel. (+31-20) 515 3220/515 3222, Telefax (+31-20) 6833 041, Telex 16479 els vi nl. *UK*: T. G. Scott & Son Ltd., Tim Blake, Portland House, 21 Narborough Road, Cosby, Leics. LE9 5TA, UK; Tel. (+44-533) 753 333, Telefax (+44-533) 750 522. *USA and Canada*: Weston Media Associates, Daniel S. Lipner, P.O. Box 1110, Greens Farms, CT 06436-1110, USA; Tel. (+1-203) 261 2500, Telefax (+1-203) 261 0101.

The most useful chiral separation column, ULTRON ES-OVM, for enantiomeric drugs.

Substance	Rs	Substance	Rs	Substance	Rs
Acetylpheneturide	2.74	Disopyramid	2.04	Nisoldipine	2.36
Alimemazine	6.06	Eperisone	1.15	Nitrendipine	1.80
Alprenolol	1.09[1)]	Ethiazide	1.42	Oxazepan	2.65[2)]
Arotinolol	1.95	Fenoprofen	0.80	Oxprenolol	1.38
Bay K 8644	5.92	Flurbiprofen	1.27	Pindolol	2.04
Benproperine	3.27	Glutethimide	1.36	2-Phenylpropionic acid	0.80
Benzoin	8.41	Glycopyrronium	1.73	Pranoprofen	0.63
Biperiden	3.17	Hexobarbital	1.70	Prenylamine	0.86
Bunitrolol	3.08	Homochlorcyclizine	3.04	Profenamine	3.31
Bupivacaine	1.26	Hydroxyzine	2.15	Promethazine	1.42
Chlormezanone	6.48	Ibuprofen	1.72	Propranolol	1.24
Chlorphenesin	2.23	Ketoprofen	1.37	Terfenadine	2.22
Chlorpheniramine	2.36	Lorazepam	2.55[2)]	Thioridazine	0.72
Chlorprenaline	2.34	Meclizine	3.71	Tolperisone	1.50
Cloperastin	2.85	Mepenzolate	1.40	Trihexyphenidyl	5.16
Dimethindene	4.33	Mephobarbital	1.70	Trimipramine	3.69
1,2-Diphenylethylamine	1.74	Methylphenidate	1.13[1)]	Verapamil	1.49

NOTE: 4.6×150mm column at room temp. except[1)] 6.0×150mm at room temp. and[2)] 6.0×150mm at 10°C

From trace analysis for metabolites

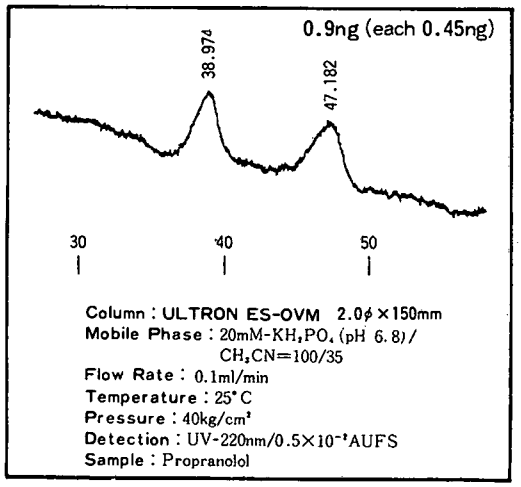

Column : ULTRON ES-OVM 2.0φ×150mm
Mobile Phase : 20mM-KH_2PO_4 (pH 6.8)/CH_3CN=100/35
Flow Rate : 0.1ml/min
Temperature : 25°C
Pressure : 40kg/cm²
Detection : UV-220nm/0.5×10⁻¹AUFS
Sample : Propranolol

to preparative scale

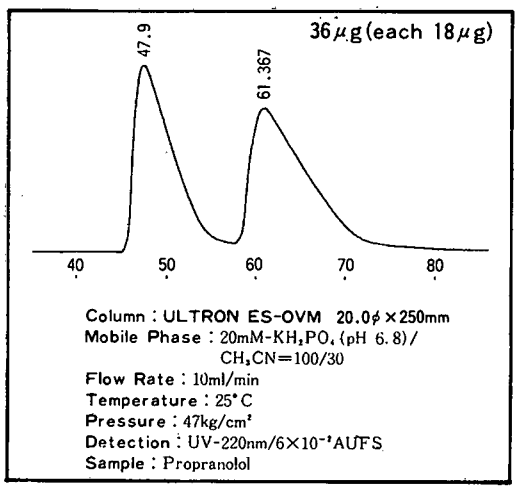

Column : ULTRON ES-OVM 20.0φ×250mm
Mobile Phase : 20mM-KH_2PO_4 (pH 6.8)/CH_3CN=100/30
Flow Rate : 10ml/min
Temperature : 25°C
Pressure : 47kg/cm²
Detection : UV-220nm/6×10⁻¹AUFS
Sample : Propranolol

SHINWA CHEMICAL INDUSTRIES, LTD

50 Kagekatsu-cho, Fushimi-ku, Kyoto 612, JAPAN

Phone: 80-75-621-2360 Fax : 80-75-602-2660

Please contact in United States of America and Europe to :

Rockland Technologies, Inc. 538 First State Boulevard, Newport, DE 19804, U.S.A.

Phone : 302-633-5880, Fax : 302-633-5893

This product is licenced by Eisai Co., Ltd.